Università Degli Studi Di Napoli

"Federico II"

Dipartimento di farmacia

Dottorato di Ricerca in
"Scienza del Farmaco"
Ciclo XXXIII 2018-2021

"Emerging toxins of European concern: identification, development of reference material and methods for their detection"

Fabio Varriale

Tutor

Prof.ssa

Carmela Dell'Aversano

Coordinator

Prof.ssa

Maria Valeria D'Auria

Alla mia famiglia,

fonte inesauribile di amore ed energia.

Table of contents

Table list

6

Figure list

13

Summary

Phytoplankton is the autotrophic component of marine and freshwater ecosystems whose activity is crucial for the well-being of all the living organisms, including terrestrial and aquatic ones. However, a certain number of species belonging to the wide group of dinoflagellates and cyanobacteria may pose a serious threat for the safety of humans and wild animals due to the production of toxic secondary metabolites known as biotoxins. These noxious microorganisms, under specific and not fully clarified environmental conditions can massively enhance their proliferation rate through the so-called harmful algal bloom (HAB). This scenario raises even more concerns as the effects of the anthropogenic pressure on the whole ecosystem are leading to tremendous environmental changes, which are promoting the incidence and the spread of HABs all over the world. The impact of HABs is drastic since the increased density of harmful algae and consequently, the presence of high toxin levels in the aquatic systems, strongly affect the economy of coastal areas and, more importantly, represents an actual risk for both environment and human health. The biotoxins can indeed accumulate in the edible tissues of a wide number of organisms within the marine trophic chain, thus ending up on the table of unaware consumers. As a consequence, the consumption of contaminated seafood can give rise to characteristic food-borne illnesses. Beside the oral route, phycotoxins can result in human poisoning following inhalation of toxic aerosols and/or direct skin contact. In order to safeguard the public health and limiting the adverse effects of HABs, governments in collaboration with food safety agencies released specific legislations to regulate the maximum permitted level of toxins in seafood. These regulations require a strict surveillance of toxins in food chain and in the environment through the implementation of routine monitoring programs which are conducted by national and local competent health protection authorities. Unfortunately, a wide range of factors are steadily increasing the proliferation of the microalgal community, with the displacement of known and unknown alien toxin-producing species in regions where they were not historically confined like the Mediterranean basin. This has determined the appearance in temperature regions of new structurally-related compounds designated as ''*Emerging Toxins*'', which are currently non-regulated in EU, thus not regularly monitored through surveillance activities. Their presence in waters and seafood is a matter of concern for competent authorities, which required efforts from

the scientific community before establishing a meaningful regulation. The development of sensitive and effective analytical methods for the detection of toxins and their metabolites in seafood, as well as the production of reference material, which is fundamental for the optimization of analytical techniques and for conducting toxicological studies, are high priority tasks for facing the emerging toxins related issues. Among the variety of instrumental techniques developed so far, the hyphenated techniques mainly based on the combination of liquid chromatography coupled to mass spectrometry (LC-MS) have proven to be effective and robust enough for monitoring phycotoxins in environmental and food samples. In addition, the employment of high-resolution multiple stage mass spectrometry (HRMS^n) demonstrated suitable for the identification and characterization of new structural analogues contained at trace levels in complex matrices.

At this regard, the aim of my PhD project was the study of the main classes of emerging toxins of European concern using LC-HRMS as method of choice. Different LC-HRMS methods were developed and optimized for each group of analytes to achieve the best analytical performances in terms of sensitivity, reproducibility and specificity. Such methods were subsequently applied to the analysis of complex matrices for determination of known compounds, as well as for identification and tentative structural characterization of new toxins and their biotransformation products. Notably:

Chapter 1 is a general introduction which reports on: i) the importance of phytoplankton in the aquatic ecosystems, ii) the real threat of harmful algal blooms for living species, iii) toxins currently regulated in EU, and iv) a detailed description of the emerging toxins.

Chapter 2 describes the development of a LC-HRMS method for the analysis of assorted cyclic imines (CIs) and its application to shellfish samples from the Mediterranean basin (Italy and Tunisia) and the Galician coastline (Spain). A mixture of CI standards containing pinnatoxin G and A (PnTX-G and -A), gymnodimine A (GYM-A) and 13desmethyl spirolide C (13desMeSPX-C) was used to optimize the chromatography, the MS parameters, and to evaluate the analytical performances and the matrix interference. The optimized HRMS^2 conditions provided for each toxin highly informative fragmentation spectra, whose complete interpretation allow to discover previously unreported fragment ions, and a new fragmentation pathway co-occurring with the main retro-Diels-Alder ring opening. The application of the implemented LC-HRMS method to the

analysis of Tunisian shellfish revealed high levels of gymnodimine A (376.5 µg/Kg) together with lower levels of five isobaric analogues of GYM-B/C and a new structural congener, which was named GYM-F, whose structure was proposed based on its fragmentation patterns. The high level of GYMs in the Tunisian sample prompted to deeply investigate the metabolic profile of the contaminated shellfish. So, a LC-HRMS data-dependent acquisition (DDA) based-approach was implemented and successfully applied, in combination with targeted HRMS[2] experiments, to the analysis of GYM fatty acid ester metabolites. The optimized methodology revealed the presence of a wide number of esters of GYM-A and -B/C, including new metabolites esterified with atypical hydroxylated, polyhydroxylated and odd-chain fatty acids. The study of the fragmentation pattern of GYM esters, in association with the finding of several isobaric ester metabolites, led to set up a new MS-based strategy, labeled as backward analysis, whose application successfully revealed the presence of new GYMs starting from the identification of their ester metabolites; the new congeners were named GYM-G, -H, -I and J. A careful interpretation of their HRMS[2] spectra allowed to propose the chemical structure of GYM-G and partially that of GYM-H, whereas only structural hints were obtained for the others due to their low relative abundance. In addition, the application of the optimized LC-HRMS method brought to the light the presence of PnTX-G (6.8 µg/Kg) for the first time in *M. galloprovincialis* from Sardinia (Thyrrenean Sea, Italy) and in mussels from the Atlantic coast of Spain (Galicia) in the range 3.1-7.7 µg/Kg. The same Spanish mussels were found to be even contaminated by 13desMeSPX-C (11.0-29.0 µg/Kg).

Chapter 3 reports on the development, the analytical comparison and the application of 3 HILIC-HRMS methods, labeled as method 1, 2 and 3, for the simultaneous determination of 13 paralytic shellfish toxins (PSTs) and tetrodotoxin (TTX) in seafood by using the Orbitrap MS. The main challenge was the implementation of a reliable and highly sensitive multi-analyte method as the reduced scan frequency due to long injection times, which are essential for the acquisition of the accurate masses, strongly affects the instrumental limits of detection and method applicability. Although methods 1 and 2 differed for chromatographic conditions and consequently, for ESI source parameters, they shared the acquisition mode, which was based on the time segmentation technique. The latter allows to select a defined number of analytes to monitor in a specific time segment, or window, thus resulting in an increased instrumental sensitivity due to the decrease of

MS^2 scans within the entire run. A rigorous comparison between method 1 and 2 revealed that: the former was characterized by higher reproducibility of retention times within and between different batches of analysis, while the latter provided the best chromatographic resolution and peak shape; both methods showed high linearity and analytical sensitivity. However, the analysis of several PST-contaminated shellfish samples revealed a low specificity for method 2, that, associated with poor chromatographic reproducibility, made it not applicable for determination of toxins in seafood. As part of method development, intriguing insight emerged in the use of the LTQ Orbitrap XL FTMS for the analysis of such compounds. A careful investigation revealed a drastic impact of the ion transmission system (LTQ-C-trap-Orbitrap) on the stability of the sulfated PST analogues in the MS analyzer, thus influencing the HRMS^2 conditions set in both methods 1 and 2. HILIC-HRMS method 3, which shared the same chromatography of method 2 but different MS conditions, was successfully applied to the analysis of environmental and food samples. Firstly, it was employed to determine the toxin profile of culture strains of *A. pacificum* originally isolated from plastic debris harvested in the Syracuse Bay (Ionian Sea, Southern Italy) in the frame of a surveillance program between 2016-2017. Secondly, it was used to confirm the presence of TTX in mussels harvested in the Marano Lagoon (Northern Adriatic Sea, Italy) during an official monitoring program between 2017-2018.

Chapter 4 reports on the developments of LC-HRMS methods for the analysis of a wide number of cyanotoxins. Notably, an effective and sensitive reverse-phase LC-HRMS method was optimized for the analysis of microcystins (MCs) and nodularins (NODs), and successfully applied to a cyanobacterial biomass sample collected from the Greek lake Kastoria. A large number of MCs were detected, with MC-RR and MC-LR being the most abundant variants. In addition, two new MC analogues were identified and named MC-prHcysR and MC-prHcys(O)R according to structural features emerging from the interpretation of their HRMS^2 spectra. The high biodiversity observed in the cyanobacterial biomass led to carefully explore the metabolic profile of the occurring cyanobacterial species. At this purpose, an effective workflow based on the combination of HRMS DDA approach with a new vendor-free published database of cyanometabolites was designed, and successfully applied. The implemented methodology turned out to be a powerful analytical tool for high throughput analysis since a large number of known and new cyanobacterial

secondary metabolites belonging to microginin, anabaenopeptin and cyanopeptoline-type peptide classes was revealed. Tentative HRMS^2-based structural characterization was conducted for all the new metabolites. In addition, the HILIC-HRMS method 1 reported in chapter 3, which was optimized for the determination of PSTs and TTX in seafood, was exploited to evaluate its suitability for the analysis of small polar cyanotoxins like anatoxin a (ATXa), cylindrospermopsin (CYN) and lynbyawolleytoxin 1 (LWTX1). As a result, a satisfactory sensitivity and linearity was achieved from the analysis of the relevant toxin standards, thus a multi-toxin HILIC-HRMS method based on time segmentation was implemented for the simultaneous analysis of a wide number of cyanotoxins (PSTs, ATXa, CYN and LWTX1).

In Chapter 5 the optimization of LC-HRMS and LC-MS^2 methods for the analysis of ciguatoxins (CTXs) on different MS instruments is reported. The untargeted approach was optimized for the analysis of Pacific (P) congeners by using a mixture of 5 reference standards. Although the method refinement still requires more efforts, which are currently hampered by the lack of adequate CRM, the optimized ESI source conditions turned out to be a valuable tool for confirmation of toxin identity. Under the implemented conditions, P-CTXs ionized through a complex pattern of in-source ions – $[M+H]^+$, $[M+H-nH_2O]^+$, $[M+Na]^+$, $[M+K]^+$, $[M+NH_4]^+$ – whose presence and relative ion abundance ratio, which was toxin-dependent, represented a characteristic fingerprint that can be exploited to detect known congeners in complex matrices, as well as for identification of new putative analogues.

The targeted approach was optimized for the analysis of Caribbean (C) CTXs on a triple quadrupole (QqQ) MS during a 6 month-period that I spent as visiting PhD student at the Centre for Environment, Fisheries and Aquaculture Science (CEFAS, Weymouth, United Kingdom) under the supervision of Dr Andrew Turner. The LC-MS^2 method was optimized by using fish extracts contaminated by C-CTX1 and -2 (lab RM) and employed to confirm and study the presence of CTXs in frozen Red Snapper fillets imported from India which were suspected to be cause of a food poisoning occurred in 2017 in Stoke-on-Trent (UK). The LC-MS^2 analysis of a wide number of fish fillets revealed the presence of peaks attributable to Caribbean (C-) or Indian (I-) CTX1 and -2 in the multiple reaction monitoring (MRM) chromatograms, whereas a noteworthy ciguatoxicity was measured by the cell-based assay (CBA-N2a). In light of these

findings, part of the contaminated production batch was used as starting material for a preparative work aimed at isolating the toxic compounds for the production of RM. At this purpose, several experiments were designed and performed to optimize a large-scale procedure to extract toxins from fish tissue with high yield and low variability. As a result, 89 Kg of homogenized fish tissue were processed on small-scale and analyzed by LC-MS^2. An aliquot of 10 Kg, identified among the most contaminated ones, was subjected to the large-scale extraction, and 74.5 g of liposoluble residue were obtained. Currently, further purification and isolation steps are ongoing using a combination of LC-MS^2 and N2a experiments for toxin/toxicity monitoring.

Chapter 6 describes the optimization and the successful application of a preparative procedure aimed at extracting, purifying and isolating ovatoxin-a (OVTX-a) with high grade of purity from 219 liters of a cultured strain of *O. ovata*. The final goal was to isolate enough material with a grade of purity greater than 90% to measure, in collaboration with national and foreign partners, in vivo acute toxicity by different routes of administration, and to support preliminary stability studies for the production of OVTX-a CRM which is not commercially available yet. LC-HRMS analysis of the toxin profile revealed the suitability of *O. ovata* cell culture for isolation of OVTX-a as it represented the main component (78%), with other analogues (OVTX-d/e) representing only 22% of the total toxin content. Starting from a previously optimized procedure, the isolation of OVTX-a was achieved through several steps including: extraction of toxin with solvents, ii) clean-up of the extracts through medium-pressure liquid chromatography (MPLC, flash chromatography), iii) a semi-preparative HPLC, iv) a final preparative HPLC, and v) multiple evaporation steps within the whole protocol. However, the procedure was strictly influenced by critical aspects which are related to the chemical-physical properties of OVTXs and palytoxin. Notably, the evaporation of solvents, which represents the most critical but unavoidable step, the irreversible adsorption of toxins to different materials and the usage of acids in the chromatographic purifications, drastically reduce recovery yields. On balance, the optimized procedure allowed to successfully isolate 3.4 mg of OVTX-a with a grade of purity of 93.3% (calculated on the total OVTXs content). The extraction procedure of toxins from cell pellets, the clean-up of the extracts by flash chromatography and the semi-preparative HPLC provided the

highest yields of recovery, whilst the concentration steps, the storage of the crude extracts and the final preparative HPLC still need to be improved.

Chapter 7 is a summary reporting two collaborative studies outside the PhD project. The first one reports on the development of an ESI⁻ HRMS direct injection method for the analysis of bisphenol (BP) AF and BPM, and its application to the analysis of beverage samples. BPs are a group of small organic molecules massively used to manufacture a wide range of commercial products. However, they are endocrine disruptors whose toxicity on living organisms is well-known. Their occurrence in foodstuff is frequent and mainly due to a migration from the packaging materials. Therefore, the HRMS approach was used to confirm the presence of BPAF and BPM in 2 processed beer samples, with the aim to support and validate the identification of different BPs in 52 beverage samples, which was conducted through a previously validated LC-fluorescence detection (FD) method.

The second collaborative study describes the optimization of a HILIC-HRMS method for the analysis of sapropterin and its structurally related compounds. Sapropterin is the active ingredient of the Kuvan®, a drug approved for the treatment of phenylalaninemia, a rare illness due to a reduced activity of the phenylalanine hydroxylase. Sapropterin-containing drugs have to guarantee high quality standards since dangerous impurities originating from the synthetic process of the active ingredient or degradation reactions may be found. In this context, the HILIC-HRMS approach was employed to corroborate the results of a LC-UV method, which was applied to identify and quantify sapropterin and its impurities in Kuvan® and Diterin ®, the branded and the generic drug, respectively.

The above studies were reported in 5 published articles, 3 articles under preparation, and seven oral/poster communications at National and International symposia that are listed below.

List of published articles

1) Plastic-associated harmful microalgal assemblages in marine environment. Casabianca S, Capellacci S, Giacobbe MG, Dell'Aversano C, Tartaglione L, Varriale F, Narizzano R,

Risso F, Moretto P, Dagnino A, Bertolotto R, Barbone E, Ungaro N, Penna A. Environ Pollut. 2019 Jan;244:617-626. doi: 10.1016/j.envpol.2018.09.110. Epub 2018 Oct.

2) Are Canned Beverages Industries Progressively Switching to Bisphenol AF? Russo G, Varriale F, Barbato F, Grumetto L. J Food Sci. 2019 Nov;84(11):3303-3311. doi: 10.1111/1750-3841.14833. Epub 2019 Oct 31

3) HPLC-Based Analysis of Impurities in Sapropterin Branded and Generic Tablets. Scudellaro E, Tartaglione L, Varriale F, Dell'Aversano C, Taglialatela-Scafati O. Pharmaceutics. 2020 Apr 3;12(4):323. doi: 10.3390/pharmaceutics12040323.

4) First occurence of Tetrodotoxin in bivalve mollusks from Northern Adriatic Sea (Italy). Bordin P, Dall'Ara S, Tartaglione L, P, Antonelli P, Calfapietra A, Varriale F, Guiatti D, Milandri A, Dell'Aversano C, Arcangeli G, Barco L. Food Control. 2021 Feb; 107510. doi: 10.1016/j.foodcont.2020.107510.

5) **Development of a Data Dependent acquisition-based approach for the identification of unknow fast-acting toxins and their ester metabolites.** Varriale F, Tartaglione L, Cinti S, Milandri A, Dall'Ara S, Calfapietra A, Dell'Aversano C. Talanta. 2021 Mar 1;224:121842. doi: 10.1016/j.talanta.2020.121842. Epub 2020 Nov 5.

Oral/Poster presentations at National/International Symposia (<u>Presenting Author</u>)

1) C. Dell'Aversano, <u>L. Tartaglione</u>, F. Varriale, A. Penna, M. Giacobbe, S. Pigozzi, A. Milandri, P. Bordin, L. Bille, A. D. Turner. Tetrodotoxin an Emerging Threat to Humans in the Mediterranean Area: First Detection in Italian Mussels. Society of Environmental Toxicology and Chemistry (SETAC) Europe. The 28th Annual Meeting Rome, 13th-17th May 2018. (Poster Presentation).

2) <u>H. David</u>, A. Laza-Martínez, M. Santos, M.F. Caeiro, L. Tartaglione, F. Varriale, C. Dell'Aversano, A. Penna, A. Amorim. Title: "Morphological, molecular and toxicological data on *Ostreopsis* cf. *siamensis* (Dinophyceae) from the Atlantic Iberian Peninsula". The 18th International Conference on Harmful Algae ICHA 2018. Nantes, France, October 21th-26th, 2018 (Oral Presentation).

3) C. Dell'Aversano, L. Tartaglione, F. Varriale, A. Penna, M. Giacobbe, S. Pigozzi, A. Milandri, P. Bordin, L. Bille, A. D. Turner. First Detection of Tetrodotoxin in Italian Mussels. Is it an Emerging Threat to Humans in the Mediterranean Area? 18th International conference on Harmful Algae. Nantes (France), 21th-26th October 2018 (Poster Presentation).

4) L. Tartaglione, F. Varriale, S. Casabianca, S. Capellacci, A. Penna, M. G. Giacobbe, A. Turner, A. Hiskia, T. Kaloudis, C. Dell'Aversano. Title: "LC- High resolution MS and LC-tandem MS as a complementary tools for a comprehensive toxin analysis in environmental and food matrices". The 18th International Conference on Harmful Algae ICHA 2018. Nantes, France, October 21th-26th, 2018 (Oral Presentation).

5) F. Varriale, L. Tartaglione, A. Milandri, S. Dall'Ara, A. Calfapietra, C. Dell'Aversano. "Looking for cyclic imines and their fatty acid derivatives in Italian, Spanish and Tunisian shellfish". 1st MS Sea Day. Livorno, Italy, June 6th-7th, 2019 (Oral Presentation).

6) S. Casabianca, S. Capellacci, M.G. Giacobbe, C. Dell'Aversano, L. Tartaglione, F. Varriale, R. Narizzano, F. Risso, P. Moretto, A. Dagnino, R. Bertolotto, E. Barbone, N. Ungaro, A. Penna. Plastic-associated harmful microalgal assemblages in marine environment. In: Biologia Marina Mediterranea, 26 (1) (2019): 429 pp. Società Italiana di Biologia Marina (SIBM) L, Livorno, June 10th-14th, 2019 (Oral Presentation).

7) S. Casabianca, S. Capellacci, M.G. Giacobbe, C. Dell'Aversano, L. Tartaglione, F. Varriale, R. Narizzano, F. Risso, P. Moretto, A. Dagnino, R. Bertolotto, E. Barbone, N. Ungaro, A. Penna. Plastic-associated harmful microalgal assemblages in marine environment. Riunione scientifica 2020. Gruppo di algologia, Società Botanica Italiana. November 20th, 2020 (Oral Presentation).

Chapter 1: Phycotoxins by harmful marine algae and freshwater cyanobacteria

1. General introduction

Seas and oceans are an extremely important source for humans for a number of different reasons, one of the most important being that they provide fishery products [1]. The consumption of seafood is vital for a healthy and balanced diet as it has a high digestibility and nutritional elements such as omega-3 fatty acids EPA and DHA (eicosapentaenoic and docosahexaenoic acid) and high-quality proteins rich in essential amino acids (e.g. lysine and methionine) which are barely contained in tubers and farinaceous-based products [2]. Seafood refers to any marine and fresh-water creature, excluding mammals, used as a source of nutrition by humans. A wide variety of edible species, classified in finfish and shellfish, come from both fishing (open seas) and farming activities (aquacultures) [3]. A key role for marine and freshwater ecosystems is certainly played by the plankton [4]. It is constituted by living species that are subjected to sea currents, improving their worldwide diffusion. One of the most important component of the plankton is the phytoplankton, the autotrophic organisms that are able to transform the inorganic carbon in organic compounds trough photosynthesis [5]. Phytoplankton is the base of the food chain in several aquatic ecosystems, [6] and produces about half of the total oxygen produced by vegetable organisms on the earth [7]. A crucial role in the phytoplankton is played by microalgae. Nowadays, more than 5000 species of marine microalgae are known and can live either in the water column or hung on a substrate [8]. Microalgae are essential for filter-feeding organisms and beneficial for aquacultures activities since they contains basic nutrients for the animal growth. Therefore, selected mixture of microalgae are usually employed as food additive to enhance the diet of aquatic animals [9]. However, about 300 species of marine microalgae are known to present a serious threat to humans [10] as, under appropriate climatic and environmental conditions, they can proliferate massively reaching high concentration in the water. This phenomenon is recognized as "*Harmful Algal Bloom*" (HAB), and it is characterized by discoloration of the water surface, scums and bad smells. HAB is a natural, world-wide spread problem that can have a negative impact both on the environment and on human life [11]. Indeed in the environment, algal biomass often causes

a substantial depletion of oxygen from the water, causing death of fish and aquatic invertebrates [12]. On the other hand, HABs result into socio-economic problems to humans as a consequence of the closure of fish and shellfish farms infested by toxic algal species and of the decline of coastal touristic activities [13-14]. Even more important is HAB's impact on human health. Harmful algae produce toxic secondary metabolites called "*phycotoxins*", that can be harmful or even lethal to humans [15]. Being the main food of several herbivorous and predatory fish and filter-feeding bivalves, microalgae and the produced phycotoxins may be accumulated in edible tissues of finfish and shellfish ending up on the table of unaware consumers that get poisoned following ingestion of contaminated seafood [16]. Besides the oral route, humans may be affected by phycotoxins even through inhalation of aerosolized toxins and direct skin contact with microalgae and/or contaminated seawaters [17]. It is still unclear why some microalgal species produce toxic compounds, since toxins do not explicit a crucial role in the internal economy of the producing organisms. However, the employment of such noxious metabolites as tool for space competition, fighting predation and a defence against the overgrowth of other organisms are among the most accredited theories on toxin production [18]. Several episodes of human poisoning linked to exposure of marine toxins are reported every year, probably related to the increase of HAB frequency, intensity and geographic distribution [19]. The conditions promoting HABs have not been fully clarified yet, even though the following are pointed as significant factors, as well as hazardous for human safety: i) eutrophication due to anthropogenic activities [20], ii) ship ballast waters which constitute an occasional vector of microalgae from a geographical area to another one [21], iii) anthropogenic contamination of sea and fresh-water ecosystems due to the presence of plastics floating to the water surface on which noxious microalgae can be absorbed [22], iv) opening of sea canals [23], v) fish import activity from tropical area where noxious species were historically confined [24], and climatic changes [23]. Notably, the increase of water temperature may favour the production and proliferation of species fitting life in warmer conditions in specific water basins where these species are historically not suitable for living [23]. The main consequence is then represented by the displacement of the microalgal community with the spreading and establishment of invasive toxin-producing algal species and toxin-bearing fish species in the environment. This phenomenon leads to the appearance and distribution of the emerging toxins,

once confined in tropical area, in the food-chain of temperate zones such as the Mediterranean area. [26].

Phycotoxins can be divided in several groups, each of them containing a certain number of structural analogues which are produced by algae or bio-transformed in seafood. Traditionally, marine toxins have been classified in five main groups according to the poisoning syndromes recorded in humans following ingestion of contaminated seafood: paralytic shellfish poisoning (PSP), amnesic shellfish poisoning (ASP), neurotoxic shellfish poisoning (NSP), azaspiracid shellfish poisoning (AZP), and diarrhetic shellfish poisoning (DSP) [27]. However, the classification based on the food-borne illness turned out to be inadequate for some groups of toxins and it does not consider other types of poisonings that are still not fully characterized. An alternative classification system, based on the chemical features of phycotoxins, was suggested by Quilliam et al. [28], and then adopted by the Joint FAO/IOC/WHO ad hoc Expert Consultation Group on Biotoxins in Bivalve Mollusks in 2005 [29]. For the first time in 2004, EC has established the maximum permitted level (MPL) for the main groups of marine toxins in bivalve molluscs, whilst one year later it settled the official methods for their detection [30-33]. As a consequence, national and local food safety authorities have instituted monitoring programs to survey the presence of phycotoxins in seafood. The establishment of regulatory limits associated with a strict surveillance of products turned out to be fundamental to decrease the impact of toxins on consumer safety, to manage the shellfish production by farm fisheries and for the trading of shellfish within and outside the EU borders [34-36]. Currently, six groups of phycotoxins are regulated and regularly monitored in EU: azaspiracids, domoic acid, okadaic acids, pectenotoxins, saxitoxins and yessotoxins (EC/853/2004) (**Table I.1**; **Fig.I.1**). Domoic acid is an amino acid derivative responsible for ASP, saxitoxins are alkaloid derivatives responsible for PSP, and the rest of them are polyketides derivatives responsible for either DSP or AZP syndromes. Most of them are lipophilic compounds, except STXs and DA which present acid and basic groups, and are therefore classified as hydrophilic compounds; yessotoxins show amphiphilic characteristics [37-38].

Table I.1 Current EU limits, the exposure levels resulting from consumption of shellfish on the EU market, the acute reference doses (ARfDs) set by EFSA, and the corresponding concentrations in shellfish meat. Extracted from the EFSA Journal (2009) 1306, 7-23.

Toxin group	Current EU limits in shellfish meat(A)	Exposure by eating a400 g portion at the EU limits [c]	Exposure from eating a 400 g portion at the 95th percentile of the concentrations in samples currently on the EU market	ARfD	Corresponding dose for a 60 kg adult	Maximum concentration in shellfish meat to avoid exceeding the ARfD, when eating a 400g portion (B)	Ratio B /A
OA and analogues	160 µg OA eq./kg SM(a)	64 µg OA eq./person (1 µg OA eq./kg b.w.)	96 µg OA eq./person (1.6 µg OA eq./kg b.w).	0.3 µg OA eq./kg b.w.	18 µg OA eq./person	45 µg OA eq./kg SM	0.28
AZA	160 µg AZA eq.[c]/kg SM	64 µg AZA1 eq./person (1 µg AZA1 eq./kg b.w.)	16 µg AZA1 eq./person (0.3 µg AZA1 eq./kg b.w.)	0.2 µg AZA1 eq./kg b.w	12 µg AZA1 eq./person	30 µg AZA1 eq./kg SM	0.19
PTX	160 µg OA eq./kg SM(a)	64 µg PTX2/person (1 µg PTX2 eq./kg b.w.)	32 µg PTX2/person (0.5 µg PTX2 eq./kg b.w.)	0.8 µg PTX2 eq./kg b.w	48 µg PTX2 eq./person	120 µg PTX2 eq./kg SM	0.75
YTX	1 mg YTX eq./kg SM	400 µg YTX eq./person (6.7 µg YTX eq./kg b.w.)	320 µg YTX eq./person (IT) (5.3 µg YTX eq./kg b.w.) 125 µg YTX eq./person(NO) (2.1 µg YTX eq./kg b.w.)	25 µg YTX eq./kg b.w	1500 µg YTX eq./person	3.75 mg YTX eq./kg SM	3.75
STX	800 µg PSP/kg SM(b)	320 µg STX eq./person (5.3 µg STX eq./kg b.w.)	< 260 µg STX eq./person (<4.3 µg STX eq./kg b.w.)	0.5 µg STX eq./kg b.w	30 µg STX eq./person	75 µg STX eq./kg SM	0.09
DA	20 mg DA/kg SM	8 mg DA[d]/person (130 µg DA/kg b.w)	1 mg DA[d]/person (17 µg DA/kg b.w)	30 µg DA[d]/kg b.w	1.8 mg DA[d]/person	4.5 mg DA[d]/kg SM	0.23

SM: shellfish meat; eq.: equivalents; b.w.: body weight; ARfD: acute reference dose; PSP: paralytic shellfish poison; EU: European Union; IT: Italy; NO: Norway; OA: okadaic acid; PTX: pectenotoxin; YTX: yessotoxin; STX: saxitoxin; DA: domoic acid. (a): For OA, dinophysistoxins and PTX, current regulation specifies a combination; however, the CONTAM Panel concluded that PTX should be considered separately. (b): In the Commission Regulation (EC) No 853/2004 a limit value of 800 µg PSP/kg SM is given. In the EFSA opinion, the CONTAM Panel adopted this figure as being expressed as µg STX equivalents/kg SM. (c): The CONTAM Panel assumed that AZA equivalent should refer to AZA1 equivalents. (d): Applies to the sum of DA and epi-DA.
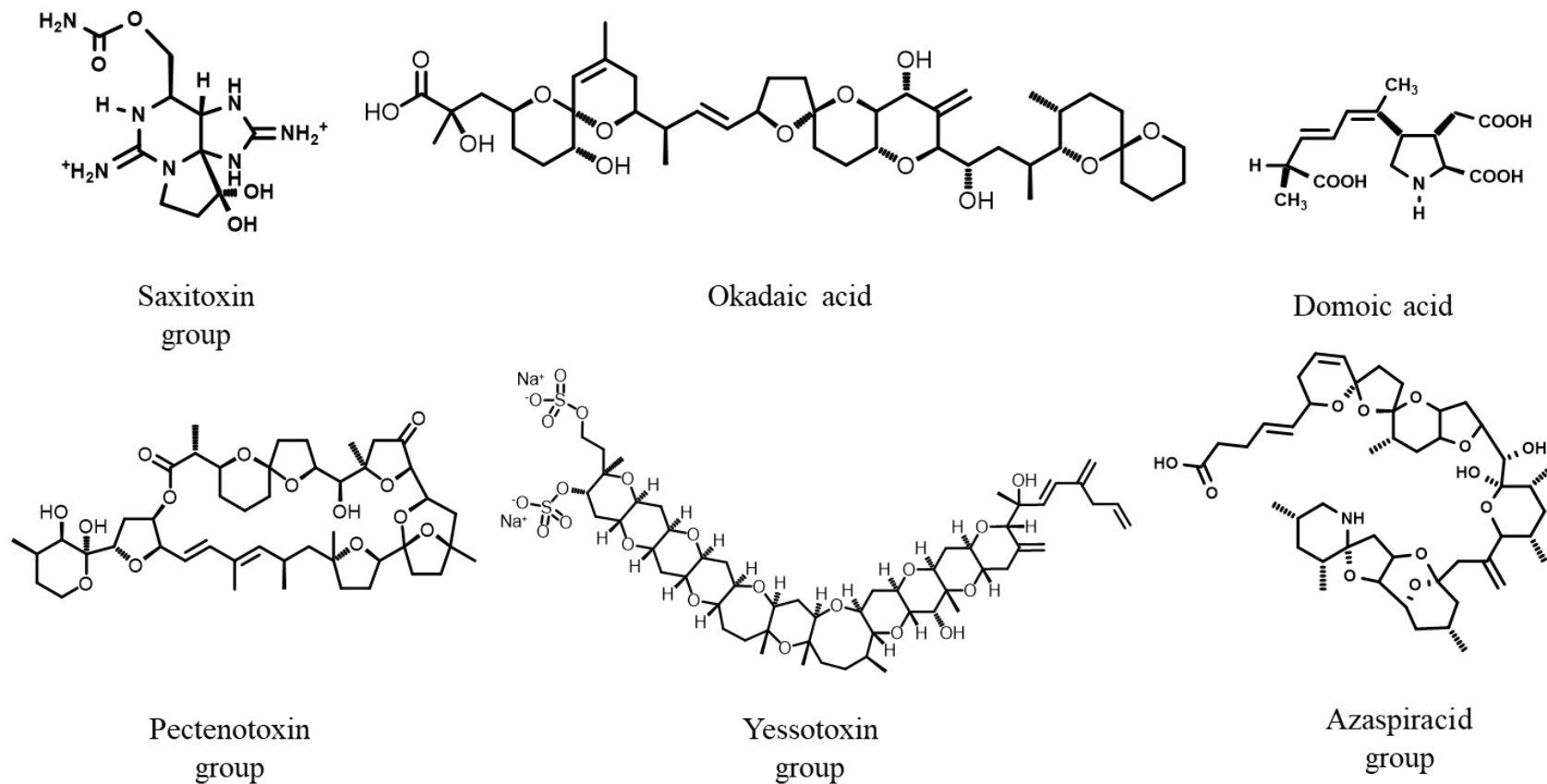
Figure I.1 Chemical structure of phycotoxin groups regularly monitored in EU (EC/853/2004).

However, new HAB-related threats once confined to tropical areas are emerging together with a plethora of new structural analogues discovered in each toxin group, following analytical advancements [39-40]. All these toxins are designated as "*Emerging Toxins*" by official organizations such as the European Commission (EC) and the European Food Safety Authority (EFSA), overall including non-regulated toxins in EU, known by scientists and a matter of concern for legislators but for which additional toxicological evidences are needed before further regulations can be established. The establishment of regulatory criteria is pointed as one of the most critical issues in the field of the emerging toxins by EC and EFSA. This requires i) determination of the MPL of each toxin group in seafood, ii) development of reliable analytical methods for their determination, iii) assessment of toxin distribution throughout the food web, and iv) collection of appropriate toxicity data. Availability of adequate amounts of reference material (RM) for each toxin is the cornerstone for both the validation of analytical techniques and the achievement of toxicity data [41-47].

Currently, cyclic imines, tetrodotoxins, ciguatoxins, maitotoxins, palytoxins and cyanotoxins are listed among the emerging toxins of European concern. A detailed description for each toxin class is reported below.

2. Emerging toxins

2.1 Cyclic imines

The cyclic imines (CIs) are a large family of about 50 polar lipophilic compounds that are produced by several species of harmful bloom-forming marine dinoflagellates and commonly grouped by structural features and toxicological properties [1]. Although they are unified by the presence of a characteristic cyclic imine unit in their structure, to which they owe their name, they are classified into different sub-groups: pinnatoxins (PnTXs), pteriatoxins (PtTXs), spirolides (SPXs), gymnodimines (GYMs), prorocentrolides, spiro-prorocentroimines, portimines and symbioimines [2]. CIs are commonly known as fast-acting toxins due to the characteristic onset of neurological symptoms and the rapid death when injected intraperitoneally in mice [3]. In fact, they are able to bind and block the muscular and neuronal nicotinic acetylcholine receptors (Ach and nAChRs) leading to asphyxia, which is consequent to the paralysis of the diaphragm [4] Although the cyclic

imine unit was found to be crucial for their activity, it turned out to be not a sufficient condition to clearly explain their toxicological properties, since different: i) lethal dose (LD_{50}) values, ii) time of onset of symptoms, iii) effects on neuromuscular transmission and iv) mode of action have been recoded across different CIs and also within the same sub-group [3,5-6]. To date, CIs have been found worldwide both in tropical and temperate regions in extracts from natural plankton, cultured dinoflagellate microalgae and contaminated seafood [7]. Although these potent toxins can accumulate in shellfish, as clearly evidenced by a wide number of monitoring studies and by algal-feeding experiments [8-9], no human intoxications linked to the consumption of CI-contaminated seafood have been reported so far, with the only exception for PnTXs. In fact, food poisoning episodes due to the consumption of shellfish of the genus *Pinna* occurred in Japan in October 1975 (1730 people affected) and in October 1980 (950 people affected), and only a few years later they were associated with the presence of noxious compounds including PnTX-A, as major component, and PnTX-B and C [10-11]. CIs are then classified as emerging toxicants due to their noticeable neurotoxicity, which poses a potential risk for consumer well-being and for seafood industries. In addition, the growing number of newly shellfish biotransformation products associated with the impact that CIs have on the neuromuscular transmission and their capacity to cross the intestinal and the blood-brain barrier (BBB) represents a warring threat for patients suffering from neuromuscular disorders [12-15]. Currently, the presence of CIs in seafood products is not regulated in Europe and in other regions of the world. In the 2010s, the EFSA Panel on Contaminants in the Food Chain released a scientific opinion on the presence of CIs in shellfish, establishing that no provisional guidelines values could be suggested since toxicological data were very poor and only limited to the acute toxicity of SPXs, GYMs and PnTXs, while chronic toxicity data were lacking [16].

2.1.1 Pinnatoxins and pteriatoxins

PnTXs are among the first sub-groups of CIs to have been discovered from the digestive glands of bivalves belonging to *Pinna* genus (from which their name derive) after shellfish poisoning episodes occurring in China and Japan where the adductor muscle of *P. attenuata* is commonly used as an ingredient for sushi [17]. Nine structural variants (PnTX A-H and PnTX 7-methyl ester;

Fig.I.2) have been described since the 1990s onwards and found in the extracts from: i) species of different bivalve families (e.g. Pinnidae, Pteriidae, Ostreidae and Mytilidae) harvested in Japan, Australia, New Zealand, Europe, Canada and China [9-11,18] and ii) indistinguishable peridinoid dinoflagellate strains collected from Australia, Japan, New Zealand, China, Qatar, and France, which were then associated with a new microalgal specie called *Vulcanodinium rugosum* [19-20]. PnTXs possess a 7-membered cyclic imine unit which is spiro-linked to a cyclohexene moiety both embedded in a 27-membered carbocyclic backbone featuring spiroketal systems and different functional groups at C21, C22, C28 and C33 (**Fig.I.2;** [21]. PnTX E-H were found to be produced by different strains of *V. rugosum*, while PnTX A-C and PnTX-D are considered derivatives of PnTX-G and PnTX E-F, respectively, due to hydrolytic and oxidative transformations occurring in shellfish [22]. The toxic profile of *V. rugosum* strongly varies among strains and this leads to different PnTX profiles in contaminated bivalves depending on which algal strains have been exposed to filter feeder organisms [22-23]. In addition, PnTXs and other CI sub-groups (SPXs and GYMs) were found to be further biotransformed in shellfish via acylation reaction, which is a common metabolic process adopted from shellfish to reduce the impact of phycotoxins on their organism [24]. As a consequence, a wide number of acyl ester derivatives of PnTX-G, 20-MeSPX-G and GYM-A have been reported and found to be the result of an esterification process between a hydroxyl group of the toxin with the carboxyl group of saturated and unsaturated fatty acids physiologically produced by shellfish [20,25-26].

Acute toxicity studies revealed that PnTXs are among the most toxic CI sub-groups since they showed the highest toxicity *per os* administration and by intraperitoneal (IP) injection, with the latter only lower to SPXs-C [5, 22, 27]. However, noticeable differences in toxicity occurred between PnTX analogues. With regards to IP administration in mice, a first study published by Takada et al. in 2001 [28] reported that PnTX-B and -C were the most toxic congeners since a mixture 1:1 of the two compounds gave a LD_{99} = 22.0 µg/Kg. More recently, the toxicity of most of the PnTX analogues was evaluated: PnTX-F turned out to be the most toxic congener (LD_{50} = 12.7 µg/Kg), followed by PnTX-G (LD_{50} = 48.0 µg/Kg), PnTX-E (LD_{50} = 57.0 µg/Kg), PnTX-H
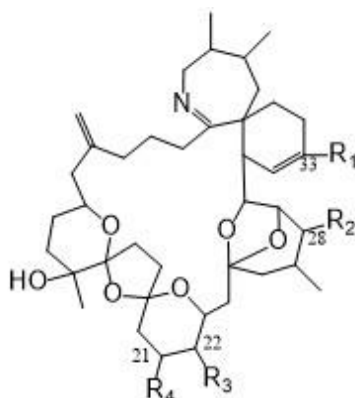
	[M+H]$^+$ m/z	R$_1$	R$_2$	R$_3$	R$_4$
PnTX-A	712.4419	—CO$_2$H	OH	H	H
PnTX-B (36*S*), -C (36*R*)	741.4685	CO$_2$H, NH$_2$	OH	H	H
PnTX-D	782.4838	CO$_2$H, O	H	OH	CH$_3$
PnTX-E	784.4994	CO$_2$H, OH	H	OH	CH$_3$
PnTX-F	766.4889	O, O	H	OH	CH$_3$
PnTX-G	694.4677		OH	H	H
PnTX-H	708.4834		H	OH	CH$_3$
PnTX-7-methyl ester	798.5151	CO$_2$CH$_3$, OH	H	OH	CH$_3$
PtTX-A	831.4824	35 S NH$_2$ 34 OH CO$_2$H	OH	H	H
PtTX-B (34*R*), -C (34*S*)	831.4824	34 S NH$_2$ 35 OH CO$_2$H	OH	H	H

Figure I.2 Planar structure and exact mass of PnTXs and PtTXs.

(LD_{50} = 67.0 µg/Kg) and PnTX-A (LD_{50} = 114.8 µg/Kg). Although PnTX-D showed the weakest acute toxicity by IP injection, it exhibited a strong cytotoxicity on leukemia cell line with IC_{50} = 2.5 µg/mL [29]. On the other hand, acute oral toxicity studies highlighted small differences between oral and IP administration, with the only exception for PnTX-E. In fact, PnTX F, -G, and -H turned out to be only 1.6 to 9.3-fold less toxic when administered orally by gavage (LD_{50} = 25.0, 150 and 163 µg/Kg, respectively), while a 49-fold decrease in potency was observed for PnTX-E (LD_{50} = 2800 µg/Kg). In addition, further studies conducted by administering PnTX-F and -G to mice through different types of food showed: i) LD_{50} values different compared to those obtained by gavage administration and ii) the oral toxicity was strongly dependent on food and/or gastric content, thus suggesting that the latter may interfere with the pharmacokinetic properties of PnTXs [23, 30-31]. A recent study conducted by Aráoz et al. [12] investigated also the mechanism of action of the acyl-ester of PnTX-G (28-*O*-palmitoyl derivative) by receptor binding assay (RBA), bringing to light that the acylation of toxin due to shellfish metabolism reduces its antagonistic behavior toward the muscular Ach receptor (700-fold) since the measured IC_{50} values for PnTX-G and its ester were 18.65 nM and 13.1 µM, respectively.

PtTX are 3 extremely toxic CI analogues described for the first time by Takada et al. [6] and found in extracts from *Pteria penguin* (origin of their name) oysters collected in Okinawa (Japan). Their structure is superimposable to that of PnTXs (**Fig. I.2**), in fact it has been supposed that PtTXs are shellfish transformation products of PnTX-G. More in detail, a metabolic pathway has been proposed: the oxidation step of PnTX-G gives rise to a common precursor for the biosynthesis of PnTX A-C and PtTX A-C. The latter are then biosynthesized via conjugation with a cysteine residue. Even though PtTX A-C are isobaric compounds, NMR experiments demonstrated that PtTX-A have a different structure since the SH group of cysteine binds C35, while PtTX B and -C, being the products of binding between the SH group of cysteine with C34, are epimers at C34 (**Fig.I.2**). To date, the toxicological data of PtTXs are extremely poor and referring only to their acute toxicity by IP administration. PtTX-A turned out to be the least toxic congener with LD_{99} = 100 µg/Kg, while a mixture of PtTX-B/C in a ratio 1:1 provided a LD_{99} = 8 µg/Kg [32].

2.1.2 Portimines

Portimines are the smallest CI sub-group composed of 3 secondary metabolites named protamine A, -B and kabirimine (**Fig.1.3**), which are produced, as well as PnTXs, by different strains of *V. rugosum*. The name portimine was derived from *Portodonium honu*, a preliminary name given to the dinoflagellate *V. rugosum*, while kabirimine own its name to Kabira Bay, the site in Okinawa where the producing microalgal strain was originally harvested [5,33-34]. Portimines feature a characteristic five-membered spirocyclic imine linked to a cyclohexene moiety, which are both embedded in a 14-membered ether macrocycle (**Fig.1.3**).

	$[M+H]^+$ m/z
Portimine A	402.2275

	$[M+H]^+$ m/z
Portimine B	418.2224

	$[M+H]^+$ m/z
Kabirimine	428.3159
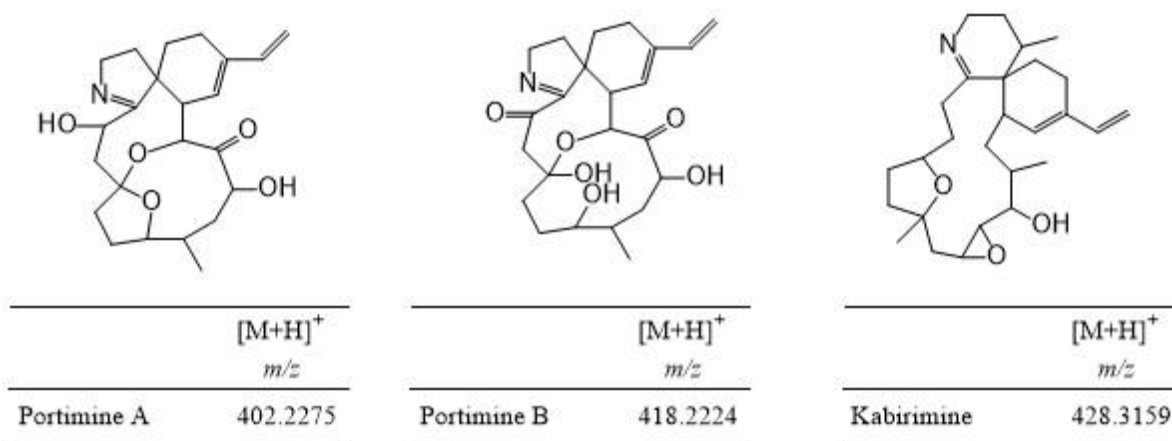
Figure I.3 Planar structure and exact mass of $[M+H]^+$ ion of portimines.

Portimine B is the open ring analogue of portimine A, since the characteristic cyclic acetal is replaced by a hemiacetal functionality. Portimine A was the first analogue to have been discovered in 2013 during the isolation of PnTXs from *V. rugosum* cell cultures, while portimine B was elucidated in 2018 from a strain of *V. rugosum* isolated in 2004 from a ballast water collected in Port Tampa (Florida). Shortly after in 2019, the structure of kabirimine has been reported. Surprisingly, all three portimines were isolated from different strains of *V. rugosum*, and only portimine A was found to be coproduced with PnTXs. This clearly evidenced as the metabolic profile of *V. rugosum* highly varies among strains, as previously reported for PnTXs. Recently, portimine A was detected for the first time in mussels harvested from Ingrill lagoon (France) at a

concentration level of 69.3 µg/Kg in association with other CI toxins such as PnTX-A and -G, 13-SPX-C and GYM-A [12].

Acute toxicity studies revealed that portimine A is one of the least potent CIs since a $LD_{50} = 1570$ µg/Kg was measured by IP injection in mice. On the other hand, portimine A exhibited a remarkable activity as antiproliferative agent and its cytotoxicity in cancer cells was about 100-fold higher than that observed for PnTX-F [5]. The anticancer mechanism of portimine A lies into the ability to induce apoptotic death in Jurkat T-lymphoma cells through caspase-3 activation [35]. Moreover, this biological activity, hitherto never reported for any of the marine natural products, configured portimine A as potent antifungal agent [36]. Portimine B displayed the same anticancer activity of portimine A, even if it was less potent [33], while kabirimine exhibited antiviral activity against the respiratory syncytial virus (RSV) [34].

2.1.3 Spirolides

SPXs are the largest CI sub-group that includes more than 20 naturally-occurring compounds found in phytoplankton and shellfish samples from Canada, Europe, North and South America New Zealand and China [18]. They are produced by marine dinoflagellates *Alexandrium ostenfeldii*, which is a microalgal specie distributed worldwide, and by *Alexandrium periuvianum*, whose toxic profiles strongly vary depending on different factors (e.g. environmental conditions, genetic factors and geographical distribution) [3]. In fact, some strains were found to be capable of producing toxins belonging to different classes or groups such as paralytic shellfish toxins (PSTs) and GYMs [37]. To date, 18 SPXs have been structurally elucidated (**Fig.I.4**), whilst the structure of 9 novel congeners, which have been recently reported by Nieva et al. [38], has been proposed on the basis of the fragmentation patterns acquired by LC-HRMS. Even though SPXs are characterized by the presence of a 7-membered spiroimine, a high chemodiversity was observed within this toxin group. The characteristic structural motif found in most of the analogues is represented by the cyclic imine unit spiro-linked to a cyclohexene which is substituted with a α-methyl butenolide moiety. This part structure displays similarities with PnTXs (7-membered cyclic imine) and GYMs (α-methyl butenolide) [2]. The spiroimine unit is embedded in a different size macrocyclic backbone containing spiroketal systems, whose structural features allow to classify

	$[M+H]^+$ m/z	R_1	R_2	R_3	R_4	R_5	
SPX-A	692.4521	CH_3	CH_3	H	H	H	$\Delta^{2,3}$
SPX-B	694.4677	CH_3	CH_3	H	H	H	
SPX-C	706.4677	CH_3	CH_3	H	H	CH_3	$\Delta^{2,3}$
iso-SPX-C	706.4677						
13-desMeSPX-C	692.4521	H	CH_3	H	H	CH_3	$\Delta^{2,3}$
27-OH-13desMeSPX-C	708.4470	H	CH_3	H	OH	CH_3	$\Delta^{2,3}$
13,19-didesMeSPX-C	678.4364	H	H	H	H	CH_3	$\Delta^{2,3}$
27-OH-13,19-didesMeSPX-C	694.4313	H	H	H	OH	CH_3	$\Delta^{2,3}$
27-Oxo-13,19-didesMeSPX-C	692.4157	H	H	H	O	CH_3	$\Delta^{2,3}$
20-OH-13,19-didesMeSPX-C	694.4313	H	H	OH	H	CH_3	$\Delta^{2,3}$
SPX-D	708.4834	CH_3	CH_3	H	H	CH_3	
13-desMeSPX-D	694.4677	H	CH_3	H	H	CH_3	
20-OH-13,19-didesMeSPX-D	696.4470	H	H	OH	H	CH_3	

	$[M+H]^+$ m/z	R	
SPX-G	692.4521	H	
20-MeSPX-G	706.4677	CH_3	

	$[M+H]^+$ m/z	
SPX-H	650.4415	$\Delta^{2,3}$
SPX-I	652.4572	

	$[M+H]^+$ m/z	
SPX-E	710.4626	$\Delta^{2,3}$
SPX-F	712.4783	

Figure I.4 Planar structure and exact mass of $[M+H]^+$ ion of SPXs.

SPXs in different sub-groups: SPX-A, -B and -C display a 5:5:6 trispiroketal ring system, SPX-G a 5:6:6 spiroketal configuration and SPX-H and -I a 5:6 dispiroketal ring system (**Fig.I.4**). The most common structural variations reported within each SPX sub-groups are: the number of methyl groups, the presence of hydroxyl or carbonyl functionalities and the saturation of the C=C between C2-C3 of the α-methyl butenolide (α-methyl-γ-butyrolactone). The most surprising structural variation was found in SPX-E and -F, which turned out to be the keto amine derivatives of SPX-A and B, respectively. The hydrolysis of the cyclic imine unit and then its opening is due to shellfish metabolism and it determines a complete loss of bioactivity [39]. In a first stage, the lack of toxicity observed for SPX-E and -F led to consider that the spiroimine unit was the pharmacophore responsible for the biological activity. However, Roach et al. in 2009 reported that SPX-H did not show toxicity when administered intraperitoneally in mice, thus suggesting that the cyclic imine unit is crucial but is not the only prerequisite for toxicity [40]. On the other hand, it was found that the presence of two methyl substituents at C31 and C32 (SPX-C, -D, -H, -I and 20MeSPX-G,) increased the stability to hydrolysis and then the potency of the toxins [41]. However, this structural characteristic is not the only requirement for the biological activity considering the lack of toxicity of SPX-H. As previously reported, the number of SPX derivatives originating from shellfish metabolism is even higher considering the fatty acid ester metabolites of 20MeSPX-G originally found in mussels from Norway [25]. Although the toxicity of SPXs is mainly due to a potent antagonistic effect on muscle and neuronal nAChRs, as well as for other CI-sub groups, *in vitro* and in *vivo* studies on human and rat models highlighted the ability of 13desMeSPX-C to bind also alternative sites giving rise to specific and different biological effects [6]. In particular, 13desMeSPX-C is capable of binding: i) the soluble Ach binding protein (AChBP), a homopentameric protein stored in glial cells of molluscs, which is released into the synaptic cleft to modulate the synaptic transmission [42-43], ii) muscarinic and nicotinic AChRs (mAChRs and nAChRs) in rat, leading to the upregulation of gene expression [44], iii) human mAChRs as irreversible competitive inhibitor [45], and iv) the L type calcium channels displaying a weak activation effect. To date, the toxicological properties of SPXs still represent a controversial issue, making critical the establishment of an accurate regulation as well as the release of provisional guidelines for their presence in shellfish. Among all the CI sub-groups, SPXs showed the highest acute toxicity by IP injection in mice, with 13desMeSPX-C being the most toxic analogue (LD_{50} = 6.9 µg/Kg), followed by 20MeSPX-G and SPX-C (LD_{50} = 8.0 µg/Kg), SPX-A

(LD$_{50}$ = 37.0 µg/Kg) and SPX-B (LD$_{50}$ = 99. µg/Kg). On the other hand, a significant reduction in potency was observed through oral toxicity studies. By way of example, the toxicity of 13desMeSPX-C was drastically reduced 19-fold and up to 72-145-fold when administered by gavage and by food, respectively. Moreover, the type of vehicles used to feed mice greatly influenced the potency of the toxin and even to a greater extent than that observed for PnTXs [2, 46]. A guidance level of 400 µg SPXs/Kg of shellfish was proposed by the European Union Reference Laboratory (EURL) [18].

2.1.4 Gymnodimines

GYMs, which are listed among the low-molecular-weight CI sub-groups, are a family of 7 analogues produced by noxious dinoflagellates belonging to *Karenia* and *Alexandrium* genus (*K. selliformis, A. ostenfeldii and A. peruvianum*) and found in extracts from phytoplankton and shellfish collected from New Zealand, Australia, Europe, North and South Africa and North America [3, 12, 18, 47-48]. Their name derives from the dinoflagellate *Gymnodinium mikimotoi,* which was originally identified as producing organism. However, few years later the new species *K. selliformis* (formerly *Gymnodinium selliforme*) was discovered and unequivocally designated as producer of the first detected GYM analogues [49-51]. GYMs feature a 6-membered spiroimine linked to a cyclohexene unit both embedded in a 16-membered macrocycle harboring 1 (GYM A, -B, and -C) or 2 (GYM-D and -E) tetrahydrofuran moieties; a α-methyl butenolide substituent is linked to the cyclohexane moiety as seen for SPXs (**Fig. I.5**). The most common variations observed within each GYM-type group are due to methyl and hydroxyl groups, and the position of a C=C moiety: $\Delta^{17,18}$ or $\Delta^{17,29}$ for GYM-A, and-B/-C, respectively, and $\Delta^{18,19}$ or $\Delta^{18,29}$ for GYM-D and -E, respectively (**Fig. I.5**). The microalgal origin of GYMs turned out to be very fascinating: i) they are produced by dinoflagellates belonging to different phylogenetic groups (*Karenia* spp to Gymnodiniales and *Alexandrium* spp to Peridiniales), and ii) analogues featuring the same type-structure are individually produced by two different microalgal organisms. Particularly, GYM-A, -B and -C were found to be produced by *K. selliformis,* while *A. ostenfeldii* and *A. peruvianum* produce their methyl congener 12-MeGYM-A and 12-MeGYM-B [37, 52-53]. On the other hand, a different strain of cultured *A. ostenfeldii* originally harvested from the Baltic Sea was found to produce the type- structure of GYM-D, 12-MeGYM-D and GYM-E; the latter turned out to be the artificial degradation product of GYM-D due to long storage in methanolic extracts [54-55].
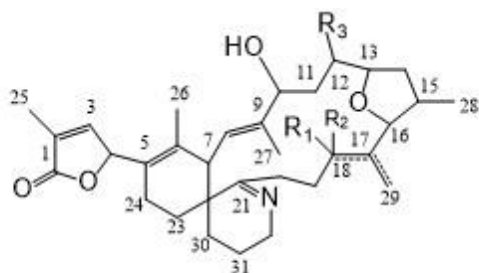
	[M+H]$^+$ m/z	R$_1$	R$_2$	R$_3$	
GYM-A	508.3417	H	H	H	$\Delta^{17,18}$
12-MeGYM-A	522.3578	H	H	CH$_3$	$\Delta^{17,18}$
GYM-B (18S)	524.3370	H	OH	H	$\Delta^{17,29}$
GYM-C (18R)	524.3370	OH	H	H	$\Delta^{17,29}$
12-MeGYM-B	538.3527	H	OH	CH$_3$	$\Delta^{17,29}$
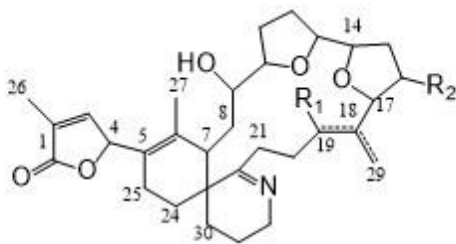
	[M+H]$^+$ m/z	R$_1$	R$_2$	
GYM-D	524.3371	H	CH$_3$	$\Delta^{18,19}$
16-desMeGYM-D	510.3214	H	H	$\Delta^{18,19}$
GYM-E	526.3163	OH	H	$\Delta^{18,29}$

Figure I.5 Planar structure and exact mass of [M+H]$^+$ ion of GYMs.

This particular behavior suggested that a common biosynthetic pathway for GYM production exists between the two different dinoflagellates. Moreover, the high variability in the toxin production and toxin profiles of *Alexandrium* species became even more evident after observing that strains of *A. peruvianum* and *A. ostenfeldii* are capable of producing, individually or together, GYMs, SPXs and PSTs [56]. Similarly to SPXs, GYMs are potent antagonist of the muscle and

neuronal nAChRs and are capable of binding the soluble AChBP [42] and the human mAChRs, even if through a competitive reversible antagonism [45]. However, a specific and characteristic effect was observed for GYMs through *in vitro* study on neuro2a cells, following which GYM-A and three synthetized structural analogues caused a remarkable sensitization of the nerve cells to the toxic effects of okadaic acid, which is a completely different phycotoxin [6]. Contrarily to SPXs, the spiroimine subunit is crucial for GYMs since a complete loss of toxicity was observed when the cyclic imine moiety is reduced to an ammine function in the synthetic derivative called gymnodamine [57]. Toxicological studies revealed that GYMs are among the least toxic CI sub-groups, even if most of data were collected only for GYM-A. The IP administration of GYM-A to mice showed a $LD_{50} = 80$ µg/Kg while the LD_{50} measured for GYM-B was 10-fold higher ($LD_{50} = 800$ µg/Kg). A remarkable decrease of potency was observed when GYM-A was administered by oral route to mice (similarly to SPXs) since: i) gavage administration provided a 10-fold reduction in toxicity with $LD_{50} = 755$ µg/Kg whilst ii) administration by food showed a $LD_{50} = 4057$ µg/Kg, corresponding to a 50-fold decrease than IP injection [47]. As observed for SPXs, acute toxicity studies demonstrated a worrying toxic potential by IP route and a very debatable toxicity *per os* administration, making even more critical the release of a provisional guidance on GYM levels in shellfish [16]. On the other hand, it has been documented that the toxic profile of shellfish samples exposed to *K. selliformis* through naturally-occurring HABs or through feeding experiments is dominated by fatty acid ester metabolites of GYMs. However, to date their acute toxicity has not been investigated yet, and it should be considered for an accurate evaluation on the exposure risk for human through the consumption of contaminated shellfish [8].

2.1.5 Prorocentrolides and spiroprorocentroimine

Prorocentrolides, the first CIs being isolated in 1988 [58], are the highest-molecular-weight CIs forming a sub-group of 8 analogues (**Fig.I.6**) [59-60]. Their structure is more complex and slightly different from other CIs since: they feature a 6-memebered cyclic imine unit (as well as GYMs) which is not connected via spiro-linkage to a cyclohexene moiety; both groups are embedded in a 26-membered macrocycle harboring one tetrahydropyran moiety and several hydroxyl groups; a further 28-membered macrocyclic lactone, arranged around the cyclohexene moiety, completes their chemical structure (**Fig.I.6**).
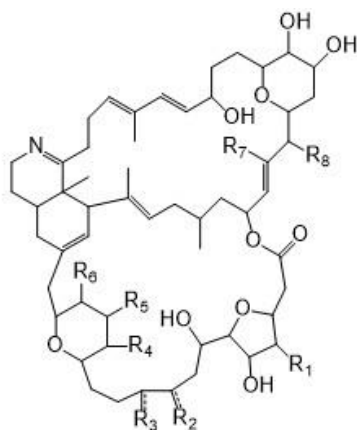
	$[M+H]^+$ m/z	R_1	R_2	R_3	R_4	R_5	R_6	R_7	R_8
Prorocentrolide-A	980.6094	H	$H_2C=$	H	OH	OH	H	CH_3	OH
30-sulfate prorocentrolide	1060.5662	H	$H_2C=$	H	OH	OH	H	CH_3	OSO_3H
4-OH prorocentrolide	996.6043	OH	$H_2C=$	H	OH	OH	H	CH_3	OH
9,51-dihydro prorocentrolide	982.6250	H	CH_3	H	OH	OH	H	CH_3	OH
14-O-acetyl-4-OH prorocetrolide	1038.6148	OH	$H_2C=$	H	$OCOCH_3$	OH	H	CH_3	OH
Prorocentrolide B	1076.5611	OSO_3H	CH_3	$H_2C=$	OH	H	OH	H	OH
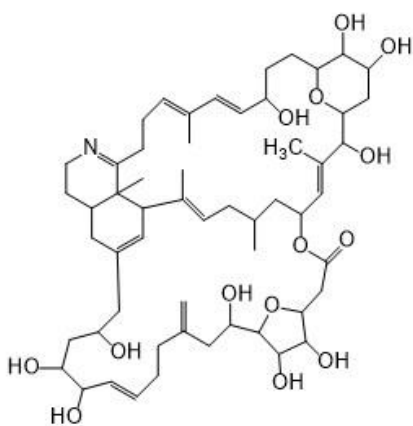
	$[M+H]^+$ m/z
Prorocentrolide C	8996.6043
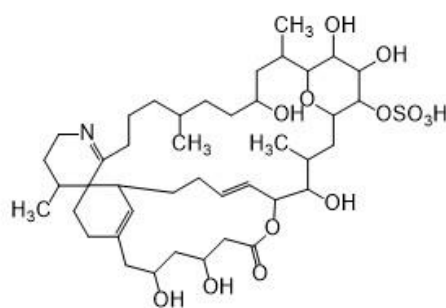
	$[M+H]^+$ m/z
Spiroprorocentrimine	828.4562

Figure I.6 Planar structure and exact mass of $[M+H]^+$ ion of prorocentrolides and spiroprorocentroimine.

Three different type-structure have been elucidated within this group and associated with: prorocentrolide A, prorocentrolide B and prorocentrolide C. The main structural difference between the first two lies into the position of a C=C moiety, which is conserved between the

structural congeners of prorocentrolide A. Contrarily, prorocentrolide C lacks the tetrahydropyran moiety in the macrocyclic lactone (**Fig.I.6**). Prorocentrolides are produced by harmful microalgal species belonging to the genus *Prorocentrum*, from which their name was derived [6]. The *Prorocentrum lima* species was already known as a toxic source since a variety of noxious secondary metabolites had previously been isolated: okadaic acid and its analogues, and the relevant dinophysistoxins (DTXs) which are responsible for the toxic syndrome commonly known as diarrheic shellfish poisoning (DSP) [61-64]. Prorocentrolide A was the first analogue to be discovered and it was isolated from *Prorocentrum lima* harvested in Japan and Taiwan, while prorocentrolide B was isolated from *P. maculosum* from tropical waters, therefore a common biosynthetic between the two microalgal species was supposed to exist [65]. In addition, a new species called *P. caipirignum* was found to be capable of coproducing prorocentrolide A and okadaic acid [66]. Although prorocentrolides were found to be ''fast acting toxins'' due to the rapid onset of neurological symptoms observed in mice during the isolation of toxins, no details have ever been reported on their mode of action. Recently, Amar et al. [60] reported that prorocentrolide A binds the muscle and neuronal AChRs, even if with a much lower affinity compared to SPXs, PnTXs and GYMs. On the other hand, 4-OH-prorocentrolide and prorocentrolide C showed cytotoxicity against human colon cancer, neuronal and hepatic cells [67]. Their anti-cancer effect was found to be related to the arrest of the cell cycle at the G2/M phase and the promotion of apoptosis [59]. Acute toxicity by IP injection to mice was measured only for prorocentrolide A ($LD_{50} = 400$ µg/Kg), which showed a toxic potential lower than other CIs [47].

Spiroprorocentroimine was originally isolated from an unknown Taiwanese strain of *Prorocentrum* species in 2001 [68]. Its chemical structure can be considered an hybrid between prorocentrolides and other CIs since: a six-membered cyclic imine unit is spiro-linked to a cyclohexene moiety both embedded in a 26-membered macrocycle harboring a tetrahydropyran moiety, 1 sulfate and 4 hydroxyl groups. A further 17-membered macrocyclic lactone in which the cyclohexene moiety is incorporated, completes the chemical structure (**Fig.I.6**). Spiroprorocentroimine is one of the least studied CI congener, in fact no data are available regarding its mechanism of action or further biological effects. Nonetheless, its toxicity was measured through IP administration and a $LD_{50} = 2500$ µg/Kg highlighted that spiroprorocentroimine is the least potent CI congener [47].

2.1.6 Symbioimines

Symbioimines are two secondary metabolites isolated in 2005 from the symbiotic marine dinoflagellate *Symbiodinium* species. They are symbioimine and its methyl congener, called neosymbioimine, which are characterized by the presence of a 6-membered cyclic imine moiety incorporated in a tricyclic structure composed of a cyclohexane and a cyclohexene, which is linked to a hydroxy phenyl sulfate moiety (**Fig.I.7**). Symbioimines are not included within the fast acting toxin group due to their biological properties, whilst are distantly considered cyclic imines due to the presence of the characteristic cyclic imine moiety. Pharmacological studies revealed that symbioimine could be used as: i) potential drug for the treatment of osteoporosis since it inhibits the osteoclastogenesis, and as ii) lead compound for the production of anti-inflammatory drugs thanks to its ability to inhibit cyclooxygenase-2 at low concentrations [69].

	$[M+H]^+$ m/z	R_1	R_2
Symbioimine	394.0964	H	H
Neosymbioimine	422.1277	CH_3	CH_3
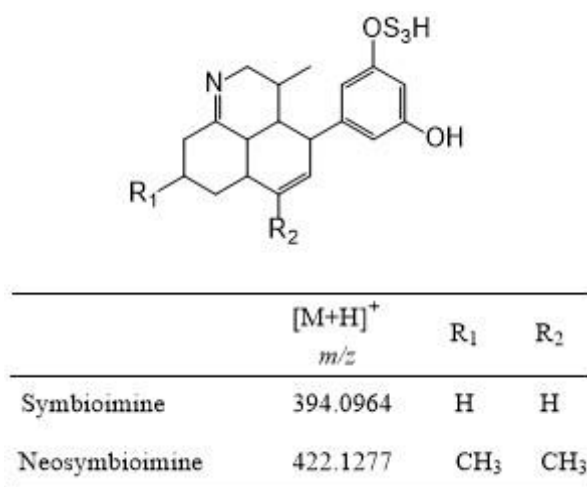
Figure I.7 Planar structure and exact mass of $[M+H]^+$ ion of symbioimines.

2.2 Tetrodotoxins

TTXs are a group of naturally occurring hydrophilic toxins including about 30 analogues described so far, among which TTX represents the first one to be discovered, as well as the most studied [70]. TTX was originally isolated in the early 1950s [71] from puffer fish (*fugu*), a marine fish belonging to the Tetraodontidae family to whom the toxin owes its name. TTX is known worldwide to cause lethal food poisoning, known as pufferfish poisoning, as the first incidents were associated with ingestion of such contaminated fish [72]. This situation has raised many

concerns as tons and tons of puffer fish are consumed every year in Japan, where *fugu* is considered a delicacy, as well as the most celebrated dish in the whole country.

Although TTX is a low-molecular weight compound, its structure hides a fascinating and complex architecture consisting of: an oxygenated backbone (2,3-dioxaadamantane) containing six hydroxyl groups and linked to a guanidinium moiety (**Fig.I.8**) [73].The large number of analogues in association with such a small structure, clearly suggested that the chemodiversity within the TTX group was mainly due to: different configuration of stereocenters, deoxygenation and oxidation. A classification system that includes the most detected congeners has been designed through 4 sub-groups [46, 75] (**Fig.I.8**): i) analogues chemically equivalent to TTX (e.g. 4-*epi*TTX, 6-*epi*TTX and 4,9-anhydroTTX), ii) deoxy analogues (e.g. 5-deoxyTTX, 11-deoxyTTX, 5,6,11-trideoxyTTX), iii) oxidized analogues (e.g. 11-oxoTTX) and iv) C11 lacking analogues (e.g. 11-norTTX-6-ol (*R*/*S* isomer). To date, even though the primary source of TTX in the marine ecosystem is still one of the most controversial issues, more than 20 endo-symbiotic bacteria are recognized to be TTX-producing species, of which those belonging to the genus *Vibrio* are the main ones. The strong influence that endo-symbiotic bacteria have on the TTX production was highly supported by a large number of reports describing the occurrence of TTX in a wide, diverse and phylogenetically unrelated organisms from Animalia (frogs, puffer fish, gastropods, starfish, worms, crabs) to dinoflagellates (*Alexandrium tamarense)* [75]. The bacterial origin of TTX was definitely confirmed by LC-ox-FLD analyses that revealed the presence of TTX in fractions obtained from cultured suspected bacteria which were first isolated from several TTX-bearing organisms [76]. This finding was further supported after observing that TTX was not detectable in the same bearing organisms when they were raised in captivity [77-78]. In addition, the amount of toxin isolated from bacteria is much less than that found in TTX-bearing animals, increasing the possibility that marine organisms can absorb and accumulate TTX through the food-web due to the presence of some inducers or enhancers, present in the host, which greatly increase the level of expression of toxin. [76].
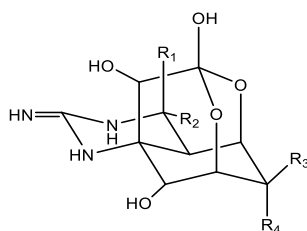
Analogue	R₁	R₂	R₃	R₄	Molecular formula
TTX	H	OH	CH_2OH	OH	$C_{11}H_{17}N_3O_8$
4-*epi*TTX	OH	H	CH_2OH	OH	$C_{11}H_{17}N_3O_8$
6-*epi*TTX	H	OH	OH	CH_2OH	$C_{11}H_{17}N_3O_8$
11-deoxyTTX	H	OH	CH_3	OH	$C_{11}H_{17}N_3O_7$
11-oxoTTX	H	OH	$CH(OH)_2$	OH	$C_{11}H_{17}N_3O_9$
11-norTTX-6(*S*)-ol	H	OH	H	OH	$C_{11}H_{15}N_3O_7$
11-norTTX-6(*R*)-ol	H	OH	OH	H	$C_{11}H_{15}N_3O_7$
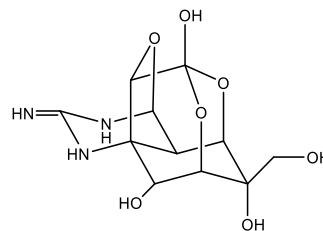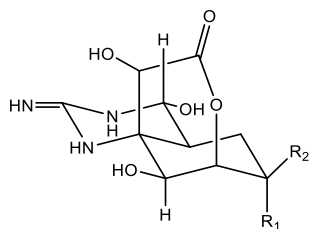
Analogue	R₁	R₂	Molecular formula	Analogue	Molecular formula
5-deoxyTTX	OH	CH_2OH	$C_{11}H_{17}N_3O_7$	4,9-anhydroTTX	$C_{11}H_{14}N_3O_7$
5,6,11-trideoxyTTX	H	CH_3	$C_{11}H_{17}N_3O_5$		

Figure I.8 General chemical structures, substituents and molecular formula of selected TTXs.

The toxic syndrome associated with the consumption of TTX-contaminated finfish and shellfish is quite similar to the PSP syndrome since TTX and PSTs share the same biological target [79]. A high toxicity was observed after intravenous injection in mammals with a median lethal dose of 2-10 µg/kg, while in humans the minimum lethal dose (MLD) reported was estimated to be as 2 mg [80-81]. A wide number of human and animal poisoning due to the consumption of TTX-

contaminated seafood have been reported from 1957 to 2009, including also some cases which fatally resulted in death. Even though most of poisoning incidents were due to the ingestion of contaminated puffer fish in tropical regions, an increasing number of poisoning due to the consumption of a wide range of contaminated marine organisms have been recorded worldwide, including European waters and temperate zones [70, 82]. Unfortunately, there are limited information about the correlation between the environmental conditions and the TTX production, which is still a matter to be explored, as well as its toxicokinetic properties [46]. Therefore, the high number of reports gave rise to even more worrying scenarios as environmental factors, which are progressively changing in relation to climate alterations, could favor the spread of TTX in all continents, increasing the growth rate of bacterial production and therefore the biosynthesis of the toxin.

Until 2017 no health-based guidance levels for TTX in seafood have been suggested globally, including the EU legislative framework which stated that all the TTX-contaminated fisheries products should not to be placed on the market [83]. However, the growing number of poisoning incidents, as well as the fact that TTXs were not monitored regularly through official programs, prompted the EU to ask EFSA for an opinion on the risk assessment for the presence of TTX in shellfish and gastropods from Europe. As a result, 44 µg TTX eq/Kg of shellfish meat have been suggested as MPL since no side effects on humans at lower levels are expected [46]. In addition, more data on the distribution of TTXs in the edible parts of marine shellfish and gastropods was required, as well as more studies on the biosynthesis, accumulation through the food chain and on acute and chronic toxicity before a magnificent regulation can be established.

2.3 Ciguatoxins

Ciguatoxins (CTXs) are a large family of complex polyether and lipid-soluble toxins that includes about 40 compounds so far described (**Table I.2**) [84-85]. The origin of their name lies into the Spanish name *cigua,* which is used to identify *Turbo pica* Linneaeus, 1758 (alternatively *Cittarium pica*), a marine gastropod mollusc (sea snail) found in the Caribbean Spanish Antilles. CTXs are high molecular weight molecules (1000-1200 Da) that feature a ladder-shape backbone composed of 13-14 contiguous ether rings, which are commonly labeled from A to M-N [86]. The CTX producing species is a benthic dinoflagellate discovered by Yasumoto et al. in 1979 and designated as *Gambierdiscus toxicus* [87]. Besides this, several new producing-microalgal species from

tropical and sub-tropical regions have been identified over the years (e.g. *G. belizeanus*, *G. yasumotoi*, *G. pacificus*, *G. australes, and G. polynesiensis* [88-90]. More recently, a new microalgal genus identified as *Fukuyoa*, which is formerly within the *Gambierdiscus* genus, was found to be capable of producing CTXs (e.*g F. yasumotoi, F. paulensis, F. ruetzeri*). To the light of this discovery, some species belonging to the *Gambierdiscus* genus were re-classified into the *Fukuyoa* genus. However, some *Fukuyoa* species were found to be unable of producing CTX, as well as some strains belonging to the same species, thus suggesting that a high variability may occur between phytoplankton samples collected from different regions of the world [91]. In addition, certain marine cyanobacterial species belonging to the genus *Trichodesmium* and *Hydrocolem* demonstrated the ability of producing CTXs [92-93]. CTXs have been detected in different Oceans, thus the scientific community has established to classify them on the basis of their geographical distribution across the oceanic regions in: Pacific (P), Indian (I) and Caribbean (C)-CTXs (**Table I.2)** [94-108].

Table I.2. MS data of known Pacific (P), Caribbean (C) and Indian (I) ciguatoxins (CTXs).

Type-structure	Congener	Molecular formula	Accurate mass $[M+H]^+$
P-CTX-1	CTX4A	$C_{60}H_{84}O_{16}$	1061.5832
or	CTX4B	$C_{60}H_{84}O_{16}$	1061.5832
CTX1B-type	M-*seco*-CTX4A or 4B	$C_{60}H_{86}O_{17}$	1079.5938
	52-*epi*-54-deoxyCTX1B	$C_{60}H_{86}O_{18}$	1095.5887
	54-deoxyCTX1B	$C_{60}H_{86}O_{18}$	1095.5887
	CTX1B	$C_{60}H_{86}O_{19}$	1111.5836
	54-*epi*CTX1B	$C_{60}H_{86}O_{19}$	1111.5836
	52-*epi*CTX1B	$C_{60}H_{86}O_{19}$	1111.5836
	54-*epi*-52-*epi*-CTX1B	$C_{60}H_{86}O_{19}$	1111.5836
	54-deoxy-50-hydroxyCTX1B	$C_{60}H_{86}O_{19}$	1111.5836
	7-oxoCTX	$C_{60}H_{86}O_{20}$	1127.5785
	7-hydroxyCTX1B	$C_{60}H_{88}O_{20}$	1129.5942
	3,4-dyhydro-3-hydroxy-7-oxoCTX	$C_{60}H_{88}O_{21}$	1145.5891
	3,4-dyhydro-4-hydroxy-7-oxoCTX	$C_{60}H_{88}O_{21}$	1145.5891

P-CTX-2	CTX3C	$C_{57}H_{82}O_{!6}$	1023.5676
or	49-*epi*CTX3C (CTX3B)	$C_{57}H_{82}O_{!6}$	1023.5676
CTX3C-type	51-hydroxyCTX3C	$C_{57}H_{82}O_{17}$	1039.5625
	M-*seco*-CTX3C or 3B	$C_{57}H_{84}O_{17}$	1041.5781
	2,3-dyhydro-2-hydroxyCTX3C	$C_{57}H_{84}O_{17}$	1041.5781
	2,3-dyhydro-3-hydroxyCTX3C	$C_{57}H_{84}O_{17}$	1041.5781
	2,3-dyhydro-51-hydroxy-2-oxoCTX3C	$C_{57}H_{82}O_{18}$	1055.5574
	51-hydroxy-2-oxoCTX3C	$C_{57}H_{82}O_{18}$	1055.5574
	51-hydroxy-3-oxoCTX3C	$C_{57}H_{82}O_{18}$	1055.5574
	M-*seco*-CTX3C methyl acetale	$C_{58}H_{86}O_{17}$	1055.5938
	M-seco-40-O-methyl-CTX3C	$C_{58}H_{86}O_{17}$	1055.5938
	2,3-dyhydro-2,3-dihydroxy-CTX3C	$C_{57}H_{84}O_{18}$	1057.5730
	A-*seco*-2,3-dihydro-51-hydroxyCTX3C	$C_{57}H_{86}O_{18}$	1059.5887
	2,3-dihydro-2,3,51-tryhydroxyCTX3C	$C_{57}H_{84}O_{19}$	1073.5680
	M-Seco-2,3-dihydro-2-hydroxy-49-O-methyl-CTX3C	$C_{58}H_{84}O_{18}$	1073.6043
	6,7-dihydro-7-hydroxyCTX	$C_{60}H_{88}O_{20}$	1129.5942
	3,4-dihydro-3-hydroxy-7-oxoCTX	$C_{60}H_{88}O_{21}$	1145.5891
	3,4-dihydro-4-hydroxy-7-oxoCTX	$C_{60}H_{88}O_{21}$	1145.5891
C-CTXs	C-CTX1	$C_{62}H_{92}O_{19}$	1141.6306
	C-CTX2	$C_{62}H_{92}O_{19}$	1141.6306
	C-CTX3	$C_{62}H_{94}O_{19}$	1143.6503
	C-CTX4	$C_{62}H_{94}O_{19}$	1143.6503
	C-CTX1127	-	1127.57[a]
	C-CTX1143	-	1143.60[a]
	C-CTX1157	-	1157.57[a]
	C-CTX1159	-	1159.58[a]
	putative C-CTX851	-	851.51[a]
	putative C-CTX857	-	857.50[a]
	putative C-CTX895	-	895.54[a]
	2 putative C-CTX875	-	875.49[a]
I-CTXs	I-CTX1	$C_{62}H_{92}O_{19}$	1141.6306
	I-CTX2	$C_{62}H_{92}O_{19}$	1141.6306

I-CTX3	$C_{62}H_{92}O_{20}$	1157.6255
I-CTX4	$C_{62}H_{92}O_{20}$	1157.6255
I-CTX5	$C_{62}H_{90}O_{19}$	1139.6149
I-CTX6	$C_{62}H_{90}O_{20}$	1155.6098

[a]= nominal mass; - = formula not assigned.

To date, CTXs are among the most studied marine toxins as they are responsible for the food poisoning syndrome, commonly known as ciguatera fish poisoning (CFP), which is estimated to affects 10.000-500.000 patients in tropical and sub-tropical regions every year [109]. CFP is a complex food-borne illness associated with the consumption of contaminated fish that have harbored CTXs [110]. The characteristic symptoms and signs associated with CFP are: gastrointestinal (e.g. abdominal pain, nausea, vomiting and diarrhea), cardiovascular (e.g. bradycardia and hypotension) and neurological (e.g. parestesia, itching, dysthesia, arthralgia and allodynia) [111-117]. It was observed that gastrointestinal disorders occur within 6-24 h from the fish consumption, and usually resolve without treatments within 1-4 days, while cardiac symptoms generally arise in the first stage of the illness and require urgent hospitalization. The neurological symptoms are among the most variable in patients: they occur in the first days of the disease, become prominent after the gastrointestinal disorders, and they may persist for long periods [110]; in absence of adequate treatments, they may become chronic [118]. A certain extent of diversity in symptomatology was observed among different tropical regions, suggesting that the structural diversity among P-, C- and I-CTXs may have influence on human disorders [84]. CFP is mainly due to the ability of CTXs to bind the voltage-gated sensitive sodium channels (VSSCs), thus increasing the Na^+ ionic current inside the cells and leading to cell disruption. The main consequences of such interaction is the disturbance of the ion conductance on nerves and muscle fibers [119-120]. Currently, CFP is diagnosed by medical evaluation of the characteristic symptoms showed by patients in association with the history of eaten fish that are commonly known to harbor CTXs (e.g. Moray eel, Barracuda, Grouper, Snapper, Kingfish, Jacks, Surgeonfish, Parrot fish, Wrasses, Hogfish, Red emperor) [110]. Notably, CTXs have been detected in more than 400 species of fish up to attaining the highest concentrations in top predatory fish, such as Barracuda, Amberjack and Grouper [121]. This phenomenon is related to the spread of the toxins through the marine food web since: large predatory fish accumulate CTXs from the

consumption of smaller herbivorous fish which have ingested the *Gambierdiscus* and/or *Fukuyoa* microalgal species [103, 122-123]. During the initial studies, there was a high degree of uncertainty on whether the toxins isolated from fish and those isolated from *Gambierdiscus* spp. were the same. Subsequently, a theory of biotransformation of the toxins following metabolism in fish was proposed, based on the evidence that the most oxygenated members of this toxin class are found at higher levels in fish whilst they are absent or produced at very low levels in dinoflagellates. Contrarily, the less polar congeners were detected at higher levels in microalgal species and at negligible concentrations in fish [86]. This consideration led to suppose that the microalgal toxins are the substrate of oxidation reactions occurring in fish due to the enzymatic activity of the cytochrome P450 aimed at excreting the toxins. However, toxicological studies revealed that the more oxidized congeners found in fish are more potent that the less polar molecules produced by microalgae, thus the oxidation pathway along the trophic chain results into an increased toxicity [96, 103, 124-126]. On the other hand, this relationship oxidation-toxicity seems to not occurs for I-CTXs, since the most polar and oxidized congeners found in organisms to the top of the food-web were less toxic than their less polar parent compounds [127]. In fact, the biotransformation pathway of CTXs was investigated and confirmed through laboratory experiments only for P-CTXs, and it cannot be applied to Caribbean and Indian congeners, whose microalgal origin remains still unknown [123]. Even though Caillaud et al. [128] reported about the putative presence of C/I-CTXs in the culture medium of a *G. pacificus* strain collected from Malaysia, their origin still represents a controversial issue, and the most accredited reports describe their finding in carnivory fish. Currently, CFP is raising high concerns within the EU borders since the global warming and anthropogenic pressure are favoring the spread of CTX-producing species even in temperate regions [84]. As a consequence, several cases of intoxication due to the consumption of contaminated fish have been recorded in Crete (Greece) and Canary Islands (Spain) [129-131]. Besides CTXs, other toxic polyether compounds have been found in extracts from *Gambierdiscus* and *Fukuyoa* spp., namely maitotoxins (MTXs), gambierol, gambieric acids (GA) gambieroxide and gambierones. Although in the past these secondary toxic metabolites have been associated with CFP syndrome, several authors have suggested that their contribute can be exclude since they exhibited different structures, toxicity and mode of action [132-136]. Insights into chemical, ecological and toxicological aspects of different CTX groups are described below.

2.3.1 Pacific CTXs

P-CTXs are the most studied CTX group in terms of chemical properties, producing organisms, distribution through the food-web and toxicity. They are about 30 structural congeners exhibiting two different type-structures, and then classified into two sub groups: P-CTX1 or CTX1B type and P-CTX-2 or CTX3C type (**Table I.2**; **Fig.I.9**) [111]. The two sub-groups are unified by the presence of a backbone composed of 13 rings (A-M), whilst the main differences lie in: i) the E ring, which is an oxygenated 7-membered ring (oxopene) in P-CTX1 and an oxygenated 8-membered ring (oxocene) in P-CTXs-2, and ii) the lack of the side-chain at A ring in P-CTX-2 group (**Fig.I.9**). All P-CTXs share the lack of the N ring (found in C-CTXs), while the M-*seco* derivatives of both sub-groups possess 12 rings (A-L) since the M ring (opened) is present as side chain substituent on the L ring. All the structural differences observed within both sub-groups involve the two side of the molecule, which are commonly labeled as R1 and R2 sides (**Fig.I.9**). Notably, differences can be due to: i) the position of the etheric oxygen at C52, ii) the position of the methylene moiety at C52, iii) the presence of additional hydroxyl groups at M ring, and iv) for P-CTX-1 the number of carbon-carbon double bond and hydroxyl group at the side chain linked to A ring (R1 side) (**Fig.I.9**).

Within P-CTX-1 type structure, a further classification can be done between A and B epimers on the basis of the configuration of the C52 at R2 side (M spiroketal ring) [103]. Type A epimers include CTX4A, M-*seco*-CTX4A and 52-*epi*-54-deoxyCTX1B, whilst B epimers include CTX4B, M-*seco*-CTX4B, 54-deoxyCTX1B and CTX1B. Different chemical-physical and toxicological properties were observed between the 2 isomer types: epimers B are more thermodynamically favored than A isomers, which are instead more polar and toxic. Nonetheless, the most potent congener described so far is CTX1B (a type B isomer) [86]. In addition, it was reported that A and B epimers are interchangeable in acidic conditions, even if the most stable B isomers are energetically favored. This interconversion may occur in the stomach of fish where toxins are further bio-transformed into more polar and toxic derivatives. In fact, for P-CTXs-1 the following oxidation pathway, which results into an increased toxicity, was proposed: CTX4B → 54-deoxyCTX1B → CTX1B for B isomers and CTX4A → 52-*epi*-54-deoxyCTX1B → 52-*epi*-CTX1B for A isomers (**Fig.I.9**).
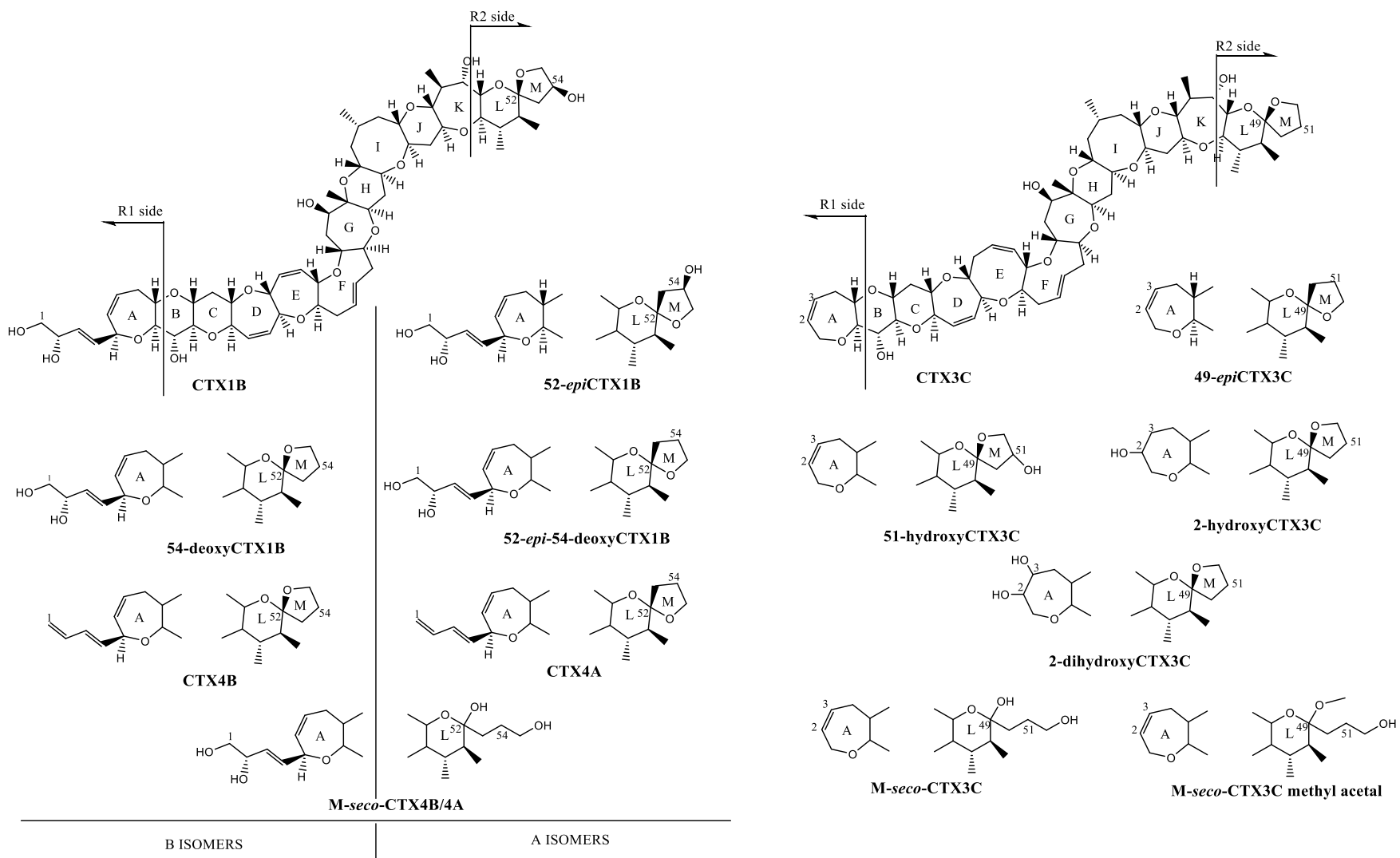
Figure I.9 Chemical structure of assorted Pacific CTXs.

CTX4A and CTX4B were thus identified as microalgal precursors, within the group of P-CTX-1, of 52-*epi*-54-deoxyCTX1B and 54-deoxyCTX1B, respectively. In fact, these two toxins were unambiguously identified both in extracts from *G. toxicus* cultures and herbivorous fish [125]. The relationship between CTX4A and CTX4B and their M-*seco* derivatives still represents a controversial issue. Indeed, in acidic conditions M-seco derivatives undergo a cyclization of the side chain leading to CTX4A and -4B [101], whilst Ikehara et al. [123] observed through laboratory trials that M-seco derivatives are biotransformation products of CTX4A and -4B. The toxicity of M-seco derivatives is still unknown even if it is reasonable to suppose that their potency is very low since they were isolated from fractions negative to the MBA. Acute toxicity studies revealed that CTX4A and CTX4B were the less toxic congeners since they exhibited a LD_{50} of 2.0 and 4.0 μg/Kg, respectively, when injected intraperitoneally to mice, whilst their oxidized derivatives, 52-*epi*-54-deoxyCTX1B and 54-deoxyCTX1B were more toxic with LD_{50} of 0.9 and 2.3 μg/Kg, respectively [43, 96, 125]. However, the most toxic congener among P-CTXs-1 is CTX1B, the most oxidized molecule for which a LD_{50} of 0.25 μg/Kg was measured [98, 137-138]. CTX1B was found at high level in carnivorous fish such as moray eels, Spanish mackerel, barracuda and snapper [139-143] whilst, differently from its less oxidized precursors, it has never been detected in microalgal samples.

Within the P-CTX-2 group, the same sub-classification in A (49-*epi*CTX3C) and B (CTX3C) epimers due to the configuration of the M ring can be done, with the only difference represented by the C atom involved, which is C49 (C52 for P-CTX-1). As a consequence, also P-CTX2 can undergo interconversion in acidic conditions [100]. The microalgal precursor of this sub-group is CTX3C, which was characterized in 1993 [144], fully synthetized in 2001 [145] and currently is commercially available as standard. The toxicity of CTX3C was lower compared to that of its oxidized derivatives such as 2,3-dihydroxyCTX3C and 51-hydroxyCTX3C. The latter represent the most toxic CTX found so far, since the measured LD_{50} by IP injection was 1.7-fold lower than that of CTX1B (190 pmol/Kg and 320 pmol/Kg, respectively) [146]. The most oxidized compounds within the P-CTX-2 group were found to be produced also by *Gambierdiscus* species in co-occurrence with CTX3C [128]. On the other hand, CTX3C showed the capacity of passing without changes through the marine food-web from the producing microalgae to fish at the top of the chain [147].

2.3.2 Caribbean CTXs

C-CTXs are a smaller group of 12 congeners of which only 4 analogues have been structurally characterized so far, namely C-CTX1-4 (**Table I.2**; **Fig.I.10**) [85-86]. Caribbean analogues possess a polyether backbone composed of 14 rings (A-N), and similarly to P-CTX-2 sub-group, the E ring is an oxocene (8-memebered ring) while the A ring lacks the side chain found in P-CTX-1 congeners (**Fig.I.10**). C-CTX1 was fully elucidated in 1998 by Lewis et al. [108] by NMR experiments on a purified fraction obtained from 51 Kg of liver, viscera and flesh of contaminated *Caranx lattus*. The structural analysis of the toxin revealed the atypical presence of a hemiketal functionality on the N ring that involves the C56 (**Fig.I.10**). Until then, this chemical feature had never been reported for any of the known CTX analogues. C-CTX2 was found to be the epimer at C56 of C-CTX1 (alternative name 56-epi C-CTX1; **Fig.I.10**) [107-108]. Differently from C-CTX1, the structure of C-CTX2 was not elucidated through NMR experiments since it was detected at lower levels than its isobaric congener, and the amount of purified toxins turned out to be too low. Therefore, its structure was brough to light storing the purified fraction of the toxin in acidic solutions and/or in organic aqueous mixtures which favored the interconversion of the anomeric C56. The LC-MS analysis of the stored fraction showed the presence of a peak eluting at the same retention time of C-CTX1 whilst that of C-CTX2 was no longer detectable [108]. Similarly, in the same experimental conditions C-CTX1 slowly rearranged to C-CTX2. Stability studies demonstrated that C-CTX1 was the lower energy epimer and only a small aliquot of the toxin underwent interconversion leading to C-CTX2. Recently, two newly congeners have been elucidated, namely C-CTX3 and-4. Their identity emerged a few years ago from the analysis of contaminated fish [148] but the purified material was not enough for NMR studies. Notably, C-CTX3 and -4 are the reduced derivatives at C56 of C-CTX1 and -2, respectively, and they lack the N ring which is opened (**Fig.I.10**). The structure of C-CTX3 and -4 was derived through LC-MS analysis in association with chemical reactions [85]. Briefly, the reduction with $NaBH_4$ of the opened form of the hemiketal moiety (CO + OH) of C-CTX1 and -2 gave rise to C-CTX3 and -4. Moreover, about 10 new C-CTX analogues have been suspected by LC-MS after the analysis of *C. latus* species, but their low level in association with a reduced yield of recovery hampered to obtain enough purified material for structural characterization [148]. Among them, three isobaric analogues of C-CTX-1 were found and named C-CTX-1141a/b/c. It has been supposed that they may be epimers of C-CTX-1 and/or 2 at the C3, C29 and C44, or regioisomers as observed for P-

CTXs. In addition, analysis of the effect of cooking of fish revealed that C-CTX-1 might interconvert to C-CTX-1141a. The IP injection to mice of C-CTX1 showed a LD_{50} of 3.6 µg/Kg, thus highlighting that it was 14-fold less toxic than P-CTX1B (LD_{50} 0.25 µg/Kg) [108].
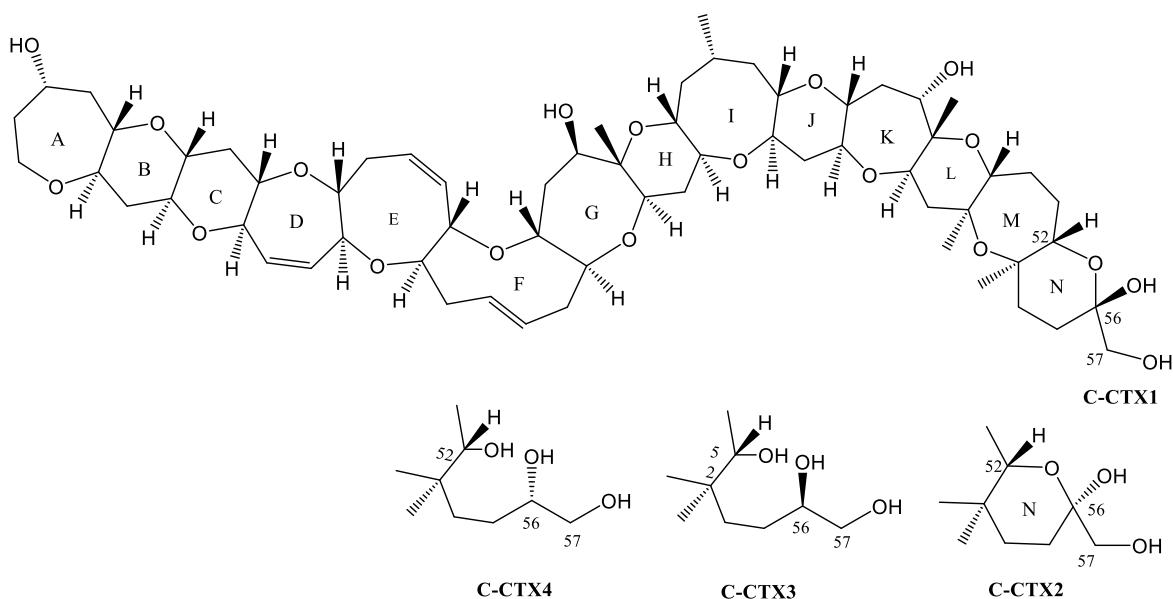
Figure I.10 Chemical structure of Caribbean CTX1-4.

2.3.3 Indian CTXs

I-CTXs are a group of 6 analogues classified from I-CTX1 to -6 (**Table I.2**). To date, none of them have been structurally characterized. LC-HRMS measurements of Indian fish species revealed that I-CTX1 and -2 are isobaric compounds, and more interestingly, they have the same exact mass of C-CTX1 and -2 [127, 149]. Nonetheless, some differences in chemical-physical properties emerged since: i) I-CTX1 and -2 showed different ionization behavior than C-CTXs when analyzed by LC-MS under the same experimental conditions, ii) contrarily to Caribbean congeners, I-CTXs did not undergo interconversion after long time storage in acidic conditions and/or organic aqueous mixtures, and iii) I-CTX1 and -2 were found to be more polar than C-CTX1 and -2 since they eluted slightly earlier when injected on a TSK HW-40S column. The lack of interconversion between I-CTX1 and -2 led to suppose that: i) I-CTX-1 and 2 could not be epimers, or ii) they could be characterized by a more stable spiroketal/hemiketal arrangement, or)

they could belong to a different class of stereoisomers. On the other hand, LC-MS analysis carried out on several Indian fish samples revealed that the ratio of I-CTX-1 and 2 is fish-dependent, thus suggesting that they may arise from different dinoflagellate precursors whose outbreak strongly affects the level of accumulated toxins in fish. LC-HRMS analysis further revealed the presence of new Indian congeners named I-CTX3 and -4, which were found to be the oxidized form of I-CTX1 and -2 [127]. They are more polar than I-CTX1 and -2, but to date, the position of the extra hydroxyl group is still unknow. Similarly to I-CTX1 and -2, I-CTX-3 and -4 showed a high stability in acidic solution or when stored for long time. Laboratory trials demonstrated that they are not degradation products of I-CTX-1 and 2 and are not epimeric compounds. It has been supposed that I-CTX-3 and 4 may originate from the oxidative metabolism in fish during attempts to detoxify and/or enhance the depuration rate of I-CTX-1 and I-CTX-2. Additionally, a comparative study between the levels of I-CTX1/2 and I-CTX3/4 determined in fish revealed that the more oxidized congeners were more concentrated in fish at the top of the food-chain, while the levels of I-CTX1 and -2 were higher in fish at the bottom of the trophic chain [150]. More recently, Diogène et al. [150] brough to light by LC-HRMS the presence of I-CTX5 and -6, which were extracted from the stomach of a shark species. Particularly, the formula assigned to I-CTX5 showed 2H less than I-CTX1/2, whilst I-CTX-6 showed 2H less than I-CTX4/5. It was supposed that they features one carbon-carbon double bond than the relevant precursor. Overall, I-CTXs were found to be less toxic than both P- and C- congeners since I-CTX1/2 and I-CTX3/4 exhibited the 60% and the 20% of the activity of CTX1B, respectively [127].

2.3.4 Regulation

Currently, there are not regulatory limits for CTXs in European and imported food products. The lack of comprehensive acute and chronic toxicity data for most of the analogues, associated with the need to implement effective and sensitive methods to study the toxin distribution within the trophic chain, did not allow for an adequate risk assessment to prevent the consumer health. EU commission established that no fishery products containing CTXs must be placed on the market (Regulation (EC) No. 854/2004). However, it was estimated that a contamination level of 0.01 µg CTX1B eq/Kg fish flesh and 0.1 C-CTX1 µg/Kg fish flesh may represent a risk for human health, therefore a safety factor of 10x has been suggested by the Food and Drugs administration (FDA-

2013-D-0269) and EFSA [46]. On the other hand, no guide levels have been proposed for I-CTXs that still represent the less studied CTX congeners.

2.4 Maitotoxins

Maitotoxins (MTXs) are a small group of complex large-size polyether toxins produced by different species belonging to the *Gambierdiscus* genus. To date, 6 MTX congeners have been reported, namely: MTX, MTX2, MTX3, MTX4 and two mono-sulfated analogues of MTX, which represents the parent compound of this toxin class [151]. The name MTX derives from the Tahitian name ''maito'' used to identify the fish *Ctenochaetus striatus* from which the toxin was first detected in the far 1976 [151]. The algal origin of the toxin was discovered only 11 years later [153], whilst the complete structural characterization was accomplished in 1993. MTX (molecular formula: $C_{164}H_{256}O_{68}S_2Na_2$; accurate mass of the di-sodium salt: 3423.5811 Da; **Fig.I.11**) is listed among the most potent marine toxins identified so far ($LD_{50} = 0.050$ µg/Kg by IP injection; [154]) and, in this context, it has also proved to be the largest non-polymeric toxic secondary metabolite of microalgal origin [155]. MTX features a ladder-shape backbone harboring 32 ether rings (A-F'), 28 hydroxyl groups, 2 methyl groups, 2 sulfate moieties and 98 stereocenters (**Fig.I.11**). The MTX-producing organism was found to be the dinoflagellate *G. australes* [156-160]. The toxicity of MTX is associated with its capability of increasing the intracellular concentration of Ca^{2+} in a large variety of cells through a voltage-independent entry mechanism [161]. Although the molecular target of MTX still remains unknown [162], the presence of one sulfate group is a prerequisite for the biological activity. In fact, lab trials demonstrated that the toxicity of MTX substantially decreases when subjected to desulfation and hydrogenation reactions [163]. Event tough MTX showed a high toxicity when intraperitoneally injected to mice, its oral potency turned out to be significantly lower [164]. Probably, this phenomenon is related to a low intestinal absorption rate due to its high molecular weight and hydrophilicity. MTX was first detected in the extracts from the digestive tracts of fish, therefore it was supposed that MTX-food poisoning could occur when guts and livers were consumed [165]. However, higher concerns about the impact of MTX on consumer safety have recently been raised by Kohli et al. [166] who demonstrated that the toxin can also accumulate in fish muscles. Even though MTXs and CTXs can be detected in the same contaminated fish since they share the same algal origin, the contribution of MTX in CFP was excluded [167-168]. MTX2 (nominal mass of the sodium salt: 3298 Da) was detected in 1990

Maitotoxin

Gambierone, R=H
44-methylgambierone, R=CH$_3$
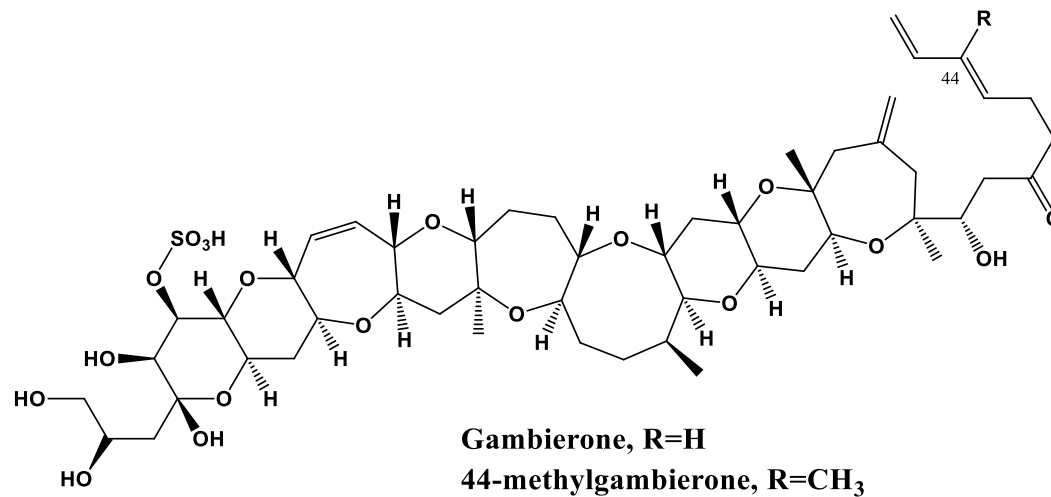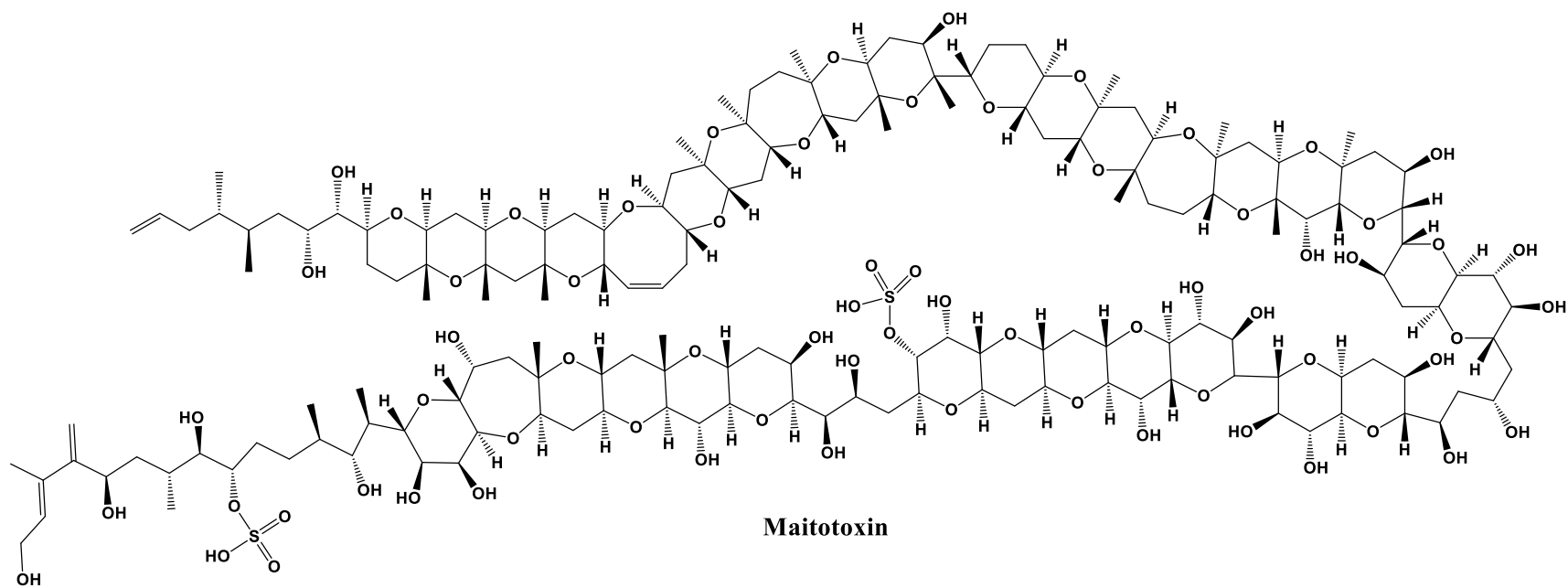
Figure I.11 Structure of maitotoxin (MTX) and 44-methylgambierone (previously identified as MTX3).

in extracts from *Gambierdiscus* strains collected from Australia [169]. Although the structure of the toxins is not elucidated yet, LC-LRMS measurements confirmed the nature of the toxin as well as the presence of 1 sulfate moiety [170-171]. Toxicological studies showed that MTX2 is less toxic than MTX1 since the LD_{50} of 0.080 µg/Kg was measured by IP injection. The reduced toxicity of MTX2 could be associated with the lack of the second sulfate group which instead is present in the structure of MTX1. MTX3 (nominal mass of the sodium salt: 1060.5 Da) was originally found in extracts from *G. australes* strains [170]. The amount of purified material was not enough to accomplish both the structural characterization and the study of the acute toxicity. However, its structure was recently elucidated, and it emerged that MTX3 is not a MTX-like compound, but it is the 44-methylgambierone (molecular formula: $C_{52}H_{78}O_{19}S$; exact mass: 1038.4858 Da), a congener of gambierone which is produced by *Gambierdiscus* dinoflagellates (**Fig.I.11**) [172-173]. MTX4 (molecular formula: $C_{157}H_{241}NO_{68}S_2$; exact mass: 3292.4872) was the latest congener to be discovered in 2017 by LC-HRMS analysis of *G. excentricus* cultures [156]. Even through the complete structure of the molecule is still unknown, Pisapia et al. [151] reported the elemental formula of the toxin and some structural features by comparing the fragmentation spectra of MTX4 with those of MTX. Currently, safety authorities still have not released guide levels for MTX in fish since it was excluded the contribution of the toxin in CFP. Nonetheless, its high acute toxicity by IP injection, combined with the ability of accumulating in muscles and in the digestive tract of fish, is raising high concerns for consumer health.

2.5 PLTX and its congeners

Palytoxin (PLTX; **Fig.I.12**) is one of the most potent non-protein and non-polymeric natural marine toxins so far known, originally identified in 1971 from the Hawaiian *Palythoa toxica*, a tropical soft coral species belonging to the *Zoanthide* family [174-176]. After the first finding, PLTX has also been detected in a large variety of *Palythoa* spp. (e.g. *P. tuberculosa, P. vestitus, P. caribaeorum, P. mammilosa and Palythoa* aff. *margaritae* and *Zoanthus* spp. (*Z. solanderi and Z. sociatus*) [174, 177-185]. The biogenetic origin of PLTX has been a controversial issue and a matter of speculations for a long time since the toxin was detected in sea anemones (*Radianthus macrodactyylus*), red algae (*Chnodria armata*), marine worms (*Hermodice carunculata*), crabs, mackerel, fish and mussels [187-190]. As a consequence, it was reasonable to assume that PLTX was produced by microorganism associated with zoanthidis [191] instead of being produced by

the zoanthidis itself. However, the finding of PLTX-like compounds produced by different species of dinoflagellates belonging to the *Ostreopsis* genus and the detection of PLTX and some congeners in cyanobacterial species (*Trichodesmium* genus*)*, made the situation even more complex [192]. Therefore, two further hypothesis on PLTX origin were postulated: i) reef-corals are able to concentrate the toxin which is produced by microalgal dinoflagellates [194-195], and/or ii) the toxin is produced by symbiotic cyanobacteria in association with the previously described organisms [196].
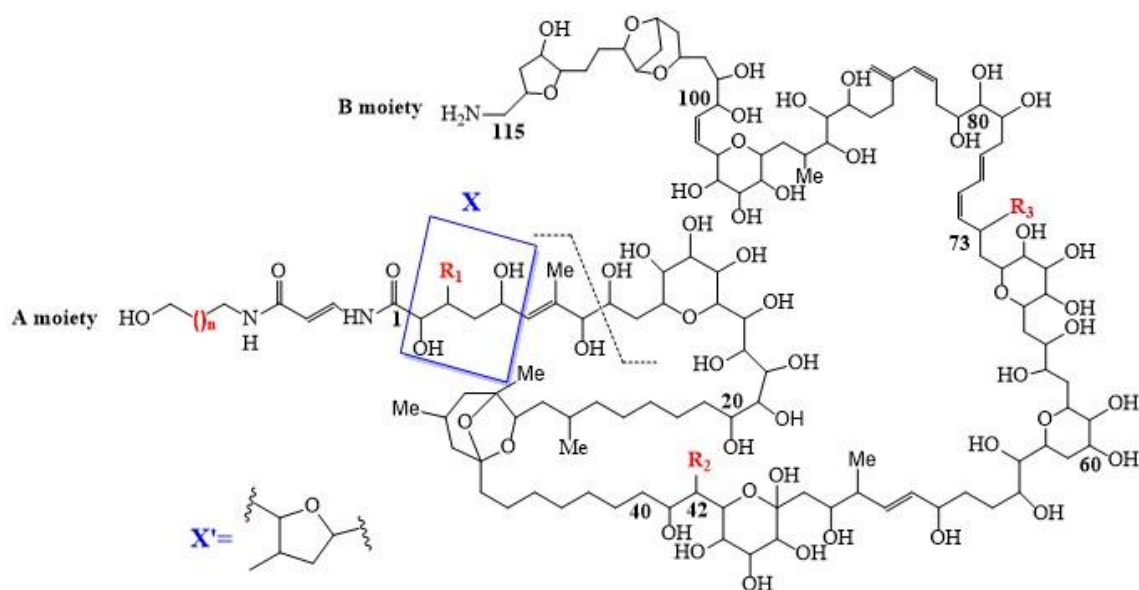
Toxin	n	R_1	R_2	R_3		Molecular formula
Palytoxin	1	Me	H	OH	X	$C_{129}H_{223}O_{54}N_3$
Homopalytoxin	2	Me	H	OH	X	$C_{130}H_{225}O_{54}N_3$
Bishomopalytoxin	3	Me	H	OH	X	$C_{131}H_{227}O_{54}N_3$
Neopalytoxin	1		H	OH	X'	$C_{129}H_{221}O_{54}N_3$
Deoxypalytoxin	1	Me	H	H	X	$C_{129}H_{223}O_{53}N_3$
42-hydroxypalytoxins (50R), (50S)	1	Me	OH	OH	X	$C_{129}H_{223}O_{55}N_3$

Figure I.12 Planar structure of PLTX and its analogues produced by *zoanthidis* species.

PLTX is a complex, amphiphilic, high molecular weight compound composed of a long and partially unsaturated aliphatic backbone harboring 64 chiral centers, 8 stereogenic double bond, 7

interspersed ether rings, 42 hydroxyl groups, two amide functions and one primary amino group ($C_{129}H_{223}O_{54}N_3$; **Fig.I.12**) [197]. Conventionally, the long alkyl chain of the toxin is split into 2 moieties, labelled as A side (C1-C8) and B side (C9-C129), since the fragmentation of the molecule through MS^2 experiments gives rise to a characteristic and intense fragment originating from cleavage between C8 and C9 (*m/z* 327) (**Fig.I.12**, [197]. To date, 6 PLTX analogues have been found in extracts from *Palythoa* spp., namely: homoPLTX, bishomoPLTX, neoPLTX, 73-deoxyPLTX and 2 diasteroisomers of 42-hydroxyPLTX (50*R* and 50*S*) **Fig.I.12** [183, 198-199]. On the other hand, the number of PLTX analogues turns out to be higher if the toxic secondary metabolites produced by dinoflagellates of the *Ostreopsis* genus are taken into consideration. *Ostreopsis* species are benthic and epiphytic microalgae originally confined in tropical and sub-tropical areas. However, their occurrence in temperate regions has become increasingly frequent, to the point of representing one of the major health problems in the Mediterranean basin due to the massive proliferation of noxious species (HABs) capable of producing PLTX-like molecules [200]. To date, several *Ostreopsis* spp. have been reported: *O. siamensis*, *O. ovata*, O. *lenticularis, O. heptagona, O. mascarenensis, O. labens, O. marina, O. belizeana, O. caribbeana* and *O. fattorussoi* [201]. It is interesting to note that not all species described so far have proved to be toxic, as well as the profile of toxin-producing species can strongly vary among different strains and in relation to different environmental factors or their geographical distribution [201-202]. The toxic secondary metabolites produced by *Ostreopsis* flagellates can be classified, on the basis of their producing-organisms, in three different sub-groups: ostreocins (OSTs), mascarenotoxins (McTXs) and ovatoxins (OVTXs) [203].

OSTs are a group of 4 analogues produced by *O. siamensis* (**Fig.I.13**). OSTD was the first congener to be discovered in 1995 in extracts from a cultured strain of *O. siamensis* collected in Okinawa (Japan), thus showing for the first time the existence of alternative biogenetic sources capable of producing PLTX-like molecules [204]. However, its structure was fully elucidated 7 years later through the combination of different techniques LC-MS^2-based [205]. Few years later, from the same toxic strain of *O. siamensis* harvested in Okinawa, 3 further OSTs were found out and structurally characterized: OSTB, OSTA and OSTE1 (**Fig.I.13**) [206-207]. Ecotoxicological studies revealed a high variability in toxin profile of *O. siamensis* collected from different geographical sites since the Japanese strains turned out to be extremely toxic whilst cell strains harvested in the Mediterranean and Atlantic basins were devoid of any toxicity [208].

PLTX = palytoxin
OVTX = ovatoxin
OVT = ovatoxin
OST = ostreocin
McTX = mascarenotoxin
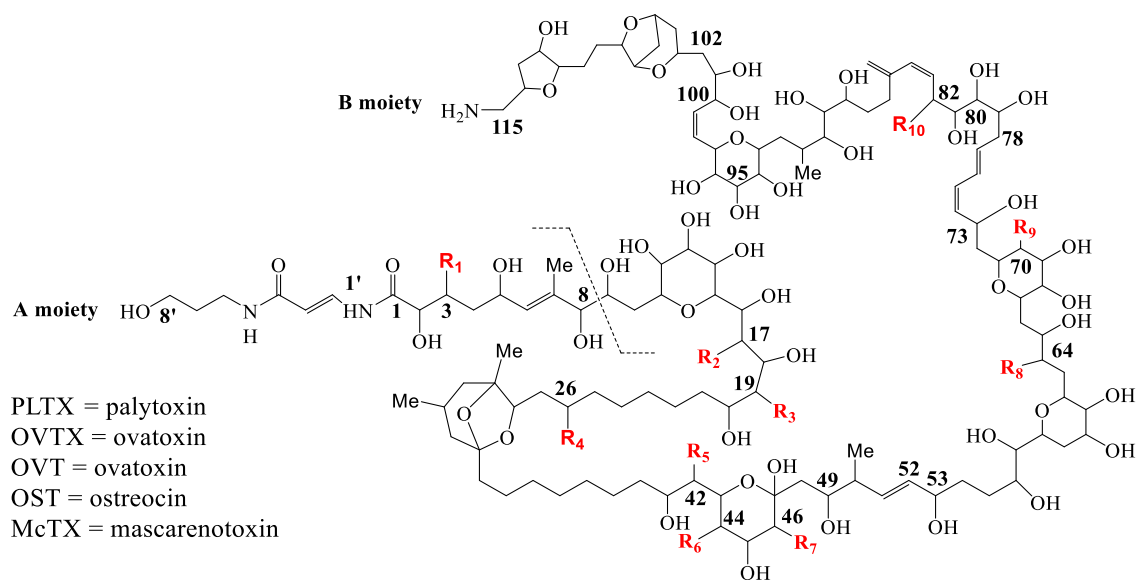
Toxin	C_3-R_1	C_{17}-R_2	C_{19}-R_3	C_{26}-R_4	C_{42}-R_5	C_{44}-R_6	C_{46}-R_7	C_{64}-R_8	C_{70}-R_9	C_{82}-R_{10}	Molecular formula	Other
PLTX	Me	OH	OH	Me	H	OH	OH	OH	OH	H	$C_{129}H_{223}O_{54}N_3$	
OVTX-a	Me	H	OH	Me	OH	H	OH	H	OH	H	$C_{129}H_{223}O_{52}N_3$	
OVTX-b	Me	H	OH	Me	OH	H	OH	H	OH	H	$C_{131}H_{227}O_{53}N_3$	+ C_2H_4O in the region N-C8'
OVTX-c	Me	H	OH	Me	OH	OH	OH	H	OH	H	$C_{131}H_{227}O_{54}N_3$	+ C_2H_4O in the region N-C8'
OVTX-d	Me	H	OH	Me	OH	OH	OH	H	OH	H	$C_{129}H_{223}O_{53}N_3$	
OVTX-e	Me	H	OH	Me	OH	H	OH	H	OH	H	$C_{129}H_{223}O_{53}N_3$	+ O in the region C8-C8'
OVTX-f	Me	H	OH	Me	OH	H	OH	H	OH	H	$C_{131}H_{227}O_{52}N_3$	+ C_2H_4 in the region C95-C102
OVTX-g	Me	H	OH	Me	OH	H	OH	H	OH	H	$C_{129}H_{223}O_{51}N_3$	
OVTX-h	Me	H	OH	Me	OH	H	H	H	OH	H	$C_{129}H_{225}O_{51}N_3$	Open ring in the region C42-C49
OVTX-i	Me	H	OH	Me	OH	H	OH	H	OH	H	$C_{131}H_{225}O_{53}N_3$	+ $C_2H_2O_2$ and 1 unsaturation in the region C49-C52 - O in the regione C53-C78
OVTX-j1	Me	H	OH	Me	OH	OH	OH	H	OH	H	$C_{131}H_{225}O_{54}N_3$	+ $C_2H_2O_2$ and 1 unsaturation in the region C49-C52 - O in the regione C53-C78
OVTX-j2	Me	H	OH	Me	OH	H	OH	H	OH	H	$C_{131}H_{225}O_{54}N_3$	+ $C_2H_2O_2$ and 1 unsaturation in the region C49-C52
OVTX-k	Me	H	OH	Me	OH	OH	OH	H	OH	H	$C_{131}H_{225}O_{55}N_3$	+ $C_2H_2O_2$ and 1 unsaturation in the region C49-C52
Isobaric PLTX	Me	H	OH	Me	OH	OH	OH	H	OH	H	$C_{129}H_{223}O_{54}N_3$	+ O in the region C8-C8'
OVTa-IK2	Me	H	OH	Me	OH	H	OH	OH	H	H	$C_{129}H_{223}O_{52}N_3$	
OVTd-IK2	Me	H	OH	Me	OH	OH	OH	OH	H	H	$C_{129}H_{223}O_{53}N_3$	
OVTe-IK2	Me	H	OH	Me	OH	H	OH	OH	H	OH	$C_{129}H_{223}O_{53}N_3$	
OSTD	H	OH	H	H	OH	H	OH	OH	OH	H	$C_{127}H_{219}O_{53}N_3$	
OSTB	H	OH	H	H	OH	OH	OH	OH	OH	H	$C_{127}H_{219}O_{54}N_3$	
OSTA	H	OH	H	H	OH	H	OH	OH	OH	OH	$C_{129}H_{219}O_{54}N_3$	
OSTE1	H	OH	H	H	OH	H	OH	OH	OH	H	$C_{129}H_{217}O_{52}N_3$	
McTX-a											$C_{127}H_{221}O_{50}N_3$	
McTX-b												
McTX-c											$C_{129}H_{221}O_{51}N_3$	

Figure I.13 Planar structure of PLTX and its analogues produced by *Ostreopsis* species.

McTXs are among the less studied PLTX analogues since only three congeners have been detected so far from *O. mascarenensis* species, and none of them have been structurally characterized. Notably, McTX-a and -b were reported for the first time in 2004 by Lenoir et al. in extracts from a cultured strain collected in 1996 in the Indian Ocean (Mauritius Island, Madagascar) [209]. The authors confirmed the identity of the 2 toxins through the acquisition of HR full-scan MS and MS^2 spectra, which were consistent with those of PLTX and its congeners. Four years later, Rossi et al. [210] reported about the presence of McTXs in *O. ovata* extracts harvested in the Gulf of Naples (Italy) in 2008. In detail, LC-HRMS and MS^2 analyses revealed and confirmed the presence of a mono-isotopic ion peak [M+H]$^+$ at *m/z* 2589.3441, which matched the MS profile of McTX-a reported by Leonir et al. [209]. The measured accurate mass allowed to assign to the toxin the following elemental formula: $C_{127}H_{221}N_3O_{50}$. However, the error in ion assignment was not within the commonly accepted mass tolerance (≤ 5 ppm) given the large difference between the accurate and the calculated exact mass of McTX-a (mono-isotopic ion peak [M+H]$^+$ at *m/z* 2589.4921). On the other hand, in lack of structural data, it cannot be excluded that McTX-a detected in *O. mascarenensis* and McTX-a detected in *O. ovata* are isobaric compounds featuring different structures. In the same study [210], the authors reported the further presence of a new analogue, named McTX-c, to which the elemental formula $C_{129}H_{221}N_3O_{51}$ was assigned on the basis of its [M+H]$^+$ mono-isotopic ion peak: i) calculated exact mass, *m/z* 2629.4870; ii) measured accurate mass, *m/z* 2629.2854.

OVTXs are the largest group of algal congeners of PLTXs considering that 17 analogues have been reported so fa (OVTX-a, b, c, d, e, f, g, h, i, j$_1$, j$_2$, k, isobaric PLTX, OVTa-IK2, OVTd-IK2 and OVTe-IK2 (**Fig.I.13)** [202,211]. Although they are mainly produced by different strains of *O. ovata*, a new producing-species called *O. fattorussoi,* has been recently reported [201, 212]. Isobaric PLTX [213] and OVTX-a [214] have been the first analogues to be discovered in in the period 2005-2006, after the occurrence of a so called ''*Ostreopsis* phenomenon'', a massive proliferation of *Ostreopsis* blooms along the Ligurian coastline (Italy), which affected hundreds of people during recreational and working activities due to their exposure to marine aerosols [215-217]. To date, OVTX-a is the only analogue whose structure was completely characterized through the employment of HRMS^2 and NMR techniques [218-220]. For all the other congeners, structural insights or tentative structural elucidations were accomplished through the LC-HRMS^2 technique (**Fig.I.13**), which turned out to be a powerful tool to achieve this goal since the structural

characterization of the algal toxins by means of NMR experiments is greatly hampered by the slow growth of dinoflagellates and the lack of standardized purification/isolation procedures characterized by high yields of recovery. As a consequence, after optimizing a mass fragmentation-based strategy to deeply investigate the structure of OVTX-a, the LC-HRMS approach has proved powerful in characterizing the toxic profile of different *O. ovata* strains from the Mediterranean area, bringing to light structural insights for OVTXs from -b to k [202, 212, 221-223]. OVTXs labelled as IK2 owe their name to their producing-*Ostreopsis* strain, namely *Ostreopsis* IK2, which was collected at Ikei Island (Okinawa, Japan). Their planar structure was proposed on the basis of the fragmentation pattern acquired by LC-HRMS^2 experiments. The tree newly Japanese analogues exhibited the same accurate mass of the Mediterranean OVTX-a, -d and -e, but different chromatographic behavior. Therefore, a different naming system for Japanese OVTXs was proposed, and the new compounds were named: OVTa-IK2, OVTd-IK2 and OVTe-IK2 [211]. As previously described for *O. siamensis*, a remarkable variability in toxicity was observed among different strains of *O. ovata*, mainly due to their geographical distribution. The highest toxin contents were found, in co-occurrence with toxic outbreaks, in strains from Brazil (60-468 pg/cell) and the Mediterranean basin (30-300 pg/cell) [202, 224]. Contrarily, *O. ovata* strains from Japan (0-16 pg/cell) and New Zealand (0.013 pg/cell) exhibited lower toxin contents [211, 225-226]. Moreover, a further variability was also found in the toxic profile of strains collected in the same area [202]. Similarly, some strains of *O. fattorussoi* from Cyprus were found to be capable of producing OVTX- i, j_1, j_2 and k, while strains from Lebanon produce only OVTX-a, -d and -e [201, 212]. However, unlike *O. ovata*, *O. fattorussoi* does not represent an actual threat to human in the Mediterranean Area considering the total toxin content measured (0.06-2.8 pg/cell) [202].

Currently, the lack of reference material as well as well-purified fractions for most of the PLTX analogues has hampered: i) the conduction of toxicological studies, ii) the development of effective analytical methods for their detection, iii) the standardization of procedures for preparative works and iv) the study of their mechanism of action. Therefore, most of the available data refers only to PLTX and a few other congeners.

The main biological target of PLTX is the transmembrane pump Na^+/K^+ ATPase, which is essential to maintain the physiological membrane potential and then the cell homeostasis [227-230]. PLTX is capable of binding the extracellular moiety of the pump, thus inducing the inhibition of the active transport of Na^+ and K^+ across the membrane. As a result, the pump is transformed

into a nonspecific monovalent cation channel which is permanently open, thus leading to a consistent ionic imbalance at cellular-level. The main consequences are: i) the increase of Ca^{2+} in the cytosol, which generally leads to cell death, and ii) the release of K^+ from different kind of cells. The latter induces the depolarization of a wide variety of tissues causing secondary pharmacological effects which include: violent contraction of skeletal, smooth and cardiac muscles, cardiovascular effects, hemolysis, release of prostaglandins and norepinephrine, platelet aggregation and inhibition of sperm motility [227-234]. PLTX exhibits toxicity to human through several routes of exposure, each of them characterized by different symptoms and signs [235-236]. The oral route, which is mainly attributable to the ingestion of contaminated seafood, is characterized by: bitter/metallic taste, vomiting, diarrhea, muscle cramps, abdominal pain, numbness of the extremities, bradycardia, difficulty and breathing [185]. In addition, the toxin has been associated to a toxic syndrome named clupeotoxism, a food-borne illness characteristic of the tropical and sub-tropical regions due to the consumption of contaminated clupeoid fish (e.g. sardines, herrings and anchovies) [237]. Beside this, fatal human poisoning have been reported worldwide [238-239]. Further exposure routes are also represented by dermal contact and inhalation of toxic marine aerosols which induce: erythema, dermatitis, fever, watery rhinorrhea, pharyngeal pain, cough, headache, and bronchoconstriction with dyspnea and conjunctivitis [235]. Moreover, the employment of mouse skin carcinogenesis model revealed that PLTX is a potent tumor promoter [240-241]. The acute toxicity of PLTX was examined by several routes of administration and through various animal models, thus showing evident differences. By way of example, the measured LD_{50} by intravenous injection was 0.045 and 0.089 µg/Kg in mice and rats, respectively. On the other hand, the IP injection of the toxin provided LD_{50} of 0.295 and 0.63 µg/Kg in mice and rats, respectively [242]. However, the oral toxicity of PLTX turned out to be much lower than that measured by parenteral administration since the intragastric administration gave $LD_{50} > 40$ and of 510 µg/Kg in rats and mice, respectively, whilst the administration by gavage did not lead mice to death at the dosage of 200 µg/Kg [243]. Although PLTX analogues showed slight structural differences compared to the parent compound, their toxicity was found to be quite different. OSTD was found to be 12.5-fold less toxic than PLTX through the cytotoxicity assay on P388 cells (2.5 pM versus 0.2 pM) and 26-fold less toxic by in vitro hemolysis assay (39.5 nM versus 1.5 nM) [204]. In addition the LD_{50} of OSTD by IP injection to mice was

64

measured at 5 μg/Kg [243]. The same trend was observed for 42-hydroxyPLTXs since preliminary cytotoxicity studies on skin HaCaT keratinocytes showed that the 50*R* and 50*S* diasteroisomers were 1 and 2 orders of magnitude, respectively, less potent than PLTX [244-247]. In addition, McTX-a exhibited the lowest toxicity by IP injection in mice since it gave a LD_{50} of 900 μg/Kg [243]. Among the OVTXs congeners, given the lacks of reference material and/or purified fractions, acute toxicological studies were performed only for OVTX-a, which provided a LD_{50} of 7 μg/Kg when administered intraperitoneally in mice [219]. However, given the high acute toxicity of PLTX and its analogues, which was measured through different in-vivo animal models, the significant differences in toxicity that emerged from the large number of reports suggest that toxicity assays still need to be adequately optimized [242]. A recent study published by Poli et al. [247] reported a detailed investigation into the toxic potential of PLTX, 42-hydroxyPLTXs, a mixture 50:50 of the latter, and OVTX-a by IP and aerosol administration in rats. The measured LD_{50} by IP injection revealed that: the mix 50:50 (0.92 μg/Kg) was the most toxic, followed by PLTX (1.81 μg/Kg), 42-hydroxyPLTXs (1.93 μg/Kg) and OVTX-a (3.26 μg/Kg). On the other hand, a noticeable higher toxicity was observed through the aerosol administration, with OVTX-a showing the highest toxicity (LD_{50} 0.031 μg/Kg), followed by PLTX (LD_{50} 0.041 μg/Kg), 42-hydroxyPLTXs (LD_{50} 0.045 μg/Kg) and the mix 50:50 (LD_{50} 0.063 μg/Kg). Overall, the measured acute inhalation toxicity was 15- to 195-fold higher than that obtained by IP injection. These data strongly suggested that the presence of PLTX and its analogues should be closely monitored not only in seafood, but also in the aquatic systems as the human exposure to toxic marine aerosols during recreational and/or working activities may also be more dangerous than the oral one.

To date, regulatory limits for PLTX and its analogues in seafood have not been established yet both in EU and in other regions of the world. The establishment of a statutory regulation still requires more efforts from the scientific community, since: i) the toxicological data are mainly limited to the acute toxicity of PLTX and few analogues, while chronic toxicological studies are lacking, ii) the development of effective and sensitive methods for detection of PLTXs in seafood are a prerequisite, as well as iii) the production of certified reference material (CRM) to conduct toxicological studies, validate analytical and biological methods within and between different laboratories, and to perform accurate quantitation of toxins in complex matrices. Nonetheless, the EFSA Panel on contaminants in the food chain (CONTAM) released in 2009 a provisional

guidance for PLTXs in seafood. Notably, taking into account an ARfD of 0.2 µg/Kg b.w. for the sum of PLTX and OSTD, for an adult of 60 Kg of b.w. a portion of 400 g of edible shellfish should not contain more than 12 µg of PLTX and OSTD, thus corresponding to a MPL of 30 µg eq. PLTXs/ Kg [185].

2.6 Cyanotoxins and cyanobacterial secondary metabolites

Cyanobacteria, also known as Cyanophyta or blue-green algae, are a huge group of photosynthetic prokaryotes including 2000 to 8000 different species [248]. Cyanobacteria have always attracted attention of the scientific community due to their unique abilities to produce bioactive compounds associated with complex metabolic pathways developed during their long history and evolution on earth (~3.5 billions of years) [249-250]. They have adapted to live in a variety of environments occupying different ecological niches; as a consequence, a high biodiversity has been observed through the description of aquatic (oceans, seas, hot spring water, fresh and brackish water), terrestrial (soils, deserts, glaciers) and symbiotic (plant, lichens and primitive animals) species [251]. It follows that cyanobacteria are characterized by extremely heterogeneous metabolic profiles, with a plethora of more than 2000 bioactive secondary cyano-metabolites that have been described so far [252-253]. Some cyanobacterial species, mainly aquatic, have demonstrated to be an effective source of newly bioactive molecules, some of which have been selected as lead compounds by pharmaceutical industry for their pharmacological properties such as antiviral and anticancer activities [254-255]. However, beside this, some cyanobacterial species are capable of producing toxic substances commonly known as cyanotoxins, whose occurrence in aquatic environment is a matter of concern for human and animal health since it has dramatic consequences on fishery, aquaculture and touristic industry worldwide [256-257].

The main criteria adopted to properly classify cyanotoxins lie in their: i) mechanism of toxicity on mammals – hepatotoxins (microcystin and nodularin), neurotoxins (anatoxins, paralytic shellfish toxins, BMAA), cytotoxins (cylindrospermopsins), dermatotoxins (lyngbyatoxins) and irritant toxins (lipopolysaccharides) -, and ii) structural features – linear and cyclic oligopeptides, alkaloids, nonproteinogenic amino acids and lipopolysaccharides [258].

2.6.1 Microcyststins and Nodularins

Microcystins (MCs) are a large family of cyanotoxins including more than 300 compounds as evidenced by hundreds of studies reported in literature since the 50's [252]. Their name derived from *Microcystis aeruginosa,* the cyanobacterium from which they were first isolated [259]. Although, freshwater cyanobacteria were found to be the main MC-producing organisms (e.g. *Anabaena, Aphanizomenon, Dolichospermum, Limnothrix, Microcystis, Nostoc, Phormidium,* and *Planktothrix*), also marine (*Geitlerinema, Leptolyngbya, Roseofilum*, and *Synecococcus*), terrestrial (e.g. *Nostoc*) and cyanobacteria-lichens symbiotic organisms (*Hapalosiphon hibernicus*) can contribute [260]. MCs are cyclic heptapeptides characterized by the presence of L-, D- and unconventional amino acids, with a high structural heterogeneity due to multiple substitutions and modifications that can involve all the amino acid residues [261]. Although a substantial chemodiversity was observed, an accurate evaluation conducted on the most substituted and conserved amino acids allowed to outline the following general structure: cyclo-(D-Ala^1-X^2-D-Masp^3-Z^4-Adda^5-D-ϒ-Glu^6-Mdha^7), were Mdha is N-methyl-dehydroalanine. L-amino acids X and Z at position 2 and 4, respectively, are the most variable, therefore their one-letter abbreviations play a key role in the naming system of such compounds (MC-XZ), while all the structural modifications involving the amino acids at positions 1,3,5,6 and 7 are separately reported in square brackets (**Fig.I.14**) [262].

Nodularins (NODs) are a smaller group of about 10 cyclic pentapeptides that are commonly associated to MCs due to their structural features and toxicity [263]. Their names originate from *Nodularia spumigena*, a saline and brackish cyanobacterium from which they were first identified. However, they were found also in benthic species such as *N. sphaerocarpa* [259]. The parent compound is NOD whose general structure is: Cyclo-(D-MeAsp^1-L-Arg^2-Adda^3-D-Glu^4-Mdhb^5), where Mdhb is 2-(methylamino)-2-dehydrobutyric acid [264] (**Fig.I.14**). Although only a limited number of structural variants have been reported so far, even NODs are characterized by structural heterogeneity, which results into variants such as: D-Asp^1, L-Val^2, L-Har^2, DMAdda^3, 6(*Z*)-Adda^3, MeAdda^3, Glu^4(OMe) and Dhb^5 *seco* derivative [260]. MCs and NODs are potent hepatotoxins that can cause internal hemorrhages and shock since they are able to inhibit the protein serine/threonine phosphatases 1 and 2A after entering into the hepatic cells through bile acids and membrane carriers [265]. Differently from NODs, MCs can also bind the molecular target through

a covalent bond. The β-amino acid Adda (3S-amino-9S-methoxy-2S,6,8S-trimethyl-10-phenyldeca-4E,6E-dienoic acid) is an unusual and characteristic residue which turned out to be crucial for the biological activity of MCs and NODs, in fact a loss of toxicity was recorded both for products of ozonolysis and for geometrical isomers (6Z) [266]. However, modifications of Adda residue at position 9 such as demethylation (desmethyl Adda; DMAdda) and acetylation (acetyl desmethyl Adda; ADMAdda;) do not affect the toxicological properties [267], whilst derivatives with esterified Glu residue, as well as *seco* analogues were found to be nontoxic [251].
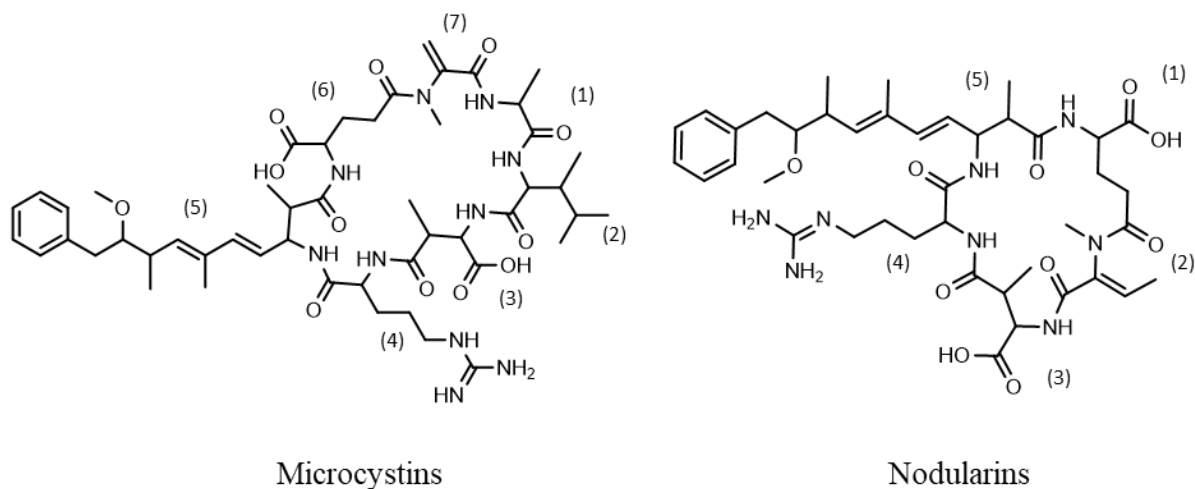
Figure I.14 Planar structure of MC-LR and NOD-R.

To date, toxicological studies have demonstrated that the most toxic variants among MCs and NODs are MC-LR and NOD-R, with LD_{50} values for both of 50 µg/Kg when intraperitoneally injected into mice [268]. On the other hand, a noteworthy decrease in potency was observed when MC-LR was administered orally to mice by gavage (LD_{50} 10.9 mg/Kg) [269]. In additions, MCs and NODs have been reported to be tumor promoters, endocrine disruptors and immunotoxicants [268-271]. To date, hepatotoxins are responsible for most of the poisoning events due to harmful cyanobacterial blooms, with MCs being the most frequently detected species. A recent review [272] described the cyanobacterium *Microcystis* as "cosmopolitan" since its presence has been practically highlighted worldwide with the exception of Antarctica. More in detail, *Microcystis* blooms were reported for 108 countries, among which 79 evidenced the occurrence of MCs.

2.6.2 Paralytic shellfish toxins

Paralytic shellfish toxins (PSTs) (**Fig.I.15**) are a complex and potent class of neurotoxins which has approximately 60 compounds described so far. They are also known as saxitoxins (STXs) in relation to the first analogue reported, called saxitoxin (STX), which was discovered in butter clams (*Saxidomus*) in the '50s [273]. PSTs are produced by marine dinoflagellates of the genera *Alexandrium, Gymnodinium* and *Pyrodinium* that naturally accumulate in filter feeding shellfish, as well as by freshwater cyanobacteria belonging to the genera *Anabaena*, *Aphanizomenon*, *Cylindrospermopsis*, *Lyngbya, Scytnema, Phormodium, Planktothrix and Raphisiopsis* [273-274]. PSTs are low molecular weight hydrophilic molecules with a common chemical core characterized by the presence of a tetrahydropurine ring containing 2 cyclic guanidine groups, which is fused to a tetrahydropyrrole moiety. The chemical diversity of this toxin class is due to multiple substitutions occurring at four site of the backbone structure, which can be hydroxyl, carbamoyl and sulfate groups. A first classification system is based on the nature of their side chain (R4) according to which PSTs can be classified into five different sub-groups: carbamoyl (R4 = – $OCONH_2$), N-sulfocarbamoyl (R4 = $-OCONHSO_3^-$), decarbamoyl (R4 = –OH), deoxydecarbamoyl (R4 = –H) and 4-hydroxybenzoate ester (R4 = $-OCOC_6H_4OH$) derivatives (**Fig.I.15**). On the other hand, taking into consideration the net charge state of the molecules, PSTs can be also categorized in neutral (0), mono-charged (+1) and bi-charged (+2) analogues according to the combination of different substituents with the characteristic chemical nucleus described before [275]. PSTs represent a serious threat to public health and aquaculture activities as they are responsible for a toxic syndrome commonly known as paralytic shellfish poisoning (PSP) [276]. The latter is due to the consumption of contaminated shellfish and it is mainly characterized by the rapid onset of neurological symptoms (15-30 min after the ingestion) that can also result in death [277-278]. Beside the risks associated with seafood consumption, another potential toxic exposure to humans is related to water-based recreational activities when harmful cyanobacteria are present in freshwater environment [273]. To date, this represents an emerging issue to face since a number of incidents describing the death of wildlife and domestic animals following the ingestion of contaminated freshwater resources have been reported [279]. In addition, the detection of PSTs in freshwater ecosystems from all continents except for Antarctica [280] makes this situation even more worrying. PSP syndrome is associated with the capacity of PSTs to be reversible blockers of

voltage-gated sensitive sodium channels (VSSCs) on nerve and muscle cells, leading so to an alteration and/or a block of the impulse conduction along the excitable cells [274, 281] which results into paralysis. To date, no antidotes have been developed yet to treat the PSP intoxication, and the artificial respiration until toxins are excreted from the body is the only palliative care adopted [282].

STX= saxitoxin
GTX= gonyautoxin
NEO= neosaxitoxin
GC= *G.catenatum* toxin
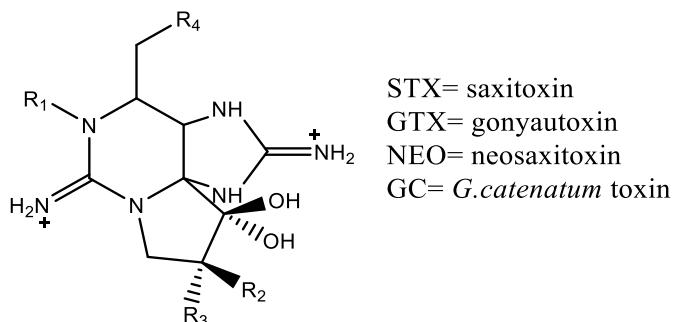
Name group	Toxin	R_1	R_2	R_3	R_4	Charge state	Molecular formula
C toxins	C1	H	H	OSO_3^-		0	$C_{10}H_{17}N_7O_{11}S_2$
	C2	H	OSO_3^-	H			$C_{10}H_{17}N_7O_{11}S_2$
	C3	OH	H	OSO_3^-			$C_{10}H_{17}N_7O_{12}S_2$
	C4	OH	OSO_3^-	H			$C_{10}H_{17}N_7O_{12}S_2$
GTXs	dcGTX2	H	H	OSO_3^-	OH	+1	$C_9H_{16}N_6O_7S$
	dcGTX3	H	OSO_3^-	H	OH		$C_9H_{16}N_6O_7S$
	dcGTX1	OH	H	OSO_3^-	OH		$C_9H_{16}N_6O_8S$
	dcGTX4	OH	OSO_3^-	H	OH		$C_9H_{16}N_6O_8S$
	GTX1	OH	H	OSO_3^-		+1	$C_{10}H_{17}N_7O_9S$
	GTX2	H	H	OSO_3^-			$C_{10}H_{17}N_7O_8S$
	GTX3	H	OSO_3^-	H			$C_{10}H_{17}N_7O_8S$
	GTX4	OH	OSO_3^-	H			$C_{10}H_{17}N_7O_9S$
	B1 (GTX5)	H	H	H		+1	$C_{10}H_{17}N_7O_7S$
	B2 (GTX5)	OH	H	H			$C_{10}H_{17}N_7O_8S$
STXs	STX	H	H	H		+2	$C_{10}H_{17}N_7O_4$
	NEO	OH	H	H			$C_{10}H_{17}N_7O_5$
	dcSTX	H	H	H	OH	+2	$C_9H_{16}N_6O_3$
	dcNEO	OH	H	H	OH		$C_{10}H_{16}N_6O_4$
	doSTX	H	H	H	H		$C_9H_{16}N_6O_2$
GC	GC1	H	OSO_3^-	H		+1	$C_{16}H_{20}N_6O_9S$
	GC2	H	H	OSO_3^-		+1	$C_{16}H_{20}N_6O_9S$
	GC3	H	H	H		+2	$C_{16}H_{20}N_6O_5$

Figure I.15. General chemical structure, substituents, charge state and molecular formula of selected PSTs.

Toxicological studies brought to the light that PST analogues are characterized by different toxicity as structural diversity affects the affinity with the biological target. The most toxic compound is STX, followed by Neosaxitoxin (NEO), gonyautoxins (GTXs), decarbamoyl derivatives (dcSTX, dcNEO, dcGTX1, -2, -3 and -4) and C toxins (C1, C2, C3 and C4) [283-284]. For this reason, EFSA has recommended to convert all the STX analogues found in seafood into STX equivalents (STX eq) through the toxicity equivalency factors (TEFs). As a results, a maximum permitted level of 800 µg STX eq/kg shellfish meat has been globally established [33] and, with the aim to protect consumer health, seafood products are regularly monitored through routine monitoring programs before reaching the market. In the last decades the reference method for detection of PSTs in shellfish has been the mouse bioassay (AOAC 959.08), but ethical matters and technical drawbacks prompted governmental organizations and monitoring laboratories to replace it with most advantageous alternatives. Currently, three AOAC official methods have been accepted for the analysis of PSTs: receptor binding assay (RBA; AOC 2011.27), pre-column oxidation (ox-LC-FLD; AOAC 2005.06) and post-column oxidation (LC-ox-FLD; AOAC 2011.02) coupled with fluorescence detection. However, since 1 January 2019, the method AOAC 2005.06 became the official reference method in the EU for determination of PSTs, replacing MBA.

2.6.3 Anatoxins

Anatoxins (ATXs) are a small group of cyanotoxins, chemically classified as alkaloids, that are produced by cyanobacteria belonging to the genera *Anabaena, Aphanizomenon, Cylindrospermopsis, Plankthotrix, Oscillatoria* and *Microcystis* [285]. The parent compound is ATX-a, which represents the first cyanobacterial toxin to be fully elucidated. ATX-a is a low-molecular weight compound (165 Da) with a tropane-related structure characterized by the presence of a secondary heterocyclic amine (**Fig.I.16**). Even though a number of structural variants has been reported so far, the simultaneous presence of ATX-a, homoanatoxin-a (HATX-a; propionyl derivative) and the nontoxic 4-OH-HATX-a was observed for *Raphidiopsis mediterranea Skuja*, a cyanobacterium isolated from Japan [286]. ATX-a and HATX-a are potent neurotoxins classified as postsynaptic cholinergic nicotinic agonists and neuromuscular blocking agents since they are able to irreversibly bind the acetylcholine receptors and are not degraded by acetylcholinesterase, causing so a rapid death by respiratory arrest (2-30 min) [287-288]. ATX-a (S), so called because of the salivation (S) induced in mice as poisoning symptom, has a completely

different structure from ATX-a, with a guanidine moiety embedded in a five-membered ring, which is linked to a tertiary ammine and a phosphate group (**Fig.I.16**). Therefore, ATX-a (S) can be classified as organophosphate compound; in fact, it binds the acetylcholinesterase causing increased amount of saliva, convulsion and death by respiratory arrest [289]. Several poisoning incidents due to cyanobacterial blooms containing ATX-producing species occurred in different countries (USA, Finland, Canada, Denmark, Scotland, Ireland, France, New Zeland) and the death of wild and domestic animals including dogs, birds, bats cows, calves, sows, pigs, fish and ducks has been documented [287].
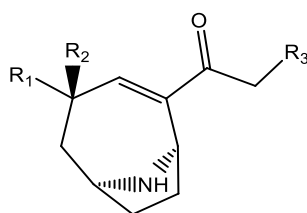
Analogue	R_1	R_2	R_3	Molecular formula
ATX-a	H	H	H	$C_{11}H_{15}NO$
HATX-a	H	H	CH_3	$C_{11}H_{17}NO$
4*R*-OH-HATX-a	H	OH	CH_3	$C_{11}H_{17}NO_2$
4*S*-OH-HATX-a	OH	H	CH_3	$C_{11}H_{17}NO_2$

ATX-a (S)

$C_{11}H_{17}N_4O_4P$
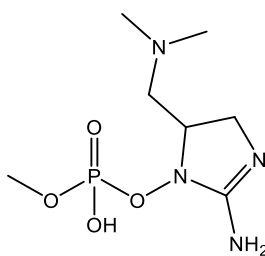
Figure I.16 General chemical structures, substituents and molecular formula of selected ATXs.

2.6.4 BMAA

BMAA is a nonprotein amino acid, β-N-methylamino-L-alanine (**Fig.I.17**), which was first detected in symbiotic cyanobacteria of *Nostoc* genus and then in a variety of cyanobacteria from freshwater, brackish and marine environments. Although BMAA is commonly known for its neurotoxicity, which is lower than that caused by neurotoxic alkaloids (STXs and ATXs), it has been suspected of playing a key role in neurodegenerative diseases in humans after accumulation through the food web [45, 290].

$C_4H_{10}N_2O_2$
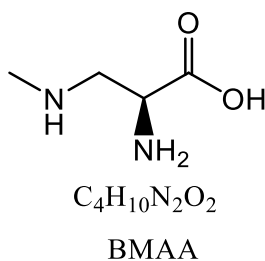
BMAA

Figure I.17 Chemical structure of β-N-methylamino-L-alanine (BMAA).

2.6.5 Cylindrospermopsins

Cilyndrispermopsins (CYNs) are low-molecular weight alkaloids produced by cyanobacteria belonging to the genera *Cylindrospermopsis, Aphanizomenon, Umezakia, Raphidiopsis* and *Anabaena* [291]. The parent compound is CYN, which features a cyclic guanidine moiety embedded in a tricyclic fused ring system which is linked to sulfate and uracil moieties (**Fig.I.18**). It was demonstrated that the guanidine and the uracil groups are essential for toxicological activity [292]. CYN is classified as cytotoxic, hepatotoxic and genotoxic compound since it is a protein synthesis inhibitor capable of damaging different organs such as kidney, spleen, intestine, thymus and heart by inducing oxidative stress in cells [289, 293]. Contrarily to neurotoxic alkaloids, CYN can lead to death very slowly as the death of mice was observed after 5-6 days after the injection of the toxin [258]. It was detected at very high levels during the outbreak of *Cylindrospermopsis* bloom in Australia, where it has caused the death of wild animals [294].
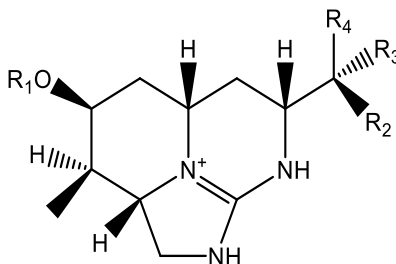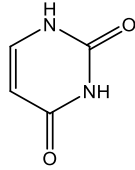
Analogue	R₁	R₂	R₃	R₄	Molecular formula
CYN	SO_3^-	H	OH		$C_{15}H_{21}N_5O_7S$
7-*epi*CYN	SO_3^-	OH	H		$C_{15}H_{21}N_5O_7S$
7-deoxy-CYN	SO_3^-	H	H		$C_{15}H_{21}N_5O_6S$
7-deoxy-desulfo-CYN	H	H	H		$C_{15}H_{21}N_5O_3$
7-deoxy-desulfo-12-acetylCYN	$COCH_3$	H	H		$C_{17}H_{23}N_5O_4$

Figure I.18 General chemical structures, substituents and molecular formula of selected CYNs.

2.6.6 Lyngbyatoxins and lyngbyawolleytoxins

Lynbyatoxins are a small group of toxins produced by cyanobacterial species of genus *Lyngbya* such as *L. wolley* and *L. majuscula* which are a fresh water and a marine species, respectively [295]. They are classified as alkaloids but a further subclassification on the basis of their structural and toxicological properties is required. The toxic compounds produced by *L. wolley* spp. are called lyngbyawolleytoxins (LWTXs) (**Fig.I.19**). They are commonly associated with STXs since they share the same backbone structure, as well as they are produced by the same cyanobacterial specie. For this reason, LWTXs are classified as neurotoxins. To date, only six analogues have been reported (LWTX1-6) [296].

On the other hand, lyngbyatoxins (L) isolated from the benthic *L. majuscula* are alkaloids featuring a 9-membered amide macrocycle containing an indole moiety linked to an alkyl chain (**Fig.I.20**). Three different analogues have been reported so far, namely lyngbyatoxin A (LA), LB and LC [297]. However, *L. majuscula* was found to produce other structurally different toxic compounds such as aplysiatoxin (AT) and debromoaplysiatoxin (DAT) (**Fig.I.20**), which cause common toxic effect on humans [45]. In addition, AT and DAT are also produced by other cyanobacterial species belonging to the genera *Schizothrix* and *Planktothrix*. LA, AT and DAT are mainly classified as dermatotoxins since several episodes of dermatitis occurred to swimmers when they come into contact with the harmful *L. majuscule* during massive algal blooms. Beside dermatotoxicity, LA,
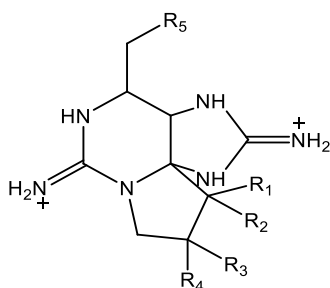
LWTX= lyngbyawolleytoxin

Toxin	R_1	R_2	R_3	R_4	R_5	Molecular formula
LWTX1	OH	H	OSO_3^-	H	$OCOCH_3$	$C_{11}H_{18}N_6O_7S$
LWTX2	OH	OH	H	OSO_3^-	$OCOCH_3$	$C_{11}H_{18}N_6O_8S$
LWTX3	OH	OH	OSO_3^-	H	$OCOCH_3$	$C_{11}H_{18}N_6O_8S$
LWTX4	H	OH	H	H	OH	$C_9H_{17}N_6O_2$
LWTX5	OH	OH	H	H	$OCOCH_3$	$C_{11}H_{19}N_6O_4$
LWTX6	H	OH	H	H	$OCOCH_3$	$C_{11}H_{19}N_6O_3$

Figure I.19 General chemical structures, substituents and molecular formula of LWTXs.

lyngbyatoxin A
$C_{28}H_{41}N_3O_2$

lyngbyatoxin B
$C_{28}H_{41}N_3O_3$

lyngbyatoxin C
$C_{28}H_{41}N_3O_3$

R_1= Br; aplysyatoxin;　　$C_{32}H_{47}O_{10}Br$
R_1= H; debromoaplysiatoxin; $C_{32}H_{48}O_{10}$
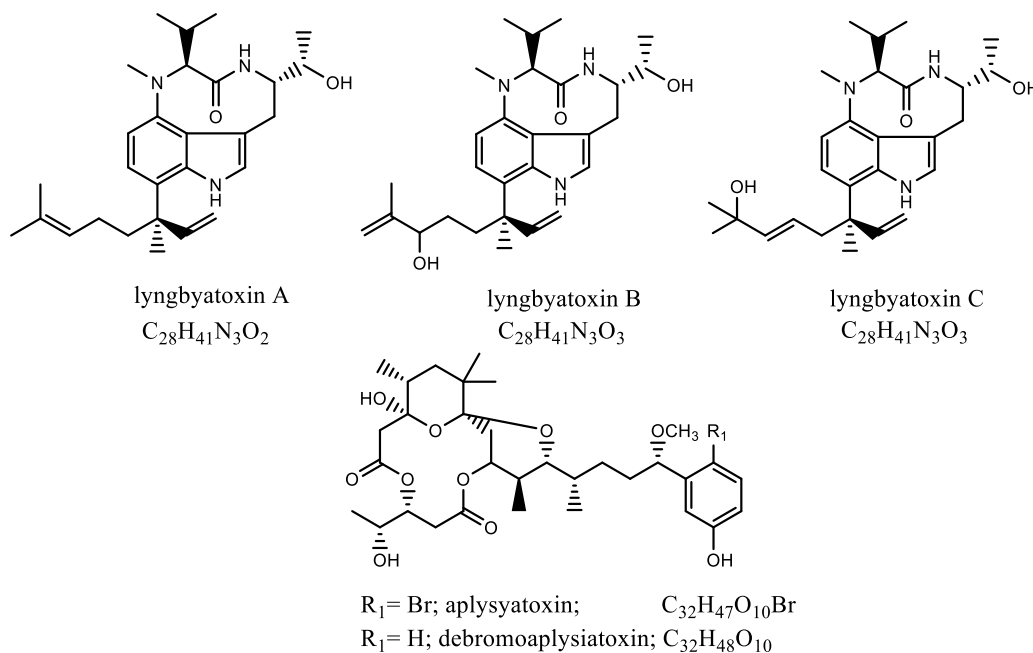
Figure I.20 Chemical structure and molecular formula of selected toxins produced by *L. majuscula*.

AT and DAT are also potent tumor promoters and cytotoxic agents since they can induce a variety of diseases such as: respiratory problem, eye infection and intestinal hemorrhaging [298].

2.6.7 Lipopolysaccharide

Lipopolysaccharide (LPS) is a component of the cell wall of the Gram negative bacteria and cyanobacteria. Cyanobacterial LPS slightly differs from that of Gram negative bacteria and it has been reported to cause a variety of pathological effects when human come into direct contact with it, including gastrointestinal and respiratory diseases, inflammation fever and eye disorders [299]. However, cyanobacterial LPS can be considered less toxic than that of other gram negative bacteria [300].

2.6.8 Microginins, anabaenopeptins and cyanopeptoline-type peptides.

Microginins (MGs) are an interesting class of cyanobacterial secondary metabolites with about 100 congeners reported so far and recognized also as oscillaginins, cyanostatins and nostoginins on the basis of the producing organism [301]. MGs are linear peptide containing three to six amino acids, some of them as N-methylated residues and/or as homo variants (**Fig.I.21**) [302]. A structural motif was found: one or more Tyr or its homo or methylated derivative are present at the C-terminus, while the N-terminus is characterized by the unconventional 3-amino-2-hydroxy-decanoic acid (Ahda) [303]. The chemovariabilty recorded within this toxin class is related to multiple amino acid substitutions along the entire peptide chain [301].

Anabaenopetins (APs) are about 100 compounds produced by freshwater, marine and terrestrial cyanobacteria, including secondary metabolites from symbiosis with marine sponges. Depending on the relevant producing organism and/or the site where they have been discovered, APs have been named also as oscillamides, nodulapeptins, ferintoic acids, lyngbyaureidamides, pompanopeptin, kermamides, konbamide, mozamide, brunsvicamides and schizopeptin (252, 304]. Anabaenopetins (APs) are cyclic hexapeptides exhibiting a cyclic moiety composed of five amino acids with a Lys connected to an exocyclic residue in position 1 through an ureido bond **Fig.I.21**. A common structural motif, excluding few exceptions, was recognized across all the congeners: a D-Lys residue in position 2, the ureido linkage between residues in position 1 and 2, homo amino acids in position 4 and N-methyl amino acids in position 5. All the other positions

are variable, ending up in a large structural diversity with a number of different analogues exhibiting masses between 750 and 950 Da. Their general chemical structure can be summarized as follows: X^1-CO-[Lys^2-X^3-X^4-MeX^5-X^6] [305-306].
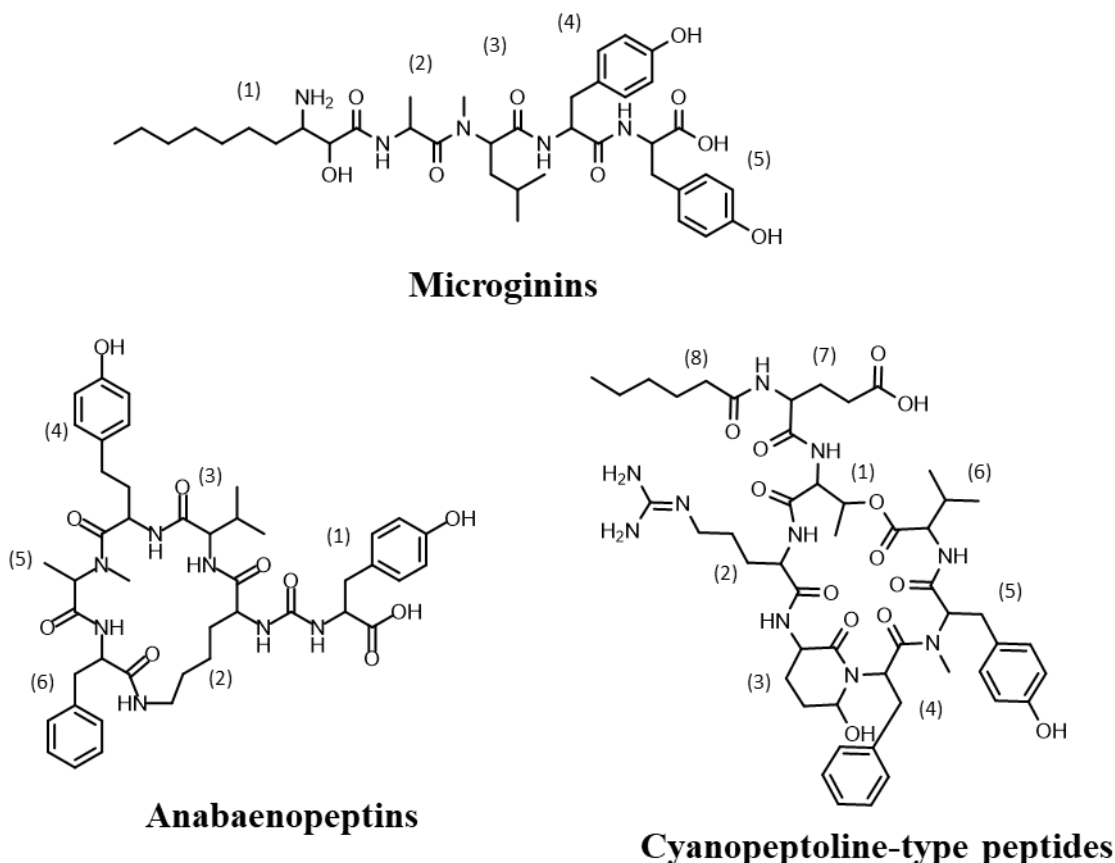
Figure I.21 Planar structures of representative cyanobacterial bioactive metabolites; microginin FR1, anabaenopeptin A, cyanopeptoline 1020.

Cyanopeptoline-type peptides (CPtps) are cyclic depsipeptides representing one of the largest family of cyanotoxins that includes more than 200 compounds hitherto reported [252]. The naming system is related to the producing cyanobacteria, so they are classified into different sub-groups: CPs, micropeptins, aeruginopeptins, microcystilide, nostopeptins, nostocyclins, oscillapeptins and somamides [307]. The common structural element is represented by the atypical non proteinaceous amino acid 3-amino-6-hydroxy-2-piperidone (Ahp) in position 3, or its methylated variant found only in few congeners, which is part of a six amino-acid membered cycle formed through the esterification of the OH group of the N-terminal Thr in position 1 (or hydroxy-methyl proline in few compounds) with the C-terminus of amino acid in position 6 (Val/Leu/Ile) **Fig.I.21**. Moreover,

the amine group of the residue in position 1 is linked to an exocyclic sidechain composed of a maximum of three residues including: amino acids and/or aliphatic fatty acid or gliceric acid or hydroxyphenyl lactic acid. Position 2 is subjected to most substitutions, thus contributing massively to the widespread structural diversity observed within this family. Position 4 can be occupied by Leu/Ile, Phe or Thr, while in position 5, N-methylated aromatic amino acids (Tyr, Phe, Trp) or they homo-variants (Htyr) or halogenated and/or methylated derivatives (Cl-/Br-MeTyr or Cl-/Br-Tyr) or kynurenine are presents [308-310].

2.6.9 Regulation and guidelines

Currently, cyanotoxins are not monitored on a regular basis in most of the countries [311]. Even though a statutory regulation is becoming a prerequisite worldwide, critical issues make this achievement an hard challenge for several reasons. An accurate health risk assessment is strictly related to different parameters such as: distribution of toxins, routes of exposure, and the study of their toxicological properties [312]. Cyanotoxins have been detected worldwide in a variety of different environmental and food samples such as fresh and salt waters, fish, shellfish and algal dietary supplements [45]. The most likely source of exposure is certainly the consumption of contaminated drinking water, that can be mainly due to the consumption of water produced using surface water as source. However, unintentional swallowing of water during recreational activities, especially in lakes and rivers, can contribute to the oral exposure [313], as well as the consumption of contaminated foods [314]. On the other hand, the inhalation of toxic aerosol and the skin contact during massive cyanobacterial blooms are routes of great concern [315]. In this context, toxicological data are often limited to few analogues for each sub-group, and a combined toxicity due to the co-occurrence of different cyanotoxins should be taken into consideration for a correct risk evaluation [316]. Moreover, the development of validated analytical methods for an accurate determination of toxins in different matrices, as well as effective extraction and clean-up methods with high yield of recovery, are prerequisites.

On the basis of the available data, the World Health Organizations (WHO) has recently released provisional guidelines for MC-LR, CYN, ATX-a and STXs for chronic and short term exposure to drinking- water, and for exposure to recreational-water (**Table I.3**) [317-320]. Although a number of countries have adopted this guidance, some other did not set alert values for any cyanotoxins in drinking and/or recreational water. Currently, Canada has been the only country to

establish a maximum permitted level of 1.5 µg/L for MC-LR in drinking-water. In other countries instead, a toxicity equivalent factor has been adopted and the sum of all the MC variants must be within 1-10 µg/L. Provisional maximum allowed levels for other cyanotoxins (ATXs, CYNs, STXs) have been released in a limited number of countries, with a high diversity observed among the US, where specific guideline levels have been suggested also for domestic animals (cats and dogs). More recently, US National Centre for Environmental Assessment suggested a stricter maximum permitted level for MC-LR in drinking water of 0.1 µg/L [321]. On the other hand, although regulations and/or recommendations for cyanotoxins in drinking and recreational waters were released in most of the countries, no maximum level has been suggested for cyanotoxins in food. In this frame, before releasing recommendations and/or establishing regulations, health institutes and governmental agencies required more data on distribution of cyanotoxins in food, detailed acute and chronic toxicity studies as well as the implementation of robust extraction procedures of toxins from complex matrices associated with the development of effective and sensitive analytical detection methods [45].

Table I.3 Provisional guideline values released by WHO in 2020 for cyanotoxins in drinking and recreational-water.

Toxin	GVc	GVs	GVr
MC-LR	1 µg/L	12 µg/L	24 µg/L
CYN	0.7 µg/L	3 µg/L	6 µg/L
ATX-a	-	30 µg/L	60 µg/L
STXs	-	3 µg/L	30 µg/L

GVc= guideline value for chronic exposure to drinking water; GVs= guideline value for short-term exposure to drinking water; GVr= guideline value for recreational exposure; - = no guideline value released.

References

1.   European Food Safety Authority. (2010). EFSA Report on Data Collection: Future Directions. *EFSA Journal*, *8*(5), 1533.

2.   Stivala, C. E., Benoit, E., Araoz, R., Servent, D., Novikov, A., Molgó, J., & Zakarian, A. (2015). Synthesis and biology of cyclic imine toxins, an emerging class of potent, globally distributed marine toxins. *Natural product reports*, *32*(3), 411-435.

3.   Molgó, J., Marchot, P., Aráoz, R., Benoit, E., Iorga, B. I., Zakarian, A., ... & Servent, D. (2017). Cyclic imine toxins from dinoflagellates: A growing family of potent antagonists of the nicotinic acetylcholine receptors. *Journal of neurochemistry*, *142*, 41-51.

4.   Hellyer, S. D., Selwood, A. I., Rhodes, L., & Kerr, D. S. (2011). Marine algal pinnatoxins E and F cause neuromuscular block in an in vitro hemidiaphragm preparation. *Toxicon*, *58*(8), 693-699.

5.   Selwood, A. I., Wilkins, A. L., Munday, R., Shi, F., Rhodes, L. L., & Holland, P. T. (2013). Portimine: A bioactive metabolite from the benthic dinoflagellate Vulcanodinium rugosum. *Tetrahedron Letters*, *54*(35), 4705-4707.

6.   Otero, A., Chapela, M. J., Atanassova, M., Vieites, J. M., & Cabado, A. G. (2011). Cyclic imines: Chemistry and mechanism of action: A review. *Chemical Research in Toxicology*, *24*(11), 1817-1829.

7.   O'Connor, P. D., & Brimble, M. A. (2007). Synthesis of macrocyclic shellfish toxins containing spiroimine moieties. *Natural product reports*, *24*(4), 869-885.

8.   Ji, Y., Che, Y., Wright, E. J., McCarron, P., Hess, P., & Li, A. (2020). Fatty acid ester metabolites of gymnodimine in shellfish collected from China and in mussels (Mytilus galloprovincialis) exposed to Karenia selliformis. *Harmful algae*, *92*, 101774.

9.   Rambla-Alegre, M., Miles, C. O., de la Iglesia, P., Fernandez-Tejedor, M., Jacobs, S., Sioen, I., ... & Diogene, J. (2018). Occurrence of cyclic imines in European commercial seafood and consumers risk assessment. *Environmental research*, *161*, 392-398.

10.   Uemura, D., Chou, T., Haino, T., Nagatsu, A., Fukuzawa, S., Zheng, S. Z., & Chen, H. S. (1995). Pinnatoxin A: a toxic amphoteric macrocycle from the Okinawan bivalve Pinna muricata. *Journal of the American Chemical Society*, *117*(3), 1155-1156.

11.   Chou, T., Osamu, K., & Uemura, D. (1996). Relative stereochemistry of pinnatoxin A, a potent shellfish poison from Pinna muricata. *Tetrahedron letters*, *37*(23), 4023-4026.

12.   Aráoz, R., Barnes, P., Séchet, V., Delepierre, M., Zinn-Justin, S., Molgó, J., ... & Servent, D. (2020). Cyclic imine toxins survey in coastal european shellfish samples: Bioaccumulation and mode of action of 28-O-palmitoyl ester of pinnatoxin-G. first report of portimine-A bioaccumulation. *Harmful Algae*, *98*, 101887.

13.   Araoz, R., Servent, D., Molgó, J., Iorga, B. I., Fruchart-Gaillard, C., Benoit, E., ... & Zakarian, A. (2011). Total synthesis of pinnatoxins A and G and revision of the mode of action of pinnatoxin A. *Journal of the American Chemical Society*, *133*(27), 10499-10511.

14.   Alonso, E., Otero, P., Vale, C., Alfonso, A., Antelo, A., Giménez-Llort, L., ... & M Botana, L. (2013). Benefit of 13-desmethyl spirolide C treatment in triple transgenic mouse model of Alzheimer disease: beta-amyloid and neuronal markers improvement. *Current Alzheimer Research*, *10*(3), 279-289.

15.   Vincent, A. (2002). Unravelling the pathogenesis of myasthenia gravis. *Nature Reviews Immunology*, *2*(10), 797-804.

16.   EFSA Panel on Contaminants in the Food Chain (CONTAM). (2010). Scientific Opinion on marine biotoxins in shellfish–Cyclic imines (spirolides, gymnodimines, pinnatoxins and pteriatoxins). *EFSA Journal*, *8*(6), 1628.

17.   Zheng, S. Z., Huang, F. L., Chen, S. C., Tan, X. F., Zuo, J. B., 822 Peng, J., and Xie, R. W. (1990). The isolation and bioactivities of pinnatoxin (in Chinese). Chinese J. Marine Drugs 33, 33–35.

18.   Davidson, K., Baker, C., Higgins, C., Higman, W., Swan, S., Veszelovszki, A., & Turner, A. D. (2015). Potential threats posed by new or emerging marine biotoxins in UK waters and examination of detection methodologies used for their control: Cyclic imines. *Marine drugs*, *13*(12), 7087-7112.

19.   Miles, C. O., Rundberget, T., Sandvik, M., Aasen, J. A., & Selwood, A. I. (2010). The presence of pinnatoxins in Norwegian mussels. *National Veterinary Institute*, 10.

20.   McCarron, P., Rourke, W. A., Hardstaff, W., Pooley, B., & Quilliam, M. A. (2012). Identification of pinnatoxins and discovery of their fatty acid ester metabolites in mussels (Mytilus edulis) from eastern Canada. *Journal of agricultural and food chemistry*, *60*(6), 1437-1446.

21.   Beaumont, S., Ilardi, E. A., Tappin, N. D., & Zakarian, A. (2010). Marine toxins with spiroimine rings: Total synthesis of pinnatoxin A. *European journal of organic chemistry*, *2010*(30), 5743.

22.   Selwood, A. I., Miles, C. O., Wilkins, A. L., van Ginkel, R., Munday, R., Rise, F., & McNabb, P. (2010). Isolation, structural determination and acute toxicity of pinnatoxins E, F and G. *Journal of agricultural and food chemistry*, *58*(10), 6532-6542.

23.   Selwood, A. I., Wilkins, A. L., Munday, R., Gu, H., Smith, K. F., Rhodes, L. L., & Rise, F. (2014). Pinnatoxin H: a new pinnatoxin analogue from a South China Sea Vulcanodinium rugosum isolate. *Tetrahedron Letters*, *55*(40), 5508-5510.

24.   Doucet, E., Ross, N. N., & Quilliam, M. A. (2007). Enzymatic hydrolysis of esterified diarrhetic shellfish poisoning toxins and pectenotoxins. *Analytical and bioanalytical chemistry*, *389*(1), 335-342.

25.   Aasen, J. A., Hardstaff, W., Aune, T., & Quilliam, M. A. (2006). Discovery of fatty acid ester metabolites of spirolide toxins in mussels from Norway using liquid chromatography/tandem mass spectrometry. *Rapid Communications in Mass Spectrometry: An International Journal Devoted to the Rapid Dissemination of Up-to-the-Minute Research in Mass Spectrometry*, *20*(10), 1531-1537.

26.   De la Iglesia, P., McCarron, P., Diogène, J., & Quilliam, M. A. (2013). Discovery of gymnodimine fatty acid ester metabolites in shellfish using liquid chromatography/mass spectrometry. *Rapid Communications in Mass Spectrometry*, *27*(5), 643-653.

27.   Arnich, N., Abadie, E., Delcourt, N., Fessard, V., Fremy, J. M., Hort, V., ... & Mattei, C. (2020). Health risk assessment related to pinnatoxins in French shellfish. *Toxicon*, *180*, 1-10.

28.   Takada, N., Umemura, N., Suenaga, K., Chou, T., Nagatsu, A., Haino, T., ... & Uemura, D. (2001). Pinnatoxins B and C, the most toxic components in the pinnatoxin series from the Okinawan bivalve Pinna muricata. *Tetrahedron Letters*, *42*(20), 3491-3494.

29.   Kuramoto, M., Arimoto, H., & Uemura, D. (2004). Bioactive alkaloids from the sea: a review. *Marine Drugs*, *2*(1), 39-54.

30.   Munday, R., Selwood, A. I., & Rhodes, L. (2012). Acute toxicity of pinnatoxins E, F and G to mice. *Toxicon*, *60*(6), 995-999.

31.   Sosa, S., Pelin, M., Cavion, F., Hervé, F., Hess, P., & Tubaro, A. (2020). Acute oral toxicity of pinnatoxin G in mice. *Toxins*, *12*(2), 87.

32.   Takada, N., Umemura, N., Suenaga, K., & Uemura, D. (2001). Structural determination of pteriatoxins A, B and C, extremely potent toxins from the bivalve Pteria penguin. *Tetrahedron Letters*, *42*(20), 3495-3497.

33.   Fribley, A. M., Xi, Y., Makris, C., Alves-de-Souza, C., York, R., Tomas, C., ... & Strangman, W. K. (2018). Identification of portimine B, a new cell permeable spiroimine that

induces apoptosis in oral squamous cell carcinoma. *ACS medicinal chemistry letters*, *10*(2), 175-179.

34.   Hermawan, I., Higa, M., Hutabarat, P. U. B., Fujiwara, T., Akiyama, K., Kanamoto, A., ... & Tanaka, J. (2019). Kabirimine, a new cyclic imine from an Okinawan dinoflagellate. *Marine drugs*, *17*(6), 353.

35.   Cuddihy, S. L., Drake, S., Harwood, D. T., Selwood, A. I., McNabb, P. S., & Hampton, M. B. (2016). The marine cytotoxin portimine is a potent and selective inducer of apoptosis. *Apoptosis*, *21*(12), 1447-1452.

36.   Brooke, D. G., Cervin, G., Champeau, O., Harwood, D. T., Pavia, H., Selwood, A. I., ... & Cahill, P. L. (2018). Antifouling activity of portimine, select semisynthetic analogues, and other microalga-derived spirocyclic imines. *Biofouling*, *34*(8), 950-961.

37.   Van de Waal, D. B., Tillmann, U., Martens, H., Krock, B., van Scheppingen, Y., & John, U. (2015). Characterization of multiple isolates from an *Alexandrium ostenfeldii* bloom in The Netherlands. *Harmful Algae*, *49*, 94-104.

38.   Nieva, J. A., Tebben, J., Tillmann, U., Wohlrab, S., & Krock, B. (2020). Mass Spectrometry-Based Characterization of New Spirolides from Alexandrium ostenfeldii (Dinophyceae). *Marine drugs*, *18*(10), 505.

39.   Hu, T., Curtis, J. M., Walter, J. A., & Wright, J. L. (1996). Characterization of biologically inactive spirolides E and F: Identification of the spirolide pharmacophore. *Tetrahedron Letters*, *37*(43), 7671-7674.

40.   Roach, J. S., LeBlanc, P., Lewis, N. I., Munday, R., Quilliam, M. A., & MacKinnon, S. L. (2009). Characterization of a dispiroketal spirolide subclass from Alexandrium ostenfeldii. *Journal of natural products*, *72*(7), 1237-1240.

41.   White, J. D., Quaranta, L., & Wang, G. (2007). Studies on the Synthesis of (−)-Gymnodimine. Subunit Synthesis and Coupling. *The Journal of organic chemistry*, *72*(5), 1717-1728.

42.   Bourne, Y., Radić, Z., Aráoz, R., Talley, T. T., Benoit, E., Servent, D., ... & Marchot, P. (2010). Structural determinants in phycotoxins and AChBP conferring high affinity binding and nicotinic AChR antagonism. *Proceedings of the National Academy of Sciences*, *107*(13), 6076-6081.

43.	Hansen, S. B., Sulzenbacher, G., Huxford, T., Marchot, P., Bourne, Y., & Taylor, P. (2006). Structural characterization of agonist and antagonist-bound acetylcholine-binding protein from Aplysia californica. *Journal of Molecular Neuroscience*, *30*(1-2), 101.

44.	Gill, S., Murphy, M., Clausen, J., Richard, D., Quilliam, M., MacKinnon, S., ... & Pulido, O. (2003). Neural injury biomarkers of novel shellfish toxins, spirolides: a pilot study using immunochemical and transcriptional analysis. *Neurotoxicology*, *24*(4-5), 593-604.

45.	Wandscheer, C. B., Vilarino, N., Espina, B., Louzao, M. C., & Botana, L. M. (2010). Human muscarinic acetylcholine receptors are a target of the marine toxin 13-desmethyl C spirolide. *Chemical research in toxicology*, *23*(11), 1753-1761.

46.	Munday, R., Quilliam, M. A., LeBlanc, P., Lewis, N., Gallant, P., Sperker, S. A., ... & MacKinnon, S. L. (2012). Investigations into the toxicology of spirolides, a group of marine phycotoxins. *Toxins*, *4*(1), 1-14.

47.	Molgó, J., Benoit, E., Aráoz, R., Zakarian, A., & Iorga, B. (2016). Spirolides and cyclic imines: toxicological profile.

48.	Krock, B., Pitcher, G. C., Ntuli, J., & Cembella, A. D. (2009). Confirmed identification of gymnodimine in oysters from the west coast of South Africa by liquid chromatography–tandem mass spectrometry. *African Journal of Marine Science*, *31*(1), 113-118.

49.	Stewart, M., Blunt, J. W., Munro, M. H., Robinson, W. T., & Hannah, D. J. (1997). The absolute stereochemistry of the New Zealand shellfish toxin gymnodimine. *Tetrahedron Letters*, *38*(27), 4889-4890.

50.	Miles, C. O., Wilkins, A. L., Stirling, D. J., & MacKenzie, A. L. (2000). New analogue of gymnodimine from a Gymnodinium species. *Journal of agricultural and food chemistry*, *48*(4), 1373-1376.

51.	Miles, C. O., Wilkins, A. L., Stirling, D. J., & MacKenzie, A. L. (2003). Gymnodimine C, an isomer of gymnodimine B, from Karenia selliformis. *Journal of agricultural and food chemistry*, *51*(16), 4838-4840.

52.	Van Wagoner, R. M., Misner, I., Tomas, C. R., & Wright, J. L. (2011). Occurrence of 12-methylgymnodimine in a spirolide-producing dinoflagellate *Alexandrium peruvianum* and the biogenetic implications. *Tetrahedron Letters*, *52*(33), 4243-4246.

53.	Strangman, W., Anttila, M., Tomas, C., & Wright, J. L. (2016). (5S)-5-[(4aR, 8aS, 9E, 11S, 13R, 14S, 16R, 17R, 19S)-11, 19-Dihydroxy-8, 10, 13, 16-tetramethyl-18-methylidene-3, 4, 5, 6,

8a, 11, 12, 13, 14, 15, 16, 17, 18, 19, 20, 21-hexadecahydro-2H-14, 17-epoxybenzo [2, 3] cyclohexadeca [1, 2-b] pyridine-7-yl]-3-methylfuran-2 (5H)-one (12-Methylgymnodimine B). *Molbank*, *2016*(2), M896.

54. Harju, K., Koskela, H., Kremp, A., Suikkanen, S., de la Iglesia, P., Miles, C. O., ... & Vanninen, P. (2016). Identification of gymnodimine D and presence of gymnodimine variants in the dinoflagellate Alexandrium ostenfeldii from the Baltic Sea. *Toxicon*, *112*, 68-76.

55. Zurhelle, C., Nieva, J., Tillmann, U., Harder, T., Krock, B., & Tebben, J. (2018). Identification of novel gymnodimines and spirolides from the marine dinoflagellate Alexandrium ostenfeldii. *Marine drugs*, *16*(11), 446.

56. Salgado, P., Riobó, P., Rodríguez, F., Franco, J. M., & Bravo, I. (2015). Differences in the toxin profiles of Alexandrium ostenfeldii (Dinophyceae) strains isolated from different geographic origins: Evidence of paralytic toxin, spirolide, and gymnodimine. *Toxicon*, *103*, 85-98.

57. Dragunow, M., Trzoss, M., Brimble, M. A., Cameron, R., Beuzenberg, V., Holland, P., & Mountfort, D. (2005). Investigations into the cellular actions of the shellfish toxin gymnodimine and analogues. *Environmental Toxicology and Pharmacology*, *20*(2), 305-312.

58. Torigoe, K., Murata, M., Yasumoto, T., & Iwashita, T. (1988). Prorocentrolide, a toxic nitrogenous macrocycle from a marine dinoflagellate, Prorocentrum lima. *Journal of the American Chemical Society*, *110*(23), 7876-7877.

59. Lee, S. M., Kim, N. H., Jeong, E. J., & Rho, J. R. (2020). Cytotoxic 4-hydroxyprorocentrolide and prorocentrolide C from cultured Dinoflagellate Prorocentrum lima induce human cancer cell death through apoptosis and cell cycle arrest. *Toxins*, *12*(5), 304

60. Amar, M., Aráoz, R., Iorga, B. I., Yasumoto, T., Servent, D., & Molgó, J. (2018). Prorocentrolide-A from cultured Prorocentrum lima dinoflagellates collected in Japan blocks sub-types of nicotinic acetylcholine receptors. *Toxins*, *10*(3), 97.

61. Murakami, Y.; Oshima, Y.; Yasumoto, T. Identification of okadaic acid as a toxic component of a marine dinoflagellate Prorocentrum lima. Nippon Suisan Gakkaishi 1982, 48, 69–72.

62. Yasumoto, T. (1989). Polyether toxins produced by dinoflagellates. *Mycotoxins and phycotoxins' 88*, 375-382.

63. Quilliam, M. A., & Ross, N. W. (1996). Analysis of Diarrhetic Shellfish Poisoning Toxins and Metabolites in Plankton and Shellfish by Ion-Spray Liquid Chromatography- Mass

Spectrometry. In Biological and Biotechnological Applications of Electrospray Ionization Mass Spectrometry; Snyder, A.P., Ed.; American Chemical Society: Washington, DC, USA, 1996; pp. 351–364.

64.   Lee, T. C. H., Fong, F. L. Y., Ho, K. C., & Lee, F. W. F. (2016). The mechanism of diarrhetic shellfish poisoning toxin production in Prorocentrum spp.: physiological and molecular perspectives. *Toxins*, *8*(10), 272.

65.   Hu, T., DeFreitas, A. S., Curtis, J. M., Oshima, Y., Walter, J. A., & Wright, J. L. (1996). Isolation and structure of prorocentrolide B, a fast-acting toxin from Prorocentrum maculosum. *Journal of natural products*, *59*(11), 1010-1014.

66.   Nascimento, S. M., Mendes, M. C. Q., Menezes, M., Rodríguez, F., Alves-de-Souza, C., Branco, S., ... & Fraga, S. (2017). Morphology and phylogeny of Prorocentrum caipirignum sp. nov.(Dinophyceae), a new tropical toxic benthic dinoflagellate. *Harmful Algae*, *70*, 73-89.

67.   Lee, S., Yang, A. R., Yoo, Y. D., Jeong, E. J., & Rho, J. R. (2019). Relative Configurational Assignment of 4-Hydroxyprorocentrolide and Prorocentrolide C Isolated from a Benthic Dinoflagellate (Prorocentrum lima). *Journal of natural products*, *82*(4), 1034-1039.

68.   Lu, C. K., Lee, G. H., Huang, R., & Chou, H. N. (2001). Spiro-prorocentrimine, a novel macrocyclic lactone from a benthic Prorocentrum sp. of Taiwan. *Tetrahedron Letters*, *42*(9), 1713-1716.

69.   Kita, M., Ohishi, N., Washida, K., Kondo, M., Koyama, T., Yamada, K., & Uemura, D. (2005). Symbioimine and neosymbioimine, amphoteric iminium metabolites from the symbiotic marine dinoflagellate Symbiodinium sp. *Bioorganic & medicinal chemistry*, *13*(17), 5253-5258.

70.   Bane, V., Lehane, M., Dikshit, M., O'Riordan, A., & Furey, A. (2014). Tetrodotoxin: Chemistry, toxicity, source, distribution and detection. *Toxins*, *6*(2), 693-755.

71.   Simidu, U., Kita-Tsukamoto, K. U. M. I. K. O., Yasumoto, T., & Yotsu, M. (1990). Taxonomy of four marine bacterial strains that produce tetrodotoxin. *International Journal of Systematic and Evolutionary Microbiology*, *40*(4), 331-336.

72.   Soong, T. W., & Venkatesh, B. (2006). Adaptive evolution of tetrodotoxin resistance in animals. *TRENDS in Genetics*, *22*(11), 621-626.

73.   Chau, R., Kalaitzis, J. A., & Neilan, B. A. (2011). On the origins and biosynthesis of tetrodotoxin. *Aquatic Toxicology*, *104*(1-2), 61-72.

74.   Yotsu-Yamashita, M., Abe, Y., Kudo, Y., Ritson-Williams, R., Paul, V. J., Konoki, K., ... & Isobe, M. (2013). First identification of 5, 11-dideoxytetrodotoxin in marine animals, and characterization of major fragment ions of tetrodotoxin and its analogs by high resolution ESI-MS/MS. *Marine drugs*, *11*(8), 2799-2813.

75.   Chau, R., Kalaitzis, J. A., & Neilan, B. A. (2011). On the origins and biosynthesis of tetrodotoxin. *Aquatic Toxicology*, *104*(1-2), 61-72.

76.   Noguch, T., & Arakawa, O. (2008). Tetrodotoxin–distribution and accumulation in aquatic organisms, and cases of human intoxication. *Marine drugs*, *6*(2), 220-242.

77.   Noguchi, T., Arakawa, O., & Takatani, T. (2006). Toxicity of pufferfish Takifugu rubripes cultured in netcages at sea or aquaria on land. *Comparative Biochemistry and Physiology Part D: Genomics and Proteomics*, *1*(1), 153-157.

78.   Noguchi, T., Arakawa, O., & Takatani, T. (2006). TTX accumulation in pufferfish. *Comparative Biochemistry and Physiology Part D: Genomics and Proteomics*, *1*(1), 145-152.

79.   Turner, A. D., Boundy, M. J., & Rapkova, M. D. (2017). Development and single-laboratory validation of a liquid chromatography tandem mass spectrometry method for quantitation of Tetrodotoxin in mussels and oysters. *Journal of AOAC International*, *100*(5), 1469-1482.

80.   DeGrasse, S., Rivera, V., Roach, J., White, K., Callahan, J., Couture, D., ... & Poli, M. (2014). Paralytic shellfish toxins in clinical matrices: extension of AOAC official method 2005.06 to human urine and serum and application to a 2007 case study in Maine. *Deep Sea Research Part II: Topical Studies in Oceanography*, *103*, 368-375.

81.   Alcaraz, A., Whipple, R. E., Gregg, H. R., Andresen, B. D., & Grant, P. M. (1999). Analysis of tetrodotoxin. *Forensic science international*, *99*(1), 35-45.

82.   Katikou, P. (2019). Public health risks associated with tetrodotoxin and its analogues in european waters: Recent advances after the EFSA scientific opinion. *Toxins*, *11*(5), 240..

83.   Council, A. (2018). Presence of Tetrodotoxin in shellfish.

84.   Costa, P. R., Estevez, P., Castro, D., Soliño, L., Gouveia, N., Santos, C., ... & Gago-Martínez, A. (2018). New insights into the occurrence and toxin profile of ciguatoxins in Selvagens Islands (Madeira, Portugal). *Toxins*, *10*(12), 524.

85.   Kryuchkov, F., Robertson, A., Miles, C. O., Mudge, E. M., & Uhlig, S. (2020). LC–HRMS and chemical derivatization strategies for the structure elucidation of Caribbean ciguatoxins: Identification of C-CTX-3 and-4. *Marine drugs*, *18*(4), 182.

86.   Soliño, L., & Costa, P. R. (2018). Differential toxin profiles of ciguatoxins in marine organisms: Chemistry, fate and global distribution. *Toxicon*, *150*, 124-143.

87.   Adachi, R., & Fukuyo, Y. (1979). The thecal structure of a marine toxic dinoflagellate Gambierdiscus toxicus gen. et sp. nov. collected in a ciguatera-endemic area. *Bull. Jpn. Soc. Sci. Fish*, *45*(1), 67-71.

88.   Faust, M. A. (1995). Observation of sand-dwelling toxic dinoflagellates (Dinophyceae) from widely differing sites, including two new species. *Journal of phycology*, *31*(6), 996-1003.

89.   Holmes, M. J. (1998). Gambierdiscus yasumotoi sp. nov.(Dinophyceae), a toxic benthic dinoflagellate from southeastern Asia. *Journal of phycology*, *34*(4), 661-668.

90.   Chinain, M., Faust, M. A., & Pauillac, S. (1999). Morphology and molecular analyses of three toxic species of Gambierdiscus (Dinophyceae): G. pacificus, sp. nov., G. australes, sp. nov., and G. polynesiensis, sp. nov. *Journal of Phycology*, *35*(6), 1282-1296.

91.   Larsson, M. E., Harwood, T. D., Lewis, R. J., SWA, H., & Doblin, M. A. (2019). Toxicological characterization of Fukuyoa paulensis (Dinophyceae) from temperate Australia. *Phycological Research*, *67*(1), 65-71.

92.   Laurent, D., Kerbrat, A. S., Darius, H. T., Girard, E., Golubic, S., Benoit, E., ... & Pauillac, S. (2008). Are cyanobacteria involved in Ciguatera Fish Poisoning-like outbreaks in New Caledonia?. *Harmful Algae*, *7*(6), 827-838.

93.   Kerbrat, A. S., Darius, H. T., Pauillac, S., Chinain, M., & Laurent, D. (2010). Detection of ciguatoxin-like and paralysing toxins in Trichodesmium spp. from New Caledonia lagoon. *Marine Pollution Bulletin*, *61*(7-12), 360-366.

94.   Tamele, I. J., Silva, M., & Vasconcelos, V. (2019). The incidence of marine toxins and the associated seafood poisoning episodes in the African countries of the Indian Ocean and the Red Sea. *Toxins*, *11*(1), 58.

95.   Murata, M., Legrand, A. M., Ishibashi, Y., & Yasumoto, T. (1989). Structures of ciguatoxin and its congener. *Journal of the American chemical Society*, *111*(24), 8929-8931-

96.   Murata, M., Legrand, A. M., Ishibashi, Y., Fukui, M., & Yasumoto, T. (1990). Structures and configurations of ciguatoxin from the moray eel Gymnothorax javanicus and its likely

precursor from the dinoflagellate Gambierdiscus toxicus. *Journal of the American Chemical Society*, *112*(11), 4380-4386.

97.   Murata, M., Legrand, A. M., Scheuer, P. J., & Yasumoto, T. (1992). 13C NMR assignments of ciguatoxin by inverse-detected 2D spectroscopy and an explanation of NMR signal broadening. *Tetrahedron letters*, *33*(4), 525-526.

98.   Lewis, R. J., Sellin, M., Poli, M. A., Norton, R. S., MacLeod, J. K., & Sheil, M. M. (1991). Purification and characterization of ciguatoxins from moray eel (Lycodontis javanicus, Muraenidae). *Toxicon*, *29*(9), 1115-1127.

99.   Lewis, R. J., Norton, R. S., Brereton, I. M., & Eccles, C. D. (1993). Ciguatoxin-2 is a diastereomer of ciguatoxin-3. *Toxicon*, *31*(5), 637-643.

100.   Yasumoto, T., Igarashi, T., Legrand, A. M., Cruchet, P., Chinain, M., Fujita, T., & Naoki, H. (2000). Structural elucidation of ciguatoxin congeners by fast-atom bombardment tandem mass spectroscopy. *Journal of the American Chemical Society*, *122*(20), 4988-4989.

101.   Yasumoto, T. (2001). The chemistry and biological function of natural marine toxins. *The Chemical Record*, *1*(3), 228-242.

102.   Blunt, J. W., & Munro, M. H. (Eds.). (2007). *Dictionary of marine natural products with CD-ROM*. CRC Press.

103.   Lewis, R. J., & Holmes, M. J. (1993). Origin and transfer of toxins involved in ciguatera. *Comparative Biochemistry and Physiology Part C: Pharmacology, Toxicology and Endocrinology*, *106*(3), 615-628

104.   Satake, M., Ishibashi, Y., Legrand, A. M., & Yasumoto, T. (1996). Isolation and structure of ciguatoxin-4A, a new ciguatoxin precursor, from cultures of dinoflagellate Gambierdiscus toxicus and parrotfish Scarus gibbus. *Bioscience, biotechnology, and biochemistry*, *60*(12), 2103-2105.

105.   Satake, M., Fukui, M., Legrand, A. M., Cruchet, P., & Yasumoto, T. (1998). Isolation and structures of new ciguatoxin analogs, 2, 3-dihydroxyCTX3C and 51-hydroxyCTX3C, accumulated in tropical reef fish. *Tetrahedron Letters*, *39*(10), 1197-1198.

106.   Yogi, K., Sakugawa, S., Oshiro, N., Ikehara, T., Sugiyama, K., & Yasumoto, T. (2014). Determination of toxins involved in ciguatera fish poisoning in the Pacific by LC/MS. *Journal of AOAC International*, *97*(2), 398-402.

107.   Vernoux, J. P., & Lewis, R. J. (1997). Isolation and characterisation of Caribbean ciguatoxins from the horse-eye jack (Caranx latus). *Toxicon*, *35*(6), 889-900.

108.   Lewis, R. J., Vernoux, J. P., & Brereton, I. M. (1998). Structure of Caribbean ciguatoxin isolated from Caranx latus. *Journal of the American Chemical Society*, *120*(24), 5914-5920.

109.   Friedman, M. A., Fernandez, M., Backer, L. C., Dickey, R. W., Bernstein, J., Schrank, K., ... & Fleming, L. E. (2017). An updated review of ciguatera fish poisoning: clinical, epidemiological, environmental, and public health management. *Marine drugs*, *15*(3), 72.

110.   Friedman, M. A., Fleming, L. E., Fernandez, M., Bienfang, P., Schrank, K., Dickey, R., ... & Reich, A. (2008). Ciguatera fish poisoning: treatment, prevention and management. *Marine drugs*, *6*(3), 456-479.

111.   Lehane, L., & Lewis, R. J. (2000). Ciguatera: recent advances but the risk remains. *International journal of food microbiology*, *61*(2-3), 91-125.

112.   Nicholson, G. M., & Lewis, R. J. (2006). Ciguatoxins: Cyclic polyether modulators of voltage-gated Iion channel function. *Marine Drugs*, *4*(3), 82-118.

113.   Bagnis, R (1968). Clinical aspects of ciguatera (fish poisoning) in French Polynesia. *Hawaii Medicinal Journal, 28(1):25-8.*

114.   Bagnis, R., Kuberski, T., & Laugier, S. (1979). Clinical observations on 3,009 cases of ciguatera (fish poisoning) in the South Pacific. *The American journal of tropical medicine and hygiene*, *28*(6), 1067-1073.

115.   Withers, N. W. (1982). Ciguatera fish poisoning. *Annual Review of Medicine,* 33:97-111

116.   Yasumoto, T.; Raj, U.; Bagnis, R. In Symposium on Seafood Toxins from Tropical Regions, Tohoku University Japan, 1984; p. 74.

117.   Calvert, G. M., Hryhorczuk, D. O., & Leikin, J. B. (1987). Treatment of Ciguatera Fish Poisoning with Amttriptyline and Nifedipine. *Journal of Toxicology: Clinical Toxicology*, *25*(5), 423-428.

118.   Baumann, F., Bourrat, M. B., & Pauillac, S. (2010). Prevalence, symptoms and chronicity of ciguatera in New Caledonia: Results from an adult population survey conducted in Noumea during 2005. *Toxicon*, *56*(5), 662-667.

119.   Bidard, J. N., Vijverberg, H. P., Frelin, C., Chungue, E., Legrand, A. M., Bagnis, R., & Lazdunski, M. (1984). Ciguatoxin is a novel type of Na+ channel toxin. *Journal of Biological Chemistry*, *259*(13), 8353-8357.

120. Lombet, A., Bidard, J. N., & Lazdunski, M. (1987). Ciguatoxin and brevetoxins share a common receptor site on the neuronal voltage-dependent Na+ channel. *FEBS letters*, *219*(2), 355-359.

121. Yasumoto, T., Seino, N., Murakami, Y., & Murata, M. (1987). Toxins produced by benthic dinoflagellates. *The Biological Bulletin*, *172*(1), 128-131.

122. BAGNIS, R. (1977). Finding of a dinoflagellate as a likely culprit of ciguatera. *日本水産学会誌*, *43*(8), 1021-1026.

123. Ikehara, T., Kuniyoshi, K., Oshiro, N., & Yasumoto, T. (2017). Biooxidation of ciguatoxins leads to species-specific toxin profiles. *Toxins*, *9*(7), 205.

124. Botana, L. M. (Ed.). (2014). *Seafood and freshwater toxins: pharmacology, physiology, and detection*. CRC Press.

125. Satake, M., Morohashi, A., Oguri, H., Oishi, T., Hirama, M., Harada, N., & Yasumoto, T. (1997). The absolute configuration of ciguatoxin. *Journal of the American Chemical Society*, *119*(46), 11325-11326.

126. Scheuer, P. J., Takahashi, W., Tsutsumi, J., & Yoshida, T. (1967). Ciguatoxin: isolation and chemical nature. *Science*, *155*(3767), 1267-1268.

127. Hamilton, B., Hurbungs, M., Jones, A., & Lewis, R. J. (2002). Multiple ciguatoxins present in Indian Ocean reef fish. *Toxicon*, *40*(9), 1347-1353.

128. Caillaud, A., de la Iglesia, P., Barber, E., Eixarch, H., Mohammad-Noor, N., Yasumoto, T., & Diogene, J. (2011). Monitoring of dissolved ciguatoxin and maitotoxin using solid-phase adsorption toxin tracking devices: Application to Gambierdiscus pacificus in culture. *Harmful Algae*, *10*(5), 433-446.

129. Sanchez-Henao, A., García-Álvarez, N., Sergent, F. S., Estévez, P., Gago-Martínez, A., Martín, F., ... & Real, F. (2020). Presence of CTXs in moray eels and dusky groupers in the marine environment of the Canary Islands. *Aquatic Toxicology*, *221*, 105427.

130. Aligizaki, K., & Nikolaidis, G. (2008). Morphological identification of two tropical dinoflagellates of the genera Gambierdiscus and Sinophysis in the Mediterranean Sea. *Journal of biological research-Thessaloniki*, *9*, 75-82.

131. Estevez, P., Sibat, M., Leão-Martins, J. M., Tudó, A., Rambla-Alegre, M., Aligizaki, K., ... & Hess, P. (2020). Use of Mass Spectrometry to determine the Diversity of Toxins Produced

by Gambierdiscus and Fukuyoa Species from Balearic Islands and Crete (Mediterranean Sea) and the Canary Islands (Northeast Atlantic). *Toxins*, *12*(5), 305.

132.   Ito, E., Suzuki-Toyota, F., Toshimori, K., Fuwa, H., Tachibana, K., Satake, M., & Sasaki, M. (2003). Pathological effects on mice by gambierol, possibly one of the ciguatera toxins. *Toxicon*, *42*(7), 733-740.

133.   Nagai, H., MIKAMI, Y., YAZAWA, K., GONOI, T., & YASUMOTO, T. (1993). Biological activities of novel polyether antifungals, gambieric acids A and B from a marine dinoflagellate Gambierdiscus toxicus. *The Journal of antibiotics*, *46*(3), 520-522.

134.   Rodríguez, I., Genta-Jouve, G., Alfonso, C., Calabro, K., Alonso, E., Sánchez, J. A., ... & Botana, L. M. (2015). Gambierone, a ladder-shaped polyether from the dinoflagellate Gambierdiscus belizeanus. *Organic letters*, *17*(10), 2392-2395.

135.   Takahashi, M., Ohizumi, Y., & Yasumoto, T. (1982). Maitotoxin, a Ca2+ channel activator candidate. *Journal of Biological Chemistry*, *257*(13), 7287-7289.

136.   Watanabe, R., Uchida, H., Suzuki, T., Matsushima, R., Nagae, M., Toyohara, Y., ... & Yasumoto, T. (2013). Gambieroxide, a novel epoxy polyether compound from the dinoflagellate Gambierdiscus toxicus GTP2 strain. *Tetrahedron*, *69*(48), 10299-10303.

137.   Ito, E., & Yasumoto, T. (1996). Morphological observations of diarrhea in mice caused by experimental ciguatoxicosis. *Toxicon*, *34*(1), 111-122.

138.   Terao, K., Ito, E., Oarada, M., Ishibashi, Y., Legrand, A. M., & Yasumoto, T. (1991). Light and electron microscopic studies of pathologic changes induced in mice by ciguatoxin poisoning. *Toxicon*, *29*(6), 633-643.

139.   Mak, Y. L., Wai, T. C., Murphy, M. B., Chan, W. H., Wu, J. J., Lam, J. C., ... & Lam, P. K. (2013). Pacific ciguatoxins in food web components of coral reef systems in the Republic of Kiribati. *Environmental science & technology*, *47*(24), 14070-14079.

140.   Meyer, L., Carter, S., & Capper, A. (2015). An updated ciguatoxin extraction method and silica cleanup for use with HPLC-MS/MS for the analysis of P-CTX-1, PCTX-2 and P-CTX-3. *Toxicon*, *108*, 249-256

141.   Hamilton, B., Whittle, N., Shaw, G., Eaglesham, G., Moore, M. R., & Lewis, R. J. (2010). Human fatality associated with Pacific ciguatoxin contaminated fish. *Toxicon*, *56*(5), 668-673.

142.	Lucas, R. E., Lewis, R. J., & Taylor, J. M. (1997). Pacific Ciguatoxin-1 associated with a large common-source outbreak of Ciguatera in East Arnhem Land, Australia. *Natural toxins*, *5*(4), 136-140.

143.	Oshiro, N., Yogi, K., Asato, S., Sasaki, T., Tamanaha, K., Hirama, M., ... & Inafuku, Y. (2010). Ciguatera incidence and fish toxicity in Okinawa, Japan. *Toxicon*, *56*(5), 656-661.

144.	Satake, M. & YASUMOTO, T. (1993). The structure of CTX3C, a ciguatoxin congener isolated from cultured Gambierdiscus toxicus." *Tetrahedron Letters,* 34: 1975-1978.

145.	Hirama, M., Oishi, T., Uehara, H., Inoue, M., Maruyama, M., Oguri, H., & Satake, M. (2001). Total synthesis of ciguatoxin CTX3C. *Science*, *294*(5548), 1904-1907.

146.	Inoue, M., Lee, N., Miyazaki, K., Usuki, T., Matsuoka, S., & Hirama, M. (2008). Critical Importance of the Nine-Membered F Ring of Ciguatoxin for Potent Bioactivity: Total Synthesis and Biological Evaluation of F-Ring-Modified Analogues. *Angewandte Chemie*, *120*(45), 8739-8742.

147.	Bottein, M. Y. D., Kashinsky, L., Wang, Z., Littnan, C., & Ramsdell, J. S. (2011). Identification of ciguatoxins in Hawaiian monk seals Monachus schauinslandi from the northwestern and main Hawaiian Islands. *Environmental science & technology*, *45*(12), 5403-5409.

148.	Pottier, I., Vernoux, J. P., Jones, A., & Lewis, R. J. (2002). Characterisation of multiple Caribbean ciguatoxins and congeners in individual specimens of horse-eye jack (Caranx latus) by high-performance liquid chromatography/mass spectrometry. *Toxicon*, *40*(7), 929-939.

149.	Hamilton, B., Hurbungs, M., Vernoux, J. P., Jones, A., & Lewis, R. J. (2002). Isolation and characterisation of Indian Ocean ciguatoxin. *Toxicon*, *40*(6), 685-693.

150.	Diogène, J., Reverté, L., Rambla-Alegre, M., Del Río, V., De La Iglesia, P., Campàs, M., ... & Turquet, J. (2017). Identification of ciguatoxins in a shark involved in a fatal food poisoning in the Indian Ocean. *Scientific reports*, *7*(1), 1-8.

151.	Pisapia, F., Sibat, M., Watanabe, R., Roullier, C., Suzuki, T., Hess, P., & Herrenknecht, C. (2020). Characterization of maitotoxin-4 (MTX4) using electrospray positive mode ionization high-resolution mass spectrometry and UV spectroscopy. *Rapid Communications in Mass Spectrometry*, *34*(19), e8859.

152.	BAGNIS, R., & P. VERNOUX, J. (1976). Toxicity of the surgeonfishes. II. Properties of the principal water-soluble toxin. *日本水産学会誌*, *42*(3), 359-365.

153.   Seliger, H. H., Tyler, M. A., & McKinley, K. R. (1979). Phytoplankton distributions and red tides resulting from frontal circulation patterns. *Toxic dinoflagellate blooms*, 239-248.

154.   Murata, M., Naoki, H., Iwashita, T., Matsunaga, S., Sasaki, M., Yokoyama, A., & Yasumoto, T. (1993). Structure of maitotoxin. *Journal of the American Chemical Society*, *115*(5), 2060-2062.

155.   Igarashi, T., Aritake, S., & Yasumoto, T. (1999). Mechanisms underlying the hemolytic and ichthyotoxic activities of maitotoxin. *Natural toxins*, *7*(2), 71-79.

156.   Pisapia, F., Sibat, M., Herrenknecht, C., Lhaute, K., Gaiani, G., Ferron, P. J., ... & Hess, P. (2017). Maitotoxin-4, a novel MTX analog produced by Gambierdiscus excentricus. *Marine drugs*, *15*(7), 220.

157.   Rhodes, L. L., Smith, K. F., Murray, S., Harwood, D. T., Trnski, T., & Munday, R. (2017). The epiphytic genus Gambierdiscus (Dinophyceae) in the Kermadec Islands and Zealandia regions of the southwestern Pacific and the associated risk of ciguatera fish poisoning. *Marine drugs*, *15*(7), 219.

158.   Rhodes, L. L., Smith, K. F., Verma, A., Murray, S., Harwood, D. T., & Trnski, T. (2017). The dinoflagellate genera Gambierdiscus and Ostreopsis from subtropical Raoul Island and North Meyer Island, Kermadec Islands. *New Zealand Journal of Marine and Freshwater Research*, *51*(4), 490-504.

159.   Munday, R., Murray, S., Rhodes, L. L., Larsson, M. E., & Harwood, D. T. (2017). Ciguatoxins and maitotoxins in extracts of sixteen Gambierdiscus isolates and one Fukuyoa isolate from the South Pacific and their toxicity to mice by intraperitoneal and oral administration. *Marine drugs*, *15*(7), 208.

160.   Rhodes, L., Harwood, T., Smith, K., Argyle, P., & Munday, R. (2014). Production of ciguatoxin and maitotoxin by strains of Gambierdiscus australes, G. pacificus and G. polynesiensis (Dinophyceae) isolated from Rarotonga, Cook Islands. *Harmful Algae*, *39*, 185-190.

161.   Gusovsky, F., & Daly, J. W. (1990). Maitotoxin: a unique pharmacological tool for research on calcium-dependent mechanisms. *Biochemical pharmacology*, *39*(11), 1633-1639.

162.   Reyes, J. G., Sánchez-Cárdenas, C., Acevedo-Castillo, W., Leyton, P., López-González, I., Felix, R., ... & Treviño, C. L. (2014). Maitotoxin: An enigmatic toxic molecule with useful applications in the biomedical sciences. *Seafood and Freshwater Toxins: Pharmacology, Physiology and Detection; Botana, LM, Ed*, 677-694.

163.   Murata, M., Gusovsky, F., Sasaki, M., Yokoyama, A., Yasumoto, T., & Daly, J. W. (1991). Effect of maitotoxin analogues on calcium influx and phosphoinositide breakdown in cultured cells. *Toxicon*, *29*(9), 1085-1096.

164.   Kelley, B. A., Jollow, D. J., Felton, E. T., Voegtline, M. S., & Higerd, T. B. (1986). Response of mice to gambierdiscus-toxicus toxin. *MARINE FISHERIES REVIEW*, *48*(4), 35-37.

165.   Ajani, P., Harwood, D. T., & Murray, S. A. (2017). Recent trends in marine phycotoxins from Australian coastal waters. *Marine drugs*, *15*(2), 33.

166.   Kohli, G. S., Papiol, G. G., Rhodes, L. L., Harwood, D. T., Selwood, A., Jerrett, A., ... & Neilan, B. A. (2014). A feeding study to probe the uptake of Maitotoxin by snapper (Pagrus auratus). *Harmful Algae*, *37*, 125-132.

167.   Tester, P. A., Litaker, R. W., & Berdalet, E. (2020). Climate change and harmful benthic microalgae. *Harmful algae*, *91*, 101655.

168.   Rossignoli, A. E., Tudó, A., Bravo, I., Díaz, P. A., Diogène, J., & Riobó, P. (2020). Toxicity characterisation of Gambierdiscus species from the Canary Islands. *Toxins*, *12*(2), 134.

169.   Holmes, M. J., Lewis, R. J., & Gillespie, N. C. (1990). Toxicity of Australian and French Polynesian strains of Gambierdiscus toxicus (Dinophyceae) grown in culture: characterization of a new type of maitotoxin. *Toxicon*, *28*(10), 1159-1172.

170.   Holmes, M. J., & Lewis, R. J. (1994). Purification and characterisation of large and small maitotoxins from cultured Gambierdiscus toxicus. *Natural toxins*, *2*(2), 64-72.

171.   Lewis, R. J., Holmes, M. J., Alewood, P. F., & Jones, A. (1994). Lonspray mass spectrometry of ciguatoxin-1, maitotoxin-2 and-3, and related marine polyether toxins. *Natural toxins*, *2*(2), 56-63.

172.   Murray, J. S., Selwood, A. I., Harwood, D. T., van Ginkel, R., Puddick, J., Rhodes, L. L., ... & Wilkins, A. L. (2019). 44-Methylgambierone, a new gambierone analogue isolated from Gambierdiscus 170. australes. *Tetrahedron Letters*, *60*(8), 621-625.

173.   Boente-Juncal, A., Álvarez, M., Antelo, Á., Rodríguez, I., Calabro, K., Vale, C., ... & Botana, L. M. (2019). Structure elucidation and biological evaluation of maitotoxin-3, a homologue of gambierone, from Gambierdiscus belizeanus. *Toxins*, *11*(2), 79.

174.   Moore, R. E., & Scheuer, P. J. (1971). Palytoxin: a new marine toxin from a coelenterate. *Science*, *172*(3982), 495-498

175.   Malo D. *Hawaiian Antiquites*, second ed. Bishop Museum Publication, Honolulu, USA. 1951, 201–226

176.   Walsh, G. E., & Bowers, R. L. (1971). A review of Hawaiian zoanthids with descriptions of three new species. *Zoological Journal of the Linnean Society*, *50*(2), 161-180.

177.   Kimura, S., Hashimoto, Y., & Yamazato, K. (1972). Toxicity of the zoanthid Palythoa tuberculosa. *Toxicon*, *10*(6), 611-617.

178.   Quinn, R. J., Moore, R. E., Kashiwagi, M., & Norton, T. R. (1974). Anticancer activity of zoanthids and the associated toxin, palytoxin, against Ehrlich ascites tumor and P-388 lymphocytic leukemia in mice. *Journal of pharmaceutical sciences*, *63*(2), 257-260.

179.   Attaway DH Ciereszko LS. Isolation and partial characterization of Caribbean palytoxin. *Proceedings of the 2ⁿᵈ International Symposium for Coral Reefs I, Great Barrier Reef Community*, Brisbane. 1974, 497-504

180.   Beress, L., Zwick, J., Kolkenbrock, H. J., Kaul, P. N., & Wassermann, O. (1983). A method for the isolation of the caribbean palytoxin (C-PTX) from the coelenterate (zooanthid) Palythoa caribaeorum. *Toxicon*, *21*(2), 285-290.

181.   Moore, R. E., & Bartolini, G. (1981). Structure of palytoxin. *Journal of the American Chemical Society*, *103*(9), 2491-2494.

182.   Moore, R. E., Woolard, F. X., & Bartolini, G. (1980). Periodate oxidation of N-(p-bromobenzoyl) palytoxin. *Journal of the American Chemical Society*, *102*(24), 7370-7372.

183.   Uemura, D., Hirata, Y., Iwashita, T., & Naoki, H. (1985). Studies on palytoxins. *Tetrahedron*, *41*(6), 1007-1017.

184.   Oku, N., Sata, N. U., Matsunaga, S., Uchida, H. O., & Fusetani, N. (2004). Identification of palytoxin as a principle which causes morphological changes in rat 3Y1 cells in the zoanthid Palythoa aff. margaritae. *Toxicon*, *43*(1), 21-25.

185.   Pelin, M., Sosa, S., & Tubaro, A. (2016). Palytoxins: toxicological profile.

186.   EFSA Panel on Contaminants in the Food Chain (CONTAM). (2009). Scientific Opinion on marine biotoxins in shellfish–Palytoxin group. *EFSA Journal*, *7*(12), 1393.

187.   Gleibs, S., Mebs, D., & Werding, B. (1995). Studies on the origin and distribution of palytoxin in a Caribbean coral reef. *Toxicon*, *33*(11), 1531-1537.

188.   Watters, M. R. (2009). Seafood Neurotoxins II: Other Ingestible Marine Biotoxins—Ciguatera, Tetrodotoxin, Cyanotoxins. *Clinical Neurotoxicology E-Book: Syndromes, Substances, Environments*, 448.

189.   Maeda M, Kodama T, Tanaka T, Yoshizumi H, Nomoto K, Takemoto T Fujiki T. Structure of insecticidal substances isolated from a red alga, Chondria armata. *Symposium Papers, 27th Symposium on the Chemistry of Natural Products*, Hiroshima, Japan. 1985:616–623.

190.   Yasumoto, T., Yasumura, D., Ohizumi, Y., Takahashi, M., Alcala, A. C., & Alcala, L. C. (1986). Palytoxin in two species of xanthid crab from the Philippines. *Agricultural and Biological chemistry*, 50(1), 163-167.

191.   Fukui, M., Murata, M., Inoue, A., Gawel, M., & Yasumoto, T. (1987). Occurrence of palytoxin in the trigger fish Melichtys vidua. *Toxicon*, *25*(10), 1121-1124.

192.   Halstead, B. W. (2002). The microbial biogenesis of aquatic biotoxins. *Toxicology mechanisms and methods*, *12*(2), 135-153..

193.   Kerbrat, A. S., Amzil, Z., Pawlowiez, R., Golubic, S., Sibat, M., Darius, H. T., ... & Laurent, D. (2011). First evidence of palytoxin and 42-hydroxy-palytoxin in the marine cyanobacterium Trichodesmium. *Marine drugs*, *9*(4), 543-560.

194.   Usami, M., Satake, M., Ishida, S., Inoue, A., Kan, Y., & Yasumoto, T. (1995). Palytoxin analogs from the dinoflagellate Ostreopsis siamensis. *Journal of the American chemical society*, *117*(19), 5389-5390.

195.   Taniyama, S., Arakawa, O., Terada, M., Nishio, S., Takatani, T., Mahmud, Y., & Noguchi, T. (2003). Ostreopsis sp., a possible origin of palytoxin (PTX) in parrotfish Scarus ovifrons. *Toxicon*, *42*(1), 29-33.

196.   Botana, L. M., Alfonso, A., Rodríguez, I., Botana, A. M., Louzao, M. D. C., & Vieytes, M. R. (2016). How safe is safe for marine toxins monitoring?. *Toxins*, *8*(7), 208.

197.   Ciminiello, P., Dell'Aversano, C., Dello Iacovo, E., Fattorusso, E., Forino, M., Grauso, L., & Tartaglione, L. (2012). High resolution LC-MSn fragmentation pattern of palytoxin as template to gain new insights into ovatoxin-a structure. The key role of calcium in MS behavior of palytoxins. *Journal of the American Society for Mass Spectrometry*, *23*(5), 952-963.

198.   Ciminiello, P., Dell'Aversano, C., Dello Iacovo, E., Fattorusso, E., Forino, M., Grauso, L., ... & Bignami, G. (2009). Stereostructure and biological activity of 42-hydroxy-palytoxin: A new

palytoxin analogue from Hawaiian Palythoa subspecies. *Chemical research in toxicology*, *22*(11), 1851-1859.

199.   Ciminiello, P., Dell'Aversano, C., Dello Iacovo, E., Forino, M., Randazzo, A., & Tartaglione, L. (2014). Identification of Palytoxin–Ca2+ Complex by NMR and Molecular Modeling Techniques. *The Journal of organic chemistry*, *79*(1), 72-79.

200.   Tichadou, L., Glaizal, M., Armengaud, A., Grossel, H., Lemée, R., Kantin, R., ... & De Haro, L. (2010). Health impact of unicellular algae of the Ostreopsis genus blooms in the Mediterranean Sea: experience of the French Mediterranean coast surveillance network from 2006 to 2009. *Clinical toxicology*, *48*(8), 839-844.

201.   Accoroni, S., Romagnoli, T., Penna, A., Capellacci, S., Ciminiello, P., Dell'Aversano, C., ... & Totti, C. (2016). Ostreopsis fattorussoi sp. nov.(Dinophyceae), a new benthic toxic Ostreopsis species from the eastern Mediterranean Sea. *Journal of phycology*, *52*(6), 1064-1084.

202.   Tartaglione, L., Dello Iacovo, E., Mazzeo, A., Casabianca, S., Ciminiello, P., Penna, A., & Dell'Aversano, C. (2017). Variability in toxin profiles of the Mediterranean Ostreopsis cf. ovata and in structural features of the produced ovatoxins. *Environmental science & technology*, *51*(23), 13920-13928.

203.   Ciminiello, P., Dell'Aversano, C., Iacovo, E. D., Fattorusso, E., Forino, M., & Tartaglione, L. (2011). LC-MS of palytoxin and its analogues: State of the art and future perspectives. *Toxicon*, *57*(3), 376-389.

204.   Usami, M., Satake, M., Ishida, S., Inoue, A., Kan, Y., & Yasumoto, T. (1995). Palytoxin analogs from the dinoflagellate Ostreopsis siamensis. *Journal of the American chemical society*, *117*(19), 5389-5390.

205.   Ukena, T., Satake, M., Usami, M., Oshima, Y., Fujita, T., Naoki, H., & Yasumoto, T. (2002). Structural confirmation of ostreocin-D by application of negative-ion fast-atom bombardment collision-induced dissociation tandem mass spectrometric methods. *Rapid communications in mass spectrometry*, *16*(24), 2387-2393.

206.   Terajima, T., Uchida, H., Abe, N., & Yasumoto, T. (2019). Structure elucidation of ostreocin-A and ostreocin-E1, novel palytoxin analogs produced by the dinoflagellate Ostreopsis siamensis, using LC/Q-TOF MS. *Bioscience, biotechnology, and biochemistry*, *83*(3), 381-390.

207.   Terajima, T., Uchida, H., Abe, N., & Yasumoto, T. (2018). Simple structural elucidation of ostreocin-B, a new palytoxin congener isolated from the marine dinoflagellate Ostreopsis

siamensis, using complementary positive and negative ion liquid chromatography/quadrupole time-of-flight mass spectrometry. *Rapid Communications in Mass Spectrometry*, *32*(12), 1001-1007.

208. Ciminiello, P., Dell'Aversano, C., Iacovo, E. D., Fattorusso, E., Forino, M., Tartaglione, L., ... & Penna, A. (2013). Investigation of toxin profile of Mediterranean and Atlantic strains of Ostreopsis cf. siamensis (Dinophyceae) by liquid chromatography–high resolution mass spectrometry. *Harmful Algae*, *23*, 19-27.

209. Lenoir, S., Ten-Hage, L., Turquet, J., Quod, J. P., & Hennion, M. C. (2006). Characterisation of new analogues of palytoxin isolated from an Ostreopsis mascarenensis bloom in the south-western Indian Ocean. *African Journal of Marine Science*, *28*(2), 389-391.

210. Rossi, R., Castellano, V., Scalco, E., Serpe, L., Zingone, A., & Soprano, V. (2010). New palytoxin-like molecules in Mediterranean Ostreopsis cf. ovata (dinoflagellates) and in Palythoa tuberculosa detected by liquid chromatography-electrospray ionization time-of-flight mass spectrometry. *Toxicon*, *56*(8), 1381-1387.

211. Uchida, H., Taira, Y., & Yasumoto, T. (2013). Structural elucidation of palytoxin analogs produced by the dinoflagellate Ostreopsis ovata IK2 strain by complementary use of positive and negative ion liquid chromatography/quadrupole time-of-flight mass spectrometry. *Rapid Communications in Mass Spectrometry*, *27*(17), 1999-2008.

212. Tartaglione, L., Mazzeo, A., Dell'Aversano, C., Forino, M., Giussani, V., Capellacci, S., ... & Ciminiello, P. (2016). Chemical, molecular, and eco-toxicological investigation of Ostreopsis sp. from Cyprus Island: structural insights into four new ovatoxins by LC-HRMS/MS. *Analytical and bioanalytical chemistry*, *408*(3), 915-932.

213. Ciminiello, P., Dell'Aversano, C., Fattorusso, E., Forino, M., Magno, G. S., Tartaglione, L., ... & Melchiorre, N. (2006). The Genoa 2005 Outbreak. Determination of Putative Palytoxin in Mediterranean Ostreopsis o vata by a New Liquid Chromatography Tandem Mass Spectrometry Method. *Analytical chemistry*, *78*(17), 6153-6159.

214. Ciminiello, P., Dell'Aversano, C., Fattorusso, E., Forino, M., Tartaglione, L., Grillo, C., & Melchiorre, N. (2008). Putative palytoxin and its new analogue, ovatoxin-a, in Ostreopsis ovata collected along the Ligurian coasts during the 2006 toxic outbreak. *Journal of the American society for mass spectrometry*, *19*(1), 111-120.

215.   Penna, A., Vila, M., Fraga, S., Giacobbe, M. G., Andreoni, F., Riobó, P., & Vernesi, C. (2005). Characterization of Ostreopsis and Coolia (Dinophyceae) isolates in the western Mediterranean Sea based on morphology, toxicity and internal transcribed spacer 5.8 S rDNA sequences 1. *Journal of phycology*, *41*(1), 212-225.

216.   Tognetto, L., Bellato, S., Moro, I., & Andreoli, C. (1995). Occurrence of Ostreopsis ovata (Dinophyceae) in the Tyrrhenian Sea during summer 1994. *Botanica marina*, *38*(1-6), 291-296.

217.   Sansoni, G., Borghini, B., Camici, G., Casotti, M., Righini, P., & Rustighi, C. (2003). Fioriture algali di Ostreopsis ovata (Gonyaulacales: Dinophyceae): un problema emergente. *Biologia ambientale*, *17*(1), 17-23.

218.   Ciminiello, P., Dell'Aversano, C., Dello Iacovo, E., Fattorusso, E., Forino, M., Grauso, L., & Tartaglione, L. (2012). High resolution LC-MSn fragmentation pattern of palytoxin as template to gain new insights into ovatoxin-a structure. The key role of calcium in MS behavior of palytoxins. *Journal of the American Society for Mass Spectrometry*, *23*(5), 952-963.

219.   Ciminiello, P., Dell'Aversano, C., Dello Iacovo, E., Fattorusso, E., Forino, M., Grauso, L., ... & Vanucci, S. (2012). Isolation and structure elucidation of ovatoxin-a, the major toxin produced by Ostreopsis ovata. *Journal of the American Chemical Society*, *134*(3), 1869-1875.

220.   Ciminiello, P., Dell'Aversano, C., Dello Iacovo, E., Fattorusso, E., Forino, M., Grauso, L., & Tartaglione, L. (2012). Stereochemical Studies on Ovatoxin-a. *Chemistry-a European Journal*, *18*(52), 16836.

221.   Ciminiello, P., Dell'Aversano, C., Iacovo, E. D., Fattorusso, E., Forino, M., Tartaglione, L., ... & Penna, A. (2012). Unique toxin profile of a Mediterranean Ostreopsis cf. ovata strain: HR LC-MS n characterization of ovatoxin-f, a new palytoxin congener. *Chemical research in toxicology*, *25*(6), 1243-1252.

222.   García-Altares, M., Tartaglione, L., Dell'Aversano, C., Carnicer, O., de la Iglesia, P., Forino, M., ... & Ciminiello, P. (2015). The novel ovatoxin-g and isobaric palytoxin (so far referred to as putative palytoxin) from Ostreopsis cf. ovata (NW Mediterranean Sea): structural insights by LC-high resolution MS n. *Analytical and bioanalytical chemistry*, *407*(4), 1191-1204.

223.   Brissard, C., Hervé, F., Sibat, M., Séchet, V., Hess, P., Amzil, Z., & Herrenknecht, C. (2015). Characterization of ovatoxin-h, a new ovatoxin analog, and evaluation of chromatographic columns for ovatoxin analysis and purification. *Journal of Chromatography A*, *1388*, 87-101.

224.   Proença, L. A. O., Boemer, G. L., Dias, J. P., Hatherly, M. M., Mendes, I. L., Mendes, L. A. M., ... & Schramm, M. A. (2010). Can the cases of airborne intoxication of beach users in south coast of Bahia (16 24'S–39 02'W) be related to microalgae. *GEOHAB OSM on Benthic HABs, Honolulu, Hawaii.*

225.   Suzuki, T., Watanabe, R., Uchida, H., Matsushima, R., Nagai, H., Yasumoto, T., ... & Adachi, M. (2012). LC-MS/MS analysis of novel ovatoxin isomers in several Ostreopsis strains collected in Japan. *Harmful algae*, *20*, 81-91.

226.   Parsons, M. L., Aligizaki, K., Bottein, M. Y. D., Fraga, S., Morton, S. L., Penna, A., & Rhodes, L. (2012). Gambierdiscus and Ostreopsis: reassessment of the state of knowledge of their taxonomy, geography, ecophysiology, and toxicology. *Harmful algae*, *14*, 107-129.

227.   Wu, C. H. (2009). Palytoxin: Membrane mechanisms of action. *Toxicon*, *54*(8), 1183-1189.

228.   Hilgemann, D. W. (2003). From a pump to a pore: how palytoxin opens the gates. *Proceedings of the National Academy of Sciences*, *100*(2), 386-388.

229.   Louzao, M. C., Ares, I. R., Vieytes, M. R., Valverde, I., Vieites, J. M., Yasumoto, T., & Botana, L. M. (2007). The cytoskeleton, a structure that is susceptible to the toxic mechanism activated by palytoxins in human excitable cells. *The FEBS journal*, *274*(8), 1991-2004.

230.   Rodrigues, A. M., Almeida, A. C. G., & Infantosi, A. F. (2008). Effect of palytoxin on the sodium–potassium pump: model and simulation. *Physical biology*, *5*(3), 036005.

231.   Morton, B. E., Fraser, C. F., Thenawidjaja, M., Albagli, L., & Rayner, M. D. (1982). Potent inhibition of sperm motility by palytoxin. *Experimental cell research*, *140*(2), 261-265.

232.   Lazzaro, M., Tshhjian JR, A. H., Fujiki, H., & Levine, L. (1987). Palytoxin: An extraordinarily potent stimulator of prostaglandin production and bone resorption in cultured mouse calvariae. *Endocrinology*, *120*(4), 1338-1345

233.   Nagase, H. I. R. O. M. I., & Karaki, H. I. D. E. A. K. I. (1987). Palytoxin-induced contraction and release of prostaglandins and norepinephrine in the aorta. *Journal of Pharmacology and Experimental Therapeutics*, *242*(3), 1120-1125.

234.   Nagase, H., Karaki, H., Ozaki, H., & Azuma, H. (1987, January). Palytoxin, a novel and potent platelet activator. In *JAPANESE JOURNAL OF PHARMACOLOGY* (Vol. 43, pp. P290-P290). EDITORIAL OFF, KANTOHYA BLDG GOKOMACHI-EBISUGAWA NAKAGYO-KU, KYOTO 604, JAPAN: JAPANESE PHARMACOLOGICAL SOC.

235.   Jonathan R, Deeds JR, Michael D, Schwartz B. Human risk associated with palytoxin exposure. *Toxicon*. 2010, 56(2):150–162.

236.   Aligizaki, K., Katikou, P., Milandri, A., & Diogène, J. (2011). Occurrence of palytoxin-group toxins in seafood and future strategies to complement the present state of the art. *Toxicon*, *57*(3), 390-399.

237.   Randall, J. E. (2005). Review of clupeotoxism, an often fatal illness from the consumption of clupeoid fishes. *Pacific science*, *59*(1), 73-77.

238.   Alcala, A. C., Alcala, L. C., Garth, J. S., Yasumura, D., & Yasumoto, T. (1988). Human fatality due to ingestion of the crab Demania reynaudii that contained a palytoxin-like toxin. *Toxicon*, *26*(1), 105-107.

239.   Noguchi T, Hwang DF, Arakawa O, Daigo K, Sato S, Ozaki H, Kawai N, Ito M, Hashimoto K. Palytoxin as the causative agent in parrotfish poisonning In: *First Asia-Pacific Congress: 1988; Sydney: Toxicon*. 1988: 34-34.

240.   Wattenberg, E. V. (2007). Palytoxin: exploiting a novel skin tumor promoter to explore signal transduction and carcinogenesis. *American Journal of Physiology-Cell Physiology*, *292*(1), C24-C32.

241.   Wattenberg, E. V., Uemura, D., Byron, K. L., Villereal, M. L., Fujiki, H., & Rosner, M. R. (1989). Structure-activity studies of the nonphorbol tumor promoter palytoxin in Swiss 3T3 cells. *Cancer Research*, *49*(21), 5837-5842.

242.   Ramos, V., & Vasconcelos, V. (2010). Palytoxin and analogs: biological and ecological effects. *Marine Drugs*, *8*(7), 2021-2037.

243.   Ito, E., & Yasumoto, T. (2009). Toxicological studies on palytoxin and ostreocin-D administered to mice by three different routes. *Toxicon*, *54*(3), 244-251-

244.   Ciminiello, P., Dell'Aversano, C., Dello Iacovo, E., Forino, M., Tartaglione, L., Pelin, M., ... & Bignami, G. (2014). Stereoisomers of 42-hydroxy palytoxin from Hawaiian Palythoa toxica and P. tuberculosa: stereostructure elucidation, detection, and biological activities. *Journal of natural products*, *77*(2), 351-357.

245.   Del Favero, G., Sosa, S., Poli, M., Tubaro, A., Sbaizero, O., & Lorenzon, P. (2014). In vivo and in vitro effects of 42-hydroxy-palytoxin on mouse skeletal muscle: Structural and functional impairment. *Toxicology letters*, *225*(2), 285-293.

246.   Pelin, M., Boscolo, S., Poli, M., Sosa, S., Tubaro, A., & Florio, C. (2013). Characterization of palytoxin binding to HaCaT cells using a monoclonal anti-palytoxin antibody. *Marine drugs*, *11*(3), 584-598.

247.   Poli, M., Ruiz-Olvera, P., Nalca, A., Ruiz, S., Livingston, V., Frick, O., ... & Deeds, J. (2018). Toxicity and pathophysiology of palytoxin congeners after intraperitoneal and aerosol administration in rats. *Toxicon*, *150*, 235-250.

248.   Nabout, J. C., da Silva Rocha, B., Carneiro, F. M., & Sant'Anna, C. L. (2013). How many species of Cyanobacteria are there? Using a discovery curve to predict the species number. *Biodiversity and conservation*, *22*(12), 2907-2918.

249.   Chaurasia, A. (2015). Cyanobacterial biodiversity and associated ecosystem services: introduction to the special issue.

250.   Paerl, H. W., & Otten, T. G. (2013). Harmful cyanobacterial blooms: causes, consequences, and controls. *Microbial ecology*, *65*(4), 995-1010.

251.   Sivonen, K., & Jones, G. (1999). Cyanobacterial toxins. *Toxic cyanobacteria in water: a guide to their public health consequences, monitoring and management*, *1*, 43-112.

252.   Jones, M. R., Pinto, E., Torres, M. A., Doerr, F., Mazur-Marzec, H., Szubert, K., ... & Janssen, E. M. L. (2020). Comprehensive database of secondary metabolites from cyanobacteria. *BioRxiv*.

253.   Gkelis, S., Lanaras, T., & Sivonen, K. (2015). Cyanobacterial toxic and bioactive peptides in freshwater bodies of Greece: Concentrations, occurrence patterns, and implications for human health. *Marine drugs*, *13*(10), 6319-6335.

254.   Costa, M., Costa-Rodrigues, J., Fernandes, M. H., Barros, P., Vasconcelos, V., & Martins, R. (2012). Marine cyanobacteria compounds with anticancer properties: A review on the implication of apoptosis. *Marine drugs*, *10*(10), 2181-2207.

255.   Zainuddin, E., Mundt, S., Wegner, U., & Mentel, R. (2002). Cyanobacteria a potential source of antiviral substances against influenza virus. *Medical microbiology and immunology*, *191*(3), 181-182.

256.   Bláha, L., Babica, P., & Maršálek, B. (2009). Toxins produced in cyanobacterial water blooms-toxicity and risks. *Interdisciplinary toxicology*, *2*(2), 36-41.

257.   Huisman, J., Codd, G. A., Paerl, H. W., Ibelings, B. W., Verspagen, J. M., & Visser, P. M. (2018). Cyanobacterial blooms. *Nature Reviews Microbiology*, *16*(8), 471-483.

258.   Ferrão-Filho, A. D. S., & Kozlowsky-Suzuki, B. (2011). Cyanotoxins: bioaccumulation and effects on aquatic animals. *Marine drugs*, *9*(12), 2729-2772.

259.   Mazur, H., & Plinski, M. (2001). Stability of cyanotoxins, microcystin-LR, microcystin-RR and nodularin in seawater and BG-11 medium of different salinity. *Oceanologia*, *43*(3), 329-339.

260.   Meriluoto, J., Spoof, L., & Codd, G. A. (Eds.). (2017). *Handbook of cyanobacterial monitoring and cyanotoxin analysis*. John Wiley & Sons.

261.   Bouaïcha, N., Miles, C. O., Beach, D. G., Labidi, Z., Djabri, A., Benayache, N. Y., & Nguyen-Quang, T. (2019). Structural diversity, characterization and toxicology of microcystins. *Toxins*, *11*(12), 714..

262.   Janssen, E. M. L. (2019). Cyanobacterial peptides beyond microcystins–a review on co-occurrence, toxicity, and challenges for risk assessment. *Water Research*, *151*, 488-499.

263.   Jokela, J., Heinilä, L. M., Shishido, T. K., Wahlsten, M., Fewer, D. P., Fiore, M. F., ... & Sivonen, K. (2017). Production of high amounts of hepatotoxin nodularin and new protease inhibitors pseudospumigins by the Brazilian benthic Nostoc sp. CENA543. *Frontiers in microbiology*, *8*, 1963.

264.   Pearson, L., Mihali, T., Moffitt, M., Kellmann, R., & Neilan, B. (2010). On the chemistry, toxicology and genetics of the cyanobacterial toxins, microcystin, nodularin, saxitoxin and cylindrospermopsin. *Marine drugs*, *8*(5), 1650-1680.

265.   Puschner, B., and Moore, C. (2013). Chapter 43 pag 533-540. *Cyanobacteria in small animal toxicology* (Third Edition), Editor(s): Michael E. Peterson, Patricia A. Talcott, W.B. Saunders, ISBN 9781455707171.

266.   Harada, K. I., Imanishi, S., Kato, H., Mizuno, M., Ito, E., & Tsuji, K. (2004). Isolation of Adda from microcystin-LR by microbial degradation. *Toxicon*, *44*(1), 107-109.

267.   Fontanillo, M., & Köhn, M. (2018). Microcystins: Synthesis and structure–activity relationship studies toward PP1 and PP2A. *Bioorganic & medicinal chemistry*, *26*(6), 1118-1126.

268.   Llana-Ruiz-Cabello, M., Jos, A., Cameán, A., Oliveira, F., Barreiro, A., Machado, J., ... & Freitas, M. (2019). Analysis of the Use of Cylindrospermopsin and/or Microcystin-Contaminated Water in the Growth, Mineral Content, and Contamination of Spinacia oleracea and Lactuca sativa. *Toxins*, *11*(11), 624.

269.   Yoshida, T., Makita, Y., Nagata, S., Tsutsumi, T., Yoshida, F., Sekijima, M., ... & Ueno, Y. (1997). Acute oral toxicity of microcystin-LR, a cyanobacterial hepatotoxin, in mice. *Natural Toxins*, *5*(3), 91-95.

270.   Mallia, V., Ivanova, L., Eriksen, G. S., Harper, E., Connolly, L., & Uhlig, S. (2020). Investigation of in vitro endocrine activities of Microcystis and Planktothrix cyanobacterial strains. *Toxins*, *12*(4), 228.

271.   Chen, C., Liu, W., Wang, L., Li, J., Chen, Y., Jin, J., ... & Zhang, X. (2016). Pathological damage and immunomodulatory effects of zebrafish exposed to microcystin-LR. *Toxicon*, *118*, 13-20.

272.   Harke, M. J., Steffen, M. M., Gobler, C. J., Otten, T. G., Wilhelm, S. W., Wood, S. A., & Paerl, H. W. (2016). A review of the global ecology, genomics, and biogeography of the toxic cyanobacterium, Microcystis spp. *Harmful algae*, *54*, 4-20.

273.   Li, J., & Persson, K. M. (2020). Quick detection method for paralytic shellfish toxins (PSTs) monitoring in freshwater-a review. *Chemosphere*, 128591-128591.

274.   Hall, S., & Strichartz, G. (1990). *Marine Toxins Origin, Structure, and Molecular Pharmacology*. ARMY MEDICAL RESEARCH INST OF INFECTIOUS DISEASES FORT DETRICK MD.

275.   Negri, A., Stirling, D., Quilliam, M., Blackburn, S., Bolch, C., Burton, I., ... & Willis, R. (2003). Three novel hydroxybenzoate saxitoxin analogues isolated from the dinoflagellate Gymnodinium catenatum. *Chemical Research in Toxicology*, *16*(8), 1029-1033.

276.   Dell'Aversano, C., Tartaglione, L., Polito, G., Dean, K., Giacobbe, M., Casabianca, S., ... & Turner, A. D. (2019). First detection of tetrodotoxin and high levels of paralytic shellfish poisoning toxins in shellfish from Sicily (Italy) by three different analytical methods. *Chemosphere*, *215*, 881-892.

277.   Bricelj, V. M., & Shumway, S. E. (1998). Paralytic shellfish toxins in bivalve molluscs: occurrence, transfer kinetics, and biotransformation. *Reviews in Fisheries Science*, *6*(4), 315-383.

278.   Llewellyn, L., Negri, A., & Robertson, A. (2006). Paralytic shellfish toxins in tropical oceans. *Toxin Reviews*, *25*(2), 159-196.

279.   Sivonen, K., & Jones, G. (1999). Cyanobacterial toxins. *Toxic cyanobacteria in water: a guide to their public health consequences, monitoring and management*, *1*, 43-112.

280. Christensen, V. G., & Khan, E. (2020). Freshwater neurotoxins and concerns for human, animal, and ecosystem health: A review of anatoxin-a and saxitoxin. *Science of the Total Environment*, *736*, 139515.

281. Kao, C. Y. (1966). Tetrodotoxin, saxitoxin and their significance in the study of excitation phenomenon. *Pharm. Rev.*, *18*, 997-1.

282. Campbell, K., Rawn, D. F., Niedzwiadek, B., & Elliott, C. T. (2011). Paralytic shellfish poisoning (PSP) toxin binders for optical biosensor technology: problems and possibilities for the future: a review. *Food Additives and Contaminants*, *28*(6), 711-725.

283. Wiese, M., D'agostino, P. M., Mihali, T. K., Moffitt, M. C., & Neilan, B. A. (2010). Neurotoxic alkaloids: saxitoxin and its analogs. *Marine drugs*, *8*(7), 2185-2211.

284. Genenah, A. A., & Shimizu, Y. (1981). Specific toxicity of paralytic shellfish poisons. *Journal of agricultural and food chemistry*, *29*(6), 1289-1291.

285. Shams, S., Capelli, C., Cerasino, L., Ballot, A., Dietrich, D. R., Sivonen, K., & Salmaso, N. (2015). Anatoxin-a producing Tychonema (Cyanobacteria) in European waterbodies. *Water research*, *69*, 68-79.

286. Namikoshi, M., Murakami, T., Watanabe, M. F., Oda, T., Yamada, J., Tsujimura, S., ... & Oishi, S. (2003). Simultaneous production of homoanatoxin-a, anatoxin-a, and a new non-toxic 4-hydroxyhomoanatoxin-a by the cyanobacterium Raphidiopsis mediterranea Skuja. *Toxicon*, *42*(5), 533-538.

287. Carmichael, W. W. (1992). Cyanobacteria secondary metabolites—the cyanotoxins. *Journal of applied bacteriology*, *72*(6), 445-459.

288. Chorus, I., & Welker, M. (2021). *Toxic cyanobacteria in water: a guide to their public health consequences, monitoring and management* (p. 858). Taylor & Francis.

289. Codd, G., Bell, S., Kaya, K., Ward, C., Beattie, K., & Metcalf, J. (1999). Cyanobacterial toxins, exposure routes and human health. *European Journal of Phycology*, *34*(4), 405-415.

290. Cox, P. A., Banack, S. A., & Murch, S. J. (2003). Biomagnification of cyanobacterial neurotoxins and neurodegenerative disease among the Chamorro people of Guam. *Proceedings of the National Academy of Sciences*, *100*(23), 13380-13383.

291. Moreira, C., Azevedo, J., Antunes, A., & Vasconcelos, V. (2013). Cylindrospermopsin: Occurrence, methods of detection and toxicology. *Journal of applied microbiology*, *114*(3), 605-620.

292.	Cartmell, C., Evans, D. M., Elwood, J. M., Fituri, H. S., Murphy, P. J., Caspari, T., ... & Rzymski, P. (2017). Synthetic analogues of cyanobacterial alkaloid cylindrospermopsin and their toxicological 286. activity. *Toxicology in Vitro*, *44*, 172-181-

293.	Humpage, A. R., Fontaine, F., Froscio, S., Burcham, P., & Falconer, I. R. (2005). Cylindrospermopsin genotoxicity and cytotoxicity: role of cytochrome P-450 and oxidative stress. *Journal of Toxicology and Environmental Health, Part A*, *68*(9), 739-753.

294.	Sivonen, K. (1996). Cyanobacterial toxins and toxin production. *Phycologia*, *35*(sup6), 12-24.

295.	Speziale, B. J., & Dyck, L. A. (1992). Lyngbya infestations: comparative taxonomy of lyngbya wollei comb. Nov.(cyanobacteria) 1. *Journal of Phycology*, *28*(5), 693-706.

296.	Smith, M. L., Westerman, D. C., Putnam, S. P., Richardson, S. D., & Ferry, J. L. (2019). Emerging Lyngbya wollei toxins: A new high resolution mass spectrometry method to elucidate a potential environmental threat. *Harmful algae*, *90*, 101700.

297.	Taylor, M. S., Stahl-Timmins, W., Redshaw, C. H., & Osborne, N. J. (2014). Toxic alkaloids in Lyngbya majuscula and related tropical marine cyanobacteria. *Harmful algae*, *31*, 1-8.

298.	Rzymski, P., & Poniedzialek, B. (2012). Dermatotoxins synthesized by blue-green algae (Cyanobacteria). *Postepy Dermatologii i Alergologii*, *29*(1), 47.

299.	Gemma, S., Molteni, M., & Rossetti, C. (2016). Lipopolysaccharides in cyanobacteria: a brief overview. *Advances in Microbiology*, *6*(5), 391-397.

300.	Raziuddin, S., Siegelman, H. W., & Tornabene, T. G. (1983). Lipopolysaccharides of the cyanobacterium Microcystis aeruginosa. *European journal of biochemistry*, *137*(1-2), 333-336.

301.	Zervou, S. K., Gkelis, S., Kaloudis, T., Hiskia, A., & Mazur-Marzec, H. (2020). New microginins from cyanobacteria of Greek freshwaters. *Chemosphere*, *248*, 125961.

302.	Lodin-Friedman, A., & Carmeli, S. (2018). Microginins from a Microcystis sp. bloom material collected from the Kishon Reservoir, Israel. *Marine drugs*, *16*(3), 78.

303.	Stewart, A. K., Ravindra, R., Van Wagoner, R. M., & Wright, J. L. (2018). Metabolomics-guided discovery of microginin peptides from cultures of the cyanobacterium Microcystis aeruginosa. *Journal of natural products*, *81*(2), 349-355.

304. Spoof, L., Błaszczyk, A., Meriluoto, J., Cegłowska, M., & Mazur-Marzec, H. (2016). Structures and activity of new anabaenopeptins produced by Baltic Sea cyanobacteria. *Marine drugs*, *14*(1), 8.

305. Christiansen, G., Philmus, B., Hemscheidt, T., & Kurmayer, R. (2011). Genetic variation of adenylation domains of the anabaenopeptin synthesis operon and evolution of substrate promiscuity. *Journal of bacteriology*, *193*(15), 3822-3831.

306. Entfellner, E., Frei, M., Christiansen, G., Deng, L., Blom, J., & Kurmayer, R. (2017). Evolution of anabaenopeptin peptide structural variability in the cyanobacterium Planktothrix. *Frontiers in microbiology*, *8*, 219.

307. Kodani, S., Komaki, H., Hemmi, H., Miyake, Y., Kaweewan, I., & Dohra, H. (2018). Streptopeptolin, a Cyanopeptolin-Type Peptide from Streptomyces olivochromogenes. *ACS omega*, *3*(7), 8104-8110.

308. Mazur-Marzec, H., Fidor, A., Cegłowska, M., Wieczerzak, E., Kropidłowska, M., Goua, M., ... & Edwards, C. (2018). Cyanopeptolins with trypsin and chymotrypsin inhibitory activity from the cyanobacterium Nostoc edaphicum CCNP1411. *Marine drugs*, *16*(7), 220.

309. Bister, B., Keller, S., Baumann, H. I., Nicholson, G., Weist, S., Jung, G., ... & Jüttner, F. (2004). Cyanopeptolin 963A, a chymotrypsin inhibitor of Microcystis PCC 7806. *Journal of natural products*, *67*(10), 1755-1757.

310. Welker, M., Maršálek, B., Šejnohová, L., & Von Doehren, H. (2006). Detection and identification of oligopeptides in Microcystis (cyanobacteria) colonies: toward an understanding of metabolic diversity. *Peptides*, *27*(9), 2090-2103.

311. United States Environmental Protection Agency (EPA). Cyanobacteria and cyanotoxins: information for drinking water systems. EPA-810F1101, September 2014.

312. More, S. J., Bampidis, V., Benford, D., Bennekou, S. H., Bragard, C., Halldorsson, T. I., ... & Hogstrand, C. (2019). Guidance on harmonised methodologies for human health, animal health and ecological risk assessment of combined exposure to multiple chemicals. *Efsa journal*, *17*(3).

313. World Health Organization (WHO). Cyanobacterial toxins: microcystin-LR in drinking-water. Background document for development of WHO Guidelines for drinking-water quality WHO/SDE/WSH/03.04/57. Originally published in *Guidelines for drinking-water quality, 2nd ed. Addendum to Vol. 2. Health criteria and other supporting information.* Geneva, 1998.

314. Papadimitriou, T., Kagalou, I., Stalikas, C., Pilidis, G., & Leonardos, I. D. (2012). Assessment of microcystin distribution and biomagnification in tissues of aquatic food web compartments from a shallow lake and evaluation of potential risks to public health. *Ecotoxicology*, *21*(4), 1155-1166..

315. Cheng, Y. S., Yue, Z., Irvin, C. M., Kirkpatrick, B., & Backer, L. C. (2007). Characterization of aerosols containing microcystin. *Marine drugs*, *5*(4), 136-150.

316. Metcalf, J. S., & Codd, G. A. (2020). Co-occurrence of cyanobacteria and cyanotoxins with other environmental health hazards: impacts and implications. *Toxins*, *12*(10), 629.

317. World Health Organization (WHO). Cyanobacterial toxins: microcystins. Background document for development of WHO Guidelines for drinking-water quality and guidelines for safe recreational water environments, WHO/HEP/ECH/WSH/2020.6.

318. World Health Organization (WHO). Cyanobacterial toxins: cylinrospermopsins. Background document for development of WHO Guidelines for drinking-water quality and guidelines for safe recreational water environments, WHO/HEP/ECH/WSH/2020.4.

319. World Health Organization (WHO). Cyanobacterial toxins: anatoxin-a and analogues. Background document for development of WHO Guidelines for drinking-water quality and guidelines for safe recreational water environments, WHO/HEP/ECH/WSH/2020.1.

320. World Health Organization (WHO). Cyanobacterial toxins: saxitoxins. Background document for development of WHO Guidelines for drinking-water quality and guidelines for safe recreational water environments, WHO/HEP/ECH/WSH/2020.8.

321. Filatova, D., Picardo, M., Núñez,, O., & Farré, M. (2020). Analysis, levels and seasonal variation of cyanotoxins in freshwater ecosystems. Trends in Environmental Analytical Chemistry, e00091.

Chapter 2: Development of a Data Dependent acquisition-based approach for the identification of unknown cyclic imines and their ester metabolites in seafood.

1. Introduction

Cyclic imines (CIs) are an assorted group of naturally-occurring toxic compounds globally distributed that share common structural motifs and toxicological properties [1]. They are produced by heterogenous species of microalgal dinoflagellates belonging to the genus *Alexandrium*, *Karenia*, *Vulcanodinium* and *Prorocentrum*, and classified into different sub-groups: pinnatoxins (PnTXs), pteriatoxins (PtTXs), spirolides (SPXs), gymnodimines (GYMs), prorocentrolides, spiroprorocentroimine and portimines [2]. CIs are characterized by a 5-membered (portimines), or 6-membered (GYMs, prorocentrolides and spiroprorocentroimines) or 7-membered (PnTXs, PtTXs and SPXs) spiroimine which is linked to a cyclohexene moiety, both harbored in a 14-27 atom-sized macrocyclic structure featuring ether rings (**Fig.I.2-6**). The only exception is represented by prorocentrolides which replace the spiroimine with a hexahydroisoquinoline group [3].

CIs are often referred to as ''fast acting-toxins'' due to the rapid beginning of neurological symptoms and fast death that occurs in mice when they are injected intraperitoneally [4]. The CI-poisoning syndrome lies into their mechanism of action: CIs are antagonists of muscle-type and neuronal nicotinic acetylcholine receptors (nAChRs) [5]. Although several intoxication episodes occurred in Japan between 1970s and '80s have been attributed to the consumption of CI-contaminated seafood, to date no human poisoning has been unequivocally linked to their presence in shellfish [6-8]. However they are frequently found in environmental and shellfish samples from Europe, and the lack of exhaustive acute and chronic toxicological data, in association with poor information on their distribution through the food chain, has prevented the EFSA from making an accurate risk assessment for consumers and no guidelines have been suggested yet [9]. Nonetheless, CIs may pose a serious threat to human well-being and more efforts are required before a meaningful regulation can be established. In addition, the growing number of new CI congeners detected in seafood, combined with the finding of their ester derivatives due to shellfish metabolism, makes the situation even more complicated [10].

CIs are polar liposoluble compounds that are co-extracted with other classes of regulated lipophilic marine biotoxins (LMBs) such as: diarrheic shellfish poisoning (DSPs; okadaic acid, dinophysistoxins and pectenotoxins) toxins, neurotoxic shellfish poisoning (NSPs; brevetoxins) toxins and Azaspiracid Shellfish Poisoning (AZP; azaspiracids) toxins. Until a few years ago, the EU reference method for monitoring the presence of LMBs in seafood was the mouse bioassay (MBA). Considering the specific and rapid onset of neurological symptoms in mice shortly after the injection of ''fast acting toxins'', the MBA has been widely employed for the detection of CIs in the frame of monitoring programs [11]. However, a questionable specificity, a poor sensitivity and the impossibility to investigate the toxic profile of contaminated shellfish represent the main drawback of such an assay [12]. To date, the MBA is no more the EU official method to survey the presence of LMBs in seafood mainly because of ethical concerns related to animal distress, and it has been replaced by a LC-MS/MS approach. As a consequence, European authorities promoted the monitoring of CIs by means of the same technique including them within the suspect list of toxins [13]. Nonetheless, a variety of techniques, each of them characterized by advantages and downsides, have been implemented during the years to monitor the presence of CIs in shellfish. Among the bio-molecular methods, fluorescent polarization [14-15] and solid-phase receptor-based assay [16] have been employed. Although these methods are quick and technically easy, they showed a number of restrictions. The impossibility to detect toxins that act with different mechanisms, the paucity of validation studies, as well as the lack of information on the toxic profile are the main disadvantages of the fluorescent polarization methods. Differently, the main drawbacks of solid-phase receptor-based assays are: the requirement of animal tissues and radiolabel, a low selectivity, matrix-interference, and the necessity to further confirm positive samples through other instrumental analytical techniques [17]. The physical-chemical properties of CIs associated with the need to monitor the presence of a wide number of structural congeners in one test run, designated the reverse-phase (RP) liquid chromatography a suitable approach to resolve complex toxin mixtures. However, the lack of chromophores in the molecules hampered to develop highly specific and sensitive RP-LC methods based on optical detection, with HPLC-UV being the only one employed [9,18]. This limitation was overcame thanks to the coupling of liquid chromatography with mass spectrometry (MS) since the presence of the imine function makes well suited CIs to the electrospray (ESI) ionization, and the usage od acidic or alkaline conditions combined with optional solid-phase extraction (SPE) greatly reduces the matrix

interference [19-20]. As a result, a wide range of sensitive and effective LC-MS and LC-MS/MS methods have been proposed [17]. Although instrumentation is expensive, and the availability of expert personnel and analytical standards are a prerequisite, LC-MS has been designated as method of choice for the determination of CIs in complex matrices [2]. In this perspective, the continuous finding of new CIs and their metabolites in shellfish, as well as the detection of known congeners for which appropriate standards are not available, make the untargeted LC-HRMS approach the most valid methodology for bringing to light new intriguing findings [21].

The present study describes the development of a high effective and sensitive LC-HRMS method for the detection of GYMs, PnTXs and SPXs in complex matrixes and its application to real shellfish samples collected from the Mediterranean basin (Tunisia and Italy) and the Atlantic coast of Spain (Galicia). The configuration of a data-dependent acquisition (DDA) based-approach allowed to discover typical and, for the first time, atypical fatty ester acid ester metabolites of GYMs in one Tunisian shellfish sample. This finding prompted to the development of a new analytical strategy, termed as ''backward analysis'', which led to the identification of new GYM analogues, for which a tentative-structural characterization was performed on the basis of their fragmentation pattern. The study of distribution of CIs along the food chain revealed the widespread presence of PnTX-G and 13desMeSPX-C in Galician mussels, the first detection of PnTX-G from raw *Mytilus galloprovincialis* harvested along the Sardinian coastline (South Italy) and a very high GYMs contamination level in Tunisian mussels.

2. Results and discussion

2.1 LC-HRMS method

2.1.1 Optimization of chromatography and MS conditions

A mixture of PnTX-G, GYM-A, 13desMeSPX-C (certified reference material; CRM) and PnTX-A (non-CRM) was prepared and used to optimize the chromatographic and MS conditions. The chromatographic method was developed by exploiting the polar lipophilic nature of such compounds, and considering the large chemical variability within the whole CI family, a versatile C8 base deactivated silica column (BDS) was exploited. The carbon-nitrogen double bond (C=N) of the cyclic imine function is mildly basic and partially polarized, thus it confers a high degree of polarity to CIs although their backbone structure is hydrophobic. Therefore, the best

chromatographic settings were achieved by using: acetonitrile as organic modifier, since it is a polar-aprotic solvent with a strong dipole moment, and additives such as formic acid, which decreases the signal suppression, and the ammonium formate, which improves the separation on column. The RP gradient-elution under the optimized chromatographic setting provided sharp and narrow peaks for each toxin, with the only exception for PnTX-A, whose higher polarity due to the presence of the COOH group gave a tailed-peak (**Fig. II.1**). Nonetheless, an excellent resolution between 2 PnTX standards was observed, and a high separation efficiency between GYM-A, 13desMeSPX-C and PnTX-G was achieved. However, the peak tailing observed for PnTX-A provided only a moderate resolution with GYM-A since their peaks were partially overlapped. Despite of that, these two toxins could be unambiguously identified and individually quantified by MS due to their different molecular masses.
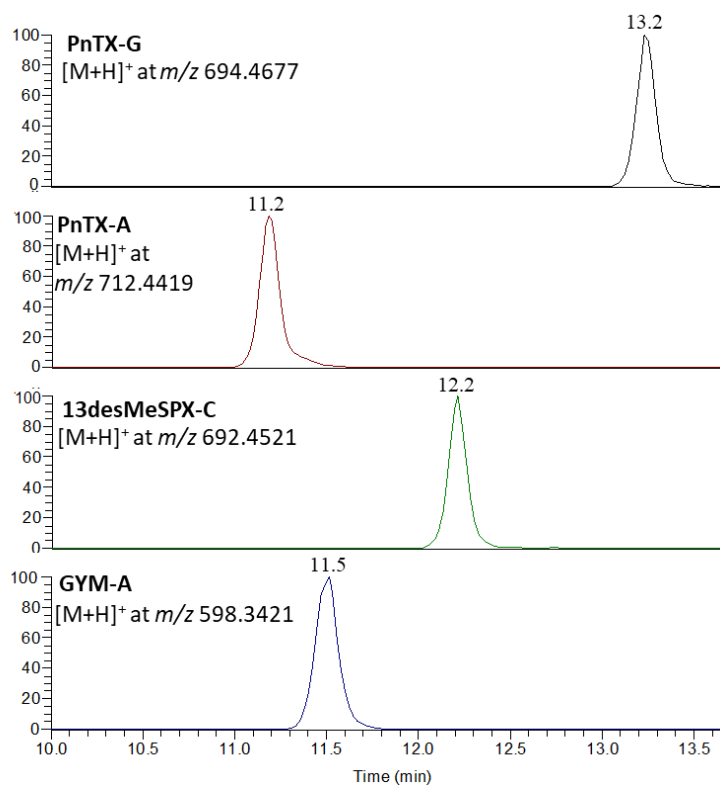
Figure II.1 Chromatographic separation of CI standards.

Under the optimized chromatographic conditions, the HR-ESI$^+$-MS spectrum of PnTX-G, -A and 13desMeSPX-C was characterized by a very intense [M+H]$^+$ ion, whilst GYM-A underwent a

significant in-source fragmentation resulting in the presence of a $[M+H-H_2O]^+$ ion and a $[M+H]^+$ ion in the relative ion ratio of 25:100 (**Fig.II2**). No in-source fragmentation occurred for PnTX-G, -A and 13desMeSPX-C, and no adduct ions were observed in the HRMS spectra of such toxins.
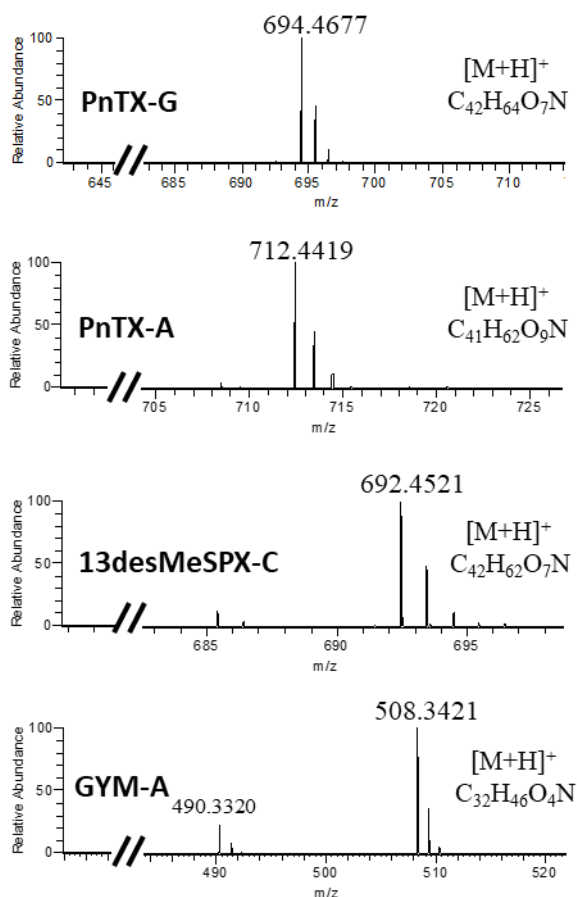
Figure II.2. HR full-scan MS spectrum of PnTX-G, -A, 13desMeSPX-C and GYM-A standard.

$HRMS^2$ conditions were investigated ramping manually the collision energies (CEs) in two different fragmentation modes: high-resolution collision induced dissociation (CID) and higher-energy collisional dissociation (HCD). For each toxin, the CID MS^2 spectrum obtained by selecting the relevant $[M+H]^+$ ion as precursor was dominated by a very intense $[M+H-H_2O]^+$ fragment, while diagnostic structural fragments were noticeably less intense. In addition, the diagnostic fragment ions at m/z 164.1432 ($C_{11}H_{18}N^+$) and 136.1119 ($C_9H_{14}N^+$) representative for 7-membered (PnTXs and SPXs) and 6-membered (GYMs) CIs [22-23] were not detectable by CID MS^2 due to the low-mass cutoff (LMCO) on the m/z range imposed by the activation Q parameter, which is

typically set on ion trap MS analyzers at 0.25 [24]. With the aim to enlarge the *m/z* range and then reduce the LMCO, the activation Q value was reduced, but a noticeable decrease in sensitivity was observed and this hampered the detection of such diagnostic fragments at appreciable levels. An alternative strategy was employed to overcome this restriction: the $[M+H-H_2O]^+$ fragment obtained through a first MS^2 scan was further fragmented through CID MS^3 experiments. As a consequence, the diagnostic fragments at *m/z* 164.1432 and 136.1119 were observed, but this approach provided less informative fragmentation patterns for each toxin and also up to 6-fold reduced sensitivity compared to that achieved by HCD MS^2 experiments. For this reason, the latter was selected as method of choice for the analysis of CIs (**Fig.II.3a-d**). A first look to the HCD fragmentation patterns revealed that the retro-Diels-Alder ring opening gave rise to most of the diagnostic fragments, including radicals, thus becoming the main fragmentation pathway for each standard. On the other hand, a careful investigation of the HCD spectra allowed to identify a further fragmentation pathway, which allowed to elucidated fragment ions that have never been reported so far (**Table II.1-4**). All these information extrapolated from the analysis of CI standards turned out to be the starting point for the toxin identification in real shellfish samples, and for designing the DDA experiment.
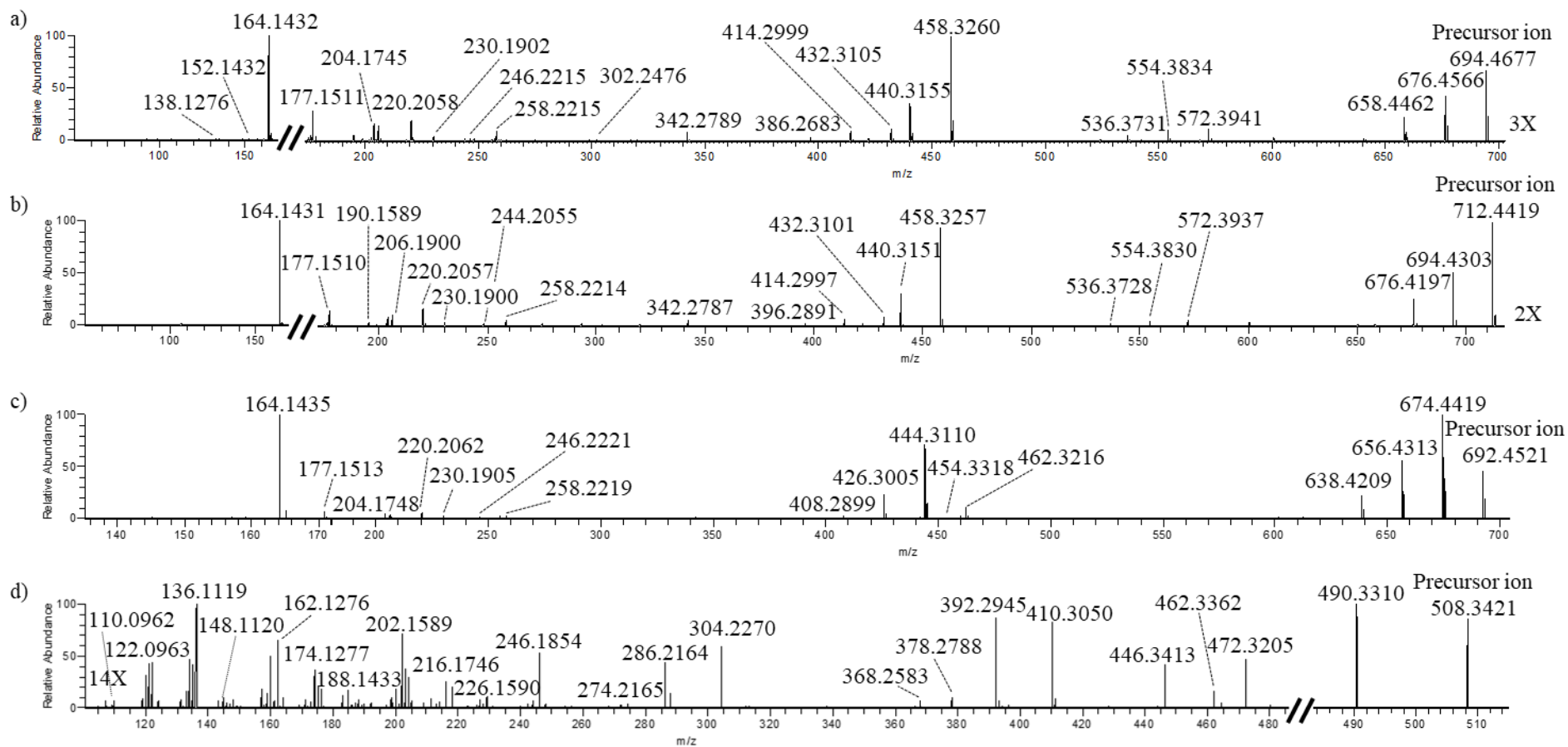
Figure II.3. HR HCD MS^2 spectrum of: a) PnTX-G, b) PnTX-A, c) 13desMeSPX-C and d) GYM-A. For ion assignment refers to tables II.1-4.

Table II.1 Assignment of fragment ions of PnTX-G to relevant cleavages. The most intense ion for each cleavage is reported in bold. Cleavages marked in red, to the best of my knowledge, have never been reported in literature.

Clv	m/z	Formula	RDB	Δ
#1	**138.1276**	$\mathbf{C_9H_{16}N^+}$	**2.5**	**-1.058**
	136.1119	$C_9H_{14}N^+$	3.5	-1.587
#2	**152.1432**	$\mathbf{C_{10}H_{18}N^+}$	**2.5**	**-0.961**
#3	166.1589	$C_{11}H_{20}N^+$	2.5	-1.060
	164.1432	$\mathbf{C_{11}H_{18}N^+}$	**3.5**	**-0.890**
	163.1354	$C_{11}H_{17}N^{\cdot+}$	4.0	-0.865
	162.1275	$C_{11}H_{16}N^+$	4.5	-1.394
#4	178.1589	$C_{12}H_{20}N^+$	3.5	-0.877
	177.1511	$\mathbf{C_{12}H_{19}N^{\cdot+}}$	**4.0**	**-0.797**
	176.1432	$C_{12}H_{18}N^+$	4.5	-0.886
#5	206.1902	$C_{14}H_{24}N^+$	3.5	-0.807
	204.1745	$\mathbf{C_{14}H_{22}N^+}$	**4.5**	**-0.814**
	202.1589	$C_{14}H_{20}N^+$	5.5	-0.674
#6	**220.2058**	$\mathbf{C_{15}H_{26}N^+}$	**3.5**	**-0.710**
	218.1902	$C_{15}H_{24}N^+$	4.5	-0.671
	217.1823	$C_{15}H_{23}N^{\cdot+}$	5.0	-0.881
	216.1746	$C_{15}H_{22}N^+$	5.5	-0.390
#7	248.2008	$C_{16}H_{26}ON^+$	4.5	-0.568
	231.1981	$C_{16}H_{25}N^{\cdot+}$	5.0	-0.006
	230.1902	$\mathbf{C_{16}H_{24}N^+}$	**5.5**	**-0.723**
	228.1749	$C_{16}H_{22}N^+$	6.5	0.981
#8	262.2163	$C_{17}H_{28}ON^+$	4.5	-1.072
	246.2215	$\mathbf{C_{17}H_{28}N^+}$	**4.5**	**-0.514**
	244.2058	$C_{17}H_{26}N^+$	5.5	-.5990
#9	276.2319	$C_{18}H_{30}ON^+$	4.5	-1.018
	274.2165	$C_{18}H_{28}ON^+$	5.5	-0.002
	260.2371	$C_{18}H_{30}N^+$	4.5	-0.794
	259.2293	$C_{18}H_{29}N^{\cdot+}$	5.0	-0.661
	258.2215	$\mathbf{C_{18}H_{28}N^+}$	**5.5**	**-0.528**
	256.2057	$C_{18}H_{26}N^+$	6.5	-1.157
#10	320.2584	$C_{20}H_{34}O_2N^+$	4.5	-0.174
	304.2634	$C_{20}H_{34}ON^+$	4.5	-0.234
	302.2476	$\mathbf{C_{20}H_{32}ON^+}$	**5.5**	**-0.632**
	286.2526	$C_{20}H_{32}N^+$	5.5	-1.211

Clv	m/z	Formula	RDB	Δ
#11	358.2732	$C_{23}H_{36}O_2N^+$	6.5	-2.277
	342.2789	$\mathbf{C_{23}H_{36}ON^+}$	**6.5**	**-0.530**
#12	404.2792	$C_{24}H_{38}O_4N^+$	6.5	-0.953
	386.2683	$\mathbf{C_{24}H_{36}O_3N^+}$	**7.5**	**-1.813**
	368.2590	$C_{24}H_{34}O_2N^+$	8.5	1.695
#13	**432.3105**	$\mathbf{C_{26}H_{42}O_4N^+}$	**6.5**	**-0.752**
	414.2999	$C_{26}H_{40}O_3N^+$	7.5	-0.750
	398.3061	$C_{26}H_{40}O_2N^+$	7.5	1.943
	396.2895	$C_{26}H_{38}O_2N^+$	8.5	-0.646
#14	460.3419	$C_{28}H_{46}O_4N^+$	6.5	-0.598
	458.3260	$\mathbf{C_{28}H_{44}O_4N^+}$	**7.5**	**-1.015**
	440.3156	$C_{28}H_{42}O_3N^+$	8.5	-0.865
	422.3050	$C_{28}H_{40}O_2N^+$	9.5	-0.867
#15	474.3576	$C_{29}H_{48}O_4N^+$	6.5	-0.328
	456.3468	$\mathbf{C_{29}H_{46}O_3N^+}$	**7.5**	**-0.988**
#16	500.3376	$C_{30}H_{46}O_5N^+$	8.5	1.119
#17	542.3837	$C_{33}H_{52}O_5N^+$	8.5	-0.627
	524.3728	$\mathbf{C_{33}H_{50}O_4N^+}$	**9.5**	**-1.212**
	506.3637	$C_{33}H_{48}O_3N^+$	10.5	1.637
#18	**572.3941**	$\mathbf{C_{34}H_{54}O_6N^+}$	**8.5**	**-0.707**
	554.3834	$C_{34}H_{52}O_5N^+$	9.5	-1.046
	536.3731	$C_{34}H_{50}O_4N^+$	10.5	-0.663
	518.3628	$C_{34}H_{48}O_3N^+$	11.5	-0.156
#19	586.4093	$C_{35}H_{56}O_6N^+$	8.5	-1.475
	568.3989	$\mathbf{C_{35}H_{54}O_5N^+}$	**9.5**	**-1.267**
	566.3850	$C_{35}H_{52}O_5N^+$	10.5	1.801
	550.3880	$C_{35}H_{52}O_4N^+$	10.5	-1.954
#20	**286.2163**	$\mathbf{C_{19}H_{28}ON^+}$	**6.5**	**-1.017**

Clv = Cleavage; RDB= Ring Double Bond equivalents; Δ= error, ppm; R= rearrangement.

Table II.2 Assignment of fragment ions of PnTX-A to relevant cleavages. The most intense ion for each cleavage is reported in bold. Cleavages marked in red, to the best of my knowledge, have never been reported in literature.

Pinnatoxin A	Clv	m/z	Formula	RDB	Δ	Clv	m/z	Formula	RDB	Δ
	#1	**152.1432**	**C$_{10}$H$_{18}$N$^+$**	**2.5**	**-1.421**	#9	320.2581	C$_{20}$H$_{34}$O$_2$N$^+$	4.5	-0.799
							302.2473	**C$_{20}$H$_{32}$ON$^+$**	**5.5**	**-1.460**
							286.2524	C$_{20}$H$_{32}$N$^+$	5.5	-1.770
	#2	166.1587	C$_{11}$H$_{20}$N$^+$	2.5	-1.662	#10	**342.2787**	**C$_{23}$H$_{36}$ON$^+$**	**6.5**	**-0.997**
		164.1431	**C$_{11}$H$_{18}$N$^+$**	**3.5**	**-1.317**					
	#3	178.1588	C$_{12}$H$_{20}$N$^+$	3.5	-1.438	#11	**432.3101**	**C$_{26}$H$_{42}$O$_4$N$^+$**	**6.5**	**-1.238**
		177.1510	**C$_{12}$H$_{19}$N$^{•+}$**	**4.0**	**-1.248**		414.2997	C$_{26}$H$_{40}$O$_3$N$^+$	7.5	-1.257
		176.1431	C$_{12}$H$_{18}$N$^+$	4.5	-1.397		396.2891	C$_{26}$H$_{38}$O$_2$N$^+$	8.5	-1.226
	#4	**206.1900**	**C$_{14}$H$_{24}$N$^+$**	**3.5**	**-1.243**	#12	458.3257	C$_{28}$H$_{44}$O$_4$N$^+$	7.5	-1.430
		204.1744	C$_{14}$H$_{22}$N$^+$	4.5	-1.157		440.3151	C$_{28}$H$_{42}$O$_3$N$^+$	8.5	-1.410
		202.1589	C$_{14}$H$_{20}$N$^+$	5.5	-0.674		**422.3050**	**C$_{28}$H$_{40}$O$_2$N$^+$**	**9.5**	**-0.796**
	#5	**220.2057**	**C$_{15}$H$_{26}$N$^+$**	**3.5**	**-1.119**	#13	542.3831	C$_{33}$H$_{52}$O$_5$N$^+$	8.5	-1.641
		218.1902	C$_{15}$H$_{24}$N$^+$	4.5	-0.671		**524.3724**	**C$_{33}$H$_{50}$O$_4$N$^+$**	**9.5**	**-1.975**
		216.1743	C$_{15}$H$_{22}$N$^+$	5.5	-1.602		506.3637	C$_{33}$H$_{48}$O$_3$N$^+$	10.5	1.637
	#6	248.2005	C$_{16}$H$_{26}$ON$^+$	4.5	-1.374	#14	**572.3937**	**C$_{34}$H$_{54}$O$_6$N$^+$**	**8.5**	**-0.690**
		230.1900	**C$_{16}$H$_{24}$N$^+$**	**5.5**	**-1.070**		554.3830	C$_{34}$H$_{52}$O$_5$N$^+$	9.5	-1.028
							536.3728	C$_{34}$H$_{50}$O$_4$N$^+$	10.5	-0.961
							518.3628	C$_{34}$H$_{48}$O$_3$N$^+$	11.5	-0.156
	#7	262.2162	C$_{17}$H$_{28}$ON$^+$	4.5	-1.339	#15	586.4093	C$_{35}$H$_{56}$O$_6$N$^+$	8.5	-1.475
		246.2215	C$_{17}$H$_{28}$N$^+$	4.5	-0.635		**568.3989**	**C$_{35}$H$_{54}$O$_5$N$^+$**	**9.5**	**-1.267**
		244.2055	**C$_{17}$H$_{26}$N$^+$**	**5.5**	**-1.787**		566.3850	C$_{35}$H$_{52}$O$_5$N$^+$	10.5	1.801
	#8	260.2370	C$_{18}$H$_{30}$N$^+$	4.5	-1.024	#16	668.4534	C$_{40}$H$_{62}$O$_7$N$^+$	10.5	2.005
		259.2291	C$_{18}$H$_{29}$N$^{•+}$	5.0	-1.240		**650.4404**	**C$_{40}$H$_{60}$O$_6$N$^+$**	**11.5**	**-1.714**
		258.2214	**C$_{18}$H$_{28}$N$^+$**	**5.5**	**-0.761**					
						#17	190.1589	C$_{13}$H$_{20}$N$^+$	4.5	-0.611

Clv = Cleavage; RDB= Ring Double Bond equivalents; Δ= error, ppm; R= rearrangement.

Table II.3 Assignment of fragment ions of 13desMeSPX-C to relevant cleavages. The most intense ion for each cleavage is reported in bold. Cleavages marked in red, to the best of my knowledge, have never been reported in literature.

13desmethylSpirolide-C	Clv	m/z	Formula	RDB	Δ	Clv	m/z	Formula	RDB	Δ
	#1	153.1515	$C_{10}H_{19}N^{\cdot+}$	2.0	2.016	#11	358.2745	$C_{23}H_{36}O_2N^+$	6.5	1.212
		152.1435	**$C_{10}H_{18}N^+$**	**2.5**	**0.551**		**342.2794**	**$C_{23}H_{36}ON^+$**	**6.5**	**0.814**
							340.2644	$C_{23}H_{34}ON^+$	7.5	2.759
	#2	166.1589	$C_{11}H_{20}N^+$	2.5	-1.060	#12	404.2791	$C_{24}H_{38}O_4N^+$	6.5	-1.052
		164.1435	**$C_{11}H_{18}N^+$**	**3.5**	**-0.890**		**386.2691**	**$C_{24}H_{36}O_3N^+$**	**7.5**	**0.232**
		162.1275	$C_{11}H_{16}N^+$	4.5	-1.394		368.2588	$C_{24}H_{34}O_2N^+$	8.5	1.152
	#3	178.1591	$C_{12}H_{20}N^+$	3.5	0.246	#13	414.3001	$C_{26}H_{40}O_3N^+$	7.5	-0.436
		177.1513	**$C_{12}H_{19}N^{\cdot+}$**	**4.0**	**0.614**		396.2895	$C_{26}H_{38}O_2N^+$	8.5	-0.444
		176.1436	$C_{12}H_{18}N^+$	4.5	1.101		**394.2746**	**$C_{26}H_{36}O_2N^+$**	**9.5**	**1.405**
	#4	206.1905	$C_{14}H_{24}N^+$	3.5	0.697	#14	446.3268	$C_{27}H_{44}O_4N^+$	6.5	0.638
		204.1748	**$C_{14}H_{22}N^+$**	**4.5**	**0.851**		**444.3110**	**$C_{27}H_{42}O_4N^+$**	**7.5**	**0.393**
		202.1592	$C_{14}H_{20}N^+$	5.5	0.761		428.3161	$C_{27}H_{42}O_3N^+$	7.5	0.512
							426.3005	$C_{27}H_{40}O_3N^+$	8.5	0.585
							408.2899	$C_{27}H_{38}O_2N^+$	9.5	0.549
	#5	**220.2062**	**$C_{15}H_{26}N^+$**	**3.5**	**0.743**	#15	**460.3426**	**$C_{28}H_{46}O_4N^+$**	**6.5**	**1.053**
		218.1907	$C_{15}H_{24}N^+$	4.5	1.896		458.3248	$C_{28}H_{44}O_4N^+$	7.5	-3.633
		216.1749	$C_{15}H_{22}N^+$	5.5	0.896		442.3320	$C_{28}H_{44}O_3N^+$	7.5	0.970
		214.1596	$C_{15}H_{20}N^+$	6.5	2.633		424.3212	$C_{28}H_{42}O_2N^+$	8.5	0.551
	#6	248.2012	$C_{16}H_{26}ON^+$	4.5	1.084	#16	472.3421	$C_{29}H_{46}O_4N^+$	7.5	-0.181
		232.2060	$C_{16}H_{26}N^+$	4.5	-0.114		**454.3318**	**$C_{29}H_{44}O_3N^+$**	**8.5**	**0.571**
		230.1905	**$C_{16}H_{24}N^+$**	**5.5**	**0.885**		436.3216	$C_{29}H_{42}O_2N^+$	9.5	1.292
		228.1748	$C_{16}H_{22}N^+$	6.5	0.718					
	#7	**246.2221**	**$C_{17}H_{28}N^+$**	**4.5**	**1.842**	#17	**522.3577**	**$C_{33}H_{48}O_4N^+$**	**10.5**	**-0.183**
		244.2063	$C_{17}H_{26}N^+$	5.5	1.448		504.3462	$C_{33}H_{46}O_3N^+$	11.5	-2.123
		242.1912	$C_{17}H_{24}N^+$	6.5	3.731					
	#8	260.2375	$C_{18}H_{30}N^+$	4.5	0.897	#18	596.4304	$C_{37}H_{58}O_5N^+$	9.5	-0.889
		259.2296	$C_{18}H_{29}N^{\cdot+}$	5.0	0.689		**577.4129**	**$C_{37}H_{55}O_4N^{\cdot+}$**	**11.0**	**0.640**
		258.2219	**$C_{18}H_{28}N^+$**	**5.5**	**0.750**		576.4047	$C_{37}H_{54}O_4N^+$	11.5	0.025
		256.2061	$C_{18}H_{26}N^+$	6.5	0.600					
	#9	320.2584	$C_{20}H_{34}O_2N^+$	4.5	-0.174	#19	630.4514	$C_{41}H_{60}O_4N^+$	12.5	-0.374
		304.2648	$C_{20}H_{34}ON^+$	4.5	4.170		613.4463	$C_{41}H_{59}O_3N^{\cdot+}$	13.0	-4.281
		302.2481	**$C_{20}H_{32}ON^+$**	**5.5**	**0.923**		**612.4418**	**$C_{41}H_{58}O_3N^+$**	**13.5**	**1.076**
		284.2376	$C_{20}H_{30}N^+$	6.5	1.208		594.4318	$C_{41}H_{56}O_2N^+$	14.5	2.126
	#10	**332.2586**	**$C_{21}H_{34}O_2N^+$**	**5.5**	**0.584**	#20	562.3898	$C_{36}H_{52}O_4N^+$	11.5	1.341
		298.2526	$C_{21}H_{32}N^+$	6.5	-1.162					

Clv = Cleavage; RDB= Ring Double Bond equivalents; Δ= error, ppm; R= rearrangement.

Table II.4 Assignment of fragment ions of GYM-A to relevant cleavages. The most intense ion for each cleavage is reported in bold. Cleavages marked in red, to the best of my knowledge, have never been reported in literature.

	m/z, formula, RDB, Δ	Clv	m/z, formula, RDB, Δ	Clv	m/z, formula, RDB, Δ
GYM-A					
[M+H]$^+$	508.3425, $C_{32}H_{46}O_4N^+$, 10.5, -0.148	#7	218.1902, $C_{15}H_{24}N^+$, 4.5, -0.350	#14	366.2791, $C_{25}H_{36}ON^+$, 8.5, -0.003
[M+H-H$_2$O]$^+$	**490.3310, $C_{32}H_{44}O_3N^+$, 11.5, -1.429**		217.1825, $C_{15}H_{23}N^{•+}$, 5.0, -0.052		**350.2842, $C_{25}H_{36}N^+$, 8.5, 0.009**
[M+H-2H$_2$O]$^+$	508.3425, $C_{32}H_{42}O_3N^+$, 12.5, -1.093		**216.1746, $C_{15}H_{22}N^+$, 5.5, -0.445**	#15	411.3130, $C_{27}H_{41}O_2N^{•+}$, 8.0, -0.537
Clv			215.1668, $C_{15}H_{21}N^{•+}$, 6.0, -0.099		410.3050, $C_{27}H_{40}O_2N^+$, 8.5, -0.843
#1	**110.0962, $C_7H_{12}N^+$, 2.5, -1.598**		214.1590, $C_{15}H_{20}N^+$, 6.5, -0.169		394.3106, $C_{27}H_{40}ON^+$, 8.5, 0.301
#2	124.1119, $C_8H_{14}N^+$, 2.5, -1.257		212.1434, $C_{15}H_{18}N^+$, 7.5, -0.076		393.3025, $C_{27}H_{39}ON^{•+}$, 9.0, -0.423
	122.0963, $C_8H_{12}N^+$, 3.5, -1.277	#8	248.2010, $C_{16}H_{26}ON^+$, 4.5, 0.318		**392.2945, $C_{27}H_{38}ON^+$, 9.5, -0.666**
	121.0884, $C_8H_{11}N^{•+}$, 4.0, -1.329		**246.1854, $C_{16}H_{24}ON^+$, 5.5, -0.207**		374.2837, $C_{27}H_{36}N^+$, 10.5, -1.514
	120.0806, $C_8H_{10}N^+$, 4.5, -1.382		244.1695, $C_{16}H_{22}ON^+$, 6.5, -0.536	#16	480.3472, $C_{31}H_{46}O_3N^+$, 9.5, -0.022
#3	**136.1119, $C_9H_{14}N^+$, 3.5, -1.073**		228.1747, $C_{16}H_{22}N^+$, 6.5, 0.236		**462.3362, $C_{31}H_{44}O_2N^+$, 10.5, -0.965**
	135.1041, $C_9H_{13}N^{•+}$, 4.0, -0.970		226.1590, $C_{16}H_{20}N^+$, 7.5, -0.337		444.3258, $C_{31}H_{42}ON^+$, 11.5, -0.543
	134.0963, $C_9H_{12}N^+$, 4.5, -1.014	#9	260.2009, $C_{17}H_{26}ON^+$, 5.5, -0.081	#17	**464.3520, $C_{31}H_{46}O_2N^+$, 9.5, -0.573**
	132.0806, $C_9H_{10}N^+$, 5.5, -1.483		246.2212, $C_{17}H_{28}N^+$, 4.5, -1.813		446.3413, $C_{31}H_{44}ON^+$, 10.5, -0.989
#4	164.1432, $C_{11}H_{18}N^+$, 3.5, -0.708		**244.2060, $C_{17}H_{26}N^+$, 5.5, -0.261**		428.3303, $C_{31}H_{42}N^+$, 11.5, -1.954
	163.1355, $C_{11}H_{17}N^{•+}$, 4.0, -0.129		242.1901, $C_{17}H_{24}N^+$, 6.5, -0.934	#18	**368.2583, $C_{24}H_{34}O_2N^+$, 8.5, -0.233**
	162.1276, $C_{11}H_{16}N^+$, 4.5, -0.593		240.1747, $C_{17}H_{22}N^+$, 7.5, 0.999	#19	396.2896, $C_{26}H_{38}O_2N^+$, 8.5, -0.192
	161.1198, $C_{11}H_{15}N^{•+}$, 5.0, -0.503	#10	**274.2165, $C_{18}H_{28}ON^+$, 5.5, -0.077**		**378.2788, $C_{26}H_{36}ON^+$, 9.5, -0.796**
	160.1120, $C_{11}H_{14}N^+$, 5.5, -0.662		272.2008, $C_{18}H_{26}ON^+$, 6.5, -0.187	#20	190.1591, $C_{13}H_{20}N^+$, 4.5, 0.651
	158.0964, $C_{11}H_{12}N^+$, 6.5, -0.038		258.2218, $C_{18}H_{28}N^+$, 5.5, 0.827		189.1512, $C_{13}H_{19}N^{•+}$, 5.0, 0.100
#5	192.1381, $C_{12}H_{18}ON^+$, 4.5, -0.889		256.2061, $C_{18}H_{26}N^+$, 6.5, 0.365		**188.1433, $C_{13}H_{18}N^+$, 5.5, -0.617**
	178.1591, $C_{12}H_{20}N^+$, 3.5, 0.358		254.1902, $C_{18}H_{24}N^+$, 7.5, -0.418		186.1278, $C_{13}H_{16}N^+$, 6.5, 0.397
	176.1433, $C_{12}H_{18}N^+$, 4.5, -0.546		252.1745, $C_{18}H_{22}N^+$, 8.5, -0.501	#21	148.1120, $C_{10}H_{14}N^+$, 4.5, -0.716
	175.1355, $C_{12}H_{17}N^{•+}$, 5.0, -0.349	#11	**304.2270, $C_{19}H_{30}O_2N^+$, 5.5, -0.413**		**146.0964, $C_{10}H_{12}N^+$, 5.5, -0.383**
	174.1277, $C_{12}H_{16}N^+$, 5.5, -0.379		302.2119, $C_{19}H_{28}O_2N^+$, 6.5, 1.371		
	172.1120, $C_{12}H_{14}N^+$, 6.5, -0.267		288.2321, $C_{19}H_{30}ON^+$, 5.5, -0.247		
#6	205.1824, $C_{14}H_{23}N^{•+}$, 4.0, -0.689		286.2164, $C_{19}H_{28}ON^+$, 6.5, -0.353		
	204.1746, $C_{14}H_{22}N^+$, 4.5, -0.520		284.2004, $C_{19}H_{26}ON^+$, 7.5, -1.798		
	203.1668, $C_{14}H_{21}N^{•+}$, 5.0, -0.449		268.2057, $C_{19}H_{26}N^+$, 7.5, -0.956		
	202.1589, $C_{14}H_{20}N^+$, 5.5, -0.476		266.1907, $C_{19}H_{24}N^+$, 8.5, 1.517		
	201.1511, $C_{14}H_{19}N^{•+}$, 6.0, -0.503	#12	**312.2375, $C_{21}H_{30}ON^+$, 7.5, 0.317**		
	200.1433, $C_{14}H_{18}N^+$, 6.5, -0.380	#13	325.2401, $C_{22}H_{31}ON^{•+}$, 8.0, 0.227		
	198.1276, $C_{14}H_{16}N^+$, 7.5, -0.434		**324.2316, $C_{22}H_{30}ON^+$, 8.5, -1.854**		

Clv = Cleavage; RDB= Ring Double Bond equivalents; Δ= error, ppm; R= rearrangement.

2.1.2 Matrix effect, limits of detection and quantification, and linearity

The CI standard mixture was used to investigate the matrix interference on the LC-HRMS response and the effectiveness of the optimized method. At this purpose, a blank matrix extract was prepared and used to get 6-points matrix-matched (MM) calibration curves. Following the same procedure, a 6-levels matrix-free (MF) calibration curve was obtained. The most concentrated level of MF and MM curves were diluted up to the lowest quantifiable and detectable level with the aim to measure the instrumental limits of quantitation (LOQ) and identification (LOD). The comparison between the LC-MS analyses of MF and MM standards revealed that chromatographic parameters were not affected by matrix since retention time and peak shape of MM and MF standards were superimposable (**Fig.II.1, Fig.II.4**), while a significant matrix interference was observed on the HRMS response (**Table II.5**).
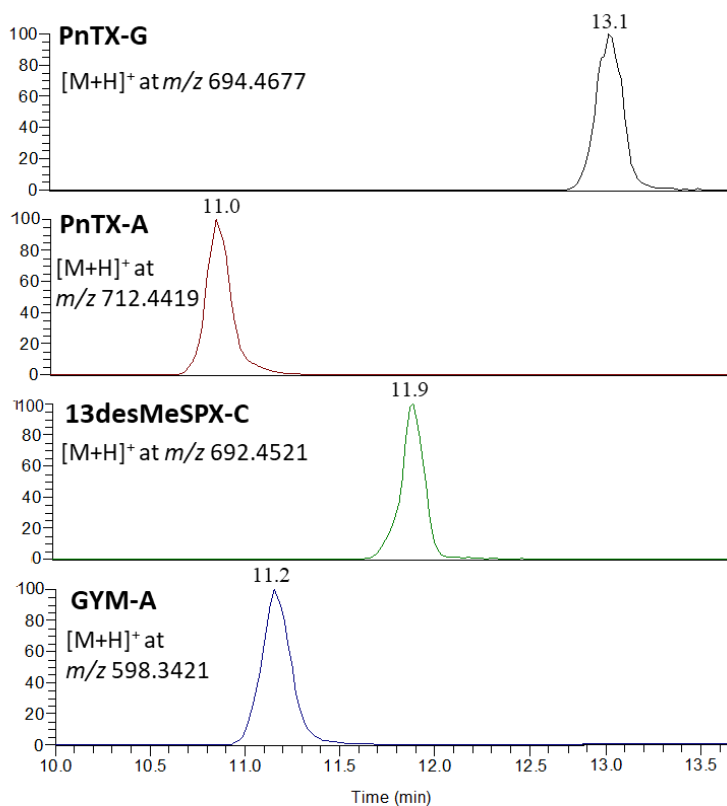
Figure II.4 Chromatographic separation of matrix-matched (MM) CI standards.

For PnTX-G a remarkable suppression of the signal (37-49%) was measured, whilst for PnTX-A the matrix-interference was almost negligible within the whole concentration range tested.

Contrarily, a concentration-dependent matrix effect was observed for GYM-A and 13desMeSPX-C. Particularly, GYM-A showed an ion enhancement effect (20%) at the most diluted point and suppression (2-19%) at the most concentrated levels, while 13-desMeSPX-C gave a noteworthy suppression (28-41%) of the signal at the most diluted points and ion enhancement at the most concentrated ones (37-64%). Considering that the instrumental LOD and LOQ may significantly vary on the base of the status of the instrument calibration, they were empirically measured. It was found that for each toxin, MF and MM standards gave the same LOD and LOQ, which were 0.2 and 0.5 ng/mL for PnTX-G, 0.6 and 1.2 ng/mL for GYM-A, 0.9 and 1.7 ng/mL for 13desMeSPX-C and 0.6 and 1.2 ng/mL for PnTX-A, respectively. All calibration curves showed a good linearity with R^2 in the range 0.998-0.999

Table II.5 Matrix effect % (+ suppression, - enhancement) at different concentration levels.

Toxin	ng/mL	Matrix effect %	
PnTX-G	240.0	37	
	120.0	49	
	60.0	47	
	30.0	48	
	15.0	44	
	7.5	41	
PnTX-A	312.5	-9	
	156.3	2	
	78.1	0	
	39.1	-3	
	19.5	-4	
	9.8	-7	

PnTX-G chart:
MF curve; y = 265480x + 427771; R² = 0.9991
MM curve; y = 165181x - 736889; R² = 0.9944

PnTX-A chart:
MF curve; y = 52273x + 178079; R² = 0.9982
MM curve; y = 56377x - 13449; R² = 0.9999

GYM-A	312.5	7
	156.3	16
	78.1	19
	39.1	11
	19.5	2
	9.8	-20

MF curve; y = 163445x + 603242
R² = 0.9984
MM curve; y = 149778x + 140148
R² = 0.9993
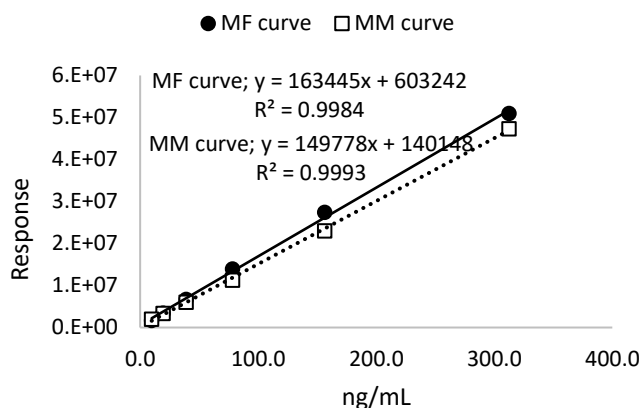
13desMeSPX-C	333.3	-61
	166.7	-47
	83.3	-64
	41.7	-37
	20.8	41
	10.4	28

MF curve; y = 9455.6x + 192.13
R² = 0.9991
MM curve; y = 15385x - 112597
R² = 0.9986
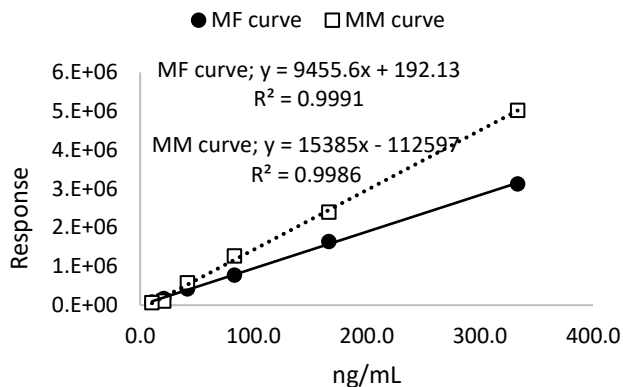
2.2 Application to shellfish samples

Background

In a frame of a collaboration with Dr. Anna Milandri of Centro Ricerche Marine, National Reference Laboratory for Marine Biotoxins (Cesenatico, Italy), 28 homogenized shellfish samples collected from the Mediterranean basin (Italy and Tunisia) and the Atlantic cost of Spain (Galicia) were analyzed. The aim of the collaboration was to investigate the distribution of CIs within the Mediterranean trophic chain. Italian samples (*M. galloprovincialis*) were collected from aquaculture sites located at Goro (Emilia-Romagna) and Tortolì (Sardinia). Spanish mussels were obtained from aquacultures located at Las Rías Baixas, a coastal area commonly known as 'Tropical Galicia', while Tunisian shellfish (*R. decussatus*) were from the gulf of Gabes (Medenine). All data are summarized in **Table II.6**.

Table II.6 List of samples analyzed in this study. Indication of shellfish species, site, GPS coordinates and date of collection, detected toxins, contamination levels (µg/kg) and codes are reported.

Code		Sample	Origin Coordinates (N,W)	Date of collection	Toxins (µg/kg)
A	1	*M. galloprovincialis*	I (Goro, Emilia-Romagna) 44.817885°, 12.272984°	2014/12/11	-
	2				-
B	1	*M. galloprovincialis*	I (Goro, Emilia-Romagna) 44.839438°, 12.309376°	2014/12/11	-
	2				-
C	1	*M. galloprovincialis*	I (Goro, Emilia-Romagna) 44.817044°, 12.345425°	2014/12/11	-
	2				-
D	1	*M. galloprovincialis*	I (Goro, Emilia-Romagna) 44.791341°, 12.348858°	2014/12/11	-
	2				-
E	1	*M. galloprovincialis*	S (Ría de Vigo) 42.28492°, -08.67636°	2014/11/20	PnTX-G (3.8) - 13desMeSPX-C (16.8)
	2				PnTX-G (4.1) - 13desMeSPX-C (28.2)
F	1	*M. galloprovincialis*	S (Ría de Vigo) 42.29749°, -08.64925°	2014/11/20	PnTX-G (4.1) - 13desMeSPX-C (11.0)
	2				PnTX-G (3.1)
G	1	*M. galloprovincialis*	S (Ría de Vigo) 42.26984°, -08.72691°	2014/11/24	PnTX-G (7.7) - 13desMeSPX-C (26.5)
	2				PnTX-G (3.6) - 13desMeSPX-C (20.8)
H	1	*M. galloprovincialis*	S (Ría de Arousa) 42.54834°, -08.89730°	2014/11/18	PnTX-G (6.6) - 13desMeSPX-C (20.4)
	2				PnTX-G (4.1)- 13desMeSPX-C (24.2)
I	1	*M. galloprovincialis*	S (Ría de Arousa) 42.60855°, -08.81869°	2014/11/19	PnTX-G (3.9) - 13desMeSPX-C (29.0)
	2				PnTX-G (3.3) - 13desMeSPX-C (24.7)
L	1	*M. galloprovincialis*	S (Ría de Arousa) 42.50596°, -08.84702°	2014/11/20	PnTX-G (4.0) - 13desMeSPX-C (18.5)
	2				PnTX-G (4.2) - 13desMeSPX-C (24.6)
M	1	*M. galloprovincialis*	S (Ría de Arousa) 42.58605°, -08.82494°	2014/11/25	PnTX-G (3.3) - 13desMeSPX-C (11.6)
	2				PnTX-G (3.6) - 13desMeSPX-C (11.5)
N	1	*M. galloprovincialis*	S (Ría de Pontevedra) 42.40809°, -08.72888°	2014/11/25	PnTX-G (3.4) - 13desMeSPX-C (27.9)
	2				13desMeSPX-C (20.3)
O		*M. galloprovincialis*	I (Cervia, Emilia-Romagna) 44.251575°, 12.338603°	2012/08/14	-
P		*R. decussatus*	T (Medenine) 33.983218°, 10.249182°	2014/03/02	GYM-A (376.5) 5 isobaric GYMs B/C (n.q.) GYM-F, -G, -H, -I,-J (n.q.)
Q		*M. galloprovincialis*	I (Tortolì, Sardegna) 39.944588°, 9.672940°	2016/05/27	PnTX-G (6.8)
R		*R. decussatus*	T (Medenine) 34.302036°, 10.177771°	2014/11/25	-

1=Hepatopancreas; 2=Total flesh; I=Italy; S=Spain; T=Tunisia; - = no toxins were found; n.q.= not quantified; N=Latitude; E=Longitude.

2.2.1 Detection of GYMs in Tunisian shellfish

The application of the LC-HRMS method brough to light the presence of a variety of GYMs in Tunisian *R. decussatus* (sample P; **Table II.6**) collected in March 2014, contrarily to the same shellfish harvested in November (sample R) for which no CIs were detected over the measured instrumental limits. The toxic profile of sample P was found to be dominated by GYM-A, with a high concentration level of 376.5 µg/Kg. The identity of the toxin was confirmed by comparing the retention time at 11.1 min (**Fig.II5a**), the exact mass of the [M+H]$^+$ ion at *m/z* 508.3425 (C$_{32}$H$_{46}$O$_4$N$^+$, RDB=10.5), the isotopic pattern and ion ratio, and the HCD MS^2 spectra (**Fig.II.6a**) with those of the relevant certified standard injected under the same experimental conditions (**Fig.II.1-4, Table II.4**).
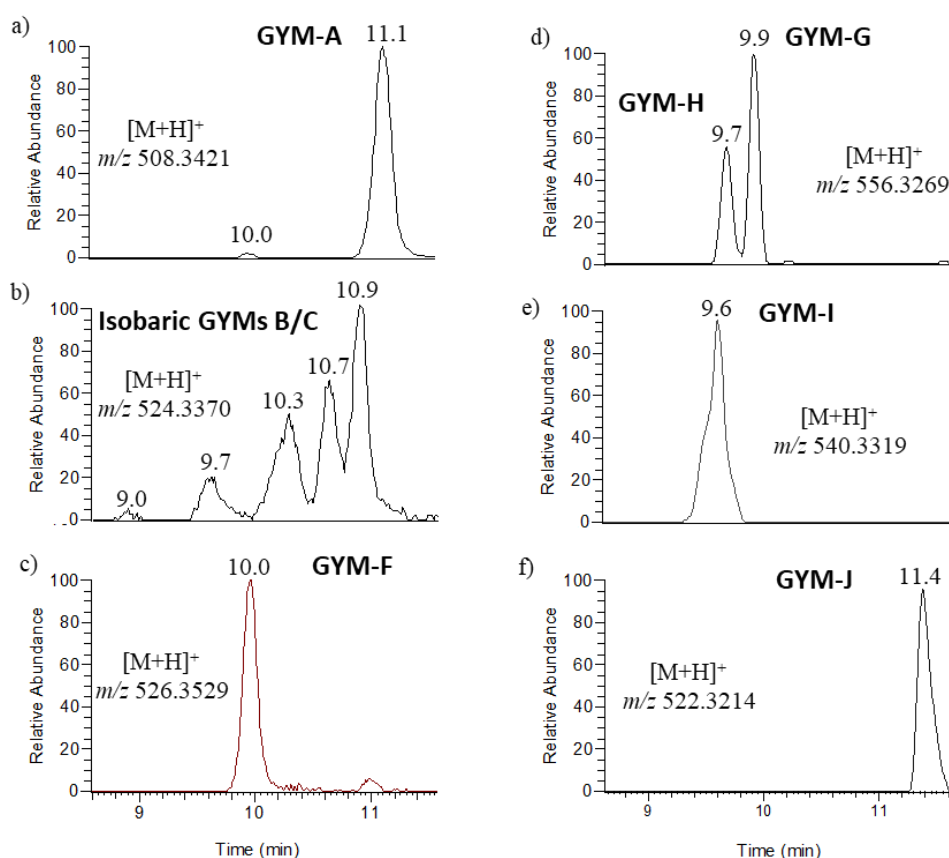
Figure II.5 XIC of: a) GYM-A, b) GYMs B/C, c) GYM-F, d) GYM-G and -H, e) GYM-I and f) GYM-J found in Tunisian sample P.
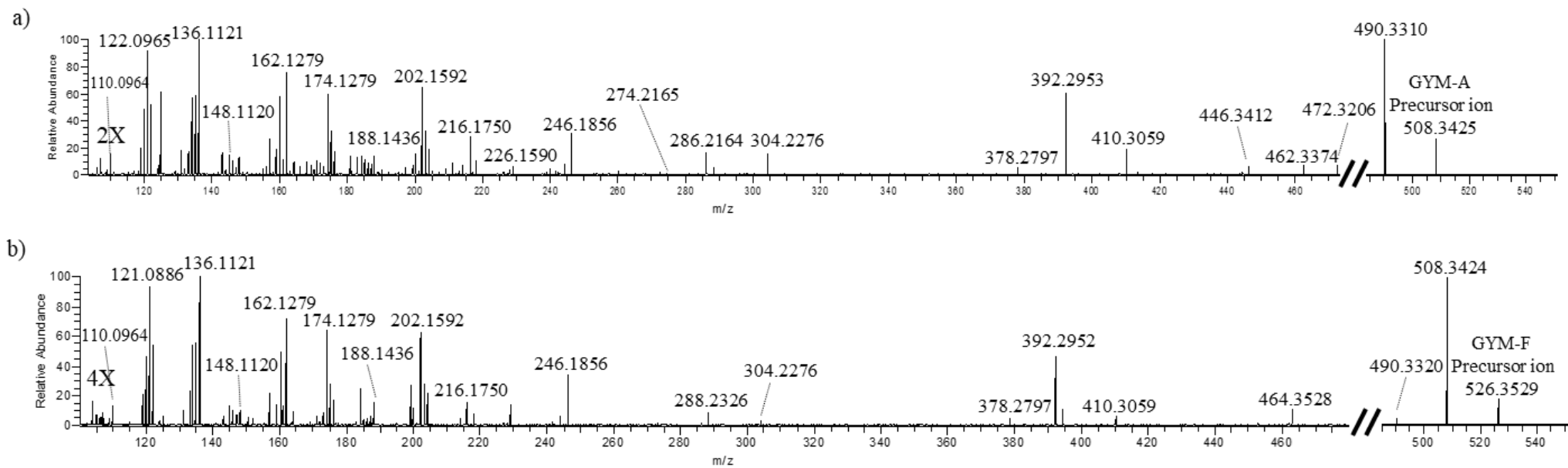
Figure II.6. HR HCD MS^2 spectra of a) GYM-A and b) GYM-F detected in Tunisian sample P. For ion assignments refer to Table II.4 (GYM-A) and Table II.8 (GYM-F).

This finding turned out to be consistent with data reported in a recent surveillance study that was conducted to monitor the presence and the persistence of GYMs in the Gulf of Gabes (North Tunisia), one of the most considerable resources for shellfish production in Tunisia. The authors described that the dinoflagellate *K.selliformis,* one of the GYM-producing organisms, periodically forms massive HABs in this area and, as a consequence, noteworthy toxic levels of GYM-A ranging from 81 to 2136 µg/Kg were found in autochthonous shellfish [25].

The XIC of the ion at *m/z* 524.3370 revealed the presence in the same Tunisian sample of five chromatographic peaks (**Fig.II.5b**) that could be associated with the presence of GYM-B/C/D and/or their new putative congeners. Although these GYMs are isobaric compounds ($C_{32}H_{46}O_5N^+$, RDB=10.5), GYM-B and -C are epimers at C18, whilst GYM-D features a different type-structure, with two tetrahydrofuran moiety in the macrocycle [26]. For this reason, $HRMS^2$ measurements were needed to confirm the identity of such toxins. Therefore, fragmentation experiments selecting the $[M+H]^+$ ion at *m/z* 524.3 as precursor were performed. All peaks showed fragmentation patterns dominated by $[M+H-nH_2O]^+$ (n=1,2) fragments and the less intense GYM diagnostic fragment at *m/z* 136.1119 (**Table II.4**, cleavage #3). None of the key fragments of GYM-D at *m/z* 316.2271 and 346.2377 were found [27], while barely detectable diagnostic fragments for GYM-B/C at *m/z* 304.2269 and 320.2226 emerged from the HCD spectra of peak eluting at 9.7, 10.3, 10.7 and 10.9 minutes (**Table.II.7**, **Fig.II.5b, Fig.II.7**). [28,29]. Nevertheless, in lack of appropriate standards for GYMs at *m/z* 524.3370, no conclusions could be drawn on the identity of those 5 peaks.
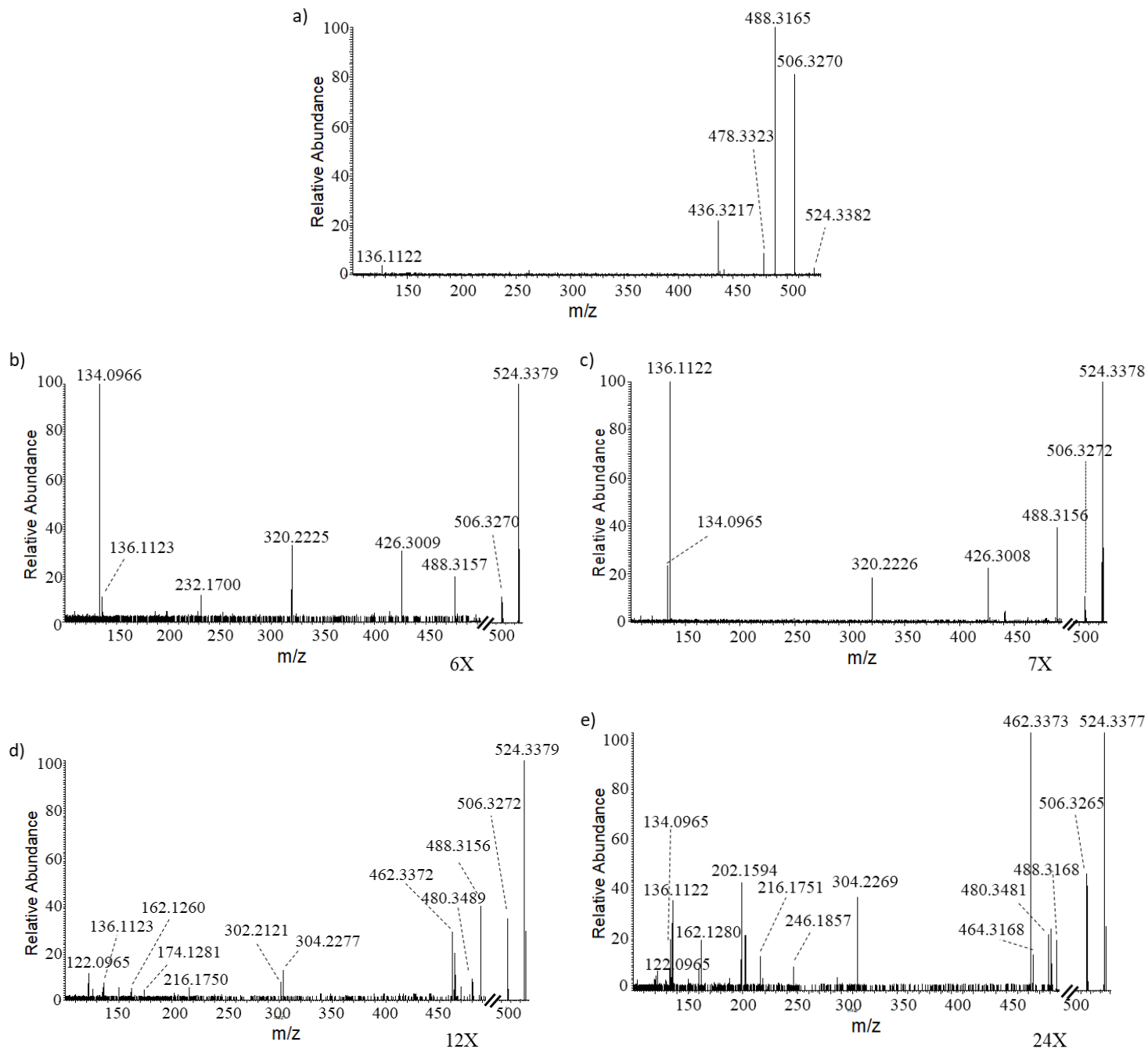
Figure II.7 HR HCD MS^2 spectrum of GYM analogues at m/z 524.3370 eluting at a) 9.0 min, b) 9.7 min, c) 10.3 min, d) 10.7 min and e) 10.9 min. For ion assignment refer to **Table II.7**.

Table II.7 Assignment of fragments contained in the LC-HRMS^2 spectra of isobaric GYMs at *m/z* 524.3370 versus GYM-B/C reported by Salgado et al., 2015. For each fragment, the relevant accurate mass, molecular formula, Ring Double Bond equivalents and error (ppm) are reported.

GYM (9.0 min)*	GYM (9.7 min)*	GYM (10.3 min)*	GYM (10.7 min)*	GYM (10.9 min)*	GYM-B/-C analogue (Salgado et al., [29]
524.3382 $C_{32}H_{46}O_5N^+$ 10.5, 2.212	524.3379 $C_{32}H_{46}O_5N^+$ 10.5, 1.716	524.3378 $C_{32}H_{46}O_5N^+$ 10.5, 1.496	524.3379 $C_{32}H_{46}O_5N^+$ 10.5, 1.697	524.3377 $C_{32}H_{46}O_5N^+$ 10.5, 1.163	524.3375 $C_{32}H_{46}O_5N^+$ 10.5, 1.240
506.3270 $C_{32}H_{44}O_4N^+$ 11.5, 1.016	506.3270 $C_{32}H_{44}O_4N^+$ 11.5, 1.550	506.3272 $C_{32}H_{44}O_4N^+$ 11.5, 1.352	506.3272 $C_{32}H_{44}O_4N^+$ 11.5, 1.431	506.3265 $C_{32}H_{44}O_4N^+$ 11.5, 1.372	506.3257 $C_{32}H_{44}O_4N^+$ 11.5, -1.551
488.3165 $C_{32}H_{42}O_3N^+$ 12.5, 1.125	488.3157 $C_{32}H_{42}O_3N^+$ 12.5, 1.137	488.3156 $C_{32}H_{42}O_3N^+$ 12.5, 1.137	488.3156 $C_{32}H_{42}O_3N^+$ 12.5, 1.137	488.3168 $C_{32}H_{42}O_3N^+$ 12.5, 1.821	488.3147 $C_{32}H_{42}O_3N^+$ 12.5, -2.500
478.3323 $C_{31}H_{44}O_3N^+$ 10.5, 1.504	426.3009 $C_{27}H_{40}O_3N^+$ 8.5, 1.688	426.3008 $C_{27}H_{40}O_3N^+$ 8.5, 1.406	480.3489 $C_{31}H_{46}O_3N^+$ 9.5, 3.454	480.3481 $C_{31}H_{46}O_3N^+$ 9.5, 1.914	470.3039 $C_{32}H_{40}O_2N^+$ 13.5, -3.096
436.3217 $C_{29}H_{42}O_2N^+$ 9.5, 1.590	320.2225 $C_{19}H_{30}O_3N^+$ 5.5, 1.592	320.2226 $C_{19}H_{30}O_3N^+$ 5.5, 1.842	464.3169 $C_{30}H_{42}O_3N^+$ 10.5, 2.195	478.3324 $C_{31}H_{44}O_3N^+$ 10.5, 1.838	462.3358 $C_{31}H_{44}O_2N^+$ 10.5, -1.852
136.1122 $C_9H_{14}N^+$ 3.5, 0.764	232.1700 $C_{15}H_{22}ON^+$ 5.5, 1.719	136.1122 $C_9H_{14}N^+$ 3.5, 0.837	462.3372 $C_{31}H_{44}O_2N^+$ 10.5, 1.198	464.3168 $C_{30}H_{42}O_3N^+$ 10.5, 1.894	368.2569 $C_{24}H_{34}O_2N^+$ 8.5, -4.089
	136.1123 $C_9H_{14}N^+$ 3.5, 0.764	134.0965 $C_9H_{12}N^+$ 4.5, 0.627	304.2277 $C_{19}H_{30}O_2N^+$ 5.5, 2.019	462.3373 $C_{31}H_{44}O_2N^+$ 10.5, 1.414	304.2266 $C_{19}H_{30}O_2N^+$ 5.5, -1.662
	134.0966 $C_9H_{12}N^+$ 4.5, 0.627		302.2121 $C_{19}H_{28}O_2N^+$ 6.5, 2.298	304.2269 $C_{19}H_{30}O_2N^+$ 5.5, -0.512	286.2159 $C_{19}H_{28}ON^+$ 6.5, -2.240
			216.1750 $C_{15}H_{22}N^+$ 5.5, 1.590	246.1857 $C_{16}H_{24}ON^+$ 5.5, 2.027	246.1848 $C_{16}H_{24}ON^+$ 5.5, -1.791
			174.1281 $C_{12}H_{16}N^+$ 5.5, 2.320	216.1751 $C_{15}H_{22}N^+$ 5.5, 1.729	216.1744 $C_{15}H_{22}N^+$ 5.5, -1.278
			162.1260 $C_{11}H_{16}N^+$ 4.5, 1.566	203.1672 $C_{14}H_{21}N^{+\bullet}$ 5.0, 1.864	202.1588 $C_{14}H_{20}N^+$ 5.5, -1.119
			136.1123 $C_9H_{14}N^+$ 3.5, 1.499	202.1594 $C_{14}H_{20}N^+$ 5.5, 1.750	174.1276 $C_{12}H_{16}N^+$ 5.5, -0.724
			122.0965 $C_8H_{12}N^+$ 3.5, 0.606	162.1280 $C_{11}H_{16}N^+$ 4.5, 1.504	162.1275 $C_{11}H_{16}N^+$ 4.5, -1.394
				160.1124 $C_{11}H_{14}N^+$ 5.5, 1.836	136.1119 $C_9H_{14}N^+$ 3.5, -1.293
				136.1122 $C_9H_{14}N^+$ 3.5, 0.690	
				134.0965 $C_9H_{12}N^+$ 4.5, 0.179	
				122.0965 $C_8H_{12}N^+$ 3.5, 0.525	

* = this study

Besides the known GYMs, intriguing findings were made through an in-depth analysis of the same Tunisian sample P. The XIC of the ion at m/z 508.3421 (GYM-A) revealed a further chromatographic peak eluting at 10.0 min, thus suggesting the presence of an isobaric GYM-A in the extract (**Fig.II.5a**). This hypothesis, that turned out to be a misidentification, was initially corroborated through the acquisition of the relevant HCD MS^2 spectrum which was superimposable to that of GYM-A. However, an in-depth analysis of the HR full-scan MS spectrum of the peak at 10.0 min revealed the presence of an intense ion at m/z 526.3529 ($C_{32}H_{48}O_5N^+$, RDB=9.5) which was found to be the [M+H]$^+$ ion of the new compound, while the ion at m/z 508.3421 ($C_{32}H_{46}O_4N^+$, RDB=10.5) was clearly interpreted as in-source fragment due to the loss of a H_2O moiety (**Fig.II.5c, Fig.II.8**). The relative ion ratio between the [M+H]$^+$ and the [M+H-H_2O]$^+$ of the new compound was 100:20. This observation was consistent with the behaviour of GYM-A standard analysed under the same experimental conditions, that presented a relative ion ratio [M+H]$^+$: [M+H-H_2O]$^+$ of 100:25 (**Fig.II.8**).
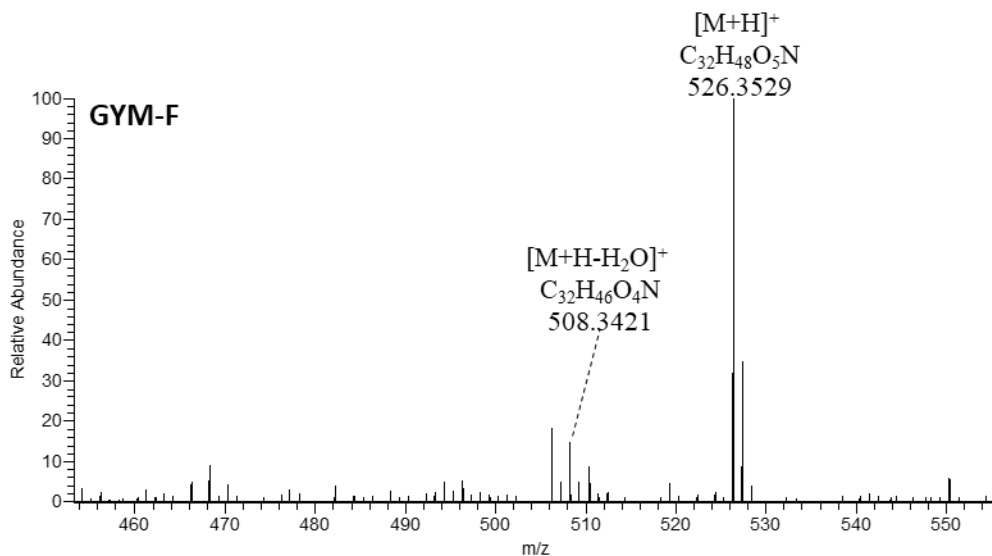
Figure II.8 HR full-scan MS spectrum of GYM-F.

The new GYM analogue at m/z 526.3529 was named GYM-F, and it presented the same nominal but different accurate mass of GYM-E ([M+H]$^+$ ion at m/z 526.3163, $C_{31}H_{44}O_6N^+$), which was recently reported by Zurhelle et al. [26]. With the aim to pull out structural insights for GYM-F, HCD HRMS^2 experiments were performed selecting the ion at m/z 526.3 as precursor. The fragmentation spectra acquired were analysed in parallel with those of GYM-A, and they turned

out to be superimposable (**Fig.II.3d, Fig.II.6b**, **Table II.4, Table II.8**), thus suggesting that the difference in elemental composition between the two compounds (H_2 + O) involved the part structure between C1 and C4, namely the α-methyl butanolide moiety (γ-lactone). This hypothesis was further corroborated by the cross interpretation of fragment ions of GYM-F at *m/z* 392.2952 ($C_{27}H_{38}ON^+$) and *m/z* 464.3528 ($C_{31}H_{46}O_2N^+$) due to the cleavage #15 and #17, respectively (**Table II.8**). Taking into account the main structural modifications so far described within the CI class, two structural hypothesis arose for GYM-F: i) it may lack the C2-C3 double bond while an additional hydroxyl group at C3 (1,4-addition of H_2O at the 2,3 unsaturated γ-lactone moiety of GYM-A) is present, as recently reported for new SPXs [30], or ii) the γ-lactone moiety of GYM-A may undergo hydrolysis, giving rise to a ring opening through the formation of a carboxyl and an hydroxyl group, as observed for PnTX-E [22]. Both reactions could be the result of the biotransformation of GYM-A in shellfish. On the other hand, Harju et al. [27] reported the presence of five isobaric analogues of GYM-F at *m/z* 526.3529 in the extracts of cultured *A. ostenfeldii* collected in the Baltic Sea. However, in lack of MS^2 data, no further correspondence between GYM-F (found in shellfish in this study) and its analogues (found in dinoflagellates by Harju et al.) can be made.

Table II.8 Assignment of fragment ions contained in HR HCD MS^2 spectra of GYM-F. The most intense ion for each cleavage is reported in bold. Inside fragments are reported in red. Proposed planar structure of GYM-F.

GYM-F			
	m/z, formula, RDB, Δ	Clv	*m/z*, formula, RDB, Δ
[M+H]$^+$	526.3529, C$_{32}$H$_{48}$O$_5$N$^+$, 9.5, 0.399	#7	218.1906, C$_{15}$H$_{24}$N$^+$, 4.5, 1.438
[M+H-H$_2$O]$^+$	**508.3424, C$_{32}$H$_{46}$O$_4$N$^+$, 10.5, 0.560**		**216.1750, C$_{15}$H$_{22}$N$^+$, 5.5, 1.405**
[M+H-2H$_2$O]$^+$	490.3320, C$_{32}$H$_{44}$O$_3$N$^+$, 11.5, 0.814		214.1594, C$_{15}$H$_{20}$N$^+$, 6.5, 1.652
[M+H-H$_2$O-CO$_2$]$^+$	**464.3528, C$_{31}$H$_{46}$O$_2$N$^+$, 9.5, 1.020**	#8	**246.1856, C$_{16}$H$_{24}$ON$^+$, 5.5, 1.296**
Clv		#9	**244.2064, C$_{17}$H$_{26}$N$^+$, 5.5, 1.612**
#1	**110.0964, C$_7$H$_{12}$N$^+$, 2.5, -0.145**	#11	304.2276, C$_{19}$H$_{30}$O$_2$N$^+$, 5.5, -1.366
#2	122.0964, C$_8$H$_{12}$N$^+$, 3.5, 0.033		**288.2326, C$_{19}$H$_{30}$ON$^+$, 5.5, 1.349**
	121.0886, C$_8$H$_{11}$N$^{+\bullet}$, 4.0, 0.075		286.2169, C$_{19}$H$_{28}$ON$^+$, 6.5, 2.163
	120.0808, C$_8$H$_{10}$N$^+$, 4.5, 0.034	#15	410.3059, C$_{27}$H$_{40}$O$_2$N$^+$, 8.5, 0.522
#3	**136.1121, C$_9$H$_{14}$N$^+$, 3.5, 0.397**		394.3108, C$_{27}$H$_{40}$ON$^+$, 8.5, 0.953
	135.1043, C$_9$H$_{13}$N$^{+\bullet}$, 4.0, 0.511		**392.2952, C$_{27}$H$_{38}$ON$^+$, 9.5, 1.067**
	134.0965, C$_9$H$_{12}$N$^+$, 4.5, 0.403	#16	**462.3369, C$_{31}$H$_{44}$O$_2$N$^+$, 10.5, 0.506**
#4	164.1435, C$_{11}$H$_{18}$N$^+$, 3.5, 0.937	#17	**464.3528, C$_{31}$H$_{46}$O$_2$N$^+$, 9.5, 1.020**
	162.1279, C$_{11}$H$_{16}$N$^+$, 4.5, 0.949	#19	**378.2797, C$_{26}$H$_{36}$ON$^+$, 9.5, 1.556**
	161.1200, C$_{11}$H$_{15}$N$^{+\bullet}$, 5.0, 0.676	#20	**188.1436, C$_{13}$H$_{18}$N$^+$, 5.5, 1.190**
	160.1122, C$_{11}$H$_{14}$N$^+$, 5.5, 0.899		187.1358, C$_{13}$H$_{17}$N$^{+\bullet}$, 6.0, 1.170
#5	176.1436, C$_{12}$H$_{18}$N$^+$, 4.5, 1.157		186.1280, C$_{13}$H$_{16}$N$^+$, 6.5, 1.472
	175.1357, C$_{12}$H$_{17}$N$^{+\bullet}$, 5.0, 0.964	#21	**148.1120, C$_{10}$H$_{14}$N$^+$, 4.5, 0.297**
	174.1279, C$_{12}$H$_{16}$N$^+$, 5.5, 0.999		146.0965, C$_{10}$H$_{12}$N$^+$, 5.5, 0.644
	172.1123, C$_{12}$H$_{14}$N$^+$, 6.5, 1.127		
#6	204.1750, C$_{14}$H$_{22}$N$^+$, 4.5, 1.439		
	203.1671, C$_{14}$H$_{21}$N$^{+\bullet}$, 5.0, 1.274		
	202.1592, C$_{14}$H$_{20}$N$^+$, 5.5, 1.008		
	200.1436, C$_{14}$H$_{18}$N$^+$, 6.5, 1.069		
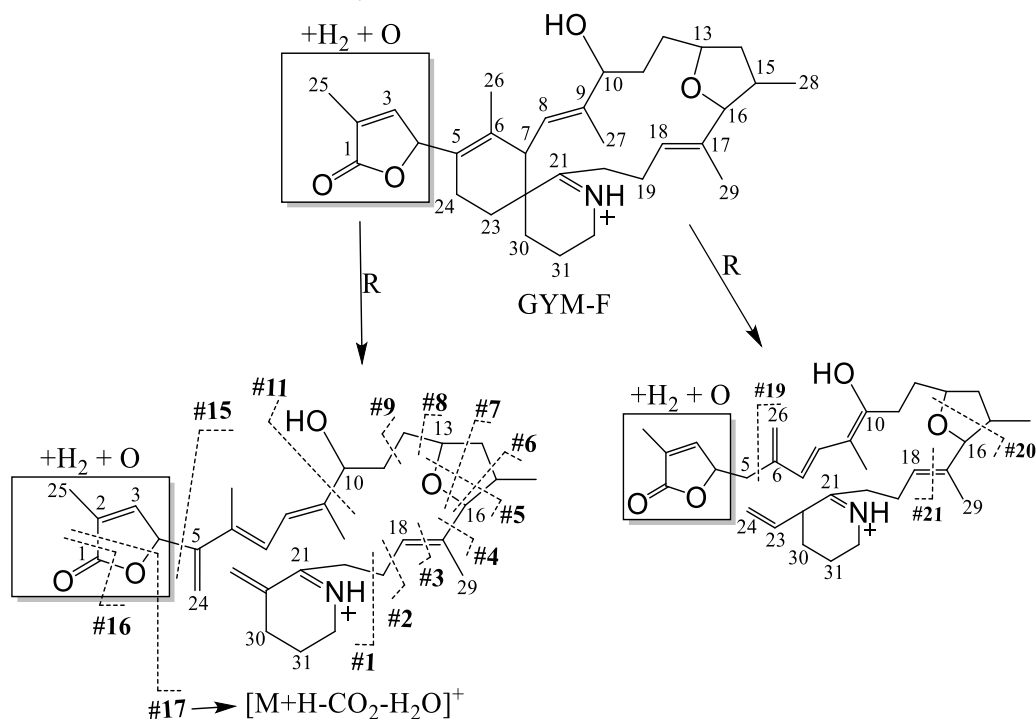
Clv = Cleavage; RDB= Ring Double Bond equivalents; Δ = error, ppm; R= rearrangement.

2.2.2 Development of a new DDA-based methodology towards the identification of new GYMs and their ester metabolites in Tunisian shellfish

The high GYM-contamination levels found in Tunisian sample P, associated with the complex toxin profile, prompted to develop a strategy to deeply investigate the metabolic profile of the shellfish sample. The necessity to implement an untargeted analytical approach for the investigation of GYM metabolites became even more evident after extracting the $[M+H-H_2O]^+$ ion of GYM-A at m/z 490.3310 from the TIC of the sample P. The obtained XIC revealed not only the presence of GYM-A, but also a large number of broad and overlapping peaks eluting between 15.5-20.5 min (**Fig.II.9a**), whose average HRMS spectrum contained an array of ions in the mass range m/z 700-900 with the $[M+H-H_2O]^+$ ion of GYM-A being the base peak (**Fig.II.9b**).
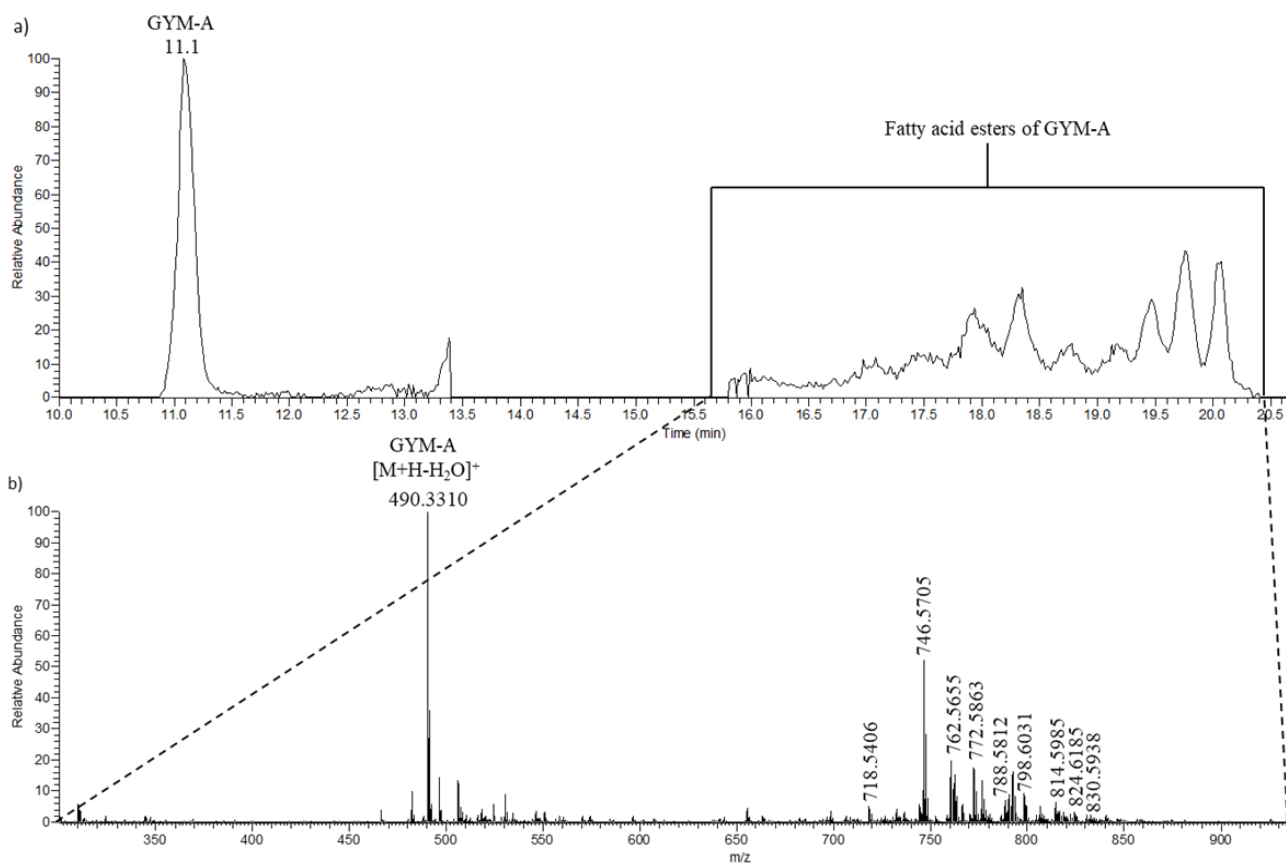
Figure II.9 a) XIC of the ion at m/z 490.3310, and b) full-scan HRMS average spectrum in the range m/z 300-940 corresponding to the peaks eluting in the time range 15.5-20.5 min.

This observation suggested the presence of fatty acid ester metabolites of GYM-A that, under the optimized experimental conditions, underwent in-source fragmentation. The breakage of the ester bond generated an intense $[M+H-AcilOH]^+$ in-source ion corresponding to the $[M+H-H_2O]^+$ ion of GYM-A at m/z 490.3310. Therefore, a HRMS data dependent acquisition (DDA) experiment in which all compounds contained in full HRMS spectrum above a defined threshold (500.0) were fragmented (no exclusion list), was designed and applied to the Tunisian sample P for the investigation of GYM ester metabolites. This kind of non-targeted experiment allows to acquire a large number of $HRMS^2$ spectra by fragmenting, at a defined collision energy, the most intense ions contained in the m/z range selected in the full-scan acquisition. The XIC of the $[M+H-AcilOH]^+$ ion of GYM-A and GYM-B/C (m/z 506.3265) from the hundreds of MS^2 scans recorded during the DDA run revealed a variety of peaks whose fragmentation spectra were characterized by: i) the $[M+H]^+$ ion of the acyl ester (precursor ion), ii) the $[M+H-AcilOH]^+$ fragment ion due to the breakage of the ester bond, namely the $[M+H-H_2O]^+$ ion of the esterified toxin, and iii) a variety of diagnostic fragments including that at m/z 136.119 due to cleavage #3. **Figure II.10** shows a characteristic HCD MS^2 spectrum of GYM-A and GYM-B/C ester metabolite at m/z 814.5985 and 830.5933, respectively.
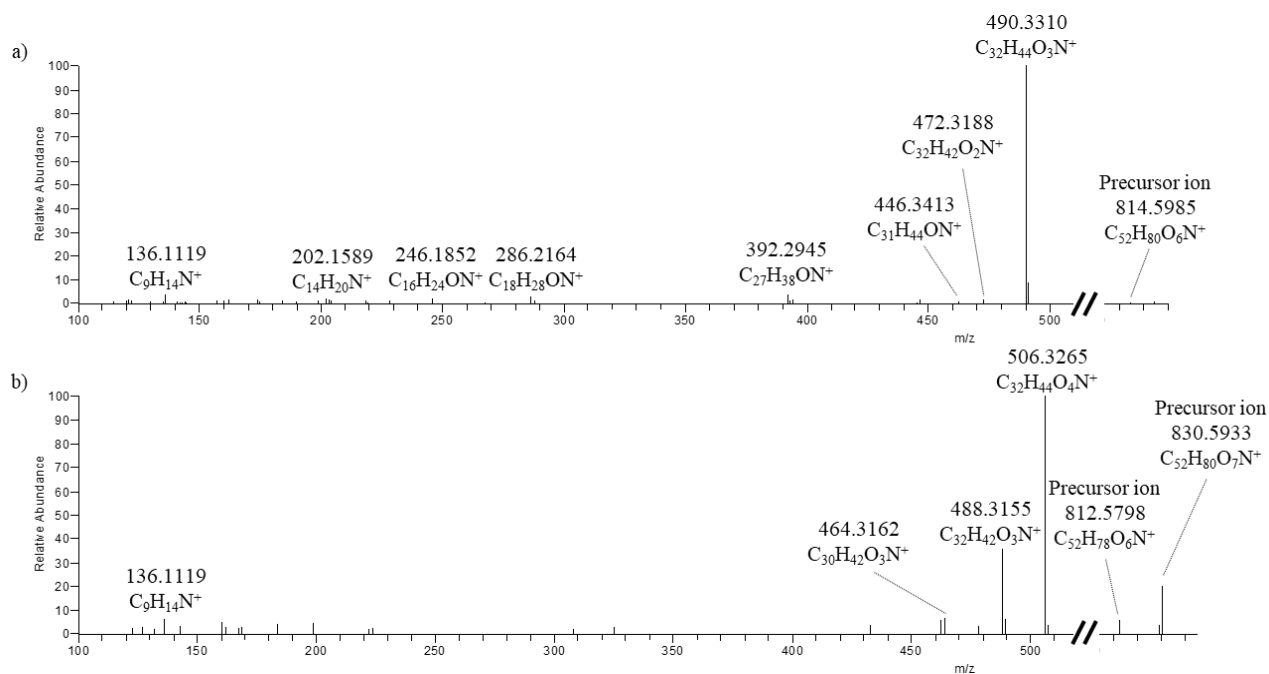
Figure II.10 HR HCD MS^2 DDA spectrum of one ester metabolite of: a) GYM-A and b) GYM-B/C detected in Tunisian sample P.

The presence of one more OH group in the structure of GYM-B/C gave more intense $[M+H-H_2O]^+$ (*m/z* 812.5798) and $[M+H-AcylOH-H_2O]^+$ (*m/z* 488.3155) fragment ions than those of GYM-A. Although HR DDA turned out to be a powerful tool for fast dereplication strategies and for the detection of unknown compounds in complex matrices, it is characterized by a reduced sensitivity due to the high number of MS^2 scans acquired in the scan time. Therefore, further investigation into the metabolic profile of the Tunisian shellfish sample was carried out through the combination of the untargeted DDA approach with targeted MS^2 experiments. As a result, a plethora of metabolites of GYM-A and GYM-B/C conjugated with: i) known naturally-occurring saturated and unsaturated fatty acids and ii) atypical hydroxylated, polyhydroxylated and iii) odd-chain fatty acids, emerged. The latter ones were brought to light for the first time in this study (**Table II.9**).

Table II.9. Measured exact mass, molecular formula and RDB of GYM esters found in sample P. For each ester: the $[M+H-AcilOH]^+$ ion, the molecular weight, the elemental composition, and the C:D of the relevant fatty acid are reported.

Acyl ester			GYM		Fatty acid	
$[M+H]^+$	Molecular Formula	RDB	$[M+H-AcilOH]^+$	C:D	Elemental composition	MW
716.5245	$C_{46}H_{70}O_5N^+$	12.5	490.3310, GYM-A	14:1	$C_{14}H_{26}O_2$	226.1933
718.5406	$C_{46}H_{72}O_5N^+$	11.5	490.3310, GYM-A	14:0	$C_{14}H_{28}O_2$	228.2089
744.5565	$C_{48}H_{74}O_5N^+$	12.5	490.3310, GYM-A	16:1	$C_{16}H_{30}O_2$	254.2246
746.5705	$C_{48}H_{76}O_5N^+$	11.5	490.3310, GYM-A	16:0	$C_{16}H_{32}O_2$	256.2402
762.5655	$C_{48}H_{76}O_6N^+$	11.5	490.3310, GYM-A	16:0	$C_{16}H_{32}O_3$	272.2351
762.5655	$C_{48}H_{76}O_6N^+$	11.5	524.3370, isobaric GYM-B/C	16:0	$C_{16}H_{32}O_2$	256.2402
768.5550	$C_{50}H_{74}O_5N^+$	14.5	490.3310, GYM-A	18:3	$C_{18}H_{30}O_2$	278.2246
770.5707	$C_{50}H_{76}O_5N^+$	13.5	490.3310, GYM-A	18:2	$C_{18}H_{32}O_2$	280.2402
772.5863	$C_{50}H_{78}O_5N^+$	12.5	490.3310, GYM-A	18:1	$C_{18}H_{34}O_2$	282.2559
774.6021	$C_{50}H_{80}O_5N^+$	11.5	490.3310, GYM-A	18:0	$C_{18}H_{36}O_2$	284.2715
776.5814	$C_{49}H_{78}O_6N^+$	11.5	490.3310, GYM-A	17:0	$C_{17}H_{34}O_3$	286.2508
776.5814	$C_{49}H_{78}O_6N^+$	11.5	524.3370, isobaric GYM-B/C	17:0	$C_{17}H_{34}O_2$	270.2559
778.5615	$C_{48}H_{76}O_7N^+$	11.5	522.3205, GYM-I	16:0	$C_{16}H_{32}O_2$	256.2402
782.5350	$C_{50}H_{72}O_6N^+$	15.5	490.3310, GYM-A	18:4	$C_{18}H_{28}O_3$	292.2038
782.5338	$C_{50}H_{72}O_6N^+$	15.5	524.3370, isobaric GYM-B/C	18:4	$C_{18}H_{28}O_2$	276.2089
784.5502	$C_{50}H_{74}O_6N^+$	14.5	490.3310, GYM-A	18:3	$C_{18}H_{30}O_3$	294.2195
784.5493	$C_{50}H_{74}O_6N^+$	14.5	524.3370, isobaric GYM-B/C	18:3	$C_{18}H_{30}O_2$	278.2246
784.5505	$C_{50}H_{74}O_6N^+$	14.5	504.3109, GYM-J	18:2	$C_{18}H_{32}O_2$	280.2402
786.5668	$C_{50}H_{76}O_6N^+$	13.5	490.3310, GYM-A	18:2	$C_{18}H_{32}O_3$	296.2351
786.5653	$C_{50}H_{76}O_6N^+$	13.5	524.3370, isobaric GYM-B/C	18:2	$C_{18}H_{32}O_2$	280.2402
786.5668	$C_{50}H_{76}O_6N^+$	13.5	504.3109, GYM-J	18:1	$C_{18}H_{34}O_2$	282.2559
788.5812	$C_{50}H_{78}O_6N^+$	12.5	490.3310, GYM-A	18:1	$C_{18}H_{34}O_3$	298.2508
788.5812	$C_{50}H_{78}O_6N^+$	12.5	524.3370, isobaric GYM-B/C	18:1	$C_{18}H_{34}O_2$	282.2559
788.5813	$C_{50}H_{78}O_6N^+$	12.5	504.3109, GYM-J	18:0	$C_{18}H_{36}O_2$	284.2715
790.5970	$C_{50}H_{80}O_6N^+$	11.5	524.3370, isobaric GYM-B/C	18:0	$C_{18}H_{36}O_2$	284.2715
798.6031	$C_{52}H_{80}O_5N^+$	13.5	490.3310, GYM-A	20:2	$C_{20}H_{36}O_2$	308.2715
808.5707	$C_{49}H_{78}O_8N^+$	11.5	490.3310, GYM-A	17:0	$C_{17}H_{34}O_5$	318.2406
808.5705	$C_{49}H_{78}O_8N^+$	11.5	524.3370, isobaric GYM-B/C	17:0	$C_{17}H_{34}O_4$	302.2457
808.5702	$C_{49}H_{78}O_8N^+$	11.5	538.3160, GYM-G/H	17:0	$C_{17}H_{34}O_2$	270.2559
812.5821	$C_{52}H_{78}O_6N^+$	14.5	490.3310, GYM-A	20:3	$C_{20}H_{34}O_3$	322.2508
814.5985	$C_{52}H_{80}O_6N^+$	13.5	490.3310, GYM-A	20:2	$C_{20}H_{36}O_3$	324.2664
814.5985	$C_{52}H_{80}O_6N^+$	13.5	524.3370, isobaric GYM-B/C	20:2	$C_{20}H_{36}O_2$	308.2715
814.5985	$C_{52}H_{80}O_6N^+$	13.5	504.3109, GYM-J	20:1	$C_{20}H_{38}O_2$	310.2072

816.6146	$C_{52}H_{82}O_6N^+$	12.5	490.3310, GYM-A	20:1	$C_{20}H_{38}O_3$	326.2821
816.6146	$C_{52}H_{82}O_6N^+$	12.5	524.3370, isobaric GYM-B/C	20:1	$C_{20}H_{38}O_2$	310.2872
816.6148	$C_{52}H_{82}O_6N^+$	12.5	504.3109, GYM-J	20:0	$C_{20}H_{40}O_2$	312.3028
818.6315	$C_{52}H_{84}O_6N^+$	11.5	490.3310, GYM-A	20:0	$C_{20}H_{40}O_3$	328.2977
818.6308	$C_{52}H_{84}O_6N^+$	11.5	524.3370, isobaric GYM-B/C	20:0	$C_{20}H_{40}O_2$	312.3028
820.5854	$C_{54}H_{78}O_5N^+$	16.5	490.3310, GYM-A	22:5	$C_{22}H_{34}O_2$	330.2559
822.5878	$C_{50}H_{80}O_8N^+$	11.5	490.3310, GYM-A	18:0	$C_{18}H_{36}O_5$	332.2563
822.5881	$C_{50}H_{80}O_8N^+$	11.5	524.3370, isobaric GYM-B/C	18:0	$C_{18}H_{36}O_4$	316.2614
822.5883	$C_{50}H_{80}O_8N^+$	11.5	538.3160GYM-G/H	18:0	$C_{18}H_{36}O_2$	284.2715
822.6013	$C_{54}H_{80}O_5N^+$	15.5	490.3310, GYM-A	22:4	$C_{22}H_{36}O_2$	332.2715
824.6185	$C_{54}H_{82}O_5N^+$	14.5	490.3310, GYM-A	22:3	$C_{22}H_{38}O_2$	334.2872
826.6343	$C_{54}H_{84}O_5N^+$	13.5	490.3310, GYM-A	22:2	$C_{22}H_{40}O_2$	336.3028
828.5773	$C_{52}H_{78}O_7N^+$	14.5	490.3310, GYM-A	20:3	$C_{20}H_{34}O_4$	338.2457
828.5760	$C_{52}H_{78}O_7N^+$	14.5	524.3370, isobaric GYM-B/C	20:3	$C_{20}H_{34}O_3$	322.2508
828.5764	$C_{52}H_{78}O_7N^+$	14.5	522.3205, GYM-I	20:3	$C_{20}H_{34}O_2$	306.2559
828.6503	$C_{54}H_{86}O_5N^+$	12.5	490.3310, GYM-A	22:1	$C_{22}H_{42}O_2$	338.3185
830.5938	$C_{52}H_{80}O_7N^+$	13.5	490.3310, GYM-A	20:2	$C_{20}H_{36}O_4$	340.2614
830.5933	$C_{52}H_{80}O_7N^+$	13.5	524.3370, isobaric GYM-B/C	20:2	$C_{20}H_{36}O_3$	324.2664
830.5931	$C_{52}H_{80}O_7N^+$	13.5	522.3205, GYM-I	20:2	$C_{20}H_{36}O_2$	308.2715
832.6104	$C_{52}H_{82}O_7N^+$	12.5	490.3310, GYM-A	20:1	$C_{20}H_{38}O_4$	342.2770
832.6096	$C_{52}H_{82}O_7N^+$	12.5	524.3370, isobaric GYM-B/C	20:1	$C_{20}H_{38}O_3$	326.2821
832.6099	$C_{52}H_{82}O_7N^+$	12.5	522.3205, GYM-I	20:1	$C_{20}H_{38}O_2$	310.2872
834.5671	$C_{54}H_{76}O_6N^+$	17.5	524.3370, isobaric GYM-B/C	22:6	$C_{22}H_{32}O_2$	328.2402
834.6278	$C_{52}H_{84}O_7N^+$	11.5	490.3310, GYM-A	20:0	$C_{20}H_{40}O_4$	344.2927
834.6250	$C_{52}H_{84}O_7N^+$	11.5	524.3370, isobaric GYM-B/C	20:0	$C_{20}H_{40}O_3$	328.2977
834.6249	$C_{52}H_{84}O_7N^+$	11.5	522.3205, GYM-I	20:0	$C_{20}H_{40}O_2$	312.3028
836.5807	$C_{54}H_{78}O_6N^+$	16.5	524.3370, isobaric GYM-B/C	22:5	$C_{22}H_{34}O_2$	330.2559
838.5965	$C_{54}H_{80}O_6N^+$	15.5	524.3370, isobaric GYM-B/C	22:4	$C_{22}H_{36}O_2$	332.2715
840.6136	$C_{54}H_{82}O_6N^+$	14.5	524.3370, isobaric GYM-B/C	22:3	$C_{22}H_{38}O_2$	334.2872
842.6281	$C_{54}H_{84}O_6N^+$	13.5	524.3370, isobaric GYM-B/C	22:2	$C_{22}H_{40}O_2$	336.3028
844.6477	$C_{54}H_{86}O_6N^+$	12.5	490.3310, GYM-A	22:1	$C_{22}H_{42}O_3$	354.3134
844.6475	$C_{54}H_{86}O_6N^+$	12.5	524.3370, isobaric GYM-B/C	22:1	$C_{22}H_{42}O_2$	338.3185
844.6476	$C_{54}H_{86}O_6N^+$	12.5	504.3109, GYM-J	22:0	$C_{22}H_{44}O_2$	340.3341
846.5886	$C_{52}H_{80}O_8N^+$	13.5	490.3310, GYM-A	20:2	$C_{20}H_{36}O_5$	356.2563
846.5886	$C_{52}H_{80}O_8N^+$	13.5	524.3370, isobaric GYM-B/C	20:2	$C_{20}H_{36}O_4$	340.2614
846.5878	$C_{52}H_{80}O_8N^+$	13.5	504.3109, GYM-J	20:1	$C_{20}H_{38}O_4$	342.2770
846.5884	$C_{52}H_{80}O_8N^+$	13.5	522.3205, GYM-I	20:2	$C_{20}H_{36}O_3$	324.2664
846.5882	$C_{52}H_{80}O_8N^+$	13.5	538.3160GYM-G/H	20:2	$C_{20}H_{36}O_2$	308.2715
848.6046	$C_{52}H_{82}O_8N^+$	12.5	490.3310, GYM-A	20:1	$C_{20}H_{38}O_5$	358.2719
848.6036	$C_{52}H_{82}O_8N^+$	12.5	524.3370, isobaric GYM-B/C	20:1	$C_{20}H_{38}O_4$	342.2770
848.6042	$C_{52}H_{82}O_8N^+$	12.5	504.3109, GYM-J	20:0	$C_{20}H_{40}O_4$	344.2927
848.6042	$C_{52}H_{82}O_8N^+$	12.5	522.3205, GYM-I	20:1	$C_{20}H_{38}O_3$	326.2821
848.6045	$C_{52}H_{82}O_8N^+$	12.5	538.3160GYM-G/H	20:1	$C_{20}H_{38}O_2$	310.2872
852.5752	$C_{54}H_{78}O_7N^+$	16.5	490.3310, GYM-A	22:5	$C_{22}H_{34}O_4$	362.2457
852.5761	$C_{54}H_{78}O_7N^+$	16.5	524.3370, isobaric GYM-B/C	22:5	$C_{22}H_{34}O_3$	346.2508
852.5783	$C_{54}H_{78}O_7N^+$	16.5	504.3109, GYM-J	22:4	$C_{22}H_{36}O_3$	348.2664
852.5750	$C_{54}H_{78}O_7N^+$	16.5	522.3205, GYM-I	22:5	$C_{22}H_{34}O_2$	330.2559
854.5911	$C_{54}H_{80}O_7N^+$	15.5	490.3310, GYM-A	22:4	$C_{22}H_{36}O_4$	364.2614
854.5905	$C_{54}H_{80}O_7N^+$	15.5	524.3370, isobaric GYM-B/C	22:4	$C_{22}H_{36}O_3$	348.2664
854.5916	$C_{54}H_{80}O_7N^+$	15.5	504.3109, GYM-J	22:3	$C_{22}H_{38}O_3$	350.2821
854.5906	$C_{54}H_{80}O_7N^+$	15.5	522.3205, GYM-I	22:4	$C_{22}H_{36}O_2$	332.2715
856.6066	$C_{54}H_{82}O_7N^+$	14.5	490.3310, GYM-A	22:3	$C_{22}H_{38}O_4$	366.2770
856.6061	$C_{54}H_{82}O_7N^+$	14.5	524.3370, isobaric GYM-B/C	22:3	$C_{22}H_{38}O_3$	350.2821
856.6077	$C_{54}H_{82}O_7N^+$	14.5	504.3109, GYM-J	22:2	$C_{22}H_{40}O_3$	352.2977
856.6066	$C_{54}H_{82}O_7N^+$	14.5	522.3205, GYM-I	22:3	$C_{22}H_{38}O_2$	334.2872
858.6227	$C_{54}H_{84}O_7N^+$	13.5	490.3310, GYM-A	22:2	$C_{22}H_{40}O_4$	368.2927
858.6228	$C_{54}H_{84}O_7N^+$	13.5	524.3370, isobaric GYM-B/C	22:2	$C_{22}H_{40}O_3$	352.2977
858.6233	$C_{54}H_{84}O_7N^+$	13.5	504.3109, GYM-J	22:1	$C_{22}H_{42}O_3$	354.3134
858.6235	$C_{54}H_{84}O_7N^+$	13.5	522.3205, GYM-I	22:2	$C_{22}H_{40}O_2$	336.3028
860.6400	$C_{54}H_{86}O_7N^+$	12.5	490.3310, GYM-A	22:1	$C_{22}H_{42}O_4$	370.3083
860.6390	$C_{54}H_{86}O_7N^+$	12.5	524.3370, isobaric GYM-B/C	22:1	$C_{22}H_{42}O_3$	354.3134
860.6392	$C_{54}H_{86}O_7N^+$	12.5	504.3109, GYM-J	22:0	$C_{22}H_{44}O_3$	356.3290
860.6407	$C_{54}H_{86}O_7N^+$	12.5	522.3205, GYM-I	22:1	$C_{22}H_{42}O_2$	338.3185

RDB= Ring Double Bond equivalents; MW = Molecular weight; C:D = Carbons : Desaturations.

The discovery of GYMs esterified with fatty acids which are unusual for shellfish metabolism can be explained through the strong relationship between environmental conditions and quality characteristic of shellfish (i.e., condition, composition, glycogen, fatty acids, etc.) [31]. Even though the diet of filter feeders organisms is mainly based on the consumption of algae (e.g. diatoms and flagellates) [32], a noticeable contribution deriving from the uptake of marine dissolved organic matter (DOM) was observed [33]. To date, the chemical composition of DOM represents a fascinating and unexplored part of the marine ecosystem [34], and it was found to be composed of terrestrial (derivatives from soils), aquatic (phytoplankton and plant derivatives) and anthropogenic (substances of industrial origins) materials [35]. Therefore, the presence of the atypical GYM fatty acid esters found in Tunisian shellfish could be due to the shellfish uptake of unusual compounds from the DOM and their involvement within the biotransformation pathways. The application of both untargeted (DDA HRMS) and targeted (HRMS^2) approaches turned out to be also the foundation for the development of a new methodology for the identification of novel GYM analogues in shellfish extract. The XIC of some identified GYM ester metabolites showed a large number of overlapping peaks which suggested the co-occurrence of isobaric esters in the Tunisian sample. Their HRMS^2 spectra not only contained the [M+H-AcilOH]$^+$ fragments of known GYMs (GYM-A and/or GYM-B/C), but also unknown signals which suggested the presence of unknown GYM congeners. By way of example, the XIC of [M+H]$^+$ ion of the ester at m/z 846.5882 (**Fig.II.11**) gave broad and un-resolved chromatographic peaks whose average MS^2 spectrum showed: i) the fragment ions at m/z 490.3310 and m/z 506.3265, corresponding to GYM-A and -B/C and ii) very intense fragments at m/z: 538.3160 (C$_{32}$H$_{44}$O$_6$N$^+$, RDB=11.5), m/z 522.3205 (C$_{32}$H$_{44}$O$_5$N$^+$, RDB=11.5) and m/z 504.3109 (C$_{32}$H$_{42}$O$_4$N$^+$, RDB=12.5), likely associated with [M+H-AcylOH]$^+$ ions of new putative GYMs; diagnostic fragments for GYM-like structures were present. This may suggest the presence of new GYM congeners esterified with different fatty acids, thus producing isobaric ester metabolites at m/z 846.5882 (**Fig.II.11**). Consequently, a new MS-based strategy, labelled as backward analysis, was conceived and structured as follows:
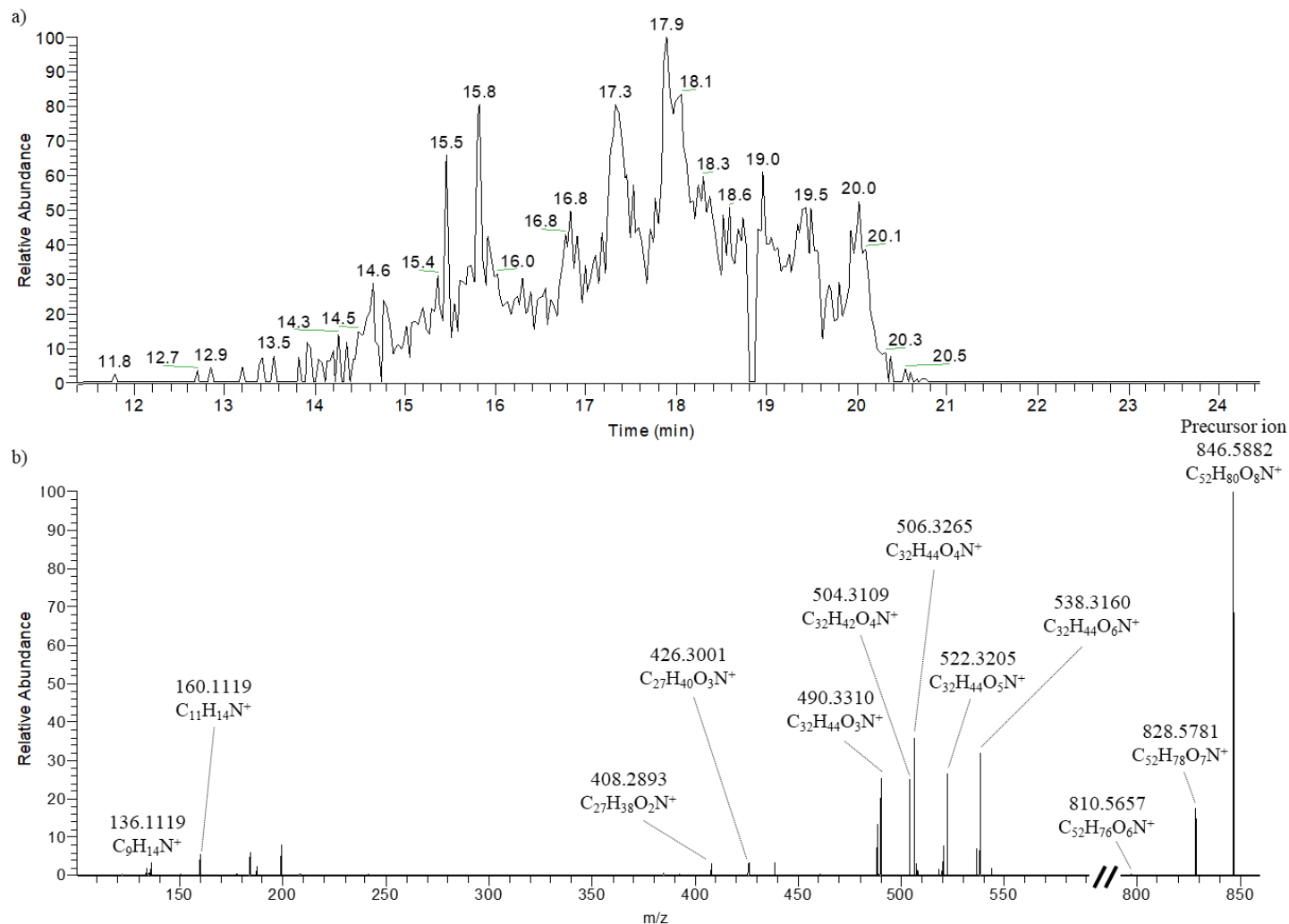
Figure II.11 Extracted Ion Chromatogram (XIC) of the [M+H]$^+$ ion at *m/z* 846.5882 in Tunisian sample P and, b) its associated HR HCD MS^2 average spectrum.

1) Unknown signals ascribable to [M+H-AcylOH]$^+$ fragments of esters of newly putative GYMs are selected from the acquired HRMS^2 spectra.

2) Formula assignment to the suspected [M+H-AcylOH]$^+$ ion applying specific constraints according to the structural properties of known GYMs; the number of C, H and O atoms are set in the range 25-40, 30-60 and 2-10, respectively, while 1 N is fixed. The RDB is even limited to a reasonable range of 8.0-13.0, and the mass tolerance is selected within 5 ppm.

3) 2H and 1O atoms are added to the elemental composition assigned to the [M+H-AcylOH]$^+$ ion (corresponding to the [M+H-H$_2$O]$^+$ ion of the toxin) with the aim of simulating the formula of the [M+H]$^+$ ion.

4) The theorical exact mass of the [M+H]$^+$ ion of the newly suspected GYM is calculated through Thermo Xcalibur Qual Browser 2.2 SP1.48 (Thermo Fisher) within 5 ppm by using the formula previously determined and selecting 1+ as the most abundant signal of the ion cluster (charge distribution).

5) A retrospective analysis of the already acquired LC-HRMS data is performed by extracting (XIC) the accurate mass of the new putative GYMs.

6) Chromatographic peaks eluting at a retention time similar to GYM-A are selected and subjected to a careful investigation. Firstly, the extracted exact mass is compared to the acquired accurate mass which generates the peak in the XIC. The elemental composition of the [M+H]$^+$ ion is assigned within 5 ppm and the obtained formula is compared to the calculated one.

7) The final confirmation of the identity of the new GYM is given by the analysis of the fragmentation spectra of the [M+H]$^+$ ion. The diagnostic fragment of GYMs at *m/z* 136.1119 (cleavage #3; **Table II.4**) clearly highlights the presence of a cyclic imine unit embedded in a six-membered ring which is the diagnostic motif within this CI sub-group.

Following the implemented methodology, the [M+H]$^+$ ions of new putative GYMs at *m/z* 556.3269 ($C_{32}H_{46}O_7N^+$, RDB=10.5), *m/z* 540.3319 ($C_{32}H_{46}O_6N^+$, RDB=10.5) and *m/z* 522.3214 ($C_{32}H_{44}O_5N^+$, RDB=11.5) were calculated and extracted from TIC. As a result, 4 chromatographic peaks eluting in close proximity of GYM-A were observed and named GYM-G, -H -I and J, with the first two being isobaric compounds (**Fig.II.5d-f**). For all new GYMs, structural hints and hypothesis were successfully formulated by interpreting the associated HCD fragmentation spectra, and in some cases, a tentative structural characterization was performed.

2.2.3 GYM-G, -H, -I and -J

The tentative structural elucidation for all new GYMs was carried out through a careful interpretation of their HCD MS^2 spectra which were analyzed in parallel with that of GYM-A, whose fragmentation patterns were assumed as template to identify the regions of the molecules were structural differences occurred.

The elemental composition assigned to the [M+H]$^+$ ion at *m/z* 556.3269 ($C_{32}H_{46}O_7N^+$) of GYM-G and GYM-H revealed the presence of three oxygen atoms more than GYM-A ($C_{32}H_{46}O_4N^+$). Contrarily to GYM-A, for which informative fragmentation patterns were acquired at CE 40%,

HRMS^2 spectra of both GYM-G and -H (**Fig.II.12**) were acquired at difference collision energies since: at CE 43%, CID MS^2 spectra were informative in the region m/z 300-600, whilst a variety of diagnostic fragments in the range m/z 100-300 emerged at CE 60%. This observation clearly suggested that GYM-G and -H featured a different backbone structure than GYM-A, and the presence of specific structural moieties greatly affected their fragmentation patterns.

The cross interpretation of fragmentation patterns of GYM-A (**Table II.4)** and GYM-G (**Table II.10**) revealed that the conserved part structures for the new compound were: i) the α-methyl butanolide moiety (γ-lactone; region C1-C4) at C5 as highlighted by the fragment ion at m/z 459.2977 ($C_{27}H_{41}O_5N^{\bullet+}$) due to cleavage #15, ii) the region ranging from C10 to C16 due to cleavages #5-7, #9, #11 and #20, and iii) the region C19-C23, which includes the 6-membered cyclic imine, as corroborated by the ion at m/z 122.0963 ($C_8H_{12}N^+$) due to cleavage #2 (**Table II.10**). The structural differences between GYM-G and GYM-A were: i) an extra hydroxyl group in the region C17-C18-C29, ii) the absence of the C=C double bond between C8-C9, and iii) an extra cyclic hemiacetal group in the region C6-C7-C8-C26 (**Table II.10**). The extra hydroxyl group in GYM-G [difference i)] emerged through a variety of fragments ions: cleavage #2 originated fragments superimposable to those of GYM-A, while #4 gave rise to a fragment at m/z 178.1227 ($C_{11}H_{16}ON^+$) which contained one more oxygen atom than that of GYM-A, clearly suggesting the presence of a OH group in the region C17-C18-C29. Taking into account the structural features of GYM-B/C (**Fig.I.5**), it can be reasonably assumed that the OH group is linked to C18 with the consequent shift of the C=C from C17-C18 (GYM-A) to C17-C29 (GYM-B/C), as also reported for GYM-E (**Fig.I.5**). This evidence was further supported by the detection of key inside fragments originating from cleavage #22 at m/z 500.3005 ($C_{29}H_{42}O_6N^+$) and associated water loss (m/z 482.2896), that are generated through the combined cleavages between C16-C17 and C18-C19 rather than from the retro-Diels-Alder rearrangement (**Table II.10**).

The absence in GYM-G of the C=C between C8-C9 [difference ii)] clearly emerged through the combined interpretation of fragment ion originating from cleavage #12, m/z 332.2583, $C_{21}H_{34}O_2N^+$ for GYM G versus m/z 312.2375, $C_{21}H_{30}ON^+$ for GYM-A (**Table II.4,10**).

For GYM-G, the remaining two additional oxygen atoms embedded in the cyclic hemiacetal function in the region C6-C7-C8-C26 [difference iii)] emerged through fragment ions at m/z 361.2619 ($C_{22}H_{35}O_3N^{\bullet+}$) and m/z 416.2795 ($C_{25}H_{38}O_4N^+$) due to cleavage #13 and #14, respectively, and from the analysis of fragment ions at m/z 387.2777 ($C_{24}H_{37}O_3N^{\bullet+}$) and m/z

386.2689 ($C_{24}H_{36}O_3N^+$) due to the loss of CO from the fragment generated through cleavage #14, as shown in **Table II.10**. The presence of the cyclic hemiacetal was also corroborated through: i) the [M+H-CO]$^+$ fragment at *m/z* 528.3315 ($C_{31}H_{46}O_6N^+$) and associated water loss (*m/z* 510.3207), which were about 15 times more intense than those observed for GYM-A (*m/z* 480.3472 and 462.3362, cleavage #16), and ii) a key inside fragment at *m/z* 470.2894 ($C_{28}H_{40}O_5N^+$), originating from cleavage #23, due to a neutral loss of $C_4H_6O_2$ from the precursor ion (**Table II.10**).
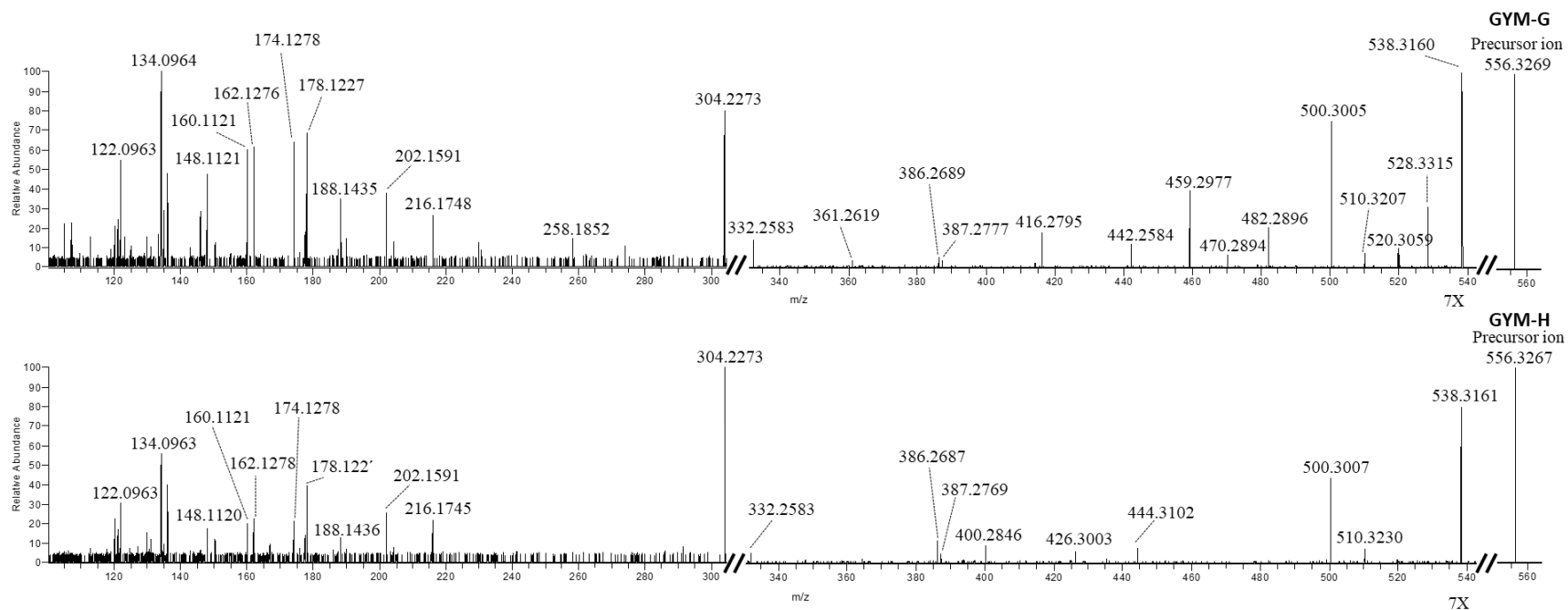
Figure II.12 HR HCD MS^2 spectra of GYM-G and -H detected in Tunisian sample P. Fragment ions in the regions *m/z* 100-305 were acquired at collision energy (CE) 60%, while fragments in the region *m/z* 330-560 at CE 43%. For ion assignment refer to Table II.10-11.

Table II.10 Assignment of fragment ions contained in HR HCD MS^2 spectra of GYM-G. The most intense ion for each cleavage is reported in bold. Inside fragments are reported in red. Proposed planar structure of GYM-G.

GYM-G			
	m/z, formula, RDB, Δ	Clv	*m/z,* formula, RDB, Δ
[M+H]$^+$	**556.3269, C$_{32}$H$_{46}$O$_7$N$^+$, 10.5, -0.502**	#9	**258.1852, C$_{17}$H$_{24}$ON$^+$, 6.5, -0.158**
[M+H-H$_2$O]$^+$	538.3160, C$_{32}$H$_{44}$O$_6$N$^+$, 11.5, -0.621	#11	**304.2273, C$_{19}$H$_{30}$O$_2$N$^+$, 5.5, 0.902**
[M+H-2H$_2$O]$^+$	520.3059, C$_{32}$H$_{42}$O$_5$N$^+$, 12.5, 0.289		286.2164, C$_{19}$H$_{28}$ON$^+$, 6.5, -0.458
[M+H-CO]$^+$	**528.3315, C$_{31}$H$_{46}$O$_6$N$^+$, 9.5, -0.898**	#12	**332.2583, C$_{21}$H$_{34}$O$_2$N$^+$, 5.5, -0.258**
[M+H-CO-H$_2$O]$^+$	510.3207, C$_{31}$H$_{44}$O$_5$N$^+$, 10.5, -1.352	#13	**361.2619, C$_{22}$H$_{35}$O$_3$N$^{\cdot+}$, 6.0, 2.089**
Clv		#14	**416.2795, C$_{25}$H$_{38}$O$_4$N$^+$, 7.5, -0.084**
#2	**122.0963, C$_8$H$_{12}$N$^+$, 3.5, -0.786**		387.2777, C$_{24}$H$_{37}$O$_3$N$^{\cdot+}$, 7.0, 2.284
	121.0886, C$_8$H$_{11}$N$^{\cdot+}$, 4.0, -0.255		386.2689, C$_{24}$H$_{36}$O$_3$N$^+$, 7.5, 0.232
	120.0807, C$_8$H$_{10}$N$^+$, 4.5, -0.799	#15	**459.2977, C$_{27}$H$_{41}$O$_5$N$^{\cdot+}$, 8.0, -0.402**
#3	136.1121, C$_9$H$_{14}$N$^+$, 3.5, -0.044	#19	**442.2584, C$_{26}$H$_{36}$O$_5$N$^+$, 9.5, -0.994**
	135.1041, C$_9$H$_{13}$N$^{\cdot+}$, 4.0, -0.822	#16	**528.3315, C$_{31}$H$_{46}$O$_6$N$^+$, 9.5, -0.898**
	134.0964, C$_9$H$_{12}$N$^+$, 4.5, -0.343	#20	204.1384, C$_{13}$H$_{18}$ON$^+$, 5.5, 0.388
#4	**178.1227, C$_{11}$H$_{16}$ON$^+$, 4.5, -0.038**		**188.1435, C$_{13}$H$_{18}$N$^+$, 5.5, 0.871**
	162.1276, C$_{11}$H$_{16}$N$^+$, 4.5, 0.212	#21	**148.1121, C$_{10}$H$_{14}$N$^+$, 4.5, 0.094**
	160.1121, C$_{11}$H$_{14}$N$^+$, 5.5, 0.389		146.0965, C$_{10}$H$_{12}$N$^+$, 5.5, 0.233
#5	190.1227, C$_{12}$H$_{16}$ON$^+$, 5.5, 0.470	**#22**	**500.3005, C$_{29}$H$_{42}$O$_6$N$^+$, 9.5, -0.249**
	174.1278, C$_{12}$H$_{16}$N$^+$, 5.5, 0.597		482.2896, C$_{29}$H$_{40}$O$_5$N$^+$, 10.5, -1.078
#6	**202.1591, C$_{14}$H$_{20}$N$^+$, 5.5, 0.513**	**#23**	472.3071, C$_{28}$H$_{42}$O$_5$N$^+$, 8.5, 2.859
	200.1435, C$_{14}$H$_{18}$N$^+$, 6.5, 0.369		**470.2894, C$_{28}$H$_{40}$O$_5$N$^+$, 9.5, -1.488**
#7	230.1543, C$_{15}$H$_{20}$ON$^+$, 6.5, 1.430		
	216.1748, C$_{15}$H$_{22}$N$^+$, 5.5, 0.480		

Clv = Cleavage; RDB= Ring Double Bond equivalents; Δ = error, ppm; R= rearrangement.

Differently from GYM-G, the structural investigation of GYM-H, its isobaric congener, was conducted analyzing in parallel the fragmentation patterns of GYM-A, GYM-G and GYM-H. Unfortunately, the low level of GYM-H in the Tunisian shellfish sample did not allow to achieve a complete structural MS-based identification like that reported above for GYM-G. Fragment ions originating from cleavage #2 and cleavages #5, #6, #7, #11 and #20, revealed that GYM-H featured the same part structures C19-C23 and C10-C16, respectively, of GYM-A and -G (**Table II.4,10,11**). The fragments ion at *m/z* 178.1227 and *m/z* 500.3007 due to cleavage #4 and #22, respectively, highlighted the presence of an extra hydroxyl group at C18 and the shift of the C=C between C17-C29, as likewise described for GYM-G (**Table II.10,11**). Moreover, also GYM-H lacked the C=C between C8-C9 as showed by fragment at *m/z* 332.2590 due to cleavage #12. On the other hand, for GYM-H cleavage #14 gave rise to fragment at *m/z* 400.2846 ($C_{25}H_{38}O_3N^+$) highlighting the presence of only one more oxygen atom in the region C6-C8, differently from GYM-G that showed 2 oxygen more embedded in the cyclic hemiacetal (**Table II.10,11**). However, the absence of the $[M+H-CO]^+$ fragment in GYM-H spectra and the same degree of unsaturation (RDB equivalents) of the fragments generated from cleavage #14 in GYM-G and GYM-H (**Table II.10,11**), led to suppose for GYM-H the presence of a tetrahydrofuran ring in the region C6-C7-C8-C26. Fragment ion at *m/z* 444.3102 ($C_{27}H_{42}O_4N^+$) due to cleavage #15 revealed that the third additional oxygen atom was located at the γ-lactone moiety (region C1-C4). However, its exact position could not be unambiguously established.

Table II.11 Assignment of fragment ions contained in HR HCD MS^2 spectra of GYM-H. The most intense ion for each cleavage is reported in bold. Inside fragments are reported in red. Proposed planar structure of GYM-H.

	GYM-H
	m/z, formula, RDB, Δ
[M+H]$^+$	**556.3267, C$_{32}$H$_{46}$O$_7$N$^+$, 10.5, -0.358**
[M+H-H$_2$O]$^+$	538.3161, C$_{32}$H$_{44}$O$_6$N$^+$, 11.5, -0.491
[M+H-2H$_2$O]$^+$	510.3230, C$_{31}$H$_{44}$O$_5$N$^+$, 10.5, 3.116
Clv	
#2	**122.0963, C$_8$H$_{12}$N$^+$, 3.5, -0.950**
	121.0885, C$_8$H$_{11}$N$^{•+}$, 4.0, -1.081
	120.0807, C$_8$H$_{10}$N$^+$, 4.5, -0.632
#3	136.1119, C$_9$H$_{14}$N$^+$, 3.5, -0.265
	135.1040, C$_9$H$_{13}$N$^{•+}$, 4.0, -1.562
	134.0963, C$_9$H$_{12}$N$^+$, 4.5, -0.790
#4	**178.1227, C$_{11}$H$_{16}$ON$^+$, 4.5, 0.389**
	162.1278, C$_{11}$H$_{16}$N$^+$, 4.5, 0.209
	160.1123, C$_{11}$H$_{14}$N$^+$, 5.5, 1.649
#5	**174.1278, C$_{12}$H$_{16}$N$^+$, 5.5, 0.310**
#6	**202.1591, C$_{14}$H$_{20}$N$^+$, 5.5, 0.316**
#7	**216.1745, C$_{15}$H$_{22}$N$^+$, 5.5, -0.677**
#11	**304.2273, C$_{19}$H$_{30}$O$_2$N$^+$, 5.5, 0.672**
#12	**332.2590, C$_{21}$H$_{34}$O$_2$N$^+$, 5.5, 1.909**
#14	400.2846, C$_{25}$H$_{38}$O$_3$N$^+$, 7.5, -0.648
	387.2769, C$_{24}$H$_{37}$O$_3$N$^{•+}$, 7.0, 0.296
	386.2687, C$_{24}$H$_{36}$O$_3$N$^+$, 7.5, -0.648
#15	**444.3102, C$_{27}$H$_{42}$O$_4$N$^+$, 7.5, -1.452**
	426.3003, C$_{27}$H$_{40}$O$_3$N$^+$, 8.5, 0.092
#20	**188.1436, C$_{13}$H$_{18}$N$^+$, 5.5, 1.243**
#21	**148.1120, C$_{10}$H$_{14}$N$^+$, 4.5, -0.378**
#22	500.3007, C$_{29}$H$_{42}$O$_6$N$^+$, 9.5, 0.131

Clv = Cleavage; RDB= Ring Double Bond equivalents; Δ = error, ppm; R= rearrangement

GYM-I and GYM-J were the least abundant analogues in the Tunisian shellfish extract, thus only structural hints were obtained from the interpretation of their HCD HMRS[2] spectra. The formula assigned to the $[M+H]^+$ of GYM-I (m/z 540.3319, $C_{32}H_{46}O_6N^+$) showed the presence of two more oxygen atoms than in GYM-A. One of them was located in the region C16-C17-C18-C29 since fragments due to cleavage #2 were superimposable between GYM-I and GYM-A, while cleavage #5 gave rise a fragment (m/z 208.1335, $C_{12}H_{18}O_2N^+$) containing one more oxygen atom in GYM-I than in GYM-A (m/z 192.1381, $C_{12}H_{18}ON^+$) (**Table II.4,12**). Further confirmation was provided by fragments due to cleavage #7 and #11 both containing one oxygen more than in relevant fragments of GYM-A. On the other hand, the poor fragmentation spectra of GYM-I did not contain useful data to identify the exact position of the second extra oxygen atom, thus it was supposed its location in the region C1-C9.

The $[M+H]^+$ of GYM-J (m/z 522.3214, $C_{32}H_{44}O_5N^+$) has a molecular formula containing one oxygen more and two hydrogen less than in GYM-A. The combined interpretation of fragments due to cleavage #4 and #6 suggested the extra oxygen could be located in the region C14-C15-C16-C28, whilst the loss of the α-methyl-butenolide moiety due to cleavage #15 pointed out that GYM-J lacked 2 H in the region C5-C13 (**Table II.4,12**).

Table II.12 Assignment of fragment ions contained in HR HCD MS[2] spectra of GYM-I and -J. The most intense ion for each cleavage is reported in bold.

	GYM-I		GYM-J
	m/z, formula, RDB, Δ		*m/z,* formula, RDB, Δ
[M+H]⁺	**540.3319, $C_{32}H_{46}O_6N^+$, 10.5, -0.138**	[M+H]⁺	**522.3214, $C_{32}H_{44}O_5N^+$, 11.5, -1.742**
[M+H-H₂O]⁺	522.3205, $C_{32}H_{44}O_5N^+$, 11.5, -1.589	[M+H-H₂O]⁺	504.3109, $C_{32}H_{42}O_4N^+$, 12.5, -0.506
[M+H-2H₂O]⁺	504.3107, $C_{32}H_{42}O_4N^+$, 12.5, -0.308		
Clv		**Clv**	
#2	**122.0964, $C_8H_{12}N^+$, 3.5, 0.033**	#3	136.1118, $C_9H_{14}N^+$, 3.5, -1.661
	120.0807, $C_8H_{10}N^+$, 4.5, -0.466		135.1040, $C_9H_{13}N^{+\cdot}$, 4.0, -1.858
#3	136.1121, $C_9H_{14}N^+$, 3.5, 0.437		**134.0962, $C_9H_{12}N^+$, 4.5, -1.909**
	135.1043, $C_9H_{13}N^{+\cdot}$, 4.0, 0.030	#4	**162.1274, $C_{11}H_{16}N^+$, 4.5, -2.073**
	134.0964, $C_9H_{12}N^+$, 4.5, -0.044	#7	**232.1694, $C_{15}H_{22}ON^+$, 5.5, -0.951**
#5	**208.1335, $C_{12}H_{18}O_2N^+$, 4.5, 1.224**	#15	**424.2841, $C_{27}H_{38}O_3N^+$, 9.5, -1.321**
#7	**232.1698, $C_{15}H_{22}ON^+$, 5.5, 0.987**		
#11	**320.2213, $C_{19}H_{30}O_3N^+$, 5.5, -2.187**		

Cleavage; RDB= Ring Double Bond equivalents; Δ = error, ppm.

2.2.4 Determination of PnTX-G in Italian and Spanish shellfish

The application of the implemented LC-HRMS method revealed the presence of PnTX-G in most of the Spanish shellfish (Galicia, Atlantic Ocean) at the contamination range of 3.1-7.7 µg/Kg, and

in the Italian sample collected in Tortolì (Sardinia, Tyrrhenian Sea) at 6.8 µg/Kg (**Table II.6**). The identity of the toxin was confirmed by comparing the retention time (**Fig.II.13**), the HR full-scan MS spectrum - containing a $[M+H]^+$ ion at m/z 694.4677 ($C_{42}H_{64}O_7N^+$, RDB=11.5) – and the fragmentation spectra (**Fig.II.13**) with those of PnTX-G standard injected under the same experimental conditions (**Fig.II.1-4**, **Table II.1**). The HR CID MS^2 spectrum of PnTX-G in contaminated samples was characterized by the presence of diagnostic fragment ions at: i) m/z 164.1432 ($C_{11}H_{18}N^+$) due to the cleavage #3, ii) m/z 458.3260 ($C_{28}H_{44}O_4N^+$) and its water loss at m/z 440.3156 ($C_{28}H_{42}O_3N^+$) due to cleavage #14, and $[M+H-nH_2O]^+$ (n=1,2) ions at m/z 676.4567 ($C_{42}H_{62}O_6N^+$) and m/z 658.4462 ($C_{42}H_{60}O_5N^+$) (**Fig.II.13**, **Table II.1**). The detection of PnTX-G in Italian *M. galloprovincialis* harvested in Sardinia in 2016 represents the first finding of the toxin in this geographical area, since Rambla-Alegre et al [8] found PnTX-G (4 µg/Kg) in Italian raw *R. decussatus* and frozen/canned *M. galloprovincialis* collected between 2014-15 from Veneto and Liguria (Adriatic and Ligurian Sea, respectively). With regard to the presence of PnTX-G in Spanish shellfish, Garcìa-Altares et al. [36] reported in 2014 the first finding of the toxin in shellfish from Catalonia (North West Mediterranean Sea), while in 2019 Moreiras et al. [13] and Lamas et al. [37] described the detection of PnTX-G in Galician shellfish (Atlantic ocean) collected in 2015 and 2017-19, respectively. Therefore, data reported in this study clearly highlight that the distribution of PnTX-G through the Galician trophic chain is pre-existing than reported in literature, since Spanish *M. galloprovincialis* analyzed in this study were collected in 2014 (**Table II.6**).

2.2.5 Determination of 13desMeSPX-C in Spanish shellfish

The study of CI distribution along the trophic chain revealed the further presence of 13desMeSPX-C in most of the Spanish samples at a contamination level within 11.0-29.0 µg/Kg (**Table II.6**). The presence of the toxin in the shellfish extracts was confirmed through the comparison of the retention time, the $[M+H]^+$ ion at m/z 692.4523 ($C_{42}H_{62}O_7N^+$, RDB=12.5) and the HCD MS^2 spectra (**Fig.II.13**) with those of 13desMeSPX-C standard analyzed under the implemented methodology (**Fig.II.1-4**). The HCD fragmentation patterns obtained from the analysis of the shellfish samples (**Fig.II.13, Table II.3**) were characterized by the presence of the diagnostic ions at: i) m/z 164.1432 ($C_{11}H_{18}N^+$) originating from cleavage #2, ii) m/z 444.3113 ($C_{27}H_{42}O_4N^+$) and

the relevant water loss ion at m/z 426.3005 ($C_{27}H_{40}O_3N^+$) due to cleavage #14, iii) m/z 674.4421 ($C_{42}H_{60}O_6N^+$), m/z 656.4315 ($C_{42}H_{58}O_5N^+$) and m/z 638.4206 ($C_{42}H_{56}O_4N^+$) originating from the loss of up to three water molecules from the precursor, respectively, and iv) the diagnostic fragment ion at m/z 462.3209 ($C_{27}H_{44}O_5N^+$) reported by Sleno et al. [38].
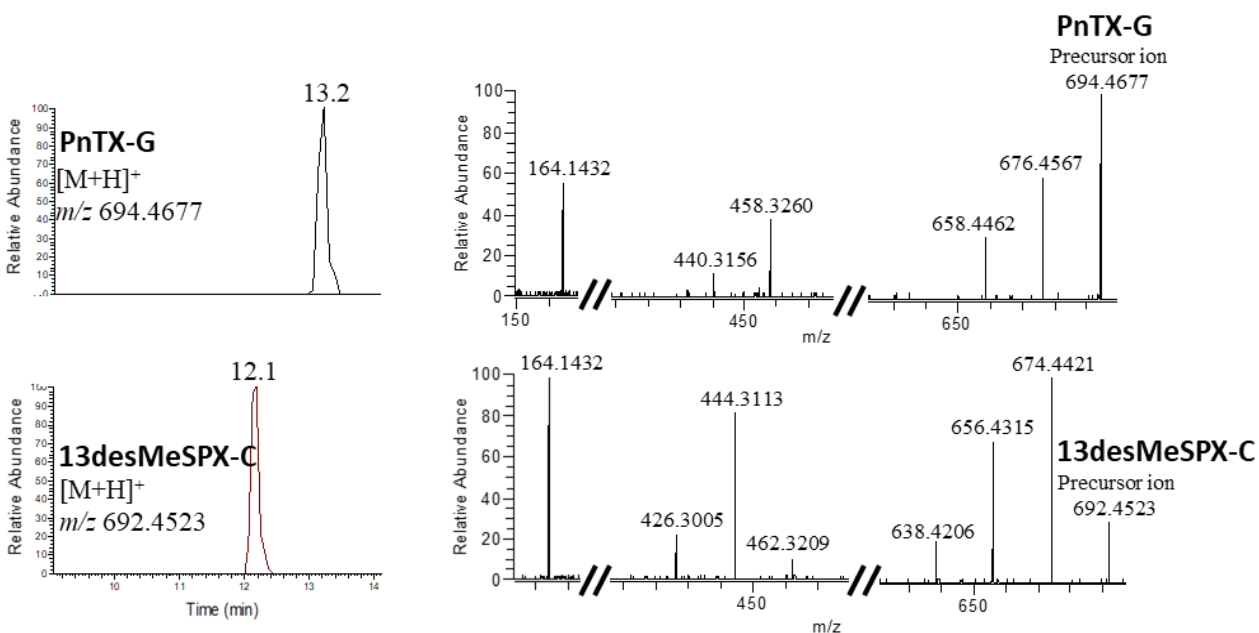
Figure II.13 LC-HRMS XIC and HR HCD MS^2 spectra of: PnTX-G in sample Q, and 13desMeSPX-C in sample I2. For ion assignment refer to Table II.1,3.

3. Materials and methods

3.1 Standards

PnTX-G, 13desMeSPX-C and GYM-A certified reference material (CRM) were purchased from the Institute of Biotoxin Metrology, National Research Council of Canada (NRCC, Halifax, Canada) whilst PnTX-A non-certified RM was purchased from Novakits (Nantes, France).

3.2 Extraction of shellfish samples

The extraction procedure of toxins from shellfish was carried out according to McCarron et al. [39]. Briefly, the edible parts of molluscs were homogenized in a waring blender and subsequently 5 g of homogenized tissue were weighted, transferred into a 50 mL PP centrifuge tube and extracted with 15 mL of MeOH (3mL for g). The mixture was well-mixed by vortex, centrifuged

at 1200 g for 5 min and the supernatant was collected and transferred into a clean 50 mL PP tube. The residue was extracted again twice under the same procedure. All supernatants were pooled together (45 mL) and dried down through a nitrogen evaporation system Evaporator®-Thermobil® (Liebisch®, Bielefeld, Germany). The minimum volume of MeOH required to completely dissolve each dried residue was added (5 mL for samples A-N, and 3 mL for samples O-R) and aliquots of 200 μL were filtered through Ultrafree® - MC – HV Durapore® PVDF 0.45 μm Centrifugal Filters (Merck Millipore Ltd., Cork, IRL) prior LC-HRMS analysis.

3.3 LC-HRMS method

LC-HRMS analyses were carried out on a hybrid linear ion trap LTQ Orbitrap XL^{TM} Fourier Transform Mass Spectrometer (FTMS) equipped with an ESI ION MAX^{TM} source coupled with a Dionex Ultimate 3000 quaternary HPLC system (Thermo-Fisher, San Jose, CA, USA). Chromatography was optimized using a HyperClone BDS C8 column 50 x 2.0 mm, 13Å, 3μm (Phenomenex, USA) eluted at room temperature with the following mobile phases: (A) water and (B) acetonitrile-water 95:5 v/v, both containing 2 mM ammonium formate and 50 mM formic acid [40]. The chromatographic separation of toxins was achieved by injecting 5 μL under a flow rate of 0.2 mL/min and the following gradient elution: time (t) 0 min, 10%B; t 10; 100%B, t 15; 100%B, t 16 10%B; re-equilibration time was 9 min. The optimized source parameters were: capillary temperature 300 °C, sheath gas 38 and auxiliary gas 26.5 (arbitrary units), spray voltage 4.5 kV, capillary voltage 47 V, and tube lens voltage 170 V. Full scan spectra were recorded at resolving power (RP) 60,000 (FWHM at m/z 400) in the range m/z 300-1200 whilst fragmentation experiments were carried at RP 30,000 (FWHM at m/z 400) at collision energy (CE) 40%, isolation width 2 m/z, activation Q 0.250 and activation time 30 ms. DDA experiment was set up through 10 scan events, with the first one being the full-scan acquisition in the range m/z 300-1200, and the others were MS^2 scans acquired fragmenting the 9 most intense ions contained in the m/z range applied in the HRMS scan. The XICs were obtained by selecting the monoisotopic peak of the [M+H]$^+$ ion of each toxin at: m/z 694.4677 (PnTX-G), m/z 712.4419 (PnTX-A), m/z 692.4521 (13desMeSPX-C) and m/z 508.3421 (GYM-A) with a mass tolerance of 5 ppm. Elemental formulae were calculated on the monoisotopic peak of the ion cluster through Thermo Xcalibur software v2.2 SP1.48 (Thermo Fisher, San Josè, CA, USA).

3.4 Evaluation of matrix effect, LOD, LOQ and toxin quantitation

A blank mussel tissue of 5 g was extracted under the same procedure in order to obtain a 5 mL blank crude extract (1 g/mL). Each standard was diluted with methanol and the blank mussel extract to prepare six-points MF and MM curves, respectively, at the following concentration levels: PnTX-G (240.0, 120.0, 60.0, 30.0, 15.0, 7.5 ng/mL), PnTX-A (312.5, 156.3, 78.1, 39.1, 19.5, 9.8 ng/mL), 13desMeSPX-C (333.3, 166.7, 83.3, 41.7, 20.8, 10.4 ng/mL) and GYM-A (312.5, 156.3, 78.1, 39.1, 19.5.0, 9.8 ng/mL). MF and MM curves were used to evaluate the matrix interference on the HRMS response (ion enhancement or suppression), which was calculated as follows:

$$100 - \left[\frac{(peak\ area\ of\ MM\ standard)}{(peak\ area\ of\ MF\ standard)} \right] X\ 100$$

Experimental LOD and LOQ were measured by preparing and injecting serial dilution point of MF and MM standard up to obtain the lowest detectable and quantifiable level. MM calibration curves were further used to quantify the toxin level in shellfish samples.

4. Conclusions

The present study has described the development of a high sensitive and effective LC-HRMS method for the analysis of assorted CIs and their determination in shellfish samples collected from Italy, Spain and Tunisia. The development of a LC-HRMS DDA approach in combination with targeted HCD MS^2 experiments revealed the presence in one Tunisian sample of a plethora of fatty acid ester metabolites of GYMs, including derivatives with atypical hydroxylated, poli-hydroxylated and odd-chain fatty acids reported for the first time in this study. This application led to the development of a new successful MS-based strategy, named backward analysis, which brought to light the presence of new GYMs in Tunisian shellfish starting from the interpretation of the fragmentation pattern of their ester metabolites. The interpretation of the HR HCD MS^2 spectra allowed to propose and/or suppose the chemical structure of the newly GYM-F, G and -H, while for GYM-I and -J only structural hints were extrapolated. Moreover, the implemented methodology revealed for the first time the presence of PnTX-G (6.8 µg/Kg) in *M. galloprovincialis* from Sardinia (Thyrrenean Sea, Italy). The study of toxin distribution along the

trophic chain showed a widespread contamination of PnTX-G (3.1-7.7 µg/Kg) and 13desMeSPX-C (11.0-29.0 µg/Kg) in Galician mussels (Atlantic Ocean, Spain), and the presence of a remarkable level of GYM-A (376.5 µg/Kg) and 5 isobaric analogues of GYM-B/C in Tunisian shellfish from Medenine (Mediterranean Sea, North Africa). The implemented analytical strategy, successfully applied in this study, may pave the way for the detection of new toxins belonging to different classes and/or xenobiotics undergoing a similar metabolic pathway in shellfish.

Results of the study reported in this chapter have been published in a research article [41].

References

1.   Otero, A., Chapela, M. J., Atanassova, M., Vieites, J. M., & Cabado, A. G. (2011). Cyclic imines: Chemistry and mechanism of action: A review. *Chemical Research in Toxicology*, *24*(11), 1817-1829

2.   Stivala, C. E., Benoit, E., Araoz, R., Servent, D., Novikov, A., Molgó, J., & Zakarian, A. (2015). Synthesis and biology of cyclic imine toxins, an emerging class of potent, globally distributed marine toxins. *Natural product reports*, *32*(3), 411-435

3.   Jeffrey, L. C. (1995). Spirolides B and D, two novel macrocycles isolated from the digestive glands of shellfish. *Journal of the chemical society, Chemical communications*, (20), 2159-2161.

4.   Molgó, J., Benoit, E., Aráoz, R., Zakarian, A., & Iorga, B. (2016). Spirolides and cyclic imines: toxicological profile.

5.   Molgó, J., Marchot, P., Aráoz, R., Benoit, E., Iorga, B. I., Zakarian, A., ... & Servent, D. (2017). Cyclic imine toxins from dinoflagellates: A growing family of potent antagonists of the nicotinic acetylcholine receptors. *Journal of neurochemistry*, *142*, 41-51.

6.   Uemura, D., Chou, T., Haino, T., Nagatsu, A., Fukuzawa, S., Zheng, S. Z., & Chen, H. S. (1995). Pinnatoxin A: a toxic amphoteric macrocycle from the Okinawan bivalve Pinna muricata. *Journal of the American Chemical Society*, *117*(3), 1155-1156

7.   Chou, T., Osamu, K., & Uemura, D. (1996). Relative stereochemistry of pinnatoxin A, a potent shellfish poison from Pinna muricata. *Tetrahedron letters*, *37*(23), 4023-4026.

8.   Rambla-Alegre, M., Miles, C. O., de la Iglesia, P., Fernandez-Tejedor, M., Jacobs, S., Sioen, I., ... & Diogene, J. (2018). Occurrence of cyclic imines in European commercial seafood and consumers risk assessment. *Environmental research*, *161*, 392-398.

9.   EFSA Panel on Contaminants in the Food Chain (CONTAM). (2010). Scientific Opinion on marine biotoxins in shellfish–Cyclic imines (spirolides, gymnodimines, pinnatoxins and pteriatoxins). *EFSA Journal*, *8*(6), 1628.

10.   Aráoz, R., Barnes, P., Séchet, V., Delepierre, M., Zinn-Justin, S., Molgó, J., ... & Servent, D. (2020). Cyclic imine toxins survey in coastal european shellfish samples: Bioaccumulation and mode of action of 28-O-palmitoyl ester of pinnatoxin-G. first report of portimine-A bioaccumulation. *Harmful Algae*, *98*, 101887.

11.   Gerssen, A., Pol-Hofstad, I. E., Poelman, M., Mulder, P. P., Van den Top, H. J., & De Boer, J. (2010). Marine toxins: Chemistry, toxicity, occurrence and detection, with special reference to the Dutch situation. *Toxins*, *2*(4), 878-904

12.   Bodero, M., Gerssen, A., Portier, L., Klijnstra, M. D., Hoogenboom, R. L., Guzmán, L., ... & Bovee, T. F. (2018). A strategy to replace the mouse bioassay for detecting and identifying lipophilic marine biotoxins by combining the Neuro-2a bioassay and LC-MS/MS analysis. *Marine drugs*, *16*(12), 501.

13.   Moreiras, G., Leão, J. M., & Gago-Martínez, A. (2020). Analysis of cyclic imines in mussels (Mytilus galloprovincialis) from Galicia (NW Spain) by LC-MS/MS. *International journal of environmental research and public health*, *17*(1), 281.

14.   Vilarino, N., Fonfría, E. S., Molgó, J., Aráoz, R., & Botana, L. M. (2009). Detection of gymnodimine-A and 13-desmethyl C spirolide phycotoxins by fluorescence polarization. *Analytical chemistry*, *81*(7), 2708-2714.

15.   Fonfría, E. S., Vilariño, N., Molgó, J., Aráoz, R., Otero, P., Espiña, B., ... & Botana, L. M. (2010). Detection of 13, 19-didesmethyl C spirolide by fluorescence polarization using Torpedo electrocyte membranes. *Analytical biochemistry*, *403*(1-2), 102-107.

16.   Aráoz, R., Ramos, S., Pelissier, F., Guérineau, V., Benoit, E., Vilariño, N., ... & Molgó, J. (2012). Coupling the Torpedo microplate-receptor binding assay with mass spectrometry to detect cyclic imine neurotoxins. *Analytical chemistry*, *84*(23), 10445-10453.

17.   Davidson, K., Baker, C., Higgins, C., Higman, W., Swan, S., Veszelovszki, A., & Turner, A. D. (2015). Potential threats posed by new or emerging marine biotoxins in UK waters and

examination of detection methodologies used for their control: Cyclic imines. *Marine drugs*, *13*(12), 7087-7112

18. Marrouchi, R., Dziri, F., Belayouni, N., Hamza, A., Benoit, E., Molgó, J., & Kharrat, R. (2010). Quantitative determination of gymnodimine-A by high performance liquid chromatography in contaminated clams from Tunisia coastline. *Marine biotechnology*, *12*(5), 579-585.

19. Gerssen, A., McElhinney, M. A., Mulder, P. P., Bire, R., Hess, P., & de Boer, J. (2009). Solid phase extraction for removal of matrix effects in lipophilic marine toxin analysis by liquid chromatography-tandem mass spectrometry. *Analytical and bioanalytical chemistry*, *394*(4), 1213-1226.

20. Gerssen, A., Mulder, P. P., McElhinney, M. A., & de Boer, J. (2009). Liquid chromatography–tandem mass spectrometry method for the detection of marine lipophilic toxins under alkaline conditions. *Journal of Chromatography A*, *1216*(9), 1421-1430.

21. Dom, I., Biré, R., Hort, V., Lavison-Bompard, G., Nicolas, M., & Guérin, T. (2018). Extended targeted and non-targeted strategies for the analysis of marine toxins in mussels and oysters by (lc-hrms). *Toxins*, *10*(9), 375

22. Selwood, A. I., Miles, C. O., Wilkins, A. L., van Ginkel, R., Munday, R., Rise, F., & McNabb, P. (2010). Isolation, structural determination and acute toxicity of pinnatoxins E, F and G. *Journal of agricultural and food chemistry*, *58*(10), 6532-6542.

23. Domènech, A., Cortés-Francisco, N., Palacios, O., Franco, J. M., Riobó, P., Llerena, J. J., ... & Caixach, J. (2014). Determination of lipophilic marine toxins in mussels. Quantification and confirmation criteria using high resolution mass spectrometry. *Journal of Chromatography A*, *1328*, 16-25.

24. Zhang, X., Fhaner, C. J., Ferguson-Miller, S. M., & Reid, G. E. (2012). Evaluation of ion activation strategies and mechanisms for the gas-phase fragmentation of sulfoquinovosyldiacylglycerol lipids from Rhodobacter sphaeroides. *International journal of mass spectrometry*, *316*, 100-107.

25. Naila, I. B., Hamza, A., Gdoura, R., Diogene, J., & de la Iglesia, P. (2012). Prevalence and persistence of gymnodimines in clams from the Gulf of Gabes (Tunisia) studied by mouse bioassay and LC–MS/MS. *Harmful Algae*, *18*, 56-64

26.   Zurhelle, C., Nieva, J., Tillmann, U., Harder, T., Krock, B., & Tebben, J. (2018). Identification of novel gymnodimines and spirolides from the marine dinoflagellate Alexandrium ostenfeldii. *Marine drugs*, *16*(11), 446.

27.   Harju, K., Koskela, H., Kremp, A., Suikkanen, S., de la Iglesia, P., Miles, C. O., ... & Vanninen, P. (2016). Identification of gymnodimine D and presence of gymnodimine variants in the dinoflagellate Alexandrium ostenfeldii from the Baltic Sea. *Toxicon*, *112*, 68-76.

28.   De la Iglesia, P., McCarron, P., Diogène, J., & Quilliam, M. A. (2013). Discovery of gymnodimine fatty acid ester metabolites in shellfish using liquid chromatography/mass spectrometry. *Rapid Communications in Mass Spectrometry*, *27*(5), 643-653.

29.   Salgado, P., Riobó, P., Rodríguez, F., Franco, J. M., & Bravo, I. (2015). Differences in the toxin profiles of Alexandrium ostenfeldii (Dinophyceae) strains isolated from different geographic origins: Evidence of paralytic toxin, spirolide, and gymnodimine. *Toxicon*, *103*, 85-98.

30.   Nieva, J. A., Tebben, J., Tillmann, U., Wohlrab, S., & Krock, B. (2020). Mass Spectrometry-Based Characterization of New Spirolides from Alexandrium ostenfeldii (Dinophyceae). *Marine drugs*, *18*(10), 505.

31.   Azpeitia, K., Ferrer, L., Revilla, M., Pagaldai, J., & Mendiola, D. (2016). Growth, biochemical profile, and fatty acid composition of mussel (Mytilus galloprovincialis Lmk.) cultured in the open ocean of the Bay of Biscay (northern Spain). *Aquaculture*, *454*, 95-108

32.   Alkanani, T., Parrish, C. C., Thompson, R. J., & McKenzie, C. H. (2007). Role of fatty acids in cultured mussels, Mytilus edulis, grown in Notre Dame Bay, Newfoundland. *Journal of Experimental Marine Biology and Ecology*, *348*(1-2), 33-45.

33.   Roditi, H. A., Fisher, N. S., & Sanudo-Wilhelmy, S. A. (2000). Uptake of dissolved organic carbon and trace elements by zebra mussels. *Nature*, *407*(6800), 78-80

34.   Dittmar, T., & Paeng, J. (2009). A heat-induced molecular signature in marine dissolved organic matter. *Nature Geoscience*, *2*(3), 175-179.

35.   K. M. G. Mostofa, C. Q. Liu, M. A. Mottaleb, G. Wan, H. Ogawa, D. Vione, T. Yoshioka, F. Wu, Dissolved Organic Matter in Natural Waters, in: K. Mostofa, T. Yoshioka, A. Mottaleb, D. Vione, (Eds) Photobiogeochemistry of Organic Matter, Environmental Science and Engineering (Environmental Engineering). Springer, Berlin, Heidelberg, 2013, pp 1-137

36.   García-Altares, M., Casanova, A., Bane, V., Diogène, J., Furey, A., & De la Iglesia, P. (2014). Confirmation of pinnatoxins and spirolides in shellfish and passive samplers from

Catalonia (Spain) by liquid chromatography coupled with triple quadrupole and high-resolution hybrid tandem mass spectrometry. *Marine drugs*, *12*(6), 3706-3732.

37.   Lamas, J. P., Arévalo, F., Moroño, Á., Correa, J., Muñíz, S., & Blanco, J. (2019). Detection and spatio-temporal distribution of pinnatoxins in shellfish from the Atlantic and Cantabrian coasts of Spain. *Toxins*, *11*(6), 340.

38.   Sleno, L., Windust, A. J., & Volmer, D. A. (2004). Structural study of spirolide marine toxins by mass spectrometry. *Analytical and bioanalytical chemistry*, *378*(4), 969-976.

39.   McCarron, P., Rourke, W. A., Hardstaff, W., Pooley, B., & Quilliam, M. A. (2012). Identification of pinnatoxins and discovery of their fatty acid ester metabolites in mussels (Mytilus edulis) from eastern Canada. *Journal of agricultural and food chemistry*, *60*(6), 1437-1446.

40.   M.A. Quilliam, P. Hess, C. Dell'Aversano, Recent development in the analysis of phycotoxins by liquid chromatography-mass spectrometry, in: W.J. deKoe, R.A. Samson, H.P. van Egmond, J. Gilbert, M.Sabino (Eds.), The Proceeding of Mycotoxins and Phycotoxins in perspective at the turn of the century, Wageningen, The Netherlands, 2001, 383-391.

41.   Varriale, F., Tartaglione, L., Cinti, S., Milandri, A., Dall'Ara, S., Calfapietra, A., & Dell'Aversano, C. (2021). Development of a data dependent acquisition-based approach for the identification of unknown fast-acting toxins and their ester metabolites. *Talanta*, *224*, 121842.

Chapter 3: Development of a hydrophilic interaction liquid chromatography-high resolution mass spectrometry (HILIC-HRMS) method for the analysis of paralytic shellfish poisoning toxins and tetrodotoxin.

1. Introduction

Paralytic shellfish poisoning toxins (PSTs) and tetrodotoxins (TTXs) are a wide group of potent naturally-occurring neurotoxins which are produced by benthic dinoflagellates and bacteria, respectively [1-3]. PSTs include more than 50 analogues, with saxitoxin (STX) being the parent compound, while TTXs are at least 30 derivatives with TTX being the first analogue to be discovered [4]. PSTs and TTXs represent a worrying threat to living beings since they can accumulate in the benthic epifauna and in a large number of edible marine organisms including fish, crustaceans, gastropods, and filter-feeding bivalves [5-7]. Surprisingly, even though PSTs and TTXs have different chemical structures, they act on the same molecular target inducing similar neurological disorders in humans which are grouped into toxic syndromes commonly known as paralytic shellfish poisoning (PSP) and tetrodotoxin shellfish poisoning (TSP) [8-10]. For this reason, the presence of such toxins in the food chain is a matter of concern for consumer health. Although shellfish products are regularly monitored in the EU for the presence of PSTs, only recently TTXs have drawn the attention of food safety authorities, which required more data on distribution through the food chain and toxicological effects before establishing a proper regulation [11]. Interestingly, PSTs and TTXs are coextracted under the same experimental conditions, thus a combined monitoring of these compounds by means of multi-toxin methods is a prerequisite. However, the development of effective, highly specific and sensitive methods for identification and quantification of PSTs and TTXs in complex matrices for long time has been a challenging issue considering: i) the high number of analogues described so far and their chemical features, ii) the limited number of commercially available standards and iii) the necessity to determine the concentration of each analogue individually for a correct health risk evaluation. Nonetheless, in the last decades a wide variety of biological and instrumental methods have been set up and proposed for the analysis of PSTs and TTXs, each having specific advantages and

drawbacks. Until December 2019, the reference method for PSTs in seafood has been the mouse bioassay (MBA) (AOAC 959.08), which has been widely employed in routine monitoring programs, as well as to monitor the presence of TTX in fish [12-14]. Although the strength of MBA is to provide a unique response resulting from the overall toxicity of an extract, ethical issues and a number of technical matters - low sensitivity, poor reproducibility and selectivity, and the impossibility of gaining information on the toxin profile, among others - make it not adequate for routine monitoring; so it has been replaced. [15-18]. Alternative biological approaches like the receptor binding assay (RBA; AOC 2011.27) and in vitro cell toxicity testing demonstrated not suitable for routine analyses because they presented drastic limitations such as poor information on toxin profile and necessity for further confirmation of positive samples [19-26].

Down sides of the biological approaches have been overcome by analytical instrumental methods that present greater sensitivity, selectivity and applicability for monitoring and research purposes. Among them, i) pre-column oxidation (ox-LC-FLD; AOAC 2005.06) [20] and ii) post-column oxidation (LC-ox-FLD; AOAC 2011.02) [27] with fluorescence detection approaches are actually accepted as official methods for the analysis of PSTs, with the first one being the EU reference method for this group of toxins. Even though ox-LC-FLD method is very sensitive and fully automated, data interpretation is quite complex and time consuming because some structurally different PSTs are oxidized into the same fluorescent product, whilst some others give rise to more than one fluorescent derivative after oxidation [28]. On the other hand, LC-ox-FLD method proved to have many advantages such as high sensitivity, an unique fluorescent chromophore formed for each PST, and the capacity to be automated. Under this approach, PSTs are analyzed by a reversed-phase (RP) chromatography using ion pairing reagents, oxidized into a specific in-line post-column reaction chamber and then detected by fluorescence. However, this method has shown a number of critical drawbacks: i) it is time consuming as two different ion-pairing RP LC runs are required for the analysis of GTXs, STXs and C toxins, ii) the instrumentation configuration is complex and requires a thorough daily maintenance, iii) ion-pairing reagents drastically reduce the RP column lifetime and iv) interfering compounds have been also identified [27, 29-33]. All the limitations of fluorescence-based detection methods have been overcome by using electrospray ionization–mass spectrometry (ESI–MS) as detector of the LC. Indeed, the basic backbone structure of PSTs and TTXs can easily ionize forming $[M+H]^+$ ions for each toxin [34-35]. Hence, a variety of separation techniques hyphenated with ESI-MS were exploited for development of new analytical

methods for PSTs and TTXs [36-38]. Among them, methods based on the combination of Capillary Electrophoresis (CE) with ESI-MS have been developed exploiting the different charge states of PSTs (mono-charged, doubly charged, and neutral) to achieve toxin separation. However, the three charge states of PST analogues require more than one analysis per sample, which makes this approach time-consuming [38-39], and the co-extraction of salts results into undesirable interferences.

Liquid chromatography (LC) coupled to ESI tandem MS is worldwide recognized as the most valid and effective alternative approach for the development of highly specific and sensitive methods for the determination of PSTs and TTXs in both environmental and food samples. Chromatographic separations can be successfully conducted in a single run using hydrophilic interaction liquid chromatography (HILIC) columns which have already proven suitable for the analysis of low molecular weight polar and ionic compounds [40-41]. In HILIC, the use of mobile phases with a high percentage of organic modifiers increases the ionization yield of the molecules, as well as improves the desolvation process (charge density) [42]. MS-detection do not require further confirmation for positive results as the possibility to perform tandem MS experiments and/or high resolution measurements (HRMS) provide additional confirmation criteria for toxin identification. All these positive aspects characterizing HILIC-MS methods allowed to overcome most of the drawbacks of the biological and analytical approaches for the determination of PSTs mentioned above, such as: i) ethical concerns (MBA), ii) the impossibility to investigate the toxin profile of samples (MBA and RBA), iii) long and complex data interpretation (ox-LC-FLD), iv) elaborate instrumentation configuration and maintenance (LC-ox-FLD), v) more than one run required for a complete analysis per sample (LC-ox-FLD and CE-MS) and vi) interference of co-extractives (all methods).

Although HILIC-MS technique has demonstrated suitable for the determination of PSTs and TTXs in complex matrices, the development of a high-performance methods is closely related to the type of mass spectrometer (MS) used. Robust and effective HILIC-MS^2 methods characterized by high sensitivity, specificity and reproducibility for the simultaneous determination of PSTs and TTXs in environmental and food samples were developed on triple quadrupole (QqQ) MS systems [3, 30, 43]. The QqQ platforms turned out to be a powerful tool for the determination of a large number of target compounds in a variety of matrices. In addition, time segmentation and dynamic MRM acquisition modes allow to monitor up to 100-120 analytes in a single run providing acceptable

levels of sensitivity even when a large number of transitions are monitored [44-45]. These features and benefits make QqQ MS the method of choice for the analysis of PSTs and TTXs. Both monitoring and research laboratories typically look for a pattern of 19 analogues per sample, among which only 15 are commercially available as certified reference materials (CRM; STX, C1, C2, GTX1, GTX2, GTX3, GTX4, dcGTX2, dcGTX3, dcNEO, NEO, B1, B2, dcSTX and TTX). The aim of this study was to develop a high-performance and sensitive HILIC-HRMS method on the LTQ Orbitrap XL™ mass spectrometer for the simultaneous analysis of 13 PST analogues and TTX. The challenging aspects of the work lie in the specifics of the mass analyzer and its application for the simultaneous analysis of a wide number of analytes in a single LC run. The strength of Orbitrap is undoubtedly represented by the high mass resolving power and the high mass accuracy. Therefore, it allows to determine the elemental composition of molecular and fragment ions with errors in the measurement of accurate masses falling well below 2 ppm [46]. Moreover, full-scan HRMS measurements allow to look for non-target compounds all at once and pave the way to retrospective analyses with no need to analyze the samples multiple times [44]. Although theses aspects make the Orbitrap platform a powerful tool for the analysis of unknown compounds at trace levels in complex matrices [47], some drawbacks make difficult the development of very sensitive multi-analyte methods. Long scan times needed for high resolution measurements make LTQ-Orbitrap XL FTMS incompatible with fast chromatography for the detection of a high number of analytes in one LC-HRMS run [48]. In addition, the long injection times required for measuring accurate masses through MS^2 experiments significantly reduce the scan frequency and the number of MS^2 scans, resulting in a reduced analytical sensitivity [49]. Keeping this in mind, this study describes analytical performances of three HILIC-HRMS methods, labeled as method 1, 2 and 3, for determination of PSTs and TTX using the Orbitrap MS. Comparison of method performance and application to the analysis of phytoplankton and shellfish samples is also reported. As part of method development, intriguing insights in the use of the LTQ Orbitrap XL FTMS for the analysis of such compounds emerged.

2. Results and discussion

2.1 HILIC-HRMS method 1

2.1.1 Optimization of chromatography

A PST mixture of CRM containing STX, C1, C2, GTX1, GTX2, GTX3, GTX4, dcGTX2, dcGTX3, dcNEO, NEO, B1 (GTX5), dcSTX and TTX standard was prepared and used to optimize the chromatographic conditions. The HILIC-MS method implemented by Dell'Aversano et al. (2000) was used as starting point for optimizing the chromatographic separation of PSTs on the available instrument. Briefly, Dell'Aversano et al. (2000) used a 5µm TSK-gel® Amide-80 column (250mm×2mmi.d.) kept at 20 °C and isocratically eluted with 65%B at 0.2 mL/min, where mobile phases were: water (A) and acetonitrile-water 95:5 v/v (B) both containing 2.0 mM ammonium formate and 3.6 mM formic acid at pH 3.5. In this study, the only difference to the above-reported conditions was the particle size of the column (3µm instead of 5 µm) and the length of the column: two TSK-gel® Amide-80 columns (250 and 150 mm) were tested, taking into account that column dimensions may affect separation efficiency, method sensitivity and analysis time.

Preliminary experiments performed under the above described conditions led to straightaway discard the isocratic elution because i) very broad chromatographic peaks were observed for STX, NEO, dcNEO and dcSTX on both columns and ii) no significant improvement in the length of the chromatographic run occurred (35 min). However, the isocratic setting provided still acceptable results in terms of peak resolution between the epimer pairs such as C1 and C2, GTX1 and GTX4, and dcGTX2 and dcGTX3. As a consequence, a gradient elution was tested on both columns: toxins were initially isocratically eluted, which allowed the separation of C toxins and GTXs, and then the %B was decreased and held to 10%B for the elution of B1, TTX, STX, NEO, dcNEO and dcSTX. Chromatographic details are reported in the experimental section. It has to be noted that while 65% B was sufficient to achieve a good toxin separation on the longer Amide-80 column (250 mm), the shorter column (150 mm) required 70%B as initial condition. Four time segments were created. As shown in **Fig.III.1-2**, C toxins were the first compounds to elute, followed by GTXs in the second time segment (GTX2, GTX1, dcGTX2, GTX3, GTX4, dcGTX3), B1 and TTX in the third one, and finally carbamoyl and decarbamoyl analogues (STX, dcNEO, dcSTX and NEO) in the last time segment. Evaluation of the peak shape indicated a number of 10 to 20 data point across each chromatographic peak which is sufficient for achieving a reliable

quantitation. Under the optimized conditions, sharp peaks were observed for C toxins (1st segment), GTXs (2nd segment), B1 and TTX (3rd segment) and STX (4th segment), whilst NEO, dcNEO and dcSTX provided broader peaks.
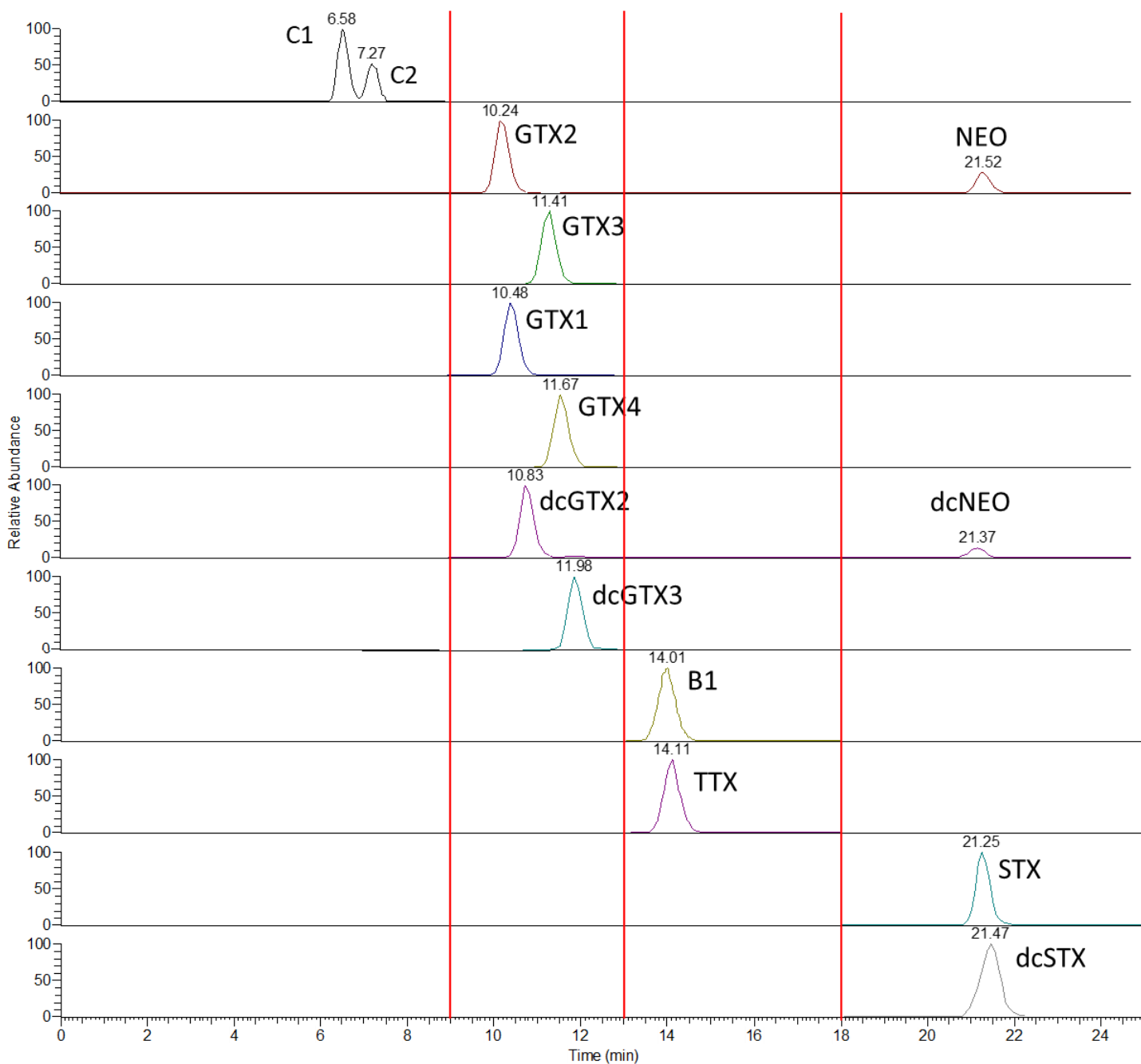
Figure III.1. Representative chromatographic separation of PSTs and TTX achieved through HILIC-HRMS method 1 and by using TSK-gel® Amide-80 of 250 mm.

Slight differences in peak shapes were observed between the two columns; the Amide-80 150 mm

provided sharper NEO and STX peaks than the 250 mm column. A good separation between the epimeric pairs (GTX2-3, GTX1-4 and dcGTX2-3) was achieved through the column of 250 mm,
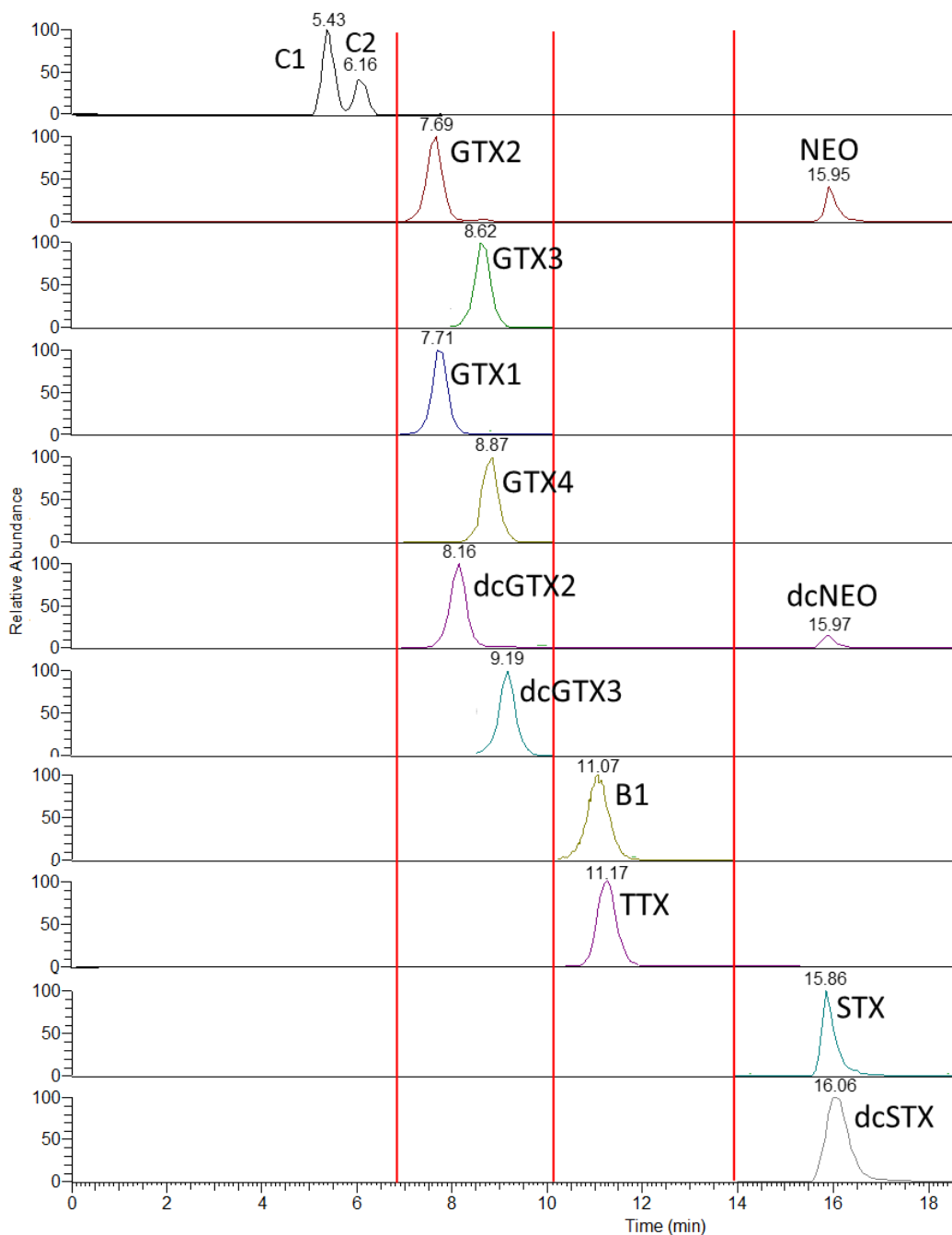
Figure III.2 Representative chromatographic separation of PSTs and TTX achieved through HILIC-HRMS method 1 and by using TSK-gel® Amide-80 of 150 mm.

except for C toxins for which only a moderate resolution was obtained. Nonetheless, the chromatographic resolution between the toxins that exist as epimeric pairs at C11 (GTX2/3 and

GTX1/4 and their dicarbamoyl derivatives) eluting in the second segment was poor since GTX2 co-eluted with GTX1 and dcGTX2 (α-group), and GTX3 co-eluted with GTX4 and dcGTX3 (β-group) (**Fig.III.1**). Moreover, GTX1 partially co-eluted with GTX3, as well as dcGTX2 with GTX3-4. Although many attempts were done to improve the separation between such toxins, they could not be chromatographically resolved, ending up in a crowded region of the chromatogram and of the associated full scan HRMS spectra that contained 6 PSTs eluting in a 2-3 min range. The employment of the 150 mm Amide-80 column gave worse results in terms of toxin separation since the resolution between the epimer pairs was only moderate with a partial co-elution between the α- and -β isomers (**Fig.III.2**). On the other hand, a poor resolution was observed also between other toxins since B1 co-eluted with TTX (third segment) and NEO co-eluted with dcNEO, STX and dcSTX (fourth segment). However, despite the poor chromatographic resolution, HRMS allowed to achieve a good selectivity in toxin identification anyway. Therefore, taking into account that only a moderate resolution was obtained between the epimeric pairs by using the 150 mm column, the employment of the 250 mm Amide-80 was preferred.hhThe necessity to implement a LC-HRMS method based on time segmentation required a careful evaluation of the reproducibility of retention times within (intra-variability) and between different batches of analysis (inter-variability). The intra-batch variability was evaluated for both Amide-80 columns by injecting a standard mixture 8 times for 30 h, and by calculating the mean and the standard deviation (sd) of retention times for each toxin. As a result, both chromatographic systems provided an excellent reproducibility with a negligible shift in retention times observed throughout the whole batch. By way of example, C1, GTX2, B1 and STX eluted, under the longer column, at 6.57±0.03, 10.28±0.08, 13.94±0.10, 21.26±0.08 min, respectively. Overall, for all the toxins the calculated sd was in the range 0.03-0.10 min, with the C toxins exhibiting the highest reproducibility (sd of 0.03 and 0.04 min for C1 and C2, respectively). This observation strongly suggested that the charge state of the molecules may have a certain influence on the chromatographic behavior as the mono and bi-charged analogues provided a slightly higher sd of retention times. The same high chromatographic reproducibility was also observed between different batches of analysis since for each toxin the calculated sd was in the range 0.04-0.12 min. On the other hand, the evaluation of the duration of time segments, together with the retention times, was taken into account for the optimization of effective methods. The 150 mm Amide-80 column provided a shorter gap between the elution of toxins in the first three segments than the 250 mm (**Fig.III.1-2**). For this reason,

even if the employment of the longer column resulted in longer analysis times than the shorter one (25 min versus 19 min), its use was preferred.

Critical issues related to MS behaviour of PSTs

PSTs are well suited to electrospray ionization providing abundant $[M+H]^+$ ions due to their basic backbone structure common to all analogues [3,34]. However, it is well-known that they undergo significant in-source fragmentation that strongly depends on: i) different types of ESI sources, ii) the ESI source parameters used, and iii) the substitution pattern and stereochemistry of different PST analogues. In this study, for the first time, the transmission of ions from LTQ to Orbitrap MS was observed to affect the stability of the ions formed in the ionization source. The crucial aspects of strong ESI^+ in-source fragmentation of PSTs lie into: i) decreased intensity of the $[M+H]^+$ ion of each analogue and ii) interference of fragment ions due to a defined PST analogue with pseudo-molecular and/or fragment ions of another analogue having the same exact mass and elemental composition: This may make difficult toxin identification based on Full scan HRMS only. By way of example, N-sulfated and C11-hydroxysulfated analogues (C1, C2, GTX1, GTX2, GTX3, GTX4, dcGTX2, dcGTX3 and B1) provide abundant $[M+H-nSO_3]^+$ (n=1,2) fragments due to the neutral loss of SO_3 (-80 Da). As a consequence, the $[M+H-SO_3]^+$ fragment at *m/z* 396.0932 of C1 and C2 might interfere with the $[M+H]^+$ ion of GTX2 and GTX3, having the same exact mass, as well as the $[M+H-2SO_3]^+$ at *m/z* 316.1364 of C toxins may interfere with the $[M+H]^+$ ion of NEO, as well as with the $[M+H-SO_3]^+$ fragment of GTX2 and GTX3. The $[M+H-SO_3]^+$ fragment at *m/z* 273.1306 of dcGTX2 and dcGTX3 may interfere with the $[M+H]^+$ ion of dcNEO, and the same is for the $[M+H-SO_3]^+$ fragment at *m/z* 300.1415 of B1 that has the same exact mass as the $[M+H]^+$ ion of STX. Although this behaviour can be exploited to select a reduced number of precursor ion to fragment within the same LC-HRMS^2 analysis, thus decreasing the number of MS^2 and increasing the instrumental sensitivity, a good resolution between closely eluting chromatographic peaks is a prerequisite for an accurate identification of the above toxins based also on retention times.

2.1.2 Optimization of HRMS conditions

As previously reported [3, 50], lower source temperatures reduce the in-source fragmentation (loss

of SO_3, H_2O and carbamoyl moieties) of individual PSTs, but at the same time reduce also the charge density of droplets, resulting in a decreased sensitivity. For this reason, a balance between the degree of fragmentation, which is toxin-dependent, and the intensity of ions was required. Therefore, influence of source parameters on the ionization of each PST analogue was evaluated under the used chromatographic conditions. An average capillary temperature of 300°C was set; indeed, the intensity of desulfated analogues such as STX and dcSTX increased with temperature up to 440°C, whilst a noticeable decrease in ion intensity was observed for C toxins and GTXs. Source voltage was set at 4.8 kV since for each toxin a stepwise decrease up to 2.5 kV resulted in a lower sensitivity. On the other hand, signal intensity greatly depended on parameters such as capillary voltage (CV) and tube lens (TL) since the highest sensitivity for C toxins was found at higher values (CV 80 and TL 210) compared to all the other PSTs (CV 20 and TL 90). These optimized source settings were then applied to the analysis of a mixture of PST and TTX standard and used to acquire their full-scan HRMS spectra. As showed in **Fig.III.3**, a high degree of in-source fragmentation occurred for all analogues, with the only exception for NEO, dcNEO and TTX, whose spectra were dominated by abundant $[M+H]^+$ ions. Although STX, dcSTX and B1 exhibited $[M+H]^+$ ions as base peak, in-source fragments due to the loss of H_2O (STX and dcSTX) and SO_3 (B1) were present in the full-scan spectrum. GTX3 and dcGTX3 gave abundant $[M+H]^+$ ions, whilst C toxins, GTX1, GTX2, GTX4 and dcGTX2 underwent a strong in-source fragmentation as their $[M+H]^+$ ions were barely (or not at all) detectable. Particularly, the $[M+H-SO_3]^+$ ion was the most intense signal in the spectra of C2, GTX2, GTX1 and dcGTX2, while the $[M+H-H_2O]^+$ and the $[M+H-2SO_3]^+$ ions were the base peaks in the spectrum of GTX4 and C1, respectively. In addition, dcGTX2, dcGTX3 dcNEO, NEO, STX and dcSTX gave $[M+Na]^+$ ions in a relative abundance ratio with the $[M+H]^+$ or in-source fragment that was toxin-dependent. Notably, for dcGTX2 the relative ratio $[M+H-SO_3]^+ : [M+Na]^+$ was 100:50; the same relation was observed between the $[M+H]^+$ and $[M+Na]^+$ ions of dcGTX3 and dcNEO, whereas for NEO, STX and dcSTX the measured relative abundance ratio $[M+H]^+ : [M+Na]^+$ was 100:30, 100:10 and 100:15, respectively. HRMS^2 experiments, ramping manually the collision energy and selecting the most intense ion as precursor, were performed for all the analogues (**Fig.III.4**).
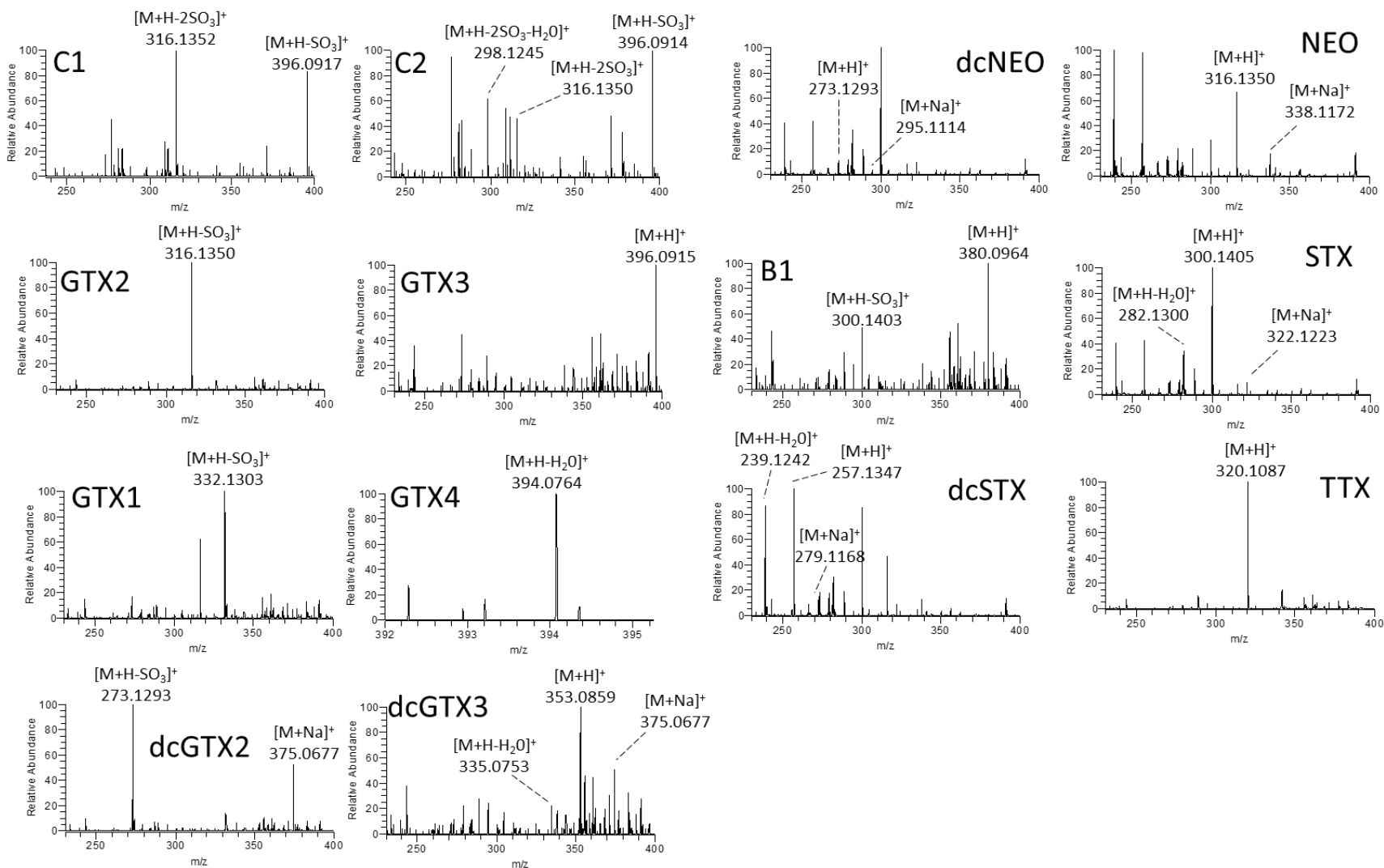
Figure III.3 HR full-scan MS spectrum of PSTs and TTX analyzed by HILIC-HRMS method 1 and by using the Amide-80 column of 250 mm.
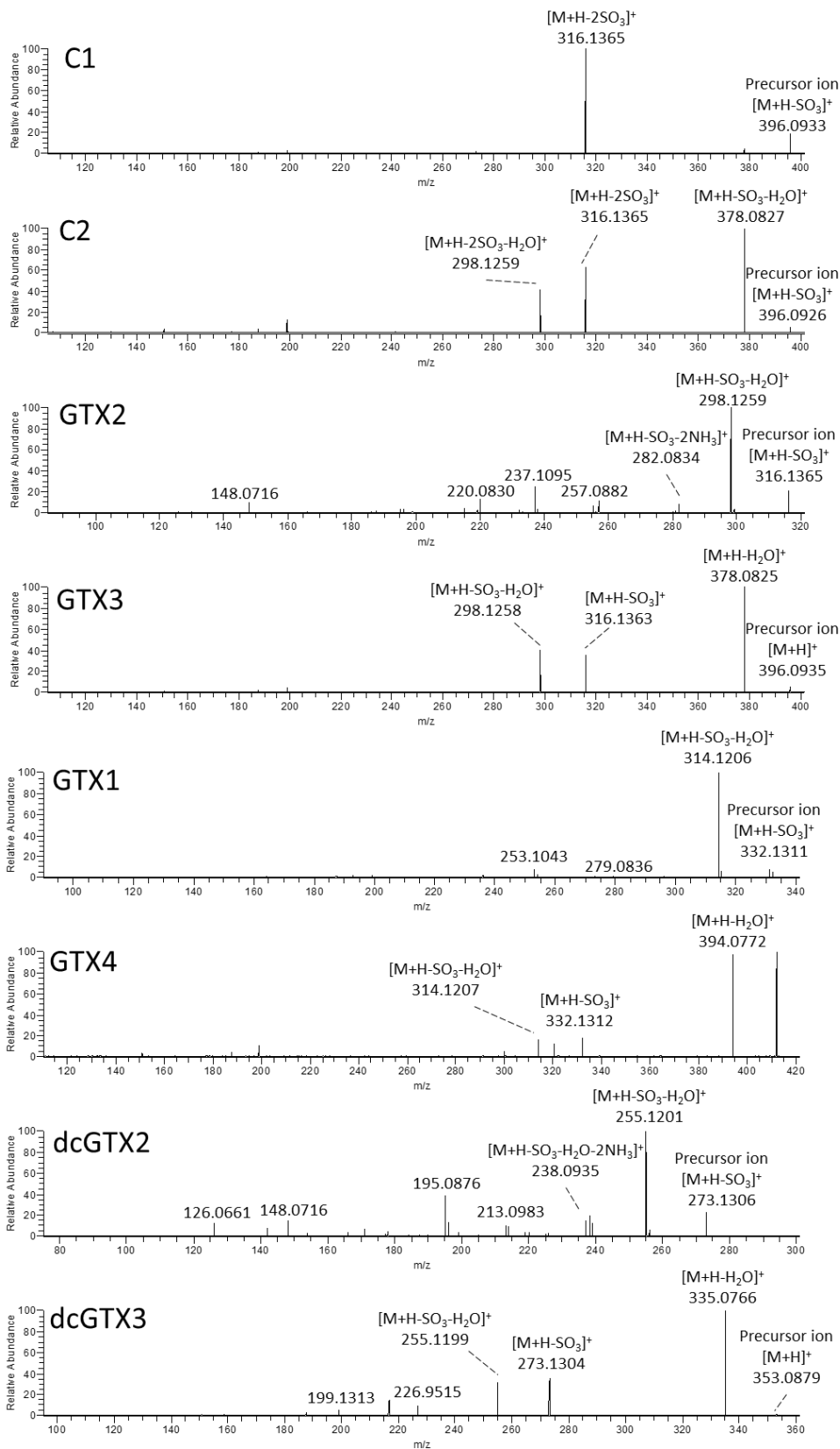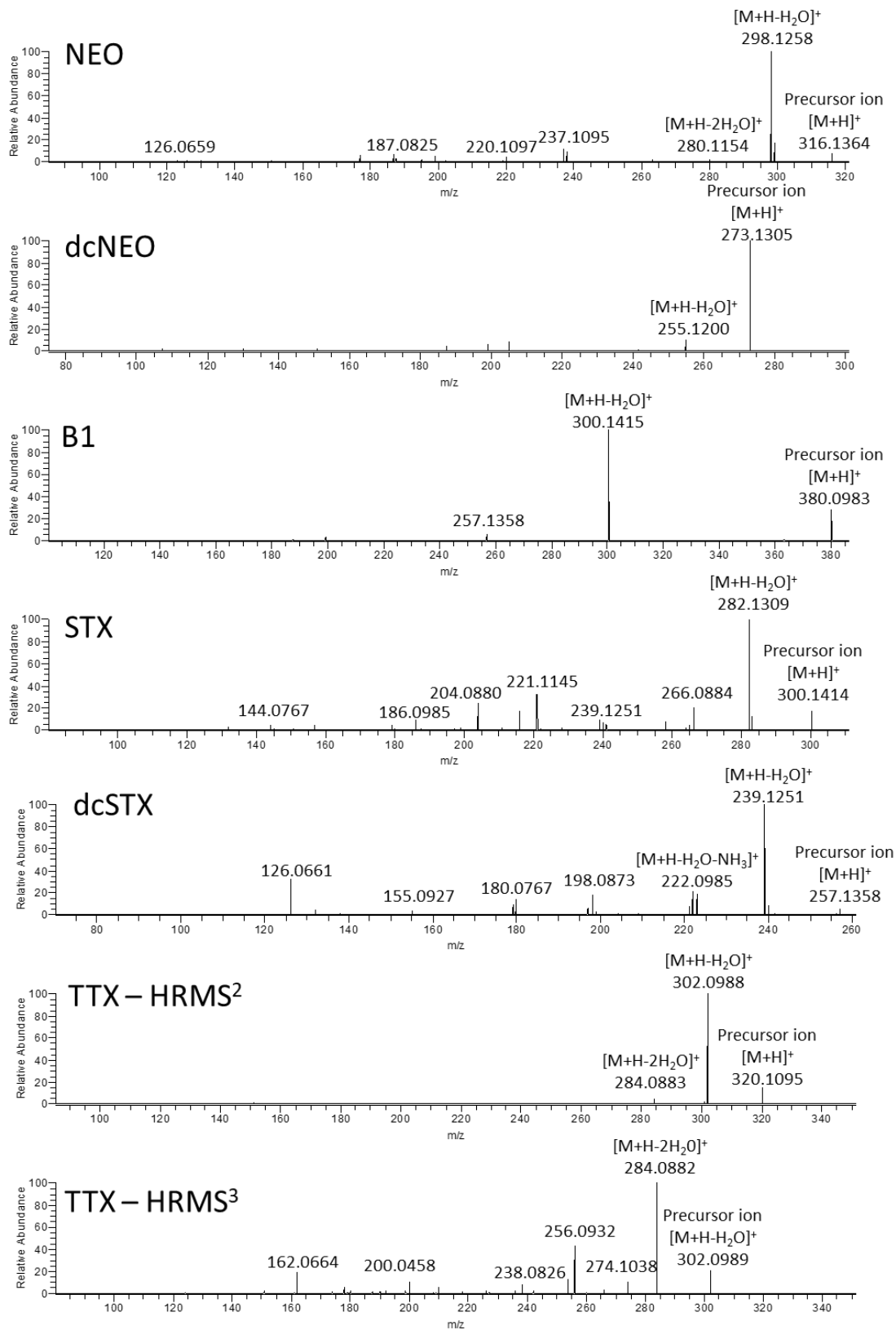
Figure III.4 CID HRMS^2 spectra of assorted PSTs and TTX. HRMS^3 spectrum of TTX.

In addition, the fragmentation of the epimer pairs provided very different HRMS^2 spectra (spectra not showed for all PSTs). Notably, differences in ionization behavior and fragmentation profiles between C11-hydroxysulfated epimers lie in the configuration of the C11 stereocenter since some analogies were observed within the 11α- (C1, GTX1, GTX2 and dcGTX2) and the 11β- (C2, GTX3, GTX4 and dcGTX3) group.

With regard to TTX, HRMS^2 experiment, selecting as precursor the [M+H]$^+$ ion, provided a fragmentation spectra dominated by a very intense [M+H-H$_2$O]$^+$ fragment at *m/z* 302.0988 and a less intense [M+H-2H$_2$O]$^+$ ion at *m/z* 284.0883 (**Fig.III.4**). Contrarily, HRMS^3 experiment, acquired by fragmenting the ion at *m/z* 302.1 which was obtained after a first MS^2 scan, showed a more informative spectrum containing a variety of diagnostic fragment ions (**Fig.III.4**). However, method sensitivity turned out to be higher when TTX was measured by HRMS^2 experiments, thus HRMS^3 approach was designated for qualitative purposes.

However, the high degree of in-source fragmentation and the absence of [M+H]$^+$ ions in the HRMS spectra of some PSTs (C toxins, GTX1 and GTX4) prompted us to carefully explore the role that the ion transmission path to the Orbitrap had. Intriguing findings emerged from this investigation and a strong influence of the analyzer (LTQ MS or LTQ-Orbitrap FTMS) on the MS behavior of individual analogues was brough to light. By way of example, the [M+H]$^+$ ion of GTX4 was not found in the HRMS spectrum (**Fig.III.3**) which contained only the low intense in-source fragments [M+H-H$_2$O]$^+$, [M+H-SO$_3$]$^+$ and [M+H-SO$_3$-H$_2$O]$^+$ at *m/z* 394.0770, 332.1310 and 314.1203, respectively, suggesting that the toxin underwent a strong in-source fragmentation. However, the low resolution full-scan MS spectrum (LRMS) of GTX4, acquired using the LTQ mass analyzer only, contained an intense [M+H]$^+$ ion, suggesting that the molecule was not fragmenting significantly in the ESI source (**Fig.III.5a**). Similarly, LR CIDMS^2 spectrum of GTX4, obtained using the ion at *m/z* 412.1 as precursor (**Fig.III.5b**) contained the same fragments as the HRMS spectrum of the toxin. Therefore, even if the [M+H]$^+$ ion of GTX4 was not found in the HR full-scan MS spectrum, pointing out that it was not detected by the Orbitrap mass analyzer, CID HRMS^2 experiments selecting as precursor the [M+H]$^+$ ion at *m/z* 412.1 (**Fig.III.4**) were successful. The presence of characteristics fragment ions of GTX4, definitely confirmed the identity of the signal emerged in the LRMS and LRMS^2 spectra. This observation suggested that the fragmentation of GTX4 was not occurring in the ESI source, as initially thought, but in the ion transmission system from LTQ to Orbitrap.
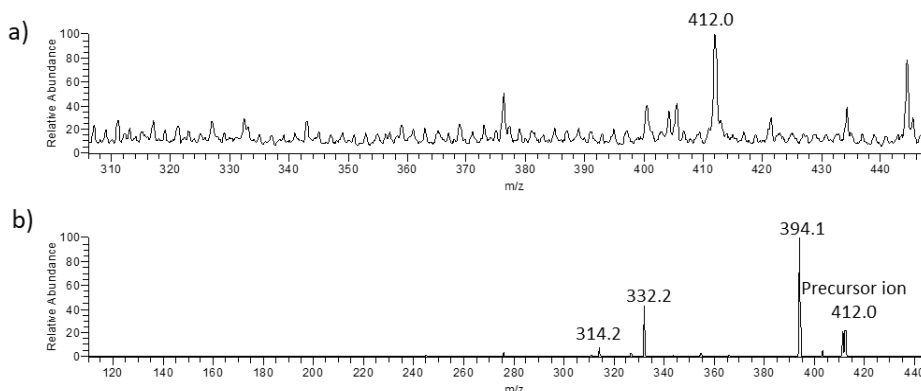
Figure III.5 a) Low-resolution (LR) full-scan MS spectrum of GTX4 CRM. b) CID LRMS^2 spectrum selecting as precursor the ion at *m/z* 412.1.

This phenomenon becomes more clear if the principle of operation of LTQ Orbitrap XL FTMS are taken into account (**Fig.III.6**; [51]. Briefly, ions generated by ESI source are injected into the LTQ, where they can be: i) scanned at LR (LRMS spectrum), ii) selected, fragmented in CID mode and scanned at LR (LRMS^2 spectrum), or iii) scanned and/or fragmented in CID mode and transferred via C-Trap to Orbitrap (transmission system) where they are captured and scanned (HRMS and/or HRMS^2 spectrum).
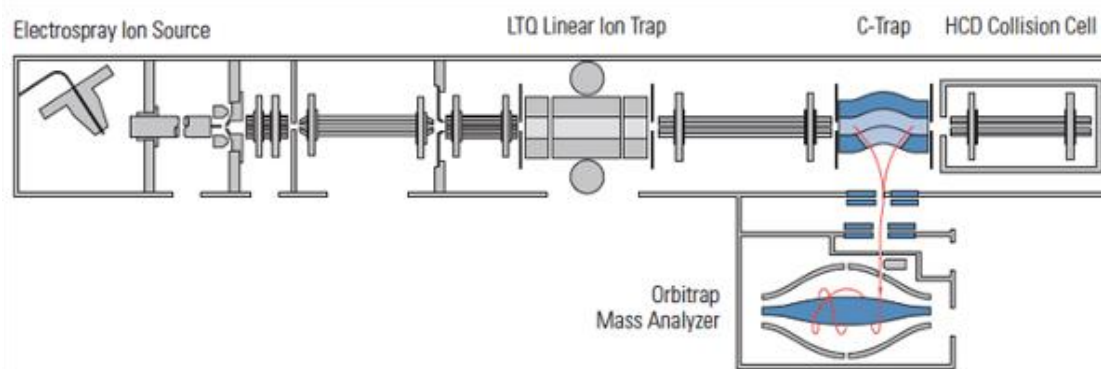
Figure III.6 Schematic representation of LTQ Orbitrap XL^{TM} Fourier Transform Mass Spectrometer (FTMS) equipped with an ESI ION MAX^{TM} source.

Therefore, the [M+H]$^+$ ion of GTX4 is quite stable when scanned by the LTQ and no spontaneous fragmentation occurs considering the absence of fragment ions in the LRMS spectrum (**FigIII.5a**). Contrarily, when the ion is transferred to Orbitrap to acquire the HR full-scan MS spectrum, it undergoes fragmentation ending up being undetectable. Contrarily, when the [M+H]$^+$ ion of GTX4

is fragmented in the LTQ mass analyzer in CID mode, the fragments are detectable both at low- and high-resolution. This means that fragment ions of GTX4, produced in the LTQ, are quite stable to be transferred via C-trap to Orbitrap, where they are scanned and detected in the HRMS^2 spectrum. Similarly, [M+H]$^+$ ions of GTX1, GTX2 and dcGTX2, which were not present in the HRMS spectrum, were present in LRMS spectra and their fragmentation spectra were acquired. However the [M+H]$^+$ ion of C toxins at *m/z* 476.0500 was not detected under any experimental conditions tested either LRMS or HRMS.

In addition, to clarify the influence that the instrument had on the stability of PSTs, and if there was a toxin-dependent relationship, further experiments were conducted. Notably, the most intense ions contained in the LRMS spectra ([M+H]$^+$ or fragment ions) were selected as precursors to acquire the relevant HRMS^2 spectra at collision energy (CE) 0%. By way of example, **Fig.III.7** showed the HRMS^2 spectrum of C2 toxin selecting as precursor the [M+H-SO$_3$]$^+$ ion at *m/z* 396.1 at CE 0. A very intense [M+H-SO$_3$-H$_2$O]$^+$ was observed, and the relative ratio between the fragment and its precursor was 90:100. This clearly evidenced the strong impact that the instrument transmission system had on the stability of the selected ions. Similarly, a significative difference was observed between the C11-α- and β- hydroxysulfated analogues. Differently from C2, the [M+H-SO$_3$]$^+$ ion of C1 at CE 0 was quite stable since the [M+H-SO$_3$-H$_2$O]$^+$ ion at *m/z* 378.0815 was barely detectable. On the other hand, the HRMS^2 spectrum, selecting as precursor the [M+H-2SO$_3$]$^+$ ion at *m/z* 316.1360, gave a less intense [M+H-2SO$_3$-H$_2$O]$^+$ fragment only for C2. However, the most intense ion for C1 was that at *m/z* 316.1360 whilst for C2 was that at *m/z* 396.0928. These investigations clearly suggested that C1 underwent a strong in-source fragmentation, and the influence of the transmission system was lower than that observed for C2. The same behavior was evidenced for the other epimeric pair (**Fig.III.7**). As a result, the C11-α-hydroxysulfated analogues (GTX2, GTX1 and dcGTX2) underwent a strongest in-source fragmentation, thus providing abundant [M+H-SO$_3$]$^+$ ions which are stable when transferred from LTQ to Orbitrap via C-trap. Their [M+H]$^+$ ions were detectable at low-resolution and not at high-resolution due to the strong impact of the ion transmission system. Contrarily, C11-β-hydroxysulfated analogues (GTX3, GTX4 and dcGTX3) underwent a lower in-source fragmentation, giving abundant [M+H]$^+$ ions that turned out to be unstable when transferred from LTQ to Orbitrap analyzer at CE 0 giving abundant [M+H-H$_2$O]$^+$ ions; their [M+H-SO$_3$]$^+$ ions were stable along the transmission system. On the other hand, desulfated analogues (STX, dcSTX, NEO

and dcNEO) did not fragment at CE 0 % differently from B1 that provided only an intense [M+H-SO$_3$]$^+$ ion at *m/z* 300.1412 while the [M+H]$^+$ ion was fragmented at CE 0%.

With the aim to develop a LC-HRMS^2 method characterized by the highest analytical sensitivity further fragmentation experiments were performed. The most intense precursor ion for each toxin was selected and the CE was ramped manually from 0 to 20% in CID mode. The peak area of C1, C2, GTX2, GTX1, dcGTX2, NEO, dcNEO, STX and dcSTX turned out to be higher at CE 0% than that obtained between CE 1-20%, even when all the produced fragments were extracted. This highlighted that, even at lower CEs, some PSTs undergo a substantial and irreversible fragmentation, with a number of fragments that ends up being undetectable, thus decreasing the instrumental sensitivity. On the other hand, GTX3, GTX4, dcGTX3, B1 and TTX provided the highest sensitivity when fragmented at CE ≠ 0%. Moreover, the method sensitivity was further increased by selecting a reduced *m/z* acquisition range that was manually configured on the basis of the fragment ions produced at specific CEs for each toxin. The best MS parameters found for the analysis of PSTs and TTX are reported in **Table III.1**. The high number of analytes to be monitored associated with: i) different source parameters found for some toxins (C1 and C2), iii) large number of precursor ions to be selected, and iii) the low scan frequency of the Orbitrap MS, clearly evidenced the need to develop a LC-HRMS^2 method that used time-segments. The configuration of time segments (or windows) allows to select a specific number of toxins (grouped on the basis of their retention times) to monitor through MS^2 scans in a defined time frame. The main advantage of this technique lies in an increased sensitivity for each detected compounds since the overall number of MS^2 scans across the entire run remarkably decreases. As a consequence, a higher number of data point for each chromatographic peak is obtained.
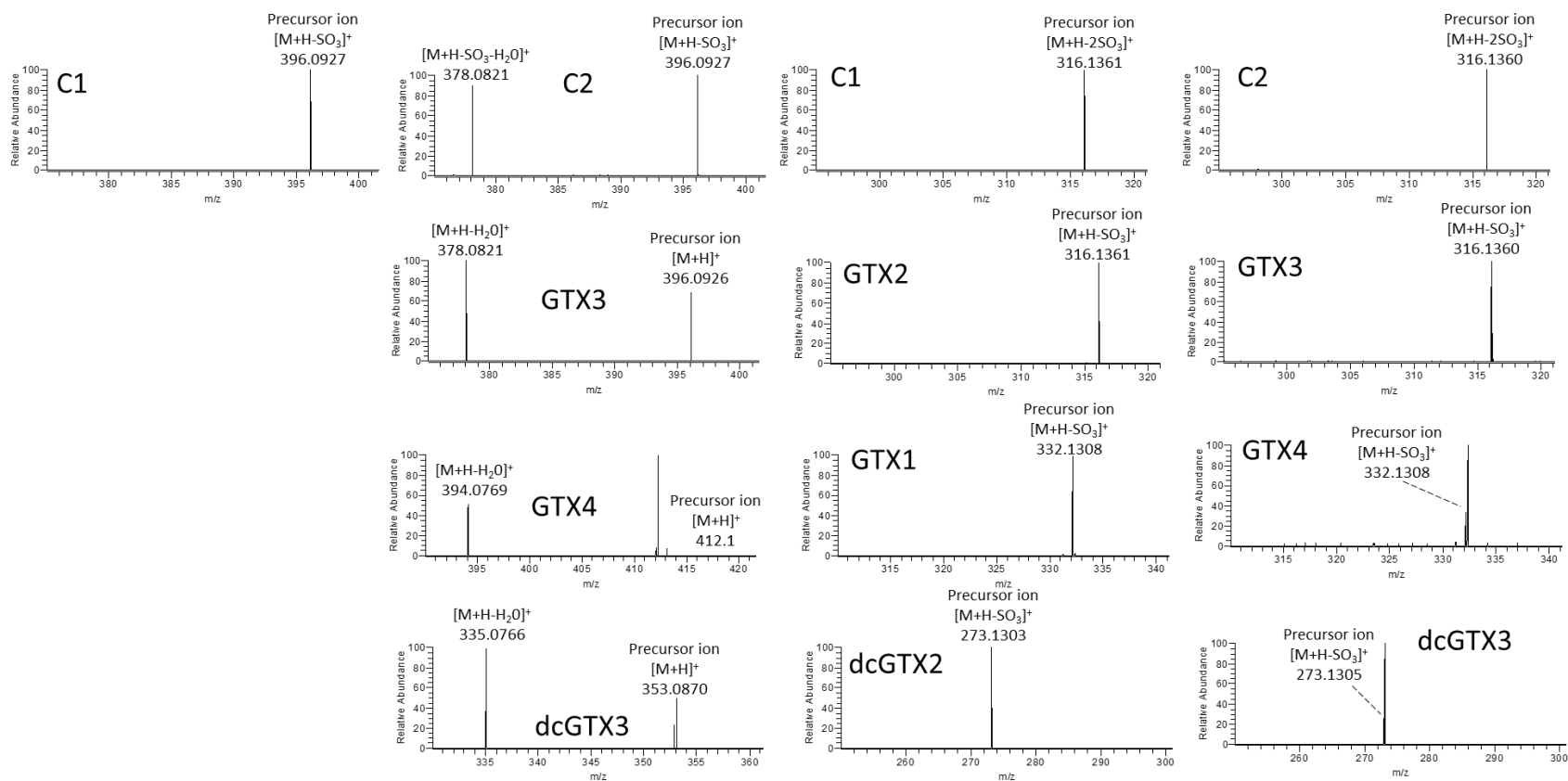
Figure III.7 CID HRMS^2 spectrum of C1,C2, GTX1-4 and dcGTX2-3 at CE 0%, selecting as precursor different ions for each toxin. The HRMS^2 spectra of α-hydroxysulfated analogues (GTX2, GTX1, dcGTX2) ,selecting as precursor the relevant [M+H]$^+$ ion, are not reported since no diagnostic ions or fragments emerged.

Table III.1. HRMS data of PST$_S$ and TTX. Optimized CID HRMS^2 conditions for method 1.

Toxin	*m/z* [M+H]$^+$ Formula	*m/z* precursor ion Formula	CID CE %	*m/z* range	Time Segment
C1	476.0500 $C_{10}H_{18}N_7O_{11}S_2^+$	316.1 - [M+H-2SO$_3$]$^+$ $C_{10}H_{18}N_7O_5^+$	0	312-320	1
C2	476.0500 $C_{10}H_{18}N_7O_{11}S_2^+$	396.1 - [M+H-SO$_3$]$^+$ $C_{10}H_{18}N_7O_8S^+$	0	374-400	1
GTX2	396.0932 $C_{10}H_{18}N_7O_8S^+$	316.1 - [M+H-SO$_3$]$^+$ $C_{10}H_{18}N_7O_5^+$	0	312-320	2
GTX3	396.0932 $C_{10}H_{18}N_7O_8S^+$	396.1 - [M+H]$^+$ $C_{10}H_{18}N_7O_8S^+$	12	294-400	2
GTX1	412.0881 $C_{10}H_{18}N_7O_9S^+$	332.1 - [M+H-SO$_3$]$^+$ $C_{10}H_{18}N_7O_6^+$	0	328-336	2
GTX4	412.0881 $C_{10}H_{18}N_7O_9S^+$	412.1 - [M+H]$^+$ $C_{10}H_{18}N_7O_9S^+$	20	310-414	2
dcGTX2	353.0874 $C_9H_{17}N_6O_7S^+$	273.1 - [M+H-SO$_3$]$^+$ $C_9H_{17}N_6O_4^+$	0	269-277	2
dcGTX3	353.0874 $C_9H_{17}N_6O_7S^+$	353.1 - [M+H]$^+$ $C_9H_{17}N_6O_7S^+$	10	251-357	2
B1	380.0983 $C_{10}H_{18}N_7O_7S^+$	380.1 - [M+H]$^+$ $C_{10}H_{18}N_7O_7S^+$	12	254-304	3
TTX	320.1095 $C_{11}H_{18}N_3O_8^+$	320.1 - [M+H]$^+$ $C_{11}H_{18}N_3O_8^+$	20	85-350	3
NEO	316.1364 $C_{10}H_{18}N_7O_5^+$	316.1 - [M+H]$^+$ $C_{10}H_{18}N_7O_5^+$	0	312-320	4
dcNEO	273.1306 $C_9H_{17}N_6O_4^+$	273.1 - [M+H]$^+$ $C_9H_{17}N_6O_4^+$	0	269-277	4
STX	300.1415 $C_{10}H_{18}N_7O_4^+$	300.1 - [M+H]$^+$ $C_{10}H_{18}N_7O_4^+$	0	296-304	4
dcSTX	257.1357 $C_9H_{17}N_6O_3^+$	239.1 - [M+H-H$_2$O]$^+$ $C_9H_{15}N_6O_2^+$	0	235-243	4

CID= collision-induced dissociation; CE= collision energy

2.1.3 Evaluation of matrix effect, limits of detection and linearity

Applicability of the implemented LC-HRMS^2 method for determination of PSTs to the analysis of real mussel samples was evaluated. At this regard, matrix-free (MF) and matrix-matched (MM) calibration curves of toxin standards were prepared at different concentration levels and analyzed by HILIC-HRMS^2 by using both TSK-gel® Amide-80 columns (150 mm and 250 mm). Notably, MM standards were prepared by diluting each toxin with an aliquot of a blank mussel extract which was subjected to a clean-up procedure by means of solid-phase extraction (SPE). Chromatographic parameters were not affected by matrix since retention time and peak shape of MF and MM

standards were almost superimposable (**Table III.2**). On the other hand, the matrix influence on the HRMS response was clearly toxin-dependent, in terms of intensity and type of effect (suppression or enhancement) (**Table III.2**). C2, GTX2, GTX1, GTX4 and STX suffered by an ion suppression effect in the whole concentration range tested, with higher suppression observed at the lowest concentration levels, whilst TTX was the only compound that underwent matrix enhancement (13.8-48.0%). For all the other toxins, a noticeable concentration-dependent matrix effect was observed. C1 and dcGTX2 underwent enhancement effect at the highest concentration levels and a suppression effect at the most diluted ones, while the opposite trend was observed for dcGTX3, B1 and dcSTX. Contrarily, for GTX3, NEO and dcNEO was not observed any trend and only a slight suppression and ion enhancement effect occurred at different concentration levels. MF and MM curves of each standard showed excellent linearity with correlation coefficients (R^2) within 0.996-0.999. Limits of detections (LODs) were experimentally measured on both Amide-80 columns (**Table III.2**) and were good for all the monitored toxins. The highest analytical sensitivity was obtained for STX, dcSTX, NEO, GTX1, GTX2 and dcGTX3, for which LODs were lower than 10 ng/mL both for MF and MM standards. A good sensitivity was also measured for GTX3, GTX4, dcGTX2, dcNEO and B1 since the LODs of MF and MM standards were within 15-28 ng/mL. The highest LODs were observed for C toxins with values of about 50 ng/mL.

Table III.2. Retention time (min) and LOD (ng/mL) of MF and MM standards measured by HILIC-HRMS[2] method 1 by using TSK-gel Amide-80 columns of different length (150 and 250 mm). Matrix effect % (+ suppression, - enhancement) at different concentration levels was measured through Amide-80 column of 250 mm.

Toxin Rt_{MF}, Rt_{MM} (min) LOD_{MF}, LOD_{MM} (ng/mL)	µg/mL	Matrix effect %	
C2	0.985	7.9	
6.16[a], 6.30[a]	0.448	5.7	
7.27[b], 7.28[b]	0.224	13.3	
56.0[a], 56.0[a]	0.112	16.2	
56.0[a], 56.0[a]	0.056	17.0	

MF curve; y = 380996x - 19885
R² = 0.9989
MM curve; y = 359938x - 23989
R² = 0.9995

GTX2	0.627	4.6	
7.69[a], 7.68[a]	0.314	5.6	
10.24[b], 10.27[b]	0.157	4.9	
2.0[a], 5.0[a]	0.078	24.0	
10.0[a], 10.0[a]	0.039	26.5	

MF curve; y = 3E+06x - 6877.5
R² = 0.9998
MM curve; y = 3E+06x - 34889
R² = 0.9996

GTX1	0.690	5.2	
7.71[a], 7.81[a]	0.345	7.2	
10.48[b], 10.49[b]	0.173	16.9	
5.0[a], 11.0[a]	0.086	-0.7	
11.0[b], 5.0[b]	0.043	12.2	

MF curve; y = 3E+06x - 19496
R² = 0.9994
MM curve; y = 3E+06x - 34717
R² = 0.9992

Toxin Rt$_{MF}$, Rt$_{MM}$ (min) LOD$_{MF}$, LOD$_{MM}$ (ng/mL)	µg/mL	Matrix effect %	
GTX4	0.450	4.2	
8.87[a], 8.87[a]	0.225	14.3	
11.67[b], 11.61[b]	0.113	21.0	
28.0[a], 56.0[a]	0.056	76.6	
56.0[b], 56.0[b]	0.028	77.1	
STX	0.343	8.9	
15.86[a], 15.86[a]	0.171	6.7	
21.25[b], 21.17[b]	0.086	6.0	
0.7[a], 0.7[a]	0.043	11.0	
3.0[b], 3.0[b]	0.021	5.8	
TTX	0.167	-13.8	
11.17[a], 11.07[a]	0.083	-15.5	
14.11[b], 14.00[b]	0.042	-23.4	
< 5.0[a]	0.021	-48.0	
< 5.0[a]	0.010	-23.6	
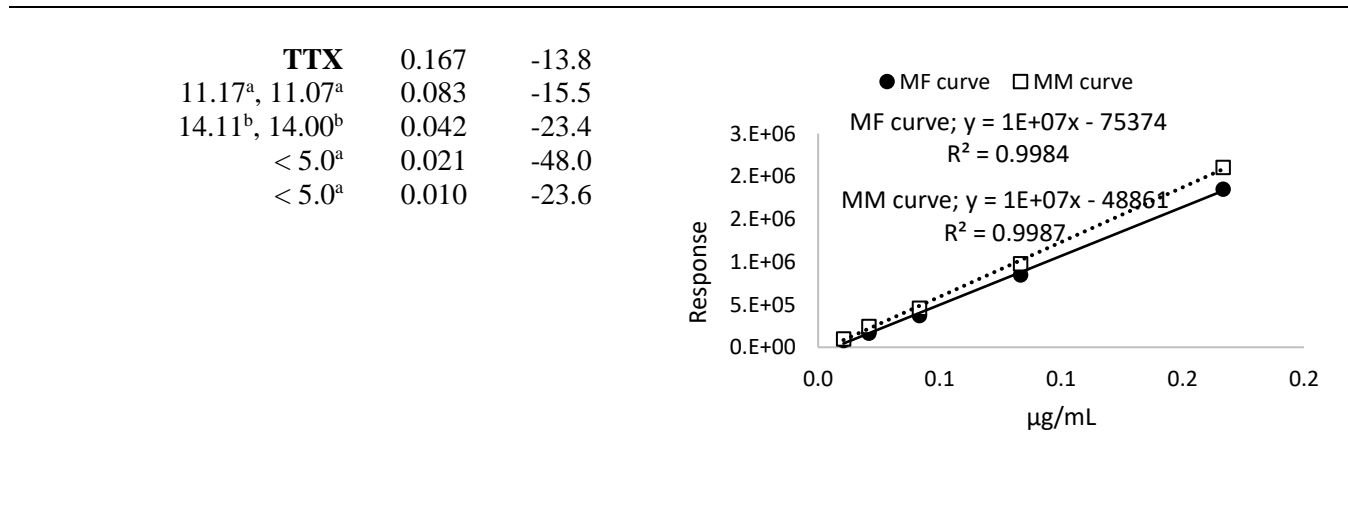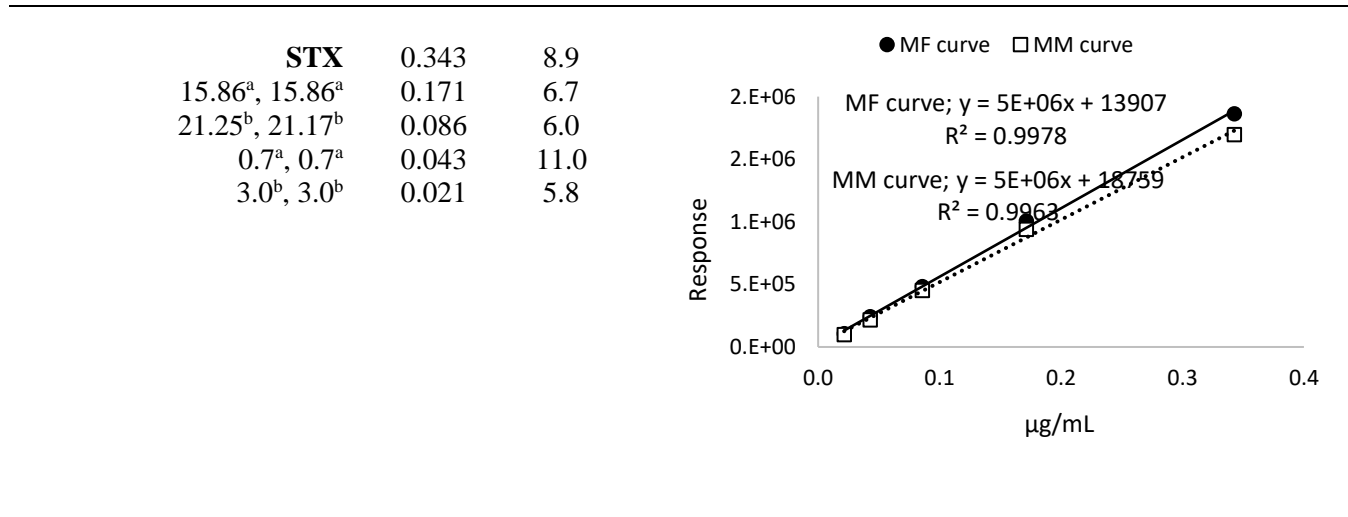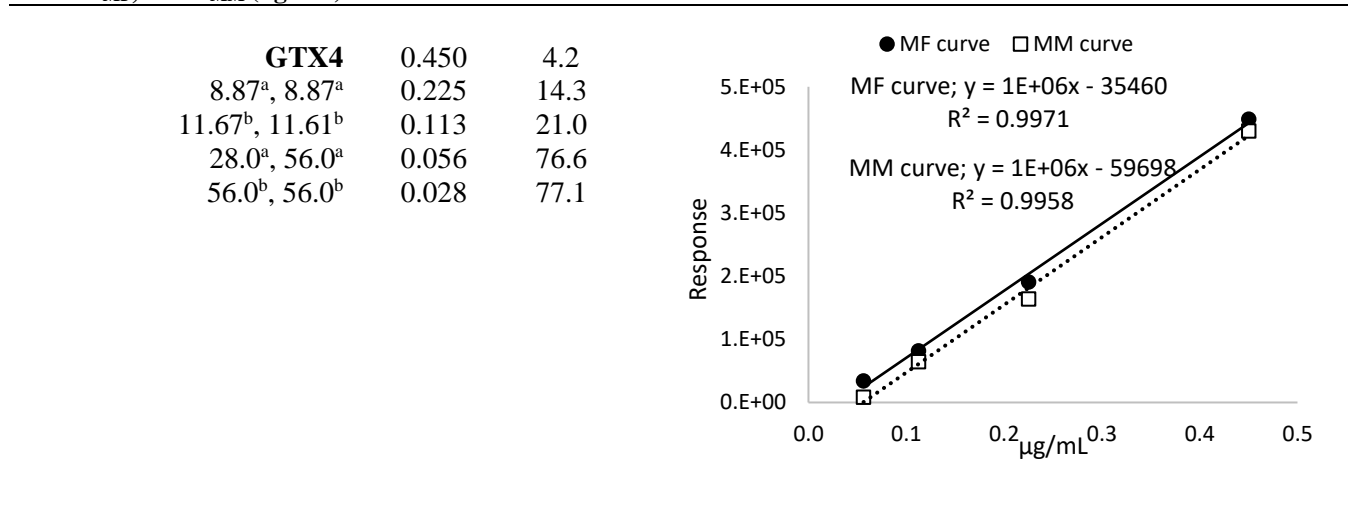
Toxin Rt_{MF}, Rt_{MM} (min) LOD_{MF}, LOD_{MM} (ng/mL)	µg/mL	Matrix effect %	
C1	0.749	-12.1	
5.43[a], 5.54[a]	0.374	-8.5	
6.58[b], 6.59[b]	0.187	4.0	
47.0[a], 47.0[a]	0.094	2.6	
47.0[b], 23.0[b]	0.047	38.8	
dcGTX2	0.490	-1.0	
8.16[a], 8.16[a]	0.245	5.3	
10.83[b], 10.83[b]	0.122	6.7	
15.0[a], 15.0[a]	0.061	10.6	
15.0[b], 15.0[b]	0.031	12.0	
dcGTX3	0.575	7.7	
9.19[a], 9.29[a]	0.288	2.1	
11.98[b], 11.94[b]	0.144	12.4	
9.0[a], 9.0[a]	0.072	-1.4	
9.0[b], 18.0[b]	0.036	-13.4	
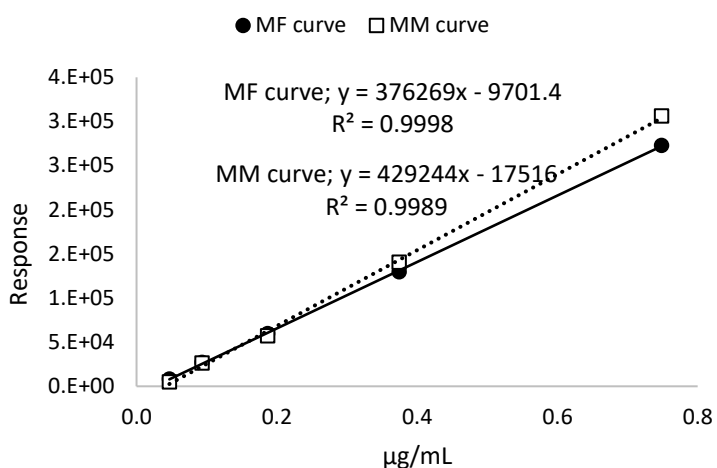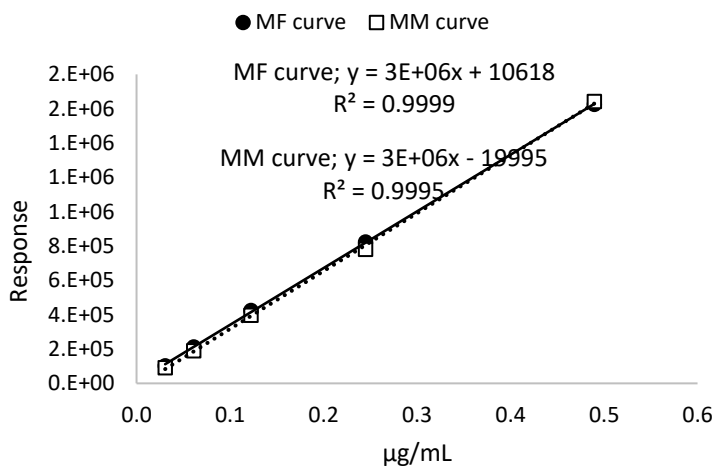
C1 graph:
MF curve; y = 376269x - 9701.4, R^2 = 0.9998
MM curve; y = 429244x - 17516, R^2 = 0.9989

dcGTX2 graph:
MF curve; y = 3E+06x + 10618, R^2 = 0.9999
MM curve; y = 3E+06x - 19995, R^2 = 0.9995

dcGTX3 graph:
MF curve; y = 3E+06x - 77750, R^2 = 0.9997
MM curve; y = 3E+06x - 63389, R^2 = 0.9987

179
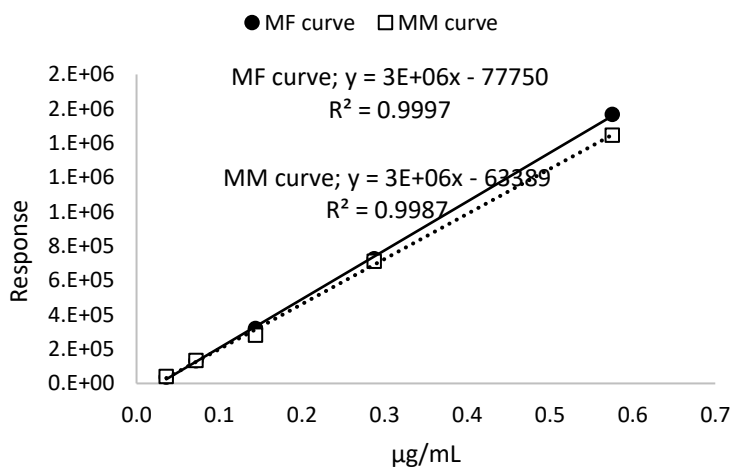
Toxin Rt_{MF}, Rt_{MM} (min) LOD_{MF}, LOD_{MM} (ng/mL)	µg/mL	Matrix effect %	
B1	0.587	1.4	
11.07[a], 11.04[a]	0.293	3.4	
14.01[b], 13.97[b]	0.147	8.4	
18.0[a], 18.0[a]	0.073	12.5	
18.0[b], 18.0[b]	0.037	-118.5	

MF curve; y = 1E+06x - 33184
R² = 0.9994

MM curve; y = 1E+06x - 33847
R² = 0.9985
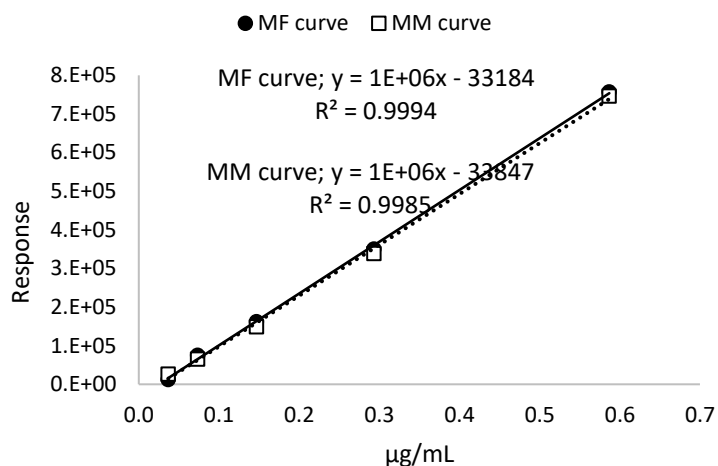
dcSTX	0.354	11.8	
16.06[a], 16.06[a]	0.177	11.2	
21.47[b], 21.41[b]	0.089	14.5	
3.0[a], c.0[a]	0.044	12.7	
6.0[b], 11.0[b]	0.022	-1.5	

MF curve; y = 7E+06x + 72589
R² = 0.9973

MM curve; y = 6E+06x + 66843
R² = 0.9987
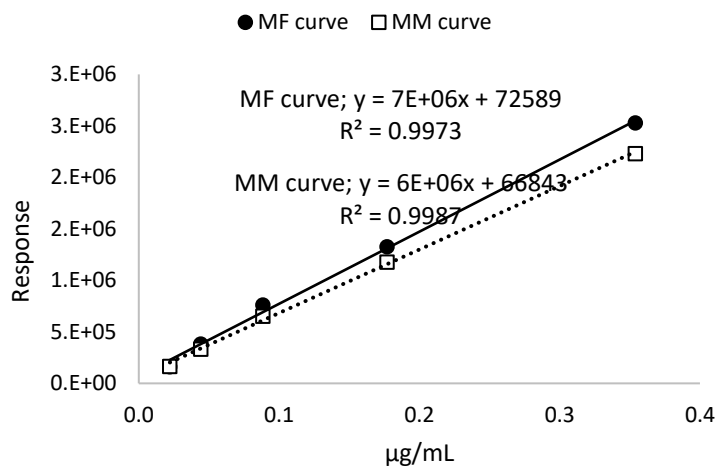
GTX3	0.477	8.7	
8.62[a], 8.73[a]	0.238	1.0	
11.41[b], 11.39[b]	0.119	16.2	
30.0[a], 15.0[a]	0.060	-12.2	
15.0[a], 30.0[a]	0.030	52.9	

MF curve; y = 2E+06x - 50354
R² = 0.9976

MM curve; y = 2E+06x - 46703
R² = 0.9993

Toxin Rt$_{MF}$, Rt$_{MM}$ (min) LOD$_{MF}$, LOD$_{MM}$ (ng/mL)	µg/mL	Matrix effect %	
NEO	0.583	5.0	
15.95[a], 15.95[a]	0.292	-3.2	
21.52[b], 21.41[b]	0.146	2.8	
2.0[a], 5.0[a]	0.073	-1.2	
5.0[a], 9.0[a]	0.036	4.7	
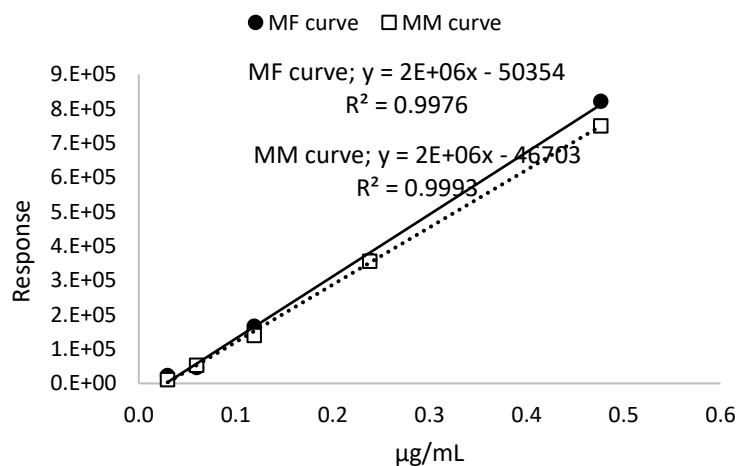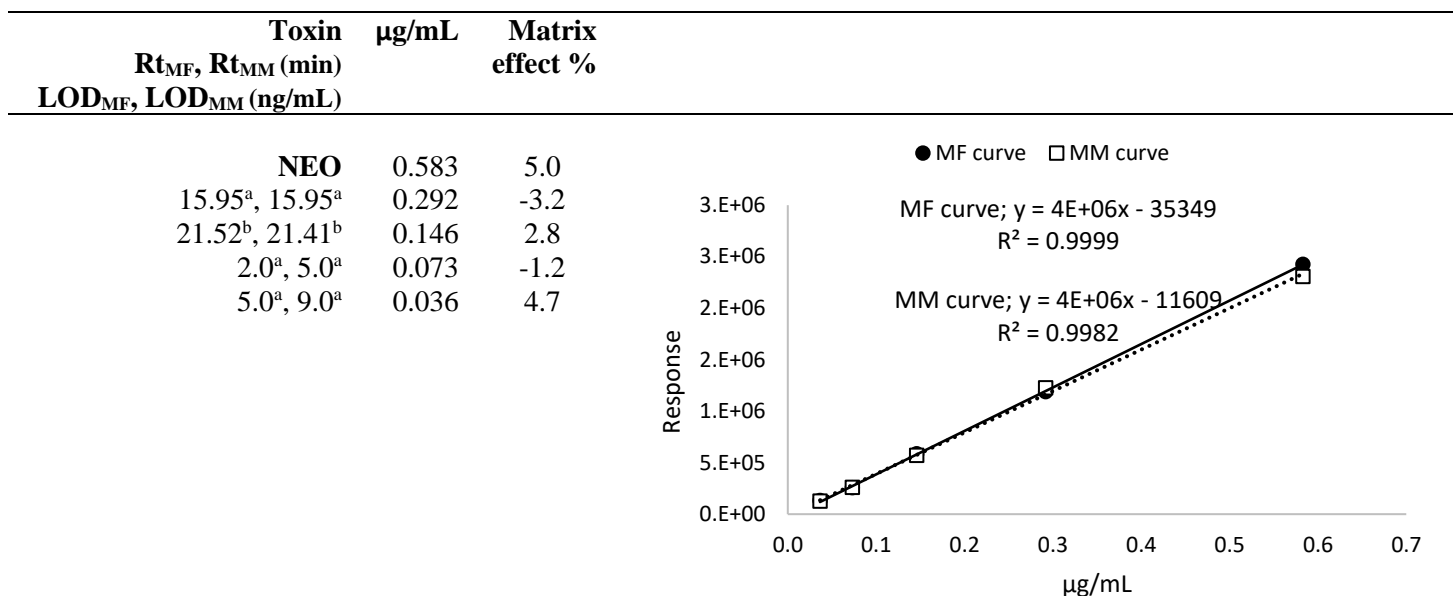
dcNEO	0.564	8.1	
15.97[a], 15.89[a]	0.282	-1.8	
21.37[b], 21.33[b]	0.141	7.4	
18.0[a], 18.0[a]	0.070	-11.9	
18.0[a], 18.0[a]	0.035	4.7	
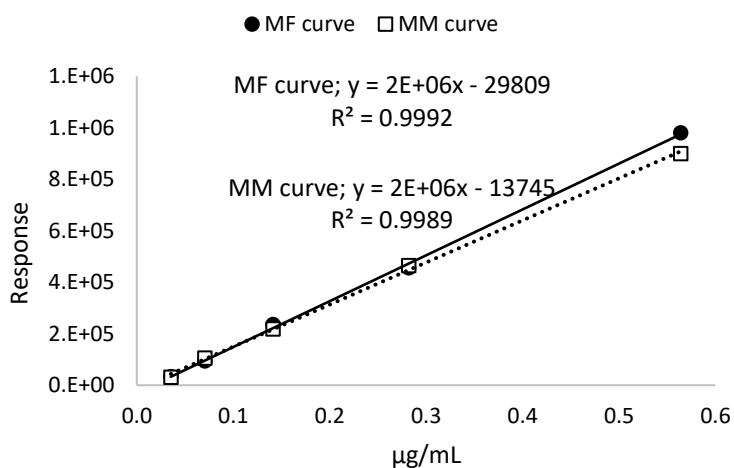
Rt$_{MF}$ = Retention time of matrix-free standards; Rt$_{MM}$ = Retention time of matrix-matched standards; LOD= limit of detection; [a]= TSK-gel® Amide-80 150 mm; [b]= TSK-gel® Amide-80 250 mm.

2.2 HILIC-HRMS method 2

General aspects

Recently, Boundy et al. [50] and Turner et al. [8,43] reported a new HILIC-HRMS[2] method on QqQ MS for the determination of PSTs and TTXs in seafood that includes also the extraction and clean-up steps. This approach gave excellent results in term of sensitivity, accuracy, and precision compared to other instrumental methods, including also the current EU official method for the analysis of PSTs in seafood (ox-LC-FLD; AOAC 2005.06). In addition, it proved suitable for

monitoring and research purposes, thus it was firstly subjected to a single laboratory validation, and then proposed for an AOAC collaborative study.

In this study, the HILIC-MS^2 method reported by Boundy et al. [50] and Turner et al. [8,43] was optimized on the LTQ Orbitrap XL MS (HILIC-HRMS method 2) and compared to the previously described HILIC-HRMS method 1.

2.2.1 Optimization of HILIC-HRMS method 2

The same PST mixture of CRM (STX, C1, C2, GTX1, GTX2, GTX3, GTX4, dcGTX2, dcGTX3, dcNEO, NEO, B1 and dcSTX) fortified with TTX standard was prepared and used to optimize the chromatographic conditions and the MS parameters. Similarly to HILIC-HRMS method 1, the chromatography reported by Boundy et al. [50] and Turner et al. [8,43] (HILIC-HRMS method 2) involves the use of water (A) and ACN (B) as mobile phases. However, some remarkable differences between the two methods are present in terms of: composition of mobile phases, additives, gradient nature and HPLC column. In the HILIC-HRMS method 1, mobile phase B is a solvent mixture of ACN-W 95:5 v/v containing as additives formic acid and ammonium formate, which are added to mobile phase A (pH =3.55). Contrarily, in method 2 mobile phase B is a mixture of ACN-W 70:30 v/v that contains formic acid, while mobile phase A is an aqueous solution composed of formic acid and NH$_3$. Therefore, differently from method 1, the principle of the chromatographic separation of method 2 is a ionic strength gradient. Although both chromatographic methods share the principle of the HILIC mechanism, the use of columns packed with different stationary phases and particle size greatly affected the toxin separation. Notably, method 1 uses a column packed with 3 μm spherical silica particles that are covalently bonded with carbamoyl groups, while the HILIC column in method 2 is packed with 1.7 μm ethylene bridged hybrid particles bonded to 2-aminobenzamide and 2-amino benzoic acid. Smaller particle size column guarantees higher resolving power and sensitivity, but the main consequence is an increased back pressure at high percentage of water during the gradient. Therefore, in method 2 the chromatographic column is kept at higher temperatures (60°C) compared to method 1 (20°C) to reduce the viscosity of solvents and prevent excessive pressure. Taking into account all these details, a chromatographic gradient for HILIC-HRMS method 2 was optimized on the available UHPLC for the separation of PSTs and TTX. Differently from method 1 (**Fig.III.1-2**), a first

isocratic step of 10 min at 99%B gave an excellent separation between epimer pairs (**Fig.III.8**) since the peak of C toxins, GTX2-3, GTX1-4 and dcGTX2-3 were completely resolved.
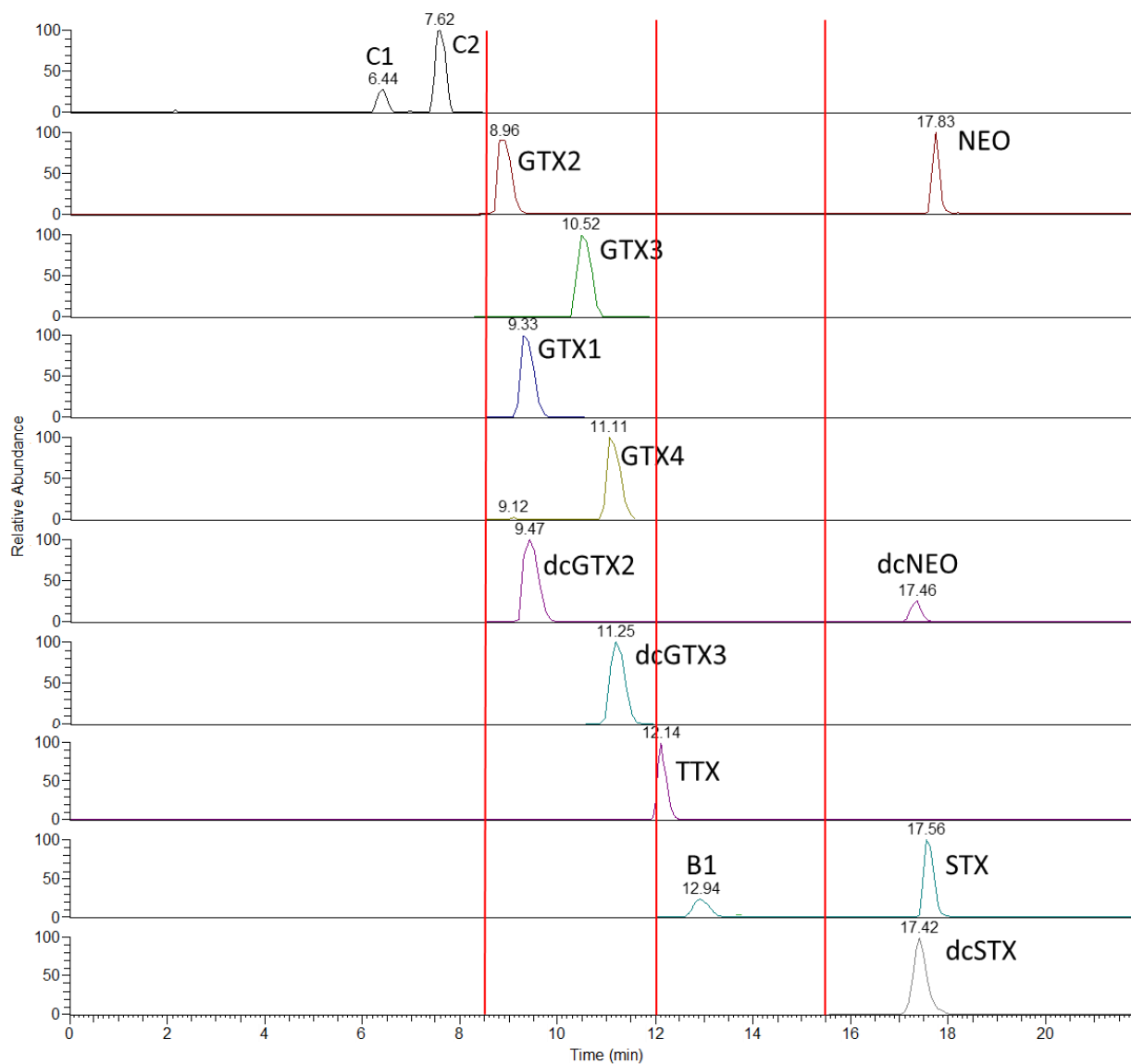
Figure III.8. Representative chromatographic separation of PSTs and TTX under HILIC-HRMS method 2.

However, similarly to method 1 (**Fig.III.1-2**) a poor resolution was obtained between the C11-α (GTX2, GTX1 and dcGTX2) and β-hydroxysulfated (GTX3, GTX4 and dcGTX3) analogues, as well as between NEO, dcNEO, STX and dcSTX that practically co-eluted (**Fig.III.8**). Although the order of elution between TTX and B1 was different between the two methods, a better

resolution (moderate) was obtained under method 2. However, the retention time of TTX represented a critical aspect for the configuration of a time-segmentation method since it eluted between the end of segment 2 and the beginning of segment 3 (**Fig.III.8**). For this reason, TTX was monitored by inserting its MS^2 scan in both chromatographic windows. With regard to peak shape, method 2 provided for most of the toxins narrower and sharper peaks than method 1, with a noticeable improvement for TTX, NEO and STX. However, similar results were obtained for B1, dcNEO and dcSTX whose peaks were wider under both methods **Fig.III.1-2,8**. Although chromatographic method 2 provided higher resolving power and a great improvement in peak shape, it showed a critical downside in terms of retention time reproducibility. The evaluation of the method variability was performed following the same procedure adopted for HILIC-HRMS method 1. As a result, a noteworthy shift of retention time was observed within the same batch of analysis, with the only exception for C toxins that, on the basis of their charge state (0), gave the highest chromatographic reproducibility (C1 6.10±0.04 min and C2 7.20±0.03 min). The worst results were obtained for NEO, dcNEO, STX and dcSTX for which the measured retention time (mean) and sd were 15.85±0.54, 14.74±0.62, 15.17±0.62 and 14.72±0.66, respectively. The same critical issue emerged from the evaluation of the variability between different batches, which involved also C toxins. By way of example, the measured sd for C1, GTX2, dcNEO and STX was 0.2, 0.5, 1.4 and 1.3 min, respectively. This pointed out as the reproducibility strongly decreased with the increase of the state of charge of the molecule. As a consequence, under the optimized conditions the configuration of a method based on time segments could not be applied to the analysis of large batches, whilst the poor long-term reproducibility made mandatory a careful evaluation of toxin retention times when the analyses spreads over different days.

The different chromatography employed in method 2 required re-optimization of ESI source parameters for the analysis of PSTs and TTX. All the intriguing findings discussed above for method 1 represented the starting point for the configuration of method 2. Although for most of the analogues a considerable degree of in-source fragmentation occurred at higher source temperatures, the highest analytical sensitivity was found setting the capillary temperature at 440°C. This represented the main difference with method 1 (source temperature 300°C) for which, under the optimized chromatography, the increase of temperatures improved the intensity of desulfated analogues (e.g. STX and dcSTX) but drastically decreased that of C toxins and GTXs. Similarly to method 1, the source voltage was kept at 4.8 kV, whilst the highest sensitivity for C

toxins was obtained setting capillary voltage (CV) and tube lens (TL) at higher values (CV 32 and TL 95) than those optimized for all the other analogues (CV 24 and TL 75). The optimized ESI MS parameters were then applied to the analysis of the standard mixture and the HR full-scan MS spectrum of each toxin was acquired (**Fig.III.9**). As expected, a strong in-source fragmentation occurred for all the analogues with the only exception of NEO, dcNEO and TTX that provided abundant $[M+H]^+$ ions. The ESI source kept at 440°C greatly influenced the spectrum of C1 which was dominated by the $[M+H-SO_3]^+$ in-source fragment, whilst the spectrum of C2 turned out to be superimposable to that obtained at 300°C (method 1) in terms of fragments and relative ion ratio between the $[M+H-SO_3]^+$, $[M+H-2SO_3]^+$ and $[M+H-2SO_3-H_2O]^+$ in-source ions (**Fig.III.3,9**). The same was observed for C11-α (GTX2, GTX1 and dcGTX2) and -β-hydroxy sulfated analogues (GTX3, GTX4 and dcGTX3) whose spectra were characterized by very intense $[M+H-SO_3]^+$ and $[M+H]^+$ ions, respectively, excepting for GTX4 that gave an intense $[M+H-H_2O]^+$ ion as well as in method 1 (**Fig.III.3,9**). STX, dcSTX and B1 ionized forming $[M+H]^+$ ions and the relevant fragments due to the loss of water or sulfate with a characteristic relative abundance ratio of the fragments which was toxin-dependent. Notably, at 440°C (method 2) the in-source fragmentation mainly affected B1 since the $[M+H-SO^3]^+$ ion was the most intense in the spectrum unlike that acquired 300°C (method 1) where the most abundant ion was the $[M+H]^+$ (**Fig.III.3,9**). In addition, the HRMS spectra acquired through method 2 contained the $[M+Na]^+$ adduct ion of dcGTX2, dcGTX3, dcNEO, NEO, STX, and dcSTX with a relative abundance similar to that observed with method 1 (**Fig.III.3,9**). HRMS^2 experiments were acquired by fragmenting the most intense ion contained in the full-scan spectrum of each toxin, and consequently, the obtained fragmentation patterns were superimposable to those recoded under method 1. In addition, the same in-source and in-C trap fragmentation behavior observed for method 1 occurred also for method 2.
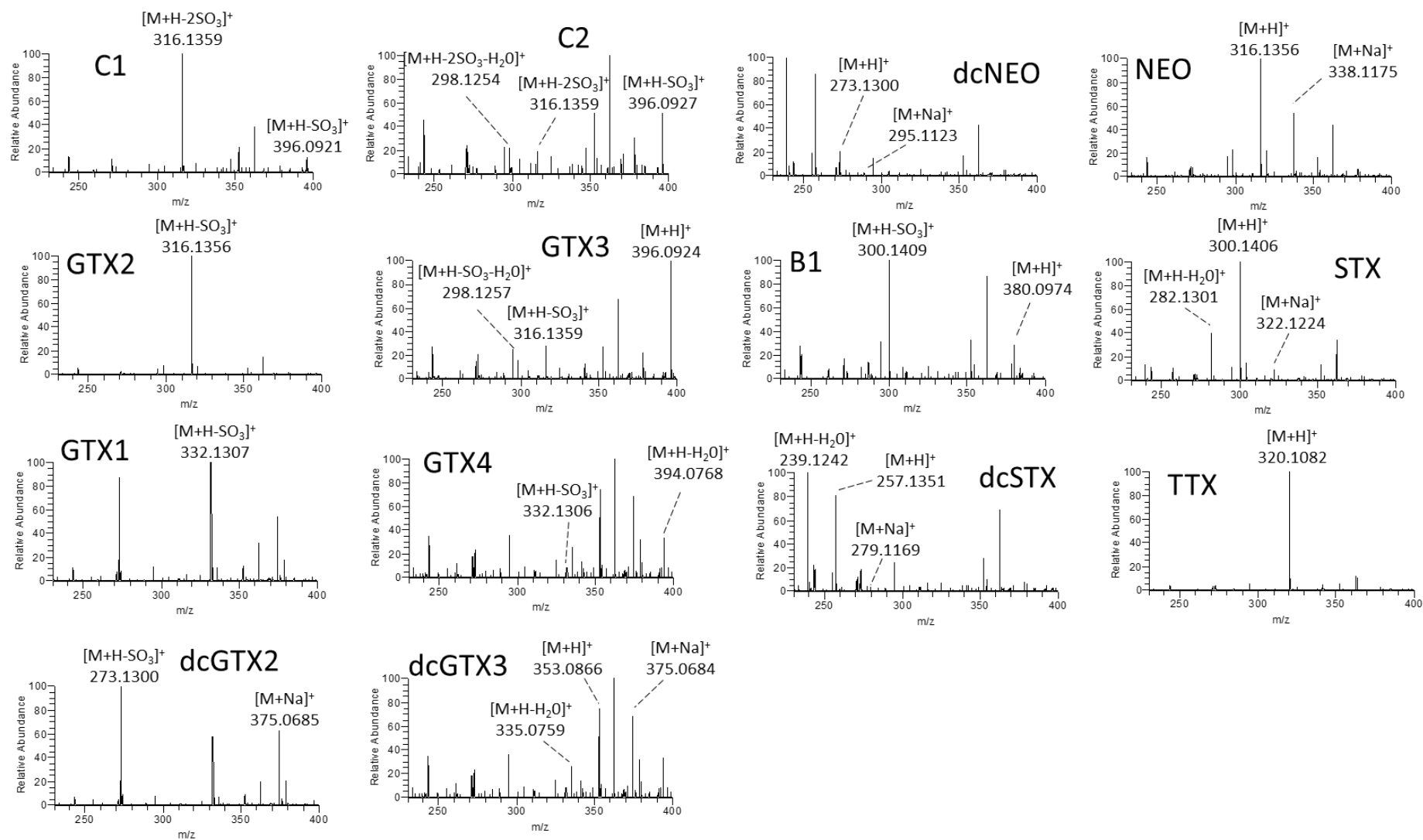
Figure III.9 HR full-scan MS spectrum of PSTs and TTX analyzed by HILIC-HRMS method 2.

The best experimental settings for the analysis of PSTs by method 2 are reported in **Table III.3**. The main differences between HILIC-HRMS method 1 and 2 were: i) the highest analytical sensitivity for B1 in method 2 that was obtained by selecting the $[M+H-SO_3]^+$ at *m/z* 300.1 instead of the $[M+H]^+$ ion at *m/z* 380.1 used in method 1, ii) the CE used to monitor the GTX3 and B1 that were different between methods, and iii) the insertion of TTX MS^2 scan in segments 2 and 3 due to its retention time **Table III.1,3**.

Table III.3 HRMS data of PST_S and TTX. Optimized CID $HRMS^2$ conditions for method 2.

Toxin	*m/z* [M+H]$^+$ Formula	*m/z* precursor ion Formula	CID CE %	*m/z* range	Time Segment
C1	476.0500 $C_{10}H_{18}N_7O_{11}S_2^+$	316.1 - $[M+H-2SO_3]^+$ $C_{10}H_{18}N_7O_5^+$	0	312-320	1
C2	476.0500 $C_{10}H_{18}N_7O_{11}S_2^+$	396.1 - $[M+H-SO_3]^+$ $C_{10}H_{18}N_7O_8S^+$	0	374-400	1
GTX2	396.0932 $C_{10}H_{18}N_7O_8S^+$	316.1 - $[M+H-SO_3]^+$ $C_{10}H_{18}N_7O_5^+$	0	312-320	2
GTX3	396.0932 $C_{10}H_{18}N_7O_8S^+$	396.1 - $[M+H]^+$ $C_{10}H_{18}N_7O_8S^+$	10	290-400	2
GTX1	412.0881 $C_{10}H_{18}N_7O_9S^+$	332.1 - $[M+H-SO_3]^+$ $C_{10}H_{18}N_7O_6^+$	0	328-336	2
GTX4	412.0881 $C_{10}H_{18}N_7O_9S^+$	412.1 - $[M+H]^+$ $C_{10}H_{18}N_7O_9S^+$	10	310-416	2
dcGTX2	353.0874 $C_9H_{17}N_6O_7S^+$	273.1 - $[M+H-SO_3]^+$ $C_9H_{17}N_6O_4^+$	0	269-277	2
dcGTX3	353.0874 $C_9H_{17}N_6O_7S^+$	353.1 - $[M+H]^+$ $C_9H_{17}N_6O_7S^+$	10	250-355	2
B1	380.0983 $C_{10}H_{18}N_7O_7S^+$	300.1 - $[M+H]^+$ $C_{10}H_{18}N_7O_4^+$	0	296-304	3
TTX	320.1095 $C_{11}H_{18}N_3O_8^+$	320.1 - $[M+H]^+$ $C_{11}H_{18}N_3O_8^+$	20	85-350	2/3
NEO	316.1364 $C_{10}H_{18}N_7O_5^+$	316.1 - $[M+H]^+$ $C_{10}H_{18}N_7O_5^+$	0	312-320	4
dcNEO	273.1306 $C_9H_{17}N_6O_4^+$	273.1 - $[M+H]^+$ $C_9H_{17}N_6O_4^+$	0	269-277	4
STX	300.1415 $C_{10}H_{18}N_7O_4^+$	300.1 - $[M+H]^+$ $C_{10}H_{18}N_7O_4^+$	0	296-304	4
dcSTX	257.1357 $C_9H_{17}N_6O_3^+$	239.1 - $[M+H-H_2O]^+$ $C_9H_{15}N_6O_2^+$	0	235-243	4

CID= collision-induced dissociation; CE= collision energy

2.2.2 Matrix effect, limits of detection and linearity

The performance of the optimized HILIC-HRMS method 2 was evaluated through the study of: i) the matrix effect on the chromatography and the HRMS response, ii) linearity and iii) instrumental

limit of detection. Similarly to method 1, MF and MM calibration curves at 5 concentration levels of a PSTs and TTX standard mixture were analyzed by LC-HRMS. The matrix effect was almost negligible on chromatographic properties since the retention times of toxins, as well as the peak shape, were almost superimposable between MF and MM curves (**Table III.4**). A noteworthy matrix suppression on the HRMS response emerged from the direct comparison between MF and MM standards. The latter were prepared as reported for HILIC-HRMS method 1. Overall, the suppression effect remained constant for most of the toxins within the whole concentration range tested, with only a slight difference observed at the most diluted points for C1, C2, GTX3, GTX1, dcGTX2, dcGTX3, dcNEO and B1, and at the highest levels for GTX1 and NEO. However, a negligible matrix enhancement effect was observed only for STX in the whole concentration range (4.0-10.2%) and TTX at 0.042 µg/mL (16.3%) (**Table III.4**). All the curves showed excellent linearity with R^2 values in the range 0.992-1 excepting for the MM curves of GTX1 (R^2 0.986) and dcNEO (R^2 0.985). A remarkable sensitivity emerged from the measurement of the instrumental LOD for each MF and MM toxin analyzed by HILIC-HRMS method 2 (**Table III.4**). The highest analytical sensitivity was measured for NEO and STX that gave LODs for MF and MM standards within 1-2 ng/mL. Very low limits were further observed for GTX1, GTX2, NEO, B1 and dcSTX with LODs < 10 ng/mL, while a moderate sensitivity was measured for C1, GTX3, dcGTX2, dcGTX3 and dcNEO that gave LODs within 10-30 ng/mL. The lowest sensitivity was obtained for C2 and GTX4 with LODs between 30-56 ng/mL. Overall, the analytical sensitivity achieved through the three HILIC-HRMS methods was comparable since slight differences can be attributed to the status of the instrument calibration when the analyses were performed. Results are summarized **in Table III.5**.

Table III.4. Retention time (min) and LOD (ng/mL) of MF and MM standards measured by HILIC-HRMS[2] method 2. Matrix effect % (+ suppression, - enhancement) at different concentration levels.

Toxin Rt_{MF}, Rt_{MM} (min) LOD_{MF}, LOD_{MM} (ng/mL)	µg/mL	Matrix effect %	
C2 **7.62, 7.59**	0.985 0.448 0.224 0.112 0.056	23.0 24.8 23.3 22.3 58.9	
GTX2 **8.96, 8.94**	0.627 0.314 0.157 0.078 0.039	15.0 20.8 22.0 17.6 28.5	
GTX1 **9.33, 9.21**	0.690 0.345 0.173 0.086 0.043	22.2 6.3 40.8 7.0 16.3	

Toxin Rt_{MF}, Rt_{MM} (min) LOD_{MF}, LOD_{MM} (ng/mL)	µg/mL	Matrix effect %	
GTX4	0.450	19.8	
11.1, 11.0	0.225	30.1	
	0.113	40.8	
	0.056	32.3	
	0.028	45.9	

●MF curve □MM curve

MF curve; y = 2E+06x - 37609
R² = 0.9956

MM curve; y = 2E+06x - 71714
R² = 0.9912

(Response vs µg/mL)
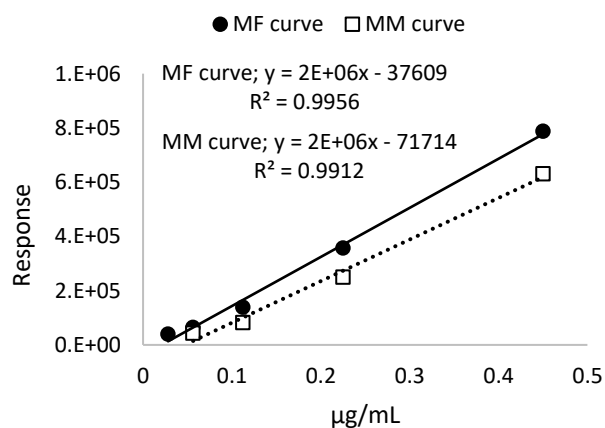
STX	0.343	-4.0	
17.56, 17.44	0.171	-5.8	
	0.086	-8.3	
	0.043	-10.2	
	0.021	-5.2	

●MF curve □MM curve

MF curve; y = 2E+07x + 116116
R² = 0.9992

MM crurve; y = 2E+07x + 173080
R² = 0.9984

(Response vs µg/mL)
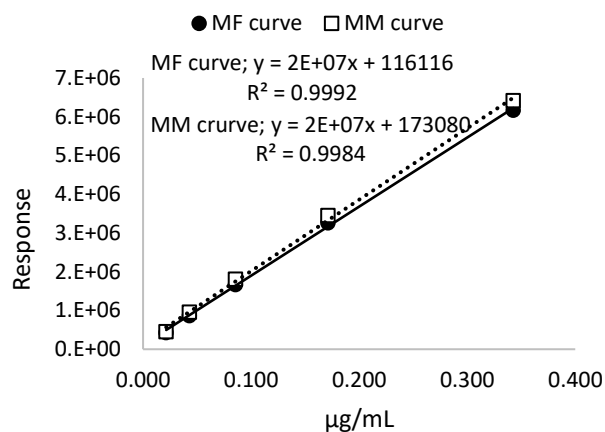
TTX	0.167	6.1	
12.14, 12.00	0.083	12.2	
	0.042	-16.3	
	0.021	9.5	
	0.010	18.1	

●MF curve □MM curve

MF curve; y = 1E+07x - 43630
R² = 0.9989

MM curve; y = 1E+07x - 26598
R² = 0.9978

(Response vs ng/mL)
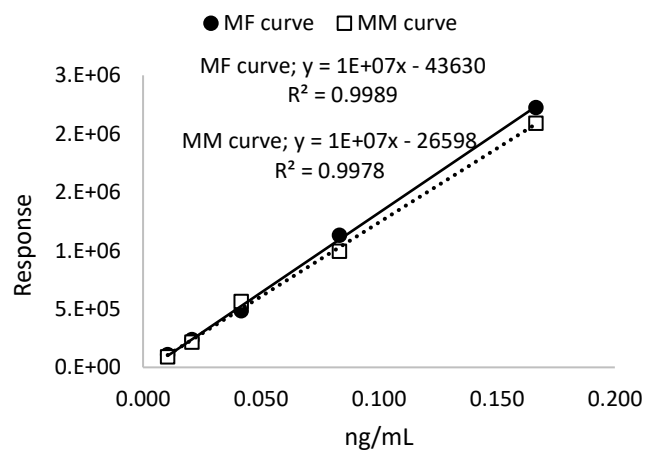
Toxin Rt$_{MF}$, Rt$_{MM}$ (min) LOD$_{MF}$, LOD$_{MM}$ (ng/mL)	µg/mL	Matrix effect %	
C1	0.749	23.3	
6.44, 6.42	0.374	22.6	
12.0, 23.0	0.187	26.2	
	0.094	29.4	
	0.047	38.1	

● MF curve □ MM curve

MF curve; y = 2E+06x - 1558.5
R² = 0.9999

MM curve; y = 1E+06x - 10704
R² = 0.9997

Response vs µg/mL
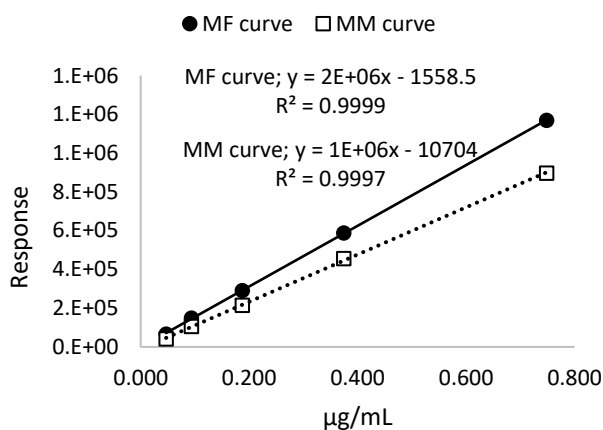
dcGTX2	0.490	17.8	
9.47, 9.24	0.245	19.9	
8.0, 15.0	0.122	40.6	
	0.061	35.7	
	0.031	35.4	

● MF curve □ MM curve

MF curve; y = 8E+06x + 358465
R² = 0.9982

MM curve; y = 7E+06x - 16271
R² = 0.9972

Response vs µg/mL
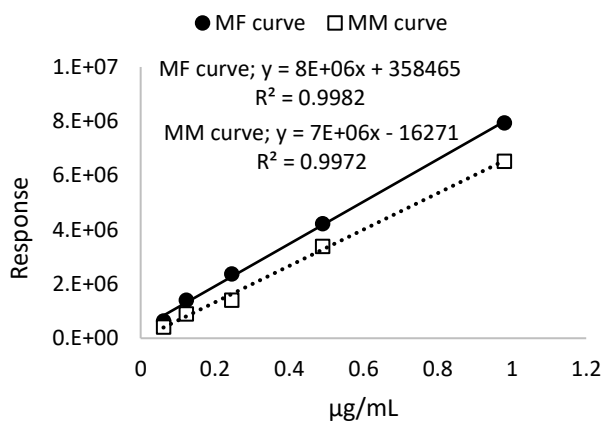
dcGTX3	0.575	18.2	
11.25, 11.11	0.288	12.7	
9.0, 18.0	0.144	29.5	
	0.072	29.0	
	0.036	44.1	

● MF curve □ MM curve

MF curve; y = 4E+06x - 51936
R² = 0.9997

MM curve; y = 4E+06x - 77489
R² = 0.9978

Response vs µg/mL
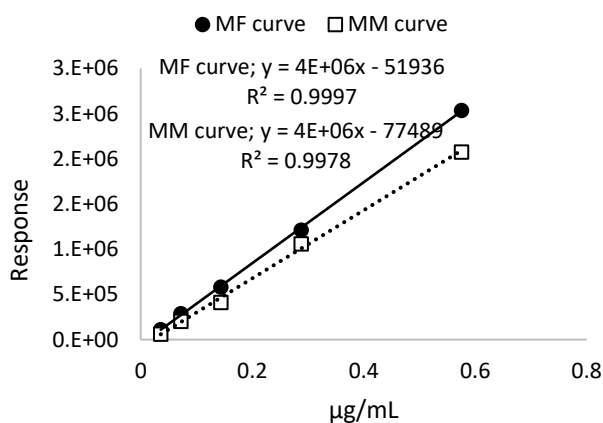
Toxin Rt$_{MF}$, Rt$_{MM}$ (min) LOD$_{MF}$, LOD$_{MM}$ (ng/mL)	µg/mL	Matrix effect %	
B1	0.587	18.9	
12.94, 12.85	0.293	21.3	
5.0, 9.0	0.147	19.7	
	0.073	24.4	
	0.037	33.6	
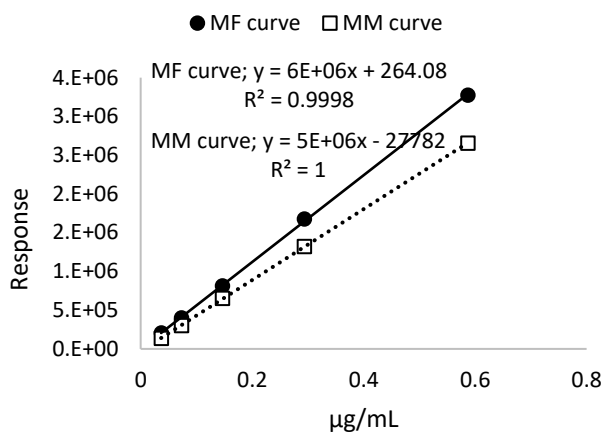
dcSTX	0.354	8.0	
17.42, 17.21	0.177	-3.2	
3.0, 3.0	0.089	1.8	
	0.044	2.7	
	0.022	20.8	
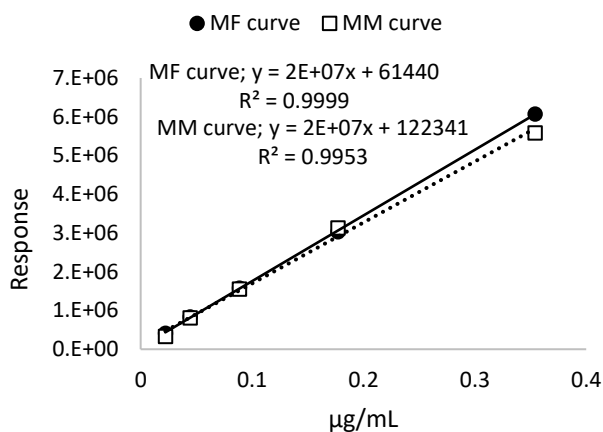
GTX3	0.477	19.5	
10.52, 10.40	0.238	24.5	
4.0, 30.0	0.119	60.0	
	0.060	59.8	
	0.030	86.4	

Toxin Rt$_{MF}$, Rt$_{MM}$ (min) LOD$_{MF}$, LOD$_{MM}$ (ng/mL)	µg/mL	Matrix effect %	
NEO 17.83, 17.79 1.0, 2.0	0.583 0.292 0.146 0.073 0.036	19.0 24.5 40.4 35.2 47.3	MF curve; y = 2E+07x - 6215.2 R² = 0.999 MM curve; y = 2E+07x - 398430 R² = 0.9977
dcNEO 17.46, 17.25 1.3, 1.3	0.564 0.282 0.141 0.070 0.035	25.8 38.6 41.1 32.5 15.4	MF curve; y = 7E+06x - 34720 R² = 0.9993 MM curve; y = 5E+06x - 96510 R² = 0.9846
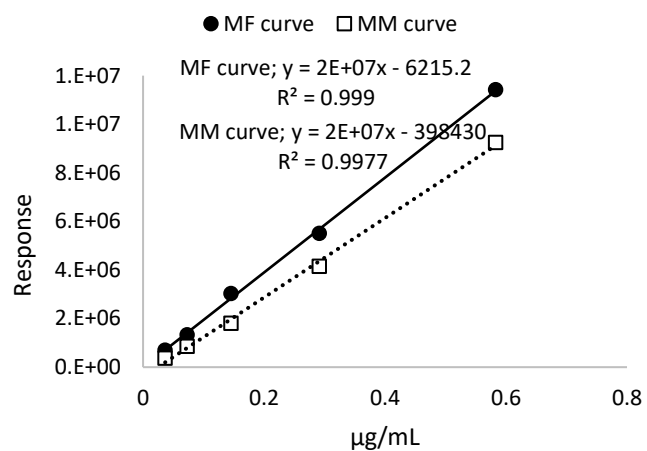
Table III.5. Instrumental limits of detection (LOD; ng/mL) of PSTs and TTX measured by HILIC-HRMS method 1 and 2.

Toxin	MF	MM	Toxin	MF	MM
C1	47.0[a]	23.0[a]	dcGTX3	9.0[a]	18.0[a]
	47.0[b]	47.0[b]		9.0[b]	9.0[b]
	12.0[c]	23.0[c]		9.0[c]	18.0[c]
C2	56.0[a]	56.0[a]	dcNEO	18.0[a]	18.0[a]
	56.0[b]	56.0[b]		18.0[b]	18.0[b]
	28.0[c]	56.0[c]		35.0[c]	35.0[c]
GTX2	10.0[a]	10.0[a]	NEO	5.0[a]	9.0[a]
	2.0[b]	5.0[b]		2.0[b]	5.0[b]
	2.0[c]	5.0[c]		1.0[c]	2.0[c]
GTX3	15.0[a]	30.0[a]	B1	18.0[a]	18.0[a]
	30.0[b]	15.0[b]		18.0[b]	18.0[b]
	4.0[c]	30.0[c]		5.0[c]	9.0[c]
GTX1	5.0[a]	11.0[a]	STX	3.0[a]	3.0[a]
	11.0[b]	15.0[b]		0.7[b]	0.7[b]
	3.0[c]	3.0[c]		1.3[c]	1.3[c]
GTX4	56.0[a]	56.0[a]	dcSTX	6.0[a]	11.0[a]
	28.0[b]	56.0[b]		3.0[b]	3.0[b]
	28.0[c]	56.0[c]		3.0[c]	3.0[c]
dcGTX2	15.0[a]	15.0[a]	TTX	< 5.0[a]	< 5.0[a]
	15.0[b]	15.0[b]		< 5.0[b]	< 5.0[b]
	8.0[c]	15.0[c]		< 5.0[c]	< 5.0[c]

[a]= HILIC-HRMS method 1, 250 mm Amide-80 column; [b]= HILIC-HRMS method 1, 150 mm Amide-80 column; [c]= HILIC-HRMS method 2.

2.3 Application to shellfish samples

Background

The shellfish samples used to evaluate the effectiveness and the applicability of the optimized HILIC-HRMS methods 1 and 2 were kindly provided by Dr. Andrew Turner of Centre for Environment Fisheries and Aquaculture Science (CEFAS; Weymouth, United Kingdom) in the

frame of a collaborative study. A total of 31 shellfish reference samples were extracted and subjected to SPE clean-up at CEFAS following the procedure reported by Boundy et al. [50] and Turner et al [8,43]. The SPE elutes were used at UniNa to test the optimized instrumental conditions.

2.3.1 HILIC-HRMS analysis of shellfish samples

The optimized HILIC-HRMS methods 1 and 2 were both used to run the shellfish samples with the aim of finding the best experimental conditions for the identification and quantification of PSTs in shellfish. The 250 mm Amide-80 column was selected to evaluate the effectiveness of HILIC-HRMS method 1. The presence of PSTs in all the analyzed samples was confirmed, even when they were contained at trace level, whilst the absence of peaks attributable to PSTs in shellfish control samples (NG1/3-rpt and MM blank-rpt) highlighted a good method specificity (**Table III.6**). The identity of each analogue was first confirmed by comparing the retention times of the peaks contained in XIC from full scan-HRMS and HRMS[2] of each toxin with those of the relevant MF and MM standards injected under the same experimental conditions. A careful analysis of HRMS and MS[2] spectra associated to the chromatographic peaks of each toxin represented further criteria for positive identification. Full-scan spectra of shellfish samples were found to be superimposable to those acquired from the analysis of PST standards in terms of measured accurate mass and relative abundance ratio between ions/in-source fragments. On the other hand, the final confirmation was obtained from the analysis of HRMS[2] spectra. More in detail, toxins monitored by fragmenting the precursor ions at CE 0% were confirmed through the accurate mass of the precursor ion (**Table III.1**; C1, GTX2, GTX3; dcGTX2, NEO, dcNEO, STX and dcSTX) and the main fragment generated ($[M+H-H_2O]^+$ fragment for C2), while PSTs monitored at CE $\neq$ 0% (**Table III.3**, **Fig.III.4**; GTX3, GTX4, dcGTX3 and B1) were corroborated by analyzing all the diagnostic fragments generated in the selected *m/z* range. The total toxin content emerged from the analysis of shellfish samples clearly highlighted that the CS sample series (CS2/13-rpt) were the most contaminated, with the highest levels of 23515 and 16217 µg eq. STX/Kg found in CS4 and CS13, respectively (**Table III.6**). Noteworthy contamination levels were also found in samples from Sicily (CA/CE) in the range 5002-14207 µg eq. STX/Kg, whilst QST and EURL PO sample series were the less contaminated ones (862-5344 and 866-1066 µg eq. STX/Kg, respectively).

Table III.6. Individual and total toxin content (µg eq. STX/Kg) found in the shellfish samples analyzed by HILIC-HRMS method 1.

Sample	C1	C2	GTX2	GTX3	GTX1	GTX4	NEO	dcGTX2	dcGTX3	dcNEO	B1	STX	dcSTX	Total
PO CRM Mix-rpt	15	0	145	0	590	933	312	0	185	0	0	285	0	2465
CS13-rpt	115	570	1072	1039	4388	1771	1900	11	0	0	0	5351	0	16217
CS12_rpt	139	587	3304	2693	0	0	0	0	0	0	332	2771	0	9827
CS11-rpt	38	0	238	0	0	0	0	12	0	0	648	643	0	1579
CS10-rpt	60	173	692	0	0	0	0	24	183	0	409	445	0	1987
CS9-rpt	0	0	110	315	0	0	0	73	0	0	0	516	238	1253
CS8-rpt	116	445	0	320	0	0	0	0	189	0	0	1092	0	2161
CS7-rpt	0	0	1243	845	1166	0	313	0	0	0	0	3204	0	6771
CS5-rpt	0	0	483	414	0	0	1109	11	0	0	0	1774	0	3790
CS4-rpt	131	590	6046	5335	827	0	559	17	0	0	87	9923	0	23515
CS3-rpt	14	176	1065	709	0	0	115	10	0	0	0	2855	0	4944
CS2-rpt	0	0	195	0	0	0	0	0	0	0	0	327	0	522
QST233-rpt	0	0	1488	499	279	0	211	0	0	0	0	2868	0	5344
QST232-rpt	0	0	0	0	0	0	0	0	0	0	0	0	862	862
QST231-rpt	0	0	381	0	464	0	81	10	0	0	0	213	439	1588
QST230-rpt	0	0	525	0	539	0	117	0	0	0	0	475	0	1657
EURL PO3-rpt	0	0	249	0	688	0	0	20	0	0	0	109	0	1066
EURL PO2-rpt	0	0	555	319	0	0	85	0	0	0	0	2371	0	3331
EURL PO1-rpt	80	209	0	0	0	0	0	20	0	0	556	0	0	866
LRM374-rpt	19	203	501	869	1724	1207	418	10	0	0	0	1293	0	6245
CRM673-rpt	12	0	133	0	1207	932	195	10	0	0	0	181	0	2671
SICILY CE-rpt	171	540	2648	1851	3462	1563	161	13	0	72	1693	2034	0	14207
SICILY CD-rpt	239	1114	1902	1610	1714	1021	159	31	0	0	2351	1510	263	11914
SICILY CC-rpt	267	990	1828	1420	1732	938	79	42	0	0	1687	1016	245	10243
SICILY CB-rpt	82	333	786	683	461	0	80	0	202	0	1243	1130	0	5002
SICILY CA-rpt	72	0	1074	931	1213	0	113	15	0	0	825	1250	0	5494
MM blank-rpt	0	0	0	0	0	0	0	0	0	0	0	0	0	0
NG3-rpt	0	0	0	0	0	0	0	0	0	0	0	0	0	0
NG2-rpt	0	0	0	0	0	0	0	0	0	0	0	0	0	0
NG1-rpt	0	0	0	0	0	0	0	0	0	0	0	0	0	0

Overall, the most common analogues were STX and GTX2 that were found in 77% and 74% of the analyzed samples, respectively, followed by NEO, dcGTX2, C1, GTX3 and GTX1 found in 50% of the shellfish. C2, GTX4, B1, dcGTX3, dcNEO and dcSTX were the less detected toxins, with dcNEO found only in one sample (SICILY CE). The analysis of the toxin profile showed a wide array of toxins between and within different sample series, with the highest variability observed for CS shellfish, while samples from Sicily provided the closest profile.

The same batch of reference shellfish samples was then analyzed by HILIC-HRMS method 2. Unfortunately, the low method reproducibility previously reported (retention times of MF and MM standards) was observed also in the analysis of real samples. This critical issue hampered the employment of the time segmentation mode for the identification of most of the analogues. On the other hand, the effectiveness of the optimized method was tested by interpreting the full-scan spectra acquired. Although the experimental conditions set turned out to be suitable and effective for the analysis of MF and MM standards, they demonstrated to be inappropriate for the analysis of contaminated shellfish. In particular, a very low method specificity emerged since the peaks observed in the full scan-XIC were broad and tailing making impossible a correct toxin identification. This in combination with the above mentioned shift of retention times of standards made method 2 unsuitable for the analysis of real samples.

Data reported in this chapter will be included in an joint manuscript under preparation.

2.4 HILIC-HRMS method 3

Background

The complete optimization of the HILIC-HRMS method was carried out between October 2020 and January 2021. However, a provisional optimization was performed between 2017-2018, and the resulting method, labelled as HILIC-HRMS method 3, was employed for the analysis of PSTs and TTXs in environmental and food samples. Even though the chromatography used for method 3 is the same as that reported for method 2, the HRMS conditions were quite different. The description of the HILIC-HRMS method 3 and its application to phytoplankton on plastics, and shellfish samples is reported in the next paragraphs.

2.4.1 Optimization of HRMS conditions

The same mixture of PST CRMs and TTX RM was prepared and used to optimize the source parameters. It should be noted that, at the time of the analysis, the possibility of exploiting the time segmentation mode was not taken into consideration. Therefore, even if the highest analytical sensitivity for some PSTs was achieved by using different source parameters, it was necessary to find common experimental conditions for all toxins. Differently from method 2, the source temperature was kept lower and set at 220°C. As a consequence, the employment of higher sheat and auxiliary gas (62.0 and 16.5 arbitrary units, respectively) was a prerequisite to achieve a good desolvation in the ESI source under the optimized chromatography. Nonetheless, similarly to methods 1 and 2 in which the ESI source was kept at 300°C and 440°C, respectively, PSTs underwent a strong in-source fragmentation even under method 2 at 220°C, whilst TTX gave an intense $[M+H]^+$ ion. The highest degree of fragmentation was observed for C toxins, GTX1-4 and B1. As expected, the full-scan spectra of C11-α and -β-hydroxysulfated epimer pairs were not superimposable since the degree of fragmentation was found to be dependent on the stereochemical properties. With the aim of achieving the highest method sensitivity, the number of MS^2 scan was reduced, thus the $HRMS^2$ experiments were optimized by selecting as precursors the $[M+H]^+$ or in-source fragment ions that could allow a combined monitoring of multiple PST analogues. This approach is based on the interference that PSTs can give due to the in-source fragmentation. As a result, C1, C2, GTX2, GTX3 and NEO were monitored through the ion at *m/z* 316.1364 that corresponds to the $[M+H-2SO_3]^+$ ion of C1 and C2, the $[M+H-SO_3]^+$ ion of GTX2 and 3, and the $[M+H]^+$ ion of NEO; GTX1 and GTX4 were monitored through the precursor ion at *m/z* 332.1313 originating from the loss of the SO_3 moiety, whilst dcGTX2, dcGTX3 and dcNEO by fragmenting the ion at *m/z* 273.1306; B1 and STX were monitored through the ion at *m/z* 300.1415 which corresponds to the $[M+H-SO_3]^+$ and $[M+H]^+$ ion, respectively, whilst two individual MS^2 scans were configured for the detection of dcSTX and TTX by fragmenting the $[M+H]^+$ precursor at *m/z* 257.1 and 320.1, respectively. The XIC of the fragment ions of the all monitored PSTs and TTX is reported in **Fig.III.10**. Although the selected precursor ions allowed a combined detection of some PSTs, the peak area of C11-β-hydroxysulfated analogues were found to be remarkably lower than those of the relevant C11-α congener. This was due not only to the different concentration levels between the commercially available standards, but also to their different fragmentation patterns. However, the selection of such precursor ions was necessary

since: the ion at *m/z* 396.0932 was the most intense in the spectrum of C2 $[M+H-SO_3]^+$ and GTX3 $[M+H]^+$, but it was barely detectable in the spectrum of C1 and GTX2, while it excluded the monitoring of NEO; the ion at *m/z* 353.0874 $[M+H]^+$ was dominant in the spectrum of dcGTX3, but it hampered the detection of dcNEO and drastically decreased the method sensitivity for dcGTX2.
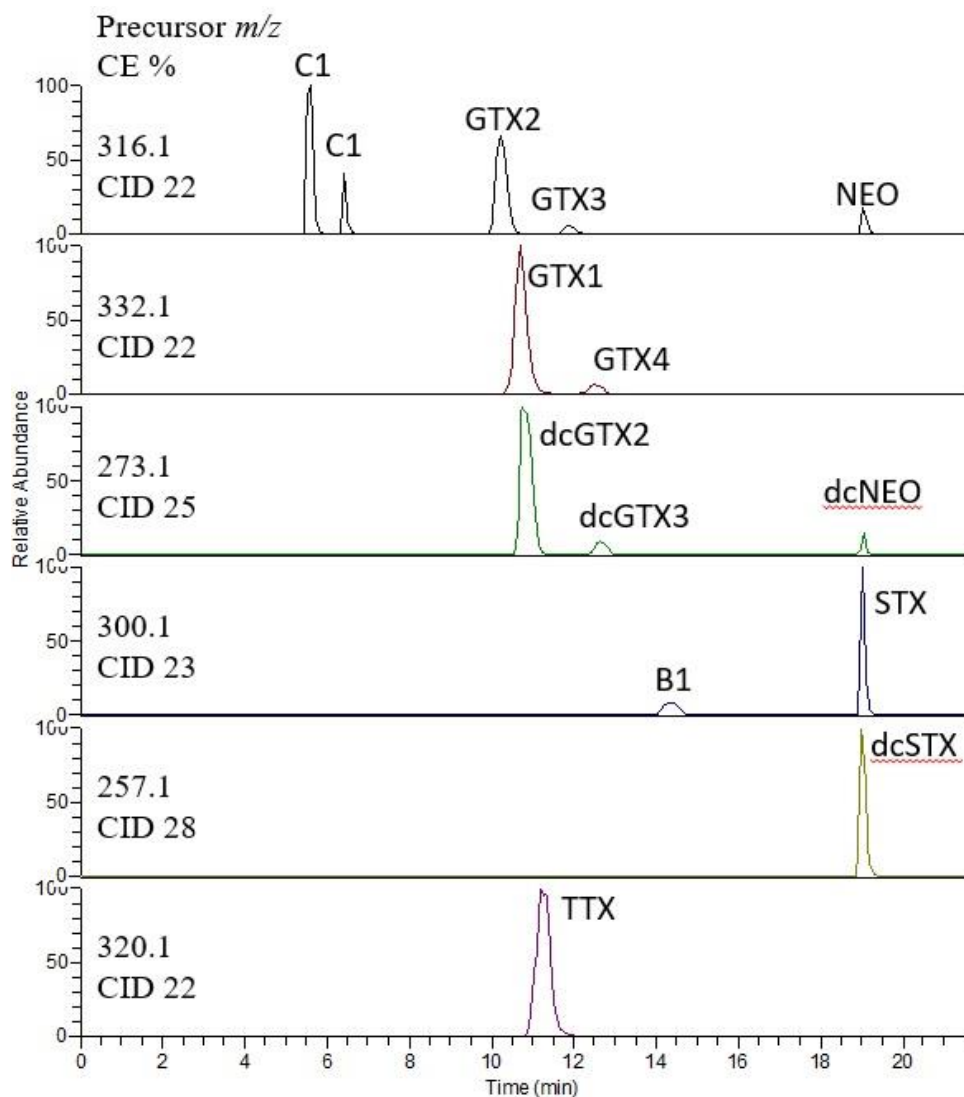
Figure III.10 XIC of PSTs and TTX standards analyzed by HILIC-HRMS method 3.

2.4.2 Application to shellfish and plankton samples: background and results

2.4.2.1 Analysis of TTX in Italian shellfish

In the frame of a collaboration with Istituto Zooprofilattico Sperimentale delle Venezie (IZSVe) and Centro Ricerche Marine (CRM) of Cesenatico - National Reference Laboratory for Marine Biotoxins, the implemented HILIC-HRMS method was used to investigate the presence of TTX in seafood. Particularly, in the context of an official monitoring program for EU regulated marine biotoxins, a number of shellfish samples collected in the area of Marano Lagoon (Northern Adriatic Sea, Italy) between 2017 and 2018 were tested positive for the presence of PSTs by the MBA screening (AOAC 959.08) with death time ranging from 8 to 43 minutes. Therefore, the presence of PSTs was investigated through the current official method in Europe (AOAC; 2005.06). Results highlighted the presence of PSTs only in two extracts, thus suggesting the need for an in-depth investigation by HILIC tandem MS. As a result, HILIC-MS^2 analyses highlighted traces of PSTs in 6 samples, and traces of TTX in most of the analyzed ones, with the highest levels of 541 and 216 µg/Kg found in sample 5-17 and 7-18, respectively [52]. An aliquot of mussel sample 5-17 was sent to UniNa, processed according to Boundy et al. [50] and Turner et al [8,43], and analyzed by HILIC-HRMS method 3 for further confirmation. As a result, the identity of TTX contained in sample 5-17 was confirmed through the presence of a chromatographic peak eluting at 11.03 min, whose associated HRMS^2 and MS^3 spectra showed the characteristic $[M+H-H_2O]^+$ and $[M+H-2H_2O]^+$ fragment ions, respectively (**Fig.III.11**). For an accurate determination of the toxin identified in the mussel sample, spiking experiments were carried out to investigate the % recovery of TTX from the entire procedure. The recovery of the extraction and the clean-up step turned out to be $68 \pm 11.3\%$ as average value of three replicates. Therefore, the quantitation of TTX conducted by using a MM standard calibration curve and including the recovery factor, revealed a contamination level of 413.0 µg/Kg. This finding represents the first evidence of TTX in shellfish from the North Adriatic Sea. However, it should be noted that TTX had been already detected in 2015-2017 in mussels from the Syracuse Bay (Ionian Sea, Southern Italy) although at lower concentration [11]. Nonetheless, the concentration of TTX found in sample 5-17 represents the highest contamination level ever found in shellfish from Europe.

More details on the experimental conditions, discussion and results are reported in a published article [52].
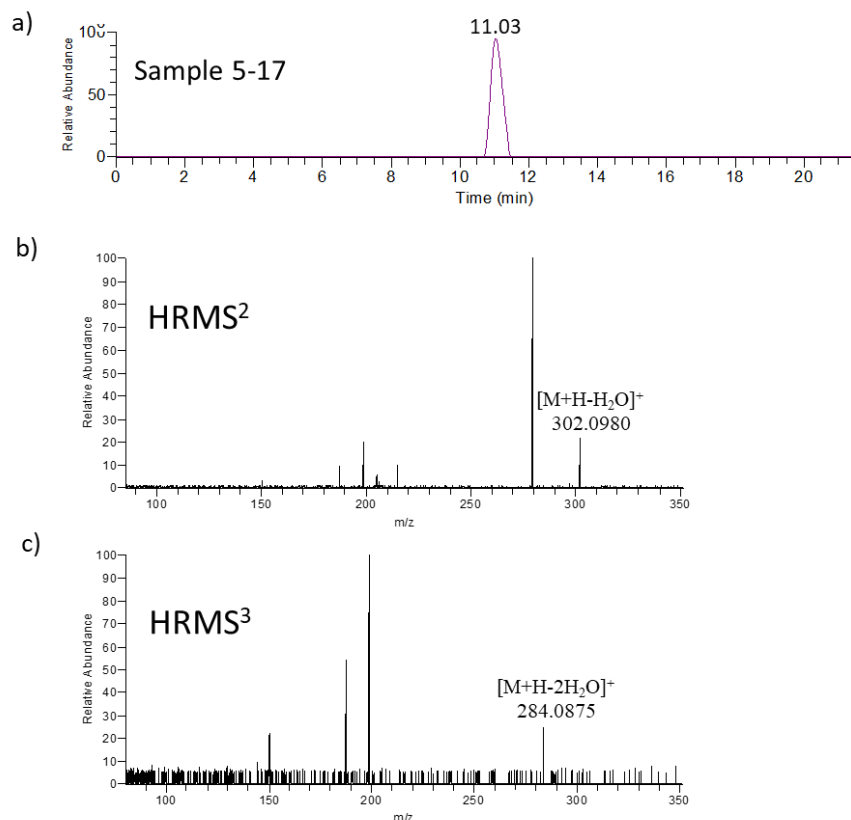
Figure III.11 a) XIC of TTX found in sample 5-17 and the associated b) HRMS^2 and c) MS^3 spectra.

2.4.2.2 Analysis of PSTs in microplastic samples

In the frame of a collaborative study with the Department of Biomolecular Sciences within the University of Urbino, the described HILIC-HRMS method was also successfully employed for the determination of PSTs in plankton samples. More in detail, in the context of a survey of plastic debris between 2016-2017, 42 plastic samples floating at the sea surface were collected from the Syracuse Bay (Ionian Sea, Southern Italy). It is well-known that floating plastics can be a substratum for the bio-adhesion of micro and macro marine organisms [53-54]. This poses high concerns for human safety since plastics can potentially act as dispersive vehicles for noxious species, favoring the accumulation of phycotoxins in the food chain. Molecular qPCR techniques allowed to identify and quantify microalgae attached to plastics and, among them, species

belonging to the harmful *Alexandrium* genus were detected in 16 samples. The harmful strains were isolated from the surface of the plastic debris, cultured and sent to UniNa for the analysis of the toxin profile and PSTs content [55]. The application of the HILIC-HRMS method 3 to the analysis of ten strains of cultured *A. pacificum* successfully revealed the presence of PSTs in all the analyzed strains by a direct comparison of the retention time and the associated HRMS^2 spectrum of each individual toxin with those of the relevant standard injected under the same experimental conditions. Quantitative analyses pointed out a total toxin content in the range 35.1-6032.2 fg/cell, with a remarkable variability in terms of toxin profile and amount of produced toxins (**Table III.7**). The most productive strain turned out to be CNR-ACAT 6FA, whilst the less productive one was CNR-ACAT5D1. The most represented toxins were C1, C2, GTX1, GTX2, GTX3, GTX4 and B1, while STX was found only in 5 strains, and dcGTX2 and NEO in one of the 10 strains; dcNEO and dcGTX3 were not found in any of the analyzed samples. The relative abundance of C2, GTX1 and GTX5 on the total toxin content, ranged from 10-56%, 14-79%, and 1-56%, respectively.

Table III.7. Individual and total toxin content (fg/cell) of the *A. pacificum* strains isolated from plastic debris.

Strains	C1	C2	GTX2	GTX3	GTX1	GTX4	dcGTX2	dcGTX3	B1	STX	NEO	Total
ACAT 5D1	n.d.	n.d.	1.63	n.d.	19.93	n.d.	n.d.	n.d.	13.28	0.29	n.d.	35.14
ACAT 6A2	n.d.	18.97	n.d.	n.d.	13.01	4.78	n.d.	n.d.	1.7	5.12	n.d.	43.58
ACAT 6FA	26.62	1413.22	10.11	n.d.	422.68	181.11	n.d.	n.d.	3978.5	n.d.	n.d.	6032.25
ACAT 15	3.84	117.76	13.11	70.11	217.57	66.8	n.d.	n.d.	320.68	n.d.	n.d.	809.87
ACAT 6D4	4.38	432.41	15.23	342.02	247.95	79.97	n.d.	n.d.	444.13	18.04	n.d.	1584.12
ACAT A1	1.77	160	10.08	2.45	227.03	64.99	n.d.	n.d.	139.56	3.21	n.d.	609.09
ACAT 7A2	0.74	114.74	1.13	n.d.	45.39	23.23	n.d.	n.d.	71.81	n.d.	n.d.	257.04
ACAT 02	52.97	388.2	1.13	3.62	119.66	112.31	n.d.	n.d.	n.d.	1.11	10.263	689.26
ACAT 6D5	32.31	887.33	35.55	n.d.	n.d.	n.d.	1.15	n.d.	844.77	n.d.	n.d.	1801.11
ACAT15P	6.25	148.76	4.62	n.d.	103.19	57.9	n.d.	n.d.	250.08	n.d.	n.d.	571.08

More details on the experimental conditions, discussion and results are reported in a published research article [55].

3. Materials and methods

3.1 Standards

Certified reference material (CRM) of STX, C1, C2, GTX1, GTX2, GTX3, GTX4, B1, dcGTX2, dcGTX3, NEO, dcNEO and dcSTX were purchased from the Institute of Biotoxin Metrology, National Research Council of Canada (NRC, Halifax, Canada). TTX standard was obtained from Enzo Life Sciences (Enzo, Exeter, United Kingdom).

3.2 Shellfish and phytoplankton samples

Shellfish from Northern Adriatic sea were collected by the Local Veterinary Authorities in the frame of the Official Control monitoring program for EU regulated marine biotoxins (Reg. EC 854/2004, Reg. EC 853/2004) and kindly provided by "Istituto Zooprofilattico Sperimentale delle Venezie" (IZSVe; Legnaro, Italy). Shellfish from UK were kindly provided by Dr. Andrew Turner of Centre for Environment Fisheries and Aquaculture Science (CEFAS; Weymouth, United Kingdom) in the frame of a collaborative study that is still ongoing. Algal pellets deriving from 10 strains of cultured *A. pacificum* were isolated from plastic debris which were collected from the Syracuse Bay (Ionian Sea, Southern Italy) between 2016-2017 in in the context of a survey of plastic debris, and provided by Prof. Antonella Penna of the Department of Biomolecular Sciences within the University of Urbino (Urbino, Italy).

3.3 Extraction of shellfish samples for TTX/PSTs

Shellfish samples were extracted according to Boundy et al. [50] and Turner et al [8,43]. Briefly, 5 g aliquots of homogenized tissue, were extracted with a 5 mL of Acetic acid 0.1% in a polypropylene tube. The mixture was mixed for 90 s and placed, first in a boiling water bath for 5 min and then in an ice bath for the same time. After being vortexed for 90 s, they were centrifuged at 4000 rpm for 10 min. Supernatants were collected, and 1.0 mL were transferred into a polypropylene tube, added of 5 uL of NH_3 25%, and then mixed. As second step, clean-up of the extracts was performed by means of solid phase extraction (SPE), using ENVI-Carb 250 mg/3mL cartridges, conditioned with 3 mL of Acetonitrile 20% + Acetic acid 1%, and then with NH_3 0,025%. 400 µL of the extracted samples were added to the cartridges, which were washed with 700 µL of HPLC water, and then eluted with 2 mL of Acetonitrile 20% + Acetic acid 1%. The

eluted fractions were collected, and 50 uL of them were diluted 1:4 with 150 uL of Acetonitrile. The obtained samples were directly analyzed by HILIC-HRMS.

3.4 Extraction of algal pellets for PSTs

A. pacificum cell pellets were separately extracted with 0.5 mL of 0.1 M acetic acid into polypropylene tube. Subsequently, each extract was sonicated for 10 min in pulse mode at 20% amplitude while kept cooled in an ice bath. The mixture was centrifuged at 8000 rpm for 10 min, the supernatant was transferred into a clean polypropylene tube while the solid residue was extracted again as reported above. The supernatants were then combined (1 mL total for sample) and an aliquot of 50 uL was diluted 1:4 with 150 uL of Acetonitrile. The obtained samples were directly analyzed by HILIC-HRMS.

3.5 Optimization of HILIC-HRMS methods

LC-HRMS analyses were carried out on a hybrid linear ion trap LTQ Orbitrap XL^{TM} Fourier Transform Mass Spectrometer (FTMS) equipped with an ESI ION MAX^{TM} source coupled with a Dionex Ultimate 3000 quaternary HPLC system (Thermo-Fisher, San Jose, CA, USA).

3.5.1 HILIC-HRMS method 1

Chromatographic conditions were optimized according to Dell'Aversano et al. [3] and slightly modified. Briefly, mobile phases were water (A) and acetonitrile-water 95:5 v/v (B) both containing 2.0 mM ammonium formate and 3.6 mM formic acid at pH 3.55. Chromatographic separation was optimized by using two TSK-gel® Amide-80 columns of different length, both packed with 5µm spherical particles, kept at 20°C and eluted at a flow rate of 0.2 mL/min; injection volumes were 5 µL. The gradient elution optimized for the longer (250mm×2mm i.d) and the shorter column (150mm×2mm i.d) were, respectively:

Method 1: time (t) 0 min, 65% B; t 13 min, 65%B; t 14, 10%B; t 23, 10%B; t 24 65%B and t 25 65% B; re-equilibration time was 9 min.

Method 2: t 0 min, 70% B; t 10 min, 70%B; t 11, 10%B; t 17, 10%B; t 18 70%B and t 19 70% B; re-equilibration time was 9 min.

The variability of the optimized chromatography was carefully evaluated by monitoring the retention times of PSTs and TTX within the same batch of analysis (intra-batch variability) and

between different batches (inter-batch variability). Notably, a standard mixture was injected 8 times within a batch of 30 h. For each toxin, the average retention time was measured and used to calculated the sd, which was employed to evaluate the method reproducibility. The LC-MS run was split into 4 time segments or windows, whose duration depended on column length:

1st segment - 9.0 and 6.9 min for column of 250 and 150 mm, respectively.

2nd segment – 4.0 and 3.2 min for column of 250 and 150 mm, respectively.

3rd segment – 5.0 and 3.8 min for column of 250 and 150 mm, respectively.

4th segment – 7.0 and 5.1 min for column of 250 and 150 mm, respectively.

ESI HRMS analyses were accomplished in positive ion mode, and source settings were optimized evaluating the response of each standard at different conditions evaluated separately. Therefore, the conserved source parameters across the entire run (4 segments) were the capillary temperature, set at 300 °C, and the spray voltage, set at 4.8 kV. In the segment 1, sheath gas and auxiliary gas were 31 and 13 (arbitrary units) respectively, whilst capillary voltage and tube lens voltage were set at 80 V and 210 V. In the segments 2-4, the following ESI source parameters were set: sheath gas 33, auxiliary gas 6, capillary voltage 20 V, and tube lens voltage 90 V. Full scan HRMS acquisition was recorded across all the run at resolving power (RP) 30,000 (FWHM at m/z 400) in the range m/z 230-500. $HRMS^2$ analyses were performed in collision-induced dissociation (CID) mode at RP 30,000 (FWHM at m/z 400), isolation width 2 m/z, activation Q 0.250, and activation time 30 ms. The precursor ion selected for each toxin including the optimized collision energy (CE) are reported in **Table III.1**. Extracted Ion Chromatograms (XICs) of analogues fragmented at CE 0 (C1, C2, GTX1, GTX2, dcGTX2, NEO, dcNEO, STX and dcSTX) were obtained by selecting the exact mass of the monoisotopic peak of each precursor ion (**Table III.1**), while XICs of analogues fragmented at CE ≠ 0 (GTX3, GTX4, dcGTX3, B1 and TTX) were obtained by selecting the most intense fragments present in the $HRMS^n$ (n=2,3) spectra **(Table III.1, Fig.III.4)**. Elemental formulae were calculated from the monoisotopic peak using a mass tolerance of 5 ppm of the ion cluster through Thermo Xcalibur software v2.2 SP1.48 (Thermo Fisher, San Josè, CA, USA).

3.5.2 HILIC-HRMS method 2

Chromatographic conditions were optimized according to Boundy et al. [50] and Turner et al. [8,43] and slightly modified. Briefly, a Water Acquity UPLC BEH Glycan 1.7 mm, 2.1 x 150 mm

column (Batch 0161) equipped with a Waters VanGuard BEH Amide cartridge 1.7 mm, 2.1 x 5mm (Waters, Massachusetts, USA) and maintained at 60°C was used. The column was eluted with water +0.015% formic acid +0.06% ammonia 25% (eluent A) and 70% acetonitrile/water +0.01% formic acid (eluent B) according to the following gradient: time (t) = 0 min, 99% B, flow 0.2 mL/min; t = 10 min, 99% B, flow 0.2 mL/min; t = 15 min, 50% B, flow 0.2 mL/min; t = 18 min, 50% B, flow 0.25 mL/min; t = 19 min, 99% B, flow 0.25 mL/min; t = 20 min, 99% B, flow 0.2 mL/min; re-equilibration time was 12 min while injection volumes were 5 µL. The variability of the optimized chromatographic method was evaluated within and between different batches as previously described for HILIC-HRMS method 1.

As reported for HILIC-HRMS method 1, the LC-MS run was divided into 4 time segments as follows: i) 1st segment – 8.5 min, ii) 2nd segment – 3.5 min, iii) 3rd segment – 3.5 min, iv) 4th segment – 6.5 min. ESI HRMS analyses were performed in positive ion mode setting the capillary temperature at 440°C and the source voltage at 4.8 kV. In the first time segment, source parameters were: sheath and auxiliary gas 30 and 3 (arbitrary units), respectively, capillary voltage 32 and tube lens 95. The same source parameters were set for segments 2-4 as follows: sheath and auxiliary gas 30 and 1, respectively, capillary voltage 24 and tube lens 75. HRMS spectra were acquired at RP 30,000 (FWHM at m/z 400) in the range m/z 230-500, whilst HRMS^2 experiments were accomplished in CID mode at RP 30,000 (FWHM at m/z 400), isolation width 2 m/z, activation Q 0.250, and activation time 30 ms. For each toxin, the precursor ion and the CE % used are reported in **Table III.3**. XICs of analogues fragmented at CE 0 % (C1, C2, GTX1, GTX2, dcGTX2, B1, NEO, dcNEO, STX and dcSTX) were obtained by selecting the exact mass of the monoisotopic peak of each precursor ion whilst analogues fragmented at CE ≠ 0 (GTX3, GTX4, dcGTX3, and TTX) were obtained by selecting the most intense fragments present in the HRMS^n (n=2,3) spectra (**Table III.3, Fig.III.4**). Elemental formulae were calculated within a mass tolerance of 5 ppm on the monoisotopic peak of the ion cluster through Thermo Xcalibur software v2.2 SP1.48 (Thermo Fisher, San Josè, CA, USA).

3.5.3 HILIC-HRMS method 3

Chromatographic conditions were the same as those reported in paragraph 3.3.2. HRMS analyses were accomplished in positive ion mode with ESI source parameters set as follows: capillary temperature 220 °C, spray voltage 4.8 kV, sheath gas 62 (arbitrary units), auxiliary gas 16.5

(arbitrary units), capillary voltage 49 V and tube lens voltage 250 V. HRMS^n experiments were performed in CID mode selecting the following parameters: RP at 30,000 (FWHM at m/z 400), isolation width 2 m/z, activation Q 0.250, and activation time 30 ms. Detection of TTX was carried out by HRMS^n (n=1,2) including two scan events as follows: i) HRMS^2 of the [M+H]$^+$ ion at m/z 320.1 - CE 23% - m/z range 85-350 - and ii) HRMS^3 selecting as precursor the [M+H-H$_2$O]$^+$ ion at m/z 302.1 – CE 20% - m/z range 80-350 - obtained through a first MS^2 scan on the [M+H]$^+$ ion. Analyses of PSTs were accomplished by HRMS^2 experiments where the following ions were selected as precursors: i) m/z 316.1 – CE 22% - m/z range 85-350 - ii) m/z 332.1 – CE 30% - m/z range 90-350 – iii) m/z 273.1 – CE 25% - m/z range 75-300 – iv) m/z 300.1 – CE 23% - m/z range 80-350 – and v) m/z 239.1 – CE 22% - m/z range 65-350. XIC of TTX was obtained by selecting the following diagnostic ions: [M+H]$^+$ at m/z 320.1068 (C$_{11}$H$_{18}$O$_8$N$_3^+$), [M+H-H$_2$O]$^+$ at m/z 302.0988 (C$_{11}$H$_{16}$O$_7$N$_3^+$) and [M+H-2H$_2$O]$^+$ at m/z 284.0882 (C$_{11}$H$_{14}$O$_6$N$_3^+$), while XIC of PSTs were obtained selecting the most intense ions reported in **Fig.III.4**, in both cases within 5 ppm mass tolerance.

3.6 Evaluation of matrix effect, instrumental limits, quantitative analyses and recovery.

The evaluation of matrix effect was conducted preparing matrix-free (MF) and matrix-matched (MM) calibration curves at levels reported in **Table III.2,4**. MF curves were prepared through serial dilution with ACN-W 3:1, while MM curves with a blank mussel tissue extracted according to the procedure reported in *paragraph 3.1*. Matrix effect (suppression and enhancement) was calculated by comparing the response (peak area) of MF and MM standards at different concentration levels as follows:

$$100 - \left[\frac{(peak\ area\ of\ MM\ standard)}{(peak\ area\ of\ MF\ standard)}\right] X\ 100$$

Experimental limits of detection (LOD) and quantitation (LOQ) were experimentally measured preparing serial dilutions of each MF and MM standard down to the lowest detectable and quantifiable concentration level, respectively. Quantitation of PSTs and TTX found in shellfish

and algal samples was performed as follows: i) MM calibration curves reported in **Table III.2** were used for determination of PSTs in shellfish samples collected from UK, ii) quantitation of TTX found out in mussels from Italy was performed through MM calibration curve, while iii) determination of PSTs in *A. pacificum* cultured strains was accomplished by comparing XIC areas of each detected toxin to the relevant standard at similar concentration levels injected under the same experimental conditions. The recovery of TTX extracted from shellfish samples was calculated through spiking experiments. Briefly, 3 blank mussel samples, each of 5 g weight, were spiked with 5µg TTX standard (1µg/1g) and then processed as reported in *paragraph 3.1*. Recovery % was calculated as follows:

$$\frac{Observed\ concentration}{Expected\ concentration} X\ 100$$

Quantitation of TTX in the spiked samples was performed by HILIC-HRMS method 3, and a percentage recovery yield of 60, 68 and 76 was calculated. The average value of 68 ± 11.3 % was used as correction factor for the accurate determination of TTX detected in shellfish from Italy.

4. Conclusions

In this study is reported the development of three HILIC-HRMS methods, named methods 1,2, and 3, for the simultaneous analysis of 13 PST analogues and TTX using the Orbitrap MS. The main drawbacks of high-resolution mass spectrometers (reduced analytical sensitivity due to long injection times and low scan frequency), when used for the configuration of multi-analyte methods, were overcome by setting up a time segmentation acquisition mode (method 1 and 2). Although both Amide-80 columns used in method 1 provided the best reproducibility in toxin retention times, the employment of the column of 250 mm was found to be preferable due to: i) a better peak resolution between epimer pairs (GTX2-3, GTX1-4 and dcGTX2-3) and ii) a longer gap between toxins eluting in different time-segments. However, method 2 gave the best results in terms of peak shape and chromatographic resolution while a high intra- and inter-batch variability was observed. The employment of the time segmentation acquisition mode allowed to set-up different source parameters for each segment, thus increasing the analytical sensitivity for each group of monitored toxins. The different chromatographic setup between method 1 and 2 strongly effected the optimization of the ESI source parameters, with the source temperature kept at 300°C and 440°C,

respectively. Nonetheless, a similar degree of in-source fragmentation was observed for most of the analogues. The absence of the $[M+H]^+$ ion of some PST congeners in the HRMS spectra led to carefully investigate the impact that the Orbitrap MS may have on the stability of the molecules in the MS analyzer. As a result, a meticulous study conducted under both methods 1 and 2 revealed a noteworthy influence of the ion transmission system (LTQ-C-trap-Orbitrap) since: i) the $[M+H]^+$ ion of GTX1, GTX2, dcGTX2 and GTX4 were found in the full-scan spectra acquired at low-resolution (LRMS) and ii) their fragmentation patterns in HRMS^2 spectra were obtained in CID mode (fragmentation occurring within the LTQ) selecting as precursor the same $[M+H]^+$ ions not detectable in the HR full-scan MS spectra. Contrarily, the high instability of C toxins was found to be associated with a strong fragmentation in the transmission from LTQ-C Trap-Orbitrap since their $[M+H]^+$ ions were not found even at Low Resolution. As further confirmation criterium of such observation, all the PST analogues were fragmented in CID mode at CE 0%. The $[M+H-SO_3]^+$ ion of C1 turned out to be more stable than that of C2, that provided an intense water loss fragment with a similar intensity. The C11-α-hydroxysulfated analogues (GTX2, GTX1 and dcGTX2) underwent the strongest fragmentation along the transmission system since none of the diagnostic ions or fragments were present in the spectra. Contrarily, their C11-β epimers (GTX3, GTX4 and dcGTX3) showed higher stability since the $[M+H]^+$ precursor ion was found in the spectra at CE 0%, with the exception of GTX4, even if the presence of intense $[M+H-H_2O]^+$ fragments pointed out the remarkable influence of the Orbitrap MS transmission system on the ion stability of toxins. On the other hand, the $[M+H-2SO_3]^+$ fragment of C toxins and the $[M+H-SO_3]^+$ fragment of both C11-α and -β epimers were not influenced during the transmission from LTQ to Orbitrap via C-trap. The same instability was observed for B1 whilst toxins lacking sulfate moieties such as: TTX, NEO, dcNEO, STX and dcSTX were not affected by transmission issue. These findings were employed for optimizing the HRMS^2 conditions for both methods 1 and 2, that were compared in terms of matrix effect, linearity and analytical sensitivity. The matrix effect did not affect the chromatographic parameters whilst a toxin-dependent influence on the MS response was observed for method 1 and a certain suppression effect was measured for method 2, except for STX that gave ion enhancement within the entire concentration range tested. Even though both methods showed a good linearity and sensitivity, method 2 was characterized by a low specificity, thus resulting not applicable to the analysis of shellfish samples. On the other hand, method 3, which shared the same chromatography of method 2 but different MS conditions (e.g.

source temperature set at 220°C, no time segmentation mode, fragmentation of common precursor ion of some PST analogues), was successfully applied to the analysis of the toxin profile of cultured *A. pacificum* strains isolated from microplastics harvested in the Syracuse Bay (Ionian Sea, Southern Italy) during a survey of plastic debris between 2016-2017. The determination of PSTs at appreciable levels highlighted as the presence of such contaminants in sea water can increase the spread of alien toxin-producing species in temperature regions and their accumulation in the food chain, thus posing concerns for human safety. HILIC-HRMS method 3 was also applied for confirming the presence of TTX in mussel samples collected in the area of Marano Lagoon (Northern Adriatic Sea, Italy) between 2017 and 2018 during an official monitoring programs. TTX was measured at the highest level ever found in shellfish from Europe 413.0 µg/Kg.

References

1.   Wiese, M., D'agostino, P. M., Mihali, T. K., Moffitt, M. C., & Neilan, B. A. (2010). Neurotoxic alkaloids: saxitoxin and its analogs. *Marine drugs*, *8*(7), 2185-2211.

2.   Li, J., & Persson, K. M. (2020). Quick detection method for paralytic shellfish toxins (PSTs) monitoring in freshwater-a review. *Chemosphere*, 128591-128591.

3.   Dell'Aversano, C., Hess, P., & Quilliam, M. A. (2005). Hydrophilic interaction liquid chromatography–mass spectrometry for the analysis of paralytic shellfish poisoning (PSP) toxins. *Journal of Chromatography A*, *1081*(2), 190-201.

4.   EFSA Panel on Contaminants in the Food Chain (CONTAM), Knutsen, H. K., Alexander, J., Barregård, L., Bignami, M., Brüschweiler, B., ... & Petersen, A. (2017). Risks for public health related to the presence of tetrodotoxin (TTX) and TTX analogues in marine bivalves and gastropods. *EFSA Journal*, *15*(4), e04752.

5.   Bates, N., Morrison, C., Flaig, L., & Turner, A. D. (2020). Paralytic shellfish poisoning and palytoxin poisoning in dogs. *Veterinary record*.

6.   Dean, K. J., Hatfield, R. G., Lee, V., Alexander, R. P., Lewis, A. M., Maskrey, B. H., ... & Turner, A. D. (2020). Multiple new paralytic shellfish toxin vectors in offshore North Sea benthos, a deep secret exposed. *Marine Drugs*, *18*(8), 400.

7.   Chau, R., Kalaitzis, J. A., & Neilan, B. A. (2011). On the origins and biosynthesis of tetrodotoxin. *Aquatic Toxicology*, *104*(1-2), 61-72.

8.   Turner, A. D., Boundy, M. J., & Rapkova, M. D. (2017). Development and single-laboratory validation of a liquid chromatography tandem mass spectrometry method for quantitation of Tetrodotoxin in mussels and oysters. *Journal of AOAC International*, *100*(5), 1469-1482.

9.   Alcaraz, A., Whipple, R. E., Gregg, H. R., Andresen, B. D., & Grant, P. M. (1999). Analysis of tetrodotoxin. *Forensic science international*, *99*(1), 35-45.

10.   Noguchi, T., Miyazawa, K., Daigo, K., & Arakawa, O. (2011). Paralytic shellfish poisoning (PSP) toxin-and/or tetrodotoxin-contaminated crabs and food poisoning by them. *Toxin Reviews*, *30*(4), 91-102.

11.   Dell'Aversano, C., Tartaglione, L., Polito, G., Dean, K., Giacobbe, M., Casabianca, S., ... & Turner, A. D. (2019). First detection of tetrodotoxin and high levels of paralytic shellfish poisoning toxins in shellfish from Sicily (Italy) by three different analytical methods. *Chemosphere*, *215*, 881-892.

12.   Anon., Paralytic Shellfish Poison. Biological Method. Final Action, AOAC OfficialMethod 959.08, AOAC International, 2005, pp. 79–80

13.   Yasumoto, T. (1991). The manual for the methods of food sanitation tests. *Vol for Chemistry, Bureau for Environmental Health, Ministry for Health and Welfare*, 232.

14.   Hungerford, J. M. (2006). Committee on natural toxins and food allergens: Marine and freshwater toxins. *Journal of AOAC International*, *89*(1), 248-269.

15.   Wiberg, G. S., & Stephenson, N. R. (1961). The effect of metal ions on the toxicity of paralytic shellfish poison. *Toxicology and applied pharmacology*, *3*(6), 707-712.

16.   McCulloch, A. W., Boyd, R. K., Freitas, A. D., Foxall, R. A., Jamieson, W. D., cock, M. L., ... & Richard, D. J. A. (1989). Zinc from oyster tissue as causative factor in mouse deaths in official bioassay for paralytic shellfish poison. *Journal of the Association of Official Analytical Chemists*, *72*(2), 384-386.

17.   Aune, T., Ramstad, H., Heidenreich, B., Landsverk, T.,Waaler, T., Egaas, E., Jul-shamn, K. (1998). Zinc accumulation in oysters giving mouse deaths in paralytic shellfishpoisoning bioassay, *Journal of Shellfish Res*earch 17, 1243–1246.

18.   Humpage, A. R., Magalhaes, V. F., & Froscio, S. M. (2010). Comparison of analytical tools and biological assays for detection of paralytic shellfish poisoning toxins. *Analytical and bioanalytical chemistry*, *397*(5), 1655-1671.

19.   Hayashi, R., Saito, H., Okumura, M., & Kondo, F. (2006). Cell bioassay for Paralytic Shellfish Poisoning (PSP): Comparison with postcolumn derivatization liquid chromatographic analysis and application to the monitoring of PSP in shellfish. *Journal of agricultural and food chemistry*, *54*(2), 269-273

20.   DeGrasse, S., Rivera, V., Roach, J., White, K., Ca.llahan, J., Couture, D., ... & Poli, M. (2014). Paralytic shellfish toxins in clinical matrices: extension of AOAC official method 2005.06 to human urine and serum and application to a 2007 case study in Maine. *Deep Sea Research Part II: Topical Studies in Oceanography*, *103*, 368-375.

21.   Ruberu, S. R., Langlois, G. W., Masuda, M., Kittredge, C., Perera, S. K., & Kudela, R. M. (2018). Receptor binding assay for the detection of paralytic shellfish poisoning toxins: Comparison to the mouse bioassay and applicability under regulatory use. *Food Additives & Contaminants: Part A*, *35*(1), 144-158.

22.   Kogure, K., Tamplin, M. L., Simidu, U., & Colwell, R. R. (1988). A tissue culture assay for tetrodotoxin, saxitoxin and related toxins. *Toxicon*, *26*(2), 191-197.

23.   Hamasaki, K., Kogure, K., & Ohwada, K. (1996). A biological method for the quantitative measurement of tetrodotoxin (TTX): tissue culture bioassay in combination with a water-soluble tetrazolium salt. *Toxicon*, *34*(4), 490-495.

24.   Hamasaki, K., Kogure, K., & Ohwada, K. (1996). An improved method of tissue culture bioassay for tetrodotoxin. *Fisheries science*, *62*(5), 825-829.

25.   Davio, S. R., & Fontelo, P. A. (1984). A competitive displacement assay to detect saxitoxin and tetrodotoxin. *Analytical biochemistry*, *141*(1), 199-204.

26.   Doucette, G. J., Powell, C. L., Do, E. U., Byon, C. Y., Cleves, F., & McClain, S. G. (2000). Evaluation of 11-[3H]-tetrodotoxin use in a heterologous receptor binding assay for PSP toxins. *Toxicon*, *38*(11), 1465-1474.

27.   Van De Riet, J., Gibbs, R. S., Muggah, P. M., Rourke, W. A., MacNeil, J. D., & Quilliam, M. A. (2011). Liquid chromatography post-column oxidation (PCOX) method for the determination of paralytic shellfish toxins in mussels, clams, oysters, and scallops: Collaborative study. *Journal of AOAC International*, *94*(4), 1154-1176.

28.   Quilliam, M. A., Janeček, M., & Lawrence, J. F. (1993). Characterization of the oxidation products of paralytic shellfish poisoning toxins by liquid chromatography/mass spectrometry. *Rapid communications in mass spectrometry*, *7*(6), 482-487.

29.   S. Sato, Y. Shimizu, in: B. Reguera, J. Blanco, M.L. Fernandez, T. Wyatt (Eds.), Proceedings of the VIII International Conference on Harmful Algae, IOC, UNESCO, Vigo, Spain, 1997, p. 465.

30.   Turner, A. D., Hatfield, R. G., Rapkova, M., Higman, W., Algoet, M., Suarez-Isla, B. A., ... & Lees, D. N. (2011). Comparison of AOAC 2005.06 LC official method with other methodologies for the quantitation of paralytic shellfish poisoning toxins in UK shellfish species. *Analytical and bioanalytical chemistry*, *399*(3), 1257-1270.

31.   Yasumoto, T., Nakamura, M., Oshima, Y., & Takahata, J. (1982) Nippon Suisan Gakkaishi 48, 1481–1483.

32.   Yasumoto, T., & Michishita, T. (1985). Fluorometric determination of tetrodotoxin by high performance liquid chromatography. *Agricultural and Biological Chemistry*, *49*(10), 3077-3080.

33.   Yotsu, M., Endo, A., & Yasumoto, T. (1989). An improved tetrodotoxin analyzer. *Agricultural and biological chemistry*, *53*(3), 893-895.

34.   Quilliam, M. A., Thomson, B. A., Scott, G. J., & Siu, K. M. (1989). Ion-spray mass spectrometry of marine neurotoxins. *Rapid Communications in Mass Spectrometry*, *3*(5), 145-150.

35.   Shoji, Y. (2001). Yotsu-Yamashita. M.; Miyazawa, T.; Yasumoto, T. Electrospray ionization mass spectrometry of tetrodotoxin and its analogs: liquid mass spectrometry, and liquid chromatography/tandem mass spectrometry. *Anal. Biochem*, *290*, 10-17.

36.   Man, C. N., Noor, N. M., Harn, G. L., Lajis, R., & Mohamad, S. (2010). Screening of tetrodotoxin in puffers using gas chromatography–mass spectrometry. *Journal of Chromatography A*, *1217*(47), 7455-7459.

37.   Locke, S. J., & Thibault, P. (1994). Improvement in detection limits for the determination of paralytic shellfish poisoning toxins in shellfish tissues using capillary electrophoresis/electrospray mass spectrometry and discontinuous buffer systems. *Analytical Chemistry*, *66*(20), 3436-3446.

38.   Ali, A. E., Arakawa, O., Noguchi, T., Miyazawa, K., Shida, Y., & Hashimoto, K. (1990). Tetrodotoxin and related substances in a ribbon worm Cephalothrix linearis (Nemertean). *Toxicon*, *28*(9), 1083-1093.

39.   Pleasance, S., Ayer, S. W., Laycock, M. V., & Thibault, P. (1992). Ionspray mass spectrometry of marine toxins. III. Analysis of paralytic shellfish poisoning toxins by flow-

injection analysis, liquid chromatography/mass spectrometry and capillary electrophoresis/mass spectrometry. *Rapid communications in mass spectrometry*, *6*(1), 14-24.

40.   Alpert, A. J. (1990). Hydrophilic-interaction chromatography for the separation of peptides, nucleic acids and other polar compounds. *Journal of chromatography A*, *499*, 177-196.

41.   Strege, M. A. (1998). Hydrophilic interaction chromatography− electrospray mass spectrometry analysis of polar compounds for natural product drug discovery. *Analytical Chemistry*, *70*(13), 2439-2445.

42.   Dell'Aversano, C., Eaglesham, G. K., & Quilliam, M. A. (2004). Analysis of cyanobacterial toxins by hydrophilic interaction liquid chromatography–mass spectrometry. *Journal of Chromatography A*, *1028*(1), 155-164.

43.   Turner, A. D., Dhanji-Rapkova, M., Fong, S. Y., Hungerford, J., McNabb, P. S., Boundy, M. J., & Harwood, D. T. (2020). Ultrahigh-performance hydrophilic interaction liquid chromatography with tandem mass spectrometry method for the determination of paralytic shellfish toxins and tetrodotoxin in mussels, oysters, clams, cockles, and scallops: Collaborative study. *Journal of AOAC International*, *103*(2), 533-562.

44.   Vanhaecke, L., Van Meulebroek, L., De Clercq, N., & Bussche, J. V. (2013). High resolution orbitrap mass spectrometry in comparison with tandem mass spectrometry for confirmation of anabolic steroids in meat. *Analytica chimica acta*, *767*, 118-127.

45.   Stone, P., Glauner, T., Kuhlmann, F., Schlabach, T., & Miller, K. (2009). New dynamic MRM mode improves data quality and triple quad quantification in complex analyses. *Agilent publication.*

46.   Ghaste, M., Mistrik, R., & Shulaev, V. (2016). Applications of Fourier transform ion cyclotron resonance (FT-ICR) and orbitrap based high resolution mass spectrometry in metabolomics and lipidomics. *International journal of molecular sciences*, *17*(6), 816.

47.   Hecht, E. S., Scigelova, M., Eliuk, S., & Makarov, A. (2006). Fundamentals and Advances of Orbitrap Mass Spectrometry. *Encyclopedia of Analytical Chemistry: Applications, Theory and Instrumentation*, 1-40.

48.   Rousu, T., Herttuainen, J., & Tolonen, A. (2010). Comparison of triple quadrupole, hybrid linear ion trap triple quadrupole, time-of-flight and LTQ-Orbitrap mass spectrometers in drug discovery phase metabolite screening and identification in vitro–amitriptyline and verapamil as model compounds. *Rapid Communications in Mass Spectrometry: An International Journal*

Devoted to the Rapid Dissemination of Up-to-the-Minute Research in Mass Spectrometry, *24*(7), 939-957.

49.   Kalli, A., Smith, G. T., Sweredoski, M. J., & Hess, S. (2013). Evaluation and optimization of mass spectrometric settings during data-dependent acquisition mode: focus on LTQ-Orbitrap mass analyzers. *Journal of proteome research*, *12*(7), 3071-3086.

50.   Boundy, M. J., Selwood, A. I., Harwood, D. T., McNabb, P. S., & Turner, A. D. (2015). Development of a sensitive and selective liquid chromatography–mass spectrometry method for high throughput analysis of paralytic shellfish toxins using graphitised carbon solid phase extraction. *Journal of Chromatography A*, *1387*, 1-12.

51.   Kalli, A., Smith, G. T., Sweredoski, M. J., & Hess, S. (2013). Evaluation and optimization of mass spectrometric settings during data-dependent acquisition mode: focus on LTQ-Orbitrap mass analyzers. *Journal of proteome research*, *12*(7), 3071-3086.

52.   Bordin, P., Dall'Ara, S., Tartaglione, L., Antonelli, P., Calfapietra, A., Varriale, F., ... & Barco, L. (2021). First occurrence of tetrodotoxins in bivalve mollusks from Northern Adriatic Sea (Italy). *Food Control*, *120*, 107510.

53.   Eriksen, M., Lebreton, L. C., Carson, H. S., Thiel, M., Moore, C. J., Borerro, J. C., ... & Reisser, J. (2014). Plastic pollution in the world's oceans: more than 5 trillion plastic pieces weighing over 250,000 tons afloat at sea. *PloS one*, *9*(12), e111913.

54.   Masó, M., Fortuño, J. M., De Juan, S., & Demestre, M. (2016). Microfouling communities from pelagic and benthic marine plastic debris sampled across Mediterranean coastal waters. *Scientia Marina*, *80*(S1), 117-127.

55.   Casabianca, S., Capellacci, S., Giacobbe, M. G., Dell'Aversano, C., Tartaglione, L., Varriale, F., ... & Penna, A. (2019). Plastic-associated harmful microalgal assemblages in marine environment. *Environmental Pollution*, *244*, 617-626.

Chapter 4 : Development of a liquid chromatography chromatography-high resolution mass spectrometry (LC-HRMS) methods for the analysis of toxic and bioactive cyanobacterial secondary metabolites.

1. Introduction

Nowadays, aquatic cyanobacteria represent one of the main global emerging issues since their impact on the whole ecosystem can causes severe and drastic consequences [1]. This concern is mainly related to their ability to massively proliferate forming dense blooms on the water surface, which are clearly visible due to characteristic colored scums (green, red, brown, yellow and pink) depending on cyanobacterial composition and their photosynthetic pigments [2-3]. Although cyano-blooms were once considered only an "aesthetic" issue, today several studies highlighted the main consequences associated with such biomass accumulation: i) increased turbidity of water which smothers the aquatic vegetation, ii) depletion of oxygen which causes hypoxia, anoxia, and subsequently death of fish, and iii) release of odorous compounds and toxic metabolites (cyanotoxins) which drastically interfere with recreational water activities (e.g. fishing, bathing and tourism), drinking water reservoirs and the consumption of edible species [4-6]. Therefore, harmful cyano-blooms (cyano-HABs) pose a serious threat to humans and other life-forms, and unfortunately, this situation is becoming even more worrying as the incidence of cyano-HABs is dramatically increasing worldwide [7]. This concerning trend is mainly related to anthropogenic pressure, with a considerable influence deriving from the global warming which not only increases the frequency, intensity and duration of cyano-blooms, but also favors the proliferation of toxic producing species, including the appearance of newly toxic secondary metabolites [8-9].

As a consequence, the availability of effective and reliable analytical methods for determining the occurrence of cyanotoxins in environmental and food samples has become a priority. However, if a variety of approaches have been developed and validated for the identification and quantitation of cyanotoxins in water, the situation is still problematic for their determination in complex matrices such as food and biological samples [10]. Overall, analytical methods can be divided into two macro-groups: biological or indirect-quantitative approaches, and chemical or direct-

quantitative techniques, each of them characterized by specific advantages and drawbacks [11]. Among the biological methods, a further diversification can be done between molecular (e.g. Polymerease-Chain Reaction, PCR; Microarray) and biochemical (e.g. Enzyme-Linked Immunosorbent Assay, ELISA) methods. PCR techniques allow a selective identification of cyanobacterial cells by using specific primers able to bind the 16S ribosomal Ribonucleic Acid (rRNA), which is a characteristic gene of prokaryotic organisms [12]. In addition, multiplex PCR techniques allow to simultaneously amplify different genes within the same run, thus the combined detection of different toxic and non-toxic cyanobacterial species is possible [13]. Quantitative measurements instead, are possible through quantitative Real-time PCR techniques (qPCR), which turned out to be also more sensitive than the classic PCR. This approach has drawn attention especially from water companies because it is not expensive and time-consuming. However, qPCR methods have been implemented for the detection of a limited number of cyanotoxin genes such as those for MC, STX and CYN [14]. Moreover, this approach has raised some doubts about its usage as an indicator of cyanotoxin risk since it can only bring to the light the presence of cyanobacterial cells in the environment while no indication is given on toxin levels. This represents a noticeable downside since the expression of toxin genes is strongly related to environmental factors, and their relationship still needs to be clarified [15]. Therefore positive results have to be confirmed by alternative approaches.

More recently, microarray technology-based methods have been developed for the analysis of cyanobacteria in environmental samples [16]. This methodology showed a great potential for high throughput analysis by simultaneously detecting a very large number of specific genes within the same run-test, making it a powerful tool for characterizing cyanobacterial biomass. However, similarly to qPCR methods, no information on toxin concentration can be obtained through this approach [17]. Among the biological approaches, quantitative measurements of cyanotoxin levels can be performed through ELISA-based methods. The usage of monoclonal, variant-specific and polyclonal antibodies allows to determine the levels of specific cyanotoxin and also specific variants within the same group [18-19]. This approach is characterized by a variety of advantages such as: experiment setting is easy, analyses are low-cost, no analytical standard are needed and unknown analogues of the same toxin family can be quantified [10,20]. A number of ELISA kits are commercially available and suitable to quantify an assorted pattern of toxins like MCs, NODs, CYNs, STXs and the BMAA [19,21-22]. For this reasons, ELISA tests have been widely employed

as primary screening tool by water companies for the analyses of raw and treated waters. However, beside the strength of such approach, the matrix effect and the large number of toxin analogues, especially for MCs, hampers accurate quantitative analyses since the cross-reactivity of the antibodies can strongly vary among different structural variants [23].

On the other side, chemical methods showed potential for direct determination of cyanotoxins in complex matrices [11]; among them, liquid chromatography coupled to mass spectrometry (LC-MS) has proven to be one of the most powerful tool since: i) cyanotoxins are thermally labile and/or nonvolatile compounds, thus not analyzable by gas chromatography (GC), ii) they are well suited to ESI ionization forming very intense $[M+H]^+$ ions and iii) MS^2 experiments do not require further confirmation through alternative methods for positive results [24-26]. Moreover, the employment of untargeted high-resolution MS approach (HRMS) not only allows to monitor and determine the presence of known cyanotoxins, but also to bring to the light new structural analogues whose presence cannot be highlighted by unit-resolution MS methods, especially in lack of commercially available reference material [27].

This study describes the optimization of a reverse-phase LC-HRMS method for the analysis of assorted cyanotoxins and its application to a real cyanobacterial biomass sample collected from a Greek lake. In this perspective, an untargeted workflow based on the combination of data dependent HRMS acquisition (DDA HRMS) and a newly vendor-free database of cyanometabolites [28] was designed. The implemented methodology allowed to identify a variety of known cyanotoxins and bioactive secondary metabolites belonging to MC, MG, AP and CPtp sub-groups and a number of unknown congeners whose chemical structures was supposed on the basis of the interpretation of their fragmentation spectra.

In addition, the implemented HILIC-HRMS method 1 for the analysis of PSTs, reported in chapter 3, was exploited to test its applicability to the analysis of hydrophilic and low-molecular weight cyanotoxins commercially available as certified reference material: ATX-a, CYN, LWTX1.

2. Results and discussion

2.1 LC-HRMS

2.1.1 Optimization of chromatography and HRMS conditions

A mixture of MC-LR, MC-RR, [Dha[7]]MC-LR and NOD-R CRM was prepared and used to optimize the MS parameters, whilst a mixture of 11 MC standards – [dAsp[3]]MC-LR, MC-LF, MC-LY, MC-HilR, [dAsp[3]]MC-RR, MC-LW, MC-YR, MC-HtyR, MC-WR and MC-LA – was used to test the chromatographic separation and the optimized MS conditions. Although MCs are rather hydrophobic compounds, the presence of polar functions such as carboxylic acids, amino and amido groups, makes these compounds well suited to be separated through reverse-phase (RP) chromatography [29]. Considering the high structural heterogeneity within the entire toxin group, a C8 base deactivated silica column (BDS) was selected for LC separation since it demonstrated suitable for the analysis of a large range of analytes with different chemical properties [30]. The presence of acids (e.g. Asp and Glu) and basic amino acid residues (e.g. Arg, Lys and His) in most of the analogues allows MCs to be easily ionized by electrospray (ESI) both in positive (ESI$^+$) and negative mode (ESI$^-$) [31]. Even though a high number of LC-MS methods were optimized providing abundant [M+H]$^+$ and/or [M+2H]$^{2+}$ ions, the choice of the ionization mode is a critical point for some reasons. Analogues having basic residue such as Arg^2 (e.g. MC-RR) and/or Arg^4 (e.g. MC-LR) can form an intramolecular salt with the carboxyl group of Glu^6 or Asp^3/MeAsp^3, thus increasing the ESI$^+$ ionization efficiency whereas ESI$^-$ provides a much lower sensitivity. On the other hand, MC variants without basic residues (e.g. MC-LA) give higher sensitivity in ESI$^-$ since the COOH functionality is not involved in intramolecular interactions with basic amino acids, while in ESI$^+$ give abundant [M+Na]$^+$ ions [32]. Based on the facts that the most common MCs contain basic amino acids and that the number of sites which undergo protonation (e.g. peptide bonds) is higher than those which can be deprotonated, ESI$^+$ ionization mode was selected as preferred channel to optimize MS parameters. As a consequence, the chromatographic separation and the optimization of the MS conditions were conducted by using as mobile phase water (A) and acetonitrile-water 95:5 v/v (B) both containing 2 mM ammonium formate and 50 mM formic acid to enhance the protonation of analytes [33].

Under the optimized conditions, MC-LR, [Dha[7]]MC-LR and NOD-R gave abundant [M+H]$^+$ ions and less intense [M+Na]$^+$ adduct ions, with a relative abundance ratio 100:10 (**Fig.IV.1a-c**). This

ionization behavior was strongly related to the presence of Arg residue in their structure. On the other hand, for MC-RR the presence of Arg^2 and Arg^4 greatly affected the ionization behavior since the bi-charged [M+2H]$^{2+}$ ion was dominant in the full-scan spectrum, showing a relative ratio with the [M+H]$^+$ ion 100:80 (**Fig.IV.1d**). This confirmed that the ionization of MCs in ESI$^+$ mode is notably dependent on the number of basic amino acids contained in their structure, with a maximum charge state being identical to the number of basic residues. Also for MC-RR the [M+Na]$^+$ ion was less intense, with a relative abundance ratio [M+Na]$^+$/ [M+H]$^+$ being 20:100.
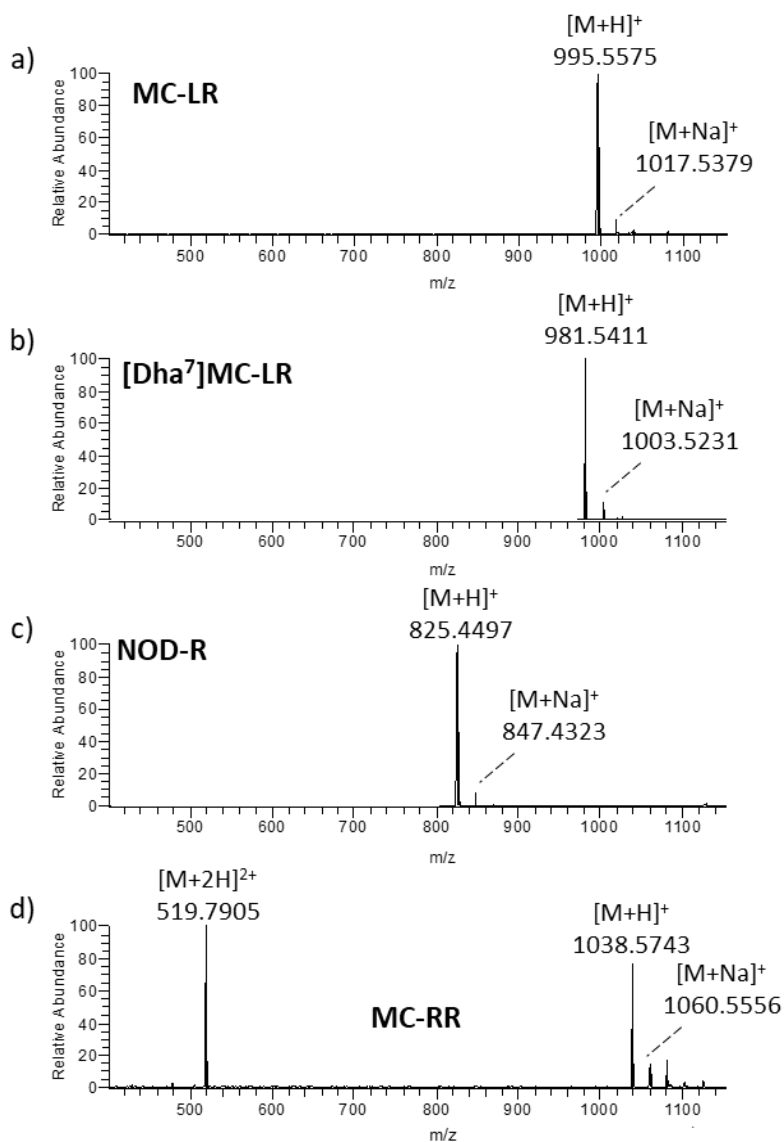
Figure IV.1 HRMS spectrum of: a) MC-LR, b) [Dha^7]MC-LR, c) NOD-R and d) MC-RR.

In addition, for all the toxins no in-source fragmentation occurred highlighting as the source temperature set at °C 350 was ideal for increasing the surface charge density of the ions without having a negative impact on their stability.

For each analogue, the optimization of HRMS^2 conditions was carried out by fragmenting the [M+H]$^+$ ion in collision-induced dissociation (CID) and higher-energy collisional dissociation (HCD) modes and ramping manually the collision energy. As shown in **Fig.IV.2**, fragmentation patterns of MC-LR acquired in CID and HCD mode turned out to be complementary since CID spectrum was characterized by the presence of diagnostic fragments in the *m/z* range 300-1000, whereas HCD spectrum provided intense fragments in the region *m/z* 100-300. This suggested that a combined interpretation of both CID and HCD spectra was necessary for both a correct identification of known MC analogues and for conducting structural hypothesis of unknown variants. CID HRMS^2 experiments gave rise to fragments related to multiple amino acid sequences, while HCD fragemtnation mode provided diagnostic fragment ions for MC and NOD group. More in detail, MCs containing Adda^5 are easily detectable by MS^2 due to the presence of an intense diagnostic fragment ion at *m/z* 135.0804 (C$_9$H$_{11}$O$^+$) originating from cleavage between C8-C9 occurring at the Adda sidechain (**Fig.IV.2a**). Contrarily, the neutral loss of C$_9$H$_{10}$O (134.0732 Da) from the [M+H]$^+$ ion gives rise to a diagnostic fragment with a *m/z* value specific for each toxin that represents an useful identification criteria for such compounds (**Fig.IV.2b**; [34]). In addition, Adda^5 represents the characteristic structural motif of MCs and NODs since it is present in most of the analogues so far known, while only few structural variants have been reported, such as: desmethyl Adda (DMAdda) and acetyl desmethyl adda (ADMAdda) [35]. However, MCs having these structural modifications can be recognized through characteristic fragment ions such as: *m/z* 121.0648 for DMAdda, due to the same cleavage between C8-C9, and *m/z* 265.1587 for ADMAdda due to the combination of the loss of the acetyl moiety and multiple cleavages occurring at the Adda^5 side chain [34,36].

The optimized LC-HRMS method was then applied to the analysis of an assorted pattern of MC standards. According to MC-LR, [Dha^7]MC-LR and NOD-R, analogues containing Arg^4 - [dAsp^3]MC-LR, MC-HilR, MC-YR, MC-HtyR and MC-WR - gave abundant [M+H]$^+$ ions and less intense [M+Na]$^+$ adduct ions with a relative abundance ratio of 100:5-15, respectively. As well as MC-RR, its desmethyl congener - [dAsp^3]MC-RR - provided a more intense [M+2H]$^{2+}$ bi-charged ion and a less intense [M+H]$^+$ ion with a relative ratio of 100:50; its [M+Na]$^+$ ion was

barely detectable. On the other hand, MCs lacking basic amino acids - MC-LF, MC-LY, MC-LA and MC-LW - provided very intense $[M+Na]^+$ and $[M+H]^+$ ions with a relative ratio of 55-65:100.
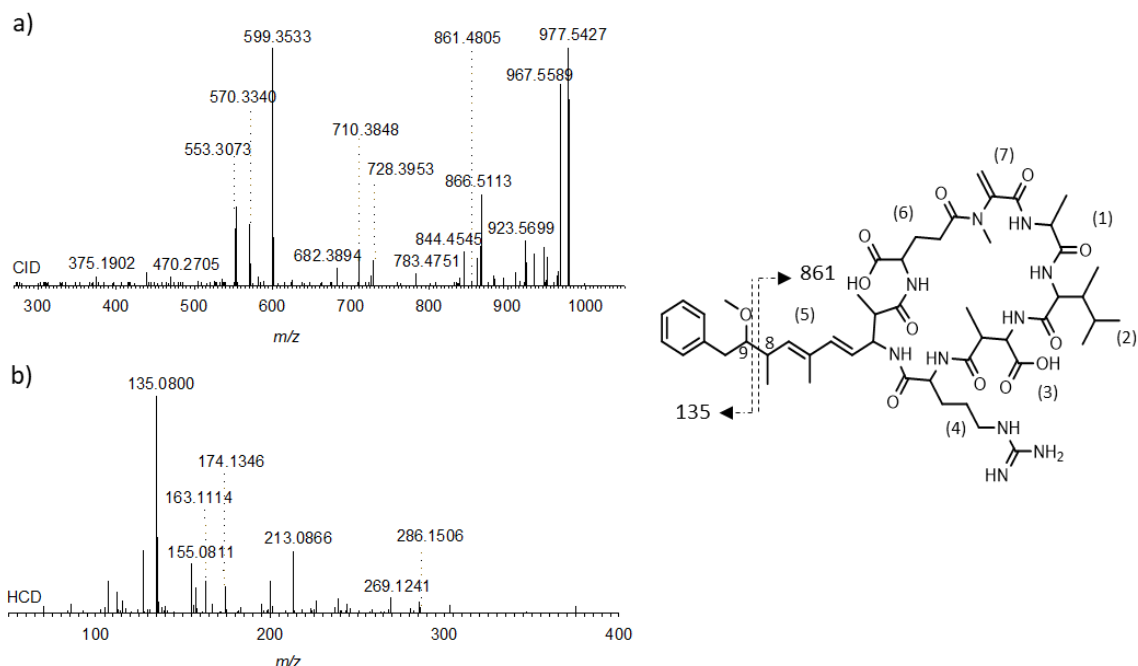
Figure IV.2 HRMS^2 spectra of MC-LR acquired in: a) CID and b) HCD mode. Representation of diagnostic cleavages originating on Adda^5. For ion assignment to relevant cleavages refer to Table IV.2.

As for chromatography, all toxins gave narrow and sharp peaks while different results were obtained in terms of resolution (**Fig.IV.3**). The isobaric congeners [dAsp^3]MC-LR and [Dha^7]MC-LR were not chromatographically separated and co-eluted with MC-LF and MC-LR; the same was observed for MC-RR and [dAsp^3]MC-RR. On the other side, an excellent resolution was obtained for all the other toxins. The co-elution of MC-LR and MC-LF with the desmethyl analogues of MC-LR, as well as the poor resolution between MC-RR and [dAsp^3]MC-RR, did not represent a critical point as a selective identification of these molecules could be conducted through measurements of exact masses. Isobaric analogues presenting the same $[M+H]^+$ ion instead ([dAsp^3]MC-LR and [Dha^7]MC-LR), could be distinguished only through the interpretation of their CID fragmentation patterns.
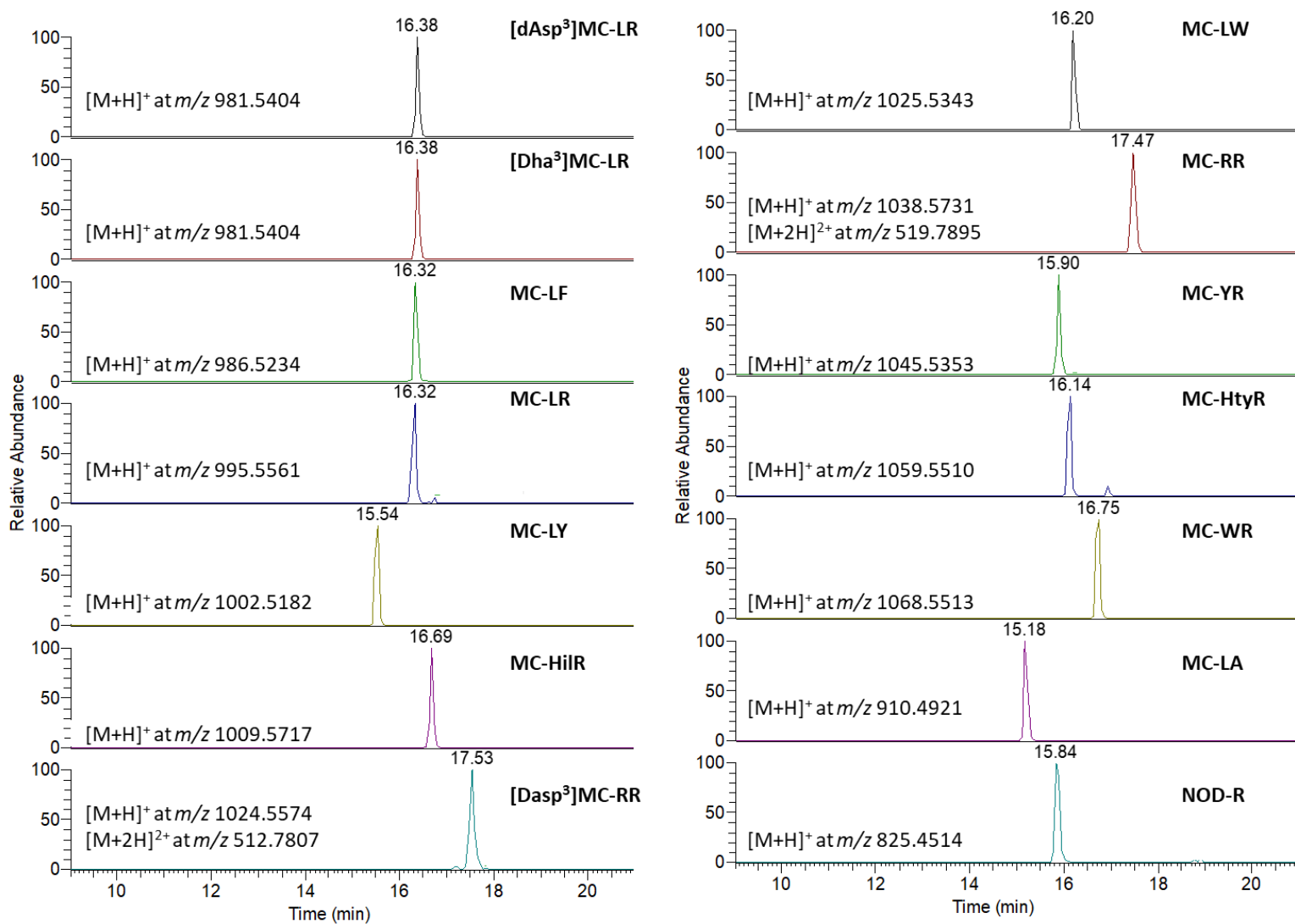
Figure IV.3 Extracted Ion Chromatogram (XIC) of: [Dha⁷]MC-LR, MC-LR, MC-RR and NOD-R certified reference material (CRM) and of [dAsp³]MC-LR, MC-LF, MC-LY, MC-HilR, [dAsp³]MC-RR, MC-LW, MC-YR, MC-HtyR, MC-WR and MC-LA non-CRM.

2.1.2 Instrumental detection limits and linearity

A mixture of MC-LR, MC-RR, [Dha⁷]MC-LR and NOD-R CRM was prepared and subjected to serial dilution in the range (15.8-280.0 ng/mL) to get 5-points matrix-free (MF) calibration curves. An excellent linearity was obtained for each standard within the entire concentration range tested with R^2 values between 0.9992-1 (**Fig.IV.4**).

Instrumental limits of detection (LOD) and quantification (LOQ) were measured by preparing a series of stepwise dilutions up to the lowest detectable and quantifiable level. As a result, the

implemented LC-HRMS method provided a remarkable sensitivity with LOD and LOQ being 2.5 and 5.0 ng/mL, respectively, for all toxin standard. Unfortunately, the limited availability of non-certified reference material for [dAsp^3]MC-LR, MC-LF, MC-LY, MC-HilR, [dAsp^3]MC-RR, MC-LW, MC-YR, MC-HtyR, MC-WR and MC-LA hampered the preparation of calibration curves and the assessment of method linearity. However, LOD and LOQ were obtained for these toxins and turned out to be, respectively: 2.5 and 5.0 ng/mL for [dAsp^3]MC-LR, MC-WR, MC-HilR and MC-HtyR, and 5.0 and 10.0 ng/mL for [dAsp^3]MC-RR, MC-YR, MC-LF, MC-LY, MC-LW and MC-LA.
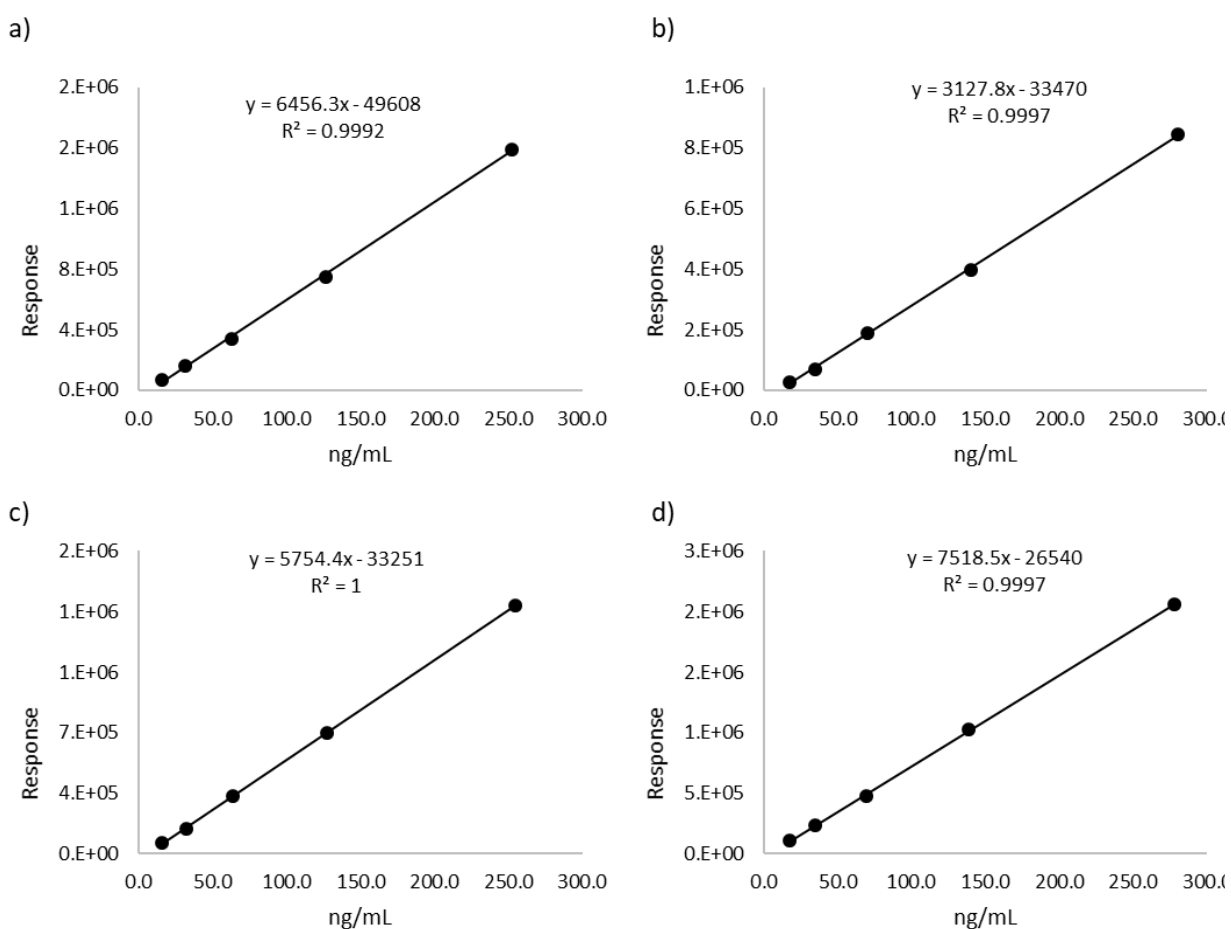
Figure IV.4 Matrix-free (MF) calibration curves of CRM: a) MC-LR, b) MC-RR, c) [dAsp^3]MC-LR and d) NOD-R.

2.2 HILIC-HRMS approach

General aspects

The high biodiversity that characterizes cyanobacteria is reflected by their metabolic profiles. Depending on the producing-organisms, cyanobacteria can produce a wide variety of secondary metabolites characterized by different chemical-physical properties [37]. This chemodiversity was also observed among the toxic compounds that they can produce since a large number of cyanotoxins with different structural features have been reported so far. Although LC-MS techniques demonstrated suitable for an accurate determination of a wide range of cyanobacterial secondary metabolites, the large diversity of produced molecules makes difficult a complete analysis in one LC-MS run under the same experimental conditions [38]. Reverse-phase (RP) LC has been successfully employed for the analysis of cyanobacterial oligopeptides (e.g. MCs, NODs, MGs, APs and CPtps), whilst its usage for the analysis of hydrophilic and low-molecular weight cyanotoxins (e.g. PSTs, ATXs, CYNs, LWTXs, BMMA) is a critical issue; the usage of ion-pairing agents is necessary to achieve an adequate retention on RP columnsm. However, these reagents do not well-suit MS since they can increase the background noise and drastically reduce the ionization efficiency. HILIC-MS approach turned out to be one of the best options for the analysis of polar cyanotoxins since a remarkable and efficient separation can be achieved without using ion-pairing agents [39]. In addition, taking into account that harmful cyano-HABs are the result of massive proliferations of different species, and that some cyanobacteria such as *Lyngbya wollei* (Farlow ex Gomont) Speziale & Dyck [40] can produce different toxins like CYNs and PST analogues, a multitoxin methods for the determination of the toxin profile of cyanobacterial biomasses is a prerequisite. In this perspective, the previously described HILIC-MS^2 method 1 (*Chapter 3*) developed for the determination of PSTs in environmental and food samples was tested for the analysis of polar cyanotoxins for which the relevant CRM is commercially available.

2.2.1 Optimization of a multi-toxin time segmented HILIC-MS method for the analysis of assorted polar cyanotoxins

A mixture of ATX-a, CYN and LWTX1 CRM was prepared and used to investigate the suitability and effectiveness of the previously described HILIC-MS method 1 for PSTs and TTX. Under the optimized conditions, ATX-a, CYN and LWTX1 gave very intense [M+H]$^+$ ions at *m/z*

166.1228 ($C_{10}H_{16}ON^+$), 416.1234 ($C_{15}H_{22}O_7N_5S^+$), and 379.1029 ($C_{11}H_{19}O_7N_6S^+$), respectively (**Fig.IV.5**).
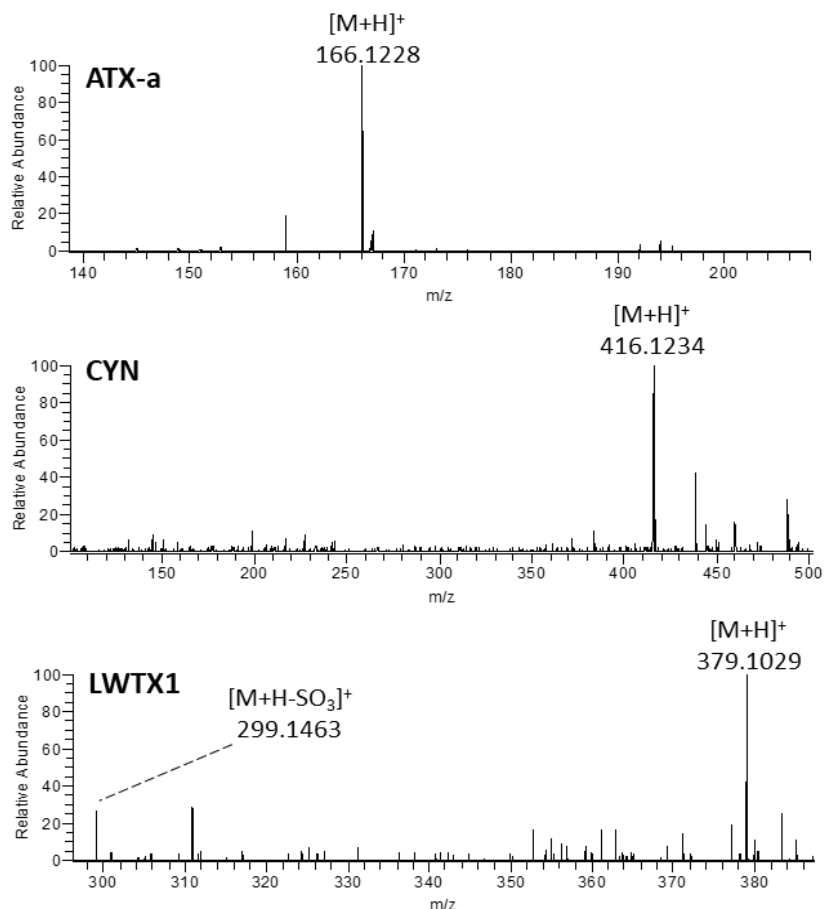
Figure IV.5 HR full-scan spectrum of ATX-a, CYN and LWTX1.

Similarly to some PSTs, CYN and LWTX1 feature a sulfate group in their structure, and taking into account that most of the sulfate PST analogues undergo a strong in-source fragmentation, a careful analysis of their full-scan spectra was carried out. CYN did not undergo in-source fragmentation since the $[M+H-SO_3]^+$ ion at m/z 336.1668 ($C_{15}H_{22}O_7N_5S^+$) was not found in the full-scan spectrum. Contrarily, an in-source loss of 79 Da (SO_3) was evidenced for LWTX1 that ionized forming the $[M+H-SO_3]^+$ ion at m/z 299.1463 ($C_{11}H_{19}O_4N_6^+$) with a relative abundance ratio $[M+H]^+$:$[M+H-SO_3]^+$ of 100:30 (**Fig.IV.5**). Considering that the source temperature is the most critical parameter that affects the stability of $[M+H]^+$ ions formed in source, an accurate evaluation of the relationship between the source temperature and the in-source fragmentation was conducted. At higher source temperatures in the range 400-440°C, the extent of the in-source

fragmentation for LWTX1 noticeably increased since the relative ratio $[M+H]^+ : [M+H-SO_3]^+$ was 100:70, while no influence was observed for CYN. On the other hand, higher temperature turned out to remarkably decrease the ionization efficiency for CYN and LWTX1 since at 300°C their ion current was 5 times more intense than that measured at 400-440°C. The same was observed for ATX-a, whose signal was 3 times more intense at 300°C whilst no in-source fragmentation occurred at higher temperatures.

$HRMS^n$ (n=2,3) conditions were optimized ramping manually the collision energies (CE) for each toxin and selecting as precursors the $[M+H]^+$ ions since they were the most intense signal in the full-scan spectra. The CID MS^2 spectrum of ATX-a acquired at CE 22 gave a variety of diagnostic fragments with ions at m/z 149.0960 ($C_{10}H_{13}O^+$) and 131.0855 ($C_{10}H_{11}O^+$), due to the neutral loss of NH_3 and NH_3+H_2O, respectively, being the most intense ones (**Fig.IV.6a**). The CID MS^2 spectrum of CYN at CE 20 was characterized by a dominant fragment at m/z 336.1667 ($C_{15}H_{22}O_4N_5^+$) due do the loss of the SO_3 moiety (79 Da) followed by a further water loss (m/z 318.1562, $C_{15}H_{20}O_3N_5^+$), and by an intense fragment at m/z 274.0857 ($C_{10}H_{16}O_4N_3S^+$) due to the loss of the side chain (uracil and CHOH moieties) (**Fig.IV.6b**). On the other hand, $HRMS^2$ spectrum of LWTX1 at CE 20 was not so informative since the only fragment obtained was that due to the neutral loss of the sulfate moiety (**Fig.IV.6c**), thus $HRMS^3$ experiment was performed by further fragmenting the ion at m/z 299.1463 ($[M+H-SO_3]^+$) at CE 15. As a result, the most intense fragment was that at m/z 239.1252 ($C_9H_{15}O_2N_6^+$) due to the loss of the side chain ($C_2H_4O_2$ moiety, 60 Da), which was followed by a further neutral loss of water (221.1148, $C_9H_{13}ON_6^+$) and of a guanidine moiety (m/z 180.0768, $C_9H_{13}ON_6^+$) (**Fig.IV.6d**). Although $HRMS^3$ approach turned out to be more informative in terms of diagnostic fragments, it led to a decreased method sensitivity. Therefore, $HRMS^2$ and MS^3 experiments were set for quantitative and qualitative purpose, respectively. The implemented HILIC-HRMS method 1 was further tested to evaluate the chromatographic separation of ATX-a, CYN and LWTX1, but differently from PSTs and TTX, chromatographic conditions were investigated using only the 250mm×2mm i.d - 5µm TSK-gel® Amide-80 column.
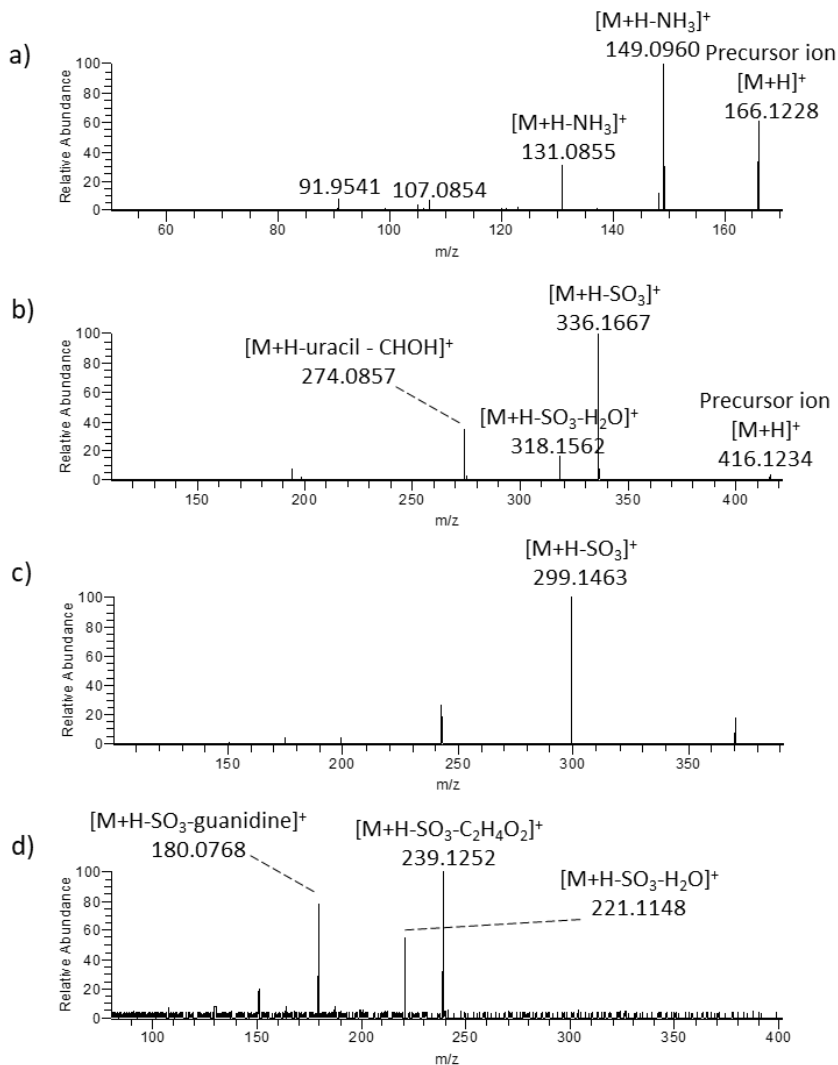
Figure IV.6 HRMS^2 spectrum of: a) ATX-a, b) CYN and c) LWTX1. d) HRMS^3 spectrum of LWTX1. Precursor ions of LWTX1 are fully fragmented and not detectable in the MS^2 and MS^3 spectra.

An excellent resolution was obtained between ATX-a, CYN and LWTX1 that eluted in the isocratic step of the gradient (65%B, t=0 → t=13) at 5.83, 4.46 and 8.26 min, respectively (**Fig.IV.7**). CYN and LWTX1 provided very sharp and narrow chromatographic peaks, whilst the peak of ATX-a was quite sharp but also tailed.

Taking into account the necessity to set up a multi-toxin method for the simultaneous analysis of a large number of polar cyanotoxins, ATX-a, CYN and LWTX1 were monitored inserting their MS^2 scans in time segments as previously shown for PSTs and TTX (chapter 3 *paragraph 3.3.1*). Therefore, a careful evaluation was conducted by considering the chromatographic behavior of

PSTs and ATX-a, CYN and LWTX1 analyzed under the same experimental conditions. ATX-a, CYN and LWTX1 eluted in the first window, as well as C toxins (**Fig.IV.7**). Even though an excellent separation was obtained between C1, C2, CYN and LWTX as their peaks were completely resolved, only a moderate resolution was achieved between C toxins and ATX-a due to the tailed peak of the latter. However, this did not represent a critical issue considering the different *m/z* values of C toxins and ATX-a that can be individually determined through HRMS and MS^2 measurements.
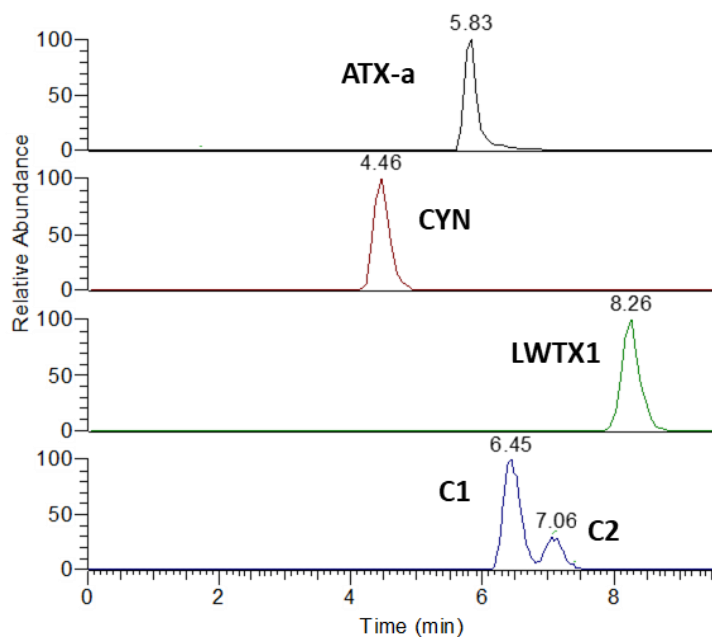
Figure IV.7 Chromatographic separation of cyanotoxins and C toxins eluting in the first time segment under the HILIC-HRMS method 1.

2.2.2 Instrumental detection limits and linearity

The same mixture of ATX-a, CYN and LWTX CRM was used to prepare a five level matrix-free (MF) calibration curve in the range 16.3-315.0 ng/mL, and subjected to serial dilution up to the lowest detectable and quantifiable level for each standard. A good linearity was achieved for each toxin with R^2 value between 0.998-0.999 (**Fig.IV.8**). In addition, the implemented multi-toxin time segmented-based HILIC-HRMS method turned out to be very sensitive. The instrumental limit of detection (LOD) and quantification (LOQ) measured for each toxin were: 0.3 and 1.3 ng/mL for ATX-a, 6.6 and 19.7 ng/mL for CYN and, 5.4 and 16.3 ng/mL for LWTX1.
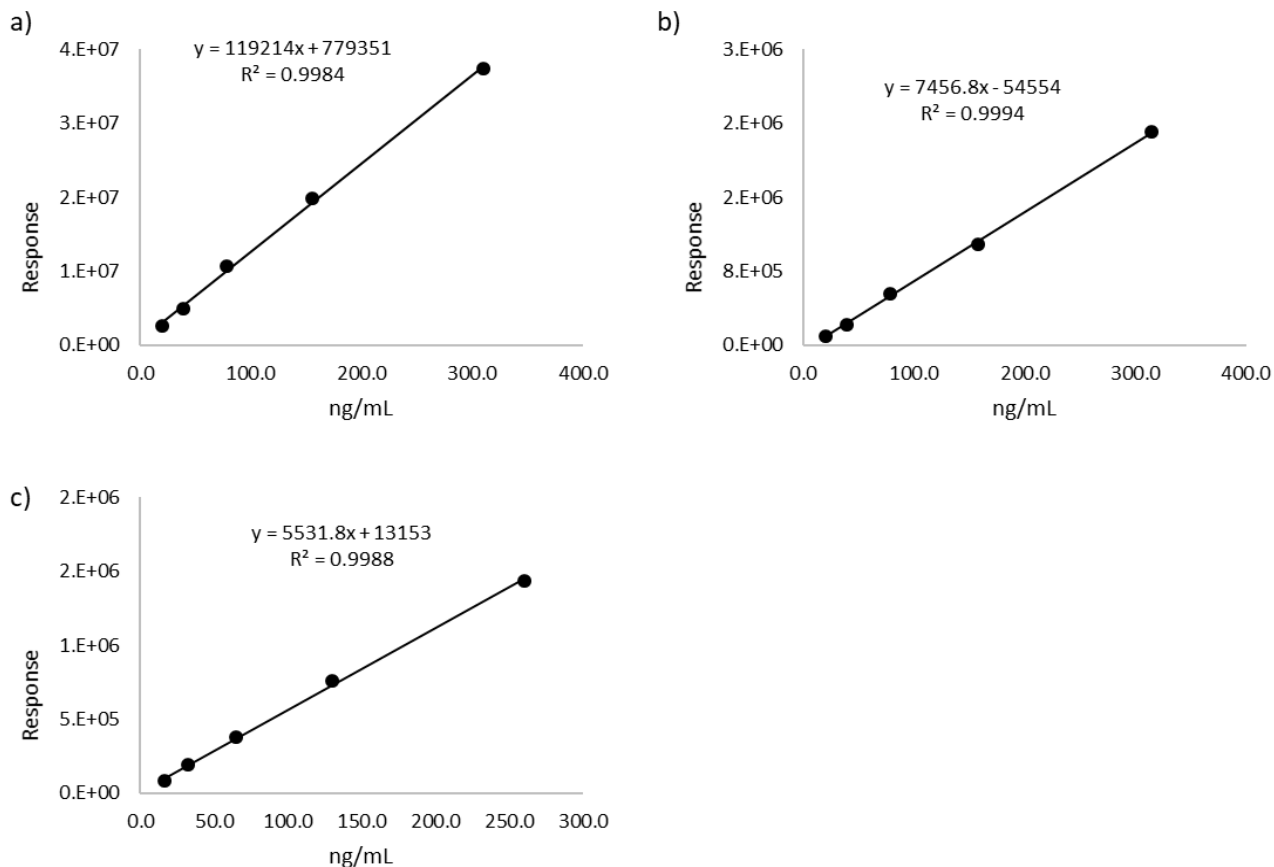
Figure IV.8 Matrix-free (MF) calibration curves of CRM: a) ATX-a, b) CYN and c) LWTX1.

2.3 Application of the LC-HRMS method to a cyanobacterial biomass

Background

In the frame of a collaboration with Dr T. Kaloudis from Athens Water Supply and Sewerage Company (EYDAP SA) and Dr A. Hiskia from Institute of Nanoscience and Nanotechnology (NCSR ''DEMOKRITOS'') of Athens, my research group received a cyanobacterial biomass sample collected from the lake Kastoria (Kastoria regional unit, Greece) during a massive cyano-HAB. The sample was previously analyzed and it was found to contain toxic cyanobacterial spp. such as: *Microcystis aeruginosa*, *Microcystis panniformis*, *Anabaena cf. flos-aquae*, *Anabaena cf. circinalis*, *Planktolyngbya limnetica*, *Aphanizomenon issatschenkoi*, *Pseudanabaena limnetica*, *Microcystis wesenbergii*, *Cyanodictyon imperfectum* and *Planktolyngbya circumcreta*. *Microcystis* and *Anabaena* spp. turned out to be the dominant organisms accounting for > 10% of the whole cyanobacterial biomass [41]. The main object of the joint study was to compare the

targeted LC-MS^2 method developed on a QqQ MS in Greece, with the untargeted LC-HRMS^2 method optimized on the LTQ Orbitrap at UniNa for the determination of MC contained in the cyanobacterial biomass sample. However this chapter will not deal with the comparison of the two instrumental methods, but describes the application of the developed LC-HRMS^2 and the optimized analytical work-flow for the determination of known and unknown cyanotoxins and cyanobacterial secondary metabolites contained in the sample.

2.3.1 Determination of known MCs

The implemented LC-HRMS^2 methods was successfully applied to the analysis of the cyanobacterial biomass sample and a large number of known MCs emerged (**Table IV.1**). More in details, the extraction from the Total Ion Current (TIC) of the [M+H]$^+$ ion of 250 analogues highlighted the presence of the following MCs: MC-LR, MC-RR, [dAsp^3]MC-LR, MC-LF, MC-LY, MC-HilR, [dAsp^3]MC-RR, MC-LW, MC-YR, MC-HtyR, MC-WR, MC-(H$_4$)YR, MC-FR, MC-MR, [MeSer^7]MC-LR, [DMAdda^5]MC-LR, and [Dha^7]MC-RR. Although for some of these MCs the relevant non-certified standard was available, quantitation was accomplished through CRM. At this purpose, all the analogues containing 1 Arg residue in their structure exhibited the same ionization behavior as MC-LR, thus they were quantified by using the MF calibration curve of MC-LR certified standard, assuming the same molar response. Similarly, MCs featuring 2 Arg were quantified through MC-RR CRM assuming the same response as MC-RR. MCs that do not have Arg residues in their structure were quantified by means of MC-LR since no adequate CRM are commercially available. As a result, MC-RR and MC-LR turned out to be the most abundant toxins with a concentration level of 523.0 and 353.3 ng/mg. It follows MC-YR at 56.8 ng/mg, while a number of variants - [dAsp^3]MC-LR, [dAsp^3]MC-RR MC-HilR, and MC-(H$_4$)YR – were found in the range 16.7 – 15.7 ng/mg. Moreover, the remaining analogues represented only the less-conspicuous part of the biomass sample with a concentration level ranging from 0.4 to 2.8 ng/mg. The structural variants of MCs whose CRM and/or RM were available, were fully confirmed using retention time, accurate mass of the [M+H]$^+$ ion, isotopic pattern, ring double bond equivalent value (RDB), CID and HCD fragmentation spectra as identification criteria. However, 7 MC analogues for which the relevant standard was not available - MC-(H$_4$)YR, MC-FR, MC-MR, [MeSer^7]MC-LR, [DMAdda^5]MC-LR, and [Dha^7]MC-RR – required interpretation of the relevant CID and HCD spectra for accurate identification. At this purpose, an effective

identification strategy was developed through the interpretation of the HRMS^2 spectra of MC-LR ([Ala^1+Leu^2+MeAsp^3+Arg^4+Adda^5+Glu^6+Mdha^7+H]$^+$, *m/z* 995.5561).

Table IV.1. List of MC congeners detected in the cyanobacterial biomass sample. The MS data, retention time (Rt), linear sequence and concentration level (ng/mg) were reported for each toxin.
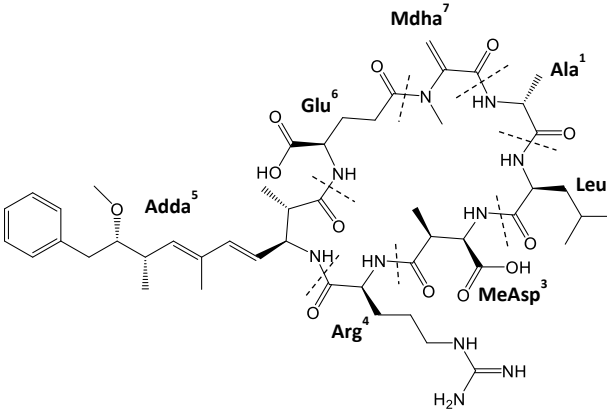
Toxin	[M+H]$^+$ [M+2H]$^{2+}$	Formula	Rt	Sequence	ng/mg
MC-RR	1038.5731 519.7895	$C_{49}H_{76}O_{12}N_{13}^+$ $C_{49}H_{77}O_{12}N_{13}^{2+}$	17.43	[Ala^1+Arg^2+MeAsp^3+Arg^4+Adda^5+Glu^6+Mdha^7+H]$^+$	523.0
MC-LR	995.5561	$C_{49}H_{75}O_{12}N_{10}^+$	16.27	[Ala^1+Leu^2+MeAsp^3+Arg^4+Adda^5+Glu^6+Mdha^7+H]$^+$	353.3
MC-YR	1045.5353	$C_{52}H_{73}O_{13}N_{10}^+$	15.91	[Ala^1+Tyr^2+MeAsp^3+Arg^4+Adda^5+Glu^6+Mdha^7+H]$^+$	56.8
[dAsp^3]MC-LR	981.5404	$C_{48}H_{73}O_{12}N_{10}^+$	16.37	[Ala^1+Leu^2+Asp^3+Arg^4+Adda^5+Glu^6+Mdha^7+H]$^+$	16.6
MC-WR	1068.5513	$C_{54}H_{74}O_{12}N_{11}^+$	16.73	[Ala^1+Trp^2+MeAsp^3+Arg^4+Adda^5+Glu^6+Mdha^7+H]$^+$	16.7
[dAsp^3]MC-RR	1024.5574 512.7807	$C_{48}H_{74}O_{12}N_{13}^+$ $C_{48}H_{75}O_{12}N_{13}^{2+}$	17.53	[Ala^1+Arg^2+Asp^3+Arg^4+Adda^5+Glu^6+Mdha^7+H]$^+$	16.6
MC-HilR	1009.5717	$C_{50}H_{77}O_{12}N_{10}^+$	16.67	[Ala^1+Hile^2+MeAsp^3+Arg^4+Adda^5+Glu^6+Mdha^7+H]$^+$	15.8
MC-(H$_4$)YR	1049.5661	$C_{52}H_{77}O_{13}N_{10}^+$	15.43	[Ala^1+H$_4$Tyr^2+MeAsp^3+Arg^4+Adda^5+Glu^6+Mdha^7+H]$^+$	15.7
[MeSer^7]MC-LR	1013.5666	$C_{49}H_{77}O_{13}N_{10}^+$	15.73	[Ala^1+Leu^2+MeAsp^3+Arg^4+Adda^5+Glu^6+MeSer^7+H]$^+$	2.8
[DMAdda^5]MC-LR	981.5404	$C_{48}H_{73}O_{12}N_{10}^+$	14.46	[Ala^1+Leu^2+MeAsp^3+Arg^4+DMAdda^5+Glu^6+Mdha^7+H]$^+$	2.3
MC-LY	1002.5182	$C_{52}H_{72}O_{13}N_7^+$	15.49	[Ala^1+Leu^2+MeAsp^3+Tyr^4+Adda^5+Glu^6+Mdha^7+H]$^+$	2.0
MC-FR	1029.5404	$C_{52}H_{73}O_{12}N_{10}^+$	16.55	[Ala^1+Phe+MeAsp^3+Arg^4+Adda^5+Glu^6+Mdha^7+H]$^+$	1.5
[Dha^7]MC-RR	1024.5574 512.7818	$C_{48}H_{74}O_{12}N_{13}^+$ $C_{48}H_{75}O_{12}N_{13}^{2+}$	17.65	[Ala^1+Arg^2+MeAsp^3+Arg^4+Adda^5+Glu^6+Dha^7+H]$^+$	1.2
MC-MR	1013.5125	$C_{48}H_{73}O_{12}N_{10}S^+$	16.03	[Ala^1+Met^2+MeAsp^3+Arg^4+Adda^5+Glu^6+Mdha^7+H]$^+$	0.8
MC-LW	1025.5343	$C_{54}H_{73}O_{12}N_8^+$	16.21	[Ala^1+Leu^2+MeAsp^3+Trp^4+Adda^5+Glu^6+Mdha^7+H]$^+$	0.8
MC-LF	986.5234	$C_{52}H_{72}O_{12}N_7^+$	16.32	[Ala^1+Leu^2+MeAsp^3+Phe^4+Adda^5+Glu^6+Mdha^7+H]$^+$	0.7
MC-HtyR	1059.5510	$C_{53}H_{75}O_{13}N_{10}^+$	16.08	[Ala^1+Htyr^2+MeAsp^3+Arg^4+Adda^5+Glu^6+Mdha^7+H]$^+$	0.4

As shown in (**Table IV.2**), Ala^1 was confirmed through a neutral loss of 101.0477 Da (Ala + CO) from the precursor ion due to the presence of the fragment #2 at *m/z* 894.5077. Following the same approach, Leu^2, MeAsp^3, Glu^6 and Mdha^7 were evidenced as specific neutral loss from the precursor ion through the presence of fragments #5, 4, 3 and 1, respectively. Adda^5 was easily confirmed, as previously discussed, due to the neutral loss of 134.0732 Da due to the presence of fragments #6 (CID) and directly (HCD) through the diagnostic ion at *m/z* 135.0799, #17. Further confirmation were obtained through fragments #18 and 19, which are characteristic for Adda

moiety. Finally, Arg^4 was confirmed through fragments #20, 21 and 22 which are characteristic for such amino acid [36]. On the other hand, the combined stepwise interpretation of fragments corresponding to specific amino acids sequences allowed to confirm the exact position of each residue in the cyclic structure. The implemented identification strategy started from the interpretation of the most intense fragment at *m/z* 599.3545 (#11) corresponding to the sequence $[Arg^4+Adda^5+Glu^6+H]^+$, which is one the most conserved part structure within the MC group, in fact analogues having structural modifications at residues 4,5 and 6 are easily identified through MS^2 experiments. Amino acid residue at position 3, which is $MeAsp^3$ for MC-LR, was confirmed through intense fragments (#9) corresponding to the sequence $[MeAsp^3+Arg^4+Adda^5+Glu^6+H]^+$, while the position of $Mdha^7$ was assessed through the fragment at *m/z* 682.3899 ($[Arg^4+Adda^5+Glu^6+Mdha^7+H]^+$, #10). Amino acid at position 1, Ala, was evidenced through fragment #8 corresponding to the sequence $[Ala^1+Arg^4+Adda^5+Glu^6+Mdha^7+H]^+$, while residue at position 2, (Leu) was evidenced by interpreting a variety of fragments (e.g. #1, 2, 3, 4, 6, 7, 12, 13, 14 and 15). Overall, this procedure was used as guidance for the confirmation of all MC analogues. However, some derivatives featuring characteristic structural modification required different approaches, especially when their fragmentation patterns were not so informative due to low concentration levels in the biomass sample. As a result, MC-(H_4)YR, MC-FR, MC-MR, [MeSer^7]MC-LR, [DMAdda^5]MC-LR, and [Dha^7]MC-RR were fully confirmed through the interpretation of the relevant CID and HCD spectra as shown in **Table IV.3-8** and **Fig.IV.9-14.**

Table IV.2 Assignment of fragment ions contained in CID and HCD spectra of MC-LR.

	m/z	Formula	Sequence	Neutral loss
$[M+H]^+$	995.5542	$C_{49}H_{75}O_{12}N_{10}^+$	$[Ala^1+Leu^2+MeAsp^3+Arg^4+Adda^5+Glu^6+Mdha^7+H]^+$	
	978.5280	$C_{49}H_{72}O_{12}N_9^+$		NH_3
	977.5452	$C_{49}H_{73}O_{11}N_{10}^+$		H_2O
	967.5608	$C_{48}H_{75}O_{11}N_{10}^+$		CO
	964.5127	$C_{48}H_{70}O_{12}N_9^+$		NH_2CH_3
	963.5297	$C_{48}H_{71}O_{11}N_{10}^+$		CH_3OH
	960.5179	$C_{49}H_{70}O_{11}N_9^+$		H_2O+NH_3
	959.5364	$C_{49}H_{71}O_{10}N_{10}^+$		$2H_2O$
	953.5344	$C_{48}H_{73}O_{12}N_8^+$		CH_3N_2 (Guanidine moiety)
	951.5663	$C_{48}H_{75}O_{10}N_{10}^+$		CO_2
	950.5344	$C_{48}H_{72}O_{11}N_9^+$		$CO+NH_3$
	949.5512	$C_{48}H_{73}O_{10}N_{10}^+$		$CO+H_2O$
	946.5028	$C_{48}H_{68}O_{11}N_9^+$		CH_3OH+NH_3
	936.5103	$C_{48}H_{70}O_{12}N_7^+$		CH_5N_3 (Guanidine)
	933.5551	$C_{48}H_{73}O_9N_{10}^+$		CO_2+H_2O
	928.4958	$C_{48}H_{66}O_{10}N_9^+$		$CH_3OH+NH_3+H_2O$
	923.5707	$C_{47}H_{75}O_9N_{10}^+$		CO_2+CO
#				
1	910.5031	$C_{45}H_{68}O_{11}N_9^+$	$[Ala^1+Leu^2+MeAsp^3+Arg^4+Adda^5+Glu^6+H]^+$	$Mdha^7$
2	894.5077	$C_{45}H_{68}O_{10}N_9^+$	$[Leu^2+MeAsp^3+Arg^4+Adda^5+Glu^6+Mdha^7+H-CO]^+$	Ala^1+CO
3	866.5126	$C_{44}H_{68}O_9N_9^+$	$[Ala^1+Leu^2+MeAsp^3+Arg^4+Adda^5+Mdha^7+H]^+$	Glu^6
	883.5394	$C_{44}H_{71}O_9N_{10}^+$	$[Ala^1+Leu^2+MeAsp^3+Arg^4+Adda^5+Mdha^7+H+NH_3]^+$	Glu^6-NH_3
	838.5180	$C_{43}H_{68}O_8N_9^+$	$[Ala^1+Leu^2+MeAsp^3+Arg^4+Adda^5+Mdha^7+H-CO]^+$	Glu^6+CO
4	866.5126	$C_{44}H_{68}O_9N_9^+$	$[Ala^1+Leu^2+MeAsp^3+Arg^4+Adda^5+Mdha^7+H]^+$	$MeAsp^3$
	883.5394	$C_{44}H_{71}O_9N_{10}^+$	$[Ala^1+Leu^2+MeAsp^3+Arg^4+Adda^5+Mdha^7+H+NH_3]^+$	$MeAsp^3-NH_3$
	838.5180	$C_{43}H_{68}O_8N_9^+$	$[Ala^1+Leu^2+MeAsp^3+Arg^4+Adda^5+Mdha^7+H-CO]^+$	$MeAsp^3+CO$
5	882.4720	$C_{43}H_{64}O_{11}N_9^+$	$[Ala^1+MeAsp^3+Arg^4+Adda^5+Glu^6+Mdha^7+H]^+$	Leu^2
6	861.4827	$C_{40}H_{65}O_{11}N_{10}^+$	$[Ala^1+Leu^2+MeAsp^3+Arg^4+Adda^5+Glu^6+Mdha^7+H-Adda moiety]^+$	$C_9H_{10}O$ (adda moiety)
	844.4555	$C_{40}H_{62}O_{11}N_9^+$	$[Ala^1+Leu^2+MeAsp^3+Arg^4+Adda^5+Glu^6+Mdha^7+H-Adda moiety-NH_3]^+$	adda moiety + NH_3
	826.4427	$C_{40}H_{60}O_{10}N_9^+$	$[Ala^1+Leu^2+MeAsp^3+Arg^4+Adda^5+Glu^6+Mdha^7+H-Adda moiety-NH_3-H_2O]^+$	adda moiety+NH_3+H_2O
7	783.4757	$C_{40}H_{63}O_8N_8^+$	$[Ala^1+Leu^2+MeAsp^3+Arg^4+Adda^5+H]^+$	Glu^6+Mdha^7
8	753.4293	$C_{38}H_{57}O_8N_8^+$	$[Ala^1+Arg^4+Adda^5+Glu^6+Mdha^7+H]^+$	$Leu^2+MeAsp^3$
9	728.3972	$C_{36}H_{54}O_9N_7^+$	$[MeAsp^3+Arg^4+Adda^5+Glu^6+H]^+$	$Ala^1+Leu^2+Mdha^7$
	710.3866	$C_{36}H_{52}O_8N_7^+$	$[MeAsp^3+Arg^4+Adda^5+Glu^6+H-H_2O]^+$	$Ala^1+Leu^2+Mdha^7+H_2O$
	700.4032	$C_{35}H_{54}O_8N_7^+$	$[MeAsp^3+Arg^4+Adda^5+Glu^6+H-CO]^+$	$Ala^1+Leu^2+Mdha^7+CO$
	682.3920	$C_{35}H_{52}O_7N_7^+$	$[MeAsp^3+Arg^4+Adda^5+Glu^6+H-H_2O-CO]^+$	$Ala^1+Leu^2+Mdha^7+ H_2O+CO$
10	682.3899	$C_{35}H_{52}O_7N_7^+$	$[Arg^4+Adda^5+Glu^6+Mdha^7+H]^+$	$Ala^1+Leu^2+MeAsp^3$
11	599.3545	$C_{31}H_{47}O_6N_6^+$	$[Arg^4+Adda^5+Glu^6+H]^+$	$Ala^1+Leu^2+MeAsp^3+Mdha^7$
	582.3282	$C_{31}H_{44}O_6N_5^+$	$[Arg^4+Adda^5+Glu^6+H-NH_3]^+$	$Ala^1+Leu^2+MeAsp^3+Mdha^7+NH_3$
	581.3438	$C_{31}H_{45}O_5N_6^+$	$[Arg^4+Adda^5+Glu^6+H-H_2O]^+$	$Ala^1+Leu^2+MeAsp^3+Mdha^7+H_2O$

	571.3597	$C_{30}H_{47}O_5N_6^+$	$[Arg^4+Adda^5+Glu^6+H-CO]^+$	$Ala^1+Leu^2+MeAsp^3+Mdha^7+CO$
12	553.3087	$C_{24}H_{41}O_7N_8^+$	$[Ala^1+Leu^2+MeAsp^3+Arg^4+Mdha^7+H]^+$	$Adda^5+Glu^6$
	570.3352	$C_{24}H_{44}O_7N_9^+$	$[Ala^1+Leu^2+MeAsp^3+Arg^4+Mdha^7+H+NH_3]^+$	$Adda^5+Glu^6-NH_3$
	552.3249	$C_{24}H_{42}O_6N_9^+$	$[Ala^1+Leu^2+MeAsp^3+Arg^4+Mdha^7+H+NH_3-H_2O]^+$	$Adda^5+Glu^6-NH_3+H_2O$
	534.3145	$C_{24}H_{40}O_5N_9^+$	$[Ala^1+Leu^2+MeAsp^3+Arg^4+Mdha^7+H+NH_3-2H_2O]^+$	$Adda^5+Glu^6-NH_3+2H_2O$
	536.2824	$C_{24}H_{38}O_7N_7^+$	$[Ala^1+Leu^2+MeAsp^3+Arg^4+Mdha^7+H-NH_3]^+$	$Adda^5+Glu^6+NH_3$
	535.2983	$C_{24}H_{39}O_6N_8^+$	$[Ala^1+Leu^2+MeAsp^3+Arg^4+Mdha^7+H-H_2O]^+$	$Adda^5+Glu^6+H_2O$
	525.3144	$C_{23}H_{41}O_6N_8^+$	$[Ala^1+Leu^2+MeAsp^3+Arg^4+Mdha^7+H-CO]^+$	$Adda^5+Glu^6+CO$
13	470.2717	$C_{20}H_{36}O_6N_7^+$	$[Ala^1+Leu^2+MeAsp^3+Arg^4+H]^+$	$Adda^5+Glu^6+Mdha^7$
	487.2972	$C_{20}H_{39}O_6N_8^+$	$[Ala^1+Leu^2+MeAsp^3+Arg^4+H+NH_3]^+$	$Adda^5+Glu^6+Mdha^7-NH_3$
	469.2881	$C_{20}H_{37}O_5N_8^+$	$[Ala^1+Leu^2+MeAsp^3+Arg^4+H+NH_3-H_2O]^+$	$Adda^5+Glu^6+Mdha^7-NH_3+H_2O$
	453.2448	$C_{20}H_{33}O_6N_6^+$	$[Ala^1+Leu^2+MeAsp^3+Arg^4+H-NH_3]^+$	$Adda^5+Glu^6+Mdha^7+NH_3$
	452.2621	$C_{20}H_{34}O_5N_7^+$	$[Ala^1+Leu^2+MeAsp^3+Arg^4+H-H_2O]^+$	$Adda^5+Glu^6+Mdha^7+H_2O$
14	446.2281	$C_{23}H_{32}O_6N_3^+$	$[Ala^1+Adda^5+Glu^6+Mdha^7+H-Adda\ moiety-NH_2]^+$	$Leu^2+MeAsp^3+Arg^4+adda\ moiety$
15	397.2077	$C_{18}H_{29}O_6N_4^+$	$[Ala^1+Leu^2+MeAsp^3+Mdha^7+H]^+$	$Arg^4+Adda^5+Glu^6$
16	375.1913	$C_{20}H_{27}O_5N_2^+$	$[Adda^5+Glu^6+Mdha^7+H-Adda\ moiety-NH_2]^+$	$Ala^1+Leu^2+MeAsp^3+Arg^4+adda\ moiety$
	347.1970	$C_{19}H_{27}O_4N_2^+$	$[Adda^5+Glu^6+Mdha^7+H-Adda\ moiety-NH_2-CO]^+$	$Ala^1+Leu^2+MeAsp^3+Arg^4+adda\ moiety+CO$
17	135.0799[a]	$C_9H_{11}O^+$	$[Adda\ moiety+H]^+$	
18	265.1579[a]	$C_{19}H_{21}O^+$	$[Adda^5-NH_2-CH_3OH+H]^+$	
19	163.1112[a]	$C_{11}H_{15}O^+$	$[Adda^5-NH_2-Adda\ moiety+H]^+$	
20	157.1080[a]	$C_6H_{13}ON_4^+$	$[Arg^4+H]^+$	
21	129.1129[a]	$C_5H_{13}N_4^+$	$Arg^4\ immonium\ ion$	
22	112.0864[a]	$C_5H_{10}N_3^+$	$[Arg^4-CO-NH_3+H]^+$	
23	n.d.			

[a]=Fragment contained in the HCD spectrum: n.d.=not detected.

Table IV.3 Assignment of fragment ions contained in CID and HCD spectra of MC-(H$_4$)YR

#	m/z	Formula	Sequence	Neutral loss
[M+H]$^+$	1049.5638	$C_{52}H_{77}O_{13}N_{10}^+$	[Ala^1+ThTyr^2+MeAsp^3+Arg^4+Adda^5+Glu^6+Mdha^7+H]$^+$	
	1032.5365	$C_{52}H_{747}O_{13}N_9^+$		NH$_3$
	1031.5529	$C_{52}H_{75}O_{12}N_{10}^+$		H$_2$O
	1021.5685	$C_{51}H_{77}O_{12}N_{10}^+$		CO
	1018.5228	$C_{51}H_{72}O_{13}N_{10}^+$		NH$_2$CH$_3$
	1017.5366	$C_{51}H_{73}O_{12}N_{10}^+$		CH$_3$OH
	1014.5262	$C_{52}H_{72}O_{12}N_9^+$		H$_2$O+NH$_3$
	1013.5419	$C_{52}H_{73}O_{11}N_{10}^+$		2H$_2$O
	1005.5735	$C_{51}H_{77}O_{11}N_{10}^+$		CO$_2$
	1004.5409	$C_{51}H_{74}O_{12}N_9^+$		CO+NH$_3$
	1003.5580	$C_{51}H_{75}O_{11}N_{10}^+$		CO+H$_2$O
	1000.5110	$C_{51}H_{70}O_{12}N_9^+$		CH$_3$OH +NH$_3$
	987.5633	$C_{51}H_{75}O_{10}N_{10}^+$		CO$_2$+H$_2$O
	982.5002	$C_{51}H_{68}O_{11}N_9^+$		CH$_3$OH +NH$_3$+H$_2$O
	977.5785	$C_{50}H_{77}O_{10}N_{10}^+$		CO$_2$+CO
1	964.5114	$C_{48}H_{70}O_{12}N_9^+$	[Ala^1+ThTyr^2+MeAsp^3+Arg^4+Adda^5+Glu^6+H]$^+$	Mdha^7
2	948.5159	$C_{48}H_{70}O_{11}N_9^+$	[ThTyr^2+MeAsp^3+Arg^4+Adda^5+Glu^6+Mdha^7+H-CO]$^+$	Ala^1 + CO
3	920.5213	$C_{48}H_{70}O_{10}N_9^+$	[Ala^1+ThTyr^2+MeAsp^3+Arg^4+Adda^5+Mdha^7+H]$^+$	Glu^6
	937.5480	$C_{48}H_{73}O_{10}N_{10}^+$	[Ala^1+ThTyr^2+MeAsp^3+Arg^4+Adda^5+Mdha^7+H+NH$_3$]$^+$	Glu^6-NH$_3$
	892.5293	$C_{47}H_{70}O_9N_9^+$	[Ala^1+ThTyr^2+MeAsp^3+Arg^4+Adda^5+Mdha^7+H-CO]$^+$	Glu^6+CO
4	920.5213	$C_{48}H_{70}O_{10}N_9^+$	[Ala^1+ThTyr^2+Arg^4+Adda^5+Glu^6+Mdha^7+H]$^+$	MeAsp^3
	937.5480	$C_{48}H_{73}O_{10}N_{10}^+$	[Ala^1+ThTyr^2+Arg^4+Adda^5+Glu^6+Mdha^7+H+NH$_3$]$^+$	MeAsp^3 -NH$_3$
	892.5293	$C_{47}H_{70}O_9N_9^+$	[Ala^1+ThTyr^2+Arg^4+Adda^5+Glu^6+Mdha^7+H-CO]$^+$	MeAsp^3 +CO
5	882.4750	$C_{43}H_{64}O_{11}N_9^+$	[Ala^1+MeAsp^3+Arg^4+Adda^5+Glu^6+Mdha^7+H]$^+$	ThTyr^2
6	915.4900	$C_{43}H_{67}O_{12}N_{10}^+$	[Ala^1+ThTyr^2+MeAsp^3+Arg^4+Adda^5+Glu^6+Mdha^7+H-Adda moiety^a]$^+$	C$_9$H$_{10}$O (adda moiety)
	898.4633	$C_{43}H_{64}O_{12}N_9^+$	[Ala^1+ThTyr^2+MeAsp^3+Arg^4+Adda^5+Glu^6+Mdha^7+H-Adda moiety-NH$_3$]$^+$	adda moiety + NH$_3$
	880.4526	$C_{43}H_{62}O_{11}N_9^+$	[Ala^1+ThTyr^2+MeAsp^3+Arg^4+Adda^5+Glu^6+Mdha^7+H-Adda moiety-NH$_3$-H$_2$O]$^+$	adda moiety +NH$_3$+H$_2$O
7	837.4832	$C_{43}H_{65}O_9N_8^+$	[Ala^1+ThTyr^2+MeAsp^3+Arg^4+Adda^5+H]$^+$	Glu^6-Mdha^7
8	n.d.			
9	728.3951	$C_{36}H_{54}O_9N_7^+$	[MeAsp^3+Arg^4+Adda^5+Glu^6+H]$^+$	Ala^1+ThTyr^2+Mdha^7
	710.3854	$C_{36}H_{52}O_8N_7^+$	[MeAsp^3+Arg^4+Adda^5+Glu^6+H-H$_2$O]$^+$	Ala^1+ThTyr^2+Mdha^7+H$_2$O
	682.3899	$C_{35}H_{52}O_7N_7^+$	[MeAsp^3+Arg^4+Adda^5+Glu^6+H-H$_2$O-CO]$^+$	Ala^1+ThTyr^2+Mdha^7+ H$_2$O+CO
10	682.3899	$C_{35}H_{52}O_7N_7^+$	[Arg^4+Adda^5+Glu^6+Mdha^7+H]$^+$	Ala^1+ThTyr^2+MeAsp^3
11	599.3530	$C_{31}H_{47}O_6N_6^+$	[Arg^4+Adda^5+Glu^6+H]$^+$	Ala^1+ThTyr^2+MeAsp^3+Mdha^7
	582.3266	$C_{31}H_{44}O_6N_5^+$	[Arg^4+Adda^5+Glu^6+H-NH$_3$]$^+$	Ala^1+ThTyr^2+MeAsp^3+Mdha^7 +NH$_3$
	571.3586	$C_{30}H_{47}O_5N_6^+$	[Arg^4+Adda^5+Glu^6+H-CO]$^+$	Ala^1+ThTyr^2+MeAsp^3+Mdha^7 +CO
12	607.3176	$C_{27}H_{43}O_8N_8^+$	[Ala^1+ThTyr^2+MeAsp^3+Arg^4+Mdha^7+H]$^+$	Adda^5+Glu^6
	624.3441	$C_{27}H_{46}O_8N_9^+$	[Ala^1+ThTyr^2+MeAsp^3+Arg^4+Mdha^7+H+NH$_3$]$^+$	Adda^5+Glu^6-NH$_3$

	606.3337	$C_{27}H_{44}O_7N_9^+$	$[Ala^1+ThTyr^2+MeAsp^3+Arg^4+Mdha^7+H+NH_3-H_2O]^+$	$Adda^5+Glu^6-NH_3+H_2O$
	588.3229	$C_{27}H_{42}O_6N_9^+$	$[Ala^1+ThTyr^2+MeAsp^3+Arg^4+Mdha^7+H+NH_3-2H_2O]^+$	$Adda^5+Glu^6-NH_3+2H_2O$
	589.3071	$C_{27}H_{41}O_7N_8^+$	$[Ala^1+ThTyr^2+MeAsp^3+Arg^4+Mdha^7+H-H_2O]^+$	$Adda^5+Glu^6+H_2O$
13	n.d.			
14	446.2275	$C_{23}H_{32}O_6N_3^+$	$[Ala^1+Adda^5+Glu^6+Mdha^7+H-Adda\ moiety-NH_2]^+$	$ThTyr^2+MeAsp^3+Arg^4+adda\ moiety$
15	n.d.			
16	375.1906	$C_{20}H_{27}O_5N_2^+$	$[Adda^5+Glu^6+Mdha^7+H-Adda\ moiety-NH_2]^+$	$Ala^1+ThTyr^2+MeAsp^3+Arg^4+adda\ moiety$
17	135.0800 [a]	$C_9H_{11}O^+$	$[Adda\ moiety+H]^+$	
18	265.1578 [a]	$C_{19}H_{21}O^+$	$[Adda^5-OCH_3-NH_2+H]^+$	
19	163.1113 [a]	$C_{11}H_{15}O^+$	$[Adda^5-NH_2-Adda\ moiety+H]^+$	
20	157.1079 [a]	$C_6H_{13}ON_4^+$	$[Arg^4+H]^+$	
21	n.d.			
22	112.0865 [a]	$C_5H_{10}N_3^+$	$[Arg^4-CO-NH_3+H]^+$	
23	n.d.			

[a]=Fragment contained in the HCD spectrum: n.d.=not detected.

Figure IV.9 HRMS^2 spectra of MC-(H4)YR acquired in CID and HCD modes.

Table IV.4 Assignment of fragment ions contained in CID and HCD spectra of MC-FR.

	m/z	Formula	Sequence		Neutral loss
[M+H]$^+$	1029.5404	C$_{52}$H$_{73}$O$_{12}$N$_{10}$$^+$	[Ala^1-Phe^2-MeAsp^3-Arg^4- Adda^5-Glu^6-Mdha^7]		
	1012.5097	C$_{52}$H$_{70}$O$_{12}$N$_9$$^+$			NH$_3$
	1011.5265	C$_{52}$H$_{71}$O$_{11}$N$_{10}$$^+$			H$_2$O
	1001.5403	C$_{51}$H$_{73}$O$_{11}$N$_{10}$$^+$			CO
	998.4947	C$_{51}$H$_{68}$O$_{12}$N$_9$$^+$			CH$_3$NH$_2$
	997.5093	C$_{51}$H$_{69}$O$_{11}$N$_{10}$$^+$			CH$_3$OH
	985.5434	C$_{51}$H$_{73}$O$_{10}$N$_{10}$$^+$			CO$_2$
	980.4814	C$_{51}$H$_{66}$O$_{11}$N$_9$$^+$			CH$_3$OH +NH$_3$
	967.5358	C$_{51}$H$_{71}$O$_9$N$_{10}$$^+$			CO$_2$+H$_2$O
	957.5514	C$_{50}$H$_{73}$O$_9$N$_{10}$$^+$			CO$_2$+CO

#	m/z	Formula	Sequence	Neutral loss
1	944.4868	C$_{48}$H$_{66}$O$_{11}$N$_9$$^+$	[Ala^1+Phe^2+MeAsp^3+Arg^4+Adda^5+Glu^6+H]$^+$	Mdha^7
2	n.d			
3	900.4937	C$_{47}$H$_{66}$O$_9$N$_9$$^+$	[Ala^1+Phe^2+MeAsp^3+Arg^4+Adda^5+Mdha^7+H]$^+$	Glu^6
	917.5153	C$_{47}$H$_{69}$O$_9$N$_{10}$$^+$	[Ala^1+Phe^2+MeAsp^3+Arg^4+Adda^5+Mdha^7+H+NH$_3$]$^+$	Glu^6-NH$_3$
4	900.4937	C$_{47}$H$_{66}$O$_9$N$_9$$^+$	[Ala^1+Phe^2+Arg^4+Adda^5+Glu^6+Mdha^7+H]$^+$	MeAsp^3
	917.5153	C$_{47}$H$_{69}$O$_9$N$_{10}$$^+$	[Ala^1+Phe^2+Arg^4+Adda^5+Glu^6+Mdha^7+H+NH$_3$]$^+$	MeAsp^3 -NH$_3$
5	n.d.			
6	895.4617	C$_{43}$H$_{63}$O$_{11}$N$_{10}$$^+$	[Ala^1+Phe^2+MeAsp^3+Arg^4+Adda^5+Glu^6+Mdha^7+H-Adda moiety^a]$^+$	C$_9$H$_{10}$O (adda moiety)
	878.4357	C$_{43}$H$_{60}$O$_{11}$N$_9$$^+$	[Ala^1+Phe^2+MeAsp^3+Arg^4+Adda^5+Glu^6+Mdha^7+H-Adda moiety-NH$_3$]$^+$	adda moiety + NH$_3$
7	817.4618	C$_{43}$H$_{61}$O$_8$N$_8$$^+$	[Ala^1+Phe^2+MeAsp^3+Arg^4+Adda^5+H]$^+$	Glu^6-Mdha^7
8	n.d.			
9	728.3940	C$_{36}$H$_{54}$O$_9$N$_7$$^+$	[MeAsp^3+Arg^4+Adda^5+Glu^6+H]$^+$	Ala^1+Phe^2+Mdha^7
	710.3826	C$_{36}$H$_{52}$O$_8$N$_7$$^+$	[MeAsp^3+Arg^4+Adda^5+Glu^6+H-H$_2$O]$^+$	Ala^1+Phe^2+Mdha^7+H$_2$O
	682.3896	C$_{35}$H$_{52}$O$_7$N$_7$$^+$	[MeAsp^3+Arg^4+Adda^5+Glu^6+H-H$_2$O-CO]$^+$	Ala^1+Phe^2+Mdha^7+ H$_2$O+CO
10	682.3896	C$_{35}$H$_{52}$O$_7$N$_7$$^+$	[Arg^4+Adda^5+Glu^6+Mdha^7+H]$^+$	Ala^1+Phe^2+MeAsp^3
11	599.3524	C$_{31}$H$_{47}$O$_6$N$_6$$^+$	[Arg^4+Adda^5+Glu^6+H]$^+$	Ala^1+Phe^2+MeAsp^3+Mdha^7
	582.3245	C$_{31}$H$_{44}$O$_6$N$_5$$^+$	[Arg^4+Adda^5+Glu^6+H-NH$_3$]$^+$	Ala^1+Phe^2+MeAsp^3+Mdha^7 +NH$_3$
	571.3575	C$_{30}$H$_{47}$O$_5$N$_6$$^+$	[Arg^4+Adda^5+Glu^6+H-CO]$^+$	Ala^1+Phe^2+MeAsp^3+Mdha^7 +CO
12	587.2911	C$_{27}$H$_{39}$O$_7$N$_8$$^+$	[Ala^1+ThTyr^2+MeAsp^3+Arg^4+Mdha^7+H]$^+$	Adda^5+Glu^6
	604.3174	C$_{27}$H$_{42}$O$_7$N$_9$$^+$	[Ala^1+ThTyr^2+MeAsp^3+Arg^4+Mdha^7+H+NH$_3$]$^+$	Adda^5+Glu^6-NH$_3$
	586.3065	C$_{27}$H$_{40}$O$_6$N$_9$$^+$	[Ala^1+ThTyr^2+MeAsp^3+Arg^4+Mdha^7+H+NH$_3$-H$_2$O]$^+$	Adda^5+Glu^6-NH$_3$+H$_2$O
	569.2814	C$_{27}$H$_{37}$O$_6$N$_8$$^+$	[Ala^1+ThTyr^2+MeAsp^3+Arg^4+Mdha^7+H-H$_2$O]$^+$	Adda^5+Glu^6+H$_2$O
13	n.d.			

14	n.d.		
15	n.d.		
16	n.d.		
17	135.0800[a]	$C_9H_{11}O^+$	[Adda moiety+H]$^+$
18	n.d.		
19	163.1113[a]	$C_{11}H_{15}O^+$	[Adda^5-NH$_2$-Adda moiety+H]$^+$
20	157.1080[a]	$C_6H_{13}ON_4^+$	[Arg^4+H]$^+$
21	n.d.		
22	112.0864 [a]	$C_5H_{10}N_3^+$	[Arg^4-CO-NH$_3$+H]$^+$
23	n.d.		

[a]=Fragment contained in the HCD spectrum: n.d.=not detected.

Figure IV.10 HRMS^2 spectra of MC-FR acquired in CID and HCD modes.

Table IV.5 Assignment of fragment ions contained in CID and HCD spectra of MC-MR.

	m/z	Formula	Sequence		Neutral loss
			MC-MR		
$[M+H]^+$	1013.5125	$C_{48}H_{73}O_{12}N_{10}S^+$	$[Ala^1+Met^2+MeAsp^3+Arg^4+Adda^5+Glu^6+Mdha^7+H]^+$		
	996.4879	$C_{48}H_{70}O_{12}N_9S^+$			NH_3
	995.5103	$C_{48}H_{71}O_{11}N_{10}S^+$			H_2O
	985.5185	$C_{47}H_{73}O_{11}N_{10}S^+$			CO
	982.4705	$C_{47}H_{68}O_{12}N_9S^+$			CH_3NH_2
	969.5208	$C_{47}H_{73}O_{10}N_{10}S^+$			CO_2
	968.4924	$C_{47}H_{70}O_{11}N_9S^+$			$CO+NH_3$
	864.4597	$C_{47}H_{76}O_{11}N_9S^+$			$CH_3OH +NH_3$
	951.5126	$C_{47}H_{71}O_9N_{10}S^+$			CO_2+H_2O
	941.5255	$C_{46}H_{73}O_9N_{10}S^+$			CO_2+CO

#					
1	n.d.				
2	n.d.				
3	884.4688	$C_{43}H_{66}O_9N_9S^+$	$[Ala^1+Met^2+MeAsp^3+Arg^4+Adda^5+Mdha^7+H]^+$		Glu^6
4	884.4688	$C_{43}H_{66}O_9N_9S^+$	$[Ala^1+Met^2+Arg^4+Adda^5+Glu^6+Mdha^7+H]^+$		$MeAsp^3$
5	n.d.				
6	879.4376	$C_{39}H_{63}O_{11}N_{10}S^+$	$[Ala^1+Met^2+MeAsp^3+Arg^4+Adda^5+Glu^6+Mdha^7+H\text{-Adda moiety}]^+$		$C_9H_{10}O$ (adda moiety)
	862.4098	$C_{39}H_{60}O_{11}N_9S^+$	$[Ala^1+Met^2+MeAsp^3+Arg^4+Adda^5+Glu^6+Mdha^7+H\text{-Adda moiety}-NH_3]^+$		adda moiety + NH_3
7	801.4304	$C_{39}H_{61}O_8N_8S^+$	$[Ala^1+Met^2+MeAsp^3+Arg^4+Adda^5+H]^+$		$Glu^6\text{-}Mdha^7$
8	n.d.				
9	728.3987	$C_{36}H_{54}O_9N_7^+$	$[MeAsp^3+Arg^4+Adda^5+Glu^6+H]^+$		$Ala^1+Met^2+Mdha^7$
	710.3853	$C_{36}H_{52}O_8N_7^+$	$[MeAsp^3+Arg^4+Adda^5+Glu^6+H\text{-}H_2O]^+$		$Ala^1+Met^2+Mdha^7+H_2O$
10	n.d.				
11	599.3536	$C_{31}H_{47}O_6N_6^+$	$[Arg^4+Adda^5+Glu^6+H]^+$		$Ala^1+Met^2+MeAsp^3+Mdha^7$
	571.3579	$C_{30}H_{47}O_5N_6^+$	$[Arg^4+Adda^5+Glu^6+H\text{-}CO]^+$		$Ala^1+Met^2+MeAsp^3+Mdha^7 +CO$
12	571.2642	$C_{23}H_{39}O_7N_8S^+$	$[Ala^1+Met^2+MeAsp^3+Arg^4+Mdha^7+H]^+$		$Adda^5+Glu^6$
	588.2912	$C_{23}H_{42}O_7N_9S^+$	$[Ala^1+Met^2+MeAsp^3+Arg^4+Mdha^7+H+NH_3]^+$		$Adda^5+Glu^6\text{-}NH_3$
	570.2798	$C_{23}H_{40}O_6N_9S^+$	$[Ala^1+Met^2+MeAsp^3+Arg^4+Mdha^7+H+NH_3-H_2O]^+$		$Adda^5+Glu^6\text{-}NH_3+H_2O$
13	n.d.				
14	n.d.				
15	n.d.				
16	n.d.				
17	135.0800^a	$C_9H_{11}O^+$	$[Adda\ moiety+H]^+$		

18	n.d.		
19	163.1117[a]	$C_{11}H_{15}O^+$	[Adda⁵-NH₂-Adda moiety+H]⁺
20	157.1085 [a]	$C_6H_{13}ON_4^+$	[Arg⁴+H]⁺
21	n.d.		
22	n.d.		
23	n.d.		

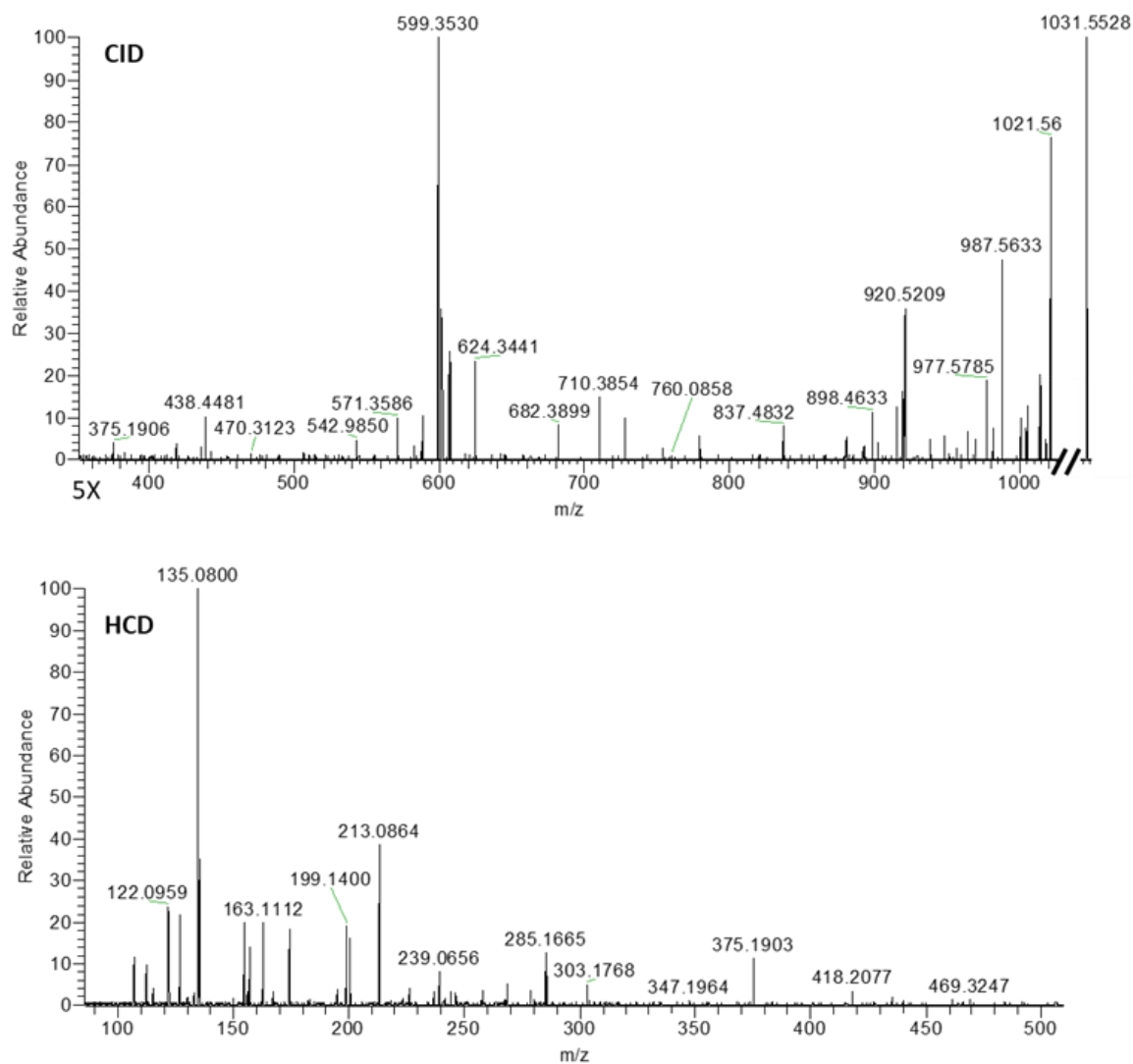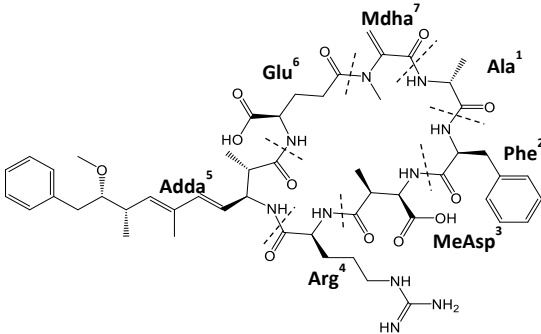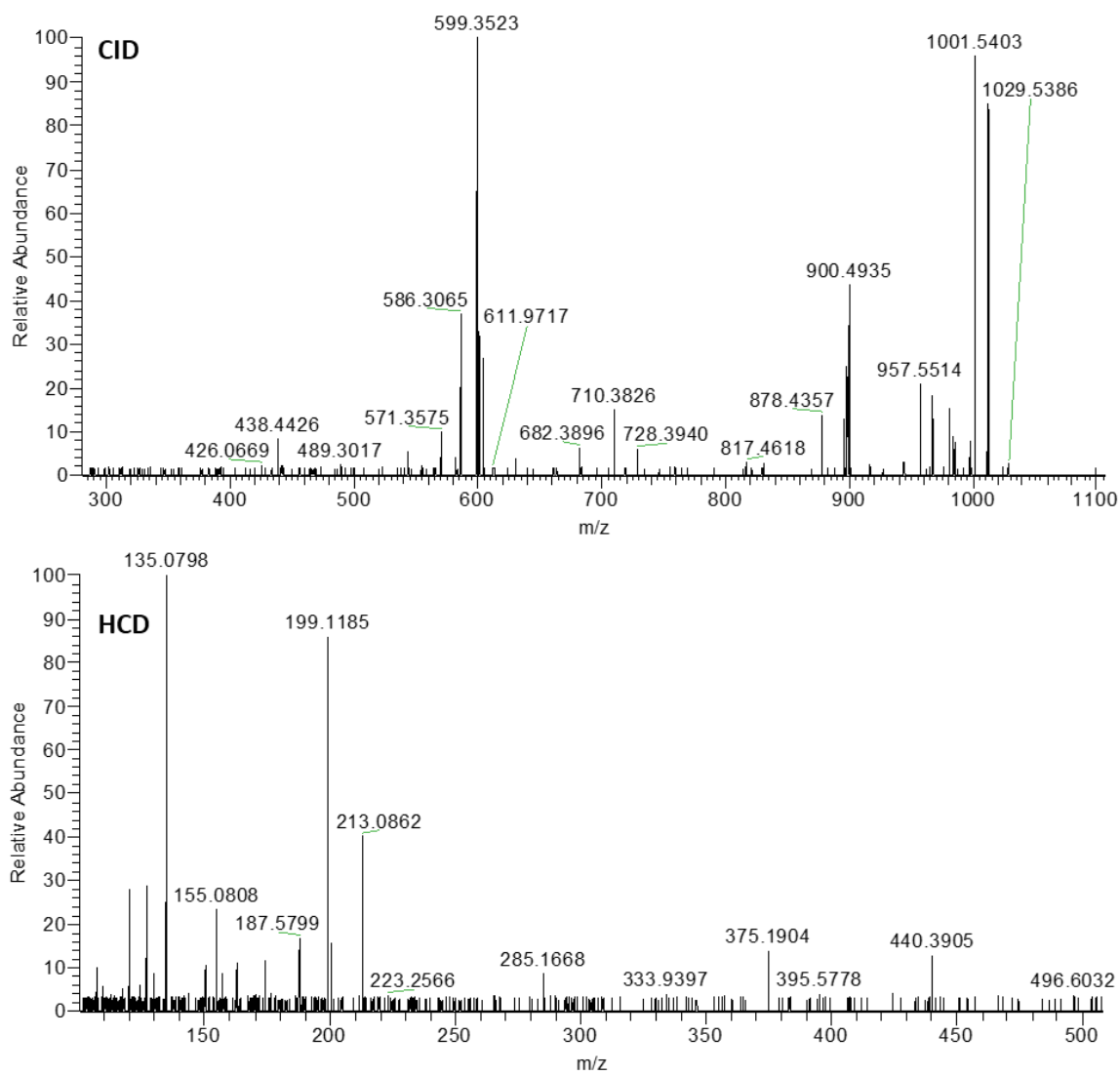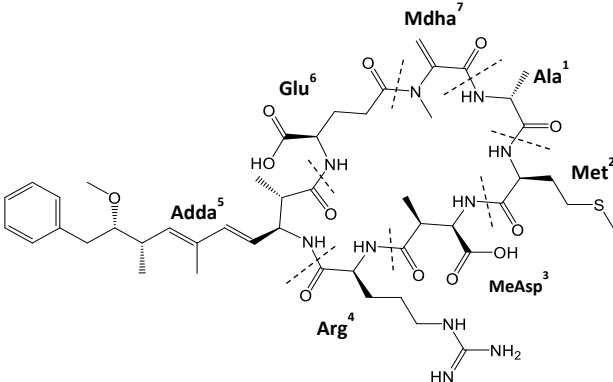[a]=Fragment contained in the HCD spectrum: n.d.=not detected.

Figure IV.11 HRMS^2 spectra of MC-MR acquired in CID and HCD modes

Table IV.6 Assignment of fragment ions contained in CID and HCD spectra of [MeSer[7]]MC-LR.

	m/z	Formula	Sequence	Neutral loss
[M+H]+	1013.5666	$C_{49}H_{77}O_{13}N_{10}^+$	[Ala[1]+Leu[2]+MeAsp[3]+Arg[4]+Adda[5]+Glu[6]+MeSer[7]+H]+	
	996.5377	$C_{49}H_{74}O_{13}N_9^+$		NH_3
	995.5537	$C_{49}H_{75}O_{12}N_{10}^+$		H_2O
	985.5692	$C_{48}H_{77}O_{12}N_{10}^+$		CO
	981.5386	$C_{48}H_{73}O_{12}N_{10}^+$		CH_3OH
	978.5267	$C_{49}H_{72}O_{12}N_9^+$		H_2O+NH_3
	977.5428	$C_{49}H_{73}O_{11}N_9^+$		$2H_2O$
	969.5750	$C_{48}H_{77}O_{11}N_{10}^+$		CO_2
	968.5412	$C_{48}H_{74}O_{12}N_9^+$		$CO+NH_3$
	967.5592	$C_{48}H_{75}O_{11}N_{10}^+$		$CO+H_2O$
	964.5115	$C_{48}H_{70}O_{12}N_9^+$		CH_3OH+NH_3
	954.5196	$C_{48}H_{72}O_{13}N_7^+$		CH_5N_3 (Guanidine)
	951.5620	$C_{48}H_{75}O_{10}N_{10}^+$		CO_2+H_2O
	946.5011	$C_{48}H_{68}O_{11}N_9^+$		$CH_3OH+NH_3+H_2O$
#	941.5790	$C_{47}H_{77}O_{10}N_{10}^+$		CO_2+CO
1	912.5163	$C_{45}H_{70}O_{11}N_9^+$	[Ala[1]+Leu[2]+MeAsp[3]+Arg[4]+Adda[5]+Glu[6]+H]+	MeSer[7]
2	912.5163	$C_{45}H_{70}O_{11}N_9^+$	[Leu[2]+MeAsp[3]+Arg[4]+Adda[5]+Glu[6]+MeSer[7]+H-CO]+	Ala[1] + CO
3	884.5215	$C_{44}H_{70}O_{10}N_9^+$	[Ala[1]+Leu[2]+MeAsp[3]+Arg[4]+Adda[5]+MeSer[7]+H]+	Glu[6]
	901.5478	$C_{44}H_{73}O_{10}N_{10}^+$	[Ala[1]+Leu[2]+MeAsp[3]+Arg[4]+Adda[5]+MeSer[7]+H+NH_3]+	Glu[6]-NH_3
	856.5288	$C_{43}H_{70}O_9N_9^+$	[Ala[1]+Leu[2]+MeAsp[3]+Arg[4]+Adda[5]+MeSer[7]+H-CO]+	Glu[6]+CO
4	884.5215	$C_{44}H_{70}O_{10}N_9^+$	[Ala[1]+Leu[2]+Arg[4]+Adda[5]+Glu[6]+MeSer[7]+H]+	MeAsp[3]
	901.5478	$C_{44}H_{73}O_{10}N_{10}^+$	[Ala[1]+Leu[2]+Arg[4]+Adda[5]+Glu[6]+MeSer[7]+H+NH_3]+	MeAsp[3]-NH_3
	856.5288	$C_{43}H_{70}O_9N_9^+$	[Ala[1]+Leu[2]+Arg[4]+Adda[5]+Glu[6]+MeSer[7]+H-CO]+	MeAsp[3]+CO
5	900.4793	$C_{43}H_{66}O_{12}N_9^+$	[Ala[1]+MeAsp[3]+Arg[4]+Adda[5]+Glu[6]+MeSer[7]+H]+	Leu[2]
6	879.4917	$C_{40}H_{67}O_{12}N_{10}^+$	[Ala[1]+Leu[2]+MeAsp[3]+Arg[4]+Adda[5]+Glu[6]+MeSer[7]+H-Adda moiety[a]]+	$C_9H_{10}O$ adda moiety
	862.4652	$C_{40}H_{64}O_{12}N_9^+$	[Ala[1]+Leu[2]+MeAsp[3]+Arg[4]+Adda[5]+Glu[6]+MeSer[7]+H-Adda moiety-NH_3]+	adda moiety + NH_3
	844.4534	$C_{40}H_{62}O_{11}N_9^+$	[Ala[1]+Leu[2]+MeAsp[3]+Arg[4]+Adda[5]+Glu[6]+MeSer[7]+H-Adda moiety-NH_3-H_2O]+	adda moiety +NH_3+H_2O
	827.4278	$C_{40}H_{59}O_{11}N_8^+$	[Ala[1]+Leu[2]+MeAsp[3]+Arg[4]+Adda[5]+Glu[6]+MeSer[7]+H-Adda moiety-2NH_3-H_2O]+	adda moiety +$2NH_3+H_2O$
7	783.4727	$C_{40}H_{63}O_8N_8^+$	[Ala[1]+Leu[2]+MeAsp[3]+Arg[4]+Adda[5]+H]+	Glu[6]-MeSer[7]
8	771.4386	$C_{38}H_{59}O_9N_8^+$	[Ala[1]+Arg[4]+Adda[5]+Glu[6]+MeSer[7]+H]+	Leu[2]+MeAsp[3]
9	729.3956	$C_{36}H_{54}O_9N_7^+$	[MeAsp[3]+Arg[4]+Adda[5]+Glu[6]+H]+	Ala[1]+Leu[2]+MeSer[7]
	710.3858	$C_{36}H_{52}O_8N_7^+$	[MeAsp[3]+Arg[4]+Adda[5]+Glu[6]+H-H_2O]+	Ala[1]+Leu[2]+MeSer[7]+H_2O
	700.4016	$C_{35}H_{54}O_8N_7^+$	[MeAsp[3]+Arg[4]+Adda[5]+Glu[6]+H-CO]+	Ala[1]+Leu[2]+MeSer[7]+CO
	682.3912	$C_{35}H_{52}O_7N_7^+$	[MeAsp[3]+Arg[4]+Adda[5]+Glu[6]+H-H_2O-CO]+	Ala[1]+Leu[2]+MeSer[7]+ H_2O+CO
10	700.4016	$C_{35}H_{54}O_8N_7^+$	[Arg[4]+Adda[5]+Glu[6]+MeSer[7]+H]+	Ala[1]+Leu[2]+MeAsp[3]
11	599.3534	$C_{31}H_{47}O_6N_6^+$	[Arg[4]+Adda[5]+Glu[6]+H]+	Ala[1]+Leu[2]+MeAsp[3]+MeSer[7]
	582.3264	$C_{31}H_{44}O_6N_5^+$	[Arg[4]+Adda[5]+Glu[6]+H-NH_3]+	Ala[1]+Leu[2]+MeAsp[3]+MeSer[7] +NH_3
12	571.3181	$C_{24}H_{43}O_8N_8^+$	[Ala[1]+Leu[2]+MeAsp[3]+Arg[4]+MeSer[7]+H]+	Adda[5]+Glu[6]

	m/z	Formula	Assignment	Complementary
	588.3443	$C_{24}H_{46}O_8N_9^+$	$[Ala^1+Leu^2+MeAsp^3+Arg^4+MeSer^7+H+NH_3]^+$	$Adda^5+Glu^6-NH_3$
	570.3341	$C_{24}H_{44}O_7N_9^+$	$[Ala^1+Leu^2+MeAsp^3+Arg^4+MeSer^7+H+NH_3-H_2O]^+$	$Adda^5+Glu^6-NH_3+H_2O$
	552.3249	$C_{24}H_{42}O_6N_9^+$	$[Ala^1+Leu^2+MeAsp^3+Arg^4+MeSer^7+H+NH_3-2H_2O]^+$	$Adda^5+Glu^6-NH_3+2H_2O$
	554.2902	$C_{24}H_{40}O_8N_7^+$	$[Ala^1+Leu^2+MeAsp^3+Arg^4+MeSer^7+H-NH_3]^+$	$Adda^5+Glu^6-NH_3+NH_3$
	553.3075	$C_{24}H_{41}O_7N_8^+$	$[Ala^1+Leu^2+MeAsp^3+Arg^4+MeSer^7+H-H_2O]^+$	$Adda^5+Glu^6+H_2O$
13	470.2709	$C_{20}H_{36}O_6N_7^+$	$[Ala^1+Leu^2+MeAsp^3+Arg^4+H]^+$	$Adda^5+Glu^6+MeSer^7$
	487.2983	$C_{20}H_{39}O_6N_8^+$	$[Ala^1+Leu^2+MeAsp^3+Arg^4+H+NH_3]^+$	$Adda^5+Glu^6+MeSer^7-NH_3$
14	446.2253	$C_{23}H_{32}O_6N_3^+$	$[Ala^1+Adda^5+Glu^6+MeSer^7+H-Adda\ moiety-NH_2-H_2O]^+$	$Leu^2+MeAsp^3+Arg^4+adda\ moiety+H_2O$
15	415.2194	$C_{18}H_{31}O_7N_4^+$	$[Ala^1+Leu^2+MeAsp^3+MeSer^7+H]^+$	$Arg^4+Adda^5+Glu^6$
16	393.2009	$C_{20}H_{29}O_6N_2^+$	$[Adda^5+Glu^6+MeSer^7+H-Adda\ moiety-NH_2]^+$	$Ala^1+Leu^2+MeAsp^3+Arg^4+adda\ moiety$
	375.1914	$C_{20}H_{27}O_5N_2^+$	$[Adda^5+Glu^6+MeSer^7+H-Adda\ moiety-NH_2-H_2O]^+$	$Ala^1+Leu^2+MeAsp^3+Arg^4+adda\ moiety+H_2O$
17	135.0801[a]	$C_9H_{11}O^+$	$[Adda\ moiety\ ^a+H]^+$	
18	n.d.			
19	163.1114[a]	$C_{11}H_{15}O^+$	$[Adda^5-NH_2-Adda\ moiety\ ^a+H]^+$	
20	157.1080[a]	$C_6H_{13}ON_4^+$	$[Arg^4+H]^+$	
21	n.d.			
22	112.0867[a]	$C_5H_{10}N_3^+$	$[Arg^4-CO-NH_3+H]^+$	
23	n.d.			

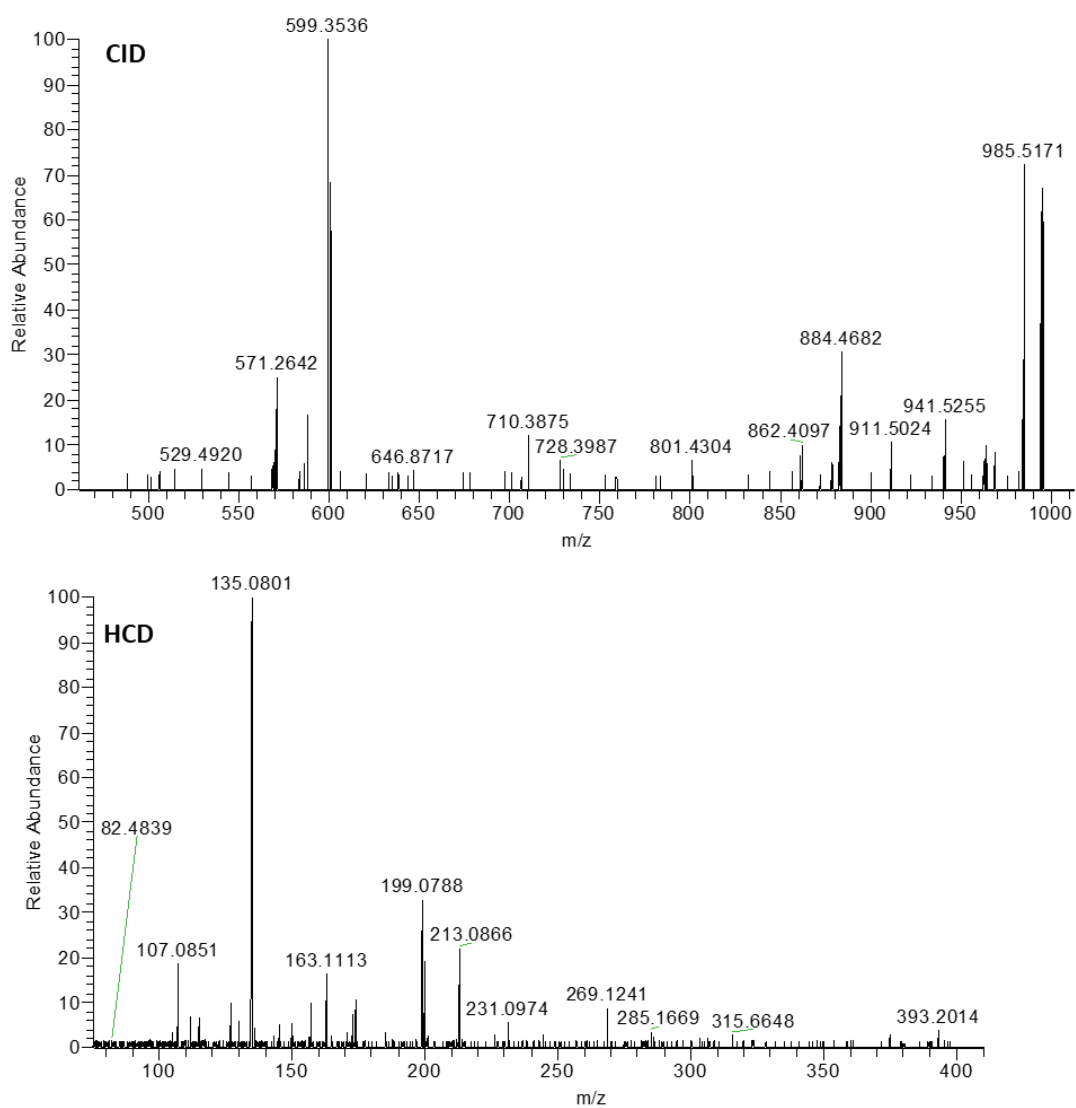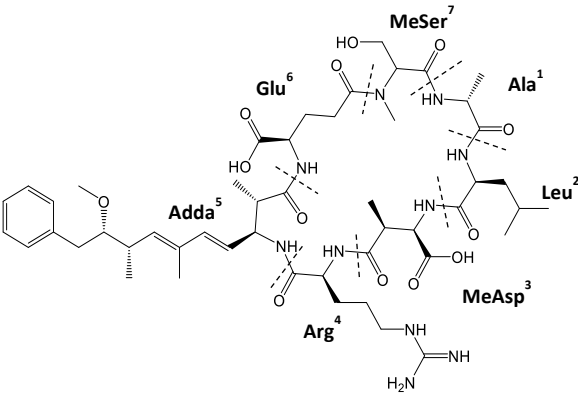[a]=Fragment contained in the HCD spectrum: n.d.=not detected.

Figure IV.12 HRMS[2] spectra of [MeSer[7]]MC-LR acquired in CID and HCD modes.

Table IV.7 Assignment of fragment ions contained in CID and HCD spectra of [DMAdda^5]MC-LR.

	m/z	Formula	Sequence	Neutral loss
			[DMAdda^5]MC-LR	
[M+H]$^+$	981.5403	C$_{48}$H$_{73}$O$_{12}$N$_{10}$$^+$	[Ala^1+Leu^2+MeAsp^3+Arg^4+DMAdda^5+Glu^6+Mdha^7+H]$^+$	
	964.5120	C$_{48}$H$_{70}$O$_{12}$N$_9$$^+$		NH$_3$
	963.5293	C$_{48}$H$_{71}$O$_{11}$N$_{10}$$^+$		H$_2$O
	953.5447	C$_{47}$H$_{73}$O$_{11}$N$_{10}$$^+$		CO
	909.5545	C$_{46}$H$_{73}$O$_9$N$_{10}$$^+$		CO$_2$+CO

#				
1	n.d.			
2	n.d.			
3	852.4960	C$_{43}$H$_{66}$O$_9$N$_9$$^+$	[Ala^1+Leu^2+MeAsp^3+Arg^4+DMAdda^5+Mdha^7+H]$^+$	Glu^6
4	852.4960	C$_{43}$H$_{66}$O$_9$N$_9$$^+$	[Ala^1+Leu^2+Arg^4+DMAdda^5+Glu^6+Mdha^7+H]$^+$	MeAsp^3
5	n.d.			
6	861.4832	C$_{40}$H$_{65}$O$_{11}$N$_{10}$$^+$	[Ala^1+Leu^2+MeAsp^3+Arg^4+DMAdda^5+Glu^6+Mdha^7+H-Adda moiety]$^+$	C$_9$H$_{10}$O (adda moiety)
	844.4533	C$_{40}$H$_{62}$O$_{11}$N$_9$$^+$	[Ala^1+Leu^2+MeAsp^3+Arg^4+DMAdda^5+Glu^6+Mdha^7+H-Adda moiety-NH$_3$]$^+$	adda moiety + NH$_3$
7	n.d.			
8	n.d.			
9	n.d.			
10	n.d.			
11	585.3386	C$_{30}$H$_{45}$O$_6$N$_6$$^+$	[Arg^4+DMAdda^5+Glu^6+H]$^+$	Ala^1+Leu^2+MeAsp^3+Mdha^7
12	n.d.			
13	n.d.			
14	n.d.			
15	n.d.			
16	n.d.			
17	n.d.			
18	n.d.			
19	163.1112^a	C$_{19}$H$_{21}$O$^+$	[Adda^5-NH$_2$-DMAdda moiety +H]$^+$	
20	157.1078^a	C$_{11}$H$_{15}$O$^+$	[Arg^4+H]$^+$	
21	n.d.			
22	112.0864^a	C$_6$H$_{13}$ON$_4$$^+$	[Arg^4-CO-NH$_3$+H]$^+$	
23	121.0642^a	C$_8$H$_9$O$^+$	[DMAdda moiety +H]$^+$	

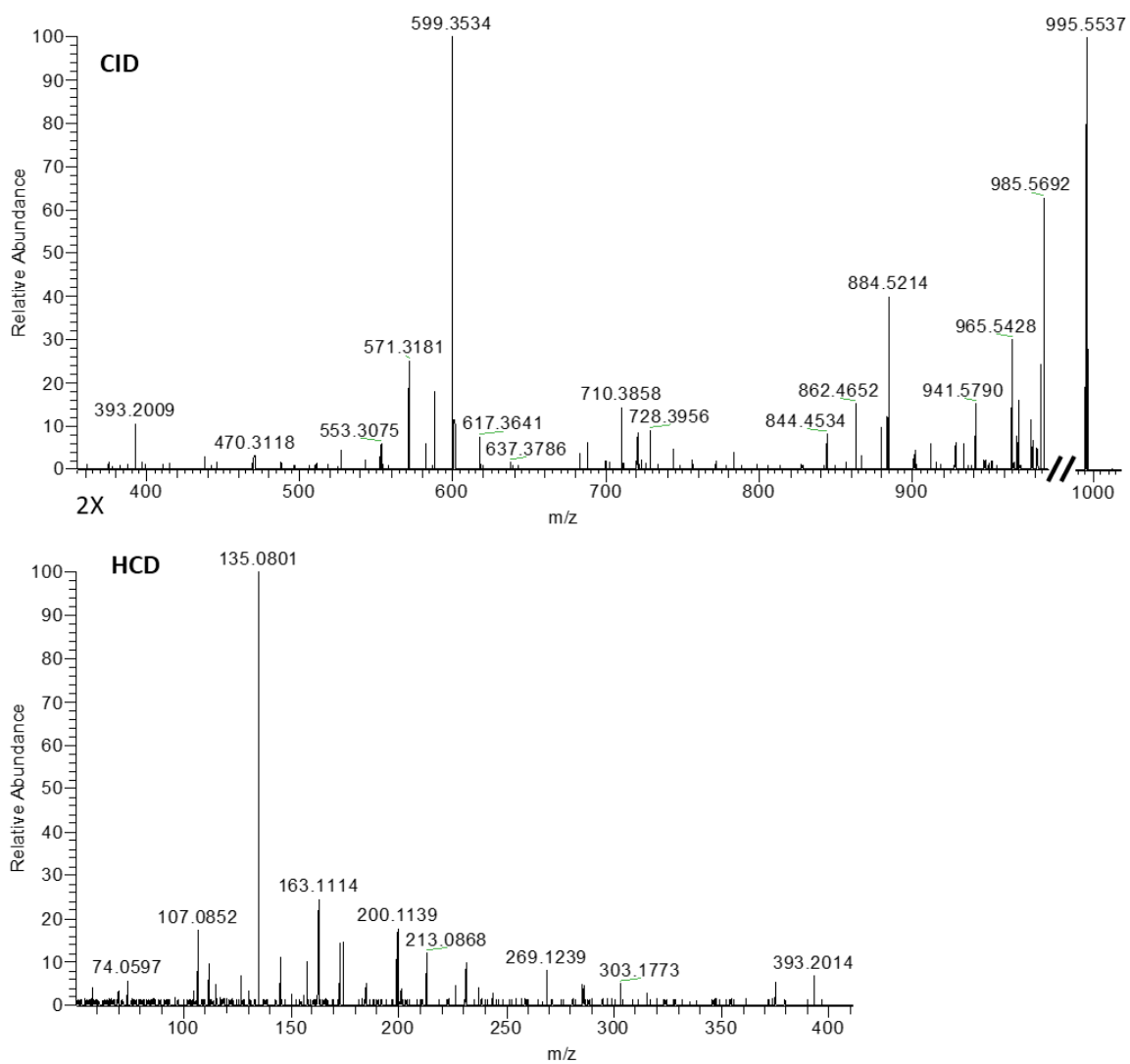^{a}=Fragment contained in the HCD spectrum: n.d.=not detected.
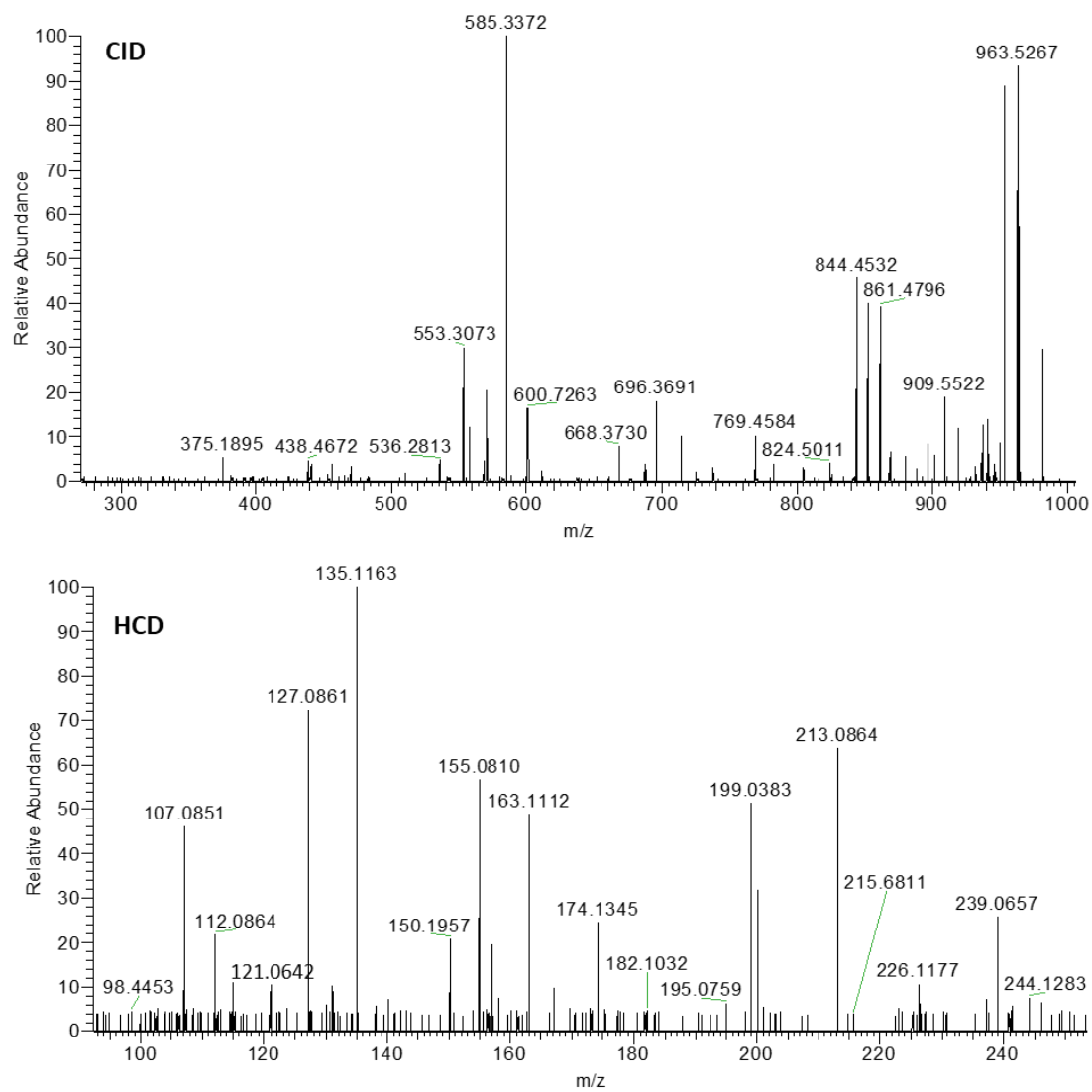
Figure IV.13 HRMS^2 spectra of [DMAdda^5]MC-LR acquired in CID and HCD modes.

Table IV.8 Assignment of fragment ions contained in CID and HCD spectra of [Dha^7]MC-RR.

	m/z	Formula	Sequence	Neutral loss
			[Dha^7]MC-RR	
[M+H]$^+$	1024.5575	C$_{48}$H$_{74}$O$_{12}$N$_{13}$$^+$	[Ala^1+Arg^2+MeAsp^3+Arg^4+Adda^5+Glu^6+Dha^7+H]$^+$	
[M+H]$^{2+}$	512.7818	C$_{48}$H$_{75}$O$_{12}$N$_{13}$$^{2+}$		
	1006.5440	C$_{48}$H$_{72}$O$_{11}$N$_{13}$$^+$		H$_2$O
	503.7757	C$_{48}$H$_{73}$O$_{11}$N$_{13}$$^{2+}$		H$_2$O
	498.7832	C$_{47}$H$_{75}$O$_{11}$N$_{13}$$^+$		CO
	490.7842	C$_{47}$H$_{75}$O$_{10}$N$_{13}$$^+$		CO$_2$
	476.7882	C$_{46}$H$_{75}$O$_9$N$_{13}$$^+$		CO+H$_2$O

#	m/z	Formula	Sequence	Neutral loss
1	n.d.			
2	n.d.			
3	895.5117	C$_{43}$H$_{67}$O$_9$N$_{12}$$^+$	[Ala^1+Arg^2+MeAsp^3+Arg^4+Adda^5+Dha^7+H]$^+$	Glu^6
4	895.5117	C$_{43}$H$_{67}$O$_9$N$_{12}$$^+$	[Ala^1+ThTyr^2+Arg^4+Adda^5+Glu^6+Mdha^7+H]$^+$	MeAsp^3
5	n.d.			
6	890.4814	C$_{39}$H$_{64}$O$_{11}$N$_{13}$$^+$	[Ala^1+Arg^2+MeAsp^3+Arg^4+Adda^5+Glu^6+Dha^7+H-Adda moiety]$^+$	C$_9$H$_{10}$O (adda moiety)
	873.4546	C$_{39}$H$_{61}$O$_{11}$N$_{12}$$^+$	[Ala^1+Arg^2+MeAsp^3+Arg^4+Adda^5+Glu^6+Dha^7+H-Adda moiety-NH$_3$]$^+$	adda moiety+ NH$_3$
	872.4706	C$_{39}$H$_{62}$O$_{10}$N$_{13}$$^+$	[Ala^1+Arg^2+MeAsp^3+Arg^4+Adda^5+Glu^6+Dha^7+H-Adda moiety-H$_2$O]$^+$	adda moiety+H$_2$O
7	n.d.			
8	n.d.			
9	728.3952	C$_{36}$H$_{54}$O$_9$N$_7$$^+$	[MeAsp^3+Arg^4+Adda^5+Glu^6+H]$^+$	Ala^1+Arg^2+Dha^7
10	n.d.			
11	599.3524	C$_{31}$H$_{47}$O$_6$N$_6$$^+$	[Arg^4+Adda^5+Glu^6+H]$^+$	Ala^1+Arg^2+MeAsp^3+Dha^7
	571.3595	C$_{30}$H$_{47}$O$_5$N$_6$$^+$	[Arg^4+Adda^5+Glu^6+H-CO]$^+$	Ala^1+Arg^2+MeAsp^3+Dha^7 +CO
12	582.3091	C$_{23}$H$_{40}$O$_7$N$_{11}$$^+$	[Ala^1+Arg^2+MeAsp^3+Arg^4+Dha^7+H]$^+$	Adda^5+Glu^6
	565.2834	C$_{23}$H$_{37}$O$_7$N$_{10}$$^+$	[Ala^1+Arg^2+MeAsp^3+Arg^4+Dha^7+H-NH$_3$]$^+$	Adda^5+Glu^6+NH$_3$
	564.2986	C$_{23}$H$_{38}$O$_6$N$_{11}$$^+$	[Ala^1+Arg^2+MeAsp^3+Arg^4+Dha^7+H-H$_2$O]$^+$	Adda^5+Glu^6+ H$_2$O
13	n.d.			
14	n.d.			
15	426.2081	C$_{17}$H$_{28}$O$_6$N$_7$$^+$	[Ala^1+Arg^2+MeAsp^3+Dha^7]$^+$	Arg^4+Adda^5+Glu^6
16	n.d.			
17	135.0800^a	C$_9$H$_{11}$O$^+$	[Adda moiety+H]$^+$	
18	n.d.			
19	n.d.			

20	157.1078[a]	$C_6H_{13}ON_4^+$	$[Arg^4+H]^+$
21	n.d.		
22	112.0863 [a]	$C_5H_{10}N_3^+$	$[Arg^4\text{-}CO\text{-}NH_3+H]^+$
23	n.d.		

[a]=Fragment contained in the HCD spectrum: n.d.=not detected

Figure IV.14 HRMS^2 spectra of [Dha^7]MC-RR acquired in CID and HCD modes.

2.3.2 Determination of new MC analogues by LC-HRMS DDA: MC-prHcysR and MC-prHcys(O)R.

The complex toxic profile of the cyanobacterial biomass sample associated with a variety of intense signals contained in the TIC requires an in-depth investigation towards the identification of unknown MC congeners. At this purpose, CID and HCD DDA HRMS[2] experiments were designed and exploited for a fast dereplication of the cyanobacterial sample. Taking into account that Adda[5] is the most conserved residue within the MC group, the diagnostic fragment at m/z 135.0804 ($C_9H_{11}O^+$) was extracted from the hundreds of HCD MS[2] scans. As a consequence, two chromatographic peaks associated with the fragmentation of precursor ions at m/z 1041.5437 and 1057.5403 emerged. The application of criteria to correctly assign the formula to $[M+H]^+$ ion of MC-like compounds [35] revealed the following ion compositions: $C_{50}H_{77}O_{12}N_{10}S^+$ for the ion at m/z 1041.5437, and $C_{50}H_{77}O_{13}N_{10}S^+$ for that at m/z 1057.5403. To date, a limited number of MCs was found to contain S in their structure, and it is mainly due to the presence of Cys and Met residues. Miles at al. [42] reported about the characteristic behavior of MCs containing methionine residue such as MC-MR. This compound can convert into its sulfoxide derivative MC-M(O)R by exposure to air. However, cyanobacteria were found to not be able to produce sulfoxides since MC-M(O)R was not detected in freshly harvested biomass samples containing MC-MR. Contrarily, MC-M(O)R was detected only after a certain period of sample storage, and its relative abundance progressively increases at the expense of MC-MR during the time. This clearly pointed out that sulfoxides are oxidation artefacts of naturally-occurring MC containing S. Therefore, considering that the formulae assigned to $[M+H]^+$ of two new MC congeners contained one S atom and differed for 1 O atom (16 Da), it was reasonable to suspect that the ion at m/z 1041.5437 was the naturally-occurring MC, whilst that at m/z 1057.5403 was its oxidized product (artefact). At this stage, a careful interpretation of the CID and HCD fragmentation spectra of two compounds was necessary to pull out structural insights and for studying the relationship between the two compounds. As shown in **Table IV.9** and **Fig.IV.15**, fragmentation spectra of the ion at m/z 1041.5437 contained the diagnostic fragment at m/z 599.3528 (#11) corresponding to the sequence [Arg[4]+Adda[5]+Glu[6]+ H]$^+$, while fragments #9 and 10 highlighted the further presence of MeAsp[3] and Mdha[7], which were also corroborated as neutral loss through fragments #1 and 4.

Table IV.9 Assignment of fragment ions contained in CID and HCD spectra of MC-prHcysR.

	m/z	Formula	Sequence	Neutral loss
MC-prHcysR				
[M+H]$^+$	1041.5437	$C_{50}H_{77}O_{12}N_{10}S^+$	[Ala^1+prHcys^2+MeAsp^3+Arg^4+Adda^5+Glu^6+Mdha^7+H]$^+$	
	1024.5132	$C_{50}H_{74}O_{12}N_9S^+$		NH$_3$
	1023.5294	$C_{50}H_{75}O_{11}N_{10}S^+$		H$_2$O
	1013.5454	$C_{49}H_{77}O_{11}N_{10}S^+$		CO
	1010.4980	$C_{49}H_{72}O_{12}N_9S^+$		NH$_2$CH$_3$
	1009.5132	$C_{49}H_{73}O_{11}N_{10}S^+$		CH$_3$OH
	1006.4990	$C_{50}H_{72}O_{11}N_9S^+$		H$_2$O+NH$_3$
	999.5143	$C_{49}H_{75}O_{12}N_8S^+$		CH$_3$N$_2$ (Guanidine moiety)
	997.5505	$C_{49}H_{77}O_{10}N_{10}S^+$		CO$_2$
	996.5190	$C_{49}H_{74}O_{11}N_9S^+$		CO+NH$_3$
	995.5348	$C_{49}H_{75}O_{10}N_{10}S^+$		CO+H$_2$O
	992.4871	$C_{49}H_{70}O_{11}N_9S^+$		CH$_3$OH+NH$_3$
	979.5398	$C_{49}H_{75}O_9N_{10}S^+$		CO$_2$+H$_2$O
	969.5557	$C_{48}H_{77}O_9N_{10}S^+$		CO$_2$+CO
#				
1	956.4871	$C_{46}H_{70}O_{11}N_9S^+$	[Ala^1+prHcys^2+MeAsp^3+Arg^4+Adda^5+Glu^6+H]$^+$	Mdha^7
2	940.4906	$C_{46}H_{70}O_{10}N_9S^+$	[prHcys^2+MeAsp^3+Arg^4+Adda^5+Glu^6+Mdha^7+H-CO]$^+$	Ala^1 + CO
3	912.4975	$C_{45}H_{70}O_9N_9S^+$	[Ala^1+prHcys^2+MeAsp^3+Arg^4+Adda^5+Mdha^7+H]$^+$	Glu^6
	929.5233	$C_{45}H_{73}O_9N_{10}S^+$	[Ala^1+prHcys^2+MeAsp^3+Arg^4+Adda^5+Mdha^7+H+NH$_3$]$^+$	Glu^6-NH$_3$
	884.5006	$C_{44}H_{70}O_8N_9S^+$	[Ala^1+prHcys^2+MeAsp^3+Arg^4+Adda^5+Mdha^7+H-CO]$^+$	Glu^6 +CO
4	912.4975	$C_{45}H_{70}O_9N_9S^+$	[Ala^1+prHcys^2+MeAsp^3+Arg^4+Adda^5+Mdha^7+H]$^+$	MeAsp^3
	929.5233	$C_{45}H_{73}O_9N_{10}S^+$	[Ala^1+prHcys^2+MeAsp^3+Arg^4+Adda^5+Mdha^7+H+NH$_3$]$^+$	MeAsp^3 -NH$_3$
	884.5006	$C_{44}H_{70}O_8N_9S^+$	[Ala^1+prHcys^2+MeAsp^3+Arg^4+Adda^5+Mdha^7+H-CO]$^+$	MeAsp^3 +CO
5	n.d.			
6	907.4667	$C_{41}H_{67}O_{11}N_{10}S^+$	[Ala^1+prHcys^2+MeAsp^3+Arg^4+Adda^5+Glu^6+Mdha^7+H-Adda moiety]$^+$	C$_9$H$_{10}$O (adda moiety)
	890.4405	$C_{41}H_{64}O_{11}N_9S^+$	[Ala^1+prHcys^2+MeAsp^3+Arg^4+Adda^5+Glu^6+Mdha^7+H-Adda moiety-NH$_3$]$^+$	adda moiety+ NH$_3$
7	829.4603	$C_{41}H_{65}O_8N_8S^+$	[Ala^1+prHcys^2+MeAsp^3+Arg^4+Adda^5+H]$^+$	Glu^6+Mdha^7
8	n.d.			
9	728.3952	$C_{36}H_{54}O_9N_7^+$	[MeAsp^3+Arg^4+Adda^5+Glu^6+H]$^+$	Ala^1+prHcys^2+Mdha^7
	710.3841	$C_{36}H_{52}O_8N_7^+$	[MeAsp^3+Arg^4+Adda^5+Glu^6+H-H$_2$O]$^+$	Ala^1+prHcys^2+Mdha^7+H$_2$O
	682.3899	$C_{35}H_{52}O_7N_7^+$	[MeAsp^3+Arg^4+Adda^5+Glu^6+H-H$_2$O-CO]$^+$	Ala^1+prHcys^2+Mdha^7+ H$_2$O+CO
10	682.3899	$C_{35}H_{52}O_7N_7^+$	[Arg^4+Adda^5+Glu^6+Mdha^7+H]$^+$	Ala^1+prHcys^2+MeAsp^3
11	599.3528	$C_{31}H_{47}O_6N_6^+$	[Arg^4+Adda^5+Glu^6+H]$^+$	Ala^1+prHcys^2+MeAsp^3+Mdha^7
	582.3266	$C_{31}H_{44}O_6N_5^+$	[Arg^4+Adda^5+Glu^6+H-NH$_3$]$^+$	Ala^1+prHcys^2+MeAsp^3+Mdha^7 +NH$_3$
	571.3580	$C_{30}H_{47}O_5N_6^+$	[Arg^4+Adda^5+Glu^6+H-CO]$^+$	Ala^1+prHcys^2+MeAsp^3+Mdha^7 +CO
12	n.d.			
13	516.2578	$C_{21}H_{38}O_6N_7S^+$	[Ala^1+prHcys^2+MeAsp^3+Arg^4+H]$^+$	Adda^5+Glu^6+Mdha^7
	499.2304	$C_{21}H_{35}O_6N_6S^+$	[Ala^1+prHcys^2+MeAsp^3+Arg^4+H+NH$_3$-H$_2$O]$^+$	Adda^5+Glu^6+Mdha^7-NH$_3$+H$_2$O
14	n.d.			
15	n.d.			
16	375.1905	$C_{20}H_{27}O_5N_2^+$	[Adda^5+Glu^6+Mdha^7+H-Adda moiety-NH$_2$]$^+$	Ala^1+ prHcys^2+MeAsp^3+Arg^4+adda moiety

17	135.0800[a]	$C_9H_{11}O^+$	[Adda moiety +H]$^+$
18	n.d.		
19	163.111[a]	$C_{11}H_{15}O^+$	[Adda^5-NH$_2$-Adda moiety +H]$^+$
20	157.1080[a]	$C_6H_{13}ON_4^+$	[Arg^4+H]$^+$
21	n.d.		
22	112.0866[a]	$C_5H_{10}N_3^+$	[Arg^4-CO-NH$_3$+H]$^+$
23	n.d.		

[a]=Fragment contained in the HCD spectrum.

Figure IV.15 HRMS^2 spectra of MC-prHcysR acquired in CID and HCD modes.

Similarly, Ala^1 was evidenced as neutral loss (Ala + CO) through fragment #2 (**Fig.IV.15**). Although fragment #5 (loss of residue in position 2) was not detected in the MS^2 spectra, the amino acid in position 2 was easily extrapolated from the data by comparing the formula assigned to the [M+H]$^+$ ion and its accurate mass with the elucidated part of the sequence: [Ala^1+X^2+MeAsp^3+Arg^4+Adda^5+Glu^6+Mdha^7+H]$^+$. As a result, residue 2 was found to have an exact mass of 177.0823 Da - $C_7H_{15}NO_2S$ corresponding to the amino acid propyl-homocysteine (prHcys). This evidence was definitely corroborated through the interpretation of a number of fragments in which prHcys was contained such as fragments #1-5 and 13 **Fig.IV.15**. In conclusion, the new MC analogue, [M+H]$^+$ ion at *m/z* 1041.5437 ($C_{50}H_{77}O_{12}N_{10}S^+$), was elucidated and it

256

corresponded to the sequence $[Ala^1+prHcys^2+MeAsp^3+Arg^4+Adda^5+Glu^6+Mdha^7+H]^+$. It was named MC-prHcysR. The interpretation of the HCD and CID spectra **Fig.IV.16** of the second unknown $[M+H]^+$ ion at *m/z* 1057.5403 $(C_{50}H_{77}O_{13}N_{10}S^+)$ **(Table IV.10)** revealed that it was the oxidized derivative of MC-prHcysR. This was clearly evidenced by key fragment ions at *m/z* 1015.4913, 997.4813 and 965.5091, lacking in the MS^2 spectra of MC-prHcysR, which corresponded to the neutral loss of C_3H_6 (propyl moiety), $C_3H_6 + H_2O$ and C_3H_8OS (propyl sulfoxide moiety), respectively. Therefore, the second newly MC analogue, having the sequence $[Ala^1+prHcys(O)^2+MeAsp^3+Arg^4+Adda^5+Glu^6+Mdha^7+H]^+$, was named MC-prHcys(O)R. Quantitation of MC-prHcysR and MC-prHcys(O)R revealed that they were present at low concentration levels of 3.8 and 2.5 ng/mg, respectively. Considering that MC-prHcys(O)R is an oxidized artefact, whose concentration increase during the storage of the extract, its measured concentration has to be added up to that of MC-prHcysR for an accurate evaluation of the toxic profile of the cyanobacterial biomass.

Table IV.10 Assignment of fragment ions contained in CID and HCD spectra of MC-prHcys(O)R.

	m/z	Formula	Sequence	Neutral loss
[M+H]$^+$	1057.5403	C$_{50}$H$_{77}$O$_{13}$N$_{10}$S$^+$	[Ala^1+prHcys(O)^2+MeAsp^3+Arg^4+Adda^5+Glu^6+Mdha^7+H]$^+$	
	1040.5118	C$_{50}$H$_{74}$O$_{13}$N$_9$S$^+$		NH$_3$
	1039.5259	C$_{50}$H$_{75}$O$_{12}$N$_{10}$S$^+$		H$_2$O
	1029.5449	C$_{49}$H$_{77}$O$_{12}$N$_{10}$S$^+$		CO
	1015.4913	C$_{47}$H$_{71}$O$_{13}$N$_{10}$S$^+$		C$_3$H$_6$
	997.4813	C$_{47}$H$_{69}$O$_{12}$N$_{10}$S$^+$		C$_3$H$_6$+H$_2$O
	995.5369	C$_{49}$H$_{75}$O$_{10}$N$_{10}$S$^+$		CO$_2$+H$_2$O
	965.5091	C$_{47}$H$_{69}$O$_{12}$N$_{10}$$^+$		C$_3$H$_8$OS

#	*m/z*	Formula	Sequence	Neutral loss
1	n.d.			
2	n.d.			
3	928.4965	C$_{45}$H$_{70}$O$_{10}$N$_9$S$^+$	[Ala^1+prHcys(O)^2+MeAsp^3+Arg^4+Adda^5+Mdha^7+H]$^+$	Glu^6
4	928.4965	C$_{45}$H$_{70}$O$_{10}$N$_9$S$^+$	[Ala^1+prHcys(O)^2+MeAsp^3+Arg^4+Adda^5+Mdha^7+H]$^+$	MeAsp^3
5	n.d.			
6	923.4720	C$_{41}$H$_{67}$O$_{12}$N$_{10}$S$^+$	[Ala^1+prHcys(O)^2+MeAsp^3+Arg^4+Adda^5+Glu^6+Mdha^7+H-Adda moiety]$^+$	C$_9$H$_{10}$O (adda moiety)
	906.4386	C$_{41}$H$_{64}$O$_{12}$N$_9$S$^+$	[Ala^1+prHcys(O)^2+MeAsp^3+Arg^4+Adda^5+Glu^6+Mdha^7+H-Adda moiety-NH$_3$]$^+$	adda moiety + NH$_3$
7	845.4591	C$_{41}$H$_{65}$O$_9$N$_8$S$^+$	[Ala^1+prHcys(O)^2+MeAsp^3+Arg^4+Adda^5+H]$^+$	Glu^6+Mdha^7
8	n.d.			
9	728.3978	C$_{36}$H$_{54}$O$_9$N$_7$$^+$	[MeAsp^3+Arg^4+Adda^5+Glu^6+H]$^+$	Ala^1+prHcys(O)^2+Mdha^7
	710.3877	C$_{36}$H$_{52}$O$_8$N$_7$$^+$	[MeAsp^3+Arg^4+Adda^5+Glu^6+H-H$_2$O]$^+$	Ala^1+prHcys(O)^2+Mdha^7+H$_2$O
	682.3930	C$_{35}$H$_{52}$O$_7$N$_7$$^+$	[MeAsp^3+Arg^4+Adda^5+Glu^6+H-H$_2$O-CO]$^+$	Ala^1+prHcys(O)^2+Mdha^7+H$_2$O+CO
10	682.3930	C$_{35}$H$_{52}$O$_7$N$_7$$^+$	[Arg^4+Adda^5+Glu^6+Mdha^7+H]$^+$	Ala^1+prHcys(O)^2+MeAsp^3
11	599.3551	C$_{31}$H$_{47}$O$_6$N$_6$$^+$	[Arg^4+Adda^5+Glu^6+H]$^+$	Ala^1+prHcys(O)^2+MeAsp^3+Mdha^7
12	615.2917	C$_{25}$H$_{43}$O$_8$N$_8$S$^+$	[Ala^1+prHcys(O)^2+MeAsp^3+Arg^4+Mdha^7+H]$^+$	Adda^5+Glu^6
	632.3180	C$_{25}$H$_{46}$O$_8$N$_9$S$^+$	[Ala^1+prHcys(O)^2+MeAsp^3+Arg^4+Mdha^7+H+NH$_3$]$^+$	Adda^5+Glu^6-NH$_3$
13	n.d.			
14	n.d.			
15	n.d.			
16	n.d.			
17	135.0804^a	C$_9$H$_{11}$O$^+$	[Adda moiety+H]$^+$	
18	265.1584^a	C$_{19}$H$_{21}$O$^+$	[Adda^5-NH$_2$-CH$_3$OH+H]$^+$	
19	163.1117^a	C$_{11}$H$_{15}$O$^+$	[Adda^5-NH$_2$-Adda moiety+H]$^+$	
20	157.1084^a	C$_6$H$_{13}$ON$_4$$^+$	[Arg^4+H]$^+$	
21	129.1135^a	C$_5$H$_{13}$N$_4$$^+$	Arg^4 immonium ion	
22	112.0868^a	C$_5$H$_{10}$N$_3$$^+$	[Arg^4-CO-NH$_3$+H]$^+$	
23	n.d.			

^{a}=Fragment contained in the HCD spectrum.

Figure IV.16 HRMS^2 spectra of MC-prHcys(O)R acquired in CID and HCD modes.

2.4 Implementation of a new work-flow for identification of cyanobacterial secondary metabolites

The large variety of cyanobacterial species found in the biomass sample, combined with the successful application of DDA experiments for the identification of new MCs, led to implement an analytical work-flow aimed to bringing to light assorted cyanobacterial secondary metabolites. Firstly, a careful analysis of the cyanobacterial biomass profile pointed out that secondary metabolites such as microginins (MGs), anabaenopeptins (APs) and cyanopeptoline-type peptides (CPtps) could be present in the extract. Therefore, an accurate study of data reported in literature was carried out with the purpose to find key structural clues for an effective MS^2-based identification strategy for such metabolites. As a result, diagnostic structural motifs within MG, AP and CPtp classes were found, and a retrospective analysis of HCD and CID DDA spectra was

performed by extracting characteristic fragment ions for each group. A large variety of chromatographic peaks was observed in the XICs, suggesting at first glance the presence of such compounds in the sample. Subsequently, each $[M+H]^+$ precursor ion was identified, the relevant formula was attributed and its presence in the vendor-free database of cyanometabolites [28] was investigated. Analogues already reported in the database were confirmed on the base of their HCD and CID fragmentation patterns, while unknown signals were classified as new metabolites and a careful interpretation of their fragmentation pattern was exploited to pull out structural insights. Unfortunately, the lack of suitable standards for most of the cyanobacterial secondary metabolites hampered a confirmation based on the retention time, and this represented a limitation since a wide range of isobaric analogues have been reported to differ for isobaric amino acids such as Leu and Ile only. Therefore, even if in some cases good quality MS^2 data were obtained and fully interpreted, these structural features hampered to achive a final confirmation.

2.4.1 Determination of microginins

The conserved part structure of MGs is represented by the characteristic N-terminus 3-amino-2-hydroxy-decanoic acid (Ahda), which is present in most of the analogues so far known. This residue can be successfully exploited for the identification of MG-like compounds since it has been reported to give a diagnostic fragment at *m/z* 128.1434 ($C_8H_{18}N^+$) due to the cleavage between C2 and C3 (**Fig.IV.17**). Although a variety of structural variants of Ahda have been reported so far, they are all detectable through specific diagnostic fragments originating from cleavages between C2-C3 and C1-C2, as shown in **Fig.IV.17** [43-44]. With the aim of investigating the presence of MGs in the cyanobacterial biomass sample, the diagnostic fragments reported in **Fig.IV.17** were extracted from the HCD and CID DDA spectra. The XIC of the diagnostic fragment at *m/z* 128.1434 (Ahda) **Fig.IV.17** revealed the presence of three chromatographic peaks eluting at 17.07, 16.46 and 16.80 min (**Fig.IV.18a,b**), of which: i) the first one was found to be originated from the precursor ion at *m/z* 728.4237 ($C_{38}H_{58}O_9N_5^+$) (**Fig.IV.19**a), whilst ii) the other two to the precursor at *m/z* 754.4392 ($C_{40}H_{60}O_9N_5^+$) (**Fig.IV.19b**). The cross interpretation of the HCD and CID DDA spectra suggested that the ion at *m/z* 728.4237 could be attributed to MG FR1 - [Ahda[1]-Ala[2]-MeLeu[3]-Tyr[4]-Tyr[5]] – (**Fig.IV.18**a; **Table IV.11**).
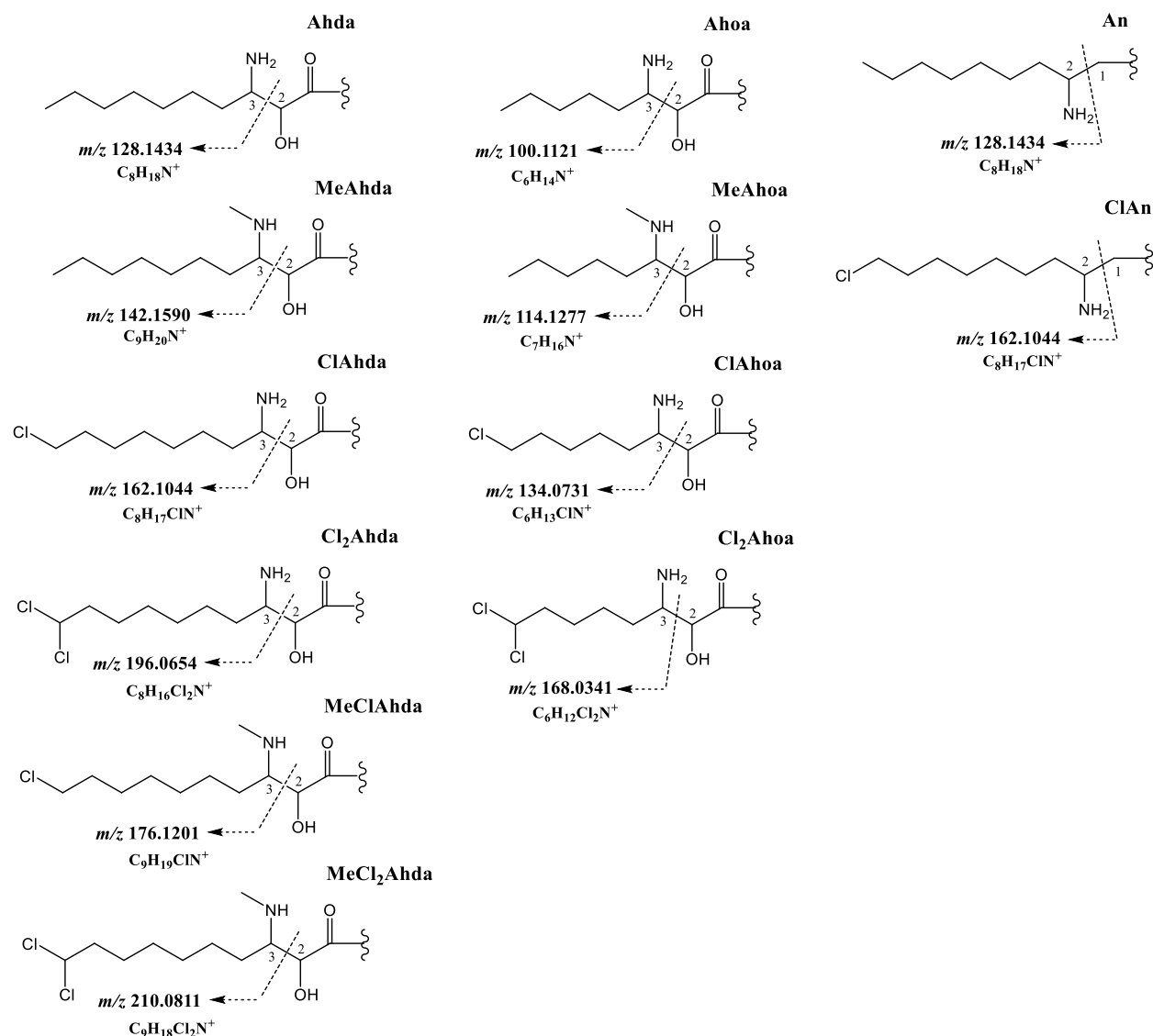
Figure IV.17 Representation of hydroxy-decanoic acid (Ahda) and its structural variants. Exact mass and formula of each diagnostic fragment. 3-amino-2-hydroxy-octanoic acid (Ahoa), 2-amino-nonane (An), Me=methyl, Cl=chloro.

Particularly, Ahda[1] was confirmed through fragments originating from cleavages #2, #3, #4 and #5, while ions at m/z 100.1120 ($C_6H_{14}N^+$, cleavage #9) and m/z 136.0756 ($C_8H_{10}NO^+$, cleavage #11 and #14) pointed out the presence of MeLeu[3] and Tyr[4,5], respectively; further evidence of Tyr[5] was given by the fragment at m/z 547.3496 ($C_{29}H_{47}N_4O_6^+$, cleavage #13) due to the neutral loss of 181.0739 Da from the $[M+H]^+$ ion, whereas cleavages #1, #6 and #7 highlighted the presence of Ala[2]. The exact position of residues was finally confirmed through: i) cleavages #10 and #15, and #8 which confirmed the sequence [Ahda[1]-Ala[2]-MeLeu[3]] and [MeLeu[3]-Tyr[4]-Tyr[5]], respectively.

Even though all amino acids and the entire sequence was confirmed on the basis of the fragmentation patterns, HRMS[2] approach do not allow to distinguish between isobaric amino acids, thus the presence of MeIle[3] cannot be excluded. This observation arises from the well-described capacity of MG-producing cyanobacteria to biosynthesize isobaric analogues that differ for MeLeu and MeIle residues. Therefore, it cannot be excluded that the peak eluting at 17.07 min could be associated with a new isobaric analogue of MG FR1 having MeIle[3]. On the other hand, the XIC of the precursor ion at *m/z* 728.4237 gave a further chromatographic peak eluting at 16.53 min (**Fig.IV.18**a). Unfortunately, its low concentration did not allow to obtain good quality MS[2] data, but an accurate investigation through the cyano-data base revealed that the same ion at *m/z* 728.4237 corresponds to cyanostatin A, a structural isomer of MG-FR1. In absence of more appropriate data, no further conclusion can be drawn.

The $[M+H]^+$ ion at *m/z* 754.4392 ($C_{40}H_{60}O_9N_5^+$) **Fig.IV.17** was found to correspond to cyanostatin B -[Ahda[1]-Tyr[2]-MeIle[3]-Pro[4]-Tyr[5]] - and no isobaric compounds have been reported so far. However, two peaks with the same exact mass emerged in the cyanobacterial biomass, thus an accurate interpretation of the relevant fragmentation patterns was a prerequisite. As reported in **Table IV.12,13**, the sequence - [Ahda[1]-Tyr[2]-MeIle[3]/MeLeu[3]-Pro[4]-Tyr[5]] – was confirmed for both peaks eluted at 16.80 and 16.46 min. This clearly suggested that a new isobaric compound of cyanostatin B, labelled in this study cyanostatin C, was present in the extract, but no match can be done between the two analogues and the chromatographic peaks emerged from the XIC. In addition, a further confirmation that the structural difference between the two isomers lies into residue 3 was given by the analysis of the full-scan spectrum. A strong in-source fragmentation due to the neutral loss of the sequence [Pro[4]-Tyr[5]] (278.1267 Da) occurred for both molecules since the most abundant in-source fragment at *m/z* 476.3150 ($C_{26}H_{42}O_5N_3^+$, cleavage #12, (**Table IV.12,13**) was found in the full-scan spectra showing a relative abundance ratio with the $[M+H]^+$ ion of 100:30, respectively (**Fig.19a**). Therefore, this ionization behavior suggested that MGs featuring [Pro[4]-Tyr[5]] can be further confirmed by analyzing their full-scan spectra due to a noticeable in-source loss of 278.1267 Da.

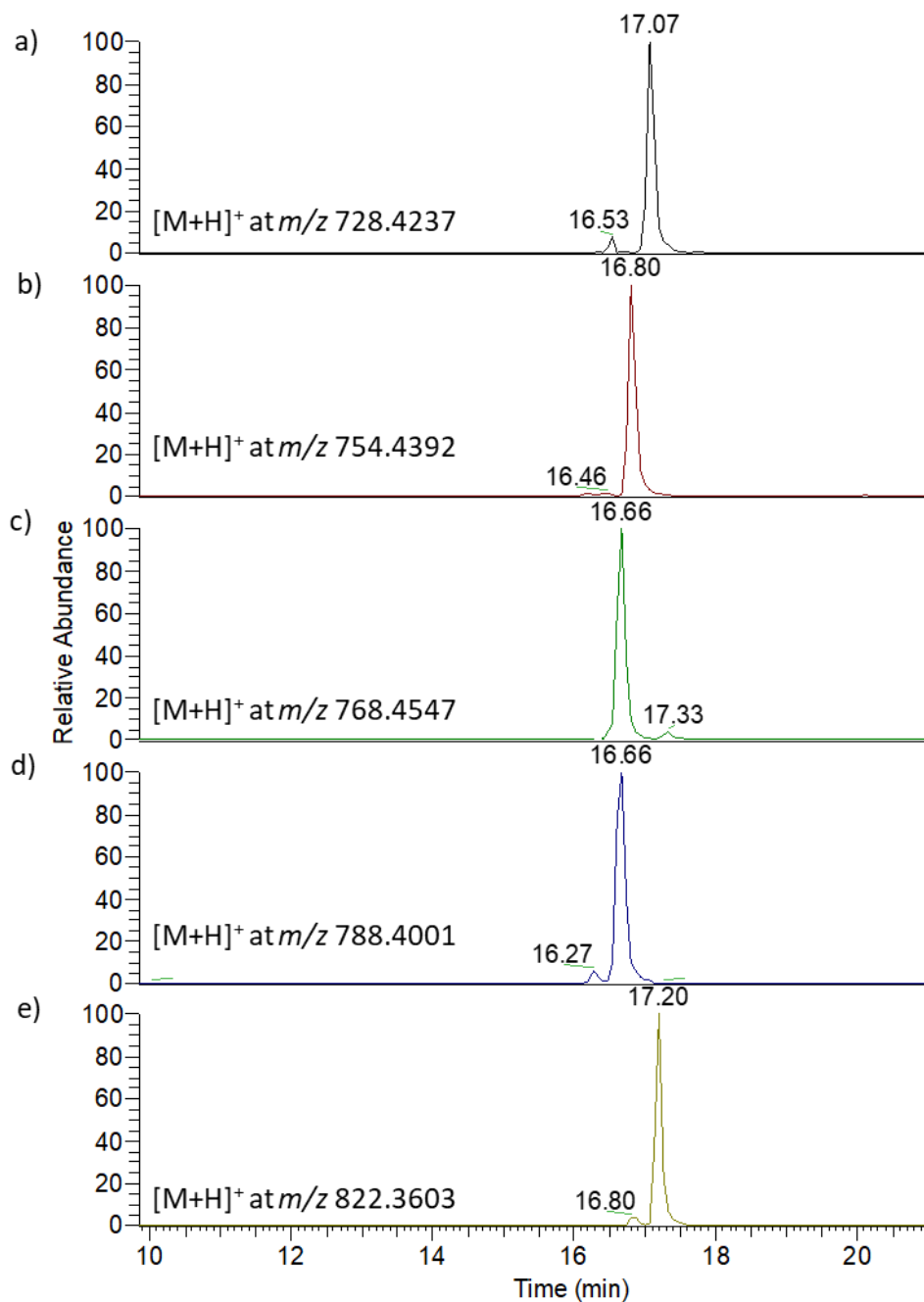**Figure IV.18** XIC of [M+H]$^+$ of known and unknown MGs emerged through the optimized analytical work-flow.

The same methodological approach was applied toward the identification of further MG congeners. The extraction of fragment at *m/z* 142.1590 (MeAhda) **Fig.IV.17** gave a peak eluting at 16.66 min (**Fig. IV.18c**),associated with the [M+H]$^+$ ion at *m/z* 768.4547 (C$_{41}$H$_{62}$O$_9$N$_5$$^+$) (**Fig.**

IV.19b), whose XIC instead, gave a further peak eluting at 17.33 (**Fig. IV.18c**). Their exact mass was found to correspond to MG 767 - [MeAhda^1-Tyr^2-MeIle^3-Pro^4-Tyr^5] and its isobaric congener MG KR767 - [MeAhda^1-Tyr^2-MeLeu^3-Pro^4-Tyr^5]. The confirmation of the sequence - [MeAhda^1-Tyr^2-MeIle^3/MeLeu^3-Pro^4-Tyr^5] - was achieved only for the most intense peak at 16.66 min (**Table IV.14**) since the low relative abundance of the peak at 17.33 min did not allow to record good MS^2 spectra. However, an intense in-source fragment at *m/z* 490.3268 (C$_{27}$H$_{44}$O$_3$N$_5^+$, cleavage #10) due to the neutral loss of [Pro^4-Tyr^5] (278 Da) was found in the full-scan spectrum of both peaks (**Fig. IV.19b**).

Similarly, the extraction of the diagnostic fragment at *m/z* 162.1044 (ClAhda) **Fig.IV.17** provided a peak eluting at 16.66 (**Fig. IV.18d**) min related to the [M+H]$^+$ ion at *m/z* 788.4001 (C$_{40}$H$_{59}$N$_5$O$_9$Cl$^+$) (**Fig. IV.19c**), whose XIC gave a further peak at 16.27 (**Fig. IV.18d**). The corresponding formula was ascribable to the isobaric MG GH787 - [ClAhda^1-Tyr^2-MeIle^3 -Pro^4-Tyr^5] – and MG KR787 - [ClAhda^1-Tyr^2- MeLeu^3-Pro^4-Tyr^5]. A complete confirmation of the sequence - [ClAhda^1-Tyr^2-MeIle^3/MeLeu^3-Pro^4-Tyr^5] – was obtained only for the most intense peak (**Table IV.15**), while the full-scan spectrum of both compounds contained the in-source fragment at *m/z* 510.2728 (C$_{26}$H$_{41}$O$_5$N$_3$Cl$^+$, cleavage #12due to the loss of [Pro^4-Tyr^5] - 278 Da (**Fig. IV.19c**).

The extraction of the diagnostic fragment at *m/z* 196.0654 (Cl$_2$Ahda) **Fig.IV.17** gave a chromatographic peak eluting at 17.20 (**Fig. IV.18e**) associated with the [M+H]$^+$ precursor ion at *m/z* 822.3603 (C$_{40}$H$_{58}$O$_9$N$_5$Cl$_2^+$) (**Fig. IV.19d,e**), while the XIC of such ion highlighted a further peak eluting at 16.80 (**Fig. IV.18e**). No MG with such accurate mass was contained in the cyano-data base. A first confirmation of the presence of two chlorine atoms for both analogues was given by the analysis of the isotopic pattern, which highlighted a relative abundance characteristic for di-chlorinated molecules between the peaks of the ion cluster (**Fig. IV.19e**). Similarly to the previously described compounds, only for the most intense peak were obtained good quality MS^2 spectra, and their interpretation confirmed the sequence [Cl$_2$Ahda^1-Tyr^2-MeIle/MeLeu^3-Pro^4-Tyr^5] (**Table IV.16**). Moreover, the in-source fragment at *m/z* 544.2332 (C$_{26}$H$_{40}$O$_5$N$_3$Cl$_2^+$, cleavage #11) due to the neutral loss of the sequence [Pro^4-Tyr^5] – 278 Da – was found in the full-scan spectrum of both peaks (**Fig. IV.19d**). These new MG analogues were named MG 822A and MG 822B.

Figure IV.19 HR full-scan spectrum of the chromatographic peaks eluting at: a) 16,46 and 16.80, b) 16.66, c) 16.66 and d) 17.20 min. Enhanced HR full-scan spectrum of the [M+H]+ ion at *m/z* 822.3606.

In addition, the application of the cyano-database highlighted the suspect presence of a variety of MG congeners such as: MG-565A (*m/z* 565.3600, $C_{29}H_{49}N_4O_7^+$), MG-FR3 (*m/z* 728.3877, $C_{37}H_{54}N_5O_{10}^+$), MG-T1 (*m/z* 732.3370, $C_{36}H_{51}N_5O_9Cl^+$), MG-T61A (*m/z* 762.3848, $C_{38}H_{57}N_5O_9Cl^+$) and MG-T65 (*m/z* 766.2984, $C_{36}H_{50}N_5O_9Cl_2^+$). Unfortunately, their low relative abundance hampered the acquisition of MS^2 spectra, thus in lack of appropriate standards, no further confirmation was drawn.

Table IV.11 Assignment of fragment ions of [M+H]$^+$ ion at *m/z* 728.4237 eluting at 17.07 min.

	m/z	Formula	Sequence	Neutral loss
[M+H]$^+$	728.4237	C$_{38}$H$_{58}$O$_9$N$_5^+$	[Ahda^1+Ala^2+MeLeu^3+Tyr^4+Tyr^5+H]$^+$	
	710.4056^b	C$_{38}$H$_{56}$O$_8$N$_5^+$		H$_2$O
Cleavage				
#1	217.1546^a	C$_{10}$H$_{21}$O$_3$N$_2^+$	[Ahda^1+Ala^2+H-C$_3$H$_6$ (Part of Ahda^1)]$^+$	MeLeu^3+Tyr^4+Tyr^5+C$_3$H$_6$
	182.1179^a	C$_{10}$H$_{16}$O$_{32}$N$^+$	[Ahda^1+Ala^2+H-C$_3$H$_6$-H$_2$O-NH$_3$]$^+$	MeLeu^3+Tyr^4+Tyr^5+C$_3$H$_6$+H$_2$O+NH$_3$
#2	146.1175^a	C$_7$H$_{16}$O$_2$N$^+$	[Ahda^1+H-C$_3$H$_6$]$^+$	Ala^2+MeLeu^3+Tyr^4+Tyr^5+C$_3$H$_6$
#3	128.1434^a	C$_8$H$_{18}$N$^+$	[Ahda^1+H-C$_2$H$_2$O$_2$]$^+$ (Ahda^1 diagnostic fragment)	Ala^2+MeLeu^3+Tyr^4+Tyr^5+C$_2$H$_2$O$_2$
#4	158.1539^a	C$_9$H$_{20}$ON$^+$	[Ahda^1+H-CO]$^+$	Ala^2+MeLeu^3+Tyr^4+Tyr^5+CO
	140.1433^a	C$_9$H$_{18}$N$^+$	[Ahda^1+H-CO-H$_2$O]$^+$	Ala^2+MeLeu^3+Tyr^4+Tyr^5+CO+H$_2$O
#5	168.1384^a	C$_{10}$H$_{18}$ON$_P^+$	[Ahda^1+H-H$_2$O]$^+$	Ala^2+MeLeu^3+Tyr^4+Tyr^5+H$_2$O
#6	211.1803^a	C$_{12}$H$_{23}$ON$_2^+$	[Ahda^1+Ala^2+H-CO-H$_2$O]$^+$	MeLeu^3+Tyr^4+Tyr^{5+}CO+H$_2$O
#7	239.1756^{a,b}	C$_{13}$H$_{23}$O$_2$N$_2^+$	[Ahda^1+Ala^2+H-H$_2$O]$^+$	MeLeu^3+Tyr^4+Tyr^5+H$_2$O
#8	472.2449^b	C$_{25}$H$_{34}$O$_6$N$_3^+$	[MeLeu^3+Tyr^4+Tyr^5+H]$^+$	Ahda^1+Ala^2
#9	100.1120^a	C$_6$H$_{14}$N$^+$	[MeLeu^3+H-CO]$^+$ (MeLeu^3 immonium ion)	Ahda^1+Ala^2+Tyr^4+Tyr^5+ CO
#10	384.2862^{a,b}	C$_{20}$H$_{38}$O$_4$N$_3^+$	[Ahda^1+Ala^2+MeLeu^3+H]$^+$	Tyr^4+Tyr^5
	366.2753^b	C$_{20}$H$_{36}$O$_3$N$_3^+$	[Ahda^1+Ala^2+MeLeu^3+H-H$_2$O]$^+$	Tyr^4+Tyr^5+H$_2$O
#11	136.0756^a	C$_8$H$_{10}$ON$^+$	[Tyr^4+H-CO]$^+$ (Tyr^4 immonium ion)	Ahda^1+Ala^2+MeLeu^3+Tyr^5+CO
#12	519.3552^b	C$_{28}$H$_{47}$O$_5$N$_4^+$	[Ahda^1+Ala^2+MeLeu^3+Tyr^4+H-CO]$^+$	Tyr^5+CO
#13	547.3496^b	C$_{29}$H$_{47}$O$_6$N$_4^+$	[Ahda^1+Ala^2+MeLeu^3+Tyr^4+H]$^+$	Tyr^5
#14	136.0756^a	C$_8$H$_{10}$ON$^+$	[Tyr^5+H-CO$_2$]$^+$	Ahda^1+Ala^2+MeLeu^3+Tyr^4+CO$_2$
#15	257.1493^a	C$_{12}$H$_{21}$O$_4$N$_2^+$	[C$_2$H$_2$O$_2$(Part of Ahda)+Ala^2+MeLeu^3+H]$^+$	Ahda^1+ Tyr^4+Tyr^5-C$_2$H$_2$O$_2$ (Part of Ahda)
	227.1395^a	C$_{11}$H$_{19}$O$_3$N$_2^+$	[C$_2$H$_2$O$_2$ (Part of Ahda)+Ala^2+MeLeu^3+H-CO]$^+$	Ahda^1+ Tyr^4+Tyr^5-C$_2$H$_2$O$_2$ (Part of Ahda)+CO

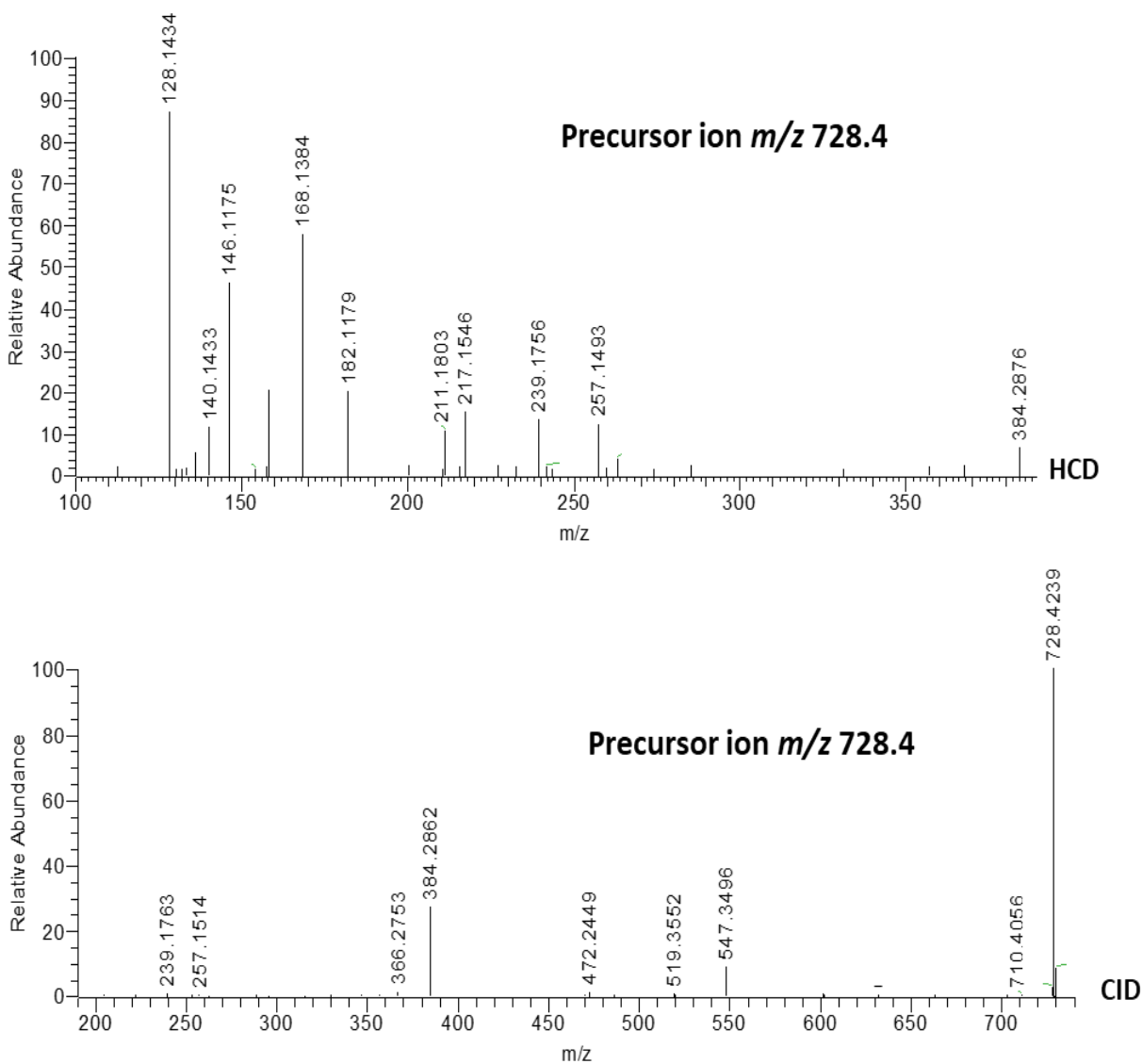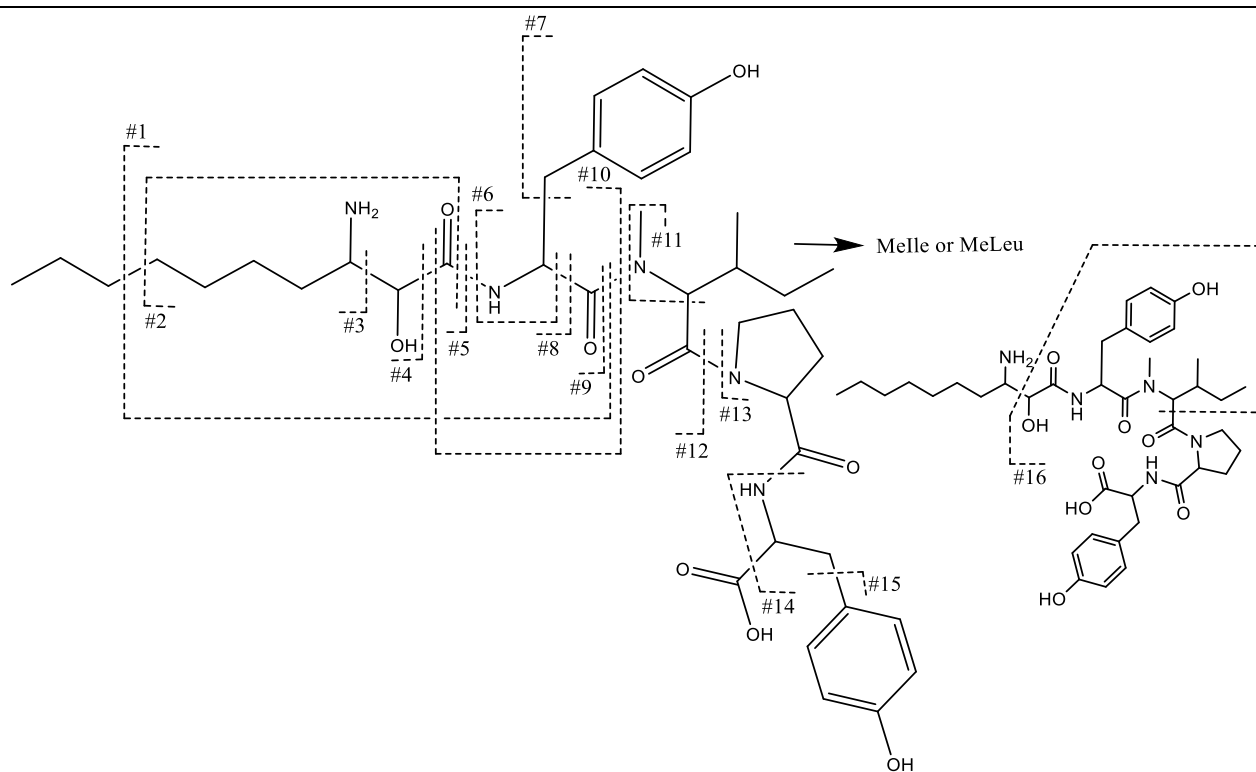a=Fragment contained in the HCD DDA spectrum; b=Fragment ion contained in the CID DDA spectrum.

Figure IV.20 HCD and CID DDA MS^2 spectrum of [M+H]$^+$ ion at *m/z* 728.4237 eluting at 17.07 min.

Table IV.12 Assignment of fragment ions of [M+H]$^+$ ion at *m/z* 754.4394 eluting at 16.80 min.

	m/z	Formula	Sequence	Neutral loss
[M+H]$^+$	754.4392	C$_{40}$H$_{60}$O$_9$N$_5$$^+$	[Ahda^1+Tyr^2+MeIle^3/MeLeu^3+Pro^4+Tyr^5+H]$^+$	
Cleavage				
#1	309.1810^{a,b}	C$_{16}$H$_{25}$O$_4$N$_2$$^+$	[Ahda^1+Tyr^2+H-C$_3$H$_6$ (Part of Ahda^1)]$^+$	MeIle^3/MeLeu^3+Pro^4+Tyr^5+C$_3$H$_6$
	274.1435^{a,b}	C$_{16}$H$_{20}$O$_3$N$^+$	[Ahda^1+Tyr^2+H-C$_3$H$_6$-H$_2$O-NH$_3$]$^+$	MeIle^3/MeLeu^3+Pro^4+Tyr^5+C$_3$H$_6$+H$_2$O+NH$_3$
	246.1492^a	C$_{15}$H$_{20}$O$_2$N$^+$	[Ahda^1+Tyr^2+H-C$_3$H$_6$-H$_2$O-NH$_3$-CO]$^+$	MeIle^3/MeLeu^3+Pro^4+Tyr^5+C$_3$H$_6$+H$_2$O+NH$_3$+CO
#2	146.1176^{a,b}	C$_7$H$_{16}$O$_2$N$^+$	[Ahda^1+H-C$_3$H$_6$]$^+$	Tyr^2+MeIle^3/MeLeu^3+Pro^4+Tyr^5+C$_3$H$_6$
#3	128.1433^a	C$_8$H$_{18}$N$^+$	[Ahda^1+H-C$_2$H$_2$O$_2$]$^+$ (Ahda^1 diagnostic fragment)	Tyr^2+MeIle^3/MeLeu^3+Pro^4+Tyr^5+C$_2$H$_2$O$_2$
#4	158.1545^a	C$_9$H$_{20}$ON$^+$	[Ahda^1+H-CO]$^+$	Tyr^2+MeIle^3/MeLeu^3+Pro^4+Tyr^5+CO
	140.1429^a	C$_9$H$_{18}$N$^+$	[Ahda^1+H-CO-H$_2$O]$^+$	Tyr^2+MeIle^3/MeLeu^3+Pro^4+Tyr^5+CO+H$_2$O
#5	168.1384^{a,b}	C$_{10}$H$_{18}$ON$^+$	[Ahda^1+H-H$_2$O]$^+$	Tyr^2+MeIle^3/MeLeu^3+Pro^4+Tyr^5+H$_2$O
#6	136.0757^a	C$_8$H$_{10}$ON$^+$	[Tyr^2+H-CO]$^+$ (Tyr^2 immonium ion)	Ahda^1+MeIle^3/MeLeu^3+Pro^4+Tyr^5+CO
#7	107.0493^a	C$_7$H$_7$O$^+$	[Tyr^2+H-C$_2$H$_2$NO]$^+$ (4-Hydroxybenzyl ion)	Ahda^1+MeIle^3/MeLeu^3+Pro^4+Tyr^5+C$_2$H$_2$NO
#8	321.2160^{a,b}	C$_{18}$H$_{29}$O$_3$N$_2$$^+$	[Ahda^1+Tyr^2+H-CO]$^+$	MeIle^3/MeLeu^3+Pro^4+Tyr^5+CO
	303.2066^{a,b}	C$_{18}$H$_{27}$O$_2$N$_2$$^+$	[Ahda^1+Tyr^2+H-CO-H$_2$O]$^+$	MeIle^3/MeLeu^3+Pro^4+Tyr^5+CO+H$_2$O
#9	349.2105^b	C$_{19}$H$_{29}$O$_4$N$_2$$^+$	[Ahda^1+Tyr^2+H]$^+$	MeIle^3/MeLeu^3+Pro^4+Tyr^5
	331.202^{a,b}	C$_{19}$H$_{27}$O$_3$N$_2$$^+$	[Ahda^1+Tyr^2+H-H$_2$O]$^+$	MeIle^3/MeLeu^3+Pro^4+Tyr^5+H$_2$O
#10	194.0816^a	C$_{10}$H$_{12}$O$_3$N$^+$	[Tyr^2+H+CO]$^+$	Ahda^1+ MeIle^3/MeLeu^3+Pro^4+Tyr^5-CO
	176.0712^a	C$_{10}$H$_{10}$O$_2$N$^+$	[Tyr^2+H+CO-H$_2$O]$^+$	Ahda^1+ MeIle^3/MeLeu^3+Pro^4+Tyr^5-CO+H$_2$O
#11	100.1120^a	C$_6$H$_{14}$N$^+$	[MeIle^3/MeLeu^3+H-CO]$^+$ (MeIle^3/MeLeu^3 immonium ion)	Ahda^1+Tyr^2+Pro^4+Tyr^5+CO
#12	476.3150^b	C$_{26}$H$_{42}$O$_5$N$_3$$^+$	[Ahda^1+Tyr^2+MeIle^3/MeLeu^3+H]$^+$	Pro^4+Tyr^5
	458.3013^b	C$_{26}$H$_{40}$O$_4$N$_3$$^+$	[Ahda^1+Tyr^2+MeIle^3/MeLeu^3+H-H$_2$O]$^+$	Pro^4+Tyr^5+H$_2$O
	448.3170^b	C$_{25}$H$_{42}$O$_4$N$_3$$^+$	[Ahda^1+Tyr^2+MeIle^3/MeLeu^3+H-CO]$^+$	Pro^4+Tyr^5+CO
	432.3218^b	C$_{25}$H$_{42}$O$_3$N$_3$$^+$	[Ahda^1+Tyr^2+MeIle^3/MeLeu^3+H-CO-OH]$^+$	Pro^4+Tyr^5+CO+OH
	430.3065^b	C$_{25}$H$_{40}$O$_3$N$_3$$^+$	[Ahda^1+Tyr^2+MeIle^3/MeLeu^3+H-CO-H$_2$O]$^+$	Pro^4+Tyr^5+CO+H$_2$O
	414.3138^b	C$_{25}$H$_{40}$O$_2$N$_3$$^+$	[Ahda^1+Tyr^2+MeIle^3/MeLeu^3+H-CO-H$_2$O-OH]$^+$	Pro^4+Tyr^5+CO+H$_2$O+OH
#13	279.1335^a	C$_{14}$H$_{19}$O$_4$N$_2$$^+$	[Pro^4+Tyr^5+H]$^+$	Ahda^1+Tyr^2+MeIle^3/MeLeu^3
#14	136.0757^a	C$_8$H$_{10}$ON$^+$	[Tyr^5+H-CO$_2$]$^+$ (Tyr^5 immonium ion)	Ahda^1+Tyr^2+MeIle^3/MeLeu^3+Pro^4+CO$_2$
#15	107.0493^a	C$_7$H$_7$O$^+$	[Tyr^5+H-C$_2$H$_2$NO$_2$]$^+$ (4-Hydroxybenzyl ion)	Ahda^1+Tyr^2+MeIle^3/MeLeu^3+Pro^4+C$_2$H$_2$NO$_2$
#16	319.1657^{a,b}	C$_{17}$H$_{23}$O$_4$N$_2$$^+$	[C$_2$H$_2$O$_2$ (Part of Ahda^1)+Tyr^2+MeIle^3/MeLeu^3+H-CO]$^+$	Ahda^1+ Pro^4+Tyr^5+CO-C$_2$H$_2$O$_2$

ᵃ=Fragment contained in the HCD DDA spectrum; ᵇ=Fragment ion contained in the CID DDA spectrum.

Figure IV.21 HCD and CID DDA MS^2 spectra of [M+H]$^+$ ion at *m/z* 754.4394 eluting at 16.80 min.

Table IV.13 Assignment of fragment ions of [M+H]$^+$ ion at *m/z* 754.4394 eluting at 16.46 min.

	m/z	Formula	Sequence	Neutral loss
[M+H]$^+$	754.4389	$C_{40}H_{60}O_9N_5^+$	[Ahda^1+Tyr^2+MeIle^3/MeLeu^3+Pro^4+Tyr^5+H]$^+$	
Cleavage				
#1	309.1798^b	$C_{16}H_{25}O_4N_2^+$	[Ahda^1+Tyr^2+H-C$_3$H$_6$ (Part of Ahda^1)]$^+$	MeIle^3/MeLeu^3+Pro^4+Tyr^5+C$_3$H$_6$
#2	146.1179^b	$C_7H_{16}O_2N^+$	[Ahda^1+H-C$_3$H$_6$]$^+$	Tyr^2+MeIle^3/MeLeu^3+Pro^4+Tyr^5+C$_3$H$_6$
#3	128.1433^a	$C_8H_{18}N^+$	[Ahda^1+H-C$_2$H$_2$O$_2$]$^+$ (Ahda^1 diagnostic fragment)	Tyr^2+MeIle^3/MeLeu^3+Pro^4+Tyr^5+C$_2$H$_2$O$_2$
#8	303.2069^b	$C_{18}H_{27}O_2N_2^+$	[Ahda^1+Tyr^2+H-CO-H$_2$O]$^+$	MeIle^3/MeLeu^3+Pro^4+Tyr^5+CO+H$_2$O
#9	331.2016^b	$C_{19}H_{27}O_3N_2^+$	[Ahda^1+Tyr^2+H-H$_2$O]$^+$	MeIle^3/MeLeu^3+Pro^4+Tyr^5+H$_2$O
#11	100.1122^a	$C_6H_{14}N^+$	[MeIle^3/MeLeu^3+H-CO]$^+$ (MeIle^3/MeLeu^3 immonium ion)	Ahda^1+Tyr^2+Pro^4+Tyr^5+CO
#12	476.3105^b	$C_{26}H_{42}O_5N_3^+$	[Ahda^1+Tyr^2+MeIle^3/MeLeu^3+H]$^+$	Pro^4+Tyr^5
	458.3013^b	$C_{26}H_{40}O_4N_3^+$	[Ahda^1+Tyr^2+MeIle^3/MeLeu^3+H-H$_2$O]$^+$	Pro^4+Tyr^5+H$_2$O
	448.3170^b	$C_{25}H_{42}O_4N_3^+$	[Ahda^1+Tyr^2+MeIle^3/MeLeu^3+H-CO]$^+$	Pro^4+Tyr^5+CO

^{a}=Fragment contained in the HCD DDA spectrum; ^{b}=Fragment ion contained in the CID DDA spectrum.
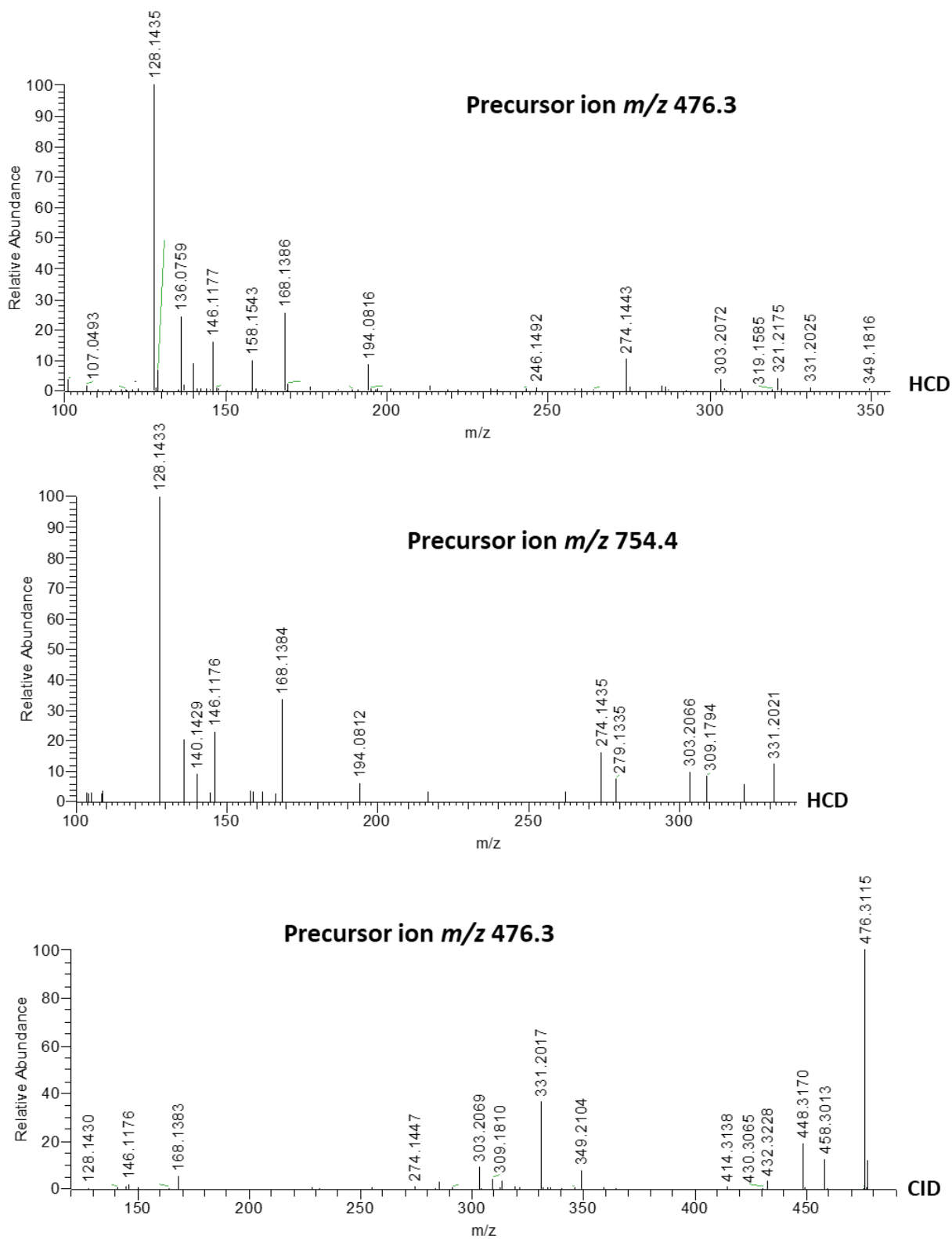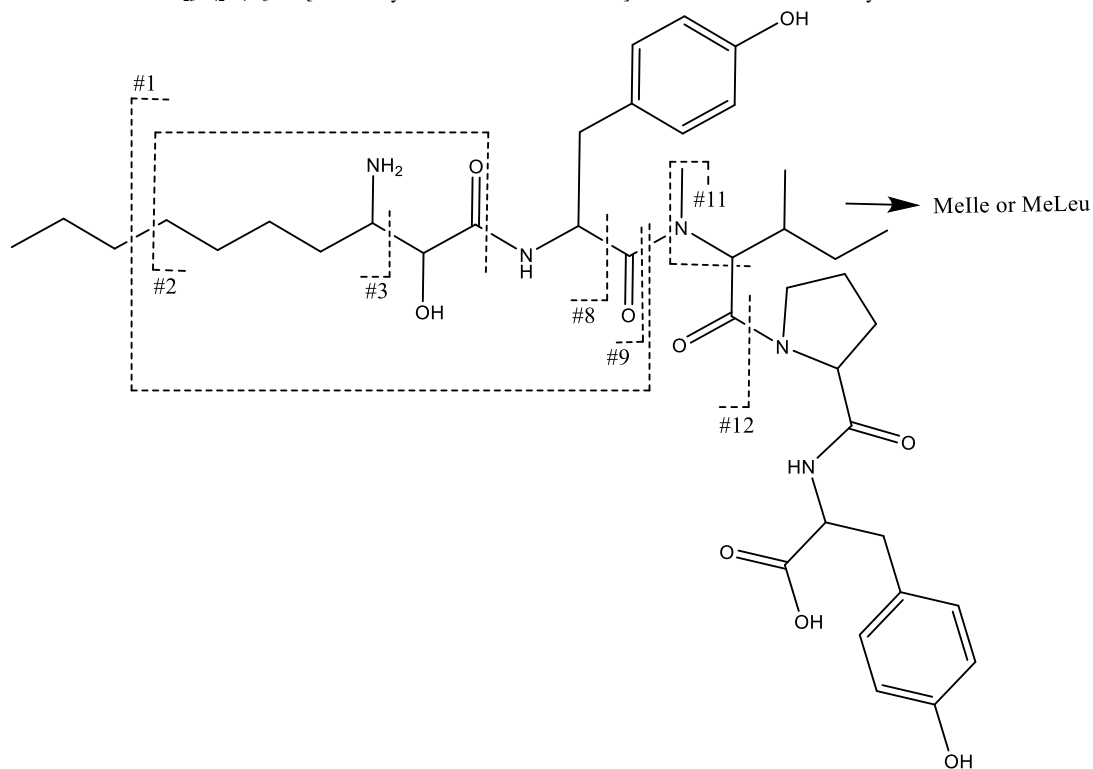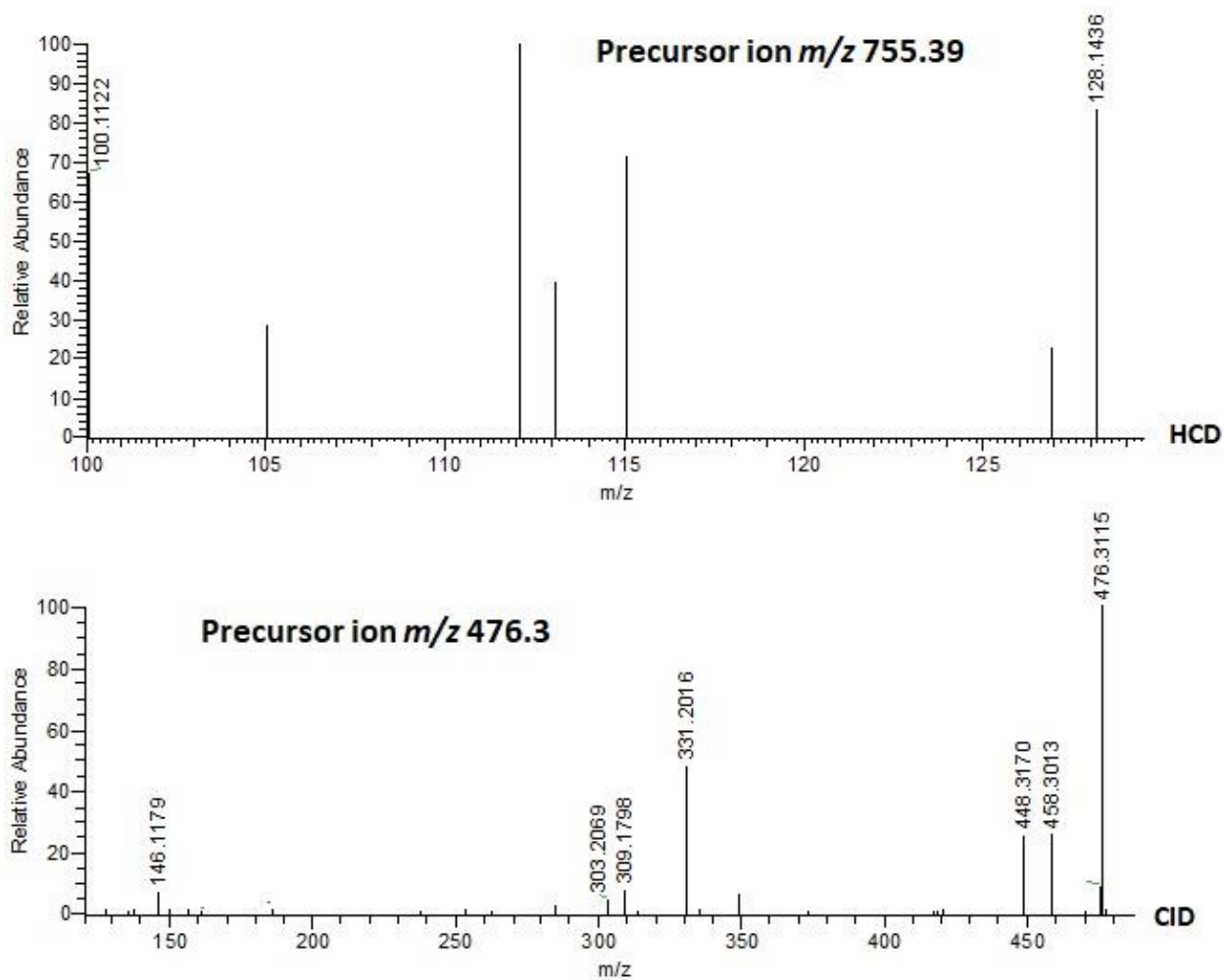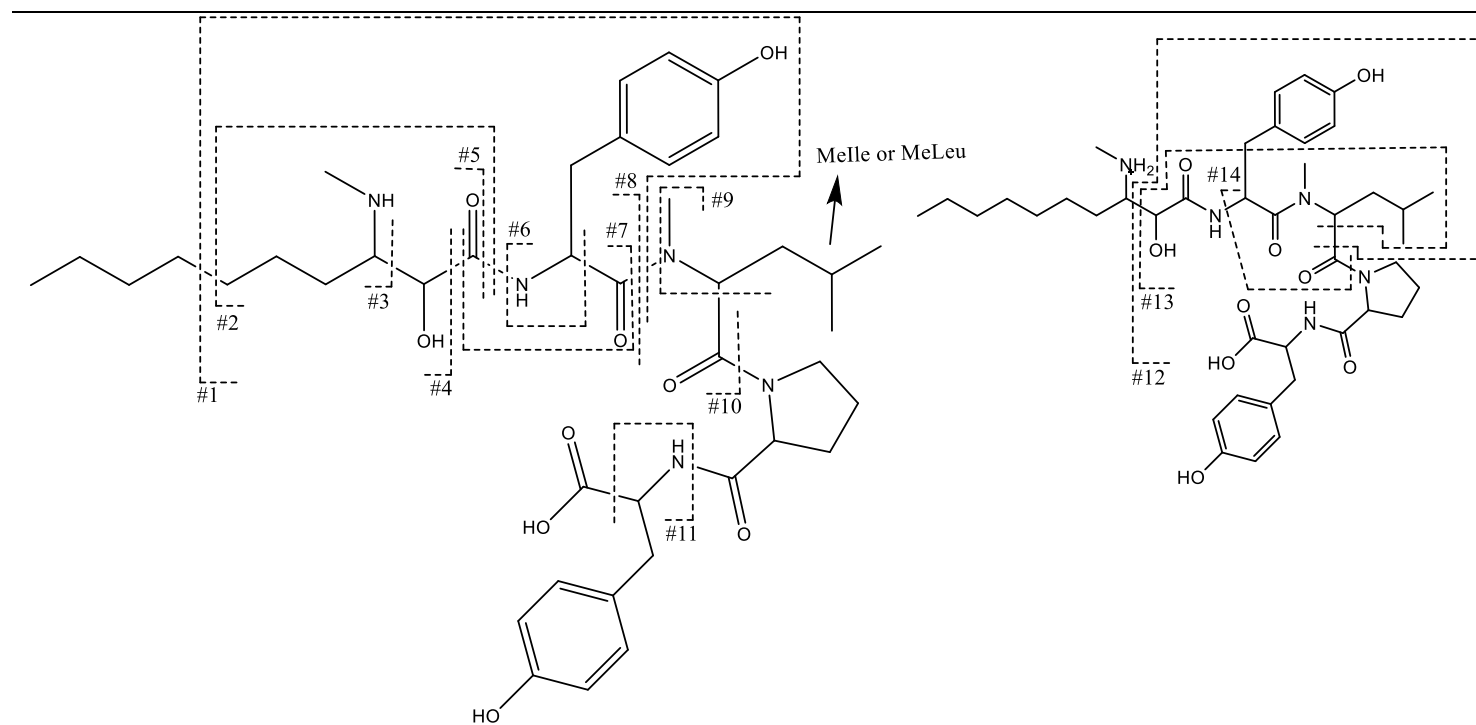
Figure IV.22 HCD and CID DDA MS^2 spectrum of [M+H]$^+$ ion at *m/z* 754.4394 eluting at 16.46 min.

Table IV.14 Assignment of fragment ions of [M+H]$^+$ ion at *m/z* 768.4547 eluting at 16.66 min.

	m/z	Formula	Sequence	Neutral loss
[M+H]$^+$	768.4547	C$_{41}$H$_{62}$O$_9$N$_5$$^+$	[MeAhda^1+Tyr^2+MeIle^3/MeLeu^3+Pro^4+Tyr^5+H]$^+$	
Cleavage				
#1	309.1803[b]	C$_{16}$H$_{25}$O$_4$N$_2$$^+$	[MeAhda^1+Tyr^2+H-C$_4$H$_8$ (Part of MeAhda^1)]$^+$	MeIle^3/MeLeu^3+Pro^4+Tyr^5+C$_4$H$_8$
#2	146.1178[a]	C$_7$H$_{16}$O$_2$N$^+$	[MeAhda^1+H-C$_4$H$_8$]$^+$	Tyr^2+MeIle^3/MeLeu^3+Pro^4+Tyr^5+C$_4$H$_8$
#3	142.1593[a]	C$_9$H$_{20}$N$^+$	[MeAhda^1+H-C$_2$H$_2$O$_2$]$^+$ (MeAhda^1 diagnostic fragment)	Tyr^2+MeIle^3/MeLeu^3+Pro^4+Tyr^5+C$_2$H$_2$O$_2$
#4	172.1702[a]	C$_{10}$H$_{22}$ON$^+$	[MeAhda^1+H-CO]$^+$	Tyr^2+MeIle^3/MeLeu^3+Pro^4+Tyr^5+CO
	154.159[a,b]	C$_{10}$H$_{20}$N$^+$	[MeAhda^1+H-CO-H$_2$O]$^+$	Tyr^2+MeIle^3/MeLeu^3+Pro^4+Tyr^5+CO+H$_2$O
#5	182.1545[a,b]	C$_{11}$H$_{20}$ON$^+$	[MeAhda^1+H-H$_2$O]$^+$	Tyr^2+MeIle^3/MeLeu^3+Pro^4+Tyr^5+H$_2$O
#6	136.076[a]	C$_8$H$_{10}$ON$^+$	[Tyr^2+H-CO]$^+$ (Tyr^2 immonium ion)	MeAhda^1+ MeIle^3/MeLeu^3+Pro^4+Tyr^5
#7	194.0812[a]	C$_{10}$H$_{12}$O$_3$N$^+$	[Tyr^2+H+CO]$^+$	MeAhda^1+MeIle^3/MeLeu^3+Pro^4+Tyr^5-CO
#8	363.228[a,b]	C$_{20}$H$_{31}$O$_4$N$_2$$^+$	[MeAhda^1+Tyr^2+H]$^+$	MeIle^3/MeLeu^3+Pro^4+Tyr^5
	345.218[a,b]	C$_{20}$H$_{29}$O$_3$N$_2$$^+$	[MeAhda^1+Tyr^2+H-H$_2$O]$^+$	MeIle^3/MeLeu^3+Pro^4+Tyr^5+H$_2$O
	317.2239[a,b]	C$_{19}$H$_{29}$O$_2$N$_2$$^+$	[MeAhda^1+Tyr^2+H-H$_2$O-CO]$^+$	MeIle^3/MeLeu^3+Pro^4+Tyr^5+H$_2$O+CO
#9	100.1121[a]	C$_6$H$_{14}$N$^+$	[MeIle^3/MeLeu^3+H-CO]$^+$	MeAhda^1+Tyr^2+Pro^4+Tyr^5+CO
#10	490.3269[b]	C$_{27}$H$_{44}$O$_5$N$_3$$^+$	[MeAhda^1+Tyr^2+MeIle^3/MeLeu^3+H]$^+$	Pro^4+Tyr^5
	472.3172[b]	C$_{27}$H$_{42}$O$_4$N$_3$$^+$	[MeAhda^1+Tyr^2+MeIle^3/MeLeu^3+H-H$_2$O]$^+$	Pro^4+Tyr^5+H$_2$O
#11	136.0764[a]	C$_8$H$_{10}$ON$^+$	[Tyr^5+H-CO$_2$]$^+$ (Tyr^5 immonium ion)	MeAhda^1+Tyr^2+MeIle^3/MeLeu^3+Pro^4+CO$_2$
#12	349.1758[b]	C$_{18}$H$_{25}$O$_5$N$_2$$^+$	[C$_2$H$_2$O$_2$ (Part of MeAhda^1)+Tyr^2+MeIle^3/MeLeu^3+H]$^+$	MeAhda^1+Pro^4+Tyr^5-C$_2$H$_2$O$_2$
	287.1749[b]	C$_{17}$H$_{23}$O$_2$N$_2$$^+$	[C$_2$H$_2$O$_2$ (Part of MeAhda^1)+Tyr^2+MeIle^3/MeLeu^3+H-CO-H$_2$O-OH]$^+$	MeAhda^1+Pro^4+Tyr^5-C$_2$H$_2$O$_2$+CO+H$_2$O+OH
#13	243.1335[a]	C$_{11}$H$_{19}$O$_4$N$_2$$^+$	[C$_2$H$_2$O$_2$ (Part of MeAhda^1)+Tyr^2+MeIle^3/MeLeu^3+H-C$_7$H$_7$O (4-Hydroxybenzyl)]$^+$	MeAhda^1+Pro^4+Tyr^5-C$_2$H$_2$O$_2$+C$_7$H$_7$O
#14	274.1432[a]	C$_{16}$H$_{20}$O$_3$N$^+$	[Tyr^2+MeIle^3/MeLeu^3+H-NH$_2$]$^+$	MeAhda^1+ Pro^4+Tyr^5+NH$_2$

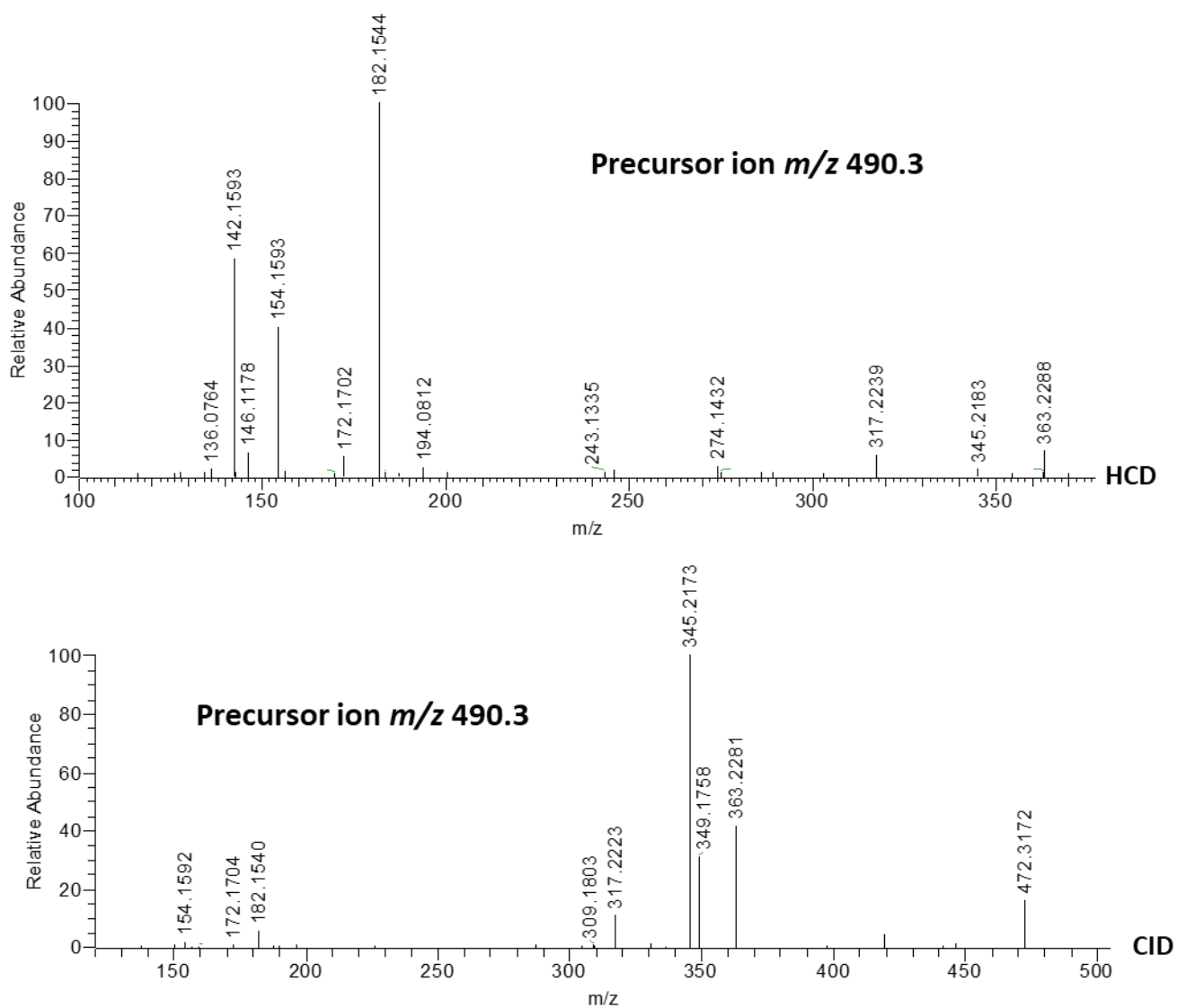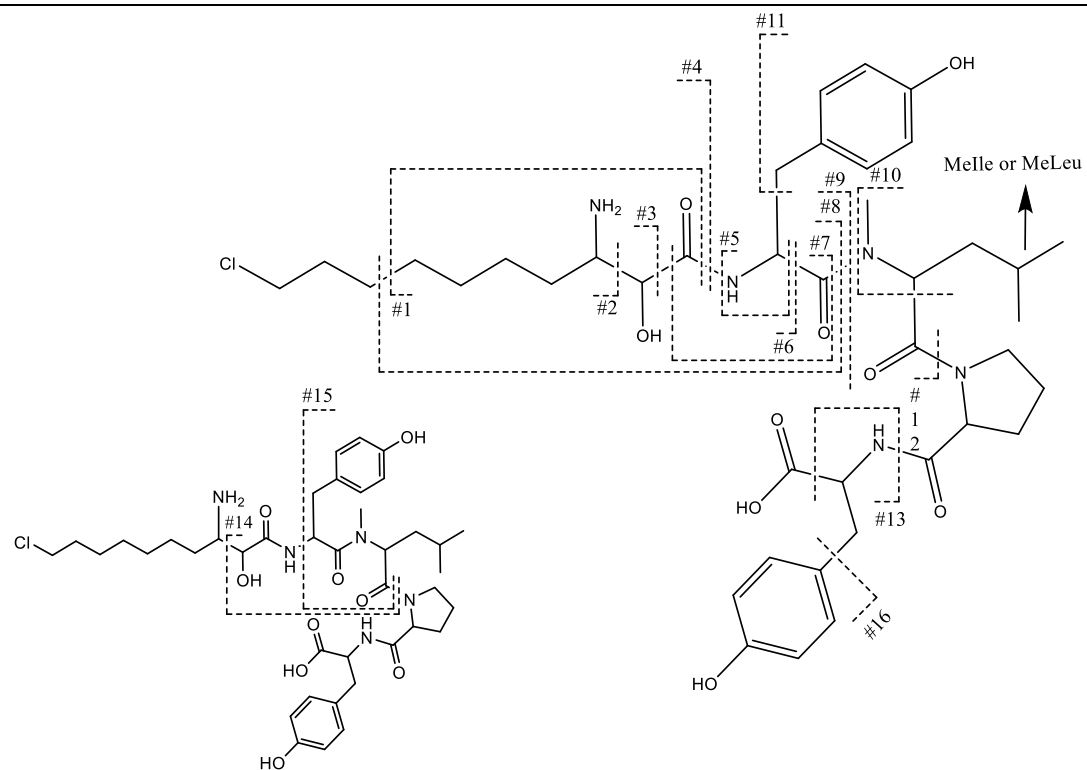Fragment contained in the HCD DDA spectrum; [b]=Fragment ion contained in the CID DDA spectrum.

Figure IV.23 HCD and CID DDA MS^2 spectrum of [M+H]$^+$ ion at *m/z* 768.4547 eluting at 16.66 min.

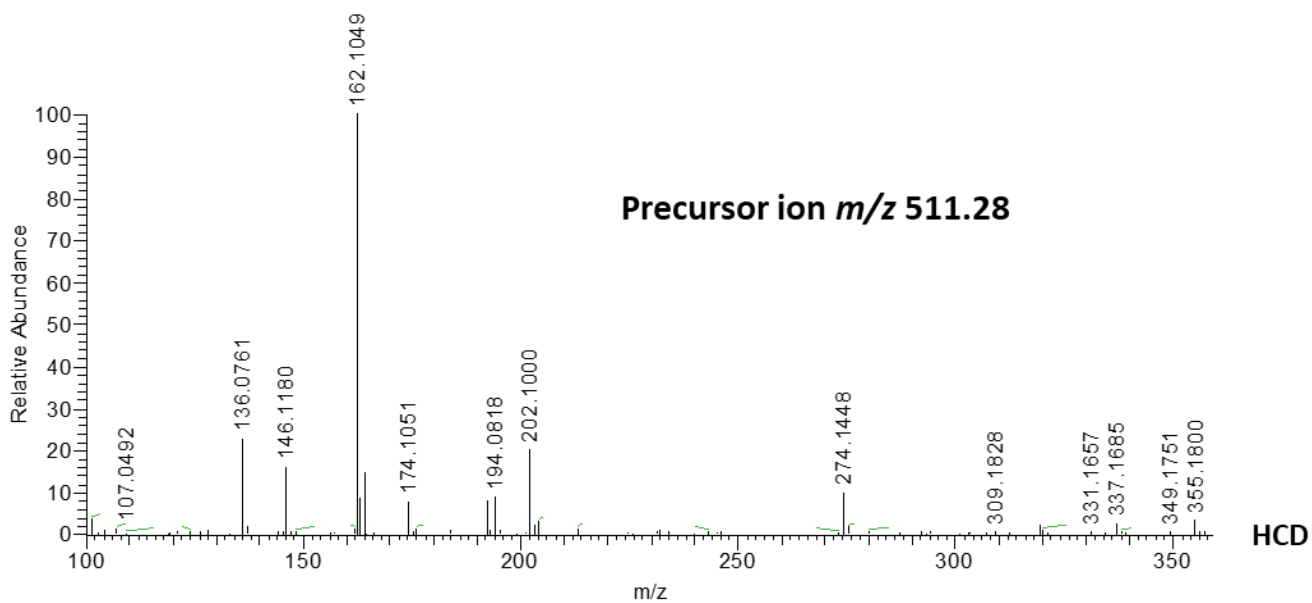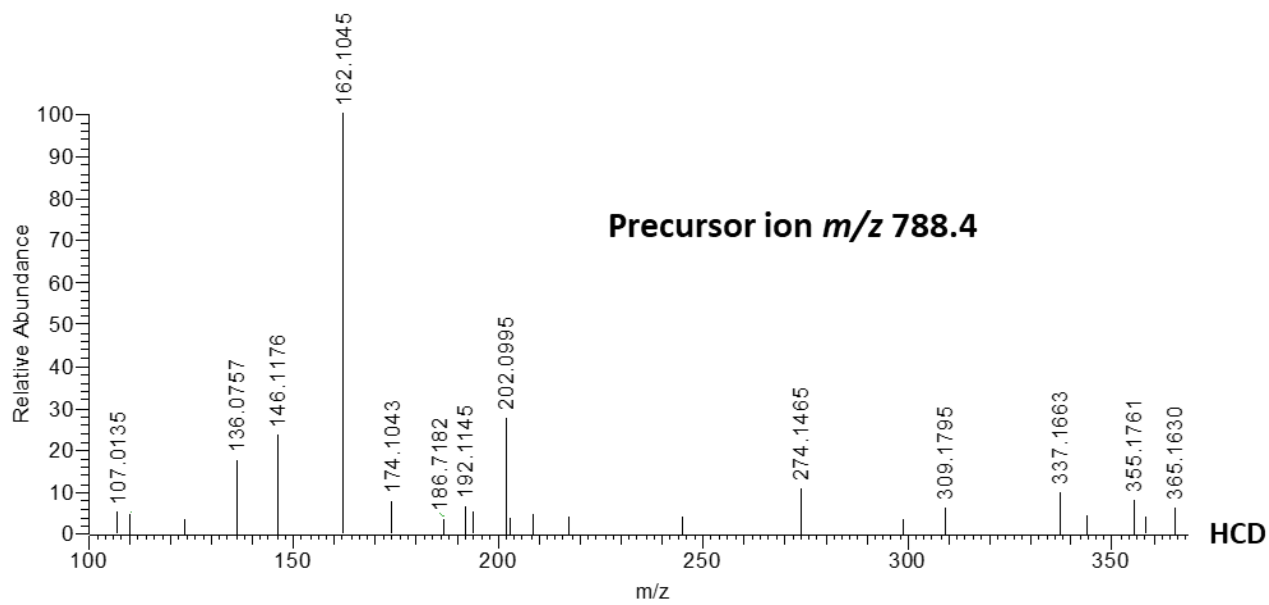**Table IV.15** Assignment of fragment ions of [M+H]$^+$ ion at *m/z* 788.4001 eluting at 16.66 min.

	m/z	Formula	Sequence	Neutral loss
[M+H]$^+$	788.4001	C$_{40}$H$_{59}$O$_9$N$_5$Cl$^+$	[ClAhda^1+Tyr^2+MeIle^3/MeLeu^3+Pro^4+Tyr^5+H]$^+$	
Cleavage				
#1	146.1176[a,b]	C$_7$H$_{16}$O$_2$N$^+$	[ClAhda^1+H-C$_3$H$_5$Cl]$^+$	Tyr^2+MeIle^3/MeLeu^3+Pro^4+Tyr^5+C$_3$H$_5$Cl
#2	162.1045[a,b]	C$_8$H$_{17}$NCl$^+$	[ClAhda^1+H-C$_2$H$_2$O$_2$]$^+$ (ClAhda^1 diagnostic fragment)	Tyr^2+MeIle^3/MeLeu^3+Pro^4+Tyr^5+C$_2$H$_2$O$_2$
#3	192.1145[a,b]	C$_9$H$_{19}$ONCl$^+$	[ClAhda^1+Tyr^2+MeIle^3/MeLeu^3+Pro^4+Tyr^5+H]$^+$	Tyr^2+MeIle^3/MeLeu^3+Pro^4+Tyr^5+CO
#4	202.0995[a,b]	C$_{10}$H$_{17}$ONCl$^+$	[ClAhda^1+H-H$_2$O]$^+$	Tyr^2+MeIle^3/MeLeu^3+Pro^4+Tyr^5+H$_2$O
	174.1043[a,b]	C$_9$H$_{17}$NCl$^+$	[ClAhda^1+H-H$_2$O-CO]$^+$	Tyr^2+MeIle^3/MeLeu^3+Pro^4+Tyr^5+H$_2$O+CO
#5	136.0757[a]	C$_8$H$_{10}$ON$^+$	[Tyr^2+H-CO]$^+$ (Tyr^2 immonium ion)	ClAhda^1+MeIle^3/MeLeu^3+Pro^4+Tyr^5+CO
#6	355.1800[a,b]	C$_{18}$H$_{28}$O$_3$N$_2$Cl$^+$	[ClAhda^1+Tyr^2+H-CO]$^+$	MeIle^3/MeLeu^3+Pro^4+Tyr^5+CO
	337.1663[a,b]	C$_{18}$H$_{26}$O$_2$N$_2$Cl$^+$	[ClAhda^1+Tyr^2+H-CO-H$_2$O]$^+$	MeIle^3/MeLeu^3+Pro^4+Tyr^5+CO+H$_2$O
#7	194.0807[a]	C$_{10}$H$_{12}$O$_3$N$^+$	[Tyr^2+H+CO]$^+$	ClAhda^1+MeIle^3/MeLeu^3+Pro^4+Tyr^5-CO
#8	309.1795[a,b]	C$_{16}$H$_{25}$O$_4$N$_2$]$^+$	[ClAhda^1+Tyr^2+H-C$_3$H$_5$Cl (Part of ClAhda^1)]$^+$	MeIle^3/MeLeu^3+Pro^4+Tyr^5+C$_3$H$_5$Cl
#9	383.1729[b]	C$_{19}$H$_{28}$O$_4$N$_2$Cl$^+$	[ClAhda^1+Tyr^2+H]$^+$	MeIle^3/MeLeu^3+Pro^4+Tyr^5
	365.163[a,b]	C$_{19}$H$_{26}$O$_3$N$_2$Cl$^+$	[ClAhda^1+Tyr^2+H-H$_2$O]$^+$	MeIle^3/MeLeu^3+Pro^4+Tyr^5+H$_2$O
#10	100.1121[a]	C$_6$H$_{14}$N$^+$	[MeIle^3/MeLeu^3+H-CO]$^+$ (MeIle^3/MeLeu^3 immonium ion)	ClAhda^1+Tyr^2+Pro^4+Tyr^5+CO
#11	107.0492[a]	C$_7$H$_7$O$^+$	[Tyr^2+H-C$_2$H$_2$NO]$^+$ (4-Hydroxybenzyl ion)	ClAhda^1+MeIle^3/MeLeu^3+Pro^4+Tyr^5+C$_2$H$_2$NO
#12	510.2728[b]	C$_{26}$H$_{41}$O$_5$N$_3$Cl$^+$	[ClAhda^1+Tyr^2+MeIle^3/MeLeu^3+H]$^+$	Pro^4+Tyr^5
	492.2623[b]	C$_{26}$H$_{39}$O$_4$N$_3$Cl$^+$	[ClAhda^1+Tyr^2+MeIle^3/MeLeu^3+H-H$_2$O]$^+$	Pro^4+Tyr^5+H$_2$O
	482.2778[b]	C$_{25}$H$_{41}$O$_4$N$_3$Cl$^+$	[ClAhda^1+Tyr^2+MeIle^3/MeLeu^3+H-CO]$^+$	Pro^4+Tyr^5+CO
	466.2847[b]	C$_{25}$H$_{41}$O$_3$N$_3$Cl$^+$	[ClAhda^1+Tyr^2+MeIle^3/MeLeu^3+H-CO-OH]$^+$	Pro^4+Tyr^5+CO+OH
#13	136.0757[a]	C$_8$H$_{10}$ON$^+$	[Tyr^5+H-CO$_2$]$^+$ (Tyr^5 immonium ion)	ClAhda^1+Tyr^2+MeIle^3/MeLeu^3+Pro^4+CO$_2$
#14	349.1751[b]	C$_{18}$H$_{25}$O$_5$N$_2^+$	[C$_2$H$_2$O$_2$ (Part of ClAhda^1)+Tyr^2+MeIle^3/MeLeu^3+H]$^+$	ClAhda^1+Pro^4+Tyr^5-C$_2$H$_2$O$_2$
	331.165[a,b]	C$_{18}$H$_{23}$O$_4$N$_2^+$	[C$_2$H$_2$O$_2$ (Part of ClAhda^1)+Tyr^2+MeIle^3/MeLeu^3+H-H$_2$O]$^+$	ClAhda^1+Pro^4+Tyr^5-C$_2$H$_2$O$_2$+H$_2$O
#15	274.1439[a,b]	C$_{16}$H$_{20}$O$_3$N$^+$	[Tyr^2+MeIle^3/MeLeu^3+H-NH$_2$]$^+$	ClAhda^1+ Pro^4+Tyr^5+NH$_2$
#16	107.0492[a]	C$_7$H$_7$O$^+$	[Tyr^5+H-C$_2$H$_2$NO$_2$]$^+$ (4-Hydroxybenzyl ion)	ClAhda^1+Tyr^2+MeIle^3/MeLeu^3+Pro^4+C$_2$H$_2$NO$_2$

a=Fragment contained in the HCD DDA spectrum; b=Fragment ion contained in the CID DDA spectrum.

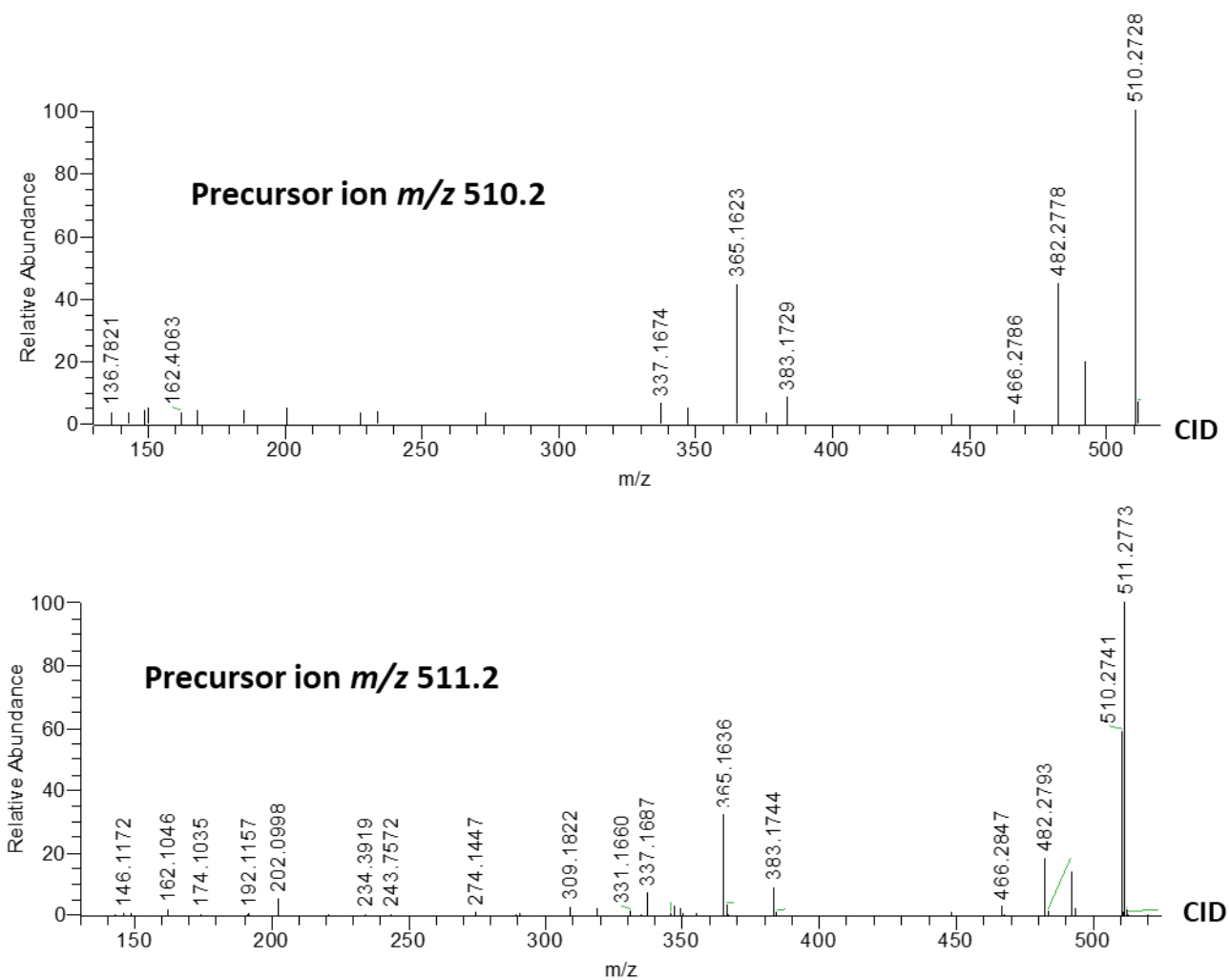**Precursor ion *m/z* 788.4**

Precursor ion *m/z* 511.28

Figure IV.24 HCD and CID DDA MS^2 spectra of [M+H]$^+$ ion at *m/z* 788.4001 eluting at 16.66 min.

Table IV.16 Assignment of fragment ions of [M+H]$^+$ ion at *m/z* 822.3603 eluting at 17.20 min.

	m/z	Formula	Sequence	Neutral loss
[M+H]$^+$	822.3603	C$_{40}$H$_{58}$O$_9$N$_5$Cl$_2$$^+$	[Cl$_2$Ahda^1+Tyr^2+MeIle^3/MeLeu^3+Pro^4+Tyr^5+H]$^+$	
Cleavage				
#1	213.1228^a	C$_{10}$H$_{17}$O$_3$N$_5$$^+$	[Cl$_2$Ahda^1+Tyr^2+H-C$_2$H$_2$Cl$_2$ (Part of Cl$_2$Ahda)-C$_7$H$_7$O (4-Hydroxybenzyl)]$^+$	MeIle^3/MeLeu^3+Pro^4+Tyr^5+C$_2$H$_2$Cl$_2$+C$_7$H$_7$O
#2	146.1178^a	C$_7$H$_{16}$O$_2$N$^+$	[Cl$_2$Ahda^1+H-C$_3$H$_4$Cl$_2$]$^+$	Tyr^2+MeIle^3/MeLeu^3+Pro^4+Tyr^5+C$_3$H$_4$Cl$_2$
#3	196.0658^{a,b}	C$_8$H$_{16}$NCl$_2$$^+$	[Cl$_2$Ahda^1+H-C$_2$H$_2$O$_2$]$^+$ (Cl$_2$Ahda^1 diagnostic fragment)	Tyr^2+MeIle^3/MeLeu^3+Pro^4+Tyr^5+C$_2$H$_2$O$_2$
	160.0889^a	C$_8$H$_{15}$NCl$^+$	[Cl$_2$Ahda^1+H-C$_2$H$_2$O$_2$-HCl]$^+$	Tyr^2+MeIle^3/MeLeu^3+Pro^4+Tyr^5+C$_2$H$_2$O$_2$+HCl
#4	226.0768^{a,b}	C$_9$H$_{18}$ONCl$_2$$^+$	[Cl$_2$Ahda^1+H-CO]$^+$	Tyr^2+MeIle^3/MeLeu^3+Pro^4+Tyr^5+CO
	190.0995^a	C$_9$H$_{17}$ONCl$^+$	[Cl$_2$Ahda^1+H-CO-HCl]$^+$	Tyr^2+MeIle^3/MeLeu^3+Pro^4+Tyr^5+CO+HCl
	172.0889^a	C$_9$H$_{15}$NCl$^+$	[Cl$_2$Ahda^1+H-CO-HCl-H$_2$O]$^+$	Tyr^2+MeIle^3/MeLeu^3+Pro^4+Tyr^5+CO+HCl+H2O
#5	236.0609^{a,b}	C$_{10}$H$_{16}$ONCl$_2$$^+$	[Cl$_2$Ahda^1+H-H$_2$O]$^+$	Tyr^2+MeIle^3/MeLeu^3+Pro^4+Tyr^5+H$_2$O
	208.0660^{a,b}	C$_9$H$_{16}$NCl$_2$	[Cl$_2$Ahda^1+H-H$_2$O-CO]$^+$	Tyr^2+MeIle^3/MeLeu^3+Pro^4+Tyr^5+H$_2$O+CO
	200.0844^{a,b}	C$_{10}$H$_{15}$ONCl$^+$	[Cl$_2$Ahda^1+H-H$_2$O-HCl]$^+$	Tyr^2+MeIle^3/MeLeu^3+Pro^4+Tyr^5+H$_2$O+HCl
#6	136.0758^a	C$_8$H$_{10}$ON$^+$	[Tyr^2+H-CO]$^+$ (Tyr^2 immonium ion)	Cl$_2$Ahda^1+MeIle^3/MeLeu^3+Pro^4+Tyr^5+CO
#7	389.1393^{a,b}	C$_{18}$H$_{27}$O$_3$N$_2$Cl$_2$$^+$	[Cl$_2$Ahda^1+Tyr^2+H-CO]$^+$	MeIle^3/MeLeu^3+Pro^4+Tyr^5+CO
	371.1295^{a,b}	C$_{18}$H$_{25}$O$_2$N$_2$Cl$_2$$^+$	[Cl$_2$Ahda^1+Tyr^2+H-CO-H$_2$O]$^+$	MeIle^3/MeLeu^3+Pro^4+Tyr^5+CO-H$_2$O
#8	194.0814^a	C$_{10}$H$_{12}$O$_3$N$^+$	[Tyr^2+H+CO]$^+$	Cl$_2$Ahda^1+ MeIle^3/MeLeu^3+Pro^4+Tyr^5-CO
	176.0712^a	C$_{10}$H$_{10}$O$_2$N$^+$	[Tyr^2+H+CO-H$_2$O]$^+$	Cl$_2$Ahda^1+ MeIle^3/MeLeu^3+Pro^4+Tyr^5-CO+H$_2$O
	148.0757^a	C$_9$H$_{10}$ON$^+$	[Tyr^2+H-CO-H$_2$O]$^+$	Cl$_2$Ahda^1+ MeIle^3/MeLeu^3+Pro^4+Tyr^5+CO+H$_2$O
#9	107.0489^a	C$_7$H$_7$O$^+$	[Tyr^2+H-C$_2$H$_2$NO]$^+$ (4-Hydroxybenzyl ion)	Cl$_2$Ahda^1+MeIle^3/MeLeu^3+Pro^4+Tyr^5+C$_2$H$_2$NO
#10	100.1121^a	C$_6$H$_{14}$N$^+$	[MeIle^3/MeLeu^3+H-CO]$^+$ (MeIle^3/MeLeu^3 immonium ion)	Cl$_2$Ahda^1+Tyr^2+Pro^4+Tyr^5+CO
#11	544.2332^b	C$_{26}$H$_{40}$O$_5$N$_3$Cl$_2$$^+$	[Cl$_2$Ahda^1+Tyr^2+MeIle^3/MeLeu^3+H]$^+$	Pro^4+Tyr^5
	526.2232^b	C$_{26}$H$_{38}$O$_4$N$_3$Cl$_2$$^+$	[Cl$_2$Ahda^1+Tyr^2+MeIle^3/MeLeu^3+H-H$_2$O]$^+$	Pro^4+Tyr^5+H$_2$O
	516.2385^b	C$_{25}$H$_{40}$O$_4$N$_3$Cl$_2$$^+$	[Cl$_2$Ahda^1+Tyr^2+MeIle^3/MeLeu^3+H-CO]$^+$	Pro^4+Tyr^5+CO
	500.2445^b	C$_{25}$H$_{40}$O$_3$N$_3$Cl$_2$$^+$	[Cl$_2$Ahda^1+Tyr^2+MeIle^3/MeLeu^3+H-CO-OH]$^+$	Pro^4+Tyr^5+CO+OH
#12	136.0758^a	C$_8$H$_{10}$ON$^+$	[Tyr^5+H-CO$_2$]$^+$ (Tyr^5 immonium ion)	Cl$_2$Ahda^1+Tyr^2+MeIle^3/MeLeu^3+Pro^4+CO$_2$
#13	309.1809^b	C$_{16}$H$_{25}$O$_4$N$_2$$^+$	[Cl$_2$Ahda^1+Tyr^2+H-C$_3$H$_4$Cl$_2$ (Part of Cl$_2$Ahda)]$^+$	MeIle^3/MeLeu^3+Pro^4+Tyr^5+C$_3$H$_4$Cl$_2$
	274.1443^{a,b}	C$_{16}$H$_{20}$O$_3$N$^+$	[Cl$_2$Ahda^1+Tyr^2+H-C$_3$H$_4$Cl$_2$ (Part of Cl$_2$Ahda)-H$_2$O-NH$_3$]$^+$	MeIle^3/MeLeu^3+Pro^4+Tyr^5+C$_3$H$_4$Cl$_2$+H$_2$O+NH$_3$
#14	417.1340^b	C$_{19}$H$_{27}$O$_4$N$_2$Cl$_2$$^+$	[Cl$_2$Ahda^1+Tyr^2+H]$^+$	MeIle^3/MeLeu^3+Pro^4+Tyr^5
	399.1234^{a,b}	C$_{19}$H$_{25}$O$_3$N$_2$Cl$_2$$^+$	[Cl$_2$Ahda^1+Tyr^2+H-H$_2$O]$^+$	MeIle^3/MeLeu^3+Pro^4+Tyr^5-H$_2$O
#15	107.0489^a	C$_7$H$_7$O$^+$	[Tyr^5+H-C$_2$H$_2$NO$_2$]$^+$ (4-Hydroxybenzyl ion)	Cl$_2$Ahda^1+Tyr^2+MeIle^3/MeLeu^3+Pro^4+C$_2$H$_2$NO$_2$
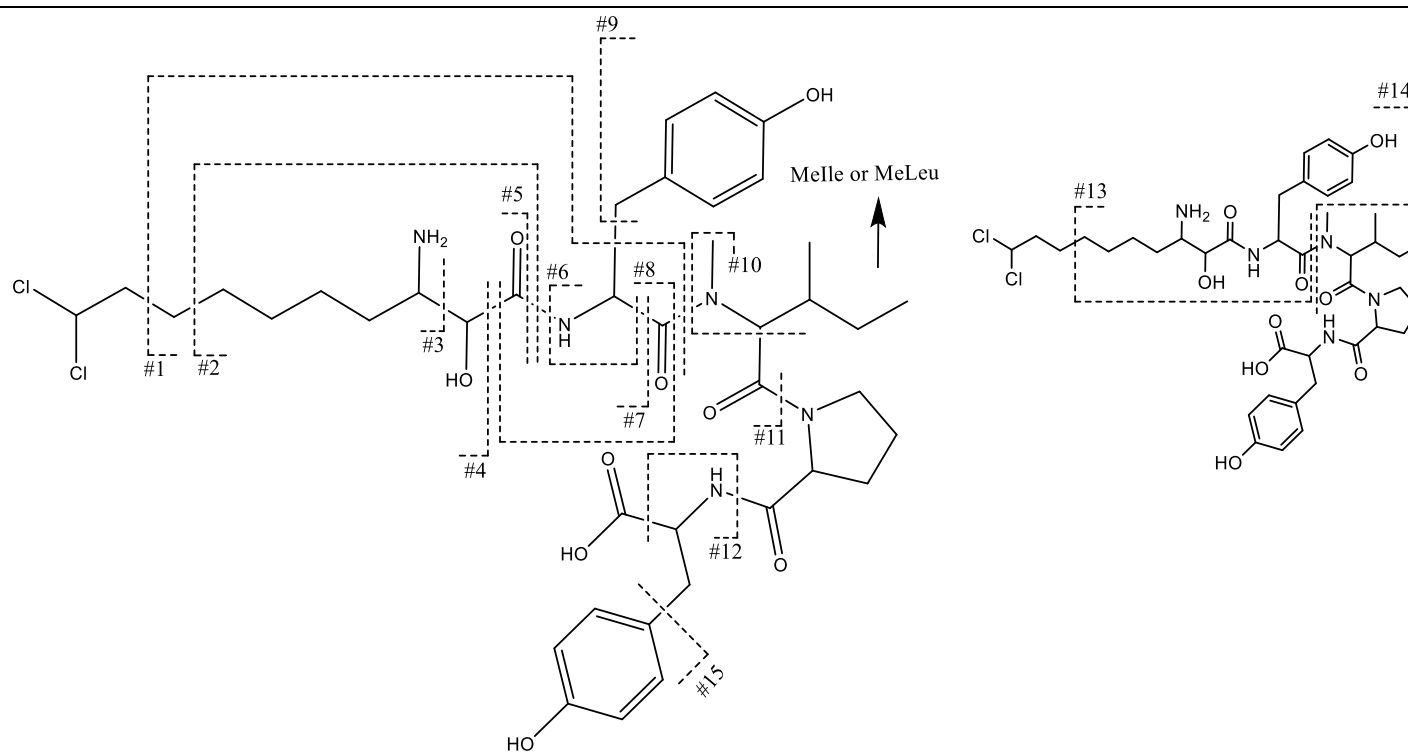
ᵃ=Fragment contained in the HCD DDA spectrum; ᵇ=Fragment ion contained in the CID DDA spectrum.
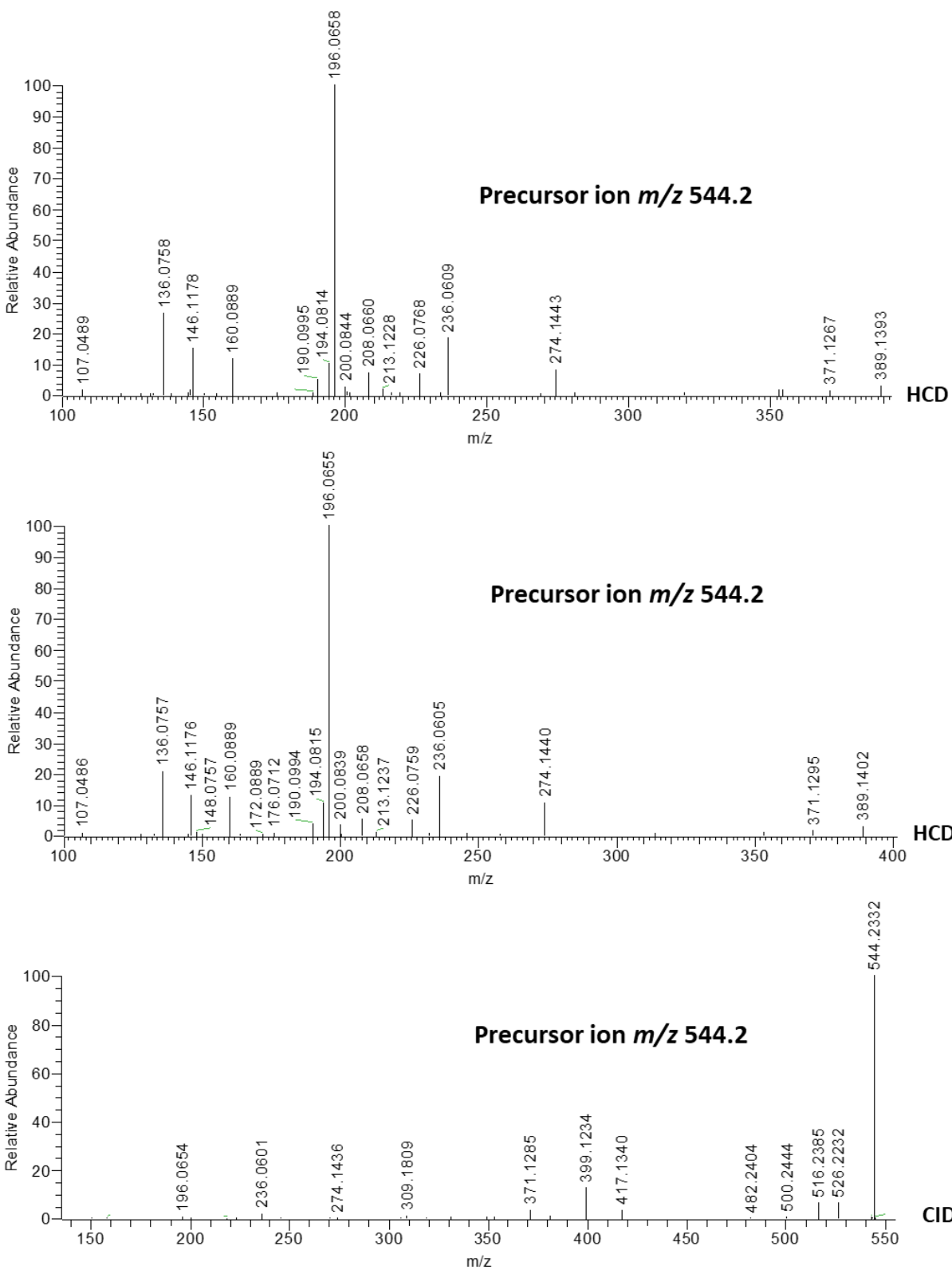
Figure IV.25 HCD and CID DDA MS^2 spectra of [M+H]$^+$ ion at *m/z* 822.3603 eluting at 17.20 min.

2.4.2 Determination of anabaenopeptins

The implemented analytical strategy was further applied for the investigation of APs in the cyanobacterial biomass sample. The structural motif of these secondary metabolites is represented by a Lys residue in position 2 (**Fig.I.21**), which is conserved in all analogues and it can be clearly evidenced by HRMS^2 experiments due to the formation of diagnostic fragment ions at *m/z* 84.0808 ($C_5H_{10}N^+$) and 129.1025 ($C_6H_{13}N_2O^+$) corresponding to Lys immonium ion and [Lys+H-H$_2$O]$^+$ ion, respectively [45-46]. However, a large variety of secondary metabolites extracted from the cyanobacterial biomass could contain a Lys residue in their structure, thus the detection of characteristic fragments of Lys represents only a first clue towards the identification of APs, making so the full interpretation of the HRMS^2 spectra a prerequisite.

The XIC of the fragment at *m/z* 129.1025 from the HCD DDA spectra highlighted the presence of four chromatographic peaks associated with the fragmentation of [M+H]$^+$ precursor ions having accurate masses and molecular formulae consistent with those of APA (*m/z* 844.4240, $C_{44}H_{58}O_{10}N_7^+$), Oscillamide Y (*m/z* 858.4396, $C_{45}H_{60}O_{10}N_7^+$), APB (*m/z* 837.4625, $C_{41}H_{61}O_9N_{10}^+$) and APF (*m/z* 851.4777, $C_{42}H_{63}O_9N_{10}^+$; **Fig.IV.26**). The identity of each AP was then confirmed by interpreting the relevant HCD and CID HRMS^2 DDA spectra, which contained a variety of fragments associated with individual residues and multiple amino acids sequences. For APA - [Tyr^1+CO+Lys^2+Val^3+HTyr^4+MeAla^5+Phe^6+H]$^+$ - **(Table IV.17)**, Tyr^1, HTyr^4 and Phe^6 were individually identified through fragments #21 and 24, #22 and 25, and #23 and 27, respectively; similarly Lys^2 through the diagnostic ion at *m/z* 129.1025 (#26) and MeAla^5 through fragment at *m/z* 114.0505 (MeAla+CO, #28). Moreover, the presence of Tyr^1, HTyr^4 and MeAla^5 was further corroborated through specific neutral losses from the precursor ion due to fragments #3, 2 and 1, respectively. The exact position of each residue instead, was confirmed through a cross-interpretation of different fragments. The sequence [CO+Lys^2+Val^3+Phe^6+H]$^+$ was confirmed through fragments #13, 15, 18 and 19, whilst the combined interpretation with fragments #20 confirmed the presence of MeAla^5. Fragments #17 and 16 corroborated HTyr^4 and Val^3, respectively, whilst fragment #14 confirmed Tyr^1 with the ureido linkage. Further confirmation was achieved through fragments #4-12.

The same approach was applied for the interpretation of HRMS^2 spectra of oscillamide Y - [Tyr^1+CO+Lys^2+Ile^3+HTyr^4+MeAla^5+Phe^6+H]$^+$ - which differs from APA for the presence of Ile^3, thus showing a mass difference of 14 Da (CH$_2$ unit). Therefore, the MS^2 spectra of oscillamide

Y were found to contain a number of fragments superimposable to those of APA, namely those that do not involve the presence of Ile^3 (#6, 8, 10, 13, 19, 20 and 21), and contrarily, a large range of fragments (#1-5, 7,9,11,12, 14-18) that differed for 14 Da than those of APA **(Table IV.18)**.
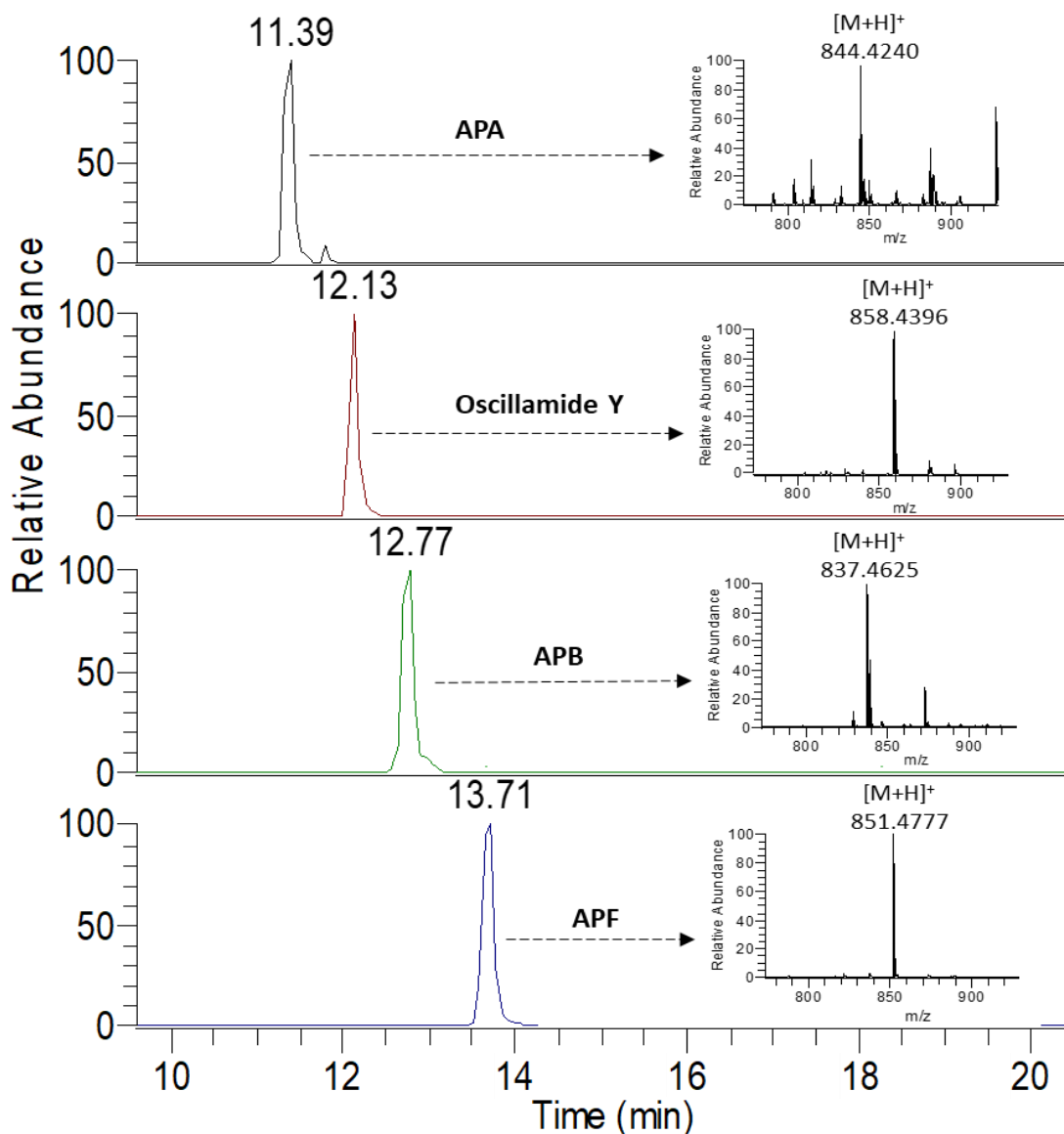
Figure IV.26 XIC of [M+H]$^+$ ion of anabaenopeptin A (APA), oscillamide Y, APB and APF with relevant full-scan HRM spectrum.
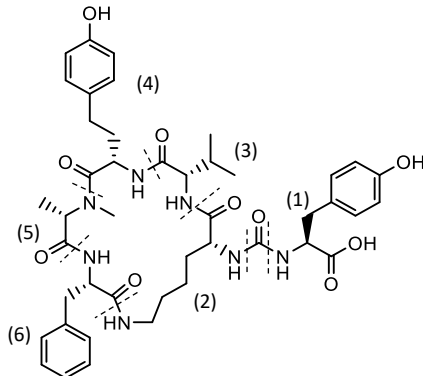
APB and APF instead, respectively differ from APA and oscillamide Y for the presence of Arg[1]. This structural variation provide significatively different fragmentation spectra, which were

dominated by the fragment ion at m/z 201.0979 ($C_7H_{13}O_3N_4^+$) related to $[Arg^1+H+CO]^+$, while the diagnostic fragment of Lys^2 (m/z 129.1025) turned out to be 2000-fold less intense. Overall, the identity of APB and APF was confirmed through the same analytical strategy adopted for APA and oscillamide Y, since they differ for 18 Da due to the presence of Val^3 and Ile^3, respectively **(Table IV.19-20)**.

Table IV.17 Assignment of fragment ions contained in CID and HCD spectra of APA.

	m/z	Formula	Sequence	Neutral loss
			Anabaenopeptin A	
$[M+H]^+$	844.4240	$C_{44}H_{58}O_{10}N_7^+$	$[Tyr^1+CO+Lys^2+Val^3+HTyr^4+MeAla^5+Phe^6+H]^+$	
	826.4132[b]	$C_{44}H_{56}O_9N_7^+$		H_2O
	816.4286[b]	$C_{43}H_{58}O_9N_7^+$		CO
	808.4019[b]	$C_{44}H_{54}O_8N_7^+$		$2H_2O$
	798.4211[b]	$C_{43}H_{56}O_8N_7^+$		$CO+H_2O$

#	m/z	Formula	Sequence	Neutral loss
1	759.3691[b]	$C_{40}H_{51}O_9N_6^+$	$[Tyr^1+CO+Lys^2+Val^3+HTyr^4+Phe^6+H]^+$	$MeAla^5$
	741.3582[b]	$C_{40}H_{49}O_8N_6^+$	$[Tyr^1+CO+Lys^2+Val^3+HTyr^4+Phe^6+H-H_2O]^+$	$MeAla^5+H_2O$
2	667.3450[b]	$C_{34}H_{47}O_8N_6^+$	$[Tyr^1+CO+Lys^2+Val^3+MeAla^5+Phe^6+H]^+$	$HTyr^4$
3	663.3498[b]	$C_{35}H_{47}O_7N_6^+$	$[CO+Lys^2+Val^3+HTyr^4+MeAla^5+Phe^6+H]^+$	Tyr^1
	635.3550[b]	$C_{34}H_{47}O_6N_6^+$	$[CO+Lys^2+Val^3+HTyr^4+MeAla^5+Phe^6+H-CO]^+$	Tyr^1+CO
	637.3702[b]	$C_{34}H_{49}O_6N_6^+$	$[CO+Lys^2+Val^3+HTyr^4+MeAla^5+Phe^6+H-CO+H_2]^+$	Tyr^1+CO-H_2
	619.3606[b]	$C_{34}H_{47}O_5N_6^+$	$[CO+Lys^2+Val^3+HTyr^4+MeAla^5+Phe^6+H-CO+H_2-H_2O]^+$	$Tyr^1+CO-H_2+H_2O$
4	649.3338[b]	$C_{34}H_{45}O_7N_6^+$	$[Tyr^1+CO+Lys^2+Val^3+MeAla^5+Phe^6+H+CO-CO_2]^+$	$HTyr^4-CO+CO_2$
5	612.3019[b]	$C_{31}H_{42}O_8N_5^+$	$[Tyr^1+CO+Lys^2+Val^3+HTyr^4+H]^+$	$MeAla^5+Phe^6$
6	568.2768[b]	$C_{29}H_{38}O_7N_5^+$	$[Tyr^1+CO+Lys^2+MeAla^5+Phe^6+H-CO+CO]^+$	$Val^3+HTyr^4+CO-CO$
7	550.3030[b]	$C_{30}H_{40}O_5N_5^+$	$[Lys^2+Val^3+HTyr^4+MeAla^5+Phe^6+H-C_4H_6NO$ (Part of Lys^2)$]^+$	$Tyr^1+CO+C_4H_6NO$
	536.2855[b]	$C_{29}H_{38}O_5N_5^+$	$[Lys^2+Val^3+HTyr^4+MeAla^5+Phe^6+H-C_5H_8NO$ (Part of Lys^2)$]^+$	$Tyr^1+CO+C_5H_8NO$
8	550.2653[b]	$C_{29}H_{36}O_6N_5^+$	$[Tyr^1+CO+Lys^2+MeAla^5+Phe^6+H-H_2O]^+$	$Val^3+HTyr^4+H_2O$
	540.2801[a]	$C_{28}H_{38}O_6N_5^+$	$[Tyr^1+CO+Lys^2+MeAla^5+Phe^6+H-CO]^+$	Val^3+HTyr^4+CO
9	509.2741[b]	$C_{28}H_{37}O_5N_4^+$	$[Val^3+HTyr^4+MeAla^5+Phe^6+H]^+$	$Tyr^1+CO+Lys^2$
10	483.2234[a]	$C_{25}H_{31}O_6N_4^+$	$[Tyr^1+CO+Lys^2+Phe^6+H]^+$	$Val^3+HTyr^4+MeAla^5$
	455.2301[a]	$C_{24}H_{31}O_5N_4^+$	$[Tyr^1+CO+Lys^2+Phe^6+H-CO]^+$	$Val^3+HTyr^4+MeAla^5-CO$
11	460.2930[b]	$C_{24}H_{38}O_4N_5^+$	$[Lys^2+Val^3+MeAla^5+Phe^6+H]^+$	$Tyr^1+CO+HTyr^4$
12	405.2134[a]	$C_{20}H_{29}O_5N_4^+$	$[CO+Lys^2+MeAla^5+Phe^6+H+CO-CH_3]^+$	$Tyr^1+Val^3+HTyr^4-2CO+CH_3$
13	403.2345[a]	$C_{21}H_{31}O_4N_4^+$	$[CO+Lys^2+Val^3+Phe^6+H]^+$	$Tyr^1+CO+HTyr^4+MeAla^5$
14	389.2173[a]	$C_{20}H_{29}O_4N_4^+$	$[Tyr^1+CO+Lys^2+Val^3+H-CO_2]^+$	$HTyr^4+MeAla^5+Phe^6+CO_2$
15	373.2239[a]	$C_{20}H_{29}O_3N_4^+$	$[Lys^2+Val^3+Phe^6+H]^+$	$Tyr^1+CO+HTyr^4+MeAla^5$
16	362.2087[a]	$C_{19}H_{28}O_4N_3^+$	$[Val^3+HTyr^4+MeAla^5+H]^+$	$Tyr^1+CO+Lys^2+Phe^6$
17	263.1389[a]	$C_{14}H_{19}O_3N_2^+$	$[HTyr^4+MeAla^5+H]^+$	$Tyr^1+CO+Lys^2+Val^3+Phe^6$
	235.1449[a]	$C_{13}H_{19}O_2N_2^+$	$[HTyr^4+MeAla^5+H-CO]^+$	$Tyr^1+CO+Lys^2+Val^3+Phe^6+CO$
18	259.1429[a]	$C_{15}H_{19}O_2N_2^+$	$[Lys^2+Phe^6+H-NH_3]^+$	$Tyr^1+CO+Val^3+HTyr^4+MeAla^5+NH_3$

19	254.1494[a]	$C_{12}H_{20}O_3N_3^+$	$[CO+Lys^2+Val^3+H]^+$	$Tyr^1+ HTyr^4+MeAla^5+Phe^6$
	226.1560[a]	$C_{11}H_{20}O_2N_3^+$	$[CO+Lys^2+Val^3+H-CO]^+$	$Tyr^1+ HTyr^4+MeAla^5+Phe^6+CO$
20	233.1288[a]	$C_{13}H_{17}O_2N_2^+$	$[MeAla^5+Phe^6+H]^+$	$Tyr^1+CO+Lys^2+Val^3+HTyr^4$
	205.1340[a]	$C_{12}H_{17}ON_2^+$	$[MeAla^5+Phe^6+H-CO]^+$	$Tyr^1+CO+Lys^2+Val^3+HTyr^4+CO$
21	182.0814[a]	$C_9H_{12}O_3N^+$	$[Tyr^1+H]^+$	$CO+Lys^2+Val^3+HTyr^4+MeAla^5+Phe^6$
22	180.1013[a]	$C_{10}H_{14}O_2N^+$	$[HTyr^4+H]^+$	$Tyr^1+CO+Lys^2+Val^3+MeAla^5+Phe^6$
23	150.0915[a]	$C_9H_{12}ON^+$	$[Phe^6+H]^+$	$Tyr^1-CO+Lys^2+Val^3+HTyr^4+MeAla^5$
24	150.0915[a]	$C_9H_{12}ON^+$	$[HTyr^4+H-CO]^+$ ($HTyr^4$ immonium ion)	$Tyr^1-CO+Lys^2+Val^3++MeAla^5+Phe^6+CO$
25	136.0758[a]	$C_8H_{10}ON^+$	$[Tyr^1+H-CO]^+$ (Tyr^1 immonium ion)	$CO+Lys^2+Val^3+HTyr^4+MeAla^5+Phe^6+CO$
26	129.1025[a]	$C_6H_{13}ON_2^+$	$[Lys^2+H]^+$	$Tyr^1-CO+ Val^3+HTyr^4+MeAla^5+Phe^6$
27	120.0808[a]	$C_8H_{10}N^+$	$[Phe^6+H-CO]^+$ Phe^6 immonium ion)	$Tyr^1-CO+Lys^2+Val^3+HTyr^4+MeAla^5+CO$
28	114.0550[a]	$C_5H_8O_2N^+$	$[MeAla^5+H+CO]^+$	$Tyr^1-CO+Lys^2+Val^3+HTyr^4+Phe^6-CO$
29	107.0488[a]	$C_7H_7O^+$	$[Tyr^1+H-C_2H_2NO_2]^+$ (4-Hydroxybenzyl ion)	$CO+Lys^2+Val^3+HTyr^4+MeAla^5+Phe^6+ C_2H_2NO_2$
30	107.0488[a]	$C_7H_7O^+$	$[HTyr^4+H-C_3H_4NO]^+$ (4-Hydroxybenzyl ion)	$Tyr^1+CO+Lys^2+Val^3+MeAla^5+Phe^6+ C_3H_4NO$

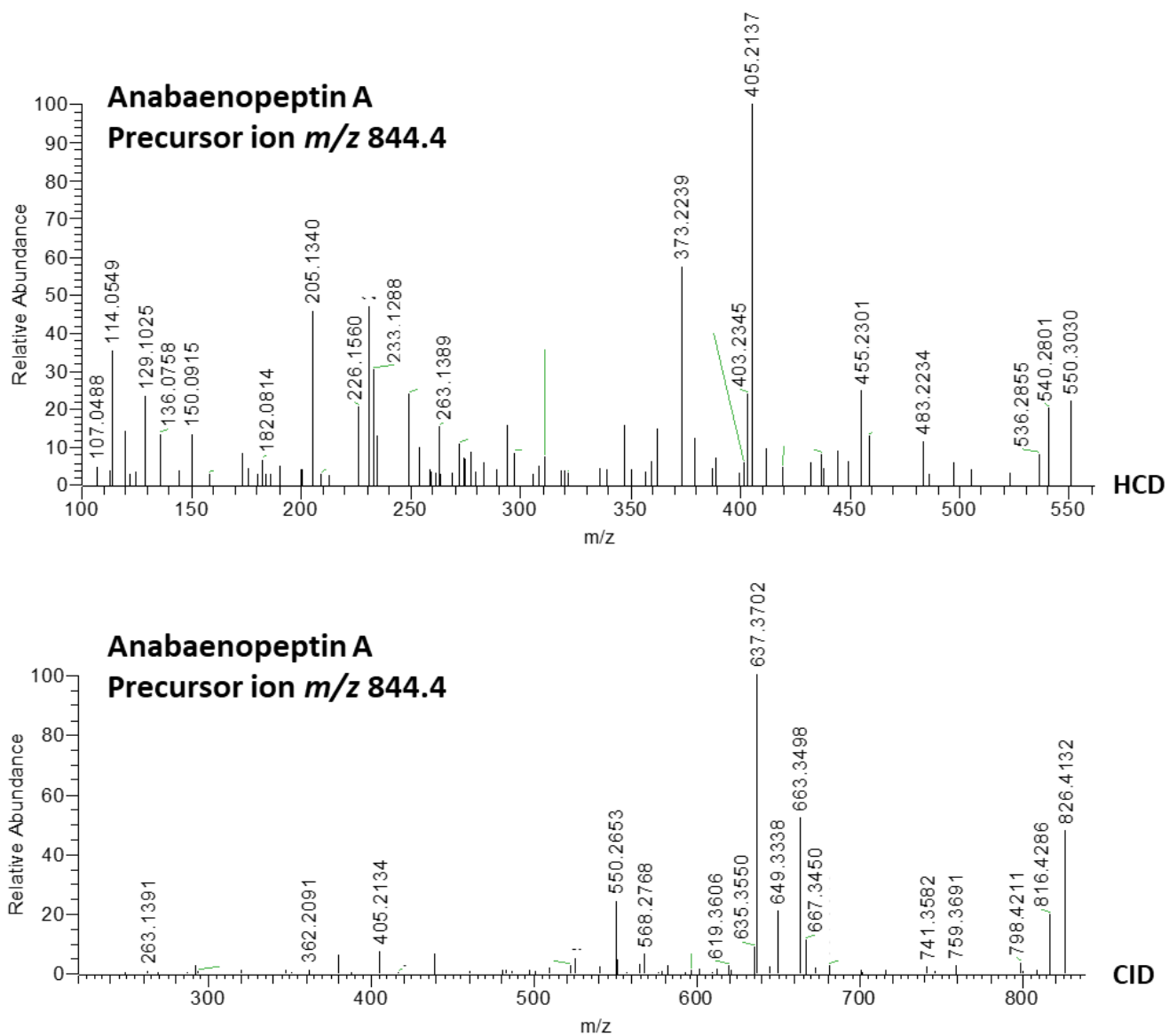[a]=Fragment contained in the HCD DDA spectrum; [b]=Fragment ion contained in the CID DDA spectrum.

Figure IV.27 HCD and CID DDA MS^2 spectrum of anabaenopeptin A.

Table IV.18 Assignment of fragment ions contained in CID and HCD spectra of oscillamide Y.

	m/z	Formula	Sequence	Neutral loss
[M+H]+	858.4396	$C_{45}H_{60}O_{10}N_7^+$	$[Tyr^1+CO+Lys^2+Ile^3+HTyr^4+MeAla^5+Phe^6+H]^+$	
	840.4296[b]	$C_{45}H_{58}O_9N_7^+$		H_2O
	830.4451[b]	$C_{44}H_{60}O_9N_7^+$		CO
	822.4152[b]	$C_{45}H_{56}O_8N_7^+$		$2H_2O$
	812.4360[b]	$C_{44}H_{58}O_8N_7^+$		$CO+H_2O$
1	773.3860[b]	$C_{41}H_{53}O_9N_6^+$	$[Tyr^1+CO+Lys^2+Ile^3+HTyr^4+Phe^6+H]^+$	$MeAla^5$
	755.3783[b]	$C_{41}H_{51}O_8N_6^+$	$[Tyr^1+CO+Lys^2+Ile^3+HTyr^4+Phe^6+H-H_2O]^+$	$MeAla^5+H_2O$
2	681.3610[b]	$C_{35}H_{49}O_8N_6^+$	$[Tyr^1+CO+Lys^2+Ile^3+MeAla^5+Phe^6+H]^+$	$HTyr^4$
3	677.3656[b]	$C_{36}H_{49}O_7N_6^+$	$[CO+Lys^2+Ile^3+HTyr^4+MeAla^5+Phe^6+H]^+$	Tyr^1
	649.3711[b]	$C_{35}H_{49}O_6N_6^+$	$[CO+Lys^2+Ile^3+HTyr^4+MeAla^5+Phe^6+H-CO]^+$	Tyr^1+CO
	651.3860[b]	$C_{35}H_{51}O_6N_6^+$	$[CO+Lys^2+Ile^3+HTyr^4+MeAla^5+Phe^6+H-CO+H_2]^+$	Tyr^1+CO-H_2
	633.3746[b]	$C_{35}H_{49}O_5N_6^+$	$[CO+Lys^2+Ile^3+HTyr^4+MeAla^5+Phe^6+H-CO+H_2-H_2O]^+$	$Tyr^1+CO-H_2+H_2O$
4	663.3500[b]	$C_{35}H_{47}O_7N_6^+$	$[Tyr^1+CO+Lys^2+Ile^3+MeAla^5+Phe^6+H+CO-CO_2]^+$	$HTyr^4-CO+CO_2$
5	626.3177[b]	$C_{32}H_{44}O_8N_5^+$	$[Tyr^1+CO+Lys^2+Ile^3+HTyr^4+H]^+$	$MeAla^5+Phe^6$
6	568.2768[b]	$C_{29}H_{38}O_7N_5^+$	$[Tyr^1+CO+Lys^2+MeAla^5+Phe^6+H-CO+CO]^+$	$Ile^3+HTyr^4+CO-CO$
7	564.3180[a]	$C_{31}H_{42}O_5N_5^+$	$[Lys^2+Ile^3+HTyr^4+MeAla^5+Phe^6+H-C_4H_6NO\ (Part\ of\ Lys^2)]^+$	$Tyr^1+CO+C_4H_6NO$
	550.3026[a]	$C_{30}H_{40}O_5N_5^+$	$[Lys^2+Ile^3+HTyr^4+MeAla^5+Phe^6+H-C_5H_8NO\ (Part\ of\ Lys^2)]^+$	$Tyr^1+CO+C_5H_8NO$
8	550.2653[b]	$C_{29}H_{36}O_6N_5^+$	$[Tyr^1+CO+Lys^2+MeAla^5+Phe^6+H-H_2O]^+$	$Ile^3+HTyr^4+H_2O$
	540.2820[a]	$C_{28}H_{38}O_6N_5^+$	$[Tyr^1+CO+Lys^2+MeAla^5+Phe^6+H-CO]^+$	Ile^3+HTyr^4+CO
9	523.2888[b]	$C_{29}H_{39}O_5N_4^+$	$[Ile^3+HTyr^4+MeAla^5+Phe^6+H]^+$	$Tyr^1+CO+Lys^2$
10	483.2234[a]	$C_{25}H_{31}O_6N_4^+$	$[Tyr^1+CO+Lys^2+Phe^6+H]^+$	$Ile^3+HTyr^4+MeAla^5$
	455.2301[a]	$C_{24}H_{31}O_5N_4^+$	$[Tyr^1+CO+Lys^2+Phe^6+H-CO]^+$	$Ile^3+HTyr^4+MeAla^5-CO$
11	474.3053[b]	$C_{25}H_{40}O_4N_5^+$	$[Lys^2+Ile^3+MeAla^5+Phe^6+H]^+$	$Tyr^1+CO+HTyr^4$
12	417.2508[b]	$C_{22}H_{33}O_4N_4^+$	$[Lys^2+Ile^3+Phe^6+H]^+$	$Tyr^1+CO+HTyr^4+MeAla^5$
13	405.2145[a]	$C_{20}H_{29}O_5N_4^+$	$[CO+Lys^2+MeAla^5+Phe^6+H+CO-CH_3]^+$	$Tyr^1+Ile^3+HTyr^4-2CO+CH_3$
14	403.2332[a]	$C_{21}H_{31}O_4N_4^+$	$[Tyr^1+CO+Lys^2+Ile^3+H-CO_2]^+$	$HTyr^4+MeAla^5+Phe^6+CO_2$
15	401.2553[a]	$C_{22}H_{33}O_3N_4^+$	$[Lys^2+Ile^3+HTyr^4+H-H_2O]^+$	$Tyr^1+CO+MeAla^5+Phe^6+H_2O$
16	387.2389[a]	$C_{21}H_{31}O_3N_4^+$	$[Lys^2+Ile^3+Phe^6+H]^+$	$Tyr^1+CO+HTyr^4+MeAla^5$

17	376.2233^a	$C_{20}H_{30}O_4N_3^+$	$[Ile^3+HTyr^4+MeAla^5+H]^+$	$Tyr^1+CO+Lys^2+Phe^6$
18	268.1648^a	$C_{13}H_{22}O_3N_3^+$	$[CO+Lys^2+Ile^3+H]^+$	$Tyr^1+ HTyr^4+MeAla^5+Phe^6$
	240.1710^a	$C_{12}H_{22}O_2N_3^+$	$[CO+Lys^2+Ile^3+H-CO]^+$	$Tyr^1+ HTyr^4+MeAla^5+Phe^6+CO$
19	263.1394^a	$C_{14}H_{19}O_3N_2^+$	$[HTyr^4+MeAla^5+H]^+$	$Tyr^1+CO+Lys^2+Ile^3+Phe^6$
	235.1455^a	$C_{13}H_{19}O_2N_2^+$	$[HTyr^4+MeAla^5+H-CO]^+$	$Tyr^1+CO+Lys^2+Ile^3+Phe^6+CO$
20	259.1429^a	$C_{15}H_{19}O_2N_2^+$	$[Lys^2+Phe^6+H-NH_3]^+$	$Tyr^1+CO+Ile^3+HTyr^4+MeAla^5+NH_3$
21	233.1288^a	$C_{13}H_{17}O_2N_2^+$	$[MeAla^5+Phe^6+H]^+$	$Tyr^1+CO+Lys^2+Ile^3+HTyr^4$
	205.1340^a	$C_{12}H_{17}ON_2^+$	$[MeAla^5+Phe^6+H-CO]^+$	$Tyr^1+CO+Lys^2+Ile^3+HTyr^4+CO$
22	182.0814^a	$C_9H_{12}O_3N^+$	$[Tyr^1+H]^+$	$CO+Lys^2+Ile^3+HTyr^4+MeAla^5+Phe^6$
23	150.0915^a	$C_9H_{12}ON^+$	$[Phe^6+H]^+$	$Tyr^1-CO+Lys^2+Ile^3+HTyr^4+MeAla^5$
24	150.0915^a	$C_9H_{12}ON^+$	$[HTyr^4+H-CO]^+$ (HTyr^4 immonium ion)	$Tyr^1-CO+Lys^2+Ile^3++MeAla^5+Phe^6+CO$
25	136.0758^a	$C_8H_{10}ON^+$	$[Tyr^1+H-CO]^+$ (Tyr^1 immonium ion)	$CO+Lys^2+Ile^3+HTyr^4+MeAla^5+Phe^6+CO$
26	129.1025^a	$C_6H_{13}ON_2^+$	$[Lys^2+H]^+$	$Tyr^1-CO+ Ile^3+HTyr^4+MeAla^5+Phe^6$
27	120.0808^a	$C_8H_{10}N^+$	$[Phe^6+H-CO]^+$ Phe^6 immonium ion)	$Tyr^1-CO+Lys^2+Ile^3+HTyr^4+MeAla^5+CO$
28	114.0550^a	$C_5H_8O_2N^+$	$[MeAla^5+H+CO]^+$	$Tyr^1-CO+Lys^2+Ile^3+HTyr^4+Phe^6-CO$
29	107.0488	$C_7H_7O^+$	$[Tyr^1+H-C_2H_2NO_2]^+$ (4-Hydroxybenzyl ion)	$CO+Lys^2+Ile^3+HTyr^4+MeAla^5+Phe^6+ C_2H_2NO_2$
30	107.0488	$C_7H_7O^+$	$[HTyr^4+H-C_3H_4NO]^+$ (4-Hydroxybenzyl ion)	$Tyr^1+CO+Lys^2+Ile^3+MeAla^5+Phe^6+ C_3H_4NO$

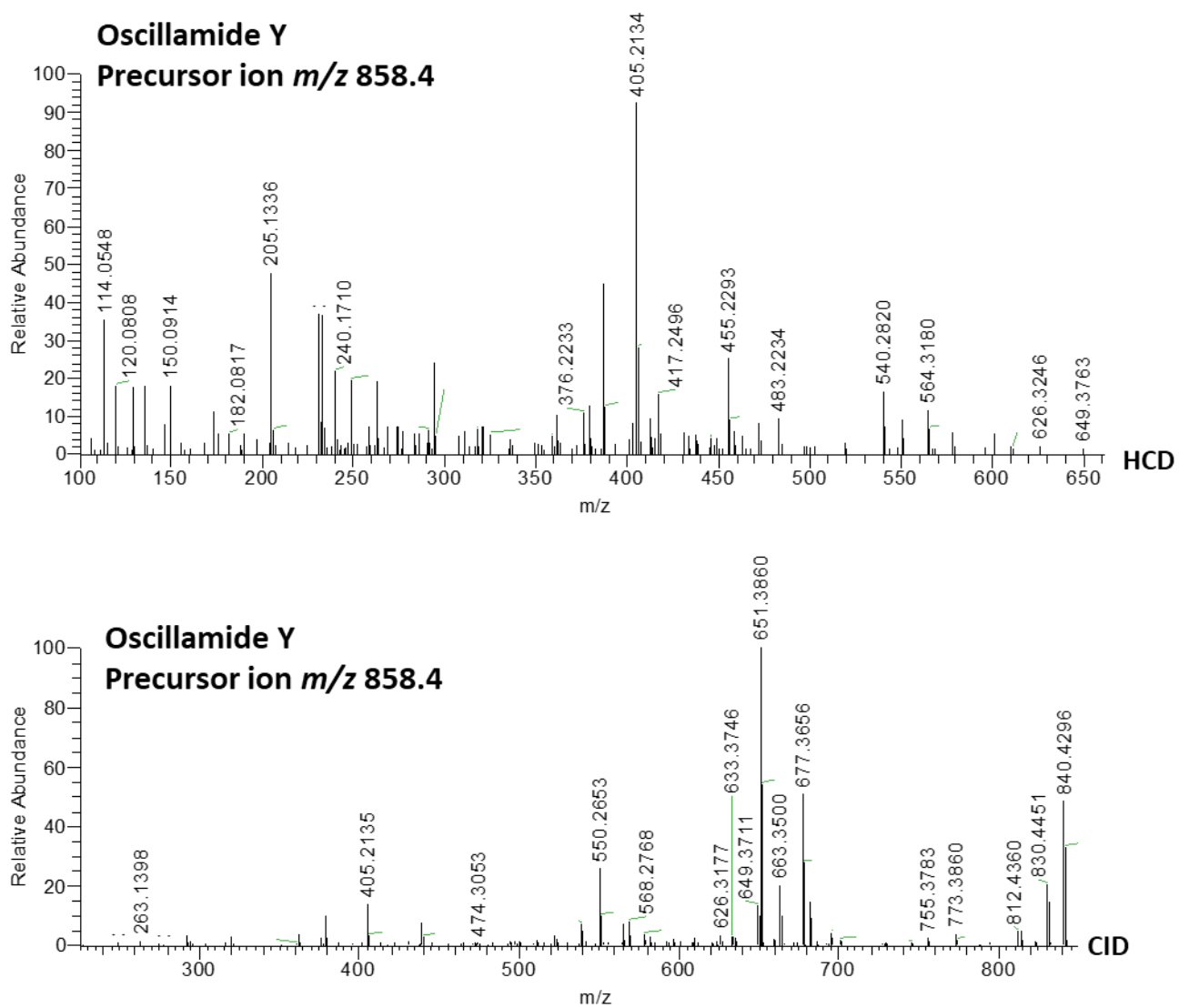^{a}=Fragment contained in the HCD DDA spectrum; ^{b}=Fragment ion contained in the CID DDA spectrum.

Figure IV.28 HCD and CID DDA MS^2 spectrum of oscillamide Y.

Table IV.19 Assignment of fragment ions contained in CID and HCD spectra of APB.

	m/z	Formula	Sequence	Neutral loss
[M+H]$^+$	837.4625	$C_{41}H_{61}O_9N_{10}^+$	[Arg^1+CO+Lys^2+Val^3+HTyr^4+MeAla^5+Phe^6+H]$^+$	
	819.4515^b	$C_{41}H_{59}O_8N_{10}^+$		H_2O
	809.4725^b	$C_{40}H_{61}O_8N_{10}^+$		CO
	802.4241^b	$C_{41}H_{56}O_8N_9^+$		H_2O+NH_3
	792.4470^b	$C_{40}H_{58}O_8N_9^+$		CO+NH_3
1	752.4126^b	$C_{37}H_{54}O_8N_9^+$	[Arg^1+CO+Lys^2+Val^3+HTyr^4+Phe^6+H]$^+$	MeAla^5
2	663.3486^b	$C_{35}H_{47}O_7N_6^+$	[CO+Lys^2+Val^3+HTyr^4+MeAla^5+Phe^6+H]$^+$	Arg^1
	635.3586^b	$C_{34}H_{47}O_6N_6^+$	[CO+Lys^2+Val^3+HTyr^4+MeAla^5+Phe^6+H-CO]$^+$	Arg^1+CO
	637.3699^b	$C_{34}H_{49}O_6N_6^+$	[CO+Lys^2+Val^3+HTyr^4+MeAla^5+Phe^6+H-CO+H_2]$^+$	Arg^1+CO-H_2
	619.3597^b	$C_{34}H_{47}O_5N_6^+$	[CO+Lys^2+Val^3+HTyr^4+MeAla^5+Phe^6+H-CO+H_2-H_2O]$^+$	Arg^1+CO-H_2+H_2O
3	561.3124^a	$C_{26}H_{41}O_6N_8^+$	[Arg^1+CO+Lys^2+Phe^6+MeAla^5+H-CO+CO]$^+$	Val^3+HTyr^4+CO-CO
4	550.3010^a	$C_{30}H_{40}O_5N_5^+$	[Lys^2+Val^3+HTyr^4+MeAla^5+Phe^6+H-C_4H_6NO (Part of Lys^2)]$^+$	Arg^1+CO+C_4H_6NO
5	509.2754^b	$C_{28}H_{37}O_5N_4^+$	[Val^3+HTyr^4+MeAla^5+Phe^6+H]$^+$	Arg^1+CO+Lys^2
6	476.2615^a	$C_{22}H_{34}O_5N_7^+$	[Arg^1+CO+Lys^2+Phe^6+H]$^+$	Val^3+HTyr^4+MeAla^5
7	460.2918^a	$C_{24}H_{38}O_4N_5^+$	[Lys^2+Val^3+MeAla^5+Phe^6+H]$^+$	Arg^1+CO+HTyr^4
8	373.2252^a	$C_{20}H_{29}O_3N_4^+$	[Lys^2+Val^3+Phe^6+H-CO]$^+$	Arg^1+CO+HTyr^4+MeAla^5+CO
9	362.2075^a	$C_{19}H_{28}O_4N_3^+$	[Val^3+HTyr^4+MeAla^5+H]$^+$	Arg^1+CO+Lys^2+Phe^6
10	263.1397^a	$C_{14}H_{19}O_3N_2^+$	[HTyr^4+MeAla^5+H]$^+$	Arg^1+CO+Lys^2+Val^3+Phe^6
11	254.1487^a	$C_{12}H_{20}O_3N_3^+$	[CO+Lys^2+Val^3+H]$^+$	Arg^1+ HTyr^4+MeAla^5+Phe^6
	226.1556^a	$C_{11}H_{20}O_2N_3^+$	[CO+Lys^2+Val^3+H-CO]$^+$	Arg^1+ HTyr^4+MeAla^5+Phe^6+CO
12	233.1284^a	$C_{13}H_{17}O_2N_2^+$	[MeAla^5+Phe^6+H]$^+$	[MeAla^5+Phe^6+H]$^+$
13	201.0979^a	$C_7H_{13}O_3N_4^+$	[Arg^1+H+CO]$^+$	CO+Lys^2+Val^3+HTyr^4+MeAla^5+Phe^6-CO
	175.1188^a	$C_6H_{15}O_2N_4^+$	[Arg^1+H]$^+$	CO+Lys^2+Val^3+HTyr^4+MeAla^5+Phe^6
	158.0922^a	$C_6H_{12}O_2N_3^+$	[Arg^1+H-NH_3]$^+$	CO+Lys^2+Val^3+HTyr^4+MeAla^5+Phe^6-NH_3
14	129.1019^a	$C_6H_{13}ON_2^+$	[Lys^2+H]$^+$	Arg^1-CO+ Val^3+HTyr^4+MeAla^5+Phe^6
15	120.0807^a	$C_8H_{10}N^+$	[Phe^6+H-CO]$^+$ Phe^6 immonium ion)	Arg^1-CO+Lys^2+Val^3+HTyr^4+MeAla^5+CO
16	114.0551^a	$C_5H_8O_2N^+$	[MeAla^5+H+CO]$^+$	Arg^1-CO+Lys^2+Val^3+HTyr^4+Phe^6-CO

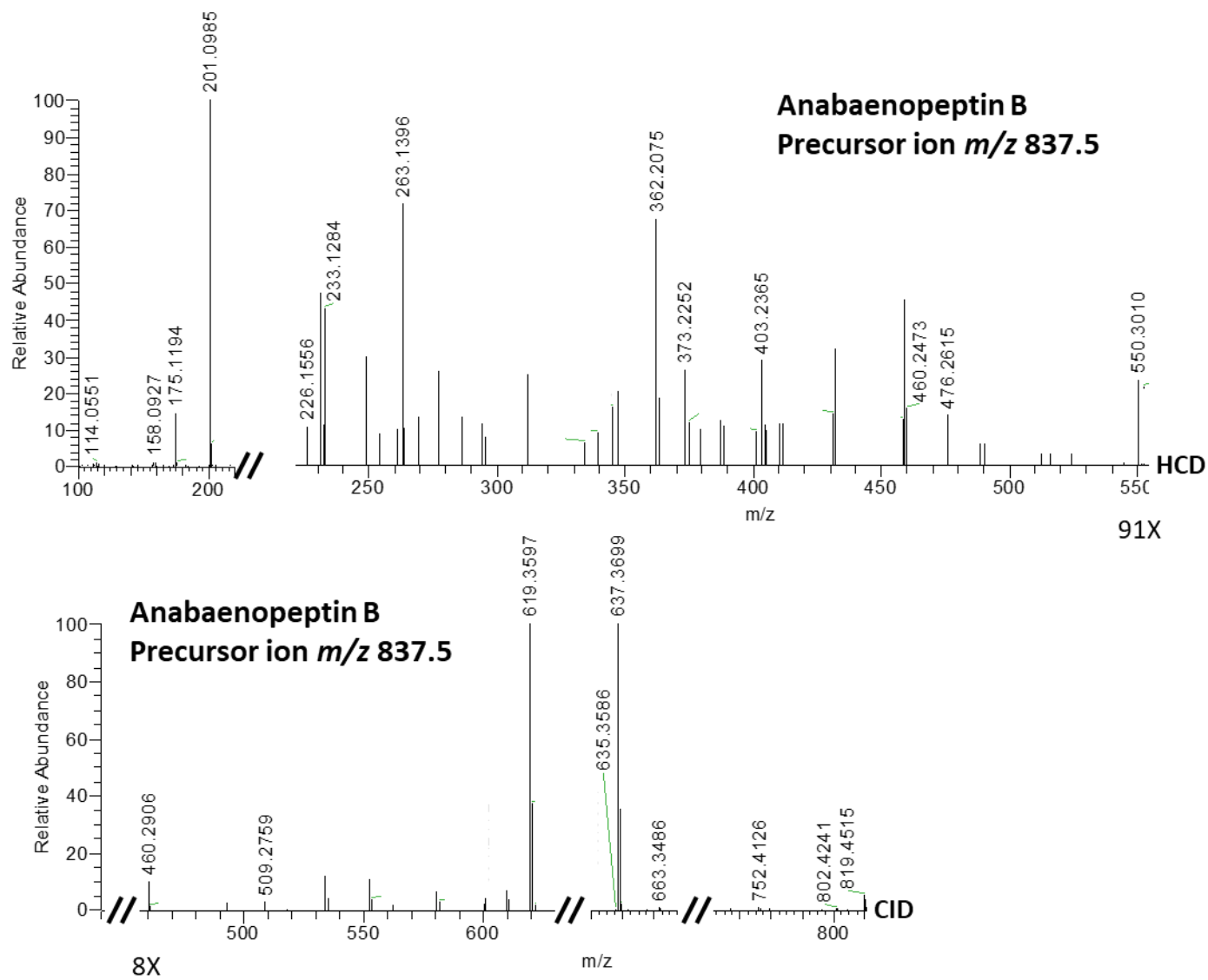^{a}=Fragment contained in the HCD DDA spectrum; ^{b}=Fragment ion contained in the CID DDA spectrum.

Figure IV.29 HCD and CID DDA MS^2 spectrum of anabaenopeptin B.

Table IV.20 Assignment of fragment ions contained in CID and HCD spectra of APF.

	m/z	Formula	Sequence		Neutral loss
			Anabaenopeptin F		
$[M+H]^+$	851.4777	$C_{42}H_{63}O_9N_{10}^+$	$[Arg^1+CO+Lys^2+Ile^3+HTyr^4+MeAla^5+Phe^6+H]^+$		
	833.4666[b]	$C_{42}H_{61}O_8N_{10}^+$			H_2O
	816.4418[b]	$C_{42}H_{58}O_8N_9^+$			H_2O+NH_3

	m/z	Formula	Sequence	Neutral loss
1	766.4242[b]	$C_{38}H_{56}O_8N_9^+$	$[Arg^1+CO+Lys^2+Ile^3+HTyr^4+Phe^6+H]^+$	$MeAla^5$
2	677.3656[b]	$C_{36}H_{49}O_7N_6^+$	$[CO+Lys^2+Ile^3+HTyr^4+MeAla^5+Phe^6+H]^+$	Arg^1
	649.3689[b]	$C_{35}H_{49}O_6N_6^+$	$[CO+Lys^2+Ile^3+HTyr^4+MeAla^5+Phe^6+H-CO]^+$	Arg^1+CO
	651.3842[b]	$C_{35}H_{51}O_6N_6^+$	$[CO+Lys^2+Ile^3+HTyr^4+MeAla^5+Phe^6+H-CO+H_2]^+$	Arg^1+CO-H_2
	633.3742[b]	$C_{35}H_{49}O_5N_6^+$	$[CO+Lys^2+Ile^3+HTyr^4+MeAla^5+Phe^6+H-CO+H_2-H_2O]^+$	$Arg^1+CO-H_2+H_2O$
3	564.3177[a]	$C_{31}H_{42}O_5N_5^+$	$[Lys^2+Ile^3+HTyr^4+MeAla^5+Phe^6+H-C_4H_6NO\ (Part\ of\ Lys^2)]^+$	$Arg^1+CO+C_4H_6NO$
4	561.3124[b]	$C_{26}H_{41}O_6N_8^+$	$[Arg^1+CO+Lys^2+Phe^6+MeAla^5+H-CO+CO]^+$	$Ile^3+HTyr^4+CO-CO$
5	523.2904[b]	$C_{29}H_{39}O_5N_4^+$	$[Ile^3+HTyr^4+MeAla^5+Phe^6+H]^+$	$Arg^1+CO+Lys^2$
6	476.2599[a]	$C_{22}H_{34}O_5N_7^+$	$[Arg^1+CO+Lys^2+Phe^6+H]^+$	$Ile^3+HTyr^4+MeAla^5$
7	474.3063[b]	$C_{25}H_{40}O_4N_5^+$	$[Lys^2+Ile^3+MeAla^5+Phe^6+H]^+$	$Arg^1+CO+HTyr^4$
8	417.2479[b]	$C_{22}H_{33}O_4N_4^+$	$[Lys^2+Ile^3+Phe^6+H+CO]^+$	$Arg^1+CO+HTyr^4+MeAla^5-CO$
	387.2378[a]	$C_{21}H_{31}O_3N_4^+$	$[Lys^2+Ile^3+Phe^6+H-CO]^+$	$Arg^1+CO+HTyr^4+MeAla^5+CO$
9	405.2126[a]	$C_{20}H_{29}O_5N_4^+$	$[CO+Lys^2+MeAla^5+Phe^6+H+CO-CH_3]^+$	$Arg^1+Ile^3+HTyr^4-2CO+CH_3$
10	376.2240[a]	$C_{20}H_{30}O_4N_3^+$	$[Ile^3+HTyr^4+MeAla^5+H]^+$	$Arg^1+CO+Lys^2+Phe^6$
11	268.1666[a]	$C_{13}H_{22}O_3N_3^+$	$[CO+Lys^2+Ile^3+H]^+$	$Arg^1+ HTyr^4+MeAla^5+Phe^6$
	240.1712[a]	$C_{12}H_{22}O_2N_3^+$	$[CO+Lys^2+Ile^3+H-CO]^+$	$Arg^1+ HTyr^4+MeAla^5+Phe^6+CO$
12	263.1394[a]	$C_{14}H_{19}O_3N_2^+$	$[HTyr^4+MeAla^5+H]^+$	$Arg^1+CO+Lys^2+Ile^3+Phe^6$
13	233.1289[a]	$C_{13}H_{17}O_2N_2^+$	$[MeAla^5+Phe^6+H]^+$	$[MeAla^5+Phe^6+H]^+$
14	201.0983[a]	$C_7H_{13}O_3N_4^+$	$[Arg^1+H+CO]^+$	$CO+Lys^2+Ile^3+HTyr^4+MeAla^5+Phe^6-CO$
	175.1191[a]	$C_6H_{15}O_2N_4^+$	$[Arg^1+H]^+$	$CO+Lys^2+Ile^3+HTyr^4+MeAla^5+Phe^6$
	158.0923[a]	$C_6H_{12}O_2N_3^+$	$[Arg^1+H-NH_3]^+$	$CO+Lys^2+Ile^3+HTyr^4+MeAla^5+Phe^6-NH_3$
15	120.1026[a]	$C_6H_{13}ON_2^+$	$[Lys^2+H]^+$	$Arg^1-CO+ Ile^3+HTyr^4+MeAla^5+Phe^6$
16	120.0811[a]	$C_8H_{10}N^+$	$[Phe^6+H-CO]^+\ Phe^6$ immonium ion)	$Arg^1-CO+Lys^2+Ile^3+HTyr^4+MeAla^5+CO$
17	114.0550[a]	$C_5H_8O_2N^+$	$[MeAla^5+H+CO]^+$	$Arg^1-CO+Lys^2+Ile^3+HTyr^4+Phe^6-CO$

[a]=Fragment contained in the HCD DDA spectrum; [b]=Fragment ion contained in the CID DDA spectrum.
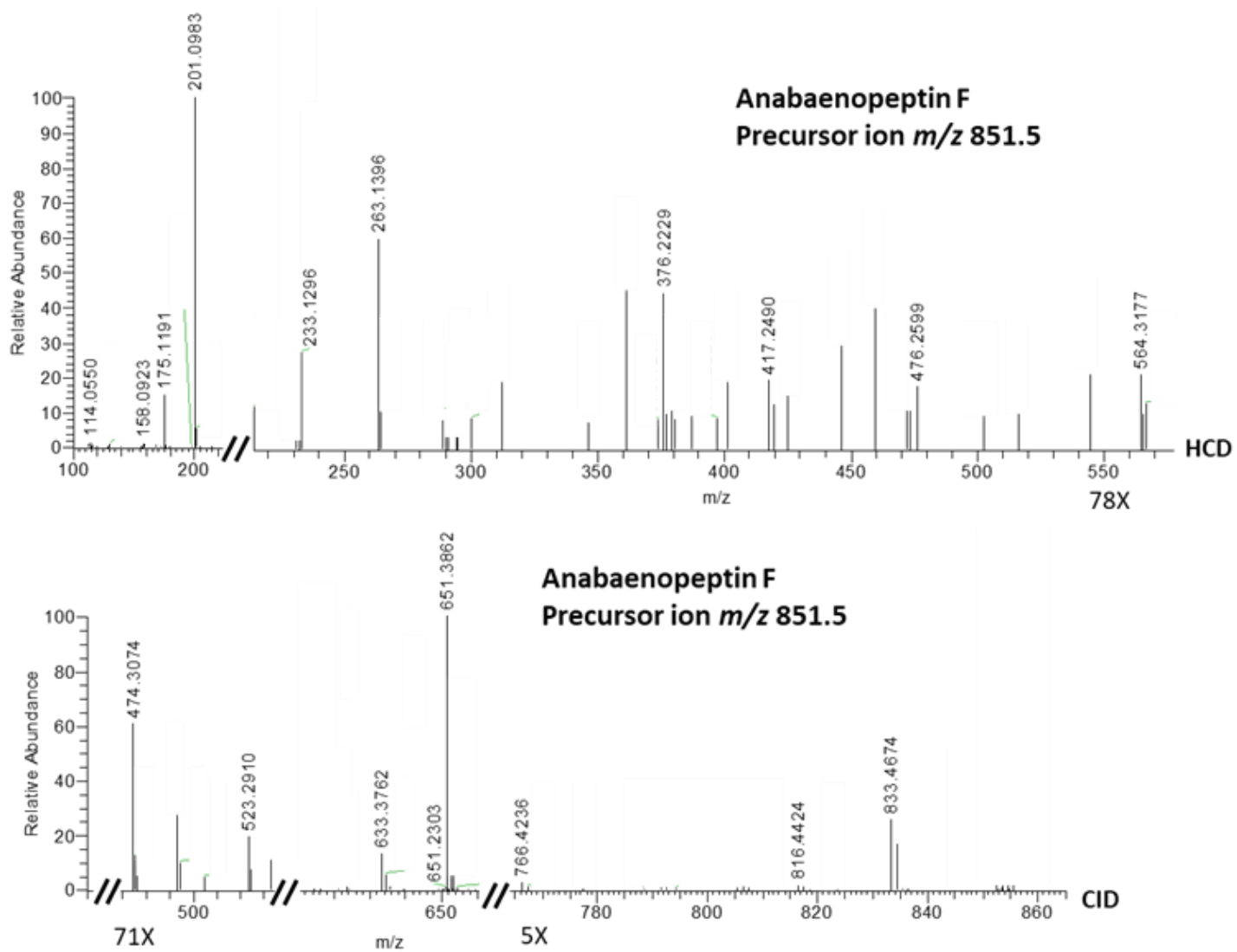
Figure IV.30 HCD and CID DDA MS^2 spectrum of anabaenopeptin F.

2.4.3 Determination of cyanopeptoline-type peptides

The last group of cyanobacterial secondary metabolites screened in the biomass samples was represented by the CPtps. Although the conserved part structure within this group is the atypical residue 3-amino-6-hydroxy-2-piperidone (Ahp) **(Fig.I.21)**, it cannot be detected individually by HRMS^2 experiments since most of the analogues are not able to produce specific Ahp fragments. However, Ahp^3 can be evidenced through diagnostic fragment ions corresponding to amino acid sequences in which it is involved. The structural motif of most of CPtps in fact is represented by Ahp^3-Leu^4/Phe^4-MeTyr^5/MePhe^5 which can form characteristic fragment ions at: i) *m/z* 386.2074, $C_{21}H_{28}N_3O_4^+$, [Ahp^3+Leu^4+MeTyr^5-H$_2$O+H]$^+$, ii) *m/z* 420.1918, $C_{24}H_{26}N_3O_4^+$, [Ahp^3+Phe^4+MeTyr^5-H$_2$O+H]$^+$, iii) *m/z* 370.2125, $C_{21}H_{28}N_3O_3^+$, [Ahp^3+Leu^4+MePhe^5-H$_2$O+H]$^+$ and iv) *m/z* 404.1969, $C_{24}H_{26}N_3O_3^+$, [Ahp^3+Phe^4+MePhe^5-H$_2$O+H]$^+$. Moreover, further key clues are represented by diagnostic fragments due to the loss of Ahp^3 from the aforementioned sequences in combination with MeTyr^5 and MePhe^5 immonium ion at *m/z* 150.0913 ($C_9H_{12}NO^+$) and *m/z* 134.0964 ($C_9H_{12}N^+$), respectively [47].

The extraction of the fragment at *m/z* 420.1918 ([Ahp^3+Phe^4+MeTyr^5-H$_2$O+H]$^+$) from the HCD and CID DDA spectra provided 3 chromatographic peaks eluting at 17.86, 16.60 and 16.60 min associated to the [M+H]$^+$ precursor ions at *m/z* 1049.5666 ($C_{52}H_{77}N_{10}O_{13}^+$), 1007.5200 ($C_{49}H_{71}N_{10}O_{13}^+$) and 1021.5353 ($C_{50}H_{73}N_{10}O_{13}^+$), respectively **Fig.IV.31**. Although two CPtp analogues have been reported to have the same exact mass with [M+H]$^+$ at *m/z* 1049.5666, the interpretation of DDA MS^2 spectra clearly confirmed the identity of Micropeptin LH1048 - Thr^1-Arg^2-Ahp^3-Phe^4-NMeTyr^5-Val^6-Glu^7-Octanoic acid^8 **(Table IV.21)**. Val^6 was highlighted as neutral loss of 99 Da from the precursor ion due to fragments #1; fragment at *m/z* 299.1655 (#12) confirmed the sequence [NMeTyr^5+Val^6+H]$^+$, and a combined interpretation between fragment #8, 11, 12 and 14, corroborated the sequence [Ahp^3+Phe^4+NMeTyr^5+Val^6+H]$^+$. Fragments #15 highlighted the sequence [Thr^1+Arg^2+H]$^+$ whilst the cross interpretation with fragments #2, 3, 4, and 6 confirmed the exact position of each residue embedded in the cyclic moiety of the molecule [Thr^1+Arg^2+ Ahp^3+Phe^4+NMeTyr^5+Val^6+H]$^+$. The exocyclic residues Glu^7 and Octanoic acid^8 were detected through fragment at *m/z* 256.1545 (#13) while the direct link between Thr^1+Glu^7 was confirmed through fragments #5, 7, 9 and 10.

Following the same analytical strategy, the [M+H]$^+$ ion at *m/z* 1021.5353 ($C_{50}H_{73}N_{10}O_{13}^+$) **Fig.IV.31** was found to correspond to cyanopeptoline 1020 -Thr^1-Arg^2-Ahp^3-Phe^4-NMeTyr^5-Val^6-

Glu[7]- Hexanoic acid[8] – which differs from Micropeptin LH1048 for 28 Da due to the presence of Hexanoic acid[8] (**Table IV.22**).
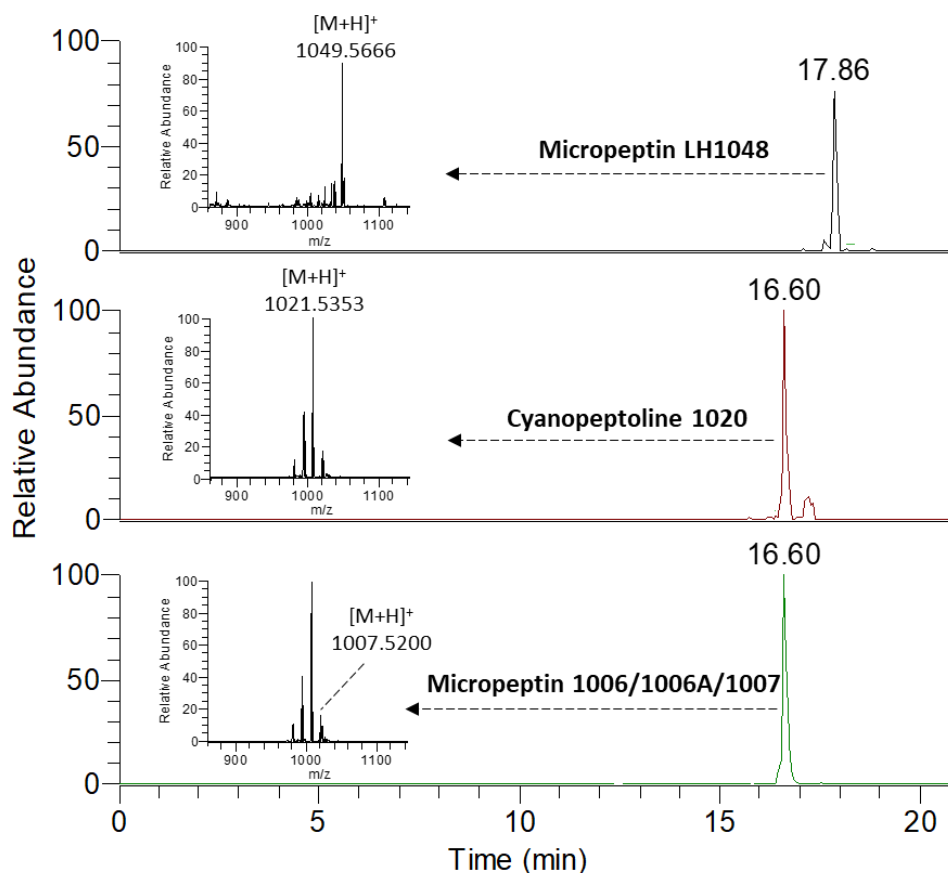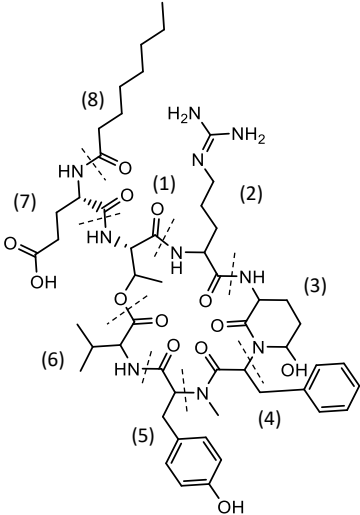

Figure IV.31 XIC and HRMS spectrum of [M+H][+] ion of micropeptin LH1048, cyanopeptolin 1020 and micropeptin 1006/1006A/1007.

The interpretation of the HRMS^2 spectra of the [M+H][+] ion at *m/z* 1007.5200 ($C_{49}H_{71}N_{10}O_{13}^+$) clearly revealed the amino acid sequence -Thr[1]-Arg[2]-Ahp[3]-Phe[4]-NMeTyr[5]-Val[6]-Asp[7]-Hexanoic cid[8]- (**Table IV.23**) since its fragmentation patterns were superimposable to those of cyanopeptoline 1020, except for the fragments involving the residue in position 7, which were characterized by 14 Da less due to the presence of Asp[7]. Nevertheless, the lack of analytical standards hampered the identity confirmation of the molecule since three different stereoisomers have been reported so far, namely Micropeptin 1006, 1006A and 1007 [28].

Table IV.21 Assignment of fragment ions contained in CID and HCD spectra of Micropeptin LH1048.

	m/z	Formula	Sequence	Neutral loss
[M+H]⁺	1049.5666	C₅₂H₇₇O₁₃N₁₀⁺	[Thr¹+Arg²+Ahp³+Phe⁴+MeTyr⁵+Val⁶+Glu⁷+Octanoic acid⁸+H]⁺	
	1031.5569[b]	C₅₂H₇₅O₁₂N₁₀⁺		H₂O
	1021.5697[b]	C₅₁H₇₇O₁₂N₁₀⁺		CO
	1014.5276[b]	C₅₂H₇₂O₁₂N₉⁺		H₂O+NH₃
	1003.5627[b]	C₅₁H₇₅O₁₁N₁₀⁺		CO+H₂O
	971.5218[b]	C₅₁H₇₁O₁₁N₈⁺		2NH₃+CO₂

#	*m/z*	Formula	Sequence	Neutral loss
1	950.4966[b]	C₄₇H₆₈O₁₂N₉⁺	[Thr¹+Arg²+Ahp³+Phe⁴+MeTyr⁵+Glu⁷+Octanoic acid⁸+H]⁺	Val⁶
	932.4833[b]	C₄₇H₆₆O₁₁N₉⁺	[Thr¹+Arg²+Ahp³+Phe⁴+MeTyr⁵+Glu⁷+Octanoic acid⁸+H-H₂O]⁺	Val⁶+H₂O
	914.4732[b]	C₄₇H₆₄O₁₀N₉⁺	[Thr¹+Arg²+Ahp³+Phe⁴+MeTyr⁵+Glu⁷+Octanoic acid⁸+H-2H₂O]⁺	Val⁶+2H₂O
	897.4507[b]	C₄₇H₆₁O₁₀N₉⁺	[Thr¹+Arg²+Ahp³+Phe⁴+MeTyr⁵+Glu⁷+Octanoic acid⁸+H-2H₂O-NH₃]⁺	Val⁶+2H₂O+NH₃
2	936.5172[b]	C₄₇H₇₀O₁₁N₉⁺	[Thr¹+Arg²+Phe⁴+MeTyr⁵+Val⁶+Glu⁷+Octanoic acid⁸+H]⁺	Ahp³
3	794.4141[b]	C₃₉H₅₆O₉N₉⁺	[Thr¹+Arg²+Ahp³+Phe⁴+MeTyr⁵+Val⁶+H]⁺	Glu⁷+Octanoic acid⁸
	776.4074[b]	C₃₉H₅₄O₈N₉⁺	[Thr¹+Arg²+Ahp³+Phe⁴+MeTyr⁵+Val⁶+H-H₂O]⁺	Glu⁷+Octanoic acid⁸+H₂O
	758.3968[b]	C₃₉H₅₂O₇N₉⁺	[Thr¹+Arg²+Ahp³+Phe⁴+MeTyr⁵+Val⁶+H-2H₂O]⁺	Glu⁷+Octanoic acid⁸+2H₂O
	741.3709[b]	C₃₉H₄₉O₇N₈⁺	[Thr¹+Arg²+Ahp³+Phe⁴+MeTyr⁵+Val⁶+H-2H₂O-NH₃]⁺	Glu⁷+Octanoic acid⁸+2H₂O+NH₃
4	711.3817[b]	C₃₅H₅₁O₈N₈⁺	[Arg²+Ahp³+Phe⁴+MeTyr⁵+Val⁶+H+H₂O]⁺	Thr¹+Glu⁷+Octanoic acid⁸-H₂O
5	612.3701[b]	C₂₈H₅₀O₈N₇⁺	[Thr¹+Arg²+Ahp³+Glu⁷+Octanoic acid⁸+H-H₂O-NH₃]⁺	Phe⁴+MeTyr⁵+Val⁶+H₂O+NH₃
6	548.2996[a]	C₂₉H₃₈O₄N₇⁺	[Arg²+Ahp³+Phe⁴+MeTyr⁵+H-H₂O-CO]⁺	Thr¹+Val⁶+Glu⁷+Octanoic acid⁸+H₂O+CO
7	513.3010[a]	C₂₃H₄₁O₇N₆⁺	[Thr¹+Arg²+Glu⁷+Octanoic acid⁸+H]⁺	Ahp³+Phe⁴+MeTyr⁵+Val⁶
	512.3209[a]	C₂₃H₄₂O₆N₇⁺	[Thr¹+Arg²+Glu⁷+Octanoic acid⁸+H-H₂O+NH₃]⁺	Ahp³+Phe⁴+MeTyr⁵+Val⁶+H₂O-NH₃
	495.2926[a]	C₂₃H₃₉O₆N₆⁺	[Thr¹+Arg²+Glu⁷+Octanoic acid⁸+H-H₂O]⁺	Ahp³+Phe⁴+MeTyr⁵+Val⁶+H₂O
	478.2651[a]	C₂₃H₃₆O₆N₅⁺	[Thr¹+Arg²+Glu⁷+Octanoic acid⁸+H-H₂O-NH₃]⁺	Ahp³+Phe⁴+MeTyr⁵+Val⁶+H₂O+NH₃
	467.2987[a]	C₂₂H₃₉O₅N₆⁺	[Thr¹+Arg²+Glu⁷+Octanoic acid⁸+H-H₂O-CO]⁺	Ahp³+Phe⁴+MeTyr⁵+Val⁶+H₂O+CO
8	420.1918[a]	C₂₄H₂₆O₄N₃⁺	[Ahp³+Phe⁴+MeTyr⁵+H-H₂O]⁺	Thr¹+Arg²+Val⁶+Glu⁷+Octanoic acid⁸+H₂O
9	339.1917[a]	C₁₇H₂₇O₅N₂⁺	[Thr¹+Glu⁷+Octanoic acid⁸+H-H₂O]⁺	Arg²+Ahp³+Phe⁴+MeTyr⁵+Val⁶+H₂O
10	352.1621[a]	C₁₅H₂₂O₅N₅⁺	[Thr¹+Arg²+Glu⁷+H-H₂O-NH₃]⁺	Ahp³+Phe⁴+MeTyr⁵+Val⁶+Octanoic acid⁸+H₂O+NH₃
	334.1509[a]	C₁₅H₂₀O₄N₅⁺	[Thr¹+Arg²+Glu⁷+H-2H₂O-NH₃]⁺	Ahp³+Phe⁴+MeTyr⁵+Val⁶+Octanoic acid⁸+2H₂O+NH₃

11	208.1278[a]	$C_{19}H_{18}O_3N^+$	$[Phe^4+MeTyr^5+H-NH_3]^+$	$Thr^1+Arg^2+Ahp^3+Val^6+Glu^7+Octanoic\ acid^8+NH_3$
12	295.1655[a]	$C_{15}H_{23}O_4N_2^+$	$[MeTyr^5+Val^6+H+H_2O]^+$	$Thr^1+Arg^2+Ahp^3+Phe^4+Glu^7+Octanoic\ acid^8-H_2O$
13	256.1545[a]	$C_{13}H_{22}O_4N^+$	$[Glu^7+Octanoic\ acid^8+H]^+$	$Thr^1+Arg^2+Ahp^3+Phe^4+MeTyr^5+Val^6$
14	243.1130[a]	$C_{14}H_{15}O_2N_2^+$	$[Ahp^3+Phe^4+H-H_2O]^+$	$Thr^1+Arg^2+MeTyr^5+Val^6+Glu^7+Octanoic\ acid^8+H_2O$
	215.1179[a]	$C_{13}H_{15}ON_2^+$	$[Ahp^3+Phe^4+H-H_2O-CO]^+$	$Thr^1+Arg^2+MeTyr^5+Val^6+Glu^7+Octanoic\ acid^8+H_2O+CO$
15	241.1306[a]	$C_{10}H_{17}O_3N_4^+$	$[Thr^1+Arg^2+H-NH_3]^+$	$Ahp^3+Phe^4+MeTyr^5+Val^6+Glu^7+Octanoic\ acid^8+NH_3$
	223.1194[a]	$C_{10}H_{15}O_2N_4^+$	$[Thr^1+Arg^2+H-NH_3-H_2O]^+$	$Ahp^3+Phe^4+MeTyr^5+Val^6+Glu^7+Octanoic\ acid^8+NH_3+H_2O$
16	150.0913[a]	$C_9H_{12}ON^+$	$[MeTyr^5+H-CO]^+$ (MeTyr[5] immonium ion)	$Thr^1+Arg^2+Ahp^3+Phe^4+Val^6+Glu^7+Octanoic\ acid^8+CO$
17	120.0807[a]	$C_8H_{10}N^+$	$[Phe^4+H-CO]^+$ (Phe[6] immonium ion)	$Thr^1+Arg^2+Ahp^3+MeTyr^5+Val^6+Glu^7+Octanoic\ acid^8+CO$
18	112.0867[a]	$C_5H_{10}N_3^+$	$[Arg^2+H-CO-NH_3]^+$	$Thr^1+Ahp^3+Phe^4+MeTyr^5+Val^6+Glu^7+Octanoic\ acid^8+CO+NH_3$
19	102.0551[a]	$C_4H_8O_2N^+$	$[Ahp^3+H-C_2H_4NO+CO]^+$	$Thr^1+Arg^2+Phe^4+MeTyr^5+Val^6+Glu^7+Octanoic\ acid^8-CO$

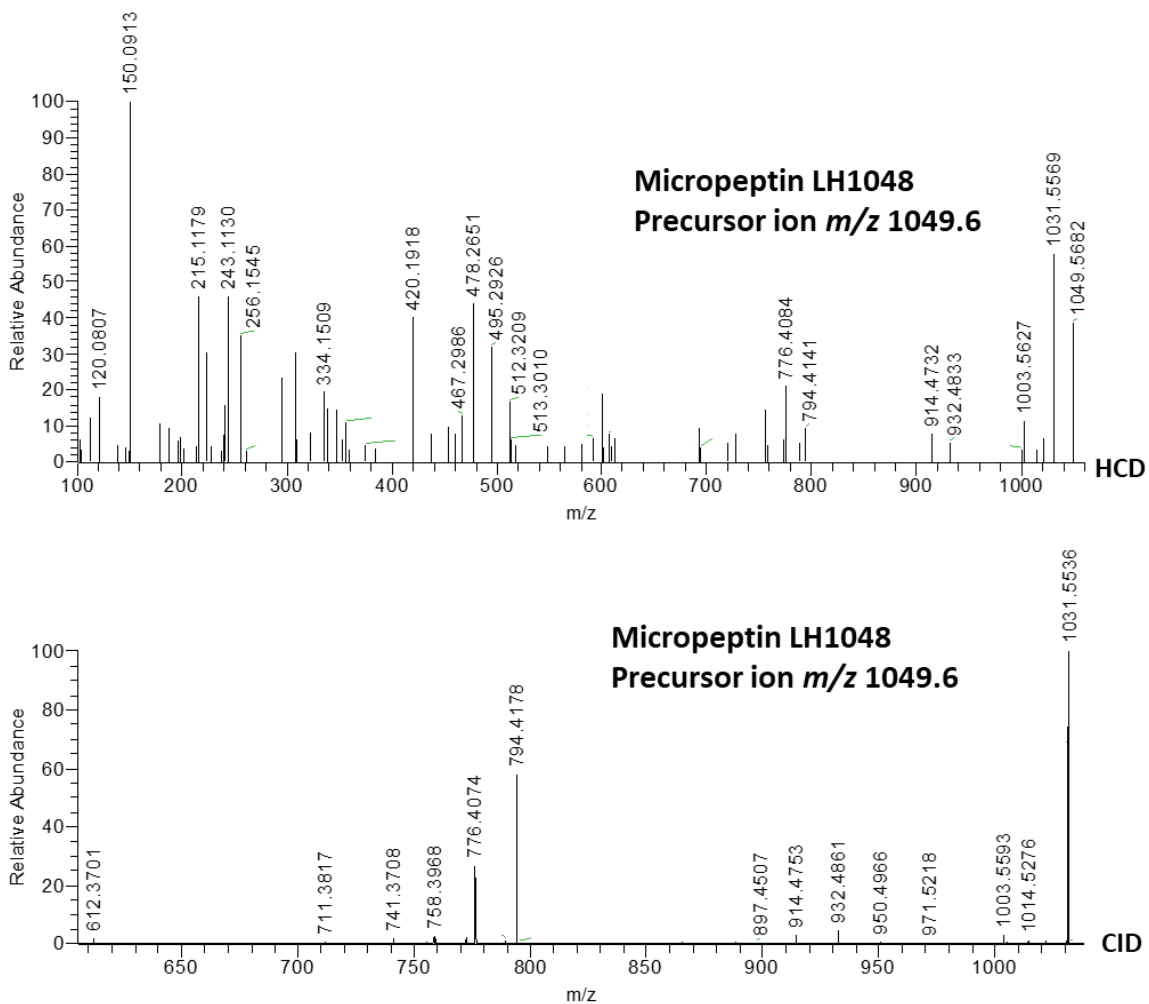[a]=Fragment contained in the HCD DDA spectrum; [b]=Fragment ion contained in the CID DDA spectrum.

Figure IV.32 HCD and CID DDA MS^2 spectrum of micropeptin LH1048.

Table IV.22 Assignment of fragment ions contained in CID and HCD spectra of Cyanopeptolin 1020.

			Cyanopeptolin 1020	
	m/z	**Formula**	**Sequence**	**Neutral loss**
$[M+H]^+$	1021.5353	$C_{50}H_{73}O_{13}N_{10}^+$	$[Thr^1+Arg^2+Ahp^3+Phe^4+MeTyr^5+Val^6+Glu^7+Hexanoic\ acid^8+H]^+$	
	1003.5212[b]	$C_{50}H_{71}O_{12}N_{10}^+$		H_2O
	993.5394[b]	$C_{49}H_{73}O_{12}N_{10}^+$		CO
	986.4914[b]	$C_{50}H_{68}O_{12}N_9^+$		H_2O+NH_3
	975.5253[b]	$C_{49}H_{71}O_{11}N_{10}^+$		H_2O+CO
	958.4982[b]	$C_{49}H_{68}O_{11}N_9^+$		CO_2+NH_3

#	*m/z*	Formula	Sequence	Neutral loss
1	904.4520[b]	$C_{45}H_{62}O_{11}N_9^+$	$[Thr^1+Arg^2+Ahp^3+Phe^4+MeTyr^5+Glu^7+Hexanoic\ acid^8+H-H_2O]^+$	Val^6+H_2O
	886.4410[b]	$C_{45}H_{60}O_{10}N_9^+$	$[Thr^1+Arg^2+Ahp^3+Phe^4+MeTyr^5+Glu^7+Hexanoic\ acid^8+H-2H_2O]^+$	Val^6+2H_2O
2	907.4426[b]	$C_{46}H_{63}O_{13}N_6^+$	$[Thr^1+Arg^2+Ahp^3+Phe^4+MeTyr^5+Val^6+Glu^7+Hexanoic\ acid^8+H-NH_3-C_4H_7N_3\ (part\ of\ Arg^2)]^+$	$NH_3+C_4H_7N_3$
	889.4308[b]	$C_{46}H_{61}O_{12}N_6^+$	$[Thr^1+Arg^2+Ahp^3+Phe^4+MeTyr^5+Val^6+Glu^7+Hexanoic\ acid^8+H-NH_3-C_4H_7N_3\ (part\ of\ Arg^2)-H_2O]^+$	$NH_3+C_4H_7N_3+H_2O$
	865.4317[b]	$C_{44}H_{61}O_{12}N_6^+$	$[Thr^1+Ahp^3+Phe^4+MeTyr^5+Val^6+Glu^7+Hexanoic\ acid^8+H]^+$	Arg^2
	848.4049[b]	$C_{44}H_{58}O_{12}N_5^+$	$[Thr^1+Ahp^3+Phe^4+MeTyr^5+Val^6+Glu^7+Hexanoic\ acid^8+H-NH_3]^+$	Arg^2+NH_3
3	794.4155[b]	$C_{39}H_{56}O_9N_9^+$	$[Thr^1+Arg^2+Ahp^3+Phe^4+MeTyr^5+Val^6+H]^+$	$Glu^7+Hexanoic\ acid^8$
	776.4048[b]	$C_{39}H_{54}O_8N_9^+$	$[Thr^1+Arg^2+Ahp^3+Phe^4+MeTyr^5+Val^6+H-H_2O]^+$	$Glu^7+Hexanoic\ acid^8+H_2O$
	758.3955[b]	$C_{39}H_{52}O_7N_9^+$	$[Thr^1+Arg^2+Ahp^3+Phe^4+MeTyr^5+Val^6+H-2H_2O]^+$	$Glu^7+Hexanoic\ acid^8+2H_2O$
	741.3672[b]	$C_{39}H_{49}O_7N_8^+$	$[Thr^1+Arg^2+Ahp^3+Phe^4+MeTyr^5+Val^6+H-2H_2O-NH_3]^+$	$Glu^7+Hexanoic\ acid^8+2H_2O+NH_3$
4	584.3372[b]	$C_{26}H_{46}O_8N_7^+$	$[Thr^1+Arg^2+Ahp^3+Glu^7+Hexanoic\ acid^8+H-H_2O-NH_3]^+$	$Phe^4+MeTyr^5+Val^6+H_2O+NH_3$
5	484.2859[a]	$C_{21}H_{38}O_6N_7^+$	$[Thr^1+Arg^2+Glu^7+Hexanoic\ acid^8+H-H_2O+NH_3]^+$	$Ahp^3+Phe^4+MeTyr^5+Val^6+H_2O-NH_3$
	467.2596[a]	$C_{21}H_{35}O_6N_6^+$	$[Thr^1+Arg^2+Glu^7+Hexanoic\ acid^8+H-H_2O]^+$	$Ahp^3+Phe^4+MeTyr^5+Val^6+H_2O$
	450.2328[a]	$C_{21}H_{32}O_6N_5^+$	$[Thr^1+Arg^2+Glu^7+Hexanoic\ acid^8+H-H_2O-NH_3]^+$	$Ahp^3+Phe^4+MeTyr^5+Val^6+H_2O+NH_3$
	439.2648[a]	$C_{20}H_{35}O_5N_6^+$	$[Thr^1+Arg^2+Glu^7+Hexanoic\ acid^8+H-H_2O-CO]^+$	$Ahp^3+Phe^4+MeTyr^5+Val^6+H_2O+CO$
6	420.1903[a]	$C_{24}H_{26}O_4N_3^+$	$[Ahp^3+Phe^4+MeTyr^5+H-H_2O]^+$	$Thr^1+Arg^2+Val^6+Glu^7+Hexanoic\ acid^8+H_2O$
7	334.1497[a]	$C_{15}H_{20}O_4N_5^+$	$[Thr^1+Arg^2+Glu^7+H-2H_2O-NH_3]^+$	$Ahp^3+Phe^4+MeTyr^5+Val^6+Hexanoic\ acid^8+2H_2O+NH_3$
8	311.1590[a]	$C_{15}H_{23}O_5N_2^+$	$[Thr^1+Glu^7+Hexanoic\ acid^8+H-H_2O]^+$	$Arg^2+Ahp^3+Phe^4+MeTyr^5+Val^6+H_2O$
9	308.1269[a]	$C_{19}H_{18}O_3N^+$	$[Phe^4+MeTyr^5+H-NH_3]^+$	$Thr^1+Arg^2+Ahp^3+Val^6+Glu^7+Hexanoic\ acid^8+NH_3$
10	295.1640[a]	$C_{15}H_{23}O_4N_2^+$	$[MeTyr^5+Val^6+H+H_2O]^+$	$Thr^1+Arg^2+Ahp^3+Phe^4\ Glu^7+Hexanoic\ acid^8-H_2O$
11	243.1119[a]	$C_{14}H_{15}O_2N_2^+$	$[Ahp^3+Phe^4+H-H_2O]^+$	$Thr^1+Arg^2+MeTyr^5+Val^6+Glu^7+Hexanoic\ acid^8+H_2O$

	215.1171[a]	$C_{13}H_{15}ON_2^+$	$[Ahp^3+Phe^4+H-H_2O-CO]^+$	$Thr^1+Arg^2+MeTyr^5+Val^6+Glu^7+Hexanoic\ acid^8+H_2O+CO$
12	241.1286[a]	$C_{10}H_{17}O_3N_4^+$	$[Thr^1+Arg^2+H-NH_3]^+$	$Ahp^3+Phe^4+MeTyr^5+Val^6+Glu^7+Hexanoic\ acid^8+NH_3$
	223.1182[a]	$C_{10}H_{15}O_2N_4^+$	$[Thr^1+Arg^2+H-NH_3-H_2O]^+$	$Ahp^3+Phe^4+MeTyr^5+Val^6+Glu^7+Hexanoic\ acid^8+NH_3+H_2O$
13	228.1222[a]	$C_{11}H_{18}O_4N^+$	$[Glu^7+Hexanoic\ acid^8+H]^+$	$Thr^1+Arg^2+Ahp^3+Phe^4+MeTyr^5+Val^6$
14	150.0907[a]	$C_9H_{12}ON^+$	$[MeTyr^5+H-CO]^+$ ($MeTyr^5$ immonium ion)	$Thr^1+Arg^2+Ahp^3+Phe^4+Val^6+Glu^7+Hexanoic\ acid^8+CO$
15	120.0802[a]	$C_8H_{10}N^+$	$[Phe^4+H-CO]^+$ (Phe^6 immonium ion)	$Thr^1+Arg^2+Ahp^3+MeTyr^5+Val^6+Glu^7+Hexanoic\ acid^8+CO$
16	112.0863[a]	$C_5H_{10}N_3^+$	$[Arg^2+H-CO-NH_3]^+$	$Thr^1+Ahp^3+Phe^4+MeTyr^5+Val^6+Glu^7+Hexanoic\ acid^8+CO+NH_3$
17	102.0545[a]	$C_4H_8O_2N^+$	$[Ahp^3+H-C_2H_4NO+CO]^+$	$Thr^1+Arg^2+Phe^4+MeTyr^5+Val^6+Glu^7+Hexanoic\ acid^8-CO$

[a]=Fragment contained in the HCD DDA spectrum; [b]=Fragment ion contained in the CID DDA spectrum
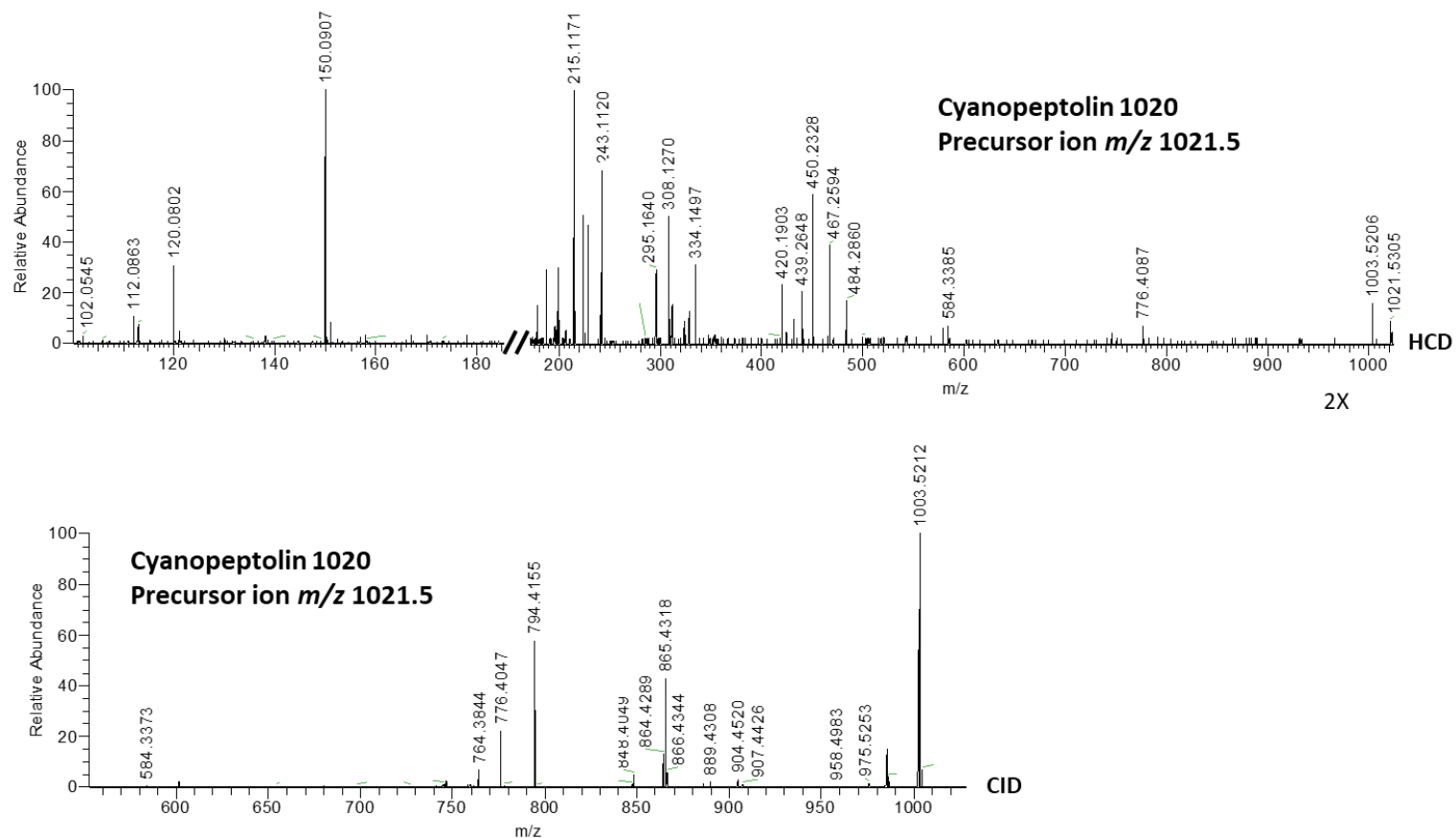
Figure IV.33 HCD and CID DDA MS^2 spectrum of cyanopeptolin 1020.

Table IV.23 Assignment of fragment ions contained in CID and HCD spectra of Micropeptin 1006/1006A/1007.

	m/z	Formula	Sequence		Neutral loss
			Micropeptin 1006/1006A/1007		
[M+H]$^+$	1007.5200	C$_{49}$H$_{71}$O$_{13}$N$_{10}$$^+$	[Thr^1+Arg^2+Ahp^3+Phe^4+MeTyr^5+Val^6+Asp^7+Hexanoic acid^8+H]$^+$		
	989.5055^b	C$_{49}$H$_{69}$O$_{12}$N$_{10}$$^+$			H$_2$O
	979.5220^b	C$_{48}$H$_{71}$O$_{12}$N$_{10}$$^+$			CO
	972.4795^b	C$_{49}$H$_{66}$O$_{12}$N$_9$$^+$			H$_2$O+NH$_3$
	961.5112^b	C$_{48}$H$_{69}$O$_{11}$N$_{10}$$^+$			H$_2$O+CO
	929.4801^b	C$_{48}$H$_{65}$O$_{11}$N$_8$$^+$			2NH$_3$+CO$_2$
1	890.4375^b	C$_{44}$H$_{60}$O$_{11}$N$_9$$^+$	[Thr^1+Arg^2+Ahp^3+Phe^4+MeTyr^5+Asp^7+Hexanoic acid^8+H-H$_2$O]$^+$		Val^6+H$_2$O
2	794.4166^b	C$_{39}$H$_{56}$O$_9$N$_9$$^+$	[Thr^1+Arg^2+Ahp^3+Phe^4+MeTyr^5+Val^6+H]$^+$		Asp^7+Hexanoic acid^8
	776.4062^b	C$_{39}$H$_{54}$O$_8$N$_9$$^+$	[Thr^1+Arg^2+Ahp^3+Phe^4+MeTyr^5+Val^6+H-H$_2$O]$^+$		Asp^7+Hexanoic acid^8+H$_2$O
	758.3960^b	C$_{39}$H$_{52}$O$_7$N$_9$$^+$	[Thr^1+Arg^2+Ahp^3+Phe^4+MeTyr^5+Val^6+H-2H$_2$O]$^+$		Asp^7+Hexanoic acid^8+2H$_2$O
	741.3709^b	C$_{39}$H$_{49}$O$_7$N$_8$$^+$	[Thr^1+Arg^2+Ahp^3+Phe^4+MeTyr^5+Val^6+H-2H$_2$O-NH$_3$]$^+$		Asp^7+Hexanoic acid^8+2H$_2$O+NH$_3$
3	470.2727^a	C$_{20}$H$_{36}$O$_6$N$_7$$^+$	[Thr^1+Arg^2+Asp^7+Hexanoic acid^8+H-H$_2$O+NH$_3$]$^+$		Ahp^3+Phe^4+MeTyr^5+Val^6+H$_2$O-NH$_3$
	453.2454^a	C$_{20}$H$_{33}$O$_6$N$_6$$^+$	[Thr^1+Arg^2+Asp^7+Hexanoic acid^8+H-H$_2$O]$^+$		Ahp^3+Phe^4+MeTyr^5+Val^6+H$_2$O
	436.2198^a	C$_{20}$H$_{30}$O$_6$N$_5$$^+$	[Thr^1+Arg^2+Asp^7+Hexanoic acid^8+H-H$_2$O-NH$_3$]$^+$		Ahp^3+Phe^4+MeTyr^5+Val^6+H$_2$O+NH$_3$
	425.2511^a	C$_{19}$H$_{33}$O$_5$N$_6$$^+$	[Thr^1+Arg^2+Asp^7+Hexanoic acid^8+H-H$_2$O-CO]$^+$		Ahp^3+Phe^4+MeTyr^5+Val^6+H$_2$O+CO
4	420.1921^a	C$_{24}$H$_{26}$O$_4$N$_3$$^+$	[Ahp^3+Phe^4+MeTyr^5+H-H$_2$O]$^+$		Thr^1+Arg^2+Val^6+Asp^7+Hexanoic acid^8+H$_2$O
5	338.1465^a	C$_{14}$H$_{20}$O$_5$N$_5$$^+$	[Thr^1+Arg^2+Asp^7+H-H$_2$O-NH$_3$]$^+$		Ahp^3+Phe^4+MeTyr^5+Val^6+Hexanoic acid^8+H$_2$O+NH$_3$
6	308.1282^a	C$_{19}$H$_{18}$O$_3$N$^+$	[Phe^4+MeTyr^5+H-NH$_3$]$^+$		Thr^1+Arg^2+Ahp^3+Val^6+Asp^7+Hexanoic acid^8+NH$_3$
7	297.1415^a	C$_{17}$H$_{21}$O$_5$N$_2$$^+$	[Thr^1+Asp^7+Hexanoic acid^8+H-H$_2$O]$^+$		Arg^2+Ahp^3+Phe^4+MeTyr^5+Val^6+H$_2$O
8	295.1650^a	C$_{15}$H$_{23}$O$_4$N$_2$$^+$	[MeTyr^5+Val^6+H+H$_2$O]$^+$		Thr^1+Arg^2+Ahp^3+Phe^4+Asp^7+Hexanoic acid^8-H$_2$O
9	243.1132^a	C$_{14}$H$_{15}$O$_2$N$_2$$^+$	[Ahp^3+Phe^4+H-H$_2$O]$^+$		Thr^1+Arg^2+MeTyr^5+Val^6+Asp^7+Hexanoic acid^8+H$_2$O
	215.1182^a	C$_{13}$H$_{15}$ON$_2$$^+$	[Ahp^3+Phe^4+H-H$_2$O-CO]$^+$		Thr^1+Arg^2+MeTyr^5+Val^6+Asp^7+Hexanoic acid^8+H$_2$O+CO
10	241.1302^a	C$_{10}$H$_{17}$O$_3$N$_4$$^+$	[Thr^1+Arg^2+H-NH$_3$]$^+$		Ahp^3+Phe^4+MeTyr^5+Val^6+Asp^7+Hexanoic acid^8+NH$_3$
	223.1191^a	C$_{10}$H$_{15}$O$_2$N$_4$$^+$	[Thr^1+Arg^2+H-NH$_3$-H$_2$O]$^+$		Ahp^3+Phe^4+MeTyr^5+Val^6+Asp^7+Hexanoic acid^8+NH$_3$+H$_2$O
11	214.1075^a	C$_{10}$H$_{16}$O$_4$N$^+$	[Asp^7+Hexanoic acid^8+H]$^+$		Thr^1+Arg^2+Ahp^3+Phe^4+MeTyr^5+Val^6
12	150.0913^a	C$_9$H$_{12}$ON$^+$	[MeTyr^5+H-CO]$^+$ (MeTyr^5 immonium ion)		Thr^1+Arg^2+Ahp^3+Phe^4+Val^6+Asp^7+Hexanoic acid^8+CO
13	120.0808^a	C$_8$H$_{10}$N$^+$	[Phe^4+H-CO]$^+$ (Phe^6 immonium ion)		Thr^1+Arg^2+Ahp^3+MeTyr^5+Val^6+Asp^7+Hexanoic acid^8+CO
14	112.0868^a	C$_5$H$_{10}$N$_3$$^+$	[Arg^2+H-CO-NH$_3$]$^+$		Thr^1+Ahp^3+Phe^4+MeTyr^5+Val^6+Asp^7+Hexanoic acid^8+CO+NH$_3$

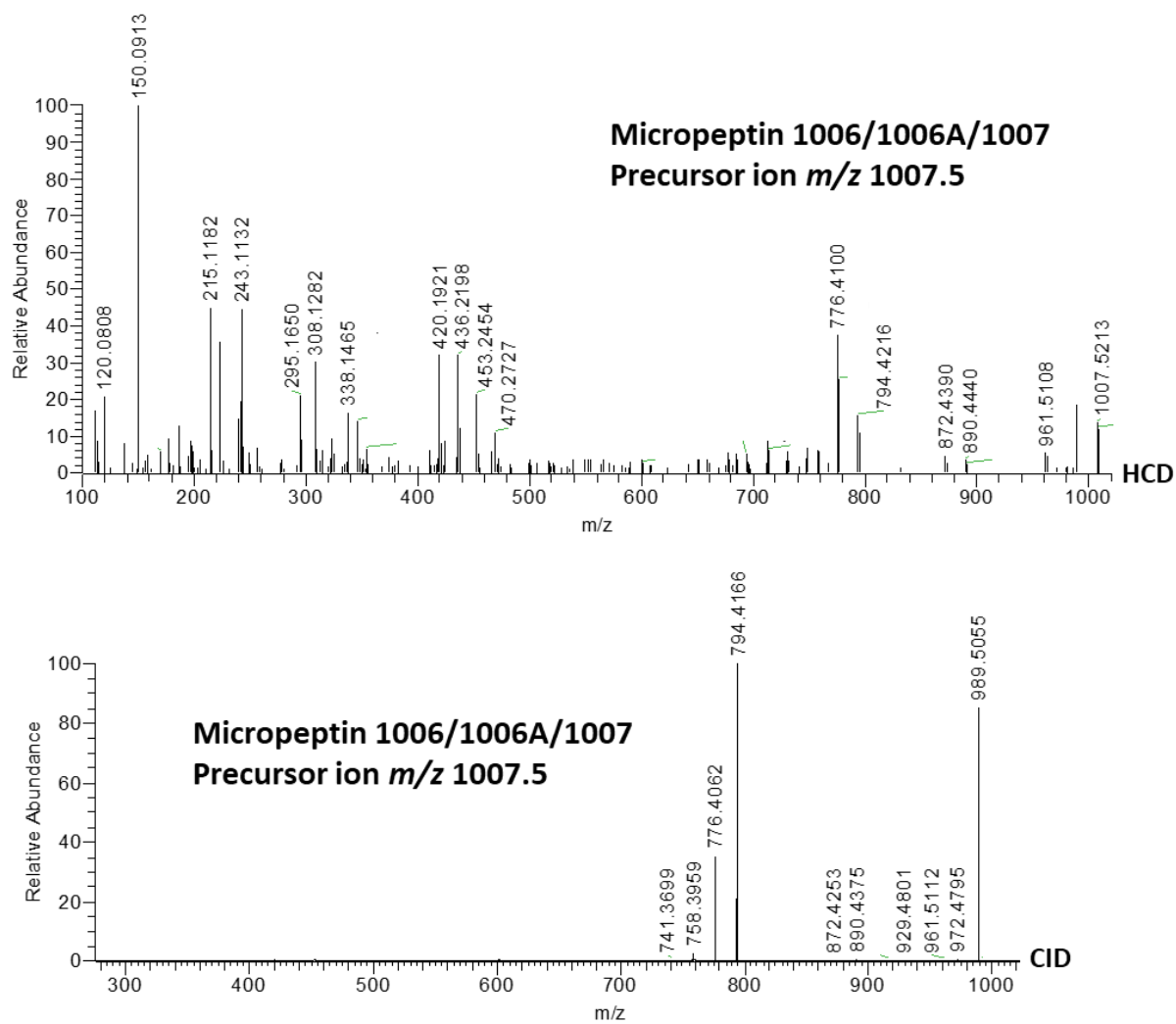^{a}=Fragment contained in the HCD DDA spectrum; ^{b}=Fragment ion contained in the CID DDA spectrum.

Figure IV.34 HCD and CID DDA MS^2 spectrum of Micropeptin 1006/1006A/1007.

The extraction of the diagnostic fragment at *m/z* 370.2125 ($C_{21}H_{28}N_3O_3^+$, [Ahp^3+Leu^4+MePhe^5-H_2O]$^+$) gave three chromatographic peaks eluting at 9.62, 11.52 and 12.45 min all associated to the precursor [M+H]$^+$ ion at *m/z* 846.4720, $C_{40}H_{64}N_9O_{11}^+$ (**Fig.IV.35a**).
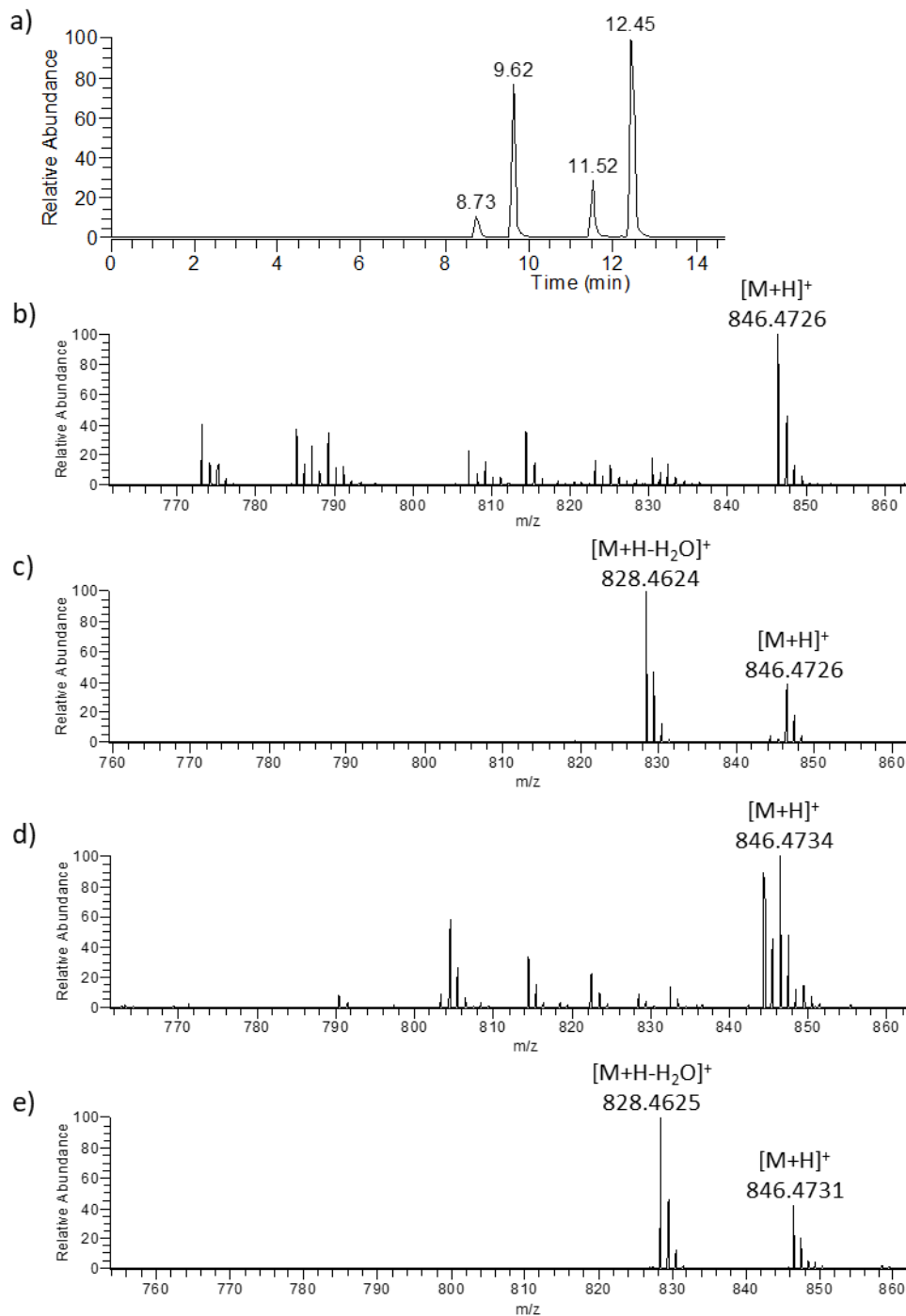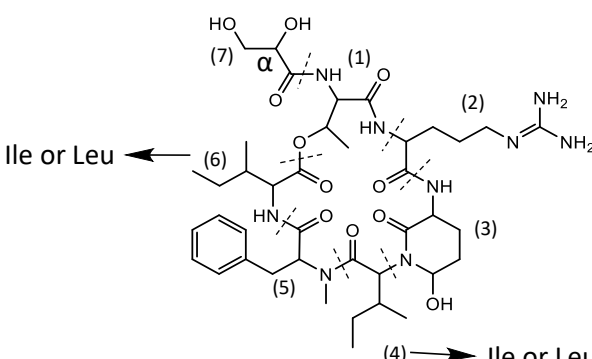

Figure IV.35 a) XIC of [M+H]$^+$ ion at *m/z* 846.4720. HR full scan MS spectrum of peak eluting at: b) 8.73 min, c) 9.62 min, d) 11.52 and e) 12.45 min.

As shown in **(Table IV.24)**, the interpretation of HCD DDA spectra of all three peaks confirmed the sequence Thr[1]-Arg[2]-Ahp[3]-Ile[4]/Leu[4]-MePhe[5]-Ile[6]/Leu[6]-Gliceric acid[7]. Moreover, the XIC of the $[M+H]^+$ ion at *m/z* 846.4720 provided a further peak eluting at 8.73 min for which no good quality MS^2 data were obtained (**Fig.IV.35a**). An in depth-investigation through the cyano-data base highlighted that only 1 compound with this exact mass had been reported so far, namely Micropeptin MZ845, which features the following sequence - Thr[1]-Arg[2]-Ahp[3]-Ile[4]-NMePhe[5]-Ile[6]-Gliceric acid[7]. However, in lack of appropriate standard and considering the impossibility of distinguishing between Ile and Leu by MS^2 approach, it was not possible to correlate Micropeptin MZ845 to any of these peaks. On the other hand, different structural hypotheses can be made for these analogues. Firstly, the four isobaric compounds at *m/z* 846.4720 (**Fig.IV.35a**) may differ each one from the others due to multiple combinations between Ile and Leu residues in position 4 and 6 since for a large number of cyanobacterial secondary metabolites this structural variation has been reported. On the other hand, it cannot be excluded the possibility that different stereoisomers are present, especially considering the structural properties of gliceric acid[7]. Its Cα is a stereocenter, thus a different configuration of the asymmetric carbon may lead to different analogues. This hypothesis arises from a careful investigation of the full-scan spectra associated with the four chromatographic peaks emerged from the XIC of the $[M+H]^+$ at *m/z* 846.4720. Isobaric analogues eluting at 9.62 and 12.45 min underwent strong in-source fragmentation since a very intense $[M+H-H_2O]^+$ ion at *m/z* 828.4624 was found in their spectrum, with a relative abundance ratio with the $[M+H]^+$ ion of 100:40, respectively (**Fig.IV.35c,e**). Contrarily, isomers eluting at 8.73 and 11.52 did not undergo in-source fragmentation since the $[M+H-H_2O]^+$ ion was not found in their spectrum (**Fig.IV.35a-b,d**). Considering that different stereoisomers may undergo to different degrees of in-source fragmentation, (e.g. epimer pairs of PSTs as reported in chapter 3), it can be supposed that isomers eluting at 9.62 and 12.45, and 8.73 and 11.52 have the same stereochemical properties, while they differ each one from the other for residue in position 4 and 6.

Table IV.24 Assignment of fragment ions contained in HCD spectrum of three isobaric Micropeptin MZ845.

	m/z			Sequence		Neutral loss
	Rt 9.62 min	Rt 11.52 min	Rt 12.45 min	Formula		
[M+H]+	846.4715	846.4711	846.4723	$C_{40}H_{64}O_{11}N_9^+$	[Thr[1]+Arg[2]+Ahp[3]+Ile[4]+MePhe[5]+Ile[6]+Gliceric acid[7]+H]+	
	828.4614	828.4645	828.4624	$C_{40}H_{62}O_{10}N_9^+$		H_2O
	818.4782	818.4777	818.4780	$C_{39}H_{64}O_{10}N_9^+$		CO
	800.4658	800.4695	800.4615	$C_{39}H_{62}O_9N_9^+$		H_2O+CO
	783.4393	n.d.	783.4420	$C_{39}H_{59}O_9N_8^+$		H_2O+CO+NH_3
	769.4125	n.d.	769.4150	$C_{39}H_{57}O_{10}N_6^+$		H_2O+CH_5N_3

#						
1	768.4370	n.d.	768.4401	$C_{40}H_{64}O_{11}N_9^+$	[Thr[1]+Arg[2]+Ahp[3]+Ile[4]+MePhe[5]+Ile[6]+Gliceric acid[7]+H-H_2O-$C_2H_4O_2$]+	H_2O+$C_2H_4O_2$ (Part of Gliceric acid[7])
2	733.3884	733.3873	n.d.	$C_{34}H_{53}O_{10}N_8^+$	[Thr[1]+Arg[2]+Ahp[3]+Ile[4]+MePhe[5]+Ile[6]+Gliceric acid[7]+H-Ile[4/6]]+	Ile[4/6]
	716.3610	716.3613	n.d.	$C_{34}H_{50}O_{10}N_7^+$	[Thr[1]+Arg[2]+Ahp[3]+Ile[4]+MePhe[5]+Ile[6]+Gliceric acid[7]+H-Ile[4/6]-NH_3]+	Ile[4/6]+NH_3
	715.3743	715.3778	715.3792	$C_{34}H_{51}O_9N_8^+$	[Thr[1]+Arg[2]+Ahp[3]+Ile[4]+MePhe[5]+Ile[6]+Gliceric acid[7]+H-Ile[4/6]-H_2O]+	Ile[4/6]+H_2O
	705.3947	705.3936	n.d.	$C_{33}H_{53}O_9N_8^+$	[Thr[1]+Arg[2]+Ahp[3]+Ile[4]+MePhe[5]+Ile[6]+Gliceric acid[7]+H-Ile[4/6]-CO]+	Ile[4/6]+CO
	698.3490	698.3532	n.d.	$C_{34}H_{48}O_9N_7^+$	[Thr[1]+Arg[2]+Ahp[3]+Ile[4]+MePhe[5]+Ile[6]+Gliceric acid[7]+H-Ile[4/6]-H_2O-NH_3]+	Ile[4/6]+H_2O+NH_3
	697.3649	n.d.	697.3674	$C_{34}H_{49}O_9N_8^+$	[Thr[1]+Arg[2]+Ahp[3]+Ile[4]+MePhe[5]+Ile[6]+Gliceric acid[7]+H-Ile[4/6]-$2H_2O$]+	Ile[4/6]+$2H_2O$
	688.3677	688.3622	n.d.	$C_{33}H_{50}O_9N_7^+$	[Thr[1]+Arg[2]+Ahp[3]+Ile[4]+MePhe[5]+Ile[6]+Gliceric acid[7]+H-Ile[4/6]-CO-NH_3]+	Ile[4/6]+CO+NH_3
3	620.3405	620.3402	620.3388	$C_{29}H_{46}O_8N_7^+$	[Thr[1]+Arg[2]+MePhe[5]+Ile[6]+Gliceric acid[7]+H]+	Ahp[3]+Ile[4]
	603.3140	603.3136	603.3132	$C_{29}H_{43}O_8N_6^+$	[Thr[1]+Arg[2]+MePhe[5]+Ile[6]+Gliceric acid[7]+H-NH_3]+	Ahp[3]+Ile[4]+NH_3
4	537.2659	537.2645	537.2703	$C_{24}H_{37}O_8N_6^+$	[Thr[1]+Arg[2]+Ahp[3]+Ile[6]+Gliceric acid[7]+H-$2NH_3$-H_2O]+	Ile[4]+MePhe[5]+$2NH_3$+H_2O
	536.2822	n.d.	536.2824	$C_{24}H_{38}O_7N_7^+$	[Thr[1]+Arg[2]+Ahp[3]+Ile[6]+Gliceric acid[7]+H-NH_3-$2H_2O$]+	Ile[4]+MePhe[5]+NH_3+$2H_2O$
	519.2559	519.2595	519.2555	$C_{24}H_{35}O_7N_6^+$	[Thr[1]+Arg[2]+Ahp[3]+Ile[6]+Gliceric acid[7]+H-$2NH_3$-$2H_2O$]+	Ile[4]+MePhe[5]+$2NH_3$+$2H_2O$
5	526.2990	526.2986	526.3038	$C_{23}H_{40}O_7N_7^+$	[Thr[1]+Arg[2]+Ahp[3]+Ile[6]+Gliceric acid[7]+H-H_2O-NHCO (part of Ahp[3])]+	Ile[4]+MePhe[5]+H_2O+NHCO
	491.2610	n.d.	491.2607	$C_{23}H_{35}O_6N_6^+$	[Thr[1]+Arg[2]+Ahp[3]+Ile[6]+Gliceric acid[7]+H-$2H_2O$-NHCO (part of Ahp[3])-NH_3]+	Ile[4]+MePhe[5]+$2H_2O$+NHCO+NH_3
6	459.2572	459.2569	459.2561	$C_{19}H_{35}O_7N_6^+$	[Thr[1]+Arg[2]+Ile[6]+Gliceric acid[7]+H]+	Ahp[3]+Ile[4]+MePhe[5]
7	440.2245	n.d.	440.2255	$C_{18}H_{30}O_6N_7^+$	[Thr[1]+Arg[2]+Ahp[3]+Gliceric acid[7]+H-$2H_2O$]+	Ile[4]+MePhe[5]+Ile[6]+$2H_2O$
	424.1822	424.1825	424.1810	$C_{18}H_{26}O_7N_5^+$	[Thr[1]+Arg[2]+Ahp[3]+Gliceric acid[7]+H-H_2O-$2NH_3$]+	Ile[4]+MePhe[5]+Ile[6]+H_2O+$2NH_3$
8	370.2125	370.2127	370.2127	$C_{21}H_{28}O_3N_3^+$	[Ahp[3]+Ile[4]+MePhe[5]+H-H_2O]+	Thr[1]+Arg[2]+Ile[6]+Gliceric acid[7]+H_2O
9	346.1698	346.1724	n.d.	$C_{13}H_{24}O_6N_5^+$	[Thr[1]+Arg[2]+Gliceric acid[7]+H]+	Ahp[3]+Ile[4]+MePhe[5]+Ile[6]
	345.1881	n.d.	345.1879	$C_{13}H_{25}O_5N_6^+$	[Thr[1]+Arg[2]+Gliceric acid[7]+H-H_2O+NH_3]+	Ahp[3]+Ile[4]+MePhe[5]+Ile[6]+H_2O-NH_3
	328.1615	328.1614	328.1617	$C_{13}H_{22}O_5N_5^+$	[Thr[1]+Arg[2]+Gliceric acid[7]+H-H_2O]+	Ahp[3]+Ile[4]+MePhe[5]+Ile[6]+H_2O
	311.1347	311.1346	311.1350	$C_{13}H_{19}O_5N_4^+$	[Thr[1]+Arg[2]+Gliceric acid[7]+H-H_2O-NH_3]+	Ahp[3]+Ile[4]+MePhe[5]+Ile[6]+H_2O+NH_3
	300.1668	300.1665	300.1669	$C_{12}H_{22}O_4N_5^+$	[Thr[1]+Arg[2]+Gliceric acid[7]+H-H_2O-CO]+	Ahp[3]+Ile[4]+MePhe[5]+Ile[6]+H_2O+CO
	286.1397	286.1406	286.1400	$C_{12}H_{20}O_5N_3^+$	[Thr[1]+Arg[2]+Gliceric acid[7]+H-H_2O-CH_2N_2 (part of Arg[2])]+	Ahp[3]+Ile[4]+MePhe[5]+Ile[6]+H_2O+CH_2N_2

| 10	293.1859	293.1862	293.1860	$C_{16}H_{25}O_3N_2^+$	[Thr[1]+MePhe[5]+Ile[6]+H][+]	Arg[2]+Ahp[3]+Ile[4]+Gliceric acid[7]
	275.1750	275.1762	275.1745	$C_{16}H_{23}O_2N_2^+$	[Thr[1]+MePhe[5]+Ile[6]+H-H_2O][+]	Arg[2]+Ahp[3]+Ile[4]+Gliceric acid[7]+H_2O
	258.1489	258.1487	258.1489	$C_{16}H_{20}O_2N^+$	[Thr[1]+MePhe[5]+Ile[6]+H-H_2O-NH_3][+]	Arg[2]+Ahp[3]+Ile[4]+Gliceric acid[7]+H_2O+NH_3
	247.1800	247.1807	247.1808	$C_{15}H_{23}ON_2^+$	[Thr[1]+MePhe[5]+Ile[6]+H-H_2O-CO][+]	Arg[2]+Ahp[3]+Ile[4]+Gliceric acid[7]+H_2O+CO
11	223.1184	233.1192	223.1189	$C_{10}H_{15}O_2N_4^+$	[Thr[1]+Arg[2]+H-H_2O-NH_3][+]	Ahp[3]+Ile[4]+MePhe[5]+Ile[6]+Gliceric acid[7]+H_2O+NH_3
12	209.1281	209.1281	209.1283	$C_{11}H_{17}O_2N_2^+$	[Ahp[3]+Ile[4]+H-H_2O][+]	Thr[1]+Arg[2]+ MePhe[5]+Ile[6]+Gliceric acid[7]+H_2O
	181.1335	181.1334	181.1336	$C_{10}H_{12}ON_2^+$	[Ahp[3]+Ile[4]+H-H_2O-CO][+]	Thr[1]+Arg[2]+ MePhe[5]+Ile[6]+Gliceric acid[7]+H_2O+CO
13	190.0862	190.0850	n.d.	$C_{11}H_{12}O_2N^+$	[MePhe[5]+H+CO][+]	Thr[1]+Arg[2]+Ahp[3]+Ile[4]+ Ile[6]+Gliceric acid[7]-CO
	162.0921	162.0920	162.0918	$C_{10}H_{12}ON^+$	[MePhe[5]+H][+]	Thr[1]+Arg[2]+Ahp[3]+Ile[4]+ Ile[6]+Gliceric acid[7]
14	172.0604	172.0604	172.0604	$C_7H_{10}O_4N^+$	[Thr[1]+Gliceric acid[7]+H-H_2O][+]	Arg[2]+Ahp[3]+Ile[4]+MePhe[5]+Ile[6]+ H_2O
15	134.0963	134.0963	134.0964	$C_9H_{12}N^+$	[MePhe[5]+H-CO][+] (MePhe[5] immonium ion)	Thr[1]+Arg[2]+Ahp[3]+Ile[4]+Ile[6]+Gliceric acid[7]+CO
16	124.1113	n.d.	124.1121	$C_8H_{14}N^+$	[Ahp[3]+Ile[4]+H-H_2O-CO-C_2H_3NO (part of Ahp[3])][+]	Thr[1]+Arg[2]+ MePhe[5]+Ile[6]+Gliceric acid[7]+H_2O+CO+C_2H_3NO
17	115.0867	115.0862	115.0863	$C_5H_{11}ON_2^+$	[Arg[2]+H-CH_2N_2 (part of Arg[2])][+]	Thr[1]+Ahp[3]+Ile[4]+MePhe[5]+Ile[6]+Gliceric acid[7]+CH_2N_2
	112.0867	112.0868	112.0868	$C_5H_{10}N_3^+$	[Arg[2]+H-NH_3-CO][+]	Thr[1]+Ahp[3]+Ile[4]+MePhe[5]+Ile[6]+Gliceric acid[7]+NH_3+CO

Rt= Retention time.
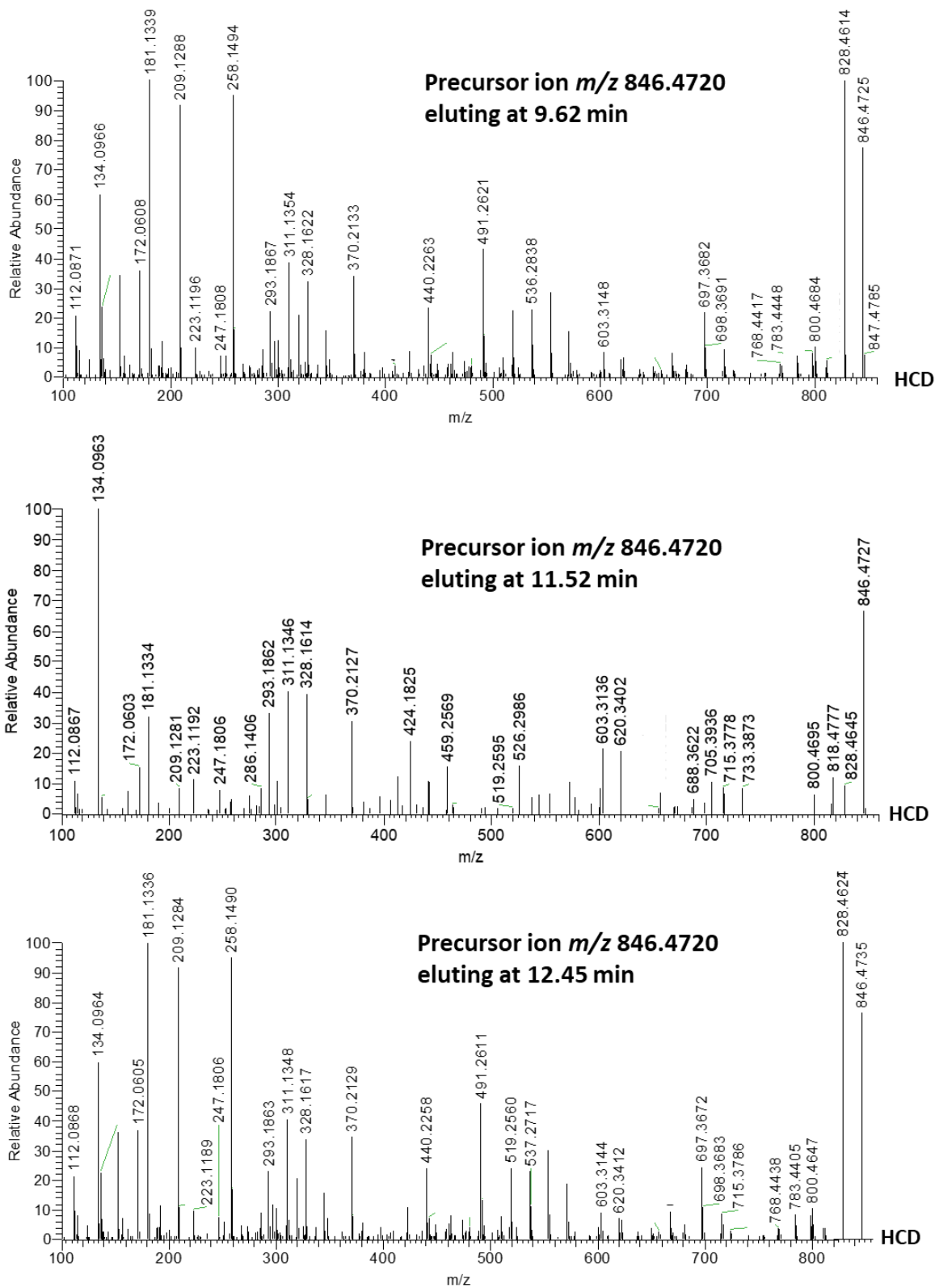
Figure IV.36 HCD DDA MS^2 spectrum of [M+H]$^+$ ion at *m/z* 846.4720 eluting at 9.62, 11.52 and 12.45 min.

3. Materials and methods

3.1 Standards

Certified reference material (CRM) of MC-LR, MC-RR, [Dha[7]]MC-LR, NOD-R, ATX-a, CYN and LWTX1 were purchased from the Institute of Biotoxin Metrology, National Research Council of Canada (NRC, Halifax, Canada). TTX standard was obtained from Enzo Life Sciences (Enzo, Exeter, United Kingdom). A mixture of [dAsp[3]]MC-RR, MC-YR, MC-HtyR,[dAsp3]MC-LR, MC-HilR, MC-WR, MC-LA, MC-LY, MC-LW and MC-LF non-certified reference material was kindly provided by National Center for Scientific Research "Demokritos'' of Athens.

3.2 Extraction of cyanobacterial biomass

The cyanobacterial biomass sample was extracted according to the procedure reported by Christophoridis et al. [41]. Briefly, an aliquot of 100 mg of lyophilized biomass was weighted, transferred into a 15 mL polypropylene (PP) centrifuge tube and extracted with 7.5 mL of a mixture methanol-water 75:25 (v/v). The mixture was sonicated in a water bath for 15 min, centrifuged for 10 min at 4500 rpm and then the supernatant was collected. The solid residue was extracted again twice, first with methanol-water 75:25 (v/v) and then with n-butanol. The three supernatants were pooled and mix together (22.5 mL) in a 50 mL PP centrifuge tube, evaporated under a gentle nitrogen stream and suspended with 2.5 mL of methanol-water 20:80 (v/v) before LC-MS analyses.

3.3 Optimization of HILIC and LC-HRMS methods

LC-HRMS analyses were carried out on a hybrid linear ion trap LTQ Orbitrap XL[TM] Fourier Transform Mass Spectrometer (FTMS) equipped with an ESI ION MAX[TM] source coupled with a Dionex Ultimate 3000 quaternary HPLC system (Thermo-Fisher, San Jose, CA, USA).

3.3.1 LC-HRMS method

Chromatographic separation was performed on a HyperClone 3μm BDS C8 13A 50 x 2.0 mm column (Phenomenex, Torrance, CA, USA) kept at room temperature and eluted at 0.2 mL/min with the following mobile phases: water (A) and acetonitrile-water 95:5 v/v (B) both containing 2.0 mM ammonium formate and 50.0 mM formic acid. The gradient elution was accomplished as

follows: time (t) 0 min, 10% B; t 10 min, 40%B; t 15, 100%B; t 20, 100%B; t 21, 10%B and t 22, 10% B; re-equilibration time was 9 min. Samples were kept in the autosampler at 4°C while the injection volume was set at 5.0 µL. ESI HRMS analyses were performed in positive ion mode, and source settings were optimized on the basis of the response of each certified standard as follows: spray voltage 4.8 kV, capillary temperature 350 °C, capillary voltage 49 V, sheath gas 35 and auxiliary gas 6 (arbitrary units), tube lens voltage 155 V. Full-scan spectra were acquired in the *m/z* range 400-1800 at resolving power (RP) 30.000 (FWHM at *m/z* 400). Higher-energy collisional dissociation (HCD) and high-resolution collision induced dissociation (CID) MS^2 experiments were recorded at RP 30.000, collision energy (CE) 15-40 %, isolation width 2 *m/z*, activation Q 0.250, activation time 30 ms, and selecting as precursors the [M+H]$^+$ ion of each toxin and/or cyanobacterial secondary metabolite. Data dependent acquisition (DDA) experiments were accomplished in positive ion mode and designed as follows: 9 scan events were set up with the scan event 1 being the HR full-scan MS in the *m/z* range 400-1800, whilst the other scans were HRMS^2 acquisitions recorded at RP 7.500 by fragmenting both in CID and HCD mode the 8 most intense ions observed within the full-scan *m/z* range selected (DDA experiment was set up similarly to that reported in chapter 2). The linearity of the method was evaluated through matrix-free (MF) calibration curves which were prepared through serial dilution with methanol/water (2:8, v/v) of a standard mixture, obtaining the following levels: MC-LR (15.8, 31.6, 63.1, 126.3, 252.5 ng/mL), MC-RR (17.5, 35.0, 70.0, 140.0, 280.0 ng/mL), [Dha^7]MC-LR (15.9, 31.9, 63.8, 127.5, 255.0 ng/mL) and NOD-R (17.3, 34.7, 69.4, 138.8, 277.5 ng/mL). Similarly, instrumental limits (LOD and LOQ) were measured through multiple dilution up to the lowest quantifiable and detectable concentration. Quantitative analysis of MCs detected in the cyanobacterial biomass sample was performed through MF calibration curves of MC-LR and MC-RR both prepared at these levels: 5.0, 10.0, 20.0 and 400.0 ng/mL. Elemental formulae were calculated on the monoisotopic peak of the ion cluster through Thermo Xcalibur software v2.2 SP1.48 (Thermo Fisher, San Josè, CA, USA) with a mass tolerance within 5 ppm.

3.3.2 HILIC-HRMS method

Chromatographic separation of ATX-a, CYN and LWTX1 was accomplished by using the TSK-gel® Amide-80 column (250mm×2mm i.d) eluted under the same experimental conditions optimized for the analysis of PSTs and TTX reported in chapter 3 *paragraph 3.3.1*. Similarly, ESI

source parameters were the same optimized for the analysis of C toxins and used in the first window of the HILIC-HRMS method time segmented-based, briefly: spray voltage 4.5 kV, capillary temperature 300 °C, capillary voltage 80 V, sheath gas 31 and auxiliary gas 13 (arbitrary units), tube lens voltage 90 V. Full-scan spectra were acquired in the m/z range 100-500 at resolving power (RP) 30,000 (FWHM at m/z 400). CID MS^n (n=2,3) experiments were recorded at RP 30,000, collision energy (CE) 20-22%, isolation width 2 m/z, activation Q 0.250, activation time 30 ms. The full-scan XIC of each toxin was obtained by selecting the exact mass of the relevant $[M+H]^+$ ion, while $HRMS^2$ XIC were performed by selecting the most intense fragments present in the CID spectra. The multi-toxin HILIC-$HRMS^2$ time segmented method for the simultaneous analysis of polar cyanotoxins (PSTs, ATX-a, CYN and LWTX1) was designed by adding the MS^2 scans for the detection of ATX-a, CYN and LWTX1 in the method HILIC-HRMS 1 previously optimized and reported in chapter 3 *paragraph 3.3.1*. On the basis of their retention time, ATX-a, CYN and LWTX1 were monitored in the first time window (0-9.5 min) through CID MS^2 experiments performed under the optimized conditions. Method linearity was assessed through MF calibration curves, which were prepared through serial dilution of a standard mixture with acetic acid 10 mM obtaining the following concentration levels: ATX-a (6.5, 19.4, 38.8, 77.5, 155.0, 310.0 ng/mL), CYN (6.6, 19.7, 39.4, 78.8, 157.5, 315.0 ng/mL) and LWTX1 (5.4, 16.3, 32.5, 65.0, 130.1, 260.1 ng/mL). LOD and LOQ were measured by preparing multiple dilution levels of the same standard mixture.

4. Conclusions

The present study has reported the development of a highly effective and sensitive reverse-phase LC-HRMS method for the analysis of cyanotoxins such as MCs and NOD. The application of the method to the analysis of a cyanobacterial biomass sample successfully highlighted a large number of MC congeners whose accurate quantitation revealed that MC-RR and MC-LR were the dominant analogues accounting for > 51% and > 34% of the total toxin content, respectively. The high biodiversity that emerged from the analysis of the cyanobacterial biomass led to the implementation of a new analytical strategy to deeply explore the metabolic profile of cyanobacterial species. The implemented methodology was designed through the combination of DDA HRMS experiments with a newly vendor-free published database of cyanometabolites. This

analytical workflow has proven to be a powerful tool for high throughput and fast screening, since the presence of a large number of known and unknown analogues within MC, MG, AP and CPtp sub-groups was brought to light. Two newly MC congeners, named in this study MC-prHcysR and MC-prHcys(O)R, were discovered; their structure was proposed on the basis of the cross interpretation of the relevant CID and HCD spectra. Following the same approach, structural insights were successfully obtained for new MG, named cyanostatin C and MG 821, and for 4 isobaric CPtps found in the cyanobacterial biomass.

In addition, the effectiveness of the HILIC-HRMS[2] method 1, which was previously optimized for the analysis of PSTs and TTX, was tested for the determination of polar and low-molecular weight cyanotoxins such as ATX-a, CYN and LWTX1. As a result, a multi-toxin time-segmented HILIC-HRMS method was developed for the analysis of assorted cyanotoxins within the same LC-MS run (PSTs, ATX-a, CYN and LWTX1) by using certified standards. However, its application to real samples is still in progress.

Results of the study reported in this chapter are reported in a manuscript under preparation.

References

1.   Bláha, L., Babica, P., & Maršálek, B. (2009). Toxins produced in cyanobacterial water blooms-toxicity and risks. *Interdisciplinary toxicology*, *2*(2), 36-41.

2.   Stomp, M., Huisman, J., Vörös, L., Pick, F. R., Laamanen, M., Haverkamp, T., & Stal, L. J. (2007). Colourful coexistence of red and green picocyanobacteria in lakes and seas. *Ecology Letters*, *10*(4), 290-298.

3.   Six, C., Thomas, J. C., Garczarek, L., Ostrowski, M., Dufresne, A., Blot, N., ... & Partensky, F. (2007). Diversity and evolution of phycobilisomes in marine Synechococcus spp.: a comparative genomics study. *Genome biology*, *8*(12), 1-22.

4.   Carmichael, W. W. (2001). Health effects of toxin-producing cyanobacteria:"The CyanoHABs". *Human and ecological risk assessment: An International Journal*, *7*(5), 1393-1407.

5.   Whitton, B. A. (Ed.). (2012). *Ecology of cyanobacteria II: their diversity in space and time*. Springer Science & Business Media.

6.   Merel, S., Walker, D., Chicana, R., Snyder, S., Baurès, E., & Thomas, O. (2013). State of knowledge and concerns on cyanobacterial blooms and cyanotoxins. *Environment international*, *59*, 303-327.

7.   Huisman, J., Codd, G. A., Paerl, H. W., Ibelings, B. W., Verspagen, J. M., & Visser, P. M. (2018). Cyanobacterial blooms. *Nature Reviews Microbiology*, *16*(8), 471-483.

8.   Wagner, C., & Adrian, R. (2009). Cyanobacteria dominance: quantifying the effects of climate change. *Limnology and Oceanography*, *54*(6part2), 2460-2468.

9.   Kleinteich, J., Wood, S. A., Küpper, F. C., Camacho, A., Quesada, A., Frickey, T., & Dietrich, D. R. (2012). Temperature-related changes in polar cyanobacterial mat diversity and toxin production. *Nature Climate Change*, *2*(5), 356-360.

10.   Testai, E., Buratti, F. M., Funari, E., Manganelli, M., Vichi, S., Arnich, N., ... & Sialehaamoa, A. (2016). Review and analysis of occurrence, exposure and toxicity of cyanobacteria toxins in food. *EFSA Supporting Publications*, *13*(2), 998E.

11.   Sanseverino, I., António, D. C., Loos, R., & Lettieri, T. (2017). Cyanotoxins: methods and approaches for their analysis and detection. *Centre, JR, Ed*.

12.   Moreira, C., Matos, A., Mendes, R. & Antunes, A. (2015). pag 1-23 in *Plant Toxins,* Editor(s): P. Gopalakrishnakone,,Célia R. Carlini, & Rodrigo Ligabue-Braun. Springer Netherlands. ISBN 978-94-007-6465-1.

13.   Auckenthaler, R., & Risch, M. (2015). Verdrängt Multiplex PCR den klassischen Kulturnachweis in der Mikrobiologie?. *Therapeutische Umschau*, *72*(2), 77-85.

14.   Pacheco, A. B. F., Guedes, I. A., & Azevedo, S. M. (2016). Is qPCR a reliable indicator of cyanotoxin risk in freshwater?. *Toxins*, *8*(6), 172.

15.   Penn, K., Wang, J., Fernando, S. C., & Thompson, J. R. (2014). Secondary metabolite gene expression and interplay of bacterial functions in a tropical freshwater cyanobacterial bloom. *The ISME journal*, *8*(9), 1866-1878.

16.   Rudi, K., Skulberg, O. M., Skulberg, R., & Jakobsen, K. S. (2000). Application of sequence-specific labeled 16S rRNA gene oligonucleotide probes for genetic profiling of cyanobacterial abundance and diversity by array hybridization. *Applied and environmental microbiology*, *66*(9), 4004-4011.

17.   Rantala, A., Rizzi, E., Castiglioni, B., De Bellis, G., & Sivonen, K. (2008). Identification of hepatotoxin-producing cyanobacteria by DNA-chip. *Environmental microbiology*, *10*(3), 653-664.

18.   Zeck, A., Eikenberg, A., Weller, M. G., & Niessner, R. (2001). Highly sensitive immunoassay based on a monoclonal antibody specific for [4-arginine] microcystins. *Analytica Chimica Acta*, *441*(1), 1-13.

19.   Metcalf, J. S., Bell, S. G., & Codd, G. A. (2000). Production of novel polyclonal antibodies against the cyanobacterial toxin microcystin-LR and their application for the detection and quantification of microcystins and nodularin. *Water Research*, *34*(10), 2761-2769.

20.   He, X., Liu, Y. L., Conklin, A., Westrick, J., Weavers, L. K., Dionysiou, D. D., ... & Walker, H. W. (2016). Toxic cyanobacteria and drinking water: Impacts, detection, and treatment. *Harmful algae*, *54*, 174-193.

21.   Moreira, C., Ramos, V., Azevedo, J., & Vasconcelos, V. (2014). Methods to detect cyanobacteria and their toxins in the environment. *Applied microbiology and biotechnology*, *98*(19), 8073-8082.

22.   Triantis, T., Tsimeli, K., Kaloudis, T., Thanassoulias, N., Lytras, E., & Hiskia, A. (2010). Development of an integrated laboratory system for the monitoring of cyanotoxins in surface and drinking waters. *Toxicon*, *55*(5), 979-989.

23.   He, X., Stanford, B. D., Adams, C., Rosenfeldt, E. J., & Wert, E. C. (2017). Varied influence of microcystin structural difference on ELISA cross-reactivity and chlorination efficiency of congener mixtures. *Water research*, *126*, 515-523.

24.   Meriluoto, J., Codd, G., Reilly, M., Metcalf, J. S., Spoof, L., Sjövall, O., ... & Tarczynska, M. (2005). TOXIC: cyanobacterial monitoring and cyanotoxin analysis.

25.   Westrick, J.A., Southwell, B., Szlag, D., Zimba, P.V., 2010b. Detection of cyanotoxins during potable water treatment. In: Gray, M.R. (Ed.), Algae: Source to Treatment. 1st ed. American Water Works Association, Denver.

26.   Lawton, L. A., & Edwards, C. (2008). Conventional laboratory methods for cyanotoxins. In *Cyanobacterial harmful algal blooms: state of the science and research needs* (pp. 513-537). Springer, New York, NY.

27.   Filatova, D., Picardo, M., Núñez, O., & Farré, M. (2020). Analysis, levels and seasonal variation of cyanotoxins in freshwater ecosystems. *Trends in Environmental Analytical Chemistry*, e00091.

28.   Jones, M. R., Pinto, E., Torres, M. A., Doerr, F., Mazur-Marzec, H., Szubert, K., ... & Janssen, E. M. L. (2020). Comprehensive database of secondary metabolites from cyanobacteria. *BioRxiv*.

29.   Rivasseau, C., Martins, S., & Hennion, M. C. (1998). Determination of some physicochemical parameters of microcystins (cyanobacterial toxins) and trace level analysis in environmental samples using liquid chromatography. *Journal of chromatography A*, *799*(1-2), 155-169.

30.   Bartó, E., Prauda, I., Kilár, F., Kiss, I., & Felinger, A. (2015). Retention behavior of resorcinarene-based cavitands on C8 and C18 stationary phases. *Journal of separation science*, *38*(17), 2975-2982.

31.   Zhang, H., Gonzales, G. B., Beloglazova, N. V., De Saeger, S., Shen, J., Zhang, S., ... & Wang, Z. (2020). Development of a validated direct injection-liquid chromatographic tandem mass spectrometric method under negative electrospray ionization for quantitation of nine microcystins and nodularin-R in lake water. *Journal of Chromatography A*, *1609*, 460432.

32.   Yuan, M., Namikoshi, M., Otsuki, A., Watanabe, M. F., & Rinehart, K. L. (1999). Electrospray ionization mass spectrometric analysis of microcystins, cyclic heptapeptide hepatotoxins: modulation of charge states and [M+ H]+ to [M+ Na]+ ratio. *Journal of the American Society for Mass Spectrometry*, *10*(11), 1138-1151.

33.   Onofrio, M. D., Mallet, C. R., Place, A. R., & Smith, J. L. (2020). A screening tool for the direct analysis of marine and freshwater phycotoxins in organic SPATT extracts from the Chesapeake Bay. *Toxins*, *12*(5), 322.

34.   Foss, A. J., Miles, C. O., Samdal, I. A., Løvberg, K. E., Wilkins, A. L., Rise, F., ... & Aubel, M. T. (2018). Analysis of free and metabolized microcystins in samples following a bird mortality event. *Harmful Algae*, *80*, 117-129.

35.   Bouaïcha, N., Miles, C. O., Beach, D. G., Labidi, Z., Djabri, A., Benayache, N. Y., & Nguyen-Quang, T. (2019). Structural diversity, characterization and toxicology of microcystins. *Toxins*, *11*(12), 714.

36.   Puddick, J., Prinsep, M. R., Wood, S. A., Cary, S. C., Hamilton, D. P., & Holland, P. T. (2015). Further characterization of glycine-containing microcystins from the McMurdo dry valleys of Antarctica. *Toxins*, *7*(2), 493-515.

37.   Huang, I. S., & Zimba, P. V. (2019). Cyanobacterial bioactive metabolites—A review of their chemistry and biology. *Harmful algae*, *86*, 139-209.

38.   Dell'Aversano, C., Eaglesham, G. K., & Quilliam, M. A. (2004). Analysis of cyanobacterial toxins by hydrophilic interaction liquid chromatography–mass spectrometry. *Journal of Chromatography A*, *1028*(1), 155-164.

39.   Smith, M. L., Westerman, D. C., Putnam, S. P., Richardson, S. D., & Ferry, J. L. (2019). Emerging Lyngbya wollei toxins: A new high resolution mass spectrometry method to elucidate a potential environmental threat. *Harmful algae*, *90*, 101700.

40.   Seifert, M., McGregor, G., Eaglesham, G., Wickramasinghe, W., & Shaw, G. (2007). First evidence for the production of cylindrospermopsin and deoxy-cylindrospermopsin by the freshwater benthic cyanobacterium, Lyngbya wollei (Farlow ex Gomont) Speziale and Dyck. *Harmful algae*, *6*(1), 73-80.

41.   Christophoridis, C., Zervou, S. K., Manolidi, K., Katsiapi, M., Moustaka-Gouni, M., Kaloudis, T., ... & Hiskia, A. (2018). Occurrence and diversity of cyanotoxins in Greek lakes. *Scientific reports*, *8*(1), 1-22.

42.   Miles, C. O., Melanson, J. E., & Ballot, A. (2014). Sulfide oxidations for LC-MS analysis of methionine-containing microcystins in Dolichospermum flos-aquae NIVA-CYA 656. *Environmental science & technology*, *48*(22), 13307-13315.

43.   Strangman, W. K., & Wright, J. L. (2016). Microginins 680, 646, and 612—New chlorinated Ahoa-containing peptides from a strain of cultured Microcystis aeruginosa. *Tetrahedron Letters*, *57*(16), 1801-1803.

44.   Zervou, S. K., Gkelis, S., Kaloudis, T., Hiskia, A., & Mazur-Marzec, H. (2020). New microginins from cyanobacteria of Greek freshwaters. *Chemosphere*, *248*, 125961.

45.   Kelstrup, C. D., Frese, C., Heck, A. J., Olsen, J. V., & Nielsen, M. L. (2014). Analytical utility of mass spectral binning in proteomic experiments by SPectral Immonium Ion Detection (SPIID). *Molecular & Cellular Proteomics*, *13*(8), 1914-1924.

46.   Flores, C., & Caixach, J. (2015). An integrated strategy for rapid and accurate determination of free and cell-bound microcystins and related peptides in natural blooms by liquid

chromatography–electrospray-high resolution mass spectrometry and matrix-assisted laser desorption/ionization time-of-flight/time-of-flight mass spectrometry using both positive and negative ionization modes. *Journal of Chromatography A*, *1407*, 76-89.

47.   Welker, M., Maršálek, B., Šejnohová, L., & Von Doehren, H. (2006). Detection and identification of oligopeptides in Microcystis (cyanobacteria) colonies: toward an understanding of metabolic diversity. *Peptides*, *27*(9), 2090-2103.

Chapter 5: Development of LC-HRMS and LC-MS^2 method for the detection of CTXs. Application of the targeted approach for the analysis of the toxic profile of Indian fish and large-scale extraction of toxic compounds.

1. Introduction

Ciguatera fish poisoning (CFP) is one of the oldest known food-born illnesses since 1500 characterized by a variety of neurological, gastrointestinal and cardiovascular disorders [1]. Epidemiological data are extremely worrying considering the strong impact that CFP have on tropical and sub-tropical populations, with an estimated number of 10,000-500,000 cases of intoxication per year [2]. This scenario raises even more concerns since a large amount of underdiagnosis and underreporting cases are assumed in areas where CFP outbreak occurs frequently. CFP is caused by the consumption of tropical and sub-tropical fish contaminated with ciguatoxins (CTXs), a class of lipophilic marine toxins which are: i) produced by benthic and epiphytic dinoflagellates belonging to the *Gambierdiscus* and *Fukuyoa* genera and ii) biotransformed in fish within the marine food web [3-4]. CTXs are complex polyether compounds that are classified according to their geographical origin in Pacific (P), Caribbean (C) and Indian (I) CTXs [5]. In the last few years the risk of ciguatera poisoning is becoming a real threat for human safety within the EU borders since CTX-producing microalgae and/or contaminated carnivorous fish have been detected in waters from Greece (Crete) [6], Macaronesia (Azores, Madeira, Canary Island and Capo Verde) [7-11] and Mediterranean basin [12-13]. Moreover, import activity of exotic fishery products from regions where CFP historically occurs to EU countries are posing high concerns for public health since a number of intoxications have already been reported [14-15]. In this context, a further alarm for consumer safety is represented by MTXs, a class of marine toxins produced by some species of *Gambierdiscus* flagellates and frequently found in co-occurrence with CTXs in extracts from algal and fish samples [16-17]. Currently, CTXs are considered emerging toxins thus: i) comprehensive data on acute and chronic toxicity, ii) studies on toxin distribution through the food web, iii) the development of high performance and sensitive methods for toxin determination and iv) the production of well-certified reference

material, are a prerequisite for achieving health and safety standards [18]. To prevent consumer health, EU commission established that no fishery products contaminated with CTXs must be placed on market (EC Regulation No. 853/2004) whilst the FDA proposed a guidance level of $<$ 0.01 µg/Kg of P-CTX1B eq. and $<$ 0.1 µg/Kg of C-CTX1 eq. in fish flesh (FDA-2013-D-0269). Nonetheless, for an accurate risk evaluation more efforts have been required from the scientific community with the aim of increasing the knowledge of such naturally-occurring marine toxicants. In the last decades, a large number of techniques characterized by specific advantages and drawbacks have been developed for detection of CTXs both in phytoplankton and food samples. Overall, the configured methodologies can be grouped in: i) in-vivo bioassay, ii) biochemical and molecular techniques (in vitro cell-based assays (CBAs), in vitro receptor binding assay (RBA) and immunoassays) iii) bioelectrochemical sensors and iii) chemical methods [4,19]. In vivo-bioassays have been widely employed in endemic regions to monitor the suspect presence of CTXs in fish. Although a wide range of models have been proposed on different animals (e.g. cats, mongooses, chickens, mosquitos, larvae of *Diptera*, crayfish and crustaceans) [20-24] administering the potentially toxic material by IP injection (fish extract) or per os (fish samples), this approach turned out unsuccessful [19]. The only exception was represented by the mouse bioassay (MBA) which demonstrated to be an useful tool to recognize CFP thanks to the onset of characteristic symptoms induced in mice after the IP injection [25-28]. However, its employments has always been a matter of ethical concerns, and the lack of specificity, reduced sensitivity, subjectivity in evaluating the toxic effects and time death, and the large number of false positives due to interferences (e.g. lipids), have favored the development of alternative approaches [19]. Among the CBAs, erythrocyte lysis assay (ELA) and neuroblastoma neuro-2a cytotoxicity assays (N2a) have been proposed. The principle of ELA is the spectrophotometric determination of hemoglobin (absorbance at 414 nm) after the lysis of erythrocytes induced by hemolytic compounds. Even though this assay was broadly exploited in the field of marine toxins [29-31], it suffers a remarkable low specificity due to the interference of a high number of hemolytic compounds such as: reactive oxygen species (ROS), poly-unsaturated fatty acids and glycolipids [32]. On the other hand, N2a turned out to be the most suitable approach among the CBAs, and one of the most sensitive and effective methods for screening the ciguatoxicity of phytoplankton and fish samples. Briefly, a suspect sample is added to neuroblastoma cell line in absence (control) and presence of ouabain and veratridine [33]. In control samples CTXs and MTXs are not able to

induce the cell death. Contrarily, the combined action of ouabain (inhibition of Na^+/K^+-ATPase pump) and veratridine (opening of Na^+ channels) increases the cell sensitivity to CTXs that activate the VGSCs, thus favoring the Na^+ influx and leading cells to death in a dose-dependent manner. Quantitation of the total content of CTXs in the screened sample is performed through the MTT assay which measures the cell metabolic activity as indicator of cell viability [34]. The main advantages of the N2a are: i) high sensitivity (sub-picograms), ii) high-throughput screening in one test run and iii) suitability for routine analysis and monitoring programs. However, the most significant limitations lie into: i) the inability of investigating the toxin profile, ii) test is time-consuming (3 days), iii) trained personnel with experience in cell culture maintenance is required and iv) the lack of an inter-lab standard procedures [19]. Nonetheless, N2a is still the most valid approach to evaluate the toxicity of CTX-contaminated material, and its combination with further instrumental analytical approaches (e.g. LC-MS) represents the most effective method for a comprehensive screening [35]. Among the biochemical approaches, radioactive (RBAr) and fluorescent (RBAf) RBAs have also been configured [36-37]. These assays are based on the competition between CTXs and brevetoxins (radiolabeled toxin) for binding the VSSCs. Although these techniques are cost-effective, rapid and useful to quantify the total toxin content, they are 10-fold less sensitive than N2a [38]. In addition, they do not provide details on toxin profile and do not measure the toxicity of a sample but the binding affinity [17]. Among the alternative biochemical approaches, anti-CTX polyclonal (pAbs) and monoclonal antibodies (mAbs) have been exploited for developing immunoassays [39-46]. Even though pAbs were exploited to configure two immunostrip tests, labeled as CiguaCheck [47-48] and Ciguatect kits [49], they did not provide satisfactory results due to high cross-reactivity with other marine toxins (okadaic acid), and false and negative positive results [50-52]. Contrarily, the employment of mAbs in immunoassays proved high specificity and sensitivity [53-56]. Recently, three different mAbs were used to develop a sandwich electrochemical immunosensor for determination of CTX_S in fish [4]. The application of this analytical tool gave excellent results in terms of sensitivity, reproducibility and matrix interference. The well-known advantages of such devices (e.g. reduced costs, user-friendliness, no maintenance and specialists are required) combined with the high analytical performance achieved, make the electrochemical biosensor a powerful tool to implement for research and monitoring purposes. Despite the fact the biological approaches gave a high sensitivity and reliability of measuring the toxic potential of samples, they suffer the

inability of evaluating the toxic profile, as well as the impossibility to elucidate the structure of new compounds. These critical drawbacks were definitely overcome by the employment of physico-chemical methods based on hyphenated techniques. Although the reverse-phase (RP) chromatography has proven suitable for separating complex mixtures of CTXs right from the very beginning, the coupling of RPLC with a sensitive detector has been a priority [17]. The lack of specific chromophores and the absence of one primary hydroxyl group for most of the analogues, made UV and fluorescence detection (FLD) methods, respectively, not adequate enough to identify and determine CTXs at very low levels [57-60]. Even though a higher sensitivity was achieved through HPLC-FLD approach, the latter still does not allow detection of CTXs in fish at the maximum permitted level suggested. As a consequence, the highest analytical power was achieved by coupling RP-HPLC with electrospray (ESI) mass spectrometry (MS). In addition, the employment of fragmentation techniques (MS/MS) remarkably improved the method sensitivity, thus making HPLC-MS/MS the method of choice for determination of toxin profile in complex matrices. However, the limited availability of toxin standards hinders the development of sensitive MS^2 methods based on the monitoring of diagnostic fragment ions, as well as the structural characterization of new compounds by high-resolution MS [19]. Nonetheless, the combination of LC-MS/MS and HRMS methods with biological assays still represents the best approach in the frame of CFP.

This study describes the development of LC-HRMS and LC-MS^2 methods on different instruments for the analysis of Pacific and Caribbean CTXs, respectively. Although the untargeted approach has not yet applied to real samples, the preliminary results obtained from the HR full-scan analysis of an assorted mixture of P-CTXs have suggested suitability for such purpose. However, the optimization of $HRMS^2$ parameters still requires further efforts since only a few CTX analogues provided fragment ions at acceptable levels (water losses from selected precursor ions). Currently, the latter represents one of the most critical aspects for optimization of sensitive MS^2 methods for monitoring CTXs in environmental and food samples, and this is mainly due to the lack of adequate reference material in terms of CTX congeners and their concentration level. On the other hand, the targeted LC-MS^2 method was configured on a triple quadrupole (QqQ) MS by using C-CTX1 and -2 contaminated fish extract as laboratory reference material (LRM). The implemented methodology was applied to the analysis of a batch of frozen fish fillets imported from India to the UK, which were suspected to be cause of a case report of CFP. The preliminary results of the

instrumental analysis suggested the presence of C/I-CTX1 and -2, while further confirmations on toxicity were obtained from the application of the N2a. In this framework, the optimized LC-MS^2 method was used to deeply investigate the toxic profile of Indian fish and the toxin distribution within each fillets. As a result, the wide spread of C/I-CTX1 and -2 in all the analyzed fish suggested that the contaminated material could be exploited to set up a preparative work aimed at extracting, purifying and isolating the toxic molecules. In this framework, it was conducted a detailed study to configure an extraction procedure, characterized by high yield of recovery and low variability, of CTXs from fish fillets. The optimized conditions were then applied for a large scale extraction and clean-up of the toxic material. However, the purification and the isolation of the toxic compounds, as well as the characterization of the toxic profile by LC-HRMS approach, are still ongoing, and more scientific efforts to achieve the fixed goals are needed.

2. Results and discussion

2.1 Development of a LC-HRMS method for the analysis of P-CTXs

CTX3C, which was the only available standard at the time of the analysis, was used to optimize the chromatographic and MS conditions, while a mixture of assorted P-CTXs including CTX1B, 51-hydroxyCTX3C, 52-*epi*-54-deoxyCTX1B, and CTX4A non-certified reference material was exploited to test the implemented conditions. The mobile phase composition turned out to be crucial for the optimization of effective methods since the use of acetonitrile or methanol as organic modifier, as well as formic acid and ammonium formate as additives, strongly affected the ionization efficiency, the quality of the full-scan spectra and method sensitivity [19]. As suggested by Yogi et al. [61], chromatography was implemented eluting a RP column with mobile phases composed of water (A) and methanol-water 95:5 *v/v* (B), both containing formic acid 0.1% *v/v* and ammonium formate 5mM. Under the described conditions, the employment of a first gradient elution from 78%B to 100%B in 11 min, and a further isocratic step at 100%B for 5 min, provided a good toxin separation (**Fig.V.1**). As showed in **Fig.V.1**, CTX1B was the first compound to elute due to its high polarity associated with the presence of 3 hydroxyl groups. Notably, the XIC of CTX1B gave two chromatographic peaks eluting at 7.72 and 8.12 min with a similar relative abundance. Their associated HRMS and MS^2 spectra turned out to be superimposable in terms of

in-source ions, fragments and relative abundance ion ratio. As a consequence, it was not possible to attribute the identity of CTX1B to any of the two peaks.
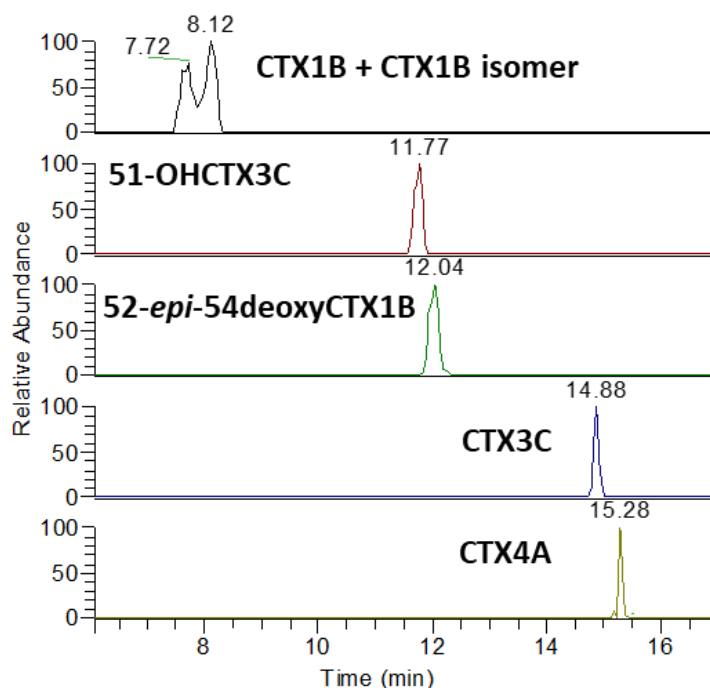

Figure V.1 Chromatographic separation of assorted P-CTXs under the optimized conditions.

Reasonably, the further presence in the non-certified standard of an isobaric congener of CTX1B (e.g. 54-*epi*CTX1B, 52-*epi*CTX1B, 54-*epi*-52-*epi*CTX1B, 54-deoxy-50-hydroxyCTX1B) was assumed. Although 51-hydroxyCTX3C and 52-*epi*-54-deoxyCTX1B belong to different P-CTX sub-groups (P-CTX1 and P-CTX-II) and have different structural features (e.g. number of OH groups, additional side chain at A ring), they almost co-eluted under the optimized chromatographic conditions (**Fig.V.1**). On the other hand, an excellent resolution was achieved for their less oxidized precursors, namely CTX3C (for 51-hydroxyCTX3C) and CTX4A (for 52-*epi*-54-deoxyCTX1B) that eluted at 14.88 and 15.28 min, respectively (**Fig.V.1**). As expected, the latter were the last CTX congeners to elute due to their highest affinity to RP stationary phase. Similarly to CTX1B, a further chromatographic peak eluting at 15.18 min was obtained in the XIC of CTX4A. However, its presence was almost negligible and reasonably attributable to the isobaric congener CTX4B. The ESI source parameters were optimized using CTX3C, and then applied to acquire the HR full-scan spectrum of each CTX congener (**Fig.V.2**).
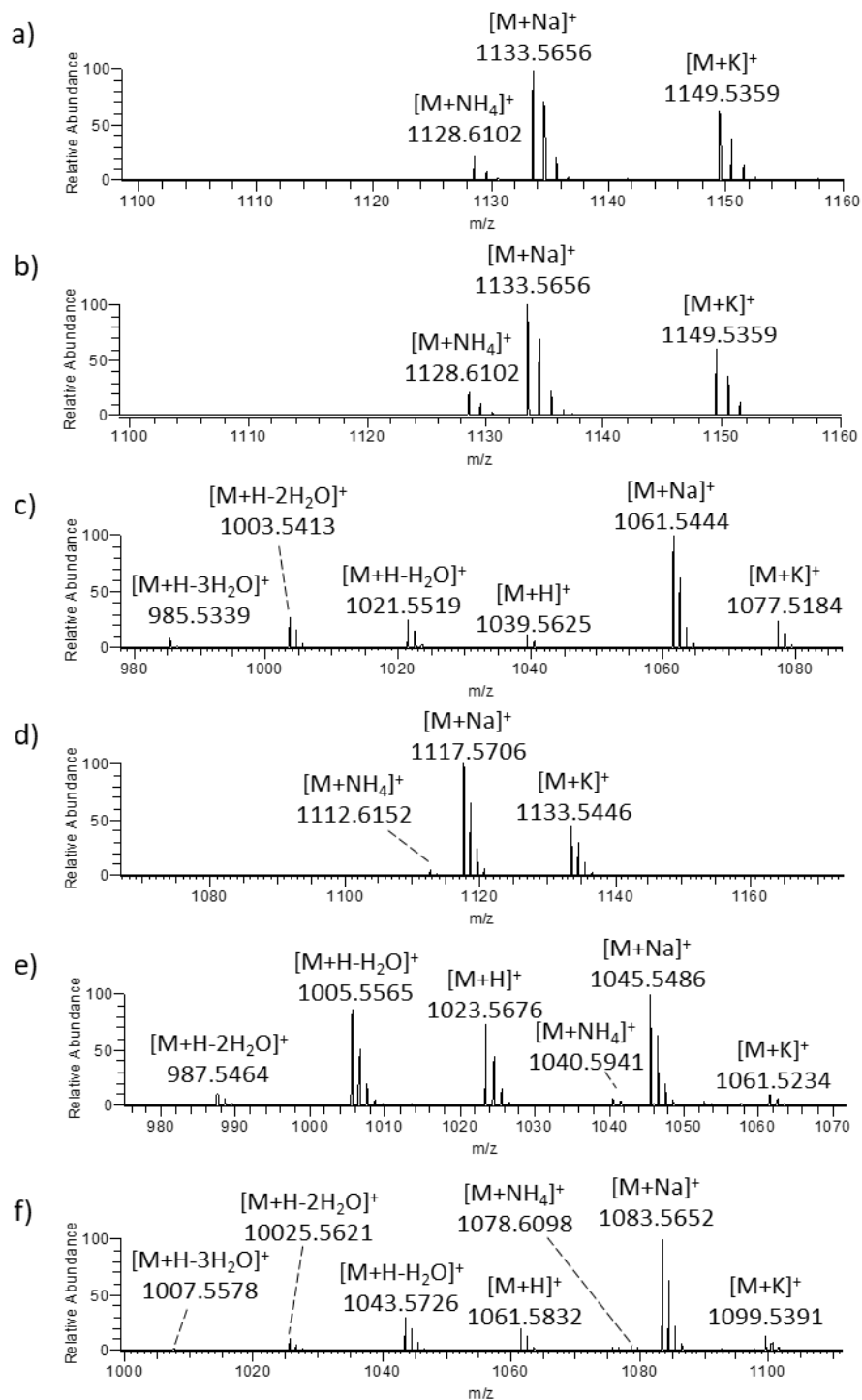
Figure V.2 HRMS spectrum of: a) peak eluting at 7.72 (CTX1B or an isobaric isomer), b) peak eluting at 8.12 (CTX1B or an isobaric isomer), c) 51hydroxyCTX3C, d) 52-*epi*-54deoxyCTX1B, e) CTX3C and f) CTX4A.

As expected, a high variability in terms of in-source ions/fragments was observed among the analyzed standards. For each toxin, the common motif was represented by the presence of the $[M+Na]^+$ ion as the base peak of the spectrum. This was ascribable to the use of methanol as mobile phase B, and formic acid as additive [19,61]. The HRMS spectrum of CTX1B, its unknown congener in the standard (**Fig.V.2a-b**), and 52-*epi*-54-deoxyCTX1B (**Fig.V.2d)** were characterized by the presence of $[M+Na]^+$, $[M+K]^+$ and $[M+NH_4]^+$ adduct ions, while the $[M+H]^+$ ion and the relevant in-source water loss fragments were not detected. The ionization behavior of CTX3C and 51-hydroxyCTX3C was quite consistent in terms of in-source formed ions: both toxins gave $[M+Na]^+$ and $[M+K]^+$ adduct ions, the $[M+H]^+$ ion and a number of $[M+H-nH_2O]^+$ (n=1,2) in-source fragments. The main difference lied into the absence of the $[M+NH_4]^+$ adduct ion in the spectrum of 51-hydroxyCTX3C, and the lack of the $[M+H-3H_2O]^+$ in spectrum of CTX3C (**Fig.V.2c-e**). The HRMS spectrum of CTX4A turned out to be the most informative since it contained all the adduct ions $[M+Na]^+$, $[M+K]^+$, $[M+NH_4]^+$, the $[M+H]^+$ ion and the in source $[M+H-nH_2O]^+$ (n=1,3) fragments (**Fig.V.2f**). However, a careful analysis of the full-scan HRMS spectra revealed some differences between toxins within the same sub-group. Considering P-CTXs-1, the relative ion ratio between the adduct ions of CTX1B and 52-*epi*-54-deoxyCTX1B was superimposable (**Fig.V.2a,b,d**), whilst remarkable differences were observed with CTX4A, since: i) the $[M+H]^+$ ion of CTX4A was clearly detected in the spectrum, and iii) although it has a lower number of OH groups than the most oxidized congeners (CTX1B), three in-source fragments due to the loss of H_2O were displayed (**Fig.V.2f**). Similarly, some differences in ionization behavior were observed within the group of P-CTX-II. For CTX3C the $[M+K]^+$ adduct ion was less intense than the $[M+H]^+$ ion and the $[M+H-H_2O]^+$ in-source fragments, whilst the opposite was observed for 51hydroxyCTX3C. Therefore, although toxins of the same sub-group share structural features, their ionization behavior can greatly vary.

On the other hand, $HRMS^2$ spectra were recorded only for CTX3C and CTX4A by selecting as precursor the $[M+H-H_2O]^+$ in-source fragments at *m/z* 1005.5565 ($C_{57}H_{81}O_{15}^+$) and 1043.5726 ($C_{60}H_{83}O_{15}^+$), respectively, which were more intense than the relevant $[M+H]^+$ ions. However, their MS^2 spectra did not contain diagnostic fragments, but only uninformative fragments due to water loss: i) $[M+H-nH_2O]^+$ (n=2,3) fragments at *m/z* 987.5465 ($C_{57}H_{79}O_{14}^+$) and 969.5359 ($C_{57}H_{77}O_{13}^+$) for CTX3C, and ii) the $[M+H-2H_2O]^+$ fragment at *m/z* 1025.5622 ($C_{60}H_{81}O_{14}^+$) for CTX4A. the lack of diagnostic fragments in the MS^2 spectra was likely due to the low concentration level of

toxins (approximately 100 ng/mL) that hampered detection of the less intense ions. To date the lack of adequate reference material (in terms of CTX analogues and concentration level) represents a critical issue for research laboratories and monitoring centers since: i) it hampers the development of high sensitive instrumental methods based on the monitoring of diagnostic fragments, and ii) the acquisition of informative HRMS^2 spectra for an accurate toxin confirmation and for the structural characterization of the unknowns. Therefore, an alternative strategy was outlined to overcome this issue. Briefly, the monitoring of CTXs can be conducted fragmenting their [M+Na]$^+$ ion, which is the prominent ion when methanol is used as solvent for mobile phase B. The characteristic of such experiment lies in the high stability of the [M+Na]$^+$ adduct that at high collision energies: i) does not provide any structural fragment, and ii) its intensity remains unchanged [61]. Therefore, the same experimental approach was applied to the analysis of the P-CTX standards. The [M+Na]$^+$ ion of each toxin was fragmented in collision induced dissociation (CID) mode at CE 20-23% (**Fig.V.3**).
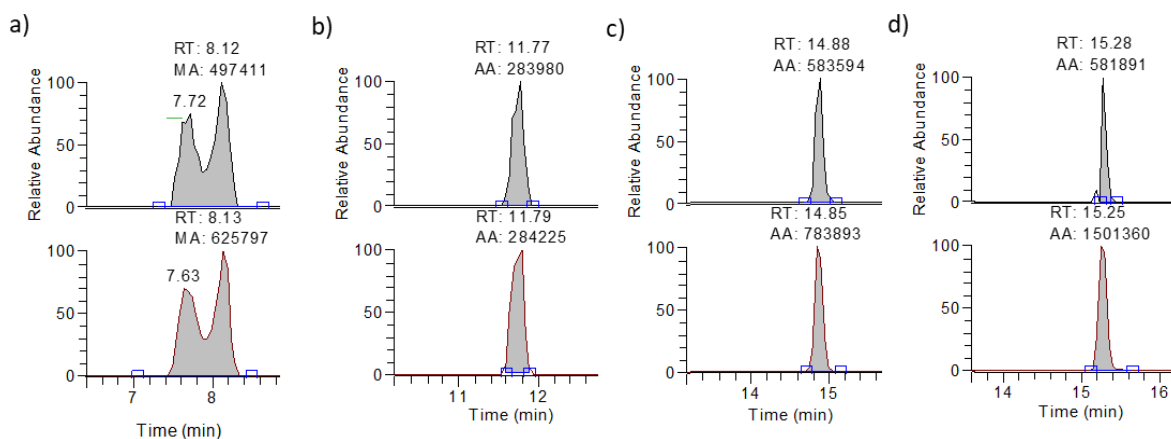
Figure V.3 Full-scan and MS^2 XIC of the [M+Na]$^+$ adduct ion of: a) CTX1B and its isomer, b) 51hydroxyCTX3C, c) CTX3C and d) CTX4A.

2.2 Analysis of Indian fish by LC-MS^2 approach

Background

Between September 2019 and March 2020 I spent a 6 month period abroad in the laboratory of Analytical Chemistry of the Centre for Environment, Fisheries and Aquaculture Science (CEFAS, Weymouth, United Kingdom). Under the supervision of Dr A. Turner, I have conducted studies on contaminated fish samples that were suspected to be the cause of a CFP in the UK. Briefly, in

June 2017, a suspected case of CFP occurred in Stoke-on-Trent (United Kingdom), where three people from the same family suffered from symptoms of food poisoning after consuming Red Snapper steaks imported from India. Two of the three family members were admitted to hospital with symptoms of diarrhea and vomiting, followed by paranesthesia and shortness of breath. The reporting doctor, in the absence of analytical confirmation, provided a presumptive diagnosis of CFP, based upon the characteristic signs and symptoms, together with the history of eating species of fish that are known to carry CTXs. One fillet of Snapper, which remained uncooked in frozen storage from the family, was retrieved and sent to CEFAS for conducting investigations into the presence of CTXs and ciguatoxicity. Preliminary analyses carried out by LC-MS^2 at CEFAS and by N2a at Dauphin Island Sea Lab (DISL, University of South Alabama, USA) under the supervision of the Prof. Alison Robertson, revealed the presence of C/I-CTXs at a 28-fold higher contamination level than that suggested by the FDA in the USA. This strongly suggested that human illness would be expected following consumption of Indian fish. Therefore, a product withdrawal was put in place for the brand associated with the intoxication after notification to the Local authority. The whole production batch of frozen Snapper fillets was consigned at Cefas with the aim to conduct further studies on toxin distribution between Snapper fillets. In case of high levels of C/I-CTXs in Indian fish, it was decided to use the toxic material to set up a preparative work with the aim to extract, purify and isolate the toxic molecules with high yield and grade of purity. With the further collaboration of Dr P. McCarron (National Research Council NRC Canada), the isolated toxins will be the starting point for the bulk production of C/I-CTX reference material not yet commercially available, that may be used to: i) develop and validate biological and analytical methods for identification of CTXs both in environmental and food samples, and ii) to conduct quality controls of commercialized products aimed at increasing the security level of customers and to preserve the public health.

2.2.1 Optimization of chromatography and MS^2 conditions

Chromatographic and MS^2 parameters were optimized using C-CTX lab reference material (LRM) prepared in-house from contaminated Barracuda fish samples collected in Antigua (Caribbean Sea). With the aim to find the best experimental conditions and the highest analytical sensitivity, three different mobile phase conditions (labeled as method A, B and C) were tested, while the gradient elution and the UPLC column were kept unchanged. Method A and B differed from

mobile phase B, which was composed of acetonitrile for method A, and methanol for B, both added of 0.1% formic acid and 5mm ammonium formate. Contrarily, both methods shared the composition of mobile phase A (0.1% formic acid and 5mm ammonium formate in water) (**Table V.1**). On the other hand, the mobile phase condition used for method C was quite different since: mobile phase A contained 1mM ammonium fluoride in water, and phase B was pure methanol. The monitoring of C-CTX1 and -2 was conducted through Multiple Reaction Monitoring (MRM) experiments selecting as precursor the $[M+H-3H_2O]^+$ ion at m/z 1087.6 ($C_{62}H_{87}O_{16}^+$), $[M+Na]^+$ ion at m/z 1163.6 ($C_{62}H_{92}O_{19}Na^+$), and the $[M+NH_4]^+$ adduct ion at m/z 1158.6 ($C_{62}H_{96}O_{19}N^+$) through the following transitions: i) 1087.6 > 1087.6, ii) 1163.6 > 1163.6 and iii) 1158.6 > 1158.6.

Table V.1 Summary of mobile phase conditions used for three detection methods.

Method	Mobile Phase A	Mobile Phase B
Method A	5 mM ammonium formate + 0.1% formic acid in water	5 mM ammonium formate + 0.1% formic acid in acetonitrile
Method B	5 mM ammonium formate + 0.1% formic acid in water	5 mM ammonium formate + 0.1% formic acid in methanol
Method C	1mM ammonium fluoride in water	Methanol

As showed in (**Fig.V.4**), all the mobile phase conditions showed the presence in the LRM of two peaks attributable to C-CTX1 and -2. Even though a baseline separation between the two toxin was not achieved, they could be individually identified through 2 sharp and narrow peaks under all the chromatographic settings tested. However, as expected the employment of different mobile phases resulted in different toxin retention times, which turned out to be more similar between method B and C due to the use of methanol as mobile phase B. The level of C-CTX1 found in LRM was higher than that of its isobaric congener C-CTX2 under each chromatographic method and MRM transition.
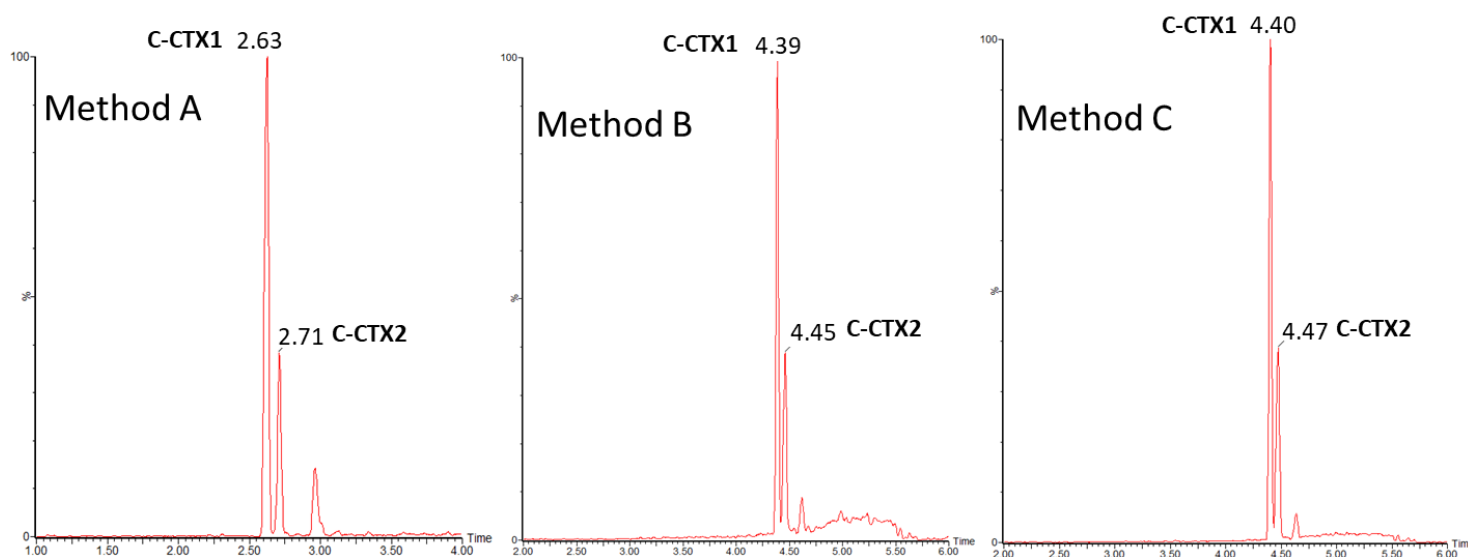
Figure V.4 Chromatographic peak of C-CTX1 and CTX-2 contained in fish LRM. Comparison between the three chromatographic methods A, B and C. The MRM transition selected was 1087.6 > 1087.6.

The highest analytical sensitivity for both Caribbean CTXs was achieved through the transition 1087.6 > 1087.6 ($[M+H-3H_2O]^+$ ion) under the chromatographic method C (**Fig.V.5**). More in detail: i) under method A, the peak of C-CTX1 originating from the transition 1087.6 > 1087.6 was 47% and 84% larger than that acquired through the transitions 1163.6 > 1163.6 ($[M+Na]^+$ ion) and 1158.6 > 1158.6 ($[M+NH_4]^+$), respectively, whilst for C-CTX2 the peak of the $[M+H-3H_2O]^+$ ion was equivalent in size to $[M+Na]^+$ and 60% higher than that of $[M+NH_4]^+$; ii) under method B, the peak area of C-CTX-1 originating from the $[M+Na]^+$ transition was less intense than the $[M+NH_4]^+$, and the same trend were observed for C-CTX2; 3) under method C, the peak area of C-CTX1 gave similar results to method A (intensity: $[M+H-3H_2O]^+$ → $[M+Na]^+$ → $[M+NH_4]^+$), whilst the peak area of CTX-2 followed the same trend observed under method B (intensity: $[M+H-3H_2O]^+$ → $[M+NH_4]^+$ → $[M+Na]^+$).

Moreover, the implemented LC-MS^2 method revealed the presence in the fish LRB of a chromatographic peak eluting shortly after C-CTX2 (**Fig.V.4**). Its presence was evidenced analyzing the reference samples under all chromatographic methods and the MRM transition. Therefore, it was reasonably suspected the presence of an isobaric congener of C-CTX1 and -2, even if further confirmations are still needed.
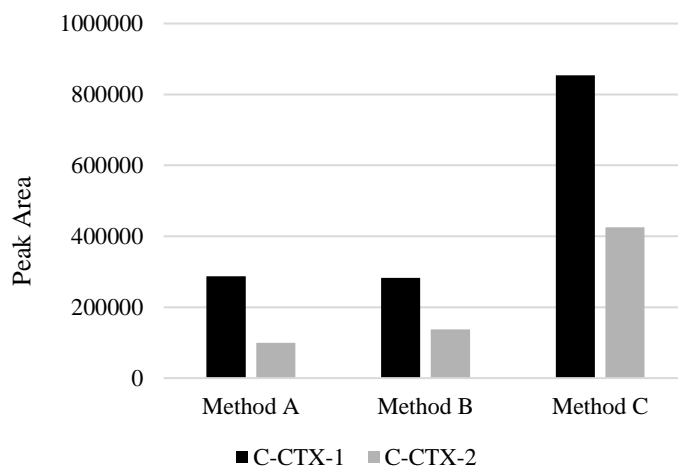
Figure V.5 Summary of C-CTX-1 and 2 peak areas (MRM, 1087.6 > 1087.6) following analysis using the three chromatographic methods A, B and C.

2.2.2 Application of the LC-MS^2 method to Indian Red Snapper fish

The configured LC-MS^2 method was applied to the analysis of Red Snapper fillets from the Indian Ocean with the aim of investigating the toxic profile of samples and assessing the degree of toxin distribution within the batch of fishery products. Taking into account the preliminary toxicological and analytical results obtained from the analysis of the fish steak implicated in the

the CFP case occurred in 2017 in Stoke-on-Trent, and the geographical distribution of CTXs in different Ocean regions, it was reasonable to assume the presence of I-CTXs in Red Snapper fillets. Therefore, 51 fish steaks (1g fish tissue analyzed for sample) were extracted under the extraction method A and analyzed by LC-MS^2 through the mobile phase condition C. As a results, the MRM transitions used to investigate the profile of C-CTX LRM revealed the presence in the Indian fish extracts of two chromatographic peaks eluting at similar retention times of C-CTX1 and -2 (**Fig.V.6**). This finding strongly suggested that the isobaric I-CTX1 and -2 contaminated the Red Snapper fillets. However, the lack of standards and LRM for I-CTXs hindered the accurate identification of those peaks on the basis of the retention time of toxins. Nonetheless, with the aim of clarifying the toxic profile of Indian fish, an in-depth investigation was conducted by comparing data on Caribbean and Indian CTXs reported in literature with those acquired in this study.
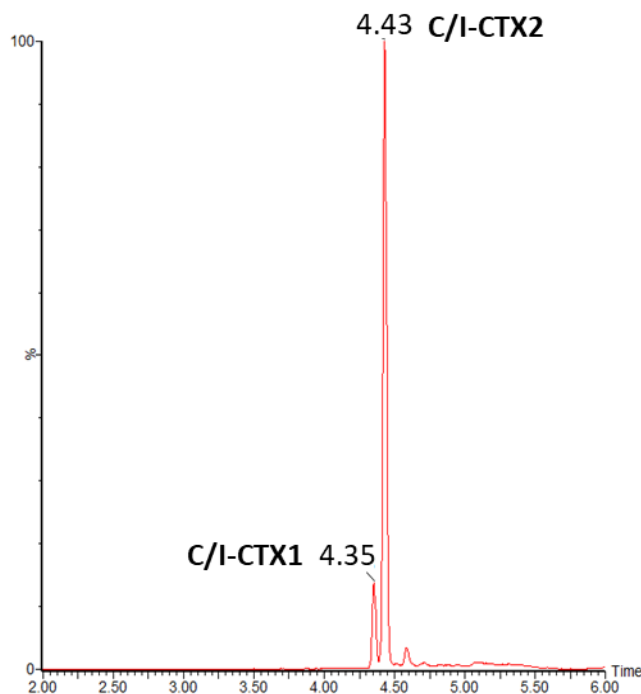
Figure V.6 Chromatographic peak of C/I-CTX1 and C/I-CTX2 contained in one Indian Red Snapper fish analyzed by LC-MS^2 method C. The following MRM transition is showed 1087.6 > 1087.6.

C-CTX1 and -2 are isobaric compounds ($C_{62}H_{92}O_{19}$), particularly epimers at C56 (*S* for C-CTX1 and *R* for C-CTX2), with C-CTX1 being the lower energy isomer. The two compounds undergo interconversion through the hemiketal group at ring N after long storage or acidic treatments. C-CTX1 was found to be the dominant isomer of the profile of contaminated carnivorous Caribbean fish. The algal origin of C-CTX1 and -2 is still unknown, but it was supposed that both toxins are produced by the same microalgal species or they are fish metabolites deriving from the same algal precursor [5,62]. On the other hand, I-CTX1 and -2 ($C_{62}H_{92}O_{19}$) are isobaric compounds of C-CTX1 and -2, but their structure is still unknown, and they do not undergo interconversion. This led to suppose that I-CTX1 and -2 are not epimers, and they lack the hemiketal group present in C-CTX1 and -2 [63]. Contrarily to C-CTXs, the relative abundance ratio between I-CTX1 and -2 found in carnivorous Indian fish turned out to be remarkably variable. This suggested that the two toxins could be produced by different microalgal species/strains, or they are fish biotransformation products originating from different algal precursors and their level in fish is associated with the exposure degree of a specific algal species [64]. In addition, ESI$^+$ HRMS analysis of purified

fractions of C- and I-CTX1 and -2 highlighted that they are able to ionize forming the same ions - $[M+H]^+$, $[M+H-nH_2O]^+$, $[M+Na]^+$, $[M+NH_4]^+$ - even if a different ion ratio was observed between the Caribbean and the Indian CTXs [63, 65] .

In this study, the comparison between the LC-MS^2 analysis of C-CTXs LRM and the 51 Indian fish extracts showed a different relative abundance ratio between the two chromatographic peaks found in Caribbean and Indian sample since: C-CTX1 is the dominant toxin in Caribbean fish LRM whilst in Indian fish the peak attributable to I-CTX2 is more intense than I-CTX1 (**Fig.V.4,6**). This trend was further confirmed analyzing the Indian fish extracts through the three chromatographic methods A,B and C, and by all the transitions set in the MRM experiment. Therefore, the different ratio between chromatographic peaks led to suppose the presence of I-CTX1 and -2 in Red Snapper fillets. However, considering that a different ionization behavior has been reported between Caribbean and Indian congeners, a detailed analysis of the peak area originating from the MRM transition was carried out. As a results, the relative ratio between the $[M+H-3H_2O]^+$, $[M+Na]^+$ and $[M+NH_4]^+$ ions measured for Indian fish extracts was superimposable to that observed for Caribbean fish LRM under the chromatographic methods A,B and C. Moreover, also for Indian CTXs, the highest analytical sensitivity (in terms of peak area of analytes) was obtained through the transition of the $[M+H-3H_2O]^+$ ion (1087.6 > 1087.6) under the three chromatographic settings. Therefore, the same ion ratio observed between C-CTXs in LRM and CTXs detected in Indian fish could suggest that: i) C- and I-CTXs undergo a similar ionization behaviour under the implemented LC-MS^2 method or ii) the two chromatographic peaks observed in Indian fish are attributable to the presence of C-CTX1 and -2. The latter hypothesis, if confirmed, would disagree the geographical classification system currently adopted for CTX congeners, as well as it would bring to light that C-CTX2 can be found at higher level than C-CTX1, pointing out a different toxic profile between fish or microalgal producing-species. Therefore, with the aim of collecting more data on the toxic profile of Indian Red Snapper fish, a wide number of frozen fish packets (467) were extracted through a different extraction method (method B2, 1g fish analysis) and analyzed through the chromatographic method C. All the MRM transitions set in the LC-MS^2 method revealed the presence in the Indian fish extracts of peaks attributable to I-CTX1 and -2, with the latter being the most abundant. The presence of the two toxins was widespread throughout different production batches of Red Snapper fillets, with a variability (total amount of toxins) of 50% (relative standard deviation RSD). The relative

abundant ratio between peak areas of I-CTX1 and -2 ranged from 1:100 to 69:100, with an average value of 29:100. Only one sample was found to not contain the peak attributable to I-CTX1. Overall, these intriguing findings suggested that all the production batch of Red Snapper fillets was contaminated by CTXs. However, the differences between Caribbean and Indian CTXs are too subtle to be distinguished using the current methodologies. Therefore, in lack of analytical confirmation, the toxins found in Indian Red Snapper fish were labelled as C/I-CTX1 and -2. In addition, the presence in the Indian fish of a further peak eluting close to C/I-CTX1 and -2 pointed out the presence of an isobaric congener as observed for C-CTXs LRM. The evaluation of such new putative compounds would require the employment of the LC-HRMS approach. Further confirmation on the toxicity of most of the analyzed samples were obtained through the employment of the N2a, which was performed by Prof. Alison Robertson of DISL. The toxicological screening revealed very high toxicity levels among all the analyzed samples, suggesting the presence of extremely potent toxins or high concentration levels of less toxic compounds. Although the N2a approach is not able to provide details on the toxic profile of the screened samples, it confirmed that Red Snapper fish are contaminated by toxins acting on VSSCs like CTXs, since: only cells treated with ouabain (O) and veratridine (V) showed toxicity when inoculated with Indian fish extracts, whilst no effects on cell viability were observed in the N2a cells non treated with OV. Therefore, toxins contained in the Red Snapper fish do not cause non-specific cell-death via a different mechanism. As a consequence, in light of analytical and toxicological results obtained from the analysis of a wide number of fish packets, the whole production batch of Red Snapper fillets showed suitable to be used as starting material for a preparative work, with the aim of obtaining purified fractions of the toxins and elucidating their structure.

To this aim, further investigations were carried out to optimize the extraction procedure of toxins from the contaminated fish to start the large-scale extraction.

2.2.3 Extraction method A: results and performance assessment.

LC-MS^2 analysis of Indian fish samples (1g fish analysis) revealed the presence of C/I-CTX-1 and -2 at variable levels (in term of peak area) within the whole production batch of Red Snapper fillets. In the frame of a large-scale extraction of the toxic material, the optimization of the experimental conditions to process a large amount of fish turned out to be a prerequisite since: i)

high recovery yields allow to obtain a large amount of toxins from fish tissue, whilst ii) a low method variability allows to correctly evaluate the total toxin content for each sample and the most toxic individuals to be included in the large-scale extraction. The first extraction method to be tested was labelled as method A, briefly: i) extraction of CTXs from 1g fish tissue with acetone, ii) precipitation of proteins by storing the acetone extract at -20°C overnight, iii) defatting of the extract through liquid-liquid partitioning with hexane, and iv) a second clean-up procedure with dichloromethane (DCM) to separate CTXs from more polar compounds.

A first experiment (*experiment 1*) (**Fig.V.7a**) conducted on three individual fish samples extracted under the described procedure, showed a high method variability since the RSD% on the total toxin content (sum of peak area of C/I-CTX1 and -2) ranged from 74 to 146%, with an average value of 95%. This strongly suggested that the extraction needed to be optimized, as well as the sampling procedure, since the toxin distribution within the fish fillet could not be homogeneous. Therefore, the homogenization of each individual fillet was considered before collecting 1g sub-sample of fish tissue.

As a conseuqence (*experiment 2*), three further fish fillets were homogenized and extracted under method A. As showed in **Fig.V.7b**, the measured RSD% ranged from 103 to 137% with an average value of 117%, underlying that the high method variability was not mainly attributable to the sampling method but to the extraction protocol A. Therefore, these preliminary results brought to light the need to deeply investigate what step or steps of method A were responsible for such a high variability.

A further experiment was designed to evaluate the contribution of the clean up procedures to the method variability (*experiment 3*). At this purpose, three individual fish fillets were homogenized, six 1g sub-samples per fillet were extracted with acetone, kept overnight at -20°C, pooled togheter to obtain an homogeneous acetone extract and then split in aliquots of equal volume. Each sub-sample was then subjected to liquid-liquid partitioning with hexane, DCM and analyzed by LC-MS^2. The measurement of RSD% showed again a very high method variability in the range 65-114%, with an average value of 93% **Fig.V.7c.** Therefore, these results allowed to reasonably exclude the contribution of the extraction process to such high method variability, which was clearly attributable to the clean-up procedures.
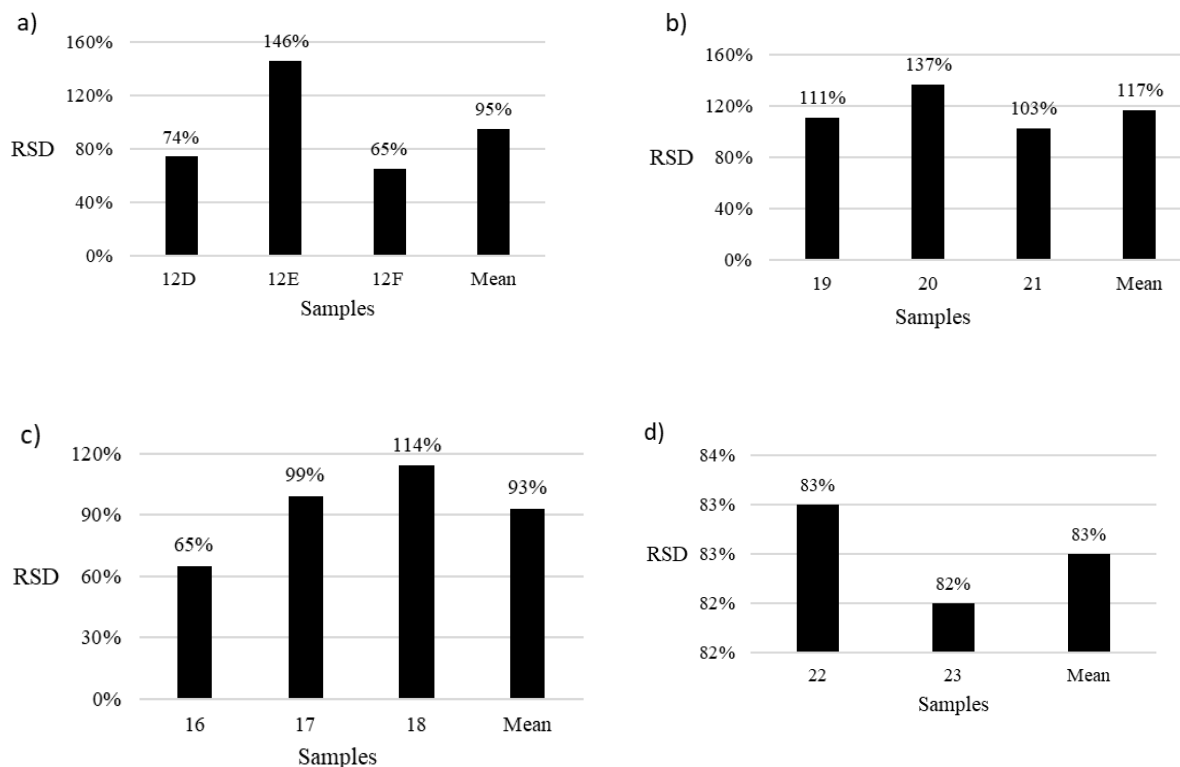
Figure V.7 Experiments performed to evaluate the variability of the extraction method A. Measured RSD% values on the total toxin content per sample. a) extraction of fish tissue without homogenization of fillets (*experiment 1*); b) extraction of fish tissue after homogenization of fillets (*experiment 2*); c) pooling of the extracs before clean-up steps (*experiment 3*); d) pooling of the extracts before partinioning with DCM (*experiment 4*).

As a consequence, a further investigation was conducted to assess the inherent variability to each individual clean-up step *(experiment 4)*. Two fish fillets were homogenized, six 1g sub-samples per fillets were collected, extracted with acetone and subjected to defatting with hexane. Susbsequently, the non liposoluble layers were pooled togheter, split in aliquots of equale volume, and individually partitioned with DCM and analyzed by LC-MS^2. As a result, a high variability of 83 and 82% (RSD) was observed **Fig.V.7d**, suggesting that both liquid-liquid partitioning steps affected the method variability, even if the highest contribution was inherent to the DCM partitioning.

Although the variability of method A was evaluated step by step, a further experiment was performed to evaluate the yield of recovery and then the loss % of the total toxin content for each step of the extraction (*experiment 5*). Therefore, two fish fillets were homogenized and six 1g sub-

samples per fillet were taken and extracted under the described procedure. After each step of the protocol (solvent extraction, defatting and DCM partitioning), samples were dried down, suspended with methanol and an aliquot of each sub-sample was analyzed by LC-MS^2. As reported in **Table V.2**, the variability inherent to the extraction with solvents was very low, with an average RSD of 16%.

Table V.2 Measured RSD% and loss% of each step within the extraction method A.

Step of the extraction method A	Variability (RSD %)	Recovery (loss%)
Extraction with solvents	16	-
1° clean-up (defatting with hexane)	51	48
2° clean-up (partitioning with DCM)	95	95

As observed before, the variability of the method increased with the first clean-up (average RSD of 51%) ending up to achieving the highest value after partitioning with DCM (average RSD of 95%). With regard to the loss% of the total toxin content, defatting with hexane gave a substantial loss of 48% (average value), whilst the liquid-liquid partitioning with DCM critically reduced the yields of recovery since it was measured an average loss of 95%. Overall, all the collected data highlighted the necessity to improve/optimize the whole extraction process since the clean-up steps, mainly partitioning with DCM, increased the variability of the method and drastically reduced the recovery yield.

2.2.4 Extraction method refinement and method comparison

Given the high variabilities and low recoveries associated with the clean-up steps within the extraction method A, work was conducted to see if refinements to the method would enable enhanced recovery and/or method precision. In addition, a new extraction method labelled as method B, was taken into account. The main differences between method A and B lied into: i) the number of steps involved in the whole procedure, ii) the mixture of solvents used for each step and iii) the ratio between the amount of fish tissue and volume of extraction solvent. Briefly, under method B: 1g of homogenized fish tissue is extracted with 3 mL of MeOH-W 3:2, then the extract is boiled at 100°C for 10 min, cooled in an ice bath for 5 min and partitioned with DCM. In order

to investigate the influence of different factors on the extraction process, slight modifications were applied to both methods A and B, resulting so in a number of different extraction sub-methods labelled as: A1, A2, A3, A4, A5, A6, B1 and B2. Main modifications, which are reported in **Table V.3**, involved: material of lab equipment (glass or plastic), solvent ratio, extraction volume and nature of solvent/mixtures used for each step.

Table V.3 Extraction methods A and B. For each sub method (A1-A5, B1-B2) all the modifications applied are reported.

Method	Procedure/modifications	Method	Procedure/modification
A	- Extraction: acetone (2mL/1g) twice - 1st Clean-up: MeOH (1mL)-hexane (2mL) 1:2 -2nd Clean-up: W (2mL)-DCM (2mL) 1:1 - Materials: Glass	**B**	- Extraction: methanol-water 3:2 (3mL/1g) - 1st Clean-up: MeOH-W 3:2- DCM 1:1 - Materials: Plastic and glass
A1	- Extraction: acetone (2mL/1g) thrice - 1st Clean-up: MeOH (1mL)-hexane (4mL) 1:4 -2nd Clean-up: W (2mL) -DCM (4mL) 1:2	**B1**	- Extraction: methanol-water 3:2 (5mL/1g)
A2	- Extraction: acetone (4mL/1g) twice - 1st Clean-up: MeOH (2mL)-hexane (4mL) 1:2 -2nd Clean-up: W (4mL)-DCM (4mL) 1:1	**B2**	- Extraction: methanol-water 3:2 (5mL/1g) - Material: Plastic
A3	- Materials: plastics		
A4	2nd Clean-up: W (2mL)-chloroform (2mL) 1:1		
A5	2nd Clean-up: methanol-water 3:2 (2mL)-DCM (2mL) 1:1		

The performance assessment of each sub-method was based on the measurement of variability within the whole protocol (RSD%) and the recovery yield of of the total toxin content (sum of peak area of C/I-CTX1 and -2). The evaluation of variability revealed a remarkable difference between methods A and B since the measured RSD ranged between 22-111% and 4-17%, respectively **(Fig.V.8a)**. Focusing on extraction methods A (RSD: A 88%, A1 97%, A2 111%, A3 86%, A4 90%, A5 22%), a direct comparison between the original method (A) and its modified versions (A2-A5) showed that: i) the triple extraction with acetone and the increase of the solvent ratio in the clean-up steps (A1) did not affect significantly the variability, as well as the substitution of glass with plastic materials (A2), ii) the same was observed when chloroform was used in the

2nd clean-up to replace DCM (A4), and iii) the increase of the extraction solvent per g of fish tissue, combined with the increased volumes in the clean-up steps while maintaining the solvent ratio (A2), drastically affects the variability with RSD higher than 100%. The most intriguing finding lied in variability measured for method A5, in which DCM is replaced by the mixture MeOH-W 3:2. This modification led to a noticeable decrease of variability, which was 4-fold lower than that measured for the original method A. Moreover, thid data represented a further confirmation that the crucial step within the extraction method A is the partitioning with DCM, as reported previously. The considerable increase in precision obtained through method A5 can be associated with the size of emulsions that MeOH-W 3:2 formed in contact with DCM, unlike the use of water which produces a larger emulsion whose size was found to be variable and sample-dependent (the same as observed between W-chloroform, method A4). Therefore, the size of the emulsion could affect the recovery of toxins especially if they are distributed in close proximity of the interface. In fact, the lowest variability was observed within methods B (RSD: A 17%, B1 10%, B2 4%), in which the mixture MeOH-W 3:2 is used for liquid-liquid partitioning with DCM. The method precision was found to progressively improve when: i) the extraction volume increased (B1) and plastic materials were used (B2). The same trend within methods A and B was observed when the total amount of extracted toxins were measured **(Fig.V.8).** Methods A-A4 provided the worst recovery, while method A5 gave results comparable to methods B. On the other hand, method B2 provided a yield of recovery which was 8%, 41% and 22% higher than method A5, B1 and B2, respectively. Overall, method B2 turned out to be the best one since it associated the lowest variability with the highest amount of extracted toxins. In addition, methods B gave further advantages, such as: i) less time-consuming than methods A since fish extracts are not kept at -20°C overnight, ii) liquid-liquid partitioning with hexane is not performed and iii) less solvents and lab equipments are consumed. These details, in association with results of variability and recovery studies, were carefully evaluated before setting up the large-scale extraction of CTXs from contaminated Red Snapper fillets. As a consequence, method B was selected as preferred method for the preparative extraction.
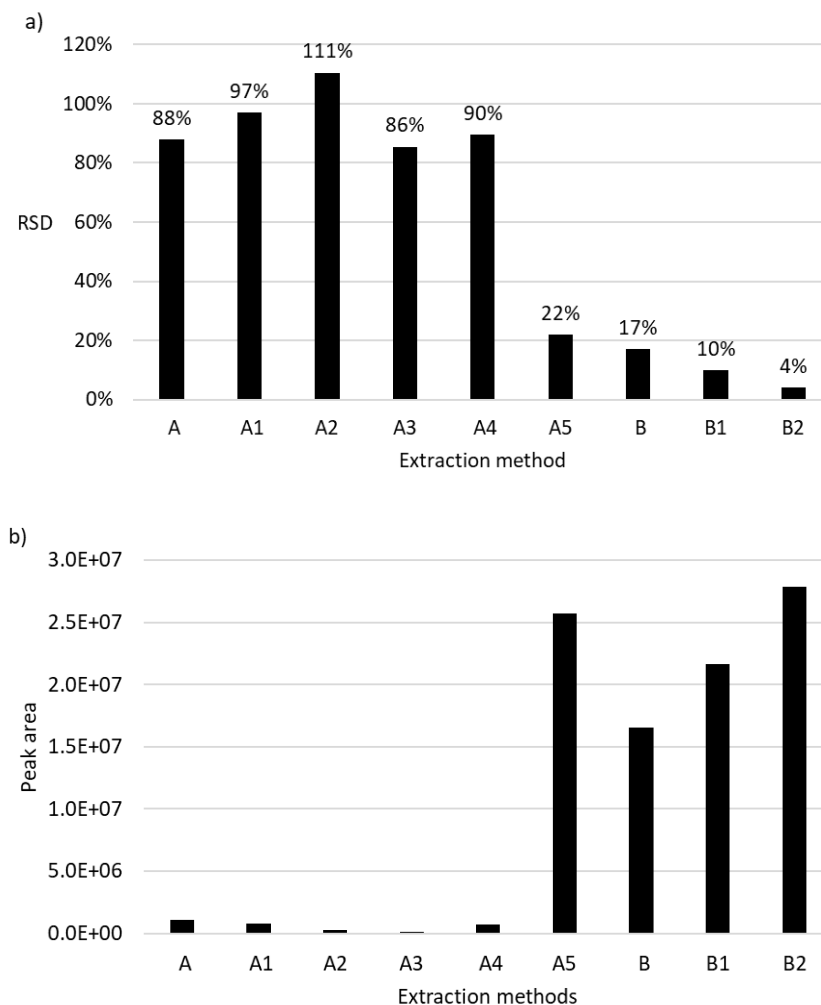
Figure V.8 a) Variability and b) total amount of extracted toxins measured for each extraction method tested.

3.2.5 Intra-fish variability

Although the high variability of method A was found to be associated with the use of water as solvent for liquid-liquid partitioning with DCM, a further study was carried out to assess the variability of toxin distribution within the fish fillet. This study turned out to be crucial to correctly select the most contaminated fish fillets to include in the large-scale extraction. At this purpose, a cross-sectional study on three fish fillets was accomplished by sampling 1g of tissue from 10 selected points across the fish steak and labelled A-J **(Fig.V.9a)**. The LC-MS^2 analysis of the ten sub-sample per fillets revealed that **(Fig.V.9b)**: i) C/I-CTX2 was the dominant toxin since it was found at higher levels than C/I-CTX1 in each point per fillet, and ii) the toxin distribution was not

homogeneous across the steak since points C-D and G-H were found to be the most contaminated. Overall the average intra-fish variability was measured at RSD 26%.
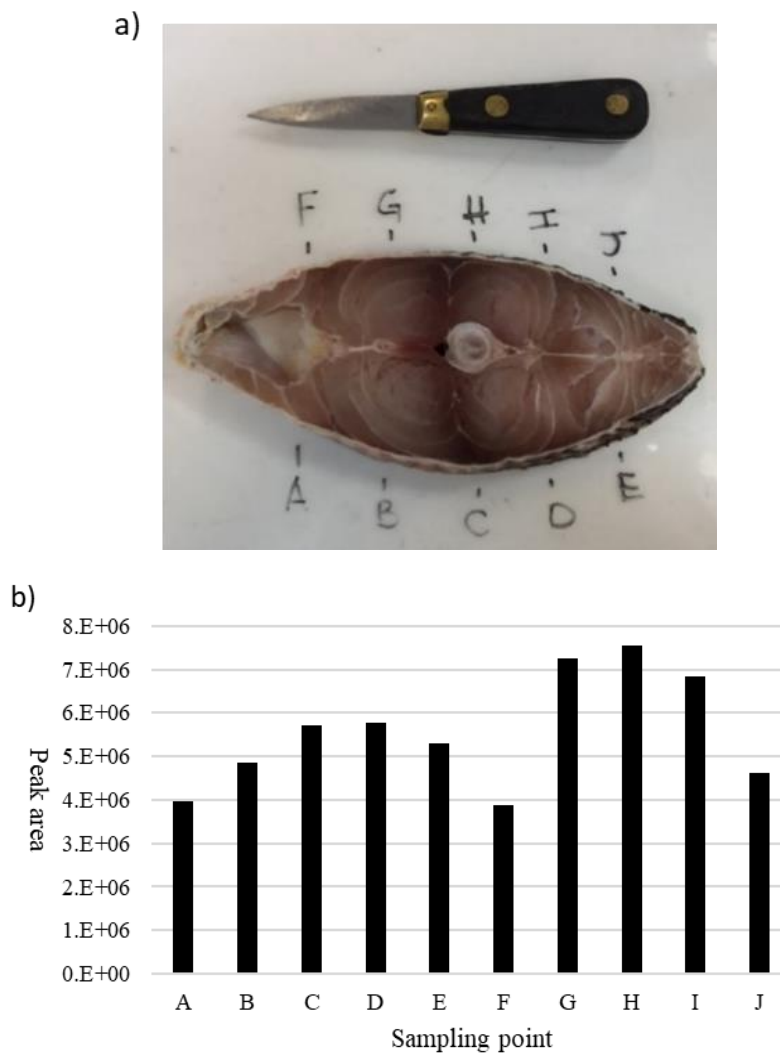

Figure V.9 a) Photo of a Red Snapper fillet used to perform the cross-sectional study. b) Average value of the sum of the peak area of C/I-CTX1 and -2 detected in each point of the cross-section.

Interestingly, a gaussian distribution of toxins was found since, for each side (A-E and F-J), the toxin content increased to the center of the steak (C-D, G-H) and decreased to the edges. This observation strongly suggested that the homogenization of the Red Snapper fillets was a prerequisite to assess the toxin content of each individual sample.

2.2.6 Instrumental and batch precision

In order to evaluate the precision of the instrument within and between different batch of analysis, six 1g samples from the same fish fillet were extracted and analyzed under the optimized experimental condition. Results showed in **Table V.4**, highlighted the high precision of the LC-MS instrument since the RSD values were ≤ 5%. Notably, a very low variability emerged by monitoring C/I-CTX1 and -2 with two different MRM transition ($1087.6 > 1087.6$ for $[M+H-3H_2O]^+$ and $1158.6 > 1158.6$ for $[M+NH_4]^+$), as well as when the single toxin or the sum of them was taken into consideration. However, it was noted that the instrument precision slightly decreased when the toxin content was low. This is observable by comparing the RSD% of C/I-CTX1, which is the minor component of the fish extract, with C/I-CTX2 or the sum of them.

Table V.4 Measured instrumental and batch precision. RSD% values refer to the individual toxin and the total toxin content.

Toxin	RSD %	
	(1087.6 > 1087.6)	(1158.6 > 1158.6)
CTX-1	5%	5%
CTX-2	3%	2%
CTX-1 + CTX-2	3%	2%

2.2.7 Large-scale extraction of Red Snapper fish and future plans

The optimized conditions were employed to homogenize, extract and analyze 467 fish packets (each of 550 g). As described before, the LC-MS^2 data (small-scale extraction, 1g fish tissue per sample) showed the presence of C/I-CTX1 and -2 at variable levels in all the analyzed samples. The selection of the most contaminated samples to include in the large-scale extraction was accomplished by considering the total peak area of toxins for each sample. Notably, among the 89 Kg of homogenized fish tissue, 10 Kg were evaluated as the most contaminated and then considered as starting material for the preparative work. Homogenized fish tissues were then subjected to a large-scale extraction under the optimized method B2 and a liposoluble residue of 74.5 g was obtained. However, the optimization of the experimental conditions for purification and isolation of the toxic compounds are still ongoing at CEFAS. Nonetheless, these steps will be conducted through the combination of different approaches: chromatographic fractionations will

be performed to obtain fraction with high degree of purity, whilst the evaluation of their toxicity will be accomplished through the employment of the N2a. Subsequently, the contaminated fractions will be subjected to an additional purification step or directly to isolation of the toxic compounds. Then, the HRMS approach will be employed to study the fragmentation pattern of the isolated compounds with the aim to conduct a structural characterization based on the interpretation of the HRMS^2 spectra. Moreover, in case of high yield of recoveries, it cannot be excluded the employment of NMR techniques to elucidate the structures of the toxins and also the production of well-characterized reference material.

3. Materials and method

3.1 Analysis of P-CTXs by LC-HRMS approach

3.1.1 Standards

The non-certified standard of CTX3C used to optimize the chromatographic and MS parameters was purchased from FUJIFILM Wako Chemicals Europe GmbH (Neuss, Germany), while CTX1B (86.6 ng/mL), 51-hydroxyCTX3C (90.6 ng/mL), 52-*epi*-54deoxyCTX1B (116.8 ng/mL), CTX3C (77 ng/mL) and CTX4A (110.2 ng/mL) standards were kindly provided by Prof. Takeshi Yasumoto of the Japan Food Research Laboratories (JFRL). C-CTX1 and -2 LRM was owned by Dr Andrew Turner of Cefas.

3.1.2 LC-HRMS method

LC-HRMS analyses were carried out on a hybrid linear ion trap LTQ Orbitrap XL^{TM} Fourier Transform Mass Spectrometer (FTMS) equipped with an ESI ION MAX^{TM} source coupled with a Dionex Ultimate 3000 quaternary HPLC system (Thermo-Fisher, San Jose, CA, USA). Chromatographic condition were optimized using a standard solution of CTX3C (Wako) at 100 ng/mL. Toxin separation was accomplished using a Kinetex C18 column (2.6 µm, 75 x 2.1 mm, 100 Å, Phenomenex) eluted at 0.2 mL/min with water (A) and methanol-water 95:5 *v/v* (B), both containing formic acid 0.1% *v/v* and ammonium formate 5mM [61]. Column was kept at 25°C while the injection volume was 10 µL. The following gradient elution was optimized: time (t) 0 min, 78% B; t 11 min, 100%B; t 16, 100%B; t 17, 78%B; re-equilibration time was 9 min. The ESI source parameters were optimized in positive ion mode using the same standard solution of

CTX3C as follows: spray voltage 4.8 kV, capillary temperature 400 °C, capillary voltage 70 V, sheath gas 50 and auxiliary gas 3 (arbitrary units), tube lens voltage 150 V. Full-scan spectra were acquired in the *m/z* range 700-1500 at resolving power (RP) 30,000 (FWHM at *m/z* 400). The HRMS[2] experiments were acquired in CID mode at RP 30,000, isolation width 2 *m/z*, activation Q 0.250, activation time 30 ms. A CE of 20-23% was used to fragment the $[M+Na]^+$ ion of each toxin, whilst the $[M+H-H_2O]^+$ ion of CTX3C and CTX4A were fragmented at CE 26%. The full-scan XIC of each toxin was obtained by selecting the exact mass of the relevant $[M+H]^+$ and $[M+Na]^+$ ion, while HRMS[2] XIC were performed by selecting the fragments present in the CID spectra. Elemental formulae were calculated on the monoisotopic peak of the ion cluster through Thermo Xcalibur software v2.2 SP1.48 (Thermo Fisher, San Josè, CA, USA) with a mass tolerance within 5 ppm.

3.2 Analysis of C/I-CTXs by LC-MS^2 approach

3.2.1 Fish samples

Fish samples were Indian Red Snapper fillets involved in the CFP case occurred in UK in 2017. Red Snapper fish were caught in the Indian Ocean FAO Zone 51, processed and packed as frozen fish fillets (550g) in India and imported into UK as final product to be commercialized. The whole production batch was composed of 99 boxes of fish. In details: 97 boxes each contained 20 packets of frozen fillets, one box contained 19 packets and the last one 14 packets. 92 boxes, classified as production batch 6L03-K1, were composed of fish packets containing small Red Snapper fillets, while seven boxes, classified as batch 6M11-K3, contained packets of large Red Snapper steaks. The total weight of the entire withdrawn production batch was 1229.6 Kg. All the boxes of fish have been stored at -20°C in a specialized food store located in Southampton (UK).

3.2.2 Extraction method A: experiments on variability and yield of recovery

Extraction method. Samples were processed as reported by Poli et al. [66]. Slight modifications were applied, briefly: fish tissue (1 ± 0.05g) was weighed and transferred into 7 mL polypropylene beadruptor tube containing 18 beads and acetone (HPLC grade, 2 mL/g tissue). Beadruptor parameters were optimized as follows: run for 30 sec, followed by a 2 minute dwell period and an additional run of 30 second (S=4.00; C=02; T = 0:30; D = 2:00). Tube was then centrifuged at

3500 rpm for 5 min at 20°C, supernatant was collected through a Pasteur pipette and placed into a 13 x 100 mm glass tube with screw cap with aluminum lining. The pellet was extracted again and supernatants (4 mL) were pooled in a glass tube, which was stored at -20°C overnight. The day after, the extract was removed from freezer, let to thaw for 20 minutes at room temperature and centrifuged at 4°C for 5 min at 3500 rpm. Supernatant was transferred into a glass tube and dried down using a Vacuum concentrator (SpeedVac^{TM}) for 2 hours at 40°C with the vacuum trap set in alcohol mode (OH). 1 mL of 90% aqueous methanol (1 mL/g tissue) was added to the dried residue and mixed for 30 seconds using a vortex. Then, 2 mL of *n*-hexane (HPLC grade, 2.0 mL/g tissue) was added for defatting the 90% methanolic extract. The emulsion was mixed by repeated inversion for 30 sec, vortexed for the same time, and then centrifuged at 20°C for 5 min at 3500 rpm. The top layer (*n*-hexane) was discarded and the bottom layer was extracted again with n-hexane. The 90% methanolic extract was then evaporated using the vacuum concentrator for 1 hour at 40°C in alcohol mode (OH). The dried residue was suspended with 2.0 mL of water, vortexed for 30 seconds and added of 2.0 mL of dichloromethane (DCM; 2.0 mL/g tissue). The emulsion water-DCM was mixed by inversion for 30 sec, vortexed for the same time, and then centrifuged at 4°C for 10 min at 3500 rpm. The bottom layer (DCM) was collected through a pasteur pipette and transferred into a glass vial. The top layer (water) was extracted again with DCM, and the bottom layers were combined and dried down with a vacuum concentrator for 20 minutes at 40°C in solvents mode. The dried residue was solubilized with 500 µL methanol and vortexed for 30 sec. 250 µL were transferred in an eppendorf tube for N2a, whilst 250 µL were transferred in a glass vial for LC-MS^2 analysis.

Assessment of variability of method A. **Experiment 1**. Three frozen fish fillets, labelled as samples 12D-F, were taken from 3 different packets of the same box (production batch 6L03-K1) and let to thaw in a water bath at room temperature for 5 min. Six 1g sub-samples were collected from the same fillet (for a total of 18 sub-samples) and processed under the described procedure (extraction method A). **Experiment 2**. Three frozen fish fillets, labelled as samples 19, 20 and 21, were taken from 3 different packets of the same box (production batch 6L03-K1) and let to thaw in a water bath at room temperature for 5 min. After removing the skin and bones through an oyster-knife, each fillet was individually cut into several pieces and homogenized through a waring blender for 1 min. Six 1g sub-samples were collected from the same homogenized fillet and processed under

the extraction method A. **Experiment 3**. Three frozen fish fillets, labelled as samples 16, 17 and 18, were taken from 3 different packets of the same box (production batch 6L03-K1) and let to thaw in a water bath at room temperature for 5 min. Fish fillets were processed as reported for experiment 2. Six 1g sub-samples per fillet were extracted under method A. The acetone extracts of each fillet (4 mL for sub-sample; total volume of 24 mL) were pooled together, mixed, split in different glass vials as individual sample (volume per sample: 4 mL) and processed following the extraction method A. **Experiment 4**. Two frozen fish fillets, labelled as samples 22 and 23, were taken from 2 different packets of the same box (production batch 6L03-K1) and let to thaw in a water bath at room temperature for 5 min. Fish fillets were processed as reported for experiment 2 and 3. Six 1g sub-samples were collected from each fillet and extracted under method A. For each fillet, after performing the liquid-liquid partitioning with *n*-hexane, the 90% MeOH extracts were pooled together (total volume of 6 mL), mixed and split in aliquots of 1 mL, which were then subjected to DCM clean-up. **Experiment 5**. Two frozen fish fillets, labelled as samples 24 and 25, were taken from 2 different packets of the same box (production batch 6L03-K1) and processed as reported for experiment 4. For each fillet, six 1g sub-samples were extracted with acetone following the described procedure. Extracts were dried down, suspended with 500 µL of MeOH and 40 µL per sample were analyzed by LC-MS^2. The remaining volumes (460 µL) were dried down, suspended with 1 mL of MeOH 90% and extracted twice with *n*-hexane. Then, methanolic extracts were dried down, suspended with 500 µL of MeOH and 40 µL per sample were analyzed by LC-MS^2. The remaining volumes were dried down, suspended with 2 mL of water, and extracted twice with DCM. DCM layers were dried down, suspended with 500 µL of MeOH and analyzed by LC-MS^2.

3.2.3 Extraction method B and alternative sub-methods

Extraction method B. Samples were processed as reported by Murray et al. [67] with slight modifications. Briefly, homogenized fish tissue (1 ± 0.01g) was weighed and transferred into a 7 mL beadruptor tube containing 18 beads and a solvent mixture MeOH-water 3:2 (3mL/g tissue). Beadruptors parameters were the same reported for extraction method A. Then, the extract was boiled at 100°C for 10 min, cooled in an ice batch at 0-4°C for 5 min, and centrifuged at 3200 rpm for 10 min at 4°C. Supernatant was collected and transferred into a 15 mL graduated polypropylene

tube containing 3 mL of DCM (3.0 mL/g tissue). The emulsion MeOH-water 3:2/DCM was mixed by inversion, vortexed for 60 sec and centrifuged for 1 minute at 4°C at 3200 rpm. The bottom layer (MeOH-water 3:2) was collected, transferred into a glass tube and then dried down in a vacuum concentrator for 30 minutes at 40°C setting the vacuum trap in solvent mode. The dried residue was solubilized with 500 µL methanol and vortexed for 30 sec. 250 µL were transferred in an eppendorf tube for N2a, whilst 250 µL were transferred in a glass vial for LC-MS[2] analysis. *Alternative sub-methods.* Extraction methods A and B were slightly modified to obtain several extraction sub-methods labelled as A1, A2, A3, A4 and A5 from method A, and B1 and B2 from method B (**Table V.3**). The performance evaluation of each extraction method was conducted by sampling six 1g sub-sample from 2 homogenized fish fillets from different packets of the same box (production batch 6L03-K1). Therefore, a total of 12 sub-samples (2 fish fillets) were extracted following each method and analyzed by LC-MS[2].

3.2.4 Sample preparation to study intra-fish variability

Three fish fillets were taken from 3 different packets of the same box (production batch 6M11-K3). Ten sampling point for fillet (A-J) were selected as reported in **Fig.V.9A,** and enough fish tissue from each point was collected through an apple corer device to have 1g sub-samples (10 sub-sample for fillet). 1g fish tissue were processed under the optimized extraction method B2.

3.2.5 Sample preparation to study instrumental and batch-precision

Three fish fillets from 3 different packets of the same box (production batch 6L03-K1) were processed under the optimized conditions (analysis of 1g fish tissue) and extracted under method B2. The final extracts were run 12 times in the same batch of LC-MS[2] analysis (intra-batch variability) and other 12 times in other two different batch (inter-batch variability).

3.2.6 Ultra-high performance liquid chromatography with tandem mass spectrometry (UHPLC-MS[2]) method

LC-MS[2] analyses were carried out on a Xevo TQ-S MS coupled to a Waters Acquity UHPLC (Manchester, UK). The instrumental method was optimized using C-CTX-contaminated reference material prepared in-house (LRM) by extracting Barracuda fish collected in Antigua, (Caribbean

sea). Chromatographic separation was performed on a 2.1x50 mm Waters Acquity UPLC column packed with 1.7 µm BEH Phenyl material, in conjunction with a Waters VanGuard BEH Phenyl 1.7 µm 2.1x5 mm guard cartridge. Column oven was set at 40°C, samples were held into the sample manager at +10°C, the injection volume was 1µL and the flow rate was 0.5 mL/min. Three different mobile phase conditions, reported in **Table V.1** were tested, whilst the gradient elution was kept unchanged as follows: time (t) 0 min, 30% B; t 5 min, 100%B; t 6, 100%B; t 6.01, 30%B; re-equilibration time was 0.9 min. Mass spectrometer parameters were set as follows: capillary voltage 2.50 kV, cone voltage 50 V, desolvation temperature 600°C, desolvation gas 1000 L/hr flow, and collision gas flow 0.15 mL/min. The instrument was operated in positive ion mode in order to confirm the presence of C-CTX1 and C-CTX2 by a Multiple Reaction Monitoring (MRM) experiment. Monitored ions of relevant toxins were: i) *m/z* 1087.6 $[M+H-3H_2O]^+$ (1087.6 > 1087.6), ii) *m/z* 1163.6 $[M+Na]^+$ (1163.6 > 1163.6) and iii) *m/z* 1158.6 $[M+NH_4]^+$ (1158.6 > 1158.6). For each transition, cone and collision voltage were set as 50V and 10 eV, respectively. All the data were acquired and processed using TargetLynx™ Application Manager software by Waters Corporation.

3.2.7 Data analysis

The variability of extraction methods, intra- and inter-fish variability and the instrumental and batch precision were measured through the following statistical parameters: the mean, standard deviation and relative standard deviation (RSD%). The RSD% was measured by calculating the sum of the peak area of C/I-CTX1 and -2 originating from the transition 1087.6 > 1087.6 for a number of 6-10 replicates per experiment. On the other hand, the yield of recovery and the total toxin level were evaluated by collecting the total peak area of C/I-CTX1 and -2 in each sample, since the lack of adequate certified or reference material did not allow to accomplish quantitative analyses by LC-MS^2.

4. Conclusions

The present study described the development of LC-HRMS and LC-MS^2 method for the analysis of CTXs. The LC-HRMS approach, optimized by using the Orbitrap MS, was developed for the analysis of P-CTXs. Although the method has not yet been applied to the analysis of real samples,

it demonstrated potential for the detection of assorted P-CTXs. The configured methodology provided a good chromatographic resolution between 5 CTX congeners (CTX1B, 52-epi-54deoxyCTX1B, 51-hydroxyCTX3C, CTX3C and CTX4A), whilst the optimized ESI source parameters turned out to be the strength of the method. Notably, under the optimized conditions, P-CTXs ionized through a complex pattern of in-source formed ions – $[M+H]^+$, $[M+H-nH_2O]^+$, $[M+Na]^+$, $[M+K]^+$, $[M+NH_4]^+$ – whose presence and relative ion ratio was toxin-dependent. Therefore, the HRMS spectra of the analyzed toxins turned out to be a valuable fingerprint to be applied to the analysis of known and unknown congeners in complex matrices. However, the unavailability of adequate CTX reference material hampered the accurate optimization of the $HRMS^2$ conditions, which still require scientific efforts and standards to be optimized. On the other hand, the $LC-MS^2$ method was optimized on QqQ MS for the analysis of C-CTXs during a research visiting at Cefas (UK). The methodology was implemented to study the toxic profile of Red Snapper fillets imported from India to UK which turned out to be cause of a CFP case in in 2017. Preliminary instrumental and biological analysis showed the presence of C/I-CTXs at level 28-fold higher than that suggested by the FDA in the USA. Therefore, the toxic material was removed from market and subjected to further analytical and toxicological investigations. The $LC-MS^2$ method for the detection of C-CTX1 and -2 was optimized by using contaminated fish as LRM. The highest analytical sensitivity was achieved by using mobile phase conditions C and by setting the transition of the $[M+H-3H_2O]^+$ ion (1087.6 > 1087.6) of C-CTX1 and -2 in the MRM experiment. The implemented method was then applied to the analysis of Indian Red Snapper fillets in order to evaluate the presence and the distribution of toxic compounds. Chromatographic peaks attributable to C/I-CTX1 and -2 were found in all the analyzed samples (467 fish packets), whilst N2a analysis performed on most of the fish fillets, revealed very high toxicity levels, suggesting the presence of extremely potent toxins or a high concentration of less toxic compounds. Therefore, the analytical and toxicological data highlighted the possibility to exploit the toxic Red Snapper fish as starting material for a preparative work, aimed at isolating the toxic compounds and obtaining purified fractions of toxins. As a consequence, further studies were overtaken with the aim of finding the best experimental conditions to use for a large-scale extraction of toxins from fish. The application of a first extraction method, labelled method A, showed high variability and low yield of recovery mainly due to the clean-up step with W-DCM 1:1. An alternative method (B) was taken into consideration, and a variety of modifications

including: extraction volume, nature of solvents, solvent ratio and materials of lab equipment, were applied to method A and B ending up to obtaining 9 extraction sub-methods (A-A5, B-B2). Method B2 gave the lowest variability and the highest yields of extraction thanks to the use of plastic material and employment of the mixture MeOH-W 3:2 for the clean-up of DCM extracts. As a consequence, it was elected as method of choice to conduct the large-scale extraction of toxins from Red Snapper fish. Moreover, cross-sectional studies highlighted that the toxin distribution is not homogeneous within the fish fillet, but it follows a gaussian distribution since the toxin content is considerably high in the center of the fillet and decreases to the edges. This suggested that the homogenization of the fish fillets was a prerequisite for evaluating the total toxin content of each sample and then for selecting the most toxic individual fillets to be included in the preparative work. Finally, the suitability of the UPLC-MS instrument for conducting such analyses was investigated. It was measured a high precision within the same batch and between different batches of analyses. Overall, the optimized procedure was applied to the analysis of 89 Kg of homogenized fish tissue and a 10 Kg aliquot was identified as most contaminated and thus selected as starting material for the preparative work. As a result 74.5 g of liposoluble residue were obtained and ready to be subjected to purification and isolation steps guided by LC-MS and N2a approaches.

References

1.   FAO, F. D. (2009). Food and Agriculture Organization of the United Nations, Rome (2004). http://www.fao.org/3/y5486e/y5486e0q.htm#bm26

2.   Friedman, M. A., Fernandez, M., Backer, L. C., Dickey, R. W., Bernstein, J., Schrank, K., ... & Fleming, L. E. (2017). An updated review of ciguatera fish poisoning: clinical, epidemiological, environmental, and public health management. *Marine drugs*, *15*(3), 72.

3.   Costa, P. R., Estevez, P., Castro, D., Soliño, L., Gouveia, N., Santos, C., ... & Gago-Martínez, A. (2018). New insights into the occurrence and toxin profile of ciguatoxins in Selvagens Islands (Madeira, Portugal). *Toxins*, *10*(12), 524.

4.   Leonardo, S., Gaiani, G., Tsumuraya, T., Hirama, M., Turquet, J., Sagristà, N., ... & Campàs, M. (2020). Addressing the analytical challenges for the detection of ciguatoxins using an electrochemical biosensor. *Analytical chemistry*, *92*(7), 4858-4865.

5.   Soliño, L., & Costa, P. R. (2018). Differential toxin profiles of ciguatoxins in marine organisms: Chemistry, fate and global distribution. *Toxicon*, *150*, 124-143.

6.   Estevez, P., Sibat, M., Leão-Martins, J. M., Tudó, A., Rambla-Alegre, M., Aligizaki, K., ... & Hess, P. (2020). Use of Mass Spectrometry to determine the Diversity of Toxins Produced by Gambierdiscus and Fukuyoa Species from Balearic Islands and Crete (Mediterranean Sea) and the Canary Islands (Northeast Atlantic). *Toxins*, *12*(5), 305.

7.   Fraga, S.; Riobó, P.; Diogène, J.; Paz, B.; Franco, J. M. 11th International Conference on harmful Algae; Capetown, 2004; p 115

8.   Fraga, S., & Rodríguez, F. (2014). Genus Gambierdiscus in the Canary Islands (NE Atlantic Ocean) with description of Gambierdiscus silvae sp. nov., a new potentially toxic epiphytic benthic dinoflagellate. *Protist*, *165*(6), 839-853.

9.   Fraga, S., Rodríguez, F., Caillaud, A., Diogène, J., Raho, N., & Zapata, M. (2011). Gambierdiscus excentricus sp. nov.(Dinophyceae), a benthic toxic dinoflagellate from the Canary Islands (NE Atlantic Ocean). *Harmful Algae*, *11*, 10-22.

10.   Bravo, I., Rodriguez, F., Ramilo, I., Rial, P., & Fraga, S. (2019). Ciguatera-causing dinoflagellate *Gambierdiscus* spp.(Dinophyceae) in a subtropical region of North Atlantic Ocean (Canary Islands): Morphological characterization and biogeography. *Toxins*, 11(7), 423.

11.   Rodríguez, F., Fraga, S., Ramilo, I., Rial, P., Figueroa, R. I., Riobó, P., & Bravo, I. (2017). Canary Islands (NE Atlantic) as a biodiversity 'hotspot'of Gambierdiscus: Implications for future trends of ciguatera in the area. *Harmful Algae*, *67*, 131-143.

12.   Aligizaki, K., & Nikolaidis, G. (2008). Morphological identification of two tropical dinoflagellates of the genera Gambierdiscus and Sinophysis in the Mediterranean Sea. *Journal of biological research-Thessaloniki*, *9*, 75-82.

13.   Laza-Martínez, A., David, H., Riobó, P., Miguel, I., & Orive, E. (2016). Characterization of a strain of Fukuyoa paulensis (Dinophyceae) from the Western Mediterranean Sea. *Journal of Eukaryotic Microbiology*, *63*(4), 481-497.

14.   Epelboin, L., Pérignon, A., Hossen, V., Vincent, R., Krys, S., & Caumes, E. (2014). Two clusters of ciguatera fish poisoning in Paris, France, related to tropical fish imported from the French Caribbean by travelers. *Journal of travel medicine*, *21*(6), 397-402.

15.   Zlotnick, B. A., Hintz, S., Park, D. L., & Auerbach, P. S. (1995). Ciguatera poisoning after ingestion of imported jellyfish: diagnostic application of serum immunoassay. *Wilderness & environmental medicine*, *6*(3), 288-294.

16.   Murata, M., Legrand, A. M., Ishibashi, Y., & Yasumoto, T. (1989). Structures of ciguatoxin and its congener. *Journal of the American chemical Society*, *111*(24), 8929-8931.

17.   Pasinszki, T., Lako, J., & Dennis, T. E. (2020). Advances in Detecting Ciguatoxins in Fish. *Toxins*, *12*(8), 494.

18.   EFSA Panel on Contaminants in the Food Chain. (2010). Scientific Opinion on marine biotoxins in shellfish–Emerging toxins: Ciguatoxin group. *EFSA journal*, *8*(6), 1627.

19.   Caillaud, A., De la Iglesia, P., Darius, H. T., Pauillac, S., Aligizaki, K., Fraga, S., ... & Diogène, J. (2010). Update on methodologies available for ciguatoxin determination: perspectives to confront the onset of ciguatera fish poisoning in Europe. *Marine Drugs*, *8*(6), 1838-1907.

20.   Bagnis, R., & Fevai, G. (1971). ciguatera feline experimentale a Tahiti. *Rev Med Vet Toulouse*.

21.   Banner, A. H., & Boroughs, H. (1958). Observations on toxins of poisonous fishes. *Proceedings of the Society for Experimental Biology and Medicine*, *98*(4), 776-778.

22.   Kosaki, T. I., & Anderson, H. H. (1968). Marine toxins from the Pacific—IV Pharmacology of ciguatoxin (s). Chungue 1984

23.   Chungue, E., Bagnis, R., & Parc, F. (1984). The use of mosquitoes (Aedes aegypti) to detect ciguatoxin in surgeon fishes (Ctenochaetus striatus). *Toxicon*, *22*(1), 161-164.*Toxicon*, *6*(1), 55-58.

24.   Labrousse, H., & Matile, L. (1996). Toxicological biotest on Diptera larvae to detect ciguatoxins and various other toxic substances. *Toxicon*, *34*(8), 881-891.

25.   Chinain, M., Darius, H. T., Ung, A., Cruchet, P., Wang, Z., Ponton, D., ... & Pauillac, S. (2010). Growth and toxin production in the ciguatera-causing dinoflagellate Gambierdiscus polynesiensis (Dinophyceae) in culture. *Toxicon*, *56*(5), 739-750.

26.   Wong, C. K., Hung, P., Lee, K. L., & Kam, K. M. (2005). Study of an outbreak of ciguatera fish poisoning in Hong Kong. *Toxicon*, 46(5), 563-571.

27.   Wong, C. K., Hung, P., Lee, K. L., & Kam, K. M. (2009). Solid-phase extraction clean-up of ciguatoxin-contaminated coral fish extracts for use in the mouse bioassay. *Food Additives and Contaminants*, 26(2), 236-247.

28.   Pottier, I., Hamilton, B., Jones, A., Lewis, R. J., & Vernoux, J. P. (2003). Identification of slow and fast-acting toxins in a highly ciguatoxic barracuda (Sphyraena barracuda) by HPLC/MS and radiolabelled ligand binding. *Toxicon*, *42*(6), 663-672.

29.   Arzul, G., Gentien, P., & Crassous, M. P. (1994). A haemolytic test to assay toxins excreted by the marine dinoflagellate Gyrodinium cf. aureolum. *Water Research*, *28*(4), 961-965.

30.   Tatters, A. O., Muhlstein, H. I., & Tomas, C. R. (2010). The hemolytic activity of Karenia selliformis and two clones of Karenia brevis throughout a growth cycle. *Journal of Applied Phycology*, *22*(4), 435-442.

31.   Holland, W. C., Litaker, R. W., Tomas, C. R., Kibler, S. R., Place, A. R., Davenport, E. D., & Tester, P. A. (2013). Differences in the toxicity of six Gambierdiscus (Dinophyceae) species measured using an in vitro human erythrocyte lysis assay. *Toxicon*, *65*, 15-33.

32.   Emura, T., Suzuki, N., Yamaguchi, M., Ohshimo, H., & Fukushima, M. (2004). A novel combination antimetabolite, TAS-102, exhibits antitumor activity in FU-resistant human cancer cells through a mechanism involving FTD incorporation in DNA. *International journal of oncology*, *25*(3), 571-578.

33.   Viallon, J., Chinain, M., & Darius, H. T. (2020). Revisiting the neuroblastoma cell-based assay (CBA-N2a) for the improved detection of marine toxins active on voltage gated sodium channels (VGSCs). *Toxins*, *12*(5), 281.

34.   Mosmann, T. (1983). Rapid colorimetric assay for cellular growth and survival: application to proliferation and cytotoxicity assays. *Journal of immunological methods*, *65*(1-2), 55-63.

35.   Darius, H. T., Roué, M., Sibat, M., Viallon, J., Vandersea, M. W., Tester, P. A., ... & Chinain, M. (2018). Tectus niloticus (Tegulidae, Gastropod) as a novel vector of ciguatera poisoning: detection of Pacific ciguatoxins in toxic samples from Nuku Hiva Island (French Polynesia). *Toxins*, *10*(1), 2.

36.   Díaz-Asencio, L., Clausing, R. J., Rañada, M. L., Alonso-Hernández, C. M., & Bottein, M. Y. D. (2018). A radioligand receptor binding assay for ciguatoxin monitoring in environmental samples: Method development and determination of quality control criteria. *Journal of environmental radioactivity*, *192*, 289-294.

37.   Hardison, D. R., Holland, W. C., McCall, J. R., Bourdelais, A. J., Baden, D. G., Darius, H. T., ... & Litaker, R. W. (2016). Fluorescent receptor binding assay for detecting ciguatoxins in fish. *PLoS One*, *11*(4), e0153348.

38.   Lewis, R. J., Inserra, M., Vetter, I., Holland, W. C., Hardison, D. R., Tester, P. A., & Litaker, R. W. (2016). Rapid extraction and identification of maitotoxin and ciguatoxin-like toxins

from Caribbean and Pacific Gambierdiscus using a new functional bioassay. *PLoS One*, *11*(7), e0160006.

39.   Hokama, Y., Banner, A. H., & Boylan, D. B. (1977). A radioimmunoassay for the detection of ciguatoxin. *Toxicon*, *15*(4), 317-325.

40.   Oguri, H., Hirama, M., Tsumuraya, T., Fujii, I., Maruyama, M., Uehara, H., & Nagumo, Y. (2003). Synthesis-based approach toward direct sandwich immunoassay for ciguatoxin CTX3C. *Journal of the American Chemical Society*, *125*(25), 7608-7612.

41.   Nagumo, Y., Oguri, H., Tsumoto, K., Shindo, Y., Hirama, M., Tsumuraya, T., ... & Kumagai, I. (2004). Phage-display selection of antibodies to the left end of CTX3C using synthetic fragments. *Journal of immunological methods*, *289*(1-2), 137-146.

42.   Tsumuraya, T., Fujii, I., & Hirama, M. (2010). Production of monoclonal antibodies for sandwich immunoassay detection of Pacific ciguatoxins. *Toxicon*, *56*(5), 797-803.

43.   Tsumuraya, T., Fujii, I., & Hirama, M. (2014). Preparation of anti-ciguatoxin monoclonal antibodies using synthetic haptens: Sandwich ELISA detection of ciguatoxins. *Journal of AOAC International*, *97*(2), 373-379.

44.   Tsumuraya, T., Fujii, I., Inoue, M., Tatami, A., Miyazaki, K., & Hirama, M. (2006). Production of monoclonal antibodies for sandwich immunoassay detection of ciguatoxin 51-hydroxyCTX3C. *Toxicon*, *48*(3), 287-294.

45.   Tsumuraya, T., Sato, T., Hirama, M., & Fujii, I. (2018). Highly sensitive and practical fluorescent sandwich ELISA for ciguatoxins. *Analytical chemistry*, *90*(12), 7318-7324.

46.   Tsumuraya, T., Takeuchi, K., Yamashita, S., Fujii, I., & Hirama, M. (2012). Development of a monoclonal antibody against the left wing of ciguatoxin CTX1B: Thiol strategy and detection using a sandwich ELISA. *Toxicon*, *60*(3), 348-357.

47.   Hokama, Y. (1985). A rapid, simplified enzyme immunoassay stick test for the detection of ciguatoxin and related polyethers from fish tissues. *Toxicon*, 23(6), 939-946.

48.   Hokama, Y., Shirai, L. K., Iwamoto, L. M., Kobayashi, M. N., Goto, C. S., & Nakagawa, L. K. (1987). Assessment of a rapid enzyme immunoassay stick test for the detection of ciguatoxin and related polyether toxins in fish tissues. *The Biological Bulletin*, *172*(1), 144-153.

49.   Park, D. L. (1995). Detection of ciguatera and diarrheic shellfish toxins in finfish and shellfish with ciguatect kit. *Journal of AOAC International*, 78(2), 533-537.

50. Paul, B., Suzanne, D., & Anne, D. (2011). Quantitative evaluation of commercially available test kit for 49. ciguatera in fish. *Food and Nutrition Sciences*, 2011.

51. Ebesu, J. S., & Campora, C. E. (2012). Comment on 'Quantitative evaluation of commercially available test kit for ciguatera in fish'. *Food and Nutrition Sciences*, 3(9), 1233-1237.

52. Dickey, R. W., Granade, H. R., & McClure, F. D. (1994). Evaluation of a solid-phase immunobead assay for detection of ciguatera-related biotoxins in Caribbean finfish. Memoirs of the Queensland Museum. Brisbane, 34(3), 481-488.

53. Oguri, H., Hirama, M., Tsumuraya, T., Fujii, I., Maruyama, M., Uehara, H., & Nagumo, Y. (2003). Synthesis-based approach toward direct sandwich immunoassay for ciguatoxin CTX3C. *Journal of the American Chemical Society*, 125(25), 7608-7612.

54. Nagumo, Y., Oguri, H., Tsumoto, K., Shindo, Y., Hirama, M., Tsumuraya, T., ... & Kumagai, I. (2004). Phage-display selection of antibodies to the left end of CTX3C using synthetic fragments. *Journal of immunological methods*, 289(1-2), 137-146.

55. Tsumuraya, T., Fujii, I., & Hirama, M. (2010). Production of monoclonal antibodies for sandwich immunoassay detection of Pacific ciguatoxins. *Toxicon*, 56(5), 797-803.

56. Tsumuraya, T., Fujii, I., & Hirama, M. (2014). Preparation of anti-ciguatoxin monoclonal antibodies using synthetic haptens: Sandwich ELISA detection of ciguatoxins. *Journal of AOAC International*, 97(2), 373-379.

57. Lewis, R. J., & Sellin, M. (1992). Multiple ciguatoxins in the flesh of fish. *Toxicon*, 30(8), 915-919.

58. Yasumoto, T., & Satake, M. (1996). Chemistry, etiology and determination methods of ciguatera toxins. *Journal of Toxicology: Toxin Reviews*, 15(2), 91-107.

59. Yasumoto, T., Fukui, M., Sasaki, K., & Sugiyama, K. (1995). Determinations of marine toxins in foods. *Journal of AOAC International*, 78(2), 574-581.

60. Vernoux, J. P., & Lewis, R. J. (1997). Isolation and characterisation of Caribbean ciguatoxins from the horse-eye jack (Caranx latus). *Toxicon*, 35(6), 889-900.

61. Yogi, K., Oshiro, N., Inafuku, Y., Hirama, M., & Yasumoto, T. (2011). Detailed LC-MS/MS analysis of ciguatoxins revealing distinct regional and species characteristics in fish and causative alga from the Pacific. *Analytical chemistry*, 83(23), 8886-8891.

62.   Lewis, R. J., Vernoux, J. P., & Brereton, I. M. (1998). Structure of Caribbean ciguatoxin isolated from Caranx latus. *Journal of the American Chemical Society*, *120*(24), 5914-5920.

63.   Hamilton, B., Hurbungs, M., Jones, A., & Lewis, R. J. (2002). Multiple ciguatoxins present in Indian Ocean reef fish. *Toxicon*, *40*(9), 1347-1353.

64.   Diogène, J., Reverté, L., Rambla-Alegre, M., Del Río, V., De La Iglesia, P., Campàs, M., ... & Turquet, J. (2017). Identification of ciguatoxins in a shark involved in a fatal food poisoning in the Indian Ocean. *Scientific reports*, *7*(1), 1-8.

65.   Hamilton, B., Hurbungs, M., Vernoux, J. P., Jones, A., & Lewis, R. J. (2002). Isolation and characterisation of Indian Ocean ciguatoxin. *Toxicon*, *40*(6), 685-693.

66.   Poli, M. A., Lewis, R. J., Dickey, R. W., Musser, S. M., Buckner, C. A., & Carpenter, L. G. (1997). Identification of Caribbean ciguatoxins as the cause of an outbreak of fish poisoning among US soldiers in Haiti. *Toxicon*, *35*(5), 733-741.

67.   Murray, J. S., Boundy, M. J., Selwood, A. I., & Harwood, D. T. (2018). Development of an LC–MS/MS method to simultaneously monitor maitotoxins and selected ciguatoxins in algal cultures and P-CTX-1B in fish. *Harmful Algae*, *80*, 80-87.

Chapter 6: Isolation of ovatoxin-a from *Ostreopsis ovata* cell cultures.

1. Introduction

Ovatoxins (OVTXs) are a group of 16 naturally-occurring secondary metabolites produced by benthic dinoflagellates belonging to the *Ostreopis* genus [1]. Although *O. ovata* was identified as the main OVTX producing-organism, a new OVTX producing-species has been recently identified and named *O. fattorussoi* [2-3]. Despite their algal origin, OVTXs are classified as structural congeners of palytoxin (PLTX), the most potent non-protein and non-polymeric marine biotoxin known to date, which is contained in soft-corals belonging to the Zoanthide family (e.g. *Palythoa* spp. and *Zoanthus* spp.) [4]. To date, the only OVTX congener whose structure has been completely elucidated is OVTX-a [5], a complex water-soluble macromolecule composed of a partially unsaturated alkyl chain that harbors 40 hydroxyl group, 2 amides functions, 1 primary amine and a number of ether/hemiketal rings (**Fig.VI.1**).
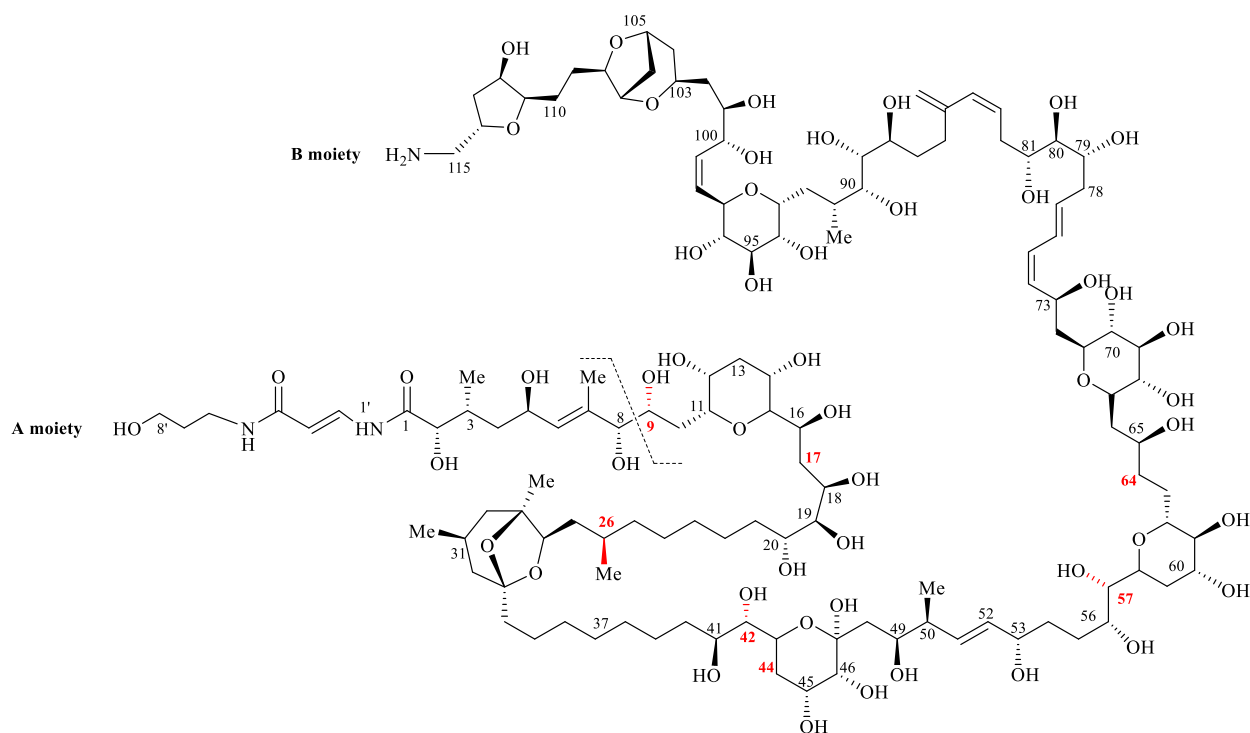

Figure VI.1 Stereostructure of OVTX-a. Differences between OVTX-a and PLTX are marked in red.

On the other hand, intriguing insights into the structure of other OVTXs were gained through the employment of HRMS[2] techniques [6]. Currently, OVTXs are emerging environmental contaminants in the Mediterranean basin and, even though they have shown able to accumulate in seafood and move into the trophic chain, they are not regulated yet [7-8]. In fact, some case of PLTX poisoning due to the consumption of contaminated seafood have been documented [9]. However, the lack of comprehensive toxicological data hampers to assess the real risks for consumers. Beside this, the toxic potential of OVTXs and their impact on human health is even greater if intoxications due to inhalation of marine aerosols and by direct contact with contaminated surfaces are taken into consideration [10]. This scenario has become alarming when in the summer 2005 along the Genoa coastline (Italy) hundreds of people showed respiratory syndromes after exposure to toxic aerosols due to a massive bloom of *O. ovata*. Instrumental analyses revealed that the implicated toxins were OVTX-a and isobaric PLTX [11]. Harmful algal blooms (HABs) of *O. ovata* have markedly increased in the last decades, and reported along the whole Italian coast [12] and in other European countries on the Mediterranean basin (e.g. France, Greece, Spain, Croatia and North Africa) [13-14]. Therefore, the scientific community made consistent efforts to develop effective methodologies to investigate and measure the presence of OVTXs in marine aerosols. As a result, the combination of PCR assays and LC-HRMS approach revealed the presence of *O. ovata* and OVTXs (2.4 pg/L) in marine aerosols collected during *O. ovata* HABs between 2009-2010 along the Tuscany coast (Italy) [15]. Moreover, the detection of PLTX and its congeners produced by soft corals in home marine aquaria, which were suspected to be the cause of poisoning for aquarium hobbyists, highlighted the relationship between *Ostreopsis*- and *Palythoa*-respiratory syndromes [16-18]. More recently, Poli et al. [10] confirmed by in-vivo rat models the high toxic potential of PLTXs and OVTX-a when administered by aerosols, with OVTX-a being the most potent with LD$_{50}$ of 0.031 µg/Kg and even 195-fold more toxic compared to IP injection (LD$_{50}$ 3.26 µg/Kg).

The toxin profile of Mediterranean strains of *O. ovata* was found to be dominated by OVTX-a followed by OVTX-b, whilst OVTX-c, -d, -e, -g, and -h, were only minor components. However, characteristic strains were found to contain OVTX-b or OVTX-f as major toxin. Moreover, a remarkable variability among different strains of *O. ovata* collected from different regions of the world, was observed. However, the highest toxic potential was identified for Brazilian and

Mediterranean strains [1]. In this context, the serious threat associated with the frequent occurrence in the Mediterranean area of *O. ovata*-HABs prompted the EU to draw guidelines for monitoring toxic blooms and the toxin profile of environmental samples and seafood [7]. Although a maximum permitted level for PLTXs in seafood has been suggested (30 µg eq. PLTX/Kg shellfish meat), more efforts have been required from the scientific community before establishing a statutory regulation. The main critical drawbacks are represented by: i) the toxicological database, since it is limited to acute toxicity studies only for a few PLTX analogues, whilst chronic toxicological data are lacking, ii) the employment of effective biological and instrumental method to properly monitor the *Ostreopsis* algal bloom and the produced OVTXs in environmental and food samples, and iii) the lack of adequate reference material. Among the variety of instrumental methods developed for detection of PLTX and OVTXs, LC-HRMS has demonstrated to be a powerful tool for in-depth investigations of toxins in complex matrices such as microalgae, seafood and marine aerosols [11,19-20]. The strength of such approach lies in the characteristic electrospray ionization behavior of PLTX and OVTXs that is used as diagnostic fingerprint for an accurate toxin identification. Notably, these toxins are able to ionize through an assorted mixture of ion species such as: mono-charged ions - $[M+H]^+$ -, bi-charged ions - $[M+2H]^{2+}$, $[M+H+Na]^+$, $[M+H+K]^+$ -, tri-charged ions - $[M+H+Ca]^{3+}$, $[M+H+Mg]^{3+}$ - and a variety of in-source water loss fragments [12]. In this context, the main limitation so far encountered is represented by the lack of reference and certified reference material (RM and CRM) for OVTXs. The latter hampers: i) the measurement of toxicological properties of toxins, and then the evaluation of the concrete risk for human health, ii) the inter-laboratory validation of analytical and biological detection methods, and iii) the accurate quantitation of toxins found in different matrices. Currently, the only standard available is PLTX standard (non-certified; FUJIFILM Wako, Japan), whilst no certified reference material has been produced so far. The main reasons lies into: i) the slow growth of dinoflagellates, when they are used as biological source, and ii) the lack of optimized procedures to isolate the produced OVTXs with high yields and grade of purity.

In this framework, this study describes the optimization and the employment of a preparative procedure to extract, purify and isolate OVTX-a at purity > 90% from 219 liters of *O. ovata* cell culture. In 2012, my research team had already optimized an isolation procedure of OVTX-a from *O. ovata* cultures, thanks to which it was possible to elucidate for the first time the structure of the toxin by NMR experiments [5]. However, the employment of such procedure including: i)

extraction of the toxin with solvents, ii) clean-up of the extract through liquid-liquid partitioning, iii) three chromatographic purifications and iv) multiple evaporation steps, brough to light some critical aspects that strongly affected the recovery yield. Therefore, an in-depth investigation aimed at elucidating the physical and chemical properties of PLTXs was carried out by using the commercially available PLTX standard. The most critical but necessary step lies in the evaporation of solvents from PLTXs containing fractions, since a strong impact on recoveries have been measured under different evaporation techniques. The adsorption of toxins on materials is a further issue, as well as the use of particular solvents and acid additives employed in the chromatographic purification steps. Moreover, the structural similarities of OVTXs make the isolation step very hard since they have a similar behavior under the used chromatographic conditions, thus resulting in toxin co-elution. Therefore, a careful choice of specific OVTX-producing strains is necessary before setting up a preparative work. In the present study, all the previously accumulated scientific evidences were taken into consideration and employed to achieve the fixed goal. Overall, even if the measured yield of recovery highlighted that the procedure still needs a further optimization, 3.4 mg of OVTX-a with a purity of 93.3% on the total OVTX content were successfully isolated from an aliquot of the *O. ovata* extracts. The complete procedure including also materials, equipment setup and troubleshooting of some of the most critical aspects is reported.

2. Results and discussion

Background

In the frame of a collaboration with Dr M. A. Poli of the Division of Diagnostic Systems within the United States Army Medical Research Institute of Infectious Diseases (USAMRIID, Maryland, USA) and Dr. D. Kulis of the Biology Department within the Woods Hole Oceanographic Institution (WHOI Massachusetts, USA), my research team received a total of 219 liters of a highly productive strain of *O. ovata* cell culture as starting material for the preparative work. The goal of such collaboration was to obtain enough purified OVTX-a (> 90%) to perform: i) development of *in-vivo* toxicity models to measure the acute inhalation toxicity of OVTX-a on primates (USAMRIID), ii) optimization of *in-vivo* mice model to measure the oral toxicity of OVTX-a, in collaboration with Prof. A. Tubaro, Dr M. Pelin and Dr S. Sosa of the University of Trieste (Italy), and iii) studies on short-term and long-term stability of the toxin in solution, which is the

prerequisite to prepare RM of this toxin class that is not commercially available yet, in collaboration with Dr P. McCarron and Dr C. Miles of the National Research Council of Canada (NRCC, Halifax, Canada).

2.1 Starting material

The starting material for the preparative work was represented by algal pellets of the same cultured strain of *O. ovata* obtained from a total of 219 liter (L) of cell culture (**Table X**).

Table VI.1 List of cultured *O. ovata* cell pellets.

Sample ID	Culture volume (L)	N° of cells	N° of pellet	N° of cells per pellet
A	1	7.44E+06	1	7.44E+06
B	3	24.4E+06	1	24.4E+06
C	3	21.1E+06	1	21.1E+06
D	3	23.2E+06	1	23.2E+06
E	3	31.2E+06	1	31.2E+06
F	1	7.00E+06*	1	7.00E+06*
G	1	7.00E+06*	1	7.00E+06*
H	51	408E+06*	3	136E+06*
I	51	408E+06*	3	136E+06*
L	51	408E+06*	3	136E+06*
M	51	408E+06*	9	45.3E+06*
Total	219	1750E+06*	25	

*Approximate number of cells.

Even though the cell counting was performed only for samples A-E, an indicative number of cells per sample could be calculated based on the available data. Notably, under the conditions employed to perform the cell culture scale-up, 1 L of *O. ovata* algal culture contained approximately 8E+06 cells. Therefore, this number of cells was estimated for pellets F and G since they were obtained from 1 L of culture. On the other hand, pellets H, I, L and M were individually obtained from 51 L of culture, thus it was reasonable to assume that each of them contained approximately 408E+06 cells. The cell pellets A-G were individually stored in 1 polypropylene (PP) tube of 50 mL, while pellets H, I and L were equally split in 3 tubes, and sample M in 9 PP tubes. By way of example, each of the 3 tubes of pellet H contained approximately 136E+06 cells.

The same was assumed for pellets I and L. Differently, each of the 9 tubes of sample M contained approximately 45.3E+06 cells. This calculations proved necessary for: i) setting up a large-scale extraction of the toxins in order to maintain the appropriate ratio number of cells/volume of extraction solvents, ii) preparing and managing the lab equipment, and for iii) minimizing times and costs associated with the set objective.

2.2 Extraction of OVTX-a from *O. ovata* cell pellets for toxin profile analysis

A small-scale extraction of each sample was accomplished to study the toxin profile of the cultured *O. ovata* strain. This analysis was needed before starting the large-scale extraction of toxins as the profile of *O. ovata* may strongly vary among different strains [1]. In addition, taking into account the aim of the preparative work, namely the isolation of OVTX-a with high grade of purity, it was necessary to investigate: i) if other OVTXs were produced by the provided cell strain, and ii) whether OVTX-a was the most abundant toxin. As previously reported, the high degree in structural similarity between the OVTX congeners can result in poor chromatographic resolutions making hard the achievement of the fixed degree of purity. At this purpose, one cell pellets per sample was extracted under a previously optimized lab-procedure, to which slight modifications were made [1]. Briefly, 1+06 of cells per sample were extracted with 3 mL of MeOH-W 1:1 (v/v), whilst no acid additives (e.g. acetic acid) were added to the extraction mixture. Taking into account the high N° of cells per pellet and the fact that they were stored in centrifuge tubes of 50 mL, for most of the samples it was not possible to extract all the cell pellet in a single extraction process due to the limited volume of the tube. The only exception was represented by sample A, G and F, which contained about 7+06 of cells per pellet, thus their tube could contain about 21 mL of MeOH-W 1:1. For the other samples, it was necessary to suspend the cell pellet with a measured volume of extraction mixture in order to obtain a homogenous cell suspension, which was then split into individual aliquots before extraction. By way of example, sample B contained 24.4E+06 cells, thus it required to be extracted with about 73 mL of MeOH-W 1:1 (3mL of mix per 1E+06) which could not be contained in a centrifuge tube of 50 mL. Therefore, 3 mL of MeOH-W 1:1 were added to sample B, ending up to obtain a homogeneous cell suspension whose concentration was 8.1E+06 cells per mL. Subsequently, 1 mL of suspension was transferred into a new PP tube of 50 mL and extracted with 25 mL of MeOH-W 1:1. Following this procedure, sample B was practically split into three homogeneous sub-samples labelled as samples B1, B2 and B3.

Similarly, samples C, D and E were suspended with 3 mL of MeOH-W 1:1, and 1 mL for sample was extracted. Contrarily, samples H, I, L and M contained the highest number of cells, thus it was necessary to add 30 mL of MeOH-W 1:1 to each of them in order to have an homogeneous cell suspension. Each sub-samples for cell pellet was then vortexed for 30 sec and then sonicated for 10 min in an ice bath setting the amplitude (AMP) at 20% in pulse mode. Subsequently, each extract was centrifuged at 900 RPM for 10 min, the supernatant was collected and transferred in a PP bottle of 100 mL. For each extract, an aliquot of 200 μL was transferred into a PP vial and analyzed by LC-HRMS.

2.3 Analysis of the toxin profile

The identification and quantitation of OVTXs produced by the *O. ovata* strain were accomplished through two optimized LC-HRMS methods [21] on a hybrid linear ion trap LTQ Orbitrap XL™ Fourier Transform Mass Spectrometer (FTMS) equipped with an ESI ION MAX™ source coupled with a Dionex Ultimate 3000 quaternary HPLC system (Thermo-Fisher, San Jose, CA, USA). Although the MS parameters and the chromatographic setting (HPLC column and mobile phase condition) were practically the same, the chromatographic gradient changed consistently based on the analysis to be performed. Notably, the investigation of the toxin profile was accomplished through the employment of a slow gradient that, associated with a smaller particle size HPLC column, guarantees high resolving power between OVTX congeners, whose peaks are completely resolved in a single chromatographic run. Briefly, a Kinetex 2.6 μm, 100Å, 100 x 2.1 mm (Phenomenex, Torrance, CA, USA) HPLC column was eluted at a flow rate of 0.2 mL/min at room temperature with water (A) and acetonitrile-water 95:5 (v/v) both containing acetic acid 30 mM. The slow gradient optimized is the following: time (t) 0 min, 25% B; t 20 min, 30%B; t 21, 100%B; t 26, 100%B; t 27 25%B; t 28 25%B; re-equilibration time was 10 min. The MS parameters were: spray voltage 4.8 kV, capillary temperature 360 °C, capillary voltage 36 V, sheath gas 60 and auxiliary gas 21 (arbitrary units), and tube lens voltage 100 V. Full-scan spectra were acquired in the *m/z* range 800-1400 at resolving power (RP) 60,000 (FWHM at *m/z* 400). Since the HRMS spectrum of PLTX and OVTXs is actually a fingerprint for this class of molecules, the HRMS[2] experiments were performed only to confirm the presence of OVTX-a by selecting the ion at *m/z* 896.1 as precursor. The experimental conditions were: RP 60,000, high-resolution collision

induced dissociation (CID) mode, collision energy (CE) 20%, isolation width 3 *m/z*, activation Q 0.250, activation time 30 ms. The full-scan XIC of each toxin was obtained by selecting the exact mass of the mono-isotopic an the most intense peak of the $[M+H+Ca]^{3+}$ ion cluster (**Table VI.2**). Elemental formulae were assigned with Thermo Xcalibur software v2.2 SP1.48 (Thermo Fisher, San Josè, CA, USA) within a mass tolerance of 5 ppm.

Table VI.2 Elemental formula of OVTXs investigated in the *O. ovata* cell culture. For each toxin the exact mass of the mono-isotopic and the most intense peak of the $[M+H+Ca]^{3+}$ cluster are reported.

Name	Acronym	Elemental formula	mono-isotopic peak	most intense peak
Palytoxin	PLTX	$C_{129}H_{223}O_{54}N_3$	906.4828	906.8172
Ovatoxin-a	OvTX-a	$C_{129}H_{223}O_{52}N_3$	895.8195	896.1540
Ovatoxin-b	OvTX-b	$C_{131}H_{227}O_{53}N_3$	910.4949	910.8294
Ovatoxin-c	OvTX-c	$C_{131}H_{227}O_{54}N_3$	915.8266	916.1610
Ovatoxin-d	OvTX-d	$C_{129}H_{223}O_{53}N_3$	901.1511	901.4856
Ovatoxin-e	OvTX-e	$C_{129}H_{223}O_{53}N_3$	901.1511	901.4856
Ovatoxin-f	OvTX-f	$C_{131}H_{227}O_{52}N_3$	905.1633	905.4977
Ovatoxin-g	OVTX-g	$C_{129}H_{223}O_{51}N_3$	890.4879	890.8223
Ovatoxin-h	OVTX-h	$C_{129}H_{225}O_{51}N_3$	891.1598	891.4942
Ovatoxin-i	OVTX-i	$C_{131}H_{225}O_{53}N_3$	909.8242	910.1572
Ovatoxin-j_1	OVTX-j_1	$C_{131}H_{225}O_{54}N_3$	915.1564	915.4908
Ovatoxin-j_2	OVTX-j_2	$C_{131}H_{225}O_{54}N_3$	915.1555	915.4877
Ovatoxin-k	OVTX-k	$C_{131}H_{225}O_{55}N_3$	920.4871	920.8189
isobaric palytoxin	isobPLTX	$C_{129}H_{223}O_{54}N_3$	906.4828	906.8172

In addition, for a careful identification of toxins, an *O. ovata* extract laboratory reference material (LRM) containing assorted OVTXs was injected under the same experimental conditions. The full-scan XIC of the OVTX-LRM showed a good chromatographic resolution between all the congeners contained in the extract (**Fig.VI.2a**). The only exception was for the isobaric OVTX-d and -e that generated two partially co-eluting peaks. The direct comparison between the XICs of the LRM and the *O.ovata* extracts revealed, for the latter, the presence of OVTX-a, OVTX-d, OVTX-e and isobaric PLTX (**Fig.VI.2a-b**).
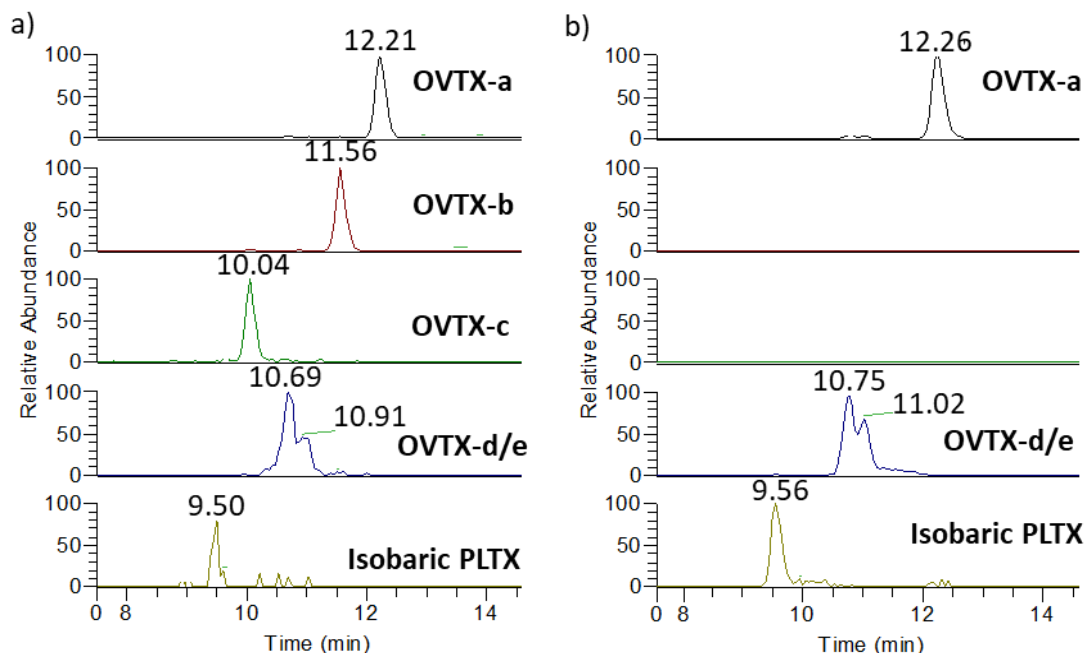
Figure VI.2 XIC of OVTX-a, b, c, d/e and isobaric PLTX contained in the: a) *O. ovata* LRM and b) *O. ovata* extract sample G analyzed through the slow gradient.

Further confirmations of the presence of OVTX-a, OVTX-d/e and isobaric PLTX in the *O. ovata* starting material were obtained from the analysis of the HR full-scan MS spectra (**Fig.VI.3**). The characteristic ionization behavior of OVTXs was clearly evidenced by the presence of diagnostic tri- and bi-charged ions in the *m/z* regions 830-910 and 1200-1400, respectively. For each toxin, the region of tri-charged ions was characterized by the presence of: i) the $[M+H+Ca]^{3+}$ ion, which was the base peak of the spectrum, ii) the $[M+H+Mg]^{3+}$ ion and iii) an assorted patterns of $[M+3H-nH_2O]^{3+}$ in-source fragments. Differently, the region of bi-charged ions contained: i) the $[M+H+K]^{2+}$ ion as the most intense, ii) the $[M+H+Na]^{2+}$ ion and, iii) a variety of $[M+2H-nH_2O]^{2+}$ in-source fragments (n=9 for OVTX-a, n= 7 for OVTX-d/e, n=2 for isobaric PLTX). For all the detected ions, the following relative ion-ratios were measured: i) $[M+H+Ca]^{3+}$: $[M+H+Mg]^{3+}$ 100:25, and ii) $[M+H+K]^{2+}$: $[M+H+Na]^{2+}$ 100:45. Contrarily, for the isobaric PLTX the ion ratio $[M+H+K]^{2+}$: $[M+H+Na]^{2+}$ was 100:15. The identity of OVTX-a was further corroborated by HRMS^2 experiments, which provided full informative fragmentation patterns (**Fig.VI.4**, **Table VI.3,** [6].
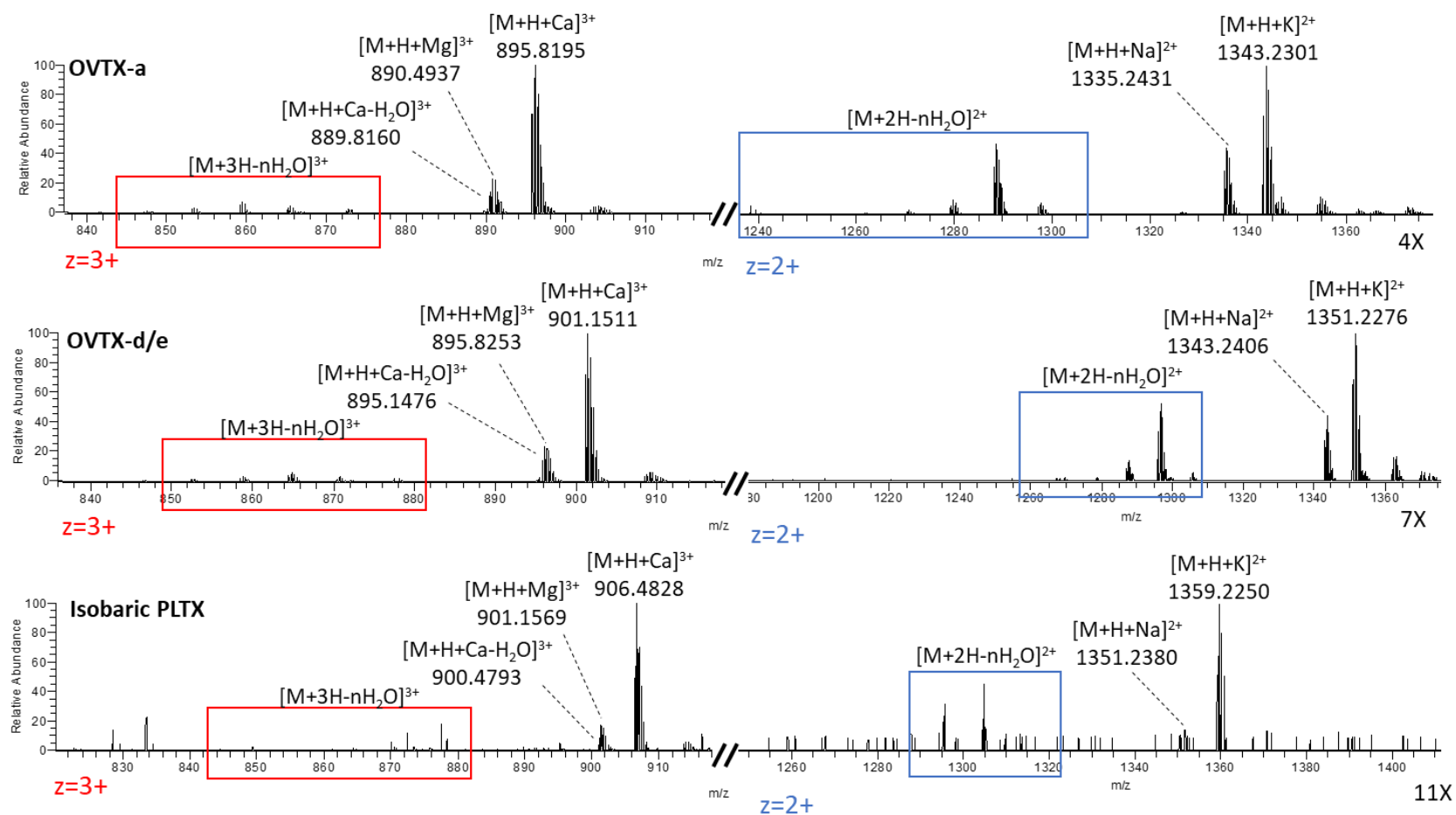
Figure VI.3 HR full-scan MS spectrum of OVTX-a, OVTX-d/e and isobaric PLTX. The *m/z* regions containing the characteristic tri- and bi-charged ions are showed.
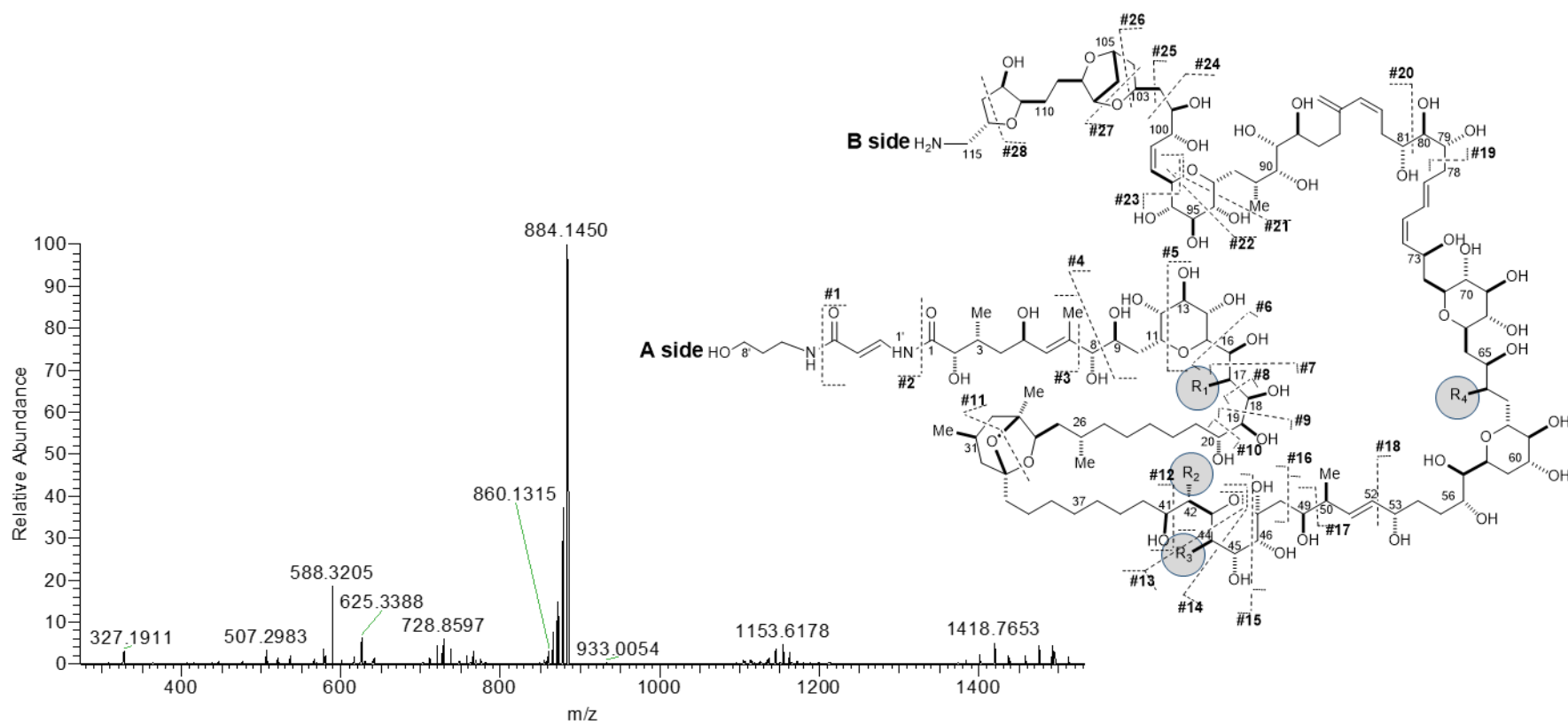
Figure VI.4 HRMS^2 spectrum and structure of OVTX-a with relevant cleavages so far reported. For ion assignment refers to Table VI.3.

Table VI.3 Assignment of A-side, B-side and internal fragments contained in the HRMS^2 spectrum of OVTX-a to relevant cleavages. For each cleavage, the mono-isotopic peak of the ion cluster is reported. The most intense ion for each cleavage is underlined.

m/z (1+, 2+, 3+)
(-nH₂O)

Precursor ion
896.1 (3+)
<u>883.8109</u> (-2H₂O)
877.8077 (-2H₂O)
871.8041 (-4H₂O)
865.8007 (-5H₂O)
859.7970 (-6H₂O)
853.7936 (-7H₂O)
847.7886 (-8H₂O)

Clv	A side m/z (1+,2+,+3) Formula, (RDB)	B side m/z (1+,2+,+3) Formula, (RDB)	Clv	A side m/z (1+,2+,+3) Formula, (RDB)	B side m/z (1+,2+,+3) Formula, (RDB)
#4	<u>327.1908 (1+)(-1H₂O)</u> C₁₆H₂₇O₅N₂ (4.5) 309.1804 (-2H₂O)	1171.1261 (2+) C₁₁₃H₁₉₅O₄₆NCa (17.0) 1162.1209 (-1H₂O) <u>1153.1158</u> (-2H₂O) 1144.1108 (-3H₂O) 1135.1062 (-4H₂O) 1126.1009 (-5H₂O) 1117.0952 (-6H₂O) 1108.0942 (-7H₂O) 781.0867 (3+) C₁₁₃H₁₉₆O₄₆NCa (16.5) <u>775.0827 (-1H₂O)</u> 769.0792 (-2H₂O) 763.0763 (-3H₂O) 757.0728 (-4H₂O) 751.0699 (-5H₂O)	**#16**	625.3387 (2+) C₅₉H₁₀₆O₂₃N₂Ca (8.0) <u>616.3335 (-1H₂O)</u> 607.3279 (-2H₂O)	737.8650 (2+) C₇₀H₁₁₇O₂₉NCa (13.0) <u>728.8596</u> (-1H₂O) 719.8543 (-2H₂O) 710.8491 (-3H₂O) 701.8436 (-4H₂O) 692.8384 (-5H₂O) 683.8331 (-6H₂O) 674.8286 (-7H₂O) 1436.7765 (1+) C₇₀H₁₁₈O₂₉N (12.5) <u>1418.7659</u> (-1H₂O) 1400.7555 (-2H₂O) 1382.7446 (-3H₂O) 1364.7341 (-4H₂O) 1346.7232 (-5H₂O) 1328.7132 (-6H₂O)
#11	<u>438.2238 (2+)</u> C₄₀H₇₂O₁₆N₂ Ca (6.0) 429.2194 (-1H₂O)		**#17**	639.3359 (2+) C₆₀H₁₀₆O₂₄N₂Ca (9.0) <u>630.3310 (-1H₂O)</u> 621.3256 (-2H₂O)	1390.7716 (1+) (-1H₂O) C₆₉H₁₁₆O₂₇N (12.5) <u>1372.7605 (-2H₂O)</u> 1354.7502 (-3H₂O)
#12	<u>536.2965 (2+)</u> C₅₂H₉₂O₁₈N₂Ca (8.0) 527.2914 (-1H₂O) 518.2858 (-2H₂O)	799.8905 (2+) (-3H₂O) C₇₇H₁₂₅O₃₁NCa (16.0) <u>790.8860 (-4H₂O)</u>	**#18**		686.8308 (2+) (-1H₂O) C₆₅H₁₀₇O₂₇NCa (13.0) <u>677.8256 (-2H₂O)</u>
#13	<u>566.3074 (2+)</u> C₅₄H₉₆O₂₀N₂Ca (8.0) 557.3021 (-1H₂O) 548.2969 (-2H₂O)	787.8919 (2+) (-1H₂O) C₇₅H₁₂₅O₃₁NCa (14.0) 778.8858 (-2H₂O) 769.8802 (-3H₂O)	**#19**	<u>932.5032 (2+)(-1H₂O)</u> C₉₀H₁₅₆O₃₅N₂Ca (14.0) 923.4983 (-2H₂O) 914.4923 (-3H₂O)	<u>804.4365(+1)</u> C₃₉H₆₆O₁₆N (7.5)
#15	<u>588.3201 (2+)</u> C₅₆H₁₀₀O₂₁N₂Ca (8.0) 579.3151 (-1H₂O) 570.3100 (-2H₂O)	774.8829 (2+) C₇₃H₁₂₃O₃₁NCa (13.0) <u>765.8781 (-1H₂O)</u> 756.8727 (-2H₂O) 747.8673 (-3H₂O) 1510.8122 (1+) C₇₃H₁₂₄O₃₁N (12.5) 1492.8023 (-1H₂O) <u>1474.7919 (-2H₂O)</u> 1456.7814 (-3H₂O)	**#21**	<u>1113.6005 (2+)</u> C₁₀₇H₁₈₆O₄₃N₂Ca (16.0) 1104.5954 (-1H₂O) 1095.5591 (-2H₂O) 1086.5866 (-3H₂O) 1077.5794 (-4H₂O)	<u>406.2216 (1+) (-3H₂O)</u> C₂₂H₃₂O₆N (7.5)

Clv	A side m/z (1+,2+,+3) Formula, (RDB)	Clv	A side m/z (1+,2+,+3) Formula, (RDB)
#22	1128.6053 (2+) $C_{108}H_{188}O_{44}N_2Ca$ (16.0) <u>1119.6021(-1H$_2$O)</u> 1110.5962 (-2H$_2$O) 1101.5869 (-3H$_2$O) 1092.5846 (-4H$_2$O)	**#4+#13**	394.2104 (2+) $C_{38}H_{68}O_{14}Ca$ (5.0)
#23	1158.6164 (2+) $C_{110}H_{192}O_{46}N_2Ca$ (16.0) <u>1149.6107(-1H$_2$O)</u> 1149.6107 (-2H$_2$O) 1140.6057 (-3H$_2$O) 1131.5990 (-4H$_2$O) 1122.5981 (-5H$_2$O)	**#4+#15**	416.2234 (2+) $C_{40}H_{72}O_{15}Ca$ (5.0)
#24	<u>1199.6367 (2+) (-1H$_2$O)</u> $C_{115}H_{198}O_{47}N_2Ca$ (18.0) 1190.6363 (-2H$_2$O)	**#4+#16**	453.2415 (2+) $C_{43}H_{78}O_{17}Ca$ (5.0)
#25	1206.6449 (2+) (-1H$_2$O) $C_{116}H_{200}O_{47}N_2Ca$ (18.0) 1197.6399 (-2H$_2$O) <u>1188.6347 (-3H$_2$O)</u> 1179.6286 (-4H$_2$O) 1170.6232 (-5H$_2$O)	**#5+#12**	641.3557 (1+) $C_{32}H_{57}O_{10}Ca$ (4.5)
		#7+#12	521.3136 (1+) $C_{28}H_{49}O_6Ca$ (4.5)
#26	1219.6517 (2+) (-1H$_2$O) $C_{118}H_{202}O_{47}N_2Ca$ (19.0) 1210.6477 (-2H$_2$O) <u>1201.6436 (-3H$_2$O)</u> 1192.6379 (-4H$_2$O) 1183.6332 (-5H$_2$O) 1174.6263 (-6H$_2$O)	**#8+#12**	507.2979 (1+) $C_{27}H_{47}O_6Ca$ (4.5)
#27	1220.6386 (2+) (-1H$_2$O) $C_{117}H_{200}O_{48}N_2Ca$ (19.0) <u>1211.6380 (-2H$_2$O)</u>	**#9+#12**	477.2875 (1+) $C_{26}H_{45}O_5Ca$ (4.5)
#4+#12	364.1999 (2+) $C_{36}H_{64}O_{12}Ca$ (5.0) 727.3924 (1+) $C_{36}H_{63}O_{12}Ca$ (5.5)	**#10+#12**	447.2771 (1+) $C_{25}H_{43}O_4Ca$ (4.5)

RDB = Ring double bond equivalent

Although the slow gradient proved to be a powerful tool for separating an assorted mixture of OVTXs, its employment is preferable only for qualitative purpose since it results into a lower sensitivity. For this reason, the quantitation of toxins contained in the *O. ovata* extracts was accomplished through a fast gradient as follows: (t) 0 min, 20% B; t 10 min, 100%B; t 15, 100%B; t 16, 20%B; t 17 20%B; re-equilibration time was 10 min. Although the fast gradient is characterized by a higher sensitivity, its resolving power turned out to be considerably lower, thus

resulting into co-elution of toxins. Nonetheless, the poor chromatographic resolution did not represent a critical issue since the acquisition of the accurate masses by the HRMS approach allowed to individually extract the peak of each toxin from the total ion current (TIC). Its performance is showed in **Fig. VI.5**.
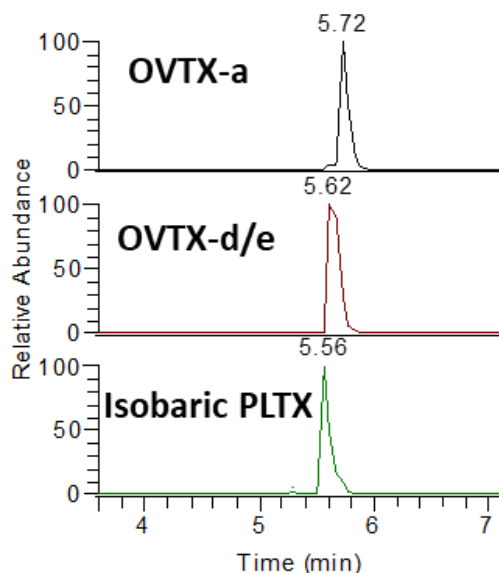

Figure VI.5 XIC of OVTX-a, -d/e and isobaric PLTX contained in the *O.ovata* extract of sample G analyzed through the fast gradient.

Overall, the quali-quantitative analyses of the extracts revealed the high potential of the selected *O. ovata* strain to be used as starting material for the preparative work focused on the isolation of OVTX-a since: i) the selected *O. ovata* strain did not produce OVTX-b, which under the optimized conditions, eluted in close proximity of OVTX-a, and ii) OVTX-a was the major component of the toxin profile accounting for 78% (OVTX-d/e and isobaric PLTX for 21, and 1% respectively. This finding allowed to start the large scale extraction of OVTX-a from the *O. ovata* cell pellets.

2.4 Extraction of OVTX-a from *O. ovata* cell pellets: optimization and toxin quantitation

The large-scale extraction of OVTX-a from *O. ovata* cell pellets was accomplished under the experimental conditions reported in in *paragraph 2.2*, even if slight modifications were applied for some pellets in terms of sample processing, in relation to the number of cells per sample. At

this purpose, the starting material was classified into: i) less concentrated (A, B, C, D, E, F and G) and ii) more concentrated samples (H, I, L and M) **(Table VI.1)**, and then two different procedures were configured. The *O. ovata* pellets A, F and G, which contained about 1+06 cells, were processed under the small-scale extraction. The same was for samples B, C, D and E, even if they were first suspended with 3 mL of the extraction mixture MeOH-W 1:1, and then 1 mL of the cell suspension was processed. Therefore, samples B, C, D and E were practically split into sub-samples labelled as B1-3, C1-3, D1-3 and E1-3, and extracted after optimizing an effective procedure. As reported in *paragraph 2.2,* each sample was first extracted with MeOH-W 1:1 (3mL for 1+06 cells) and then sonicated for 10 min in pulse mode in an ice-bath. The sonication step was accomplished through the ultrasonic homogenizer Bandelin GmbH 2200.2 (Berlin, Germany). Considering that the volume of each extract ranged between 20-30 mL, the optimization of the parameters was performed through the probe sonicator KE76 (Bandelin), which allowed to extract a total volume of 10-350 mL. Although the probe KE76 can ensure an amplitude up to 75%, this parameter was carefully considered in relation to the objective to achieve since: greater is the amplitude of the waves, higher is the energy associated. The physico-chemical phenomenon on which sonication is based is the cavitation. Briefly, an alternating current generator applies a potential difference to a transducer that converts the energy to high frequency mechanical waves. The produced ultrasounds are amplified and transmitted to a liquid sample, where small vacuum bubbles (cavities) are formed when the pressure reaches the liquid's vapor pressure. As a consequence, the bubbles collapse generating shock waves that are able to release an enormous energy concurrently to the increase of the solvent temperature. This phenomenon can be exploited to disrupt the cell membrane favoring the release of the secondary metabolites in the extraction solvent. However, the main risk is associated with the destruction of the molecules if the time and amplitude of the sonication are not well optimized. At this purpose, the optimization of the extraction procedure of OVTX-a from *O. ovata* cell pellets was conducted by setting the amplitude at 20%, and emitting ultrasounds in pulse mode with 1 sec on/off. The effectiveness of the sonication was first evaluated analyzing the effects on cells with an optical microscope. The number of intact cells after 1 extraction cycle of 5 min were considerably higher (qualitative evaluation), whilst an effective cell lysis was achieved after 10 minutes. Subsequently, the extract was centrifuged to separate the cell pellets from the supernatant containing the extracted algal metabolites. Centrifugation was accomplished through a Hermle labortechnik GmbH Z326

(Gosheim, Germany) centrifuge. The best experimental conditions were found by setting the centrifuge at 9000 RPM for 10 min since the employment of lower RPM or reduced centrifugation times provided uncleaned fractions. The resulting supernatant was then transferred into PP bottle of 100 mL by means of a Gilson PIPETMAN® P10 (1-10 mL) equipped with D10mL sterile tips (Delaware Country, Ohio, USA). The cell pellet was extracted again twice following the same procedure, and the three supernatants were pooled together. In order to evaluate the effectiveness of the extraction method, each pellet was subjected to 2 further extractions (fourth and fifth extraction cycle) and supernatants were collected separately. From each extract, an aliquot of 200 µL was taken and transferred by means of a Gilson PIPETMAN® P100 (20-100 µL) equipped with D1000mL sterile tips (Delaware Country, Ohio, USA) into PP vials of 300 µL. The quantitation of the extracted OVTX-a and the measurement of the extraction yield was accomplished through LC-HRMS analyses using: i) the fast gradient described before and ii) a 6-points calibration curve of PLTX standard (Wako Chemicals GmbH, Germany) at 31, 62.5, 125, 250, 500 and 1000 ng/mL, assuming that OVTX-a and PLTX have the same molar response. For samples A-G, the amount of OVTX-a obtained from 8+06 of *O. ovata* cells was in the range: i) 1.7-2.8 mg after three extraction cycles, ii) 0.02-0.1 mg for the fourth extraction and iii) 1-4 µg after the fifth extraction. These data strongly suggested that, under the optimized conditions, three cycles were suitable to maximize the extraction yield. Therefore, the aliquots obtained from the further two extractions were not included in the preparative work as the amount of OVTX-a was too low compared to the extraction volume. This choice was associated to the next step: the concentration of the extracts. As mentioned before, preliminary stability studies conducted by using PLTX standard revealed that the evaporation of solvents from PLTXs containing fractions strongly affected the yield of recovery, which strongly depended on: the nature of solvent, the material of the container and the evaporation technique. Moreover, the evaporation of large volumes of extracts was time-consuming and not properly effective for a preparative work. For this reason, *O. ovata* extracts containing a reduced quantity of OVTX-a were not purified but stored separately and used to optimize the experimental conditions of other steps. Similarly, an extraction procedure was configured for the most concentrated samples H, I, L and M. Considering that the cell counting was not performed for such samples, the number of cells contained in each pellet was supposed on the basis of the volume of the starting cell culture **(Table VI.1)**. Each of the three pellets of samples H (H1-3), I (I1-I3) and L (L1-L3) was suspended with 30 mL of

MeOH-W 1:1, and an approximate concentration of 4.5+06 of cell per mL was assumed. Similarly, the 9 cell pellets M (M1-9) were suspended with 30 mL of the mixture and a concentration of 1.5+06 cell per mL was supposed. However, the first experiments conducted by extracting 1 mL of cell suspension with about 15 mL (H1, I1 and L1) and 5 mL (M1) of MeOH-W 1:1 revealed that the volume of the extraction mixture used was not enough to maximize the extraction yield of OVTX-a, thus a higher number of cells was supposed to be in such samples. Among the variety of lab trials performed by increasing stepwise the extraction volume, the best experimental condition was found by extracting 1 mL of cell suspension with 30 mL of MeOH-W 1:1. Notably, 0.6 mg of OVTX-a were obtained after three extraction cycles, whilst only 0.01 and 0.002 mg were measured after the fourth and fifth cycle, respectively. Taking into account the large volume of cell suspensions to be processed, namely 570 mL (H1-3, I1-3, L1-3, M1-9), the configuration of a large-scale extraction turned out to be a pre-requisite. More in detail, 6 mL of cell suspension were split and transferred into 6 PP tubes of 50 mL by means of a Gilson PIPETMAN® P1000 (100-1000 µL) equipped with D1000 mL sterile tips (Delaware Country, Ohio, USA). Each tube was added of 30 mL of MeOH-W 1:1 and vortexed for 30 sec. The content of the 6 tubes (180 mL) was pooled into a PP becker of 500 mL and sonicated in an ice-batch at 20% AMP with 1 sec on/off. The optimization of the sonication for the large scale-extraction was conducted using the probe sonicator VS 70T (Bandelin), which allowed to sonicate volumes between 20-900 mL. However, this probe can ensure the highest performance for cell membrane lysis only when the volumes to be extracted are between 20-400 mL. Similarly to the small scale-extraction, the optimization of the sonication time was qualitatively performed observing, by means of an optical microscope, the state of cells after measured intervals of sonication (each of 10 min). A satisfactory cell disruption was achieved after 40 min of sonication. Subsequently, the extract (180 mL) was equally split into 6 PP tubes of 50 mL and centrifuged at 9000 RPM for 10 min. All six supernatants were collected through the pipette P10 and transferred into a PP bottle of 1 L. The same extraction procedure was repeated again twice and a final crude extract of 540 mL was obtained after three extraction cycles. On the other hand, further two extractions (fourth and fifth) were conducted and the supernatants (180 mL each) were collected separately in PP bottles of 250 mL. Aliquot of 200 µL for each extract were transferred into PP vials of 300 µL and analyzed by LC-HRMS as reported previously. As a result, 2.4 mg of OVTX-a were measured after three extraction cycles, whilst only 5 and 4 µg were obtained from the fourth and fifth extraction, respectively. Therefore,

similarly to the small-scale extraction, only the first three extracts were selected for the purification of OVTX-a. The direct comparison between the OVTX-a extracted under the small-scale (0.6 mg from 1 mL of cell suspension) and the large-scale (2.4 mg from 6 mL of cell suspension) procedure highlighted a loss of 0.2 mg for mL of cell suspension. This loss could be reasonably attributed to a higher adsorption of OVTX-a to the surfaces of materials since, under the large-scale extractions, the crude extracts were inevitably transferred through a high number of lab containers (PP tubes → Becker → PP tubes → PP bottles).

The application of the optimized procedures to the cell pellets allowed to obtain about 50 L of *O. ovata* crude extracts. The quantitation of OVTX-a was accomplished by LC-HRMS analysis through the preparation of aliquots of 200 μL per extract which were transferred through the P100 pipette into PP vials of 300 μL. Then, each aliquots was subjected to three stepwise dilutions of a factor 1:10 with MeOH-W 1:1 up to obtain 4 points for extract: i) crude extract, ii) extract diluted 1:10, iii) extract diluted 1:100 and iv) extract diluted 1:1000. This operation turned out to be indispensable for conducting an accurate toxin quantitation since the response recorded by LC-HRMS of OVTX-a contained in the crude extracts was much higher than of PLTX standards used to build up the calibration curve. Overall, the schematic work-flow applied for the small- and large-scale extraction of *O. ovata* cell pellets and the amount of extracted OVTX-a per sample are reported in **Fig.VI.6**. The total quantity of extracted OVTX-a was 428.1 mg.
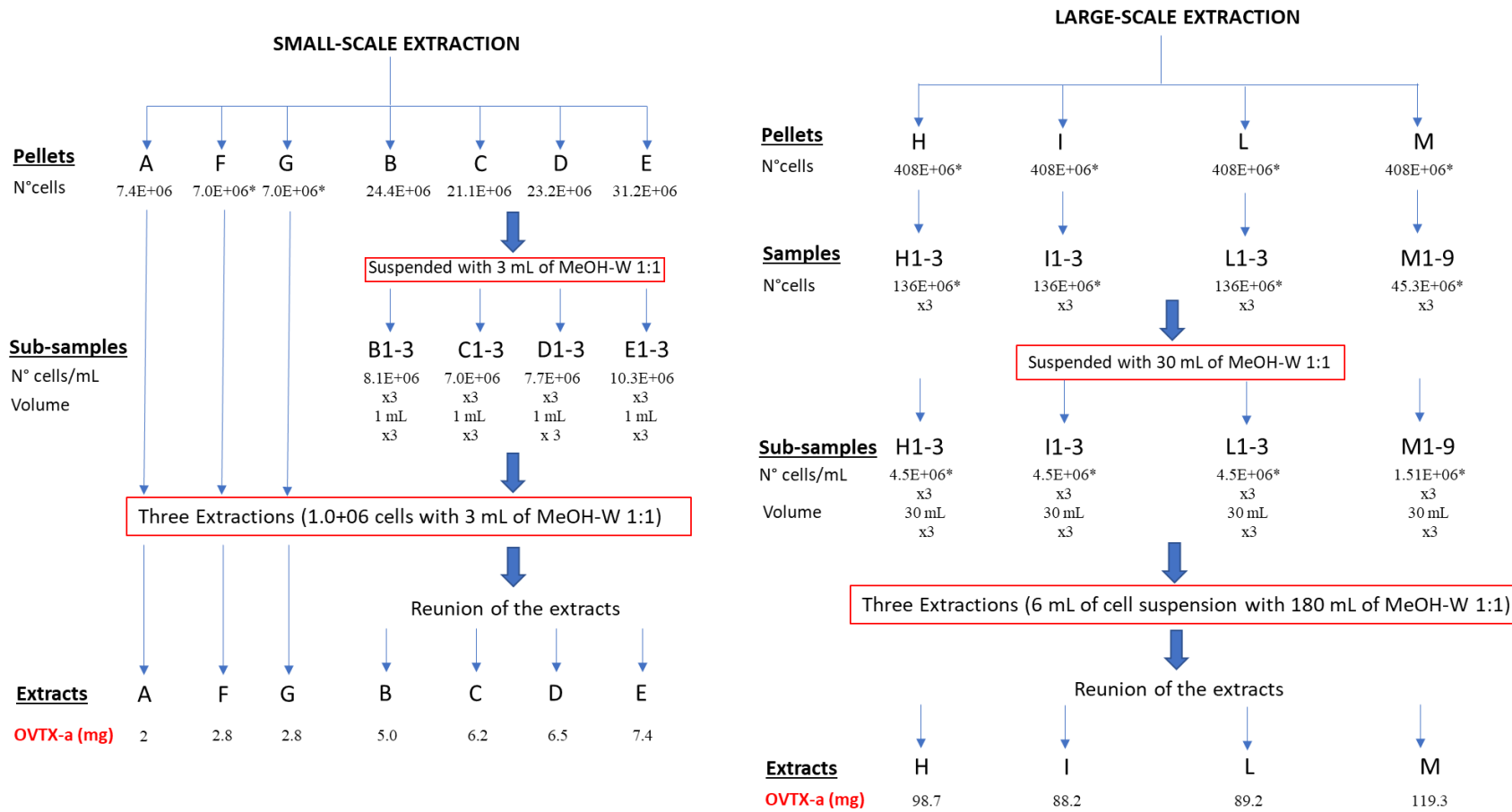
Figure VI.6 Schematic work-flow applied in the small- and large-scale extraction of OVTX-a from *O. ovata* cell pellets. Final amount of extracted OVTX-a per sample. * Approximate number of cells.

2.5 Concentration of *O. ovata* crude extracts

A total volume of about 50 L of *O. ovata* crude extract was obtained from 219 L of cell culture as starting material. Before proceeding with the clean-up step, each crude extract was concentrated under nitrogen (N_2). In particular, the less concentrated extracts - A, B, C, D, E, F and G – were pooled together in a PP bottle of 2.0 L, and an homogeneous reunion of 1.2 L, labelled as A-G, was obtained **(Table VI.4)**. On the other hand, all the other crude extracts obtained from pellets H, I, L and M were stored in PP bottle of 1 or 2 L at +4°C.

As mentioned before, preliminary stability studies conducted on PLTX standard highlighted that the evaporation of solvents is one of the most critical but unavoidable steps that drastically decreases the yield of recovery. It was found that the loss % strongly depends on different: i) physico-chemical parameters (e.g. nature of solvents, degree of concentration and solvents used to re-dissolve the dried residue), ii) evaporation techniques (N_2 flow, rotary evaporation and freeze-drying) and iii) the material in which the sample is stored. Although the best recovery was obtained through the freeze-drying, its employment was not applicable to the concentration of MeOH-W 1:1 crude extracts since: i) extracts were stored in PP bottles, whose material is characterized by low thermal conductivity, thus defrosting of the sample and/or reduced sublimation of the solid are expected, ii) the freezing point of the mixture MeOH-W 1:1 in considerably lower, thus it cannot be easily achieved through common laboratory freeze dryers, especially for large volume extracts, and iii) it is time-consuming. Although the most time-effective approach was the concentration of the extracts through the rotary evaporation, its use provides the lowest yield of recovery. On balance, the concentration under N_2 stream was selected as method of choice since the measured loss % was higher than the freeze-drying but lower than the rotary evaporation, even if it takes more time than the latter.

The objectives of the concentration step were: i) to combine all the extracts per sample (H, I, L and M) and ii) concentrate each sample to a volume of 100 mL. Therefore, considering that: i) the degree of adsorption of PLTX to the surfaces of materials may increase during the evaporation of solvents, and ii) the loss % drastically increases when samples are dried down, the optimization of the concentration step was mandatory. In detail, for each original pellet (H, I, L and M), a large number of PP bottle of 1 and 2 L were used to store the crude extracts. Starting from a bottle of 1 L, it was concentrated under N_2 stream while it was kept in a water bath at room temperature. The employment of temperature has to be carefully considered since it allows fast evaporation of

solvents (especially for less volatile solvents as water and methanol) with the positive effect of keeping low N_2 consumption, but it could favor the appearance of degradation products, especially for less stable compounds, thus affecting drastically the yield of recovery. For this reason, the temperature of the water bath was set between 25-30°C. Considering that extracts did not have to be dried down, when the volume of the extract under concentration was halved to 500 mL, the bottle was filled up with additional 500 mL of the same extract stored in a different bottle. When all the extracts for each pellet were concentrated in a single PP bottle of 1 L, the volume was reduced to 100 mL and the resulting extract was transferred into a PP bottle of the same volume using the pipette P10. As a result, this procedure allowed to obtain 5 concentrated crude extracts of 100 mL which were representative for the original pellet A-G, H, I, L and M. The influence of the evaporation step on the yield of recovery was carefully monitored during the whole process by preparing aliquots of each extract in two different stages: i) when about half of the total extract was evaporated, and ii) when each extract was concentrated to 100 mL. Notably, 4 aliquots for each extract were prepared through serial dilution of a 1:10 factor as follows: i) crude extract, ii) extract diluted 1:10, iii) extract diluted 1:100 and iv) extract diluted 1:1000. Although all 4 aliquots were analyzed by LC-HRMS, only the one that gave a response (peak area) similar to the dilution levels of PLTX standards prepared for the calibration curve was considered to accurately quantify OVTX-a. As showed in **Table VI.4**, the concentration of the extracts turned out to be a critical step since an average loss of 42.5% was measured The total amount of OVTX-a decreased from 428.1 mg (measured in the starting extracts) to 234.5 mg in the samples concentrated at 100 mL. The evaporation of about half the volume showed higher toxin loss (average 26.9 %) compared to the final concentration to 100 mL (average 21.6 %). The only exception was observed for sample M, for which the final concentration of the extract to 100 mL gave a toxin loss (43.6 %) higher than the pre-concentration step (25.2 %). The lowest toxin loss was observed for sample L (23.0 %). Although the total amount of OVTX-a contained in the concentrated samples was enough to conduct the next steps of purification and isolation, these data strongly suggested that the concentration of large volumes of extracts still needed to be optimized.

Table VI.4 Loss % of OVTX-a due to the extract concentration. The total volume, the quantity of OVTX-a (marked in red) and its loss % were measured for: i) the starting extracts, ii) pre-concentrated, and iii) concentrated extracts.

Extracts	A-G	H	I	L	M	Total
Volume (L)	1.2	11.6	8.0	9.0	19.8	49.6
OVTX-a (mg)	32.7	98.7	88.2	89.2	119.3	428.1
Volume (L)	0.65	6.95	4.55	5.3	10.66	28.1
OVTX-a (mg)	23.9	63.2	59.4	77.0	89.2	312.8
Loss %	26.9	35.9	32.6	13.7	25.2	26.9*
Volume (L)	0.1	0.1	0.1	0.1	0.1	0.5
OVTX-a (mg)	22.6	45.0	47.9	68.7	50.3	234.5
Loss %	5.4	28.9	19.4	10.8	43.6	21.6*
Total loss %	30.9	54.4	45.7	23.0	57.8	42.5*

* Average values

2.6 Clean-up of the extracts: flash chromatography

Among all the concentrated extracts, sample H was selected to be used as a starting material for the purification and isolation of OVTX-a.

The first purification step of the preparative work was accomplished using the flash chromatography, a medium-pressure liquid chromatography (MPLC) technique which is widely employed to separate a large variety of organic compounds. A measured aliquot of an extract is loaded onto the top of a prepacked preparative columns, which is eluted isocratically or through a chromatographic gradient with specific mobile phases (depending on the nature of the stationary phase, reverse or silica) and with the help of air pressure. Under optimized conditions, analytes are separated from matrix and collected in a certain number of fractions. A variety of detectors can be coupled to the chromatographic system, depending on the nature of the molecules to monitor. Compound featuring chromophores in their structure can be revealed through: i) UV (200-400 nm) and UV-Vis (200-800 nm) lamps. Specific wavelength can be selected through diode array UV detectors. Contrarily, for compounds lacking of functional groups capable of absorbing in the UV-Vis spectrum, the following detectors can be exploited: evaporative light scattering (ELSD) and mass spectrometers (MS). The clean-up of concentrated *O. ovata* crude extracts was accomplished through a Combiflash® *Rf* 200 (Teledyne Isco, Nebraska, USA) equipped with the UV detector. The flash column employed was the RediSep ® *Rf* C18 360g, 40-63 µm, 60 Å, mesh 230-400,

column volume 361.1 mL (Teledyne Isco). The flash column was equilibrated (2 column volumes; CV; 720 mL) with water (A) 60% and isopropanol (isoPrOH; B) 40% at a flow rate of 7.0 mL/min. The clean-up of the extract was performed through the following ladder-like gradient **(Table VI.5)**:

Table VI.5 Ladder-like gradient optimized for clean-up step of *O. ovata* crude extracts by flash chromatography.

Time	A % (water)	B % (isoPrOH)	Flow (mL/min)	CV - mL
0	60	40	7	-
10	60	40	7	0.2 - 72
0	30	70	7	-
15	30	70	7	0.3 - 108
0	10	90	25	-
25	10	90	25	2.0 - 720
0	5	95	25	-
25	5	95	25	2.0 – 720
0	10	90	25	-
10	10	90	25	0.7 - 252

The sample loading volume was 50 mL. The UV detector was set at $\lambda 233$ and $\lambda 263$ nm which correspond to the absorption bands of conjugated diene and α,β-unsaturated carbonyl groups, respectively. Fractions of 10 mL were collected according to volume in PP tube of 15 mL through a fraction collector. Before performing the re-equilibration, the column was subjected to 2 flush operations: i) 3 CV (1080 mL) with water (A) 10% - isoPrOH (B) 90% at 100 mL/min and ii) 1 CV (360 mL) with the same mobile phase composition at 150 mL/min. Fractions of 50 mL were collected according to volume in PP tube of the same volume. As previously described for crude extracts, toxin identification and quantitation was accomplished through LC-HRMS, and using the fast gradient due to the higher instrumental sensitivity compared to that achievable with UV lamp coupled to the MPLC chromatograph. To this aim, OVTXs (OVTX-a, d/e and isobaric PLTX) eluting through the ladder-like gradient were revealed by preparing representative samples of 10

contiguous fractions (total volume 100 mL). In particular, for each individual fraction 20 μL were taken through the pipette P100 and transferred into a PP vial for LC-MS analysis of 300 μL. The final volume of each vial was 200 μL (20 μL x 10 fractions). Differently, detection of OVTXs eluting after 2 flushes of the column was accomplished by preparing representative samples for 2 contiguous fractions by collecting 50 μL (total volume 100 μL).

Since the clean-up procedure of the crude extract by flash chromatography was accomplished after a period of 5 months from the end of the extraction and concentration steps, sample H was analyzed again by LC-HRMS. As a result, a total amount of 24.8 mg of OVTX-a was measured, thus highlighting a high instability of the toxin in the extract due to the long storage at 4°C since the starting quantity was 45 mg. Therefore, this data revealed that a loss of 44.7 % occurred for the crude extract H after a 5-month period.

Sample H (100 mL) was then purified in 2 flash chromatography steps injecting 50 mL of crude extract per step onto the column. Overall, an excellent recovery (89.4 %) was achieved through the MPLC approach since 22.2 mg of OVTX-a with a higher degree of purity were obtained. More in detail, the LC-HRMS analysis of the collected fractions revealed that most of the OVTX-a was recovered when column was eluted at 90%B. In addition, the first flush of the column at 100 mL/min considerably increased the toxin recovery since about 2.5 mg of OVTX-a were measured. Contrarily, from the second flush only 0.4 mg (average value) were obtained. On the other hand, even if the flash chromatography turned out to be a powerful tool for performing the clean-up of the *O. ovata* extracts, the high degree of structural similarity between OVTXs hampered their chromatographic separation. Therefore, OVTX-a, d/e and isobaric PLTX were recovered in the same fractions. Subsequently, the most concentrated fractions containing OVTXs (2.6 L) were selected and concentrated under N_2 stream in order to obtain a concentrated sample to use for the next semipreparative and preparative steps. Fractions were concentrated under N_2 stream at room temperature through the evaporator Labortechnik TM-130-36 (Liebisch GmbH & Co, Bielefeld, Germany). More in detail, fractions of 10 mL were pooled together in PP tubes of 50 mL. When the volume was concentrated to 25 mL, the tube was then refilled with other selected fractions. This operation was stopped when two fractions of 10 mL were obtained. Subsequently, each fraction was transferred through a P1000 pipette in a PP tube of 15 mL and concentrated to 2.0 mL. During the evaporation of solvents, measured aliquots of acetonitrile (ACN) were added in

order to have approximately mixtures of ACN-W 2:8. Overall, the two fractions contained 13.5 mg of OVTX-a. Other MPLC fractions containing OVTXs were not included in the next preparative steps, but stored at -4°C.

2.7 Semipreparative HPLC

The two concentrated fractions obtained from the clean-up step were further purified through a semipreparative procedure by using a UHPLC Dionex Ultimate® 3000 coupled to a hybrid linear ion trap LTQ Orbitrap XL™ Fourier Transform Mass Spectrometer (FTMS) equipped with an ESI ION MAX™ (Thermo-Fisher, San Jose, CA, USA). The chromatographic purification was accomplished by using a Gemini C18 250 x 10 mm, 10 μm, 110 Å, column eluted at 2.0 mL/min and at 25°C with water (A) and acetonitrile (ACN; B) both containing acetic acid 0.1 % v/v. The elution of toxins was achieved through the following gradient: time (t) 0, B20%; t 40, B100%; t 45, B100%; t 46, B20%; t 47, B20%; re-equilibration time was 10 min. The injection volume was 100 μL. The MS was used as detector for collecting manually fractions containing OVTXs. The MS parameters employed were the same reported in *paragraph 2.3*. The column outflow was split between the ESI source, for the MS-based fractionation, and the container for fraction collection. Notably, a flow of 1.9 mL/min was directed to the collection system (PP bottles of 100 mL), while a flow of 0.1 mL/min was directed to the MS system for real-time toxin detection. Under the optimized conditions, a purified fraction of 300 mL containing OVTX-a, d/e and isobaric PLTX was obtained. The employment of a 10 μm particle size HPLC column did not allow to separate OVTXs in single chromatographic fractions since they co-eluted under the same peak between 11.4-14.4 min **(Fig.VI.7)**. The purified fraction of 300 mL was concentrated at room temperature under N₂ stream to 2.0 mL. During the evaporation of solvents, measured aliquots of ACN were added to obtain approximately, a final mixture of ACN-W 2:8. The purified fraction was first concentrated in the collection container and then transferred through a pipette P1000 into a PP tube of 15 mL, in which the volume was concentrated to 2.0 mL. For an accurate toxin quantitation, an aliquot of 20 μL was taken from the concentrated fraction and diluted with 180 μL of ACN-W 2:8 (dilution factor 1:10). A further stepwise dilutions of a factor 1:10 was performed in order to prepare a representative sample diluted 1:100. These aliquots were prepared similarly to what described before, and analyzed by LC-HRMS. The peak area of OVTX-a contained in 1:100

diluted sample was comparable to the instrumental response of the PLTX standards used for building the calibration curve, thus it was used for quantitative purpose.
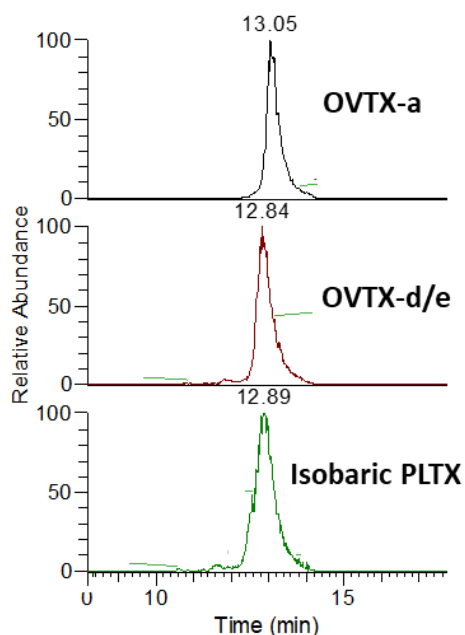

Fig. VI.7 Representative XIC of OVTXs collected and purified through the semipreparative procedure. The diagnostic ions reported in Table VI.2 and Fig.VI.3 were extracted.

Quantitative analysis revealed that 8.8 mg of purified OVTX-a were obtained. The yield of recovery within the semipreparative step was found to be 65% since the concentrated fraction obtained from the clean-up step contained 13.5 mg of OVTX-a.

2.8 Preparative HPLC: isolation of OVTXs

Finally, the purified fraction from the semipreparative HPLC was subjected to a preparative procedure in order to isolate the contained OVTXs.

Preparative HPLC is an extremely important chromatographic technique which is widely employed for purification and isolation of organic compounds from a large variety of complex matrices. This approach is based on the chromatographic purification of fractions, previously subjected to clean-up and semipreparative purification procedures, by using HPLC columns with narrower diameters. Samples to be purified are dried down (when possible) and re-suspended with

a solvent mixture superimposable to that used as starting condition of the chromatographic gradient.

The isolation of OVTXs from the already purified fraction of 2.0 mL (8.8 mg of OVTX-a) was accomplished through the same experimental setting used for the semipreparative HPLC. The Orbitrap MS, which was coupled to the UHPLC system, was employed as real-time detector for the guided fractionation of toxins. Notably, the isolation of toxins was conducted by using a Kinetex C18 100 x 4.6 mm, 2.6 μm, 10 Å, column eluted at 0.9 mL/min and at 25°C with water (A) and acetonitrile (ACN; B) both containing acetic acid 0.1 % v/v. The chromatographic gradient employed was the following: time (t) 0, B25%; t 30, B30%; t 31, B100%; t 36, B100%; t 37, B25%; t 38, B25%; re-equilibration time was 10 min. The injection volume was 100 μL. The ESI source parameters were the same described before. Chromatographic fractions containing OVTXs were collected manually by splitting the column outflow between the ESI source (0.020 mL/min) and the collection containers (0.880 mL/min), which were PP tube of 50 mL. The starting fraction of 2 mL containing OVTX-a (8.8 mg), -d/e and isobaric PLTX was fully purified through 22 injections. The employment of a HPLC column having a narrower diameter and a smaller particle size allowed to separate all the OVTXs, which were collected in different containers. The chromatographic gradient employed for the isolation procedure was the same slow gradient (*paragraph 2.3)* already optimized for the analysis of the toxin profile of OVTXs from *O. ovata* extracts. The only difference lied in the flow rate used due to the smaller particle size and the narrower diameter of the analytical HPLC column. Under the optimized conditions, OVTX-a eluted through a broad chromatographic peak between 7.1-11.9 min (**Fig.VI.8a**). However, it was collected a fraction eluting from 7.8 to 11.3 since: i) isobaric-PLTX and OVTX-d/e eluted shortly before OVTX-a between 6.15-8.2 min, whilst ii) a degradation product of OVTX-a was found to elute shortly after between 11.3-12.4 min (**Fig.VI.8a**). The latter was identified as dehydrated derivative of OVTX-a since its HRMS spectrum showed as base peak the $[M+H+Ca-H_2O]^{3+}$ tri-charged ion at *m/z* 889.8158 (mono-isotopic peak of the ion cluster) rather than the characteristic $[M+H+Ca]^{3+}$ tri-charged ion, which is the dominant peak for each OVTX under the optimized conditions (**Fig.VI.8b**). Therefore, with the aim of isolating OVTX-a with a degree of purity greater than 90%, the tails of its peak were not collected in the same fraction due to the overlap of other OVTXs/degradation products.
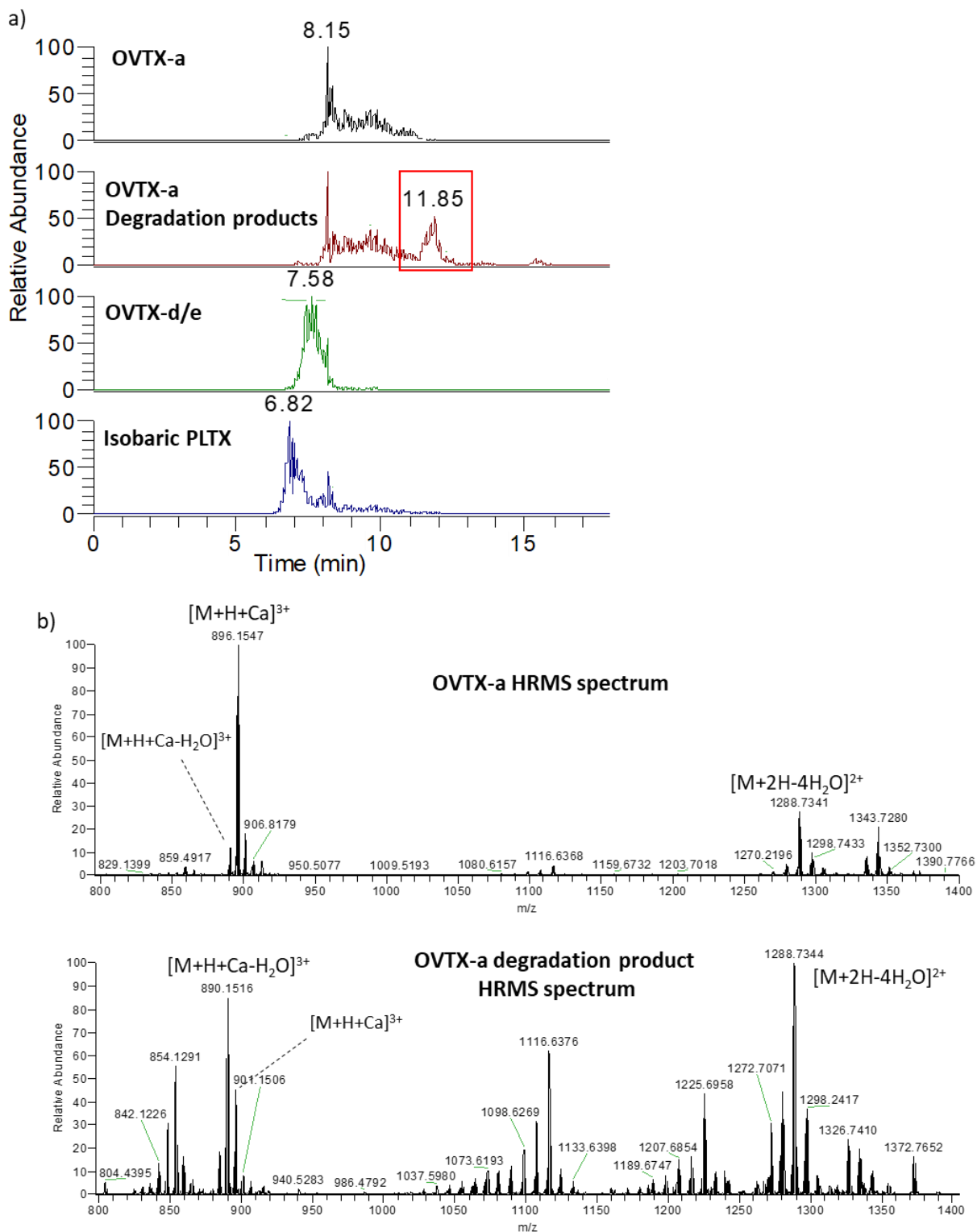
Figure VI.8 a) XIC of OVTXs eluting during the preparative HPLC. b) HRMS spectrum of OVTX-a and its degradation product.

Overall, a fraction of 50 mL containing OVTX-a was collected and quantified by LC-HRMS. Samples for quantitative analysis were prepared similarly to what described before. Briefly, 20 µL of the isolated fraction were taken and diluted 1:10 with 180 µL of ACN-W 2:8, and then a further dilution 1:10 was made to obtain a fraction diluted 1:00. The latter gave a peak area within the range of instrumental response of PLTX standards (used to build the calibration curve), thus it was used for quantitative purpose. On the other hand, the most concentrated sample (fraction diluted 1:10) was used to measure the grade of purity of the toxin. Differently from the procedure followed for quantifying toxins from crude extracts, flash chromatography and semipreparative HPLC, the quantitation of the isolated OVTX-a was carried out by using the slow analytical gradient. This choice was due to the necessity of quantifying the isolated toxin and simultaneously measure the degree of purity. As a result, the LC-HRMS analysis revealed that 3.4 mg of OVTX-a were successfully isolated with a grade of purity of 93.3 % on the total OVTXs content (**Fig.XI.9**).
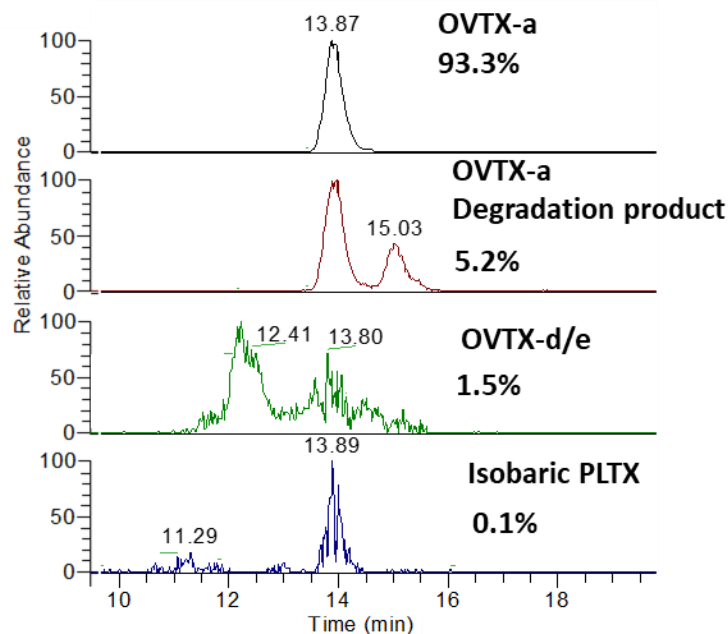

Figure VI.9 a) XIC of OVTXs eluting in the fraction of OVTX-a collected from the preparative HPLC.

The concentration of the toxin was 68.3 µg/mL. The fraction of OVTX-a contained only traces of OVTX-d/e, isobaric PLTX and OVTX-a degradation product which accounted for 1.5, 0.1 and 5.2

%, respectively, of the total toxin content. However, the yield of recovery throughout the isolation step (39.8%) suggested that a further optimization is still needed.

3. Conclusion

The present study reported the optimization of a procedure, and its successful application, for isolation of OVTX-a with a grade of purity greater than 90% from of *O. ovata* cell culture. 219 liters of a cultured strain were the starting material for the preparative work, which was aimed at obtaining sufficient purified OVTX-a to measure in-vivo toxicity and study the toxin stability in solution, which is indispensable for the preparation of reference material that is not available yet. The toxin profile of the *O. ovata* cell pellets analyzed by LC-HRMS highlighted the suitability of the starting material for the set purposes, as: i) OVTX-a accounted for 78% of the total toxin content, thus being the major compound, and ii) interfering OVTXs eluting in close proximity of OVTX-a, such as OVTX-b, were not produced. Two extraction procedures were optimized on the basis of the number of cells per sample. The less concentrated ones (A-G) were extracted on a small-scale with a mixture MeOH-W 1:1 (3 mL for 1+06 cells), sonicated for 10 min in an ice-bath at 20% AMP and then centrifuged at 9000 RPM. The extraction was repeated twice and supernatants collected together. Extracts A-G were then pooled and 32.7 mg of OVTX-a were measured. The most concentrated samples (H, I, L and M) were suspended with 30 mL of MeOH-W 1:1 and processed on a large-scale. Six mL of cell suspension were extracted with 180 mL of extraction solvents, sonicated for 40 min in an ice-bath at 20% AMP and then centrifuged at 9000 RPM. Two further extraction cycles were performed and supernatants were collected together. Overall, all the starting material was extracted and 49.6 L of crude extracts containing 428 mg of OVTX-a were obtained. The next step was the concentration of the crude extracts to a small volume of 100 mL. Preliminary stability studies conducted on PLTX standard (under publication) identified the evaporation of solvents as the most critical step which drastically affected the yield of recovery mainly due to the absorption of the toxin to the surfaces of materials. The concentration under N_2 stream was selected as method of choice in terms of recovery yields and time effectiveness. A specific procedure was then optimized, and 5 samples of 100 mL (A-G, H, I, L and M) were obtained. The recovery of OVTX-a was strictly monitored during the evaporation process and, as expected, a loss of 26.9 and 21.6 % was measured after the pre-concentration and

the final concentration of the extracts, respectively. Overall, 234.5 mg of OVTX-a were quantified with an average loss of 42.5 %. Sample H was selected for the next purification steps since it contained a high level of OVTX-a (45 mg). The storage of the extract at 4°C for a period of 5 months showed a considerable toxin loss as the content of OVTX-a in one of the most concentrated samples decreased from 45.0 mg to 24.8 mg (loss 44.7 %). This strongly suggested that the storage conditions are critical as well as the evaporation stage. Subsequently, the concentrated crude extract H was subjected to a clean-up procedure by flash chromatography. The optimized experimental conditions allowed to obtain, after 2 runs, purified fractions containing 22.2 mg of OVTX-a, thus highlighting an excellent yield of recovery (89.4%). The most concentrated fractions (2.6 L) were selected and concentrated under N_2 stream up to obtain two fractions of 2.0 mL containing 13.5 mg of OVTX-a. Then, both samples were purified through an optimized semipreparative HPLC by using the Orbitrap MS as real-time toxin detection system. The employment of a large-size column allowed to collect all the extracted OVTXs in one fraction, which contained 8.8 mg of OVTX-a. Overall a good recovery of 65% was measured within this step. The fraction containing the eluted OVTXs was then concentrated under N2 stream to 2.0 mL and subjected to a final preparative HPLC. The employment of a narrower and small particle-size column, in association with already optimized chromatographic conditions, allowed to separate all the OVTXs, which were collected in different fractions. In addition, a degradation product of OVTX-a was detected and collected separately. Overall, after 22 injections on column, a fraction of 50 mL containing 3.4 mg of OVTX-a with a grade of purity of 93.3 % of the total OVTX content was obtained. On balance, the configured procedure to isolate OVTX-a from *O. ovata* cell culture proved effective since enough purified material with a high grade of purity was obtained. Nonetheless, further studies are required to achieve higher yields of recoverie, which are actually hampered by the concentration of the crude extracts (loss 42.5 %), the storage of the extracted material (44.7 %) and the final isolation step (loss 60.2 %). On the other hand, the optimized extraction process (428 mg from 219 L of culture), the clean-up by flash chromatography (recovery 89.4 %) and the semipreparative HPLC (65 %) represented the strength of the method.

Data reported in this chapter will be included in a manuscript under preparation.

References

1.   Tartaglione, L., Dello Iacovo, E., Mazzeo, A., Casabianca, S., Ciminiello, P., Penna, A., & Dell'Aversano, C. (2017). Variability in toxin profiles of the Mediterranean Ostreopsis cf. ovata and in structural features of the produced ovatoxins. *Environmental science & technology*, *51*(23), 13920-13928.

2.   Accoroni, S., Romagnoli, T., Penna, A., Capellacci, S., Ciminiello, P., Dell'Aversano, C., ... & Totti, C. (2016). Ostreopsis fattorussoi sp. nov.(Dinophyceae), a new benthic toxic Ostreopsis species from the eastern Mediterranean Sea. *Journal of phycology*, *52*(6), 1064-1084.

3.   Tartaglione, L., Mazzeo, A., Dell'Aversano, C., Forino, M., Giussani, V., Capellacci, S., ... & Ciminiello, P. (2016). Chemical, molecular, and eco-toxicological investigation of Ostreopsis sp. from Cyprus Island: structural insights into four new ovatoxins by LC-HRMS/MS. *Analytical and bioanalytical chemistry*, *408*(3), 915-932.

4.   Gleibs, S., Mebs, D., & Werding, B. (1995). Studies on the origin and distribution of palytoxin in a Caribbean coral reef. *Toxicon*, *33*(11), 1531-1537.

5.   Ciminiello, P., Dell'Aversano, C., Dello Iacovo, E., Fattorusso, E., Forino, M., Grauso, L., ... & Vanucci, S. (2012). Isolation and structure elucidation of ovatoxin-a, the major toxin produced by Ostreopsis ovata. *Journal of the American Chemical Society*, *134*(3), 1869-1875.

6.   Ciminiello, P., Dell'Aversano, C., Dello Iacovo, E., Fattorusso, E., Forino, M., Grauso, L., & Tartaglione, L. (2012). High resolution LC-MSn fragmentation pattern of palytoxin as template to gain new insights into ovatoxin-a structure. The key role of calcium in MS behavior of palytoxins. *Journal of the American Society for Mass Spectrometry*, *23*(5), 952-963.

7.   EFSA Panel on Contaminants in the Food Chain (CONTAM). (2009). Scientific Opinion on marine biotoxins in shellfish–Palytoxin group. *EFSA Journal*, *7*(12), 1393.

8.   Amzil, Z., Sibat, M., Chomerat, N., Grossel, H., Marco-Miralles, F., Lemee, R., ... & Sechet, V. (2012). Ovatoxin-a and palytoxin accumulation in seafood in relation to Ostreopsis cf. ovata blooms on the French Mediterranean coast. *Marine drugs*, *10*(2), 477-496.

9.   Deeds, J. R., & Schwartz, M. D. (2010). Human risk associated with palytoxin exposure. *Toxicon*, *56*(2), 150-162.

10.   Poli, M., Ruiz-Olvera, P., Nalca, A., Ruiz, S., Livingston, V., Frick, O., ... & Deeds, J. (2018). Toxicity and pathophysiology of palytoxin congeners after intraperitoneal and aerosol administration in rats. *Toxicon*, *150*, 235-250.

11.   Ciminiello, P., Dell'Aversano, C., Fattorusso, E., Forino, M., Magno, G. S., Tartaglione, L., ... & Melchiorre, N. (2006). The Genoa 2005 Outbreak. Determination of Putative Palytoxin in Mediterranean Ostreopsis o vata by a New Liquid Chromatography Tandem Mass Spectrometry Method. *Analytical chemistry*, *78*(17), 6153-6159.

12.   Ciminiello, P., Dell'Aversano, C., Iacovo, E. D., Fattorusso, E., Forino, M., & Tartaglione, L. (2011). LC-MS of palytoxin and its analogues: State of the art and future perspectives. *Toxicon*, *57*(3), 376-389.

13.   Rhodes, L. (2011). World-wide occurrence of the toxic dinoflagellate genus Ostreopsis Schmidt. *Toxicon*, *57*(3), 400-407.

14.   Brahim, M. B., Feki, M., & Bouain, A. (2015). Occurrences of the toxic dinoflagellate Ostreopsis ovata in relation with environmental factors in Kerkennah Island (Southern coast of Tunisia). *Journal of Coastal Life Medicine*, *3*(8), 596-599.

15.   Ciminiello, P., Dell'Aversano, C., Iacovo, E. D., Fattorusso, E., Forino, M., Tartaglione, L., ... & Penna, A. (2014). First finding of Ostreopsis cf. ovata toxins in marine aerosols. *Environmental science & technology*, *48*(6), 3532-3540.

16.   Tartaglione, L., Pelin, M., Morpurgo, M., Dell'Aversano, C., Montenegro, J., Sacco, G., ... & Tubaro, A. (2016). An aquarium hobbyist poisoning: Identification of new palytoxins in Palythoa cf. toxica and complete detoxification of the aquarium water by activated carbon. *Toxicon*, *121*, 41-50.

17.   Tartaglione, L., Dell'Aversano, C., Mazzeo, A., Forino, M., Wieringa, A., & Ciminiello, P. (2016). Determination of palytoxins in soft coral and seawater from a home aquarium. comparison between Palythoa-and Ostreopsis-related inhalatory poisonings. *Environmental science & technology*, *50*(2), 1023-1030.

18.   Deeds, J. R., Handy, S. M., White, K. D., & Reimer, J. D. (2011). Palytoxin found in Palythoa sp. zoanthids (Anthozoa, Hexacorallia) sold in the home aquarium trade. *PLoS One*, *6*(4), e18235.

19.   Ciminiello, P., Dell'Aversano, C., Fattorusso, E., Forino, M., Tartaglione, L., Grillo, C., & Melchiorre, N. (2008). Putative palytoxin and its new analogue, ovatoxin-a, in Ostreopsis ovata collected along the Ligurian coasts during the 2006 toxic outbreak. *Journal of the American society for mass spectrometry*, *19*(1), 111-120.

20. Ciminiello, P., Dell'Aversano, C., Iacovo, E. D., Fattorusso, E., Forino, M., Grauso, L., ... & Pistocchi, R. (2010). Complex palytoxin-like profile of Ostreopsis ovata. Identification of four new ovatoxins by high-resolution liquid chromatography/mass spectrometry. *Rapid Communications in Mass Spectrometry*, *24*(18), 2735-2744.

21. Ciminiello, P., Dell'Aversano, C., Iacovo, E. D., Forino, M., & Tartaglione, L. (2015). Liquid chromatography–high-resolution mass spectrometry for palytoxins in mussels. *Analytical and bioanalytical chemistry*, *407*(5), 1463-1473.

Chapter 7: Summary on collaborative studies outside the PhD project.

1. Development of an ESI⁻ HRMS direct injection method for the detection of bisphenol M and AF in canned beverages.

Bisphenols (BPs) are a group of low-molecular weight organic compounds featuring a backbone structure based on diphenylmethane, with the exception of some analogues that have a different skeleton (e.g. BPS, BPP and BPM) **(Fig.VII.1)** [1]. The structural motif within this class of molecules is represented by two hydroxyphenyl groups which can be further substituted with alkyl (e.g. methyl and isopropyl), halogens (e.g. bromine), phenyl and nitro groups at meta positions. Among the most frequent structural variations, the two hydrogen atoms of the diphenylmethane moiety can be replaced by alkyl, phenyl and/or trifluoromethyl groups (BPA, BPAP, BPAF, BPB, BPBP, BPC, BPC2, BPE, BPG, BPPH, BPTMC, BPZ, dinitroBPA and tetrabromoBPA), while for BPZ and BPTMC the carbon atom is embedded in a six-membered ring. A unique modification can be found in BPS, since the carbon atom of the diphenylmethane moiety is replaced by a sulfonyl functionality **(Fig.VII.1).** BPA represents the parent compound of BP group [2]; it has been widely employed by industries as basic building block to manufacture plastic and coatings such as epoxy resins and polycarbonate which are high-performance materials largely used in the everyday life [3]. Therefore, BPA occurs in a large amount of commercial products such as: food packaging, DVDs, medical equipment, toys and automotive parts, lining of beverage and food cans, dental cements, thermal receipt papers etc. [4]. However, the toxicological and adverse health effects of BPA on living organisms are well-known. It is a synthetic xenoestrogen capable of acting as endocrine disrupting chemical (EDC) that mimes estrogen in the body [5]. As a consequence, the toxicity of BPA is mainly due to the homeostatic imbalance of the sexual and thyroid hormone activities [6]. Also, it is a mutagenic and carcinogenic compound which is supposed to remarkably increase the risk of different illnesses such as: obesity, diabetes, infertility and cardiovascular diseases [7]. Human can be exposed to BPA through several routes: oral, dermal and respiratory [8]. Specifically, the oral exposure due to the consumption of contaminated

food after migration of BPA from packaging material has raised even higher concerns for human safety.
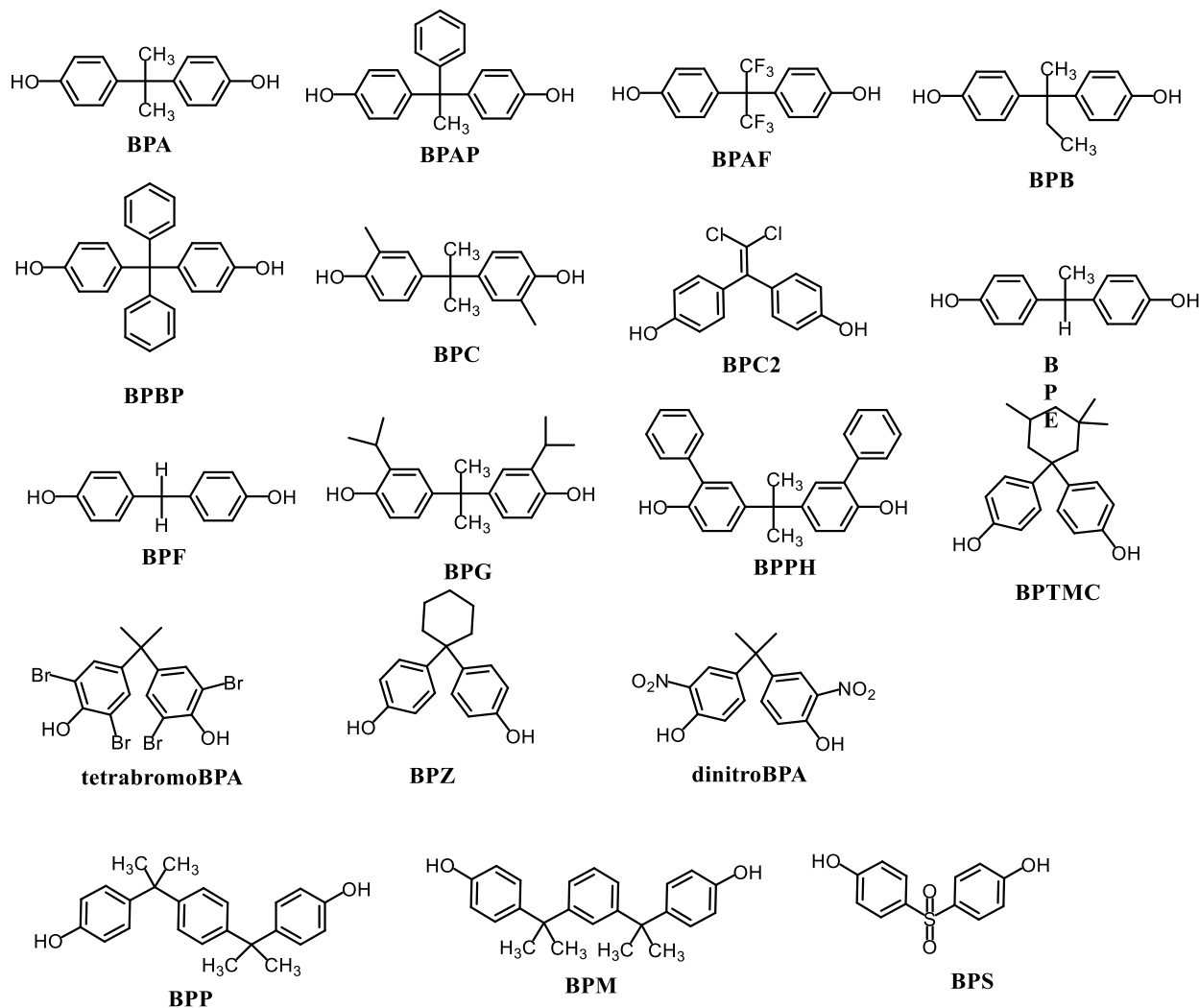

Figure VII.1 Planar structures of assorted bisphenols (BPs).

This evidence prompted the food safety authorities to assess the real risk for consumers [9], and stringent regulations were established to limit the production and the usage of BPA with the aim to preserve the consumer health and to reduce its impact on population [10-13]. As a consequence, industries, especially food manufacturers, are progressively switching to chemical alternatives to BPA, starting to use its structural analogues (BPs) as their chemistry is similar to the parent compound. In this way, industrial products, as well as the industrial procedures can be kept unmodified [14-16].

In the frame of a collaboration with Prof. L. Grumetto, Prof. F. Barbato and Dr. G. Russo from the Department of Pharmacy at UniNa, I took part in a monitoring study focused on detection and quantitation of assorted BPs in beers and energy drinks, marketed in Italy, of national and foreign production. Notably, I optimized an ESI⁻ HRMS direct injection method for the analysis of BPAF and BPM standards that was then employed to confirm the presence of such compounds in canned beverage samples. The HRMS approach was used to corroborate the presence of BPAF and BPM only in two canned beers since its aim was to validate and support the positive identification of assorted BPs in 52 samples, which was carried out by means of a previously validated liquid-chromatography - fluorescence detection (LC-FD) method [17]. Briefly, the ESI⁻ HRMS method was optimized by infusing separately BPAF (25 µg/mL) and BPM (10 µg/mL) standard solutions at a flow rate of 10 µL/min. Under the optimized experimental conditions, the HR full-scan MS spectrum of BPM and BPAF was characterized by the presence of $[M-H]^-$ ion, as base peak, at m/z 345.1860 ($C_{24}H_{25}O_2$, RDB = 12.5) and 335.0513 ($C_{15}H_9O_2F_6$, RDB= 8.5), respectively **(Fig.VII.2)**. In addition, BPAF underwent in-source fragmentation since the characteristic fragment at m/z 265.0486 ($C_{14}H_8O_2F_3$, Rdb= 9.5) due to the loss of CHF_3 moiety was found in the full-scan spectrum with a relative abundance ion ratio with the $[M-H]^-$ ion of 10:100. The intense $[M-H]^-$ ion of BPM and BPAF was then selected as precursors to acquire the relevant HRMS² spectra in high-energy collision-induced dissociation (CID) mode **(Fig.VII.2)**. A full interpretation of the fragmentation patterns of BPM and BPAF was reported in **Table VII.1**. The application of the optimized HRMS and MS² method to the analysis of beverage samples confirmed the presence of BPM and BPAF in beer#34 and beer#4, respectively. The presence in the HRMS spectra of the in-source ion at m/z 345.1860 for BPM, and m/z 335.0515 and 275.0325 for BPAF, as well as the diagnostic fragments in CID spectra were used as confirmation criteria **(Table VII.1)**. Therefore, the direct comparison between HRMS and MS² spectra of BPM and BPAF standards with those detected in beer#34 and beer#4, acquired under the same experimental conditions, confirmed the presence of BPs in canned products. More details on experimental conditions and results are reported in the published research article [18].
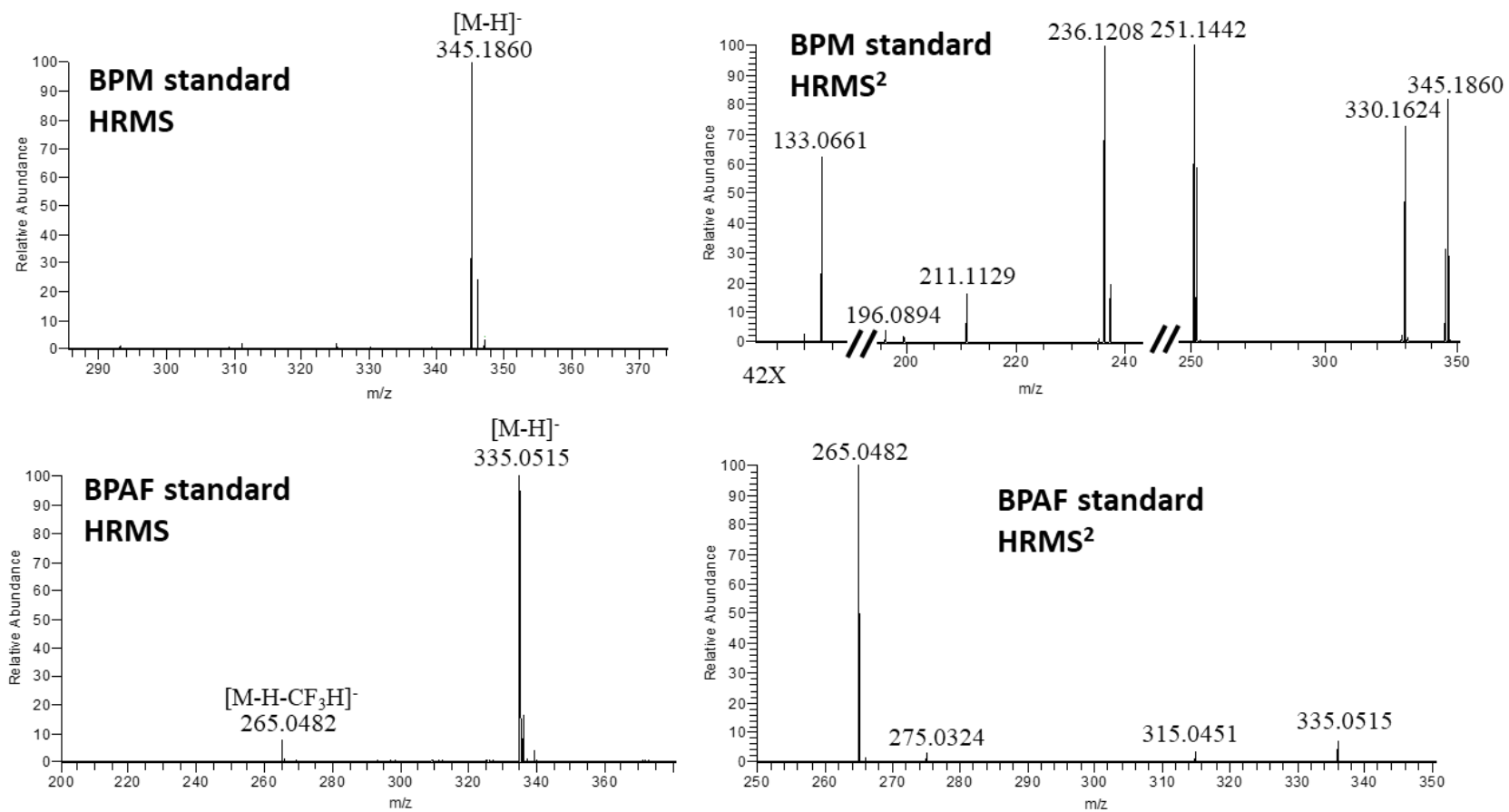
Figure VII.2 HRMS and CID MS^2 spectra of BPM and BPAF standards.

Table VII.1 Assignment of fragment ions contained in the CID HRMS^2 spectra of BPM and BPAF standards. Direct comparison with BPM and BPAF found in canned beer samples.

Samples	BPM standard	Beer#34	BPAF standard	Beer#4
m/z	345.1860	345.1860	335.0513	335.0515
Formula	$C_{24}H_{25}O_2^+$	$C_{24}H_{25}O_2^+$	$C_{15}H_9O_2F_6^+$	$C_{15}H_9O_2F_6^+$
Rdb, Δppm	12.5, 0.048	12.5, 1.468	8.5, 0.262	8.5, 0.859
Loss	H	H	H	H
m/z	330.1624	330.1624	315.0451	315.0450
Formula	$C_{23}H_{22}O_2^{+\bullet}$	$C_{23}H_{22}O_2$	$C_{15}H_8O_2F_5^+$	$C_{15}H_8O_2F_5^+$
Rdb, Δppm	13.0, -0.510	13.0, -0.267	9.5, 0.337	9.5, -0.107
Loss	$\bullet CH_3$	$\bullet CH_3$	HF	HF
m/z	251.1442	251.1442	275.0324	275.0325
Formula	$C_{18}H_{19}O^+$	$C_{18}H_{19}O^+$	$C_{15}H_6O_2F_3^+$	$C_{15}H_6O_2F_3^+$
Rdb, Δppm	9.5, 0.125	9.5, 0.125	11.5, -0.463	11.5, -0.245
Loss	C_6H_6O	C_6H_6O	3HF	3HF
m/z	236.1208	236.1207	265.0482	265.0482
Formula	$C_{17}H_{16}O^{+\bullet}$	$C_{17}H_{16}O^{+\bullet}$	$C_{14}H_8O_2F_3^+$	$C_{14}H_8O_2F_3^+$
Rdb, Δppm	10.0, 0.451	10.0, 0.112	9.5, 0.161	9.5, 0.123
Loss	$\bullet C_7H_9O$	$\bullet C_7H_9O$	CHF_3	CHF_3
m/z	211.1129	211.1131		
Formula	$C_{15}H_{15}O^+$	$C_{15}H_{15}O^+$		
Rdb, Δppm	8.5, 0.339	8.5, 1.381		
Loss	$C_9H_{10}O$	$C_9H_{10}O$		
m/z	196.0894	133.0661		
Formula	$C_{14}H_{12}O^{+\bullet}$	$C_9H_9O^+$		
Rdb, Δppm	9.0, 0.391	5.5, 1.215		
Loss	$\bullet C_{10}H_{13}O$	$C_{15}H_{16}O$		
m/z	133.0661	n.d.		
Formula	$C_9H_9O^+$			
Rdb, Δppm	5.5, 1.366			
Loss	$C_{15}H_{16}O$			

Rdb= Ring Double Bond Equivalent, Δppm= error

2. HILIC-HRMS method for the analysis of impurities in sapropterin branded and generic tablets.

Sapropterin dihydrochloride (BH$_4$·2HCl), also known as sapropterin, is an active compound of synthetic origin which corresponds to the *6R*-isomer of tetrahydrobiopterin (BH$_4$), the natural cofactor of the phenylalanine hydroxylase (PHA) [19]. The latter, is an hepatic enzyme capable of transforming phenylalanine in tyrosine, an essential amino acid which represents the substrate for the synthesis of neurotransmitters and melatonin [20]. Sapropterin is the active ingredient of the Kuvan®, a drug approved by the European Medicines Agency (EMA; Procedure No. EMEA/H/C/000943/II/0033) and the Food and Drug Administration (FDA; APPLICATION NUMBER:205065Orig1s000) for the treatment of phenylalaninemia, a rare illness due to a reduced activity of the PHA. It follows that patients affected by this disease have mild or high concentration of phenylalanine in the blood [21]. In addition, mutations in the PHA gene can further cause the phenylketonuria (PKU), a medical condition characterized by a reduced metabolism of the phenylalanine amino acid that, if untreated, may lead to different disorders (e.g. mental disorders, behavioral problems, intellectual disability) [22-23]. However, only the 2% of the PHA patients showed defects in the biosynthesis or recycling of the BH$_4$ [24]. Therefore, sapropterin was approved to treat PHA in patients over 4 years old with BH$_4$-responsive PKU, in adults and young people having a BH$_4$ deficiency, and to reduce the blood level of phenylalanine PHA [25]. Although sapropterin is a small-size molecule, its chemistry is quite complex since it showed a remarkable instability in solution, as well as its synthesis is made difficult by the presence of three continuous chiral centers [26-27] (**Fig.VII.3**). The stereochemistry of sapropterin is essential for the biological activity since only the *6R* isomer is active while the *6S* isomer was found to cause an irreversible inactivation of PHA in rat [28]. Therefore, pharmaceutical formulations of sapropterin have to be characterized by a life-long stability and a very low content of putative dangerous impurities which can originate from the synthetic process of the active ingredient , as well as from its degradation (**Fig.VII.3**).

In the frame of a collaboration with Prof. O. Taglialatela Scafati of the Department of Pharmacy of the University of Napoli Federico II, I developed a HILIC-HRMS[2] method to analyze sapropterin and a large number of structurally related compounds that can be found as impurities in sapropterin tablets. The HRMS approach was used to corroborate and support the application

of a LC-UV method exploited to investigate the composition and the stability of the life-long treatment of Kuvan® and Diterin®, which are the branded and a generic sapropterin-containing drug, respectively. It is mandatory to state that Dipharma S.A., which was the sponsor of the study and producer of Diterin®, provided the products without having any role in the development of the study as well as in the data interpretation.
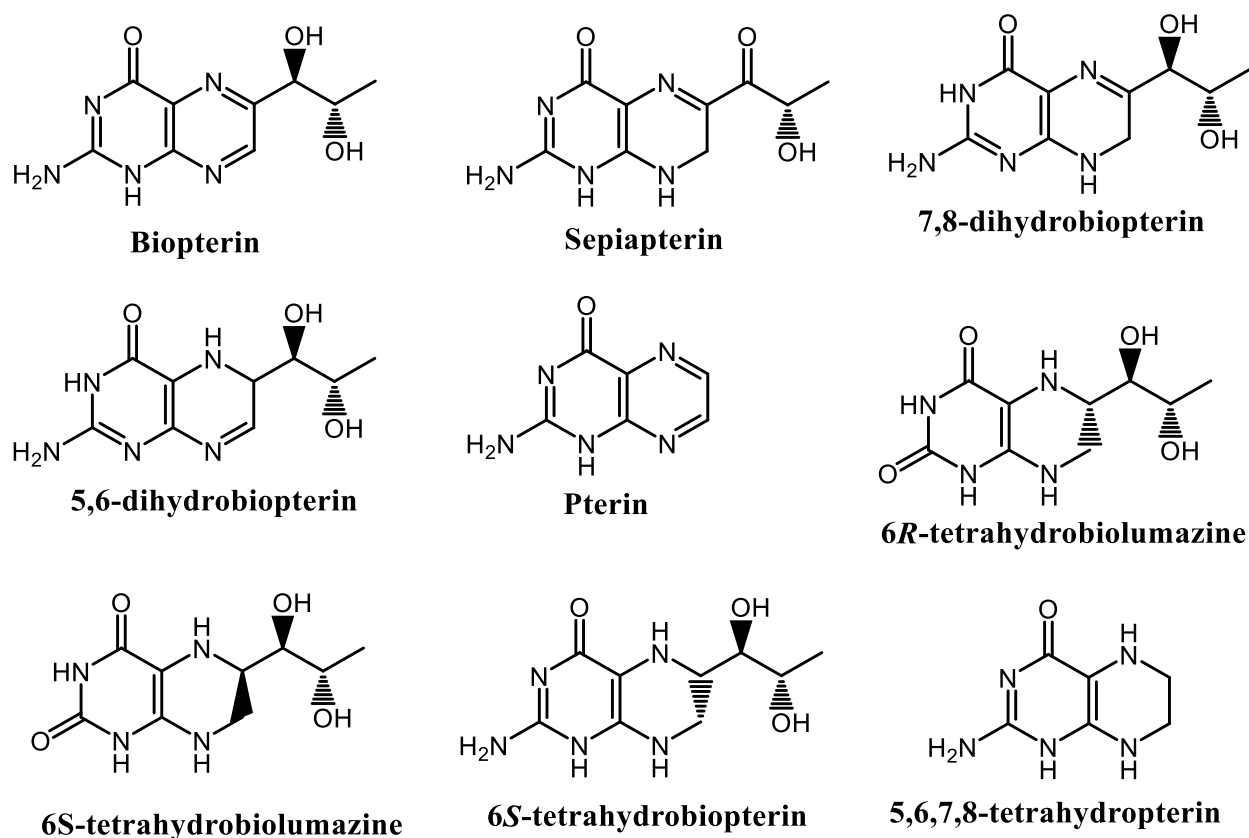

Figure VII.3 Chemical structure of Sapropterin and its structurally-related analogues.

To date, a very low number of LC-MS^2 methods have been optimized for the analysis of sapropterin (BH$_4$) and its impurities [29-32], and even less HRMS^2 data are available. Most of the LC-UV methods rely on ion-exchange chromatographic columns, which are frequently eluted with phosphate buffers [33-35]. Unfortunately, the monosodium phosphate (NaH$_2$PO$_4$) is incompatible with LC-MS systems since it is a non-volatile salt. Therefore, taking into account the chemical-physical properties of sapropterin and its structurally-related compounds (sapropterins), which are small polar molecules, the optimization of the LC conditions was performed by exploiting the

principles of the hydrophilic interaction liquid chromatography (HILIC). This approach allowed to resolve a mixture of 9 compounds: (biopterin, sepiapterin, 7,8-dihydrobiopterin, pterin, 6*S*- and 6*R*-tetrahydrobiolumazine, 6S-tetrahydrobiopterin and 5,6,7,8-tetrahydropterin; **Fig.VII.4**), while the employment of the high mass accuracy turned out to be indispensable for a selective and specific identification of different molecules for which only a moderate or poor chromatographic resolution was achieved.
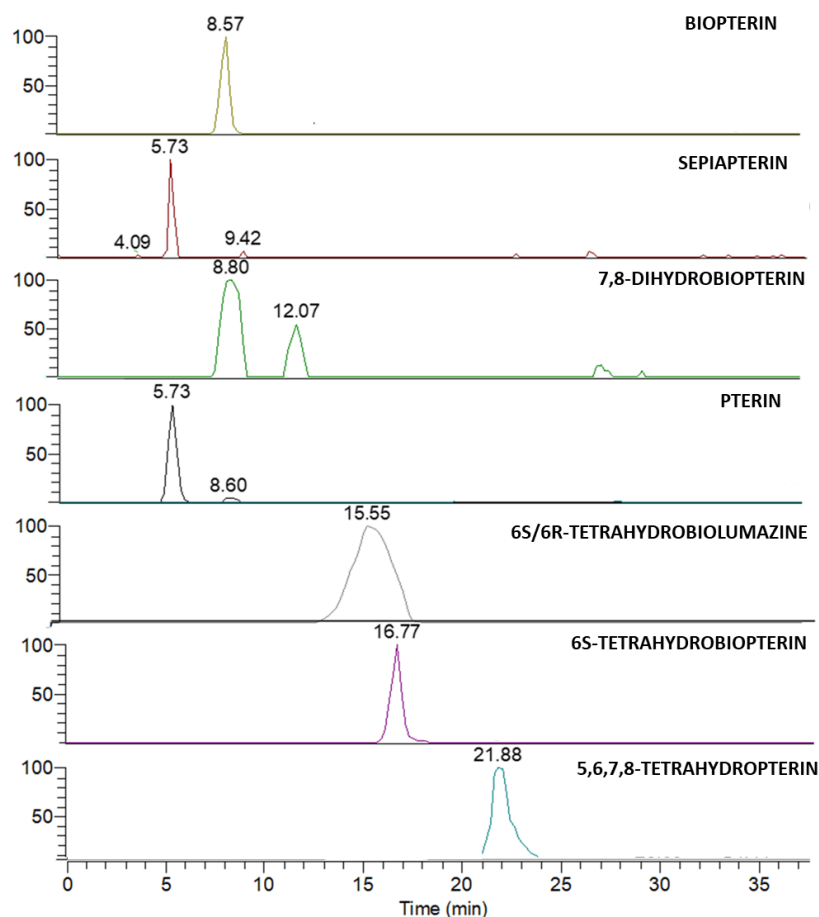

Figure VII.4 XIC of compounds by selecting the accurate mass of the relevant [M+H]⁺ and [M+Na]⁺ ions reported in Table VII.2.

The ESI source parameters and the HRMS^2 conditions were optimized by using sapropterin standard solution at 10 µg/mL. Overall, the application of the developed HILIC-HRMS method to the analysis of standards revealed a characteristic behavior for all the compounds, since their HR full-scan spectra were characterized by the presence of a [M+H]⁺ ion, as base peak for most of the

compounds, and a $[M+Na]^+$ adduct ion with a relative abundance ion ratio being specific for each analyte **(Table VII.2)**. Moreover, the acquisition of $HRMS^2$ spectra in CID mode showed characteristic fragmentation patterns for each molecule, for which a complete interpretation was carried out. In conclusion, the optimized $HILIC\text{-}HRMS^2$ method turned out to be a powerful tool for supporting the LC-UV approach used for identification and quantitation of sapropterin and its impurities contained in Kuvan® and Diterin® tablets. More details on the experimental conditions and results are reported in the published research article [36].

Table VII.2 Exact mass, molecular formula (MF), Ring Double Bond Equivalents (RDB) and errors (ppm) measured for the $[M+H]^+$ and $[M+Na]^+$ of each compound.

Compound	$[M+H]^+$ (m/z) MF, RDB, ppm	$[M+Na]^+$ (m/z) MF, RDB, ppm	$[M+H]^+$: $[M+Na]^+$ relative abundance ion ratio
Biopterin	238.0936 $C_9H_{12}O_3N_5$, 6.5, (0.480)	260.0755 $C_9H_{11}O_3N_5Na$, 6.5, (0.344)	60 : 100
Biopterin	238.0936 $C_9H_{12}O_3N_5$, 6.5, (0.480)	260.0755 $C_9H_{11}O_3N_5Na$, 6.5, (0.344)	60 : 100
7,8-dyhydrobiopterin	240.1093 $C_9H_{14}O_3N_5$, 5.5, (0.725)	262.0909 $C_9H_{13}O_3N_5Na$, 5.5, (-0.154)	100 : 80
Pterin	164.0567 $C_6H_6ON_5$, 6.5, (0.571)	186.0387 $C_6H_5ON_5Na$, 6.5, (0.478)	100 : 30
6R/6S-tetrahydrobiolumazine	243.1088 $C_9H_{15}O_4N_4$, 4.5 (1.022)	265.0910 $C_9H_{14}O_4N_4Na$, 4.5 (0.995)	100 : 20
6S-tetrahydrobiopterin	242.1248 $C_9H_{16}O_3N_5$, 4.5, (1.752)	264.1072 $C_9H_{15}O_3N_5Na$, 4.5, (1.815)	100 : 90
5,6,7,8- tetrahydropterin	168.0880 $C_6H_{10}ON_5$, 4.5, (0.437)	190.0700 $C_6H_9ON_5Na$, 4.5, (0.362)	100 : 80

References

1.   Fiege, H., Voges, H. W., Hamamoto, T., Umemura, S., Iwata, T., Miki, H., ... & Paulus, W. (2000). Phenol derivatives. *Ullmann's Encyclopedia of Industrial Chemistry*.

2.   Noszczyńska, M., & Piotrowska-Seget, Z. (2018). Bisphenols: Application, occurrence, safety, and biodegradation mediated by bacterial communities in wastewater treatment plants and rivers. *Chemosphere*, *201*, 214-223.

3.   Shah, P. N., Acharige, M. J. T., Kim, N., Ryan, D. K., DeSisto, W., & Lee, Y. (2020). Green Bisphenol A: A High Valued Building Block Isolated from Lignin Biowaste. *Waste and Biomass Valorization*, 1-10.

4.   Ben-Jonathan, N., & Hugo, E. R. (2016). Bisphenols come in different flavors: is "S" better than "A"?.

5.   Rubin, B. S. (2011). Bisphenol A: an endocrine disruptor with widespread exposure and multiple effects. *The Journal of steroid biochemistry and molecular biology*, *127*(1-2), 27-34.

6.   Nagel, S. C., & Bromfield, J. J. (2013). Bisphenol A: a model endocrine disrupting chemical with a new potential mechanism of action.

7.   Michałowicz, J. (2014). Bisphenol A–sources, toxicity and biotransformation. *Environmental toxicology and pharmacology*, *37*(2), 738-758.

8.   Ma, Y., Liu, H., Wu, J., Yuan, L., Wang, Y., Du, X., ... & Zhang, H. (2019). The adverse health effects of bisphenol A and related toxicity mechanisms. *Environmental research*, *176*, 108575.

9.   World Health Organization (WHO). (2010, November). Toxicological and health aspects of bisphenol A. In *Proceedings of the Joint FAO/WHO Expert Meeting, Ottawa, ON, Canada* (pp. 2-5).

10.   Additives, I. F. (2013). Adhesives and Components of Coatings. *Final Rule Food and Drug Administration*, *78*.

11.   FDA, U. (2012). Indirect food additives: Polymers.

12.   Cwiek-Ludwicka, K. (2015). Bisphenol A (BPA) in food contact materials-new scientific opinion from EFSA regarding public health risk. *Roczniki Państwowego Zakładu Higieny*, *66*(4).

13.   Bolognesi, C., Castle, L., Cravedi, J. P., Engel, K. H., Fowler, P. A. F., Franz, R., ... & Zorn, H. (2015). Scientific Opinion on the risks to public health related to the presence of bisphenol A (BPA) in foodstuffs: Executive summary. *Efsa Journal*.

14.   Gallo, P., Pisciottano, I. D. M., Esposito, F., Fasano, E., Scognamiglio, G., Mita, G. D., & Cirillo, T. (2017). Determination of BPA, BPB, BPF, BADGE and BFDGE in canned energy drinks by molecularly imprinted polymer cleaning up and UPLC with fluorescence detection. *Food chemistry*, *220*, 406-412.

15.   Regueiro, J., & Wenzl, T. (2015). Determination of bisphenols in beverages by mixed-mode solid-phase extraction and liquid chromatography coupled to tandem mass spectrometry. *Journal of Chromatography A*, *1422*, 230-238.

16.   Danish, E. P. A. (2014). Alternative technologies and substances to bisphenol A (BPA) in thermal paper receipts. *Environmental project*, (1553).

17.   Russo, G., Barbato, F., & Grumetto, L. (2016). Development and validation of a LC-FD method for the simultaneous determination of eight bisphenols in soft drinks. *Food Analytical Methods*, *9*(10), 2732-2740.

18.   Russo, G., Varriale, F., Barbato, F., & Grumetto, L. (2019). Are canned beverages industries progressively switching to bisphenol AF?. *Journal of food science*, *84*(11), 3303-3311.

19.   Muntau, A. C., Röschinger, W., Habich, M., Demmelmair, H., Hoffmann, B., Sommerhoff, C. P., & Roscher, A. A. (2002). Tetrahydrobiopterin as an alternative treatment for mild phenylketonuria. *New England Journal of Medicine*, *347*(26), 2122-2132.

20.   Kobe, B., Jennings, I. G., House, C. M., Michell, B. J., Goodwill, K. E., Santarsiero, B. D., ... & Kemp, B. E. (1999). Structural basis of autoregulation of phenylalanine hydroxylase. *Nature structural biology*, *6*(5), 442-448.

21.   Vockley, J., Andersson, H. C., Antshel, K. M., Braverman, N. E., Burton, B. K., Frazier, D. M., ... & Berry, S. A. (2014). Phenylalanine hydroxylase deficiency: diagnosis and management guideline. *Genetics in Medicine*, *16*(2), 188.

22.   Fusetti, F., Erlandsen, H., Flatmark, T., & Stevens, R. C. (1998). Structure of tetrameric human phenylalanine hydroxylase and its implications for phenylketonuria. *Journal of Biological Chemistry*, *273*(27), 16962-16967.

23.   Blau, N., & van Spronsen, F. J. (2014). Disorders of phenylalanine and tetrahydrobiopterin metabolism. In *Physician's Guide to the Diagnosis, Treatment, and Follow-Up of Inherited Metabolic Diseases* (pp. 3-21). Springer, Berlin, Heidelberg.

24.   de Baulny, H. O., Abadie, V., Feillet, F., & de Parscau, L. (2007). Management of phenylketonuria and hyperphenylalaninemia. *The Journal of nutrition*, *137*(6), 1561S-1563S.

25.   Stanford, M., & Veating, G. (2009). Sapropterin: a review of its use in the treatment of primary hyperphenylalaninemia. *Drugs*, *69*(4), 461-476.

26.   Davis, M. D., Kaufman, S., & Milstien, S. (1988). The auto-oxidation of tetrahydrobiopterin. *European journal of biochemistry*, *173*(2), 345-351..

27.   Murata, S., Ichinose, H., & Urano, F. (2007). Tetrahydrobiopterin and related biologically important pterins. In *Bioactive Heterocycles II* (pp. 127-171). Springer, Berlin, Heidelberg.

28.   Mitchell, J. J., Trakadis, Y. J., & Scriver, C. R. (2011). Phenylalanine hydroxylase deficiency. *Genetics in medicine*, *13*(8), 697-707.

29.   Schmidt, H., Tegeder, I., & Geisslinger, G. (2006). Determination of neopterin and biopterin by liquid chromatography coupled to tandem mass spectrometry (LC-MS/MS) in rat and human plasma, cell extracts and tissue homogenates.

30.   Zhao, Y., Cao, J., Chen, Y. S., Zhu, Y., Patrick, C., Chien, B., ... & Foehr, E. D. (2009). Detection of tetrahydrobiopterin by LC–MS/MS in plasma from multiple species. *Bioanalysis*, *1*(5), 895-903.

31.   Musson, D. G., Kramer, W. G., Foehr, E. D., Bieberdorf, F. A., Hornfeldt, C. S., Kim, S. S., & Dorenbaum, A. (2010). Relative bioavailability of sapropterin from intact and dissolved sapropterin dihydrochloride tablets and the effects of food: a randomized, open-label, crossover study in healthy adults. *Clinical therapeutics*, *32*(2), 338-346.

32.   Schmitz, K., Trautmann, S., Hahnefeld, L., Fischer, C., Gurke, R., Schreiber, Y., ... & Tegeder, I. (2020). Sapropterin (BH4) aggravates autoimmune encephalomyelitis in mice. *Authorea Preprints*.

33.   Nichol, C. A., Smith, G. K., & Duch, D. S. (1985). Biosynthesis and metabolism of tetrahydrobiopterin and molybdopterin. *Annual review of biochemistry*, *54*(1), 729-764.

34.   Milstien, S., & Kaufman, S. (1989). The biosynthesis of tetrahydrobiopterin in rat brain: Purification and characterization of 6-pyruvoyl tetrahydropterin (2′-oxo) reductase. *Journal of Biological Chemistry*, *264*(14), 8066-8073.

35.   Lambruschini, N., Pérez-Dueñas, B., Vilaseca, M. A., Mas, A., Artuch, R., Gassió, R., ... & Campistol, J. (2005). Clinical and nutritional evaluation of phenylketonuric patients on tetrahydrobiopterin monotherapy. *Molecular genetics and metabolism*, *86*, 54-60.

36.   Scudellaro, E., Tartaglione, L., Varriale, F., Dell'Aversano, C., & Taglialatela-Scafati, O. (2020). HPLC-Based Analysis of Impurities in Sapropterin Branded and Generic Tablets. *Pharmaceutics*, *12*(4), 323.

Ringraziamenti

Ringrazio infinitamente la Prof.ssa Dell'Aversano e la Prof.ssa Tartaglione per avermi dato la possibilità di crescere nel loro gruppo di ricerca, per la fiducia che ogni giorno mi hanno concesso, per aver contribuito allo sviluppo di quello spirito critico ed analitico indispensabile non solo nel settore scientifico, e per le conoscenze trasmesse durante tutto il percorso di dottorato.

Un ringraziamento speciale va alla Prof.ssa Varra, colei che con infinita saggezza ed affetto ha contribuito al raggiungimento di questo traguardo.

Un grazie di cuore al Dr. Andrew Turner, una persona magnifica che con gentilezza e semplicità ha reso unica la mia esperinza nel Regno Unito, umanamente e lavorativamente. Un sentito grazie a tutto lo staff del Cefas, con il quale ho trascorso dure giornate di lavoro ed indimenticabili momenti che mai potrò dimenticare.

Ringrazio affettuosamente tutti gli studenti, colleghi, docenti ed amici con i quali ho condiviso un'importante parte di questo percorso.

Infine, dedico questa tesi alla mia famiglia, quella luce che non si spegne mai nemmeno nelle notti più buie.